Aqueous Concentration Ratios to Estimate Mass of Multi-Component NAPL Residual in Porous Media

by

Stanley Feenstra

A thesis
presented to the University of Waterloo
in fulfilment of the
thesis requirement for the degree of
Doctor of Philosophy
in
Earth Sciences

Waterloo, Ontario, Canada, 1997

The University of Waterloo requires the signatures of all persons using or photocopying this thesis. Please sign below, and give address and date.

Abstract

A method was developed and evaluated for estimating the mass of chemicals contained in NAPL residual zones based on temporal changes in the ratios of the dissolved contaminants derived from the dissolution of multi-component NAPL residual.

The Effective Solubility Model (ESM) was developed as a tool to describe the changes in aqueous concentration ratios of organic contaminants emitted from the dissolution of a multi-component zone of NAPL residual. The model is based on the principle that temporal changes in the ratios of aqueous-phase concentrations in groundwater can be related to the degree of chemical mass depletion of NAPL residual. The ESM utilizes a series of linked equilibration cells to calculate the dissolution of multi-component NAPL according to Raoult's Law.

ESM simulations compared favourably to the results of three published laboratory dissolution experiments and two controlled field experiments. A method was developed using the ESM, together with groundwater monitoring data, to estimate the quantity of chemical mass contained in NAPL zones at sites of NAPL contamination. As an example application, monitoring results of the groundwater pump-and-treat system at the Emplaced-Source experiment were used to estimate the mass of the NAPL source. The NAPL mass estimated using the ESM method was within 20% of the actual NAPL mass. The mass estimate was made using only the measured aqueous concentrations in extraction well PW-2, and the physical and chemical properties for the NAPL components and aquifer. No specific assumptions were required regarding the dimensions or geometry of the source zone, groundwater flow conditions, or dissolution mass transfer coefficients. This research has illustrated the potential for the ESM method to provide useful estimates of the chemical mass contained in multi-component NAPL residual zones in porous media.

Acknowledgments

Our present ability is determine the mass of chemicals contained in NAPL source zones in the subsurface was described succinctly by Jennifer Warnes, in her song - The Hunter:

You never know,

you never know,

you never know when, you never know.

(Attic Records Limited, 1992)

It is hoped that the work described here will improve this ability.

This research was supported financially by the University Consortium Solvents-in-Groundwater Research Program at the University of Waterloo which was funded by The Boeing Company, Ciba-Geigy, Dow Chemical Company, Eastman Kodak Company, General Electric, Laidlaw, Inc., Mitre Corporation, Motorola, PPG Industries, United Technologies, the Natural Science and Engineering Research Council (NSERC), and the Ontario University Research Incentive Fund (URIF).

Many individuals at the University of Waterloo also contributed to the completion of the two controlled field experiments at the Borden site. Dr. Michael Rivett, post-doctoral fellow from the UK, was instrumental in the design and implementation of the Emplaced-Source experiment. Field activities such as the installation of monitoring devices, the collection of cores and plumbing of the groundwater treatment system could not have been completed without the efforts of Bob Ingleton and Paul Johnson. Installation of the source zone was far more challenging than anticipated, and the contributions of Mette Broholm and Sam Vales are gratefully

acknowledged. Doug Morton provided many days of effort in sampling and analysis of groundwater samples from the experiment.

The opportunity to use information from the Free-Release experiment was provided by Dr. Kim Broholm, post-doctoral fellow from Denmark, who was assisted in the implementation of the experiment by Mette Broholm, Paul Johnson, Bert Habicher, Andre Unger, Scott Vales, Sam Vales, Dave Baerg and Jeff Murphy.

Mary Feenstra coded the Excel macro for the Effective Solubility Model and assisted in preparation of the computer graphics.

This thesis has benefited from the review and suggestions of my thesis examination committee of Drs. Jim Barker, Rick Devlin, Doug Mackay and Neil Thomson of the University of Waterloo, and Dr. David Burris of the US Air Force.

Of most significance, I am grateful to my thesis advisor Dr. John Cherry for the opportunity to have pursued this research on a part-time basis, in an unorthodox manner, over an extended period of time, at the University of Waterloo.

Dedication

Dr. Robert N. Farvolden

This thesis is dedicated to the memory of Bob Farvolden. In 1973, it was the enthusiasm of his lectures on introductory geology at Waterloo that woke me, figuratively (and in class on one occasion - literally), to the many fascinating challenges to be found in the study of earth sciences. As I proceeded through my years of undergraduate study at Waterloo, it was he that encouraged me and guided me to graduate work in hydrogeology at Waterloo. Although the hydrogeology program was smaller in 1978-1980 than it is today, it was a stimulating place to study, and the timing was perfect to be among the first wave of hydrogeologists that focused on groundwater contamination. Since then, I have had the opportunity to be involved in consulting on groundwater contamination problems throughout Canada and the United States, and the privilege of pursuing my doctoral studies at Waterloo. These endeavours have been as fulfilling and rewarding as can be hoped for in one's professional career. For Bob's encouragement and direction in leading me to this path, I will be always grateful.

Table of Contents

		Page
Chapter 1. Introduction		
1.1	Objective	1
1.2	Existing Methods for Estimation of NAPL Mass	1
1.3	Aqueous Concentration Ratios for Estimation of NAPL Mass	3
1.4	Conceptual Models for NAPL Source Zones	5
1.5	Chemical Composition of NAPLs	8
Chapter 2. Determination of Effective Solubility		
2.1	Introduction	21
2.2	Solubility of a Single-Component NAPL	21
2.3	Effective Solubility of Multi-Component NAPLs	23
	2.3.1 Ideal Behaviour	23
	2.3.2 Non-Ideal Behaviour	26
2.4	Solubility of Solid-Phase Organic Compounds	27
2.5	Applicability of Raoult's Law for Simple NAPLs	29
	2.5.1 Chlorinated Solvent Mixtures	29
	2.5.2 Chlorinated Benzene Mixtures	32
	2.5.3 Petroleum Hydrocarbon Mixtures	34
	2.5.4 Conclusions on Raoult's Law for Simple NAPLs	36
2.6	Applicability of Raoult's Law for Complex NAPLs	37
	2.6.1 Gasoline	38
	2.6.2 Diesel Fuel	40
	2.6.3 Creosote and Coal Tar	41

Table of Contents

		Page
	2.6.4 Effect of Uncharacterized Portion of NAPL	44
	2.6.5 Conclusions on Raoult's Law for Complex NAPLs	46
2.7	Prediction of Effective Solubility using UNIFAC	47
	2.7.1 Chlorinated Solvent Mixtures	48
	2.7.2 Chlorinated Benzene Mixtures	48
	2.7.3 Petroleum Hydrocarbon Mixtures	49
	2.7.4 Gasoline	49
	2.7.5 Diesel Fuel	50
	2.7.6 Creosote and Coal Tar	50
	2.7.7 Conclusions on UNIFAC for NAPL Mixtures	50
2.8	Other Factors Influencing Solubility	51
	2.8.1 Temperature	51
	2.8.2 pH	51
	2.8.3 Dissolved Inorganics	55
	2.8.4 Miscible Co-Solvents	57
	2.8.5 Surfactants	57
	2.8.6 Dissolved Organic Matter	63
2.9	Overall Conclusions Regarding Effective Solubility	64
Chapter 3. Principles for Dissolution of Multi-Component NAPL		
3.1	Introduction	167
3.2	Dissolution of NAPL Residual	167
	3.2.1 Pore-Scale Mass Transfer Models	167
	3.2.2 Laboratory-Scale Mass Transfer Models	172

TABLE OF CONTENTS

		Page
3.3	Non-Equilibrium Mass Transfer for Multi-Component NAPL	175
3.4	Chromatographic Effect in Multi-Component NAPL Zones	178
3.5	Dissolution of NAPL Pools	179
3.6	Conceptual Models for Dissolution of Multi-Component NAPL	183

Chapter 4. Description of Effective Solubility Model (ESM)

4.1	Principles	195
4.2	Calculation Method	196
	4.2.1 Input Parameters	196
	4.2.2 Iterative Calculations	199
	4.2.3 Output	204
4.3	Sensitivity Analyses	205
	4.3.1 Overview	205
	4.3.2 Effect of Solubility of Components	207
	4.3.3 Effect of Number of Cells	208
	4.3.4 Effect of Soil Organic Carbon	209
	4.3.5 Effect of Porosity	210
	4.3.6 Effect of Initial NAPL Content	210
4.4	Error Analyses	211
4.5	Conclusions Regarding the ESM	213

TABLE OF CONTENTS

		Page
Chapter 5. Comparison of Results of Laboratory Studies to ESM		
5.1	Chlorinated Benzene Mixture	247
	5.1.1 Experimental Conditions	247
	5.1.2 Comparison to ESM	248
5.2	Petroleum Hydrocarbon Mixture	250
	5.2.1 Experimental Conditions	250
	5.2.2 Comparison to ESM	251
5.3	Benzene-Toluene Mixture	252
	5.3.1 Experimental Conditions	252
	5.3.2 Comparison to ESM	253
5.4	Conclusions Regarding Comparison to Laboratory Studies	253
Chapter 6. Controlled Field Study: Emplaced-Source Experiment		
6.1	Overview	287
6.2	Experimental Conditions	289
	6.2.1 Source Installation	289
	6.2.2 Site Layout and Study Program	291
6.3	Investigation and Monitoring Methods	292
	6.3.1 Water Table Monitoring	292
	6.3.2 Groundwater Sampling	292
	6.3.3 Aquifer Cores	294
6.4	Hydrogeological Conditions	295
	6.4.1 Hydraulic Conductivity	295
	6.4.2 Groundwater Flow Direction	296

		Page
	6.4.3 Hydraulic Gradient	297
	6.4.4 Source Zone Composition	297
6.5	Overall Plume Migration	298
6.6	Source Zone Dissolution	300
	6.6.1 Overview	300
	6.6.2 Magnitude of Aqueous Concentrations	300
	6.6.3 Temporal Changes in Aqueous Concentrations	301
	6.6.4 Averaged Aqueous Concentrations	303
6.7	Determination of NAPL Mass Remaining	304
	6.7.1 Mass Flux Crossing the 1 m Fence	305
	6.7.2 Source Cores	306
	6.7.3 Pump-and-Treat System	307
6.8	Temporal Variation in Aqueous Concentration Ratios	307
6.9	Comparison of Measured Ratios to ESM	309
6.10	Conclusions Regarding Emplaced-Source Experiment	310

Chapter 7. Controlled Field Study: Free-Release Experiment

7.1	Overview	379
7.2	Test Cell Layout and Study Program	380
7.3	Investigation and Monitoring Methods	382
	7.3.1 Water Table Monitoring	382
	7.3.2 Groundwater Sampling	382
	7.3.3 Aquifer Cores	384
	7.3.4 Chloride Tracer Test	384

		Page
	7.3.5 Cell Excavation	384
7.4	Hydrogeological Conditions	385
	7.4.1 Hydraulic Conductivity	385
	7.4.2 Hydraulic Gradient	386
	7.4.3 Calculated Groundwater Velocity	387
	7.4.4 Position of NAPL Source Zone	388
7.5	Plume Migration	389
	7.5.1 Overview	389
	7.5.2 Magnitude of Aqueous Concentrations	390
	7.5.3 Temporal Changes in Aqueous Concentrations	390
	7.5.4 Averaged Aqueous Concentrations	392
7.6	Determination of NAPL Mass Remaining	392
7.7	Temporal Variation in Aqueous Concentration Ratios	393
7.8	Comparison of Measured Ratios to ESM	394
7.9	Conclusions Regarding Free-Release Experiment	396

Chapter 8. Application of the ESM Method for Evaluation of NAPL Sites

8.1	Methodology	457
	8.1.1 Overview	457
	8.1.2 Required Field Data	457
	8.1.3 Required Model Parameters	461
	8.1.4 Model Simulations	462
8.2	Example: Emplaced-Source Experiment PW-2	464

		Page
8.3	Dayton Case Study	467
	8.3.1 Site Conditions	467
	8.3.2 DNAPL Source Zone	471
	8.3.3 Aqueous Concentrations and Ratios in GW-32	472
8.4	Conditions for the Application of the ESM Method	474

Chapter 9. Summary and Conclusions

9.1	Determination of Effective Solubility	501
9.2	Principles for Dissolution of Multi-Component NAPL	501
9.3	Effective Solubility Model (ESM)	504
9.4	Comparison to Laboratory Studies	505
9.5	Comparison to the Emplaced-Source Experiment	505
9.6	Comparison to the Free-Release Experiment	506
9.7	Application of the ESM Method for Evaluation of NAPL Sites	507

Chapter 10. References 513

Appendix A.

Evaluation of the Assumption that $\gamma_{aq}^{i} = \gamma_{aq}^{p}$ 527

Appendix B.

ESM Implementation 533

List of Tables

Page

Chapter 1

1-1. Composition of waste solvent DNAPL recovered from monitoring wells at the Savannah River Plant, Aiken, South Carolina. 12

1-2. Composition of waste solvent DNAPL recovered from monitoring wells at the Tyson's Superfund site, King of Prussia, Pennsylvania. 12

1-3. Average composition of DNAPL recovered from nine monitoring wells at the S-Area landfill, Niagara Falls, New York. 13

1-4. Major components of gasoline. 14

1-5. Major components of coal tar. 15

1-6. Isomer composition of PCB Aroclors. 16

Chapter 2

2-1. Solubility of water in selected liquid organic compounds. 70

2-2. Solid-phase solubility and supercooled liquid solubility values for selected PAH compounds. 71

2-3. Pure-phase solubility of chlorinated solvents at 23°C to 24°C determined by Broholm and Feenstra (1995). 72

2-4. Deviation of aqueous concentrations predicted by Raoult's Law from measured aqueous concentrations for laboratory experiments of Broholm and Feenstra (1995). 73

2-5. Pure-phase solubility of chlorinated benzenes at 25°C determined by Banerjee (1984). 74

2-6. Deviation of aqueous concentrations predicted by Raoult's Law from the measured aqueous concentrations for the laboratory experiments of Banerjee (1984). 75

2-7. Pure-phase solubility of selected hydrocarbons at 20°C determined by Burris and MacIntyre (1986b). 76

2-8. Deviation of aqueous concentrations predicted by Raoult's Law from the measured aqueous concentrations for the laboratory experiments by Leinonen and Mackay (1973). 77

2-9. Deviation of aqueous concentrations predicted by Raoult's Law from the measured aqueous concentrations from the laboratory experiments by Burris and MacIntyre. 78

2-10. Deviation of aqueous concentrations predicted by Raoult's Law from measured aqueous concentrations for laboratory experiments on gasoline. 79

2-11. Deviation of aqueous concentrations predicted by Raoult's Law from measured aqueous concentrations for laboratory experiments on diesel fuels. 80

2-12. Deviation of aqueous concentrations predicted by Raoult's Law from measured aqueous concentrations for laboratory experiments on creosote and coal tars. 81

List of Tables

		Page
2-13.	Examples of the uncertainty imparted to the calculated effective solubilities of the characterized components of NAPL for different values of the molecular mass of the UC (uncharacterized) portion.	82
2-14.	Deviation in aqueous concentrations predicted by Raoult's Law and UNIFAC from measured aqueous concentrations for laboratory experiments of Broholm and Feenstra (1995).	83
2-15.	Deviation of aqueous concentrations predicted by Raoult's Law and UNIFAC from measured aqueous concentrations for laboratory experiments of Banerjee (1984).	84
2-16.	Deviation of aqueous concentrations predicted by Raoult's Law and UNIFAC from the measured aqueous concentrations for laboratory experiments by Leinonen and Mackay (1973).	85
2-17.	Deviation of aqueous concentrations predicted by Raoult's Law and UNIFAC from the measured aqueous concentrations for laboratory experiments by Burris and MacIntyre.	86
2-18.	Deviation of aqueous concentrations predicted by Raoult's Law and UNIFAC from the measured aqueous concentrations for laboratory experiments on gasolines.	87
2-19.	Deviation of aqueous concentrations predicted by Raoult's Law and UNIFAC from the measured aqueous concentrations for laboratory experiments on diesel fuels.	88
2-20.	Deviation of aqueous concentrations predicted by Raoult's Law and UNIFAC from the measured aqueous concentrations for laboratory experiments on creosotes and coal tars.	89
2-21	Pure-phase solubility values of selected organic compounds at 0°C and 25°C.	90
2-22.	Organic acids and bases which can be important groundwater contaminants.	91
2-23.	Comparison of solubility of various organic compounds in distilled water and seawater at 25°C.	92
2-24.	Salting Constants for various organic compounds in seawater and sodium chloride solutions.	93
2-25.	Total molecular surface area (TSA) for various organic compounds.	94
2-26.	Examples of the uncertainty associated with the chemical analyses of organic contaminants in groundwater by commercial analytical laboratories.	95

Chapter 3

3-1.	Calculated values for aqueous-phase diffusion coefficients for selected organic contaminants common in groundwater.	187
3-2.	Measured values for mass transfer coefficients determined for the dissolution of coal tars.	188

List of Tables

Page

Chapter 5

5-1. Composition and properties of chlorinated benzene mixture. 256

5-2. Comparison of measured initial aqueous concentrations to effective solubility values calculated by Raoult's Law for the chlorinated benzene mixture. 256

5-3. Composition and properties of petroleum hydrocarbon mixture. 257

5-4. Comparison of measured initial aqueous concentrations to effective solubility values calculated by Raoult's Law for the petroleum hydrocarbon mixture. 257

5-5. Composition and properties of benzene-toluene mixture. 258

5-6. Comparison of measured initial aqueous concentrations to effective solubility values calculated by Raoult's Law for the benzene-toluene mixture. 258

Chapter 6

6-1. Summary of initial source composition based on source core analyses. 312

6-2. Calculation of initial effective solubility values of solvents based on initial NAPL source composition and Raoult's Law. 313

6-3. Composition and properties of the components in the NAPL in the source zone used as input parameters in the ESM simulations. 314

Chapter 7

7-1. Calculation of initial effective solubility values of solvents based on initial NAPL source composition and Raoult's Law. 397

7-2. Composition and properties of the components in the NAPL in the source zone used as input parameters in the ESM simulations. 398

Chapter 8

8-1. Calculation of initial NAPL source composition based on aqueous concentrations in PW-2. 478

8-2. Composition and properties of the components in the NAPL in the source zone used as input parameters in the ESM simulations for the PW-2 data. 479

8-3. Calculation of initial NAPL source composition based on aqueous concentrations in GW-32. 480

8-4. Composition and properties of the components in the NAPL in the source zone used as input parameters in the ESM simulations for the Dayton site. 481

List of Figures

Page

Chapter 1

1-1. Example of changes in measured aqueous concentration ratios observed at the Dayton, New Jersey site, and aqueous concentration ratios predicted by a 1-cell ESM. 17

1-2. Conceptual model for LNAPL contamination in the subsurface. 18

1-3. Conceptual model for DNAPL contamination in the subsurface. 19

Chapter 2

2-1. Relationship between supercooled liquid solubility and solid-phase solubility versus melting point. 96

2-2. Comparison of measured aqueous concentrations to aqueous concentrations calculated by Raoult's Law for trichloroethylene - chloroform mixtures. 97

2-3. Comparison of measured aqueous concentrations to aqueous concentrations calculated by Raoult's Law for trichloroethylene - carbon tetrachloride mixtures. 98

2-4. Comparison of measured aqueous concentrations to aqueous concentrations calculated by Raoult's Law for trichloroethylene - 1,1,1-trichloroethane mixtures. 99

2-5. Comparison of measured aqueous concentrations to aqueous concentrations calculated by Raoult's Law for trichloroethylene - tetrachloroethylene mixtures. 100

2-6. Comparison of measured aqueous concentrations to aqueous concentrations calculated by Raoult's Law for tetrachloroethylene - chloroform mixtures. 101

2-7. Comparison of measured aqueous concentrations to aqueous concentrations calculated by Raoult's Law for tetrachloroethylene - carbon tetrachloride mixtures. 102

2-8. Comparison of measured aqueous concentrations to aqueous concentrations calculated by Raoult's Law for tetrachloroethylene - 1,1,1-trichloroethane mixtures. 103

2-9. Comparison of measured aqueous concentrations to aqueous concentrations calculated by Raoult's Law for chloroform - trichloroethylene-tetrachloroethylene mixtures. 104

2-10. Comparison of measured aqueous concentrations to aqueous concentrations calculated by Raoult's Law for chlorobenzene - 1,3-dichlorobenzene mixtures. 105

2-11. Comparison of measured aqueous concentrations to aqueous concentrations calculated by Raoult's Law for chlorobenzene - 1,2,4-trichlorobenzene mixtures. 106

2-12. Comparison of measured aqueous concentrations to aqueous concentrations calculated by Raoult's Law for chlorobenzene - 1,3-dichlorobenzene - 1,2,4-trichlorobenzene mixtures. 107

List of Figures

		Page
2-13.	Comparison of measured aqueous concentrations to aqueous concentrations calculated by Raoult's Law for chlorobenzene - 1,2,4,5-tetrachlorobenzene mixtures.	108
2-14.	Comparison of measured aqueous concentrations to aqueous concentrations calculated by Raoult's Law for benzene - 2-methyl pentane mixtures.	109
2-15.	Comparison of measured aqueous concentrations to aqueous concentrations calculated by Raoult's Law for n-octane - 1-methyl naphthalene mixtures.	110
2-16.	Comparison of measured aqueous concentrations to aqueous concentrations calculated by Raoult's Law for tetralin - methylcyclohexane mixtures.	111
2-17.	Comparison of measured aqueous concentrations to aqueous concentrations calculated by Raoult's Law for ethyl benzene - n-octane mixtures.	112
2-18.	Comparison of measured aqueous concentrations to aqueous concentrations calculated by Raoult's Law for 4-component hydrocarbon mixture.	113
2-19.	Comparison of measured aqueous concentrations to aqueous concentrations calculated by Raoult's Law for a simulated JP-4 jet fuel mixture.	114
2-20.	Comparison of measured aqueous concentrations to aqueous concentrations calculated by Raoult's Law for a PS-6 gasoline.	115
2-21.	Comparison of measured aqueous concentrations to aqueous concentrations calculated by Raoult's Law for a PS-6 gasoline.	116
2-22.	Comparison of measured aqueous concentrations to aqueous concentrations calculated by Raoult's Law for the average composition of 31 gasolines.	117
2-23.	Comparison of measured aqueous concentrations to aqueous concentrations calculated by Raoult's Law for a sample of diesel fuel (#1).	118
2-24.	Comparison of measured aqueous concentrations to aqueous concentrations calculated by Raoult's Law for a sample of diesel fuel (#2).	119
2-25.	Comparison of measured aqueous concentrations to aqueous concentrations calculated by Raoult's Law for a sample of diesel fuel (#3).	120
2-26.	Comparison of measured aqueous concentrations to aqueous concentrations calculated by Raoult's Law for a sample of diesel fuel (#4).	121
2-27.	Comparison of measured aqueous concentrations to aqueous concentrations calculated by Raoult's Law for a sample of creosote.	122
2-28.	Comparison of measured aqueous concentrations to aqueous concentrations calculated by Raoult's Law for a sample of coal tar (#1).	123
2-29.	Comparison of measured aqueous concentrations to aqueous concentrations calculated by Raoult's Law for a sample of coal tar (#4).	124
2-30.	Comparison of measured aqueous concentrations to aqueous concentrations calculated by Raoult's Law for a sample of coal tar (#5).	125
2-31.	Illustration of the sensitivity of the calculated effective solubility to the assumed molecular mass (MM) of the uncharacterized (UC) portion of a multi-component NAPL. For a ratio of MM of the UC portion to average MM of characterized portion equal to 1.	126

List of Figures

		Page
2-32.	Illustration of the sensitivity of the calculated effective solubility to the assumed molecular mass (MM) of the uncharacterized (UC) portion of a multi-component NAPL. For a ratio of MM of the UC portion to average MM of characterized portion equal to 1.5	127
2-33.	Illustration of the sensitivity of the calculated effective solubility to the assumed molecular mass (MM) of the uncharacterized (UC) portion of a multi-component NAPL. For a ratio of MM of the UC portion to average MM of characterized portion equal to 0.5.	128
2-34.	Comparison of measured aqueous concentrations to aqueous concentrations calculated by Raoult's Law and UNIFAC for trichloroethylene - chloroform mixtures.	129
2-35.	Comparison of measured aqueous concentrations to aqueous concentrations calculated by Raoult's Law and UNIFAC for trichloroethylene - carbon tetrachloride mixtures.	130
2-36.	Comparison of measured aqueous concentrations to aqueous concentrations calculated by Raoult's Law and UNIFAC for trichloroethylene - 1,1,1-trichloroethane mixtures.	131
2-37.	Comparison of measured aqueous concentrations to aqueous concentrations calculated by Raoult's Law and UNIFAC for trichloroethylene - tetrachloroethylene mixtures.	132
2-38.	Comparison of measured aqueous concentrations to aqueous concentrations calculated by Raoult's Law and UNIFAC for tetrachloroethylene - chloroform mixtures.	133
2-39.	Comparison of measured aqueous concentrations to aqueous concentrations calculated by Raoult's Law and UNIFAC for tetrachloroethylene - carbon tetrachloride mixtures.	134
2-40.	Comparison of measured aqueous concentrations to aqueous concentrations calculated by Raoult's Law and UNIFAC for tetrachloroethylene - 1,1,1-trichloroethane mixtures.	135
2-41.	Comparison of measured aqueous concentrations to aqueous concentrations calculated by Raoult's Law and UNIFAC for chloroform - trichloroethylene - tetrachloroethylene mixtures.	136
2-42.	Comparison of measured aqueous concentrations to aqueous concentrations calculated by Raoult's Law and UNIFAC for chlorobenzene - 1,3-dichlorobenzene mixtures.	137
2-43.	Comparison of measured aqueous concentrations to aqueous concentrations calculated by Raoult's Law and UNIFAC for chlorobenzene - 1,2,4-trichlorobenzene mixtures.	138
2-44.	Comparison of measured aqueous concentrations to aqueous concentrations calculated by Raoult's Law and UNIFAC for chlorobenzene - 1,3-dichlorobenzene - 1,2,4-trichlorobenzene mixtures.	139
2-45.	Comparison of measured aqueous concentrations to aqueous concentrations calculated by Raoult's Law and UNIFAC for benzene - 2-methyl pentane mixtures.	140

List of Figures

		Page
2-46.	Comparison of measured aqueous concentrations to aqueous concentrations calculated by Raoult's Law and UNIFAC for n-octane - 1-methyl naphthalene mixtures.	141
2-47.	Comparison of measured aqueous concentrations to aqueous concentrations calculated by Raoult's Law and UNIFAC for tetralin - methylcyclohexane mixtures.	142
2-48.	Comparison of measured aqueous concentrations to aqueous concentrations calculated by Raoult's Law and UNIFAC for ethyl benzene - n-octane mixtures.	143
2-49.	Comparison of measured aqueous concentrations to aqueous concentrations calculated by Raoult's Law and UNIFAC for a 4-component hydrocarbon mixture.	144
2-50.	Comparison of measured aqueous concentrations to aqueous concentrations calculated by Raoult's Law and UNIFAC for a simulated JP-4 jet fuel mixture.	145
2-51.	Comparison of measured aqueous concentrations to aqueous concentrations calculated by Raoult's Law and UNIFAC for a PS-6 gasoline.	146
2-52.	Comparison of measured aqueous concentrations to aqueous concentrations calculated by Raoult's Law and UNIFAC for a PS-6 gasoline.	147
2-53.	Comparison of measured aqueous concentrations to aqueous concentrations calculated by Raoult's Law and UNIFAC for the average composition of 31 gasolines.	148
2-54.	Comparison of measured aqueous concentrations to aqueous concentrations calculated by Raoult's Law and UNIFAC for a sample of diesel fuel (#1).	149
2-55.	Comparison of measured aqueous concentrations to aqueous concentrations calculated by Raoult's Law and UNIFAC for a sample of diesel fuel (#2).	150
2-56.	Comparison of measured aqueous concentrations to aqueous concentrations calculated by Raoult's Law and UNIFAC for a sample of diesel fuel (#3).	151
2-57.	Comparison of measured aqueous concentrations to aqueous concentrations calculated by Raoult's Law and UNIFAC for a sample of diesel fuel (#4).	152
2-58.	Comparison of measured aqueous concentrations to aqueous concentrations calculated by Raoult's Law and UNIFAC for a sample of creosote.	153
2-59.	Comparison of measured aqueous concentrations to aqueous concentrations calculated by Raoult's Law and UNIFAC for a sample of coal tar (#1).	154
2-60.	Comparison of measured aqueous concentrations to aqueous concentrations calculated by Raoult's Law and UNIFAC for a sample of coal tar (#4).	155
2-61.	Comparison of measured aqueous concentrations to aqueous concentrations calculated by Raoult's Law and UNIFAC for a sample of coal tar (#5).	156
2-62.	Solid-phase solubility of pentachlorophenol (PCP) versus pH.	157
2-63.	Solubility of organic compounds with increasing concentration of dissolved salts.	158
2-64.	Increase in solubility of trichloroethylene (TCE), 1,2,4-trichlorobenzene (124-TCBz) and pyrene in a methanol-water system.	159

List of Figures

Page

2-65. Increase in solubility of trichloroethylene (TCE), 1,2,4-trichlorobenzene (124-TCBz) and pyrene in an acetone-water system. 160

2-66. Example of the effect of the surfactant, sodium dodecyl sulfate, on the solubility of 1,2,3-trichlorobenzene. 161

2-67. Increase in solubility of 1,2-dichloroethylene, trichloroethylene and tetrachloroethylene in the presence of various surfactants. 162

2-68. Increase in solubility of naphthalene, phenanthrene and pyrene in the presence of various surfactants. 163

2-69. Increase in solubility of 1,2,3-trichlorobenzene and DDT in the presence of various surfactants. 164

2-70. Values of CMC for a set of 125 typical surfactant compounds. 165

2-71. Increase in solubility of organic contaminants due to the presence of dissolved organic matter. 166

Chapter 3

3-1. Consistency in relative aqueous concentrations during approach to solubility limits for dissolution of mixture of methylcyclohexane and 1-methyl naphthalene. 189

3-2. Consistency in relative aqueous concentrations during approach to solubility limits for dissolution of mixture of methylcyclohexane, ethyl benzene, tetralin and 1-methyl naphthalene. 190

3-3. Consistency in relative aqueous concentrations during approach to solubility limits for dissolution of mixture of ethyl benzene and tetralin. 191

3-4. Aqueous concentrations and concentration ratios above a multi-component NAPL pool of TCM and PCE. 192

3-5. Schematic diagram of conceptual conditions for dissolution of multi-component NAPL. 193

Chapter 4

4-1. Schematic of calculation sequence for the Effective Solubility Model. 215

4-2. Aqueous concentration ratios predicted by ESM for binary NAPL mixture with differing pure-phase solubility, for 1-cell configuration. 216

4-3. Aqueous concentration ratios predicted by ESM for binary NAPL mixture with pure-phase solubilities of 1,000 mg/L (component A) and 500 mg/L (component B) for 1-cell, 10-cell and 100-cell configurations. 217

4-4. Aqueous concentration ratios predicted by ESM for binary NAPL mixture with pure-phase solubilities of 1,000 mg/L (component A) and 100 mg/L (component B) for 1-cell, 10-cell and 100-cell configurations. 218

4-5. Aqueous concentration ratios predicted by ESM for binary NAPL mixture with pure-phase solubilities of 1,000 mg/L (component A) and 10 mg/L (component B) for 1-cell, 10-cell and 100-cell configurations. 219

List of Figures

		Page
4-6.	Aqueous concentration ratios predicted by ESM for binary NAPL mixture with pure-phase solubilities of 1,000 mg/L (component A) and 1 mg/L (component B) for 1-cell, 10-cell and 100-cell configurations.	220
4-7.	Aqueous concentration ratios predicted by ESM for binary NAPL mixture with pure-phase solubilities of 1,000 mg/L (component A) and 500 mg/L (component B) for f_{OC} values of 0.0001, 0.001 and 0.01.	221
4-8.	Aqueous concentration ratios predicted by ESM for binary NAPL mixture with pure-phase solubilities of 1,000 mg/L (component A) and 100 mg/L (component B) for f_{OC} values of 0.0001, 0.001 and 0.01.	222
4-9.	Aqueous concentration ratios predicted by ESM for binary NAPL mixture with pure-phase solubilities of 1,000 mg/L (component A) and 10 mg/L (component B) for f_{OC} values of 0.0001, 0.001 and 0.01.	223
4-10.	Aqueous concentration ratios predicted by ESM for binary NAPL mixture with pure-phase solubilities of 1,000 mg/L (component A) and 1 mg/L (component B) for f_{OC} values of 0.0001, 0.001 and 0.01.	224
4-11.	Aqueous concentration ratios predicted by ESM for binary NAPL mixture with pure-phase solubilities of 100 mg/L (component A) and 10 mg/L (component B) for f_{OC} values of 0.0001, 0.001 and 0.01.	225
4-12.	Aqueous concentration ratios predicted by ESM for binary NAPL mixture with pure-phase solubilities of 1,000 mg/L (component A) and 500 mg/L (component B) for porosity values of 0.2, 0.3 and 0.4.	226
4-13.	Aqueous concentration ratios predicted by ESM for binary NAPL mixture with pure-phase solubilities of 1,000 mg/L (component A) and 100 mg/L (component B) for porosity values of 0.2, 0.3 and 0.4.	227
4-14.	Aqueous concentration ratios predicted by ESM for binary NAPL mixture with pure-phase solubilities of 1,000 mg/L (component A) and 10 mg/L (component B) for porosity values of 0.2, 0.3 and 0.4.	228
4-15.	Aqueous concentration ratios predicted by ESM for binary NAPL mixture with pure-phase solubilities of 1,000 mg/L (component A) and 1 mg/L (component B) for porosity values of 0.2, 0.3 and 0.4.	229
4-16.	Aqueous concentration ratios predicted by ESM for binary NAPL mixture with pure-phase solubilities of 100 mg/L (component A) and 10 mg/L (component B) for porosity values of 0.2, 0.3 and 0.4.	230
4-17.	Aqueous concentration ratios predicted by ESM for binary NAPL mixture with pure-phase solubilities of 1,000 mg/L (component A) and 500 mg/L (component B) for NAPL residual contents of 5 L/m^3, 15 L/m^3 and 50 L/m^3.	231
4-18.	Aqueous concentration ratios predicted by ESM for binary NAPL mixture with pure-phase solubilities of 1,000 mg/L (component A) and 100 mg/L (component B) for NAPL residual contents of 5 L/m^3, 15 L/m^3 and 50 L/m^3.	232
4-19.	Aqueous concentration ratios predicted by ESM for binary NAPL mixture with pure-phase solubilities of 1,000 mg/L (component A) and 10 mg/L (component B) for NAPL residual contents of 5 L/m^3, 15 L/m^3 and 50 L/m^3.	233

Page

4-20. Aqueous concentration ratios predicted by ESM for binary NAPL mixture with pure-phase solubilities of 1,000 mg/L (component A) and 1 mg/L (component B) for NAPL residual contents of 1 L/m^3, 5 L/m^3 and 15 L/m^3. 234

4-21. Aqueous concentration ratios predicted by ESM for binary NAPL mixture with pure-phase solubilities of 100 mg/L (component A) and 10 mg/L (component B) for NAPL residual contents of 5 L/m^3, 15 L/m^3 and 50 L/m^3. 235

4-22. Aqueous concentration ratios predicted by ESM for binary NAPL mixture with pure-phase solubilities of 1,000 mg/L (component A) and 500 mg/L (component B) for +15% and -15% error in the solubility of component A. 236

4-23. Aqueous concentration ratios predicted by ESM for binary NAPL mixture with pure-phase solubilities of 1,000 mg/L (component A) and 500 mg/L (component B) for +15% and -15% error in the solubility of component B. 237

4-24. Aqueous concentration ratios predicted by ESM for binary NAPL mixture with pure-phase solubilities of 1,000 mg/L (component A) and 100 mg/L (component B) for +15% and -15% error in the solubility of component A. 238

4-25. Aqueous concentration ratios predicted by ESM for binary NAPL mixture with pure-phase solubilities of 1,000 mg/L (component A) and 100 mg/L (component B) for +15% and -15% error in the solubility of component B. 239

4-26. Aqueous concentration ratios predicted by ESM for binary NAPL mixture with pure-phase solubilities of 1,000 mg/L (component A) and 10 mg/L (component B) for +15% and -15% error in the solubility of component A. 240

4-27. Aqueous concentration ratios predicted by ESM for binary NAPL mixture with pure-phase solubilities of 1,000 mg/L (component A) and 10 mg/L (component B) for +15% and -15% error in the solubility of component B. 241

4-28. Aqueous concentration ratios predicted by ESM for binary NAPL mixture with pure-phase solubilities of 1,000 mg/L (component A) and 1 mg/L (component B) for +15% and -15% error in the solubility of component A. 242

4-29. Aqueous concentration ratios predicted by ESM for binary NAPL mixture with pure-phase solubilities of 1,000 mg/L (component A) and 1 mg/L (component B) for +15% and -15% error in the solubility of component B. 243

4-30. Aqueous concentration ratios predicted by 1-cell ESM for NAPL mixtures having an unknown component with different pure-phase solubility values. 244

4-31. Aqueous concentration ratios predicted by 10-cell ESM for NAPL mixtures having an unknown component with different pure-phase solubility values. 245

Chapter 5

5-1. Measured aqueous concentrations for mixture of chlorobenzenes in a laboratory column dissolution experiment. 259

5-2. Measured trichlorobenzene/chlorobenzene ratios for dissolution of a mixture of chlorobenzenes. 260

5-3. Measured tetrachlorobenzene/chlorobenzene ratios for dissolution of a mixture of chlorobenzenes. 261

List of Figures

		Page
5-4.	Measured tetrachlorobenzene/trichlorobenzene ratios for dissolution of a mixture of chlorobenzenes.	262
5-5.	Measured trichlorobenzene/chlorobenzene ratios versus NAPL remaining for dissolution of a mixture of chlorobenzenes.	263
5-6.	Measured tetrachlorobenzene/chlorobenzene ratios versus NAPL remaining for dissolution of a mixture of chlorobenzenes.	264
5-7.	Measured tetrachlorobenzene/trichlorobenzene ratios versus NAPL remaining for dissolution of a mixture of chlorobenzenes.	265
5-8.	Comparison of measured aqueous concentrations to aqueous concentrations predicted using the ESM for 1-cell configuration.	266
5-9.	Comparison of measured aqueous concentrations to aqueous concentrations predicted using the ESM for 2-cell configuration.	267
5-10.	Comparison of measured aqueous concentrations to aqueous concentrations predicted using ESM for 4-cell configuration.	268
5-11.	Comparison of measured trichlorobenzene/chlorobenzene ratios to ratios predicted using the ESM for 1-cell, 2-cell and 4-cell configurations.	269
5-12.	Comparison of measured tetrachlorobenzene/chlorobenzene ratios to ratios predicted using the ESM for 1-cell, 2-cell and 4-cell configurations.	270
5-13.	Comparison of measured tetrachlorobenzene/trichlorobenzene ratios to ratios predicted using the ESM for 1-cell, 2-cell and 4-cell configurations.	271
5-14.	Measured aqueous concentrations for mixture of hydrocarbons in a laboratory column dissolution experiment.	272
5-15.	Measured hexane/cyclohexane ratios for dissolution of a mixture of hydrocarbons.	273
5-16.	Measured hexane/dimethyl butane ratios for dissolution of a mixture of hydrocarbons.	274
5-17.	Measured dimethyl butane/cyclohexane ratios for dissolution of a mixture of hydrocarbons.	275
5-18.	Measured hexane/cyclohexane ratios versus NAPL remaining for dissolution of a mixture of hydrocarbons.	276
5-19.	Measured hexane/dimethyl butane ratios versus NAPL remaining for dissolution of a mixture of hydrocarbons.	277
5-20.	Measured dimethyl butane/cyclohexane ratios versus NAPL remaining for dissolution of a mixture of hydrocarbons.	278
5-21.	Comparison of measured hexane/cyclohexane ratios to ratios predicted using ESM for 1-cell, 5-cell and 10-cell configurations.	279
5-22.	Comparison of measured hexane/dimethyl butane ratios to ratios predicted using ESM for 1-cell, 5-cell and 10-cell configurations.	280
5-23.	Comparison of measured dimethyl butane/cyclohexane ratios to ratios predicted using ESM for 1-cell, 5-cell and 10-cell configurations.	281
5-24.	Measured aqueous concentrations for benzene-toluene mixture in a laboratory column dissolution experiment.	282

Page

5-25. Measured toluene/benzene ratios for dissolution of a benzene-toluene mixture. 283

5-26. Measured toluene/benzene ratios versus NAPL remaining for dissolution of a benzene-toluene mixture. 284

5-27. Comparison of measured toluene/benzene ratios to ratios predicted using ESM for 1-cell, 2-cell and 3-cell configurations. 285

Chapter 6

6-1. Location of Canadian Forces Base Borden, Ontario. 315

6-2. Location of Emplaced-Source experimental site at the Canadian Forces Base Borden. 316

6-3. Schematic diagram of source zone configuration for the Emplaced-Source experiment. 317

6-4. Layout of groundwater monitoring points and water table monitoring wells for the Emplaced-Source experiment. 318

6-5. Location of groundwater monitoring points along the centre line of the aqueous-phase plumes. 319

6-6. Section diagram of monitoring points located along the 1 m Fence, viewed looking upgradient toward the source. 320

6-7. Hydraulic conductivity profiles for the aquifer at the 1m Fence and in the source zone. 321

6-8. Temporal change in hydraulic head and groundwater flow direction. 322

6-9. Temporal change in horizontal hydraulic gradient. 323

6-10. Initial composition of emplaced source based on the results of a soil core taken immediately after source emplacement. 324

6-11. Extents of aqueous-phase plumes emitted from the source zone at 322 days after emplacement. 325

6-12. Longitudinal section of chloroform (TCM) aqueous-phase plume at 322 days. 326

6-13. Layout of groundwater pump-and-treat and *in situ* treatment wall installed to control the aqueous-phase plumes emitted from the source zone. 327

6-14. Shrinkage of TCE (trichloroethylene) plume downgradient of PW-2 in response to operation of the pump-and-treat system. 328

6-15. Temporal variation in aqueous concentrations at monitoring point ES-2-8. 329

6-16. Aqueous-phase plumes along the 1 m Fence. 330

6-17. Temporal variation in aqueous concentrations at monitoring point ES-3-9. 331

6-18. Temporal variation in aqueous concentrations at monitoring point ES-2-12. 332

6-19. Temporal variation in aqueous concentrations averaged for monitoring location ES-4. 333

6-20. Temporal variation in aqueous concentrations averaged for monitoring location ES-3. 334

List of Figures

		Page
6-21.	Temporal variation in aqueous concentrations averaged for monitoring location ES-2.	335
6-22.	Temporal variation in aqueous concentrations averaged for monitoring location ES-1.	336
6-23.	Temporal variation in aqueous concentrations averaged for monitoring location ES-28.	337
6-24.	Temporal variation in aqueous concentrations averaged for all the monitoring locations along the 1 m Fence.	338
6-25.	Hydraulic gradient values used for calculation of chemical mass flux crossing the 1 m Fence.	339
6-26.	Temporal variation in chemical mass flux crossing the 1 m Fence.	340
6-27.	Change in NAPL mass remaining versus time based on calculated cumulative mass crossing the 1 m Fence.	341
6-28.	Change in chloroform (TCM) concentrations in source zone based on analysis of core samples.	342
6-29.	Change in trichloroethylene (TCE) concentrations in source zone based on analysis of core samples.	343
6-30.	Change in tetrachloroethylene (PCE) concentrations in source zone based on analysis of core samples.	344
6-31.	Change in NAPL mass remaining versus time based on calculated chemical mass crossing the 1 m Fence, compared to source cores.	345
6-32.	Aqueous-phase concentrations in PW-2 during operation of the pump-and-treat system.	346
6-33.	Calculated chemical mass flux from PW-2 during operation of the pump-and-treat system.	347
6-34.	Temporal variation in aqueous concentration ratios for concentrations averaged for the 1 m Fence.	348
6-35.	Change in aqueous concentration ratios versus NAPL mass remaining for concentrations averaged for the 1 m Fence.	349
6-36.	Temporal variation in aqueous concentration ratios for concentrations averaged for monitoring location ES-2.	350
6-37.	Change in aqueous concentration ratios versus NAPL mass remaining for concentrations averaged for monitoring location ES-2.	351
6-38.	Temporal variation in aqueous concentration ratios for concentrations averaged for monitoring location ES-1.	352
6-39.	Change in aqueous concentration ratios versus NAPL mass remaining for concentrations averaged for monitoring location ES-1.	353
6-40.	Temporal variation in aqueous concentration ratios at monitoring point ES-2-8.	354
6-41.	Change in aqueous concentration ratios versus NAPL mass remaining at monitoring point ES-2-8.	355

List of Figures

		Page
6-42.	Temporal variation in aqueous concentration ratios for concentrations averaged for monitoring location ES-3.	356
6-43.	Change in aqueous concentration ratios versus NAPL mass remaining for concentrations averaged for monitoring location ES-3.	357
6-44.	Temporal variation in aqueous concentration ratios at monitoring point ES-3-9.	358
6-45.	Change in aqueous concentration ratios versus NAPL mass remaining at monitoring point ES-3-9.	359
6-46.	Temporal variation in aqueous concentration ratios for concentrations averaged for monitoring location ES-4.	360
6-47.	Change in aqueous concentration ratios versus NAPL mass remaining for concentrations averaged for monitoring location ES-4.	361
6-48.	Temporal variation in aqueous concentration ratios for concentrations averaged for monitoring location ES-28.	362
6-49.	Change in aqueous concentration ratios versus NAPL mass remaining for concentrations averaged for monitoring location ES-28.	363
6-50.	Change in TCE/TCM ratio versus NAPL remaining predicted by ESM.	364
6-51.	Change in PCE/TCM ratio versus NAPL remaining predicted by ESM.	365
6-52.	Change in PCE/TCE ratio versus NAPL remaining predicted by ESM.	366
6-53.	Measured TCE/TCM ratios versus NAPL remaining for concentrations averaged over the 1 m Fence compared to ratios predicted by the ESM.	367
6-54.	Measured PCE/TCM ratios versus NAPL remaining for concentrations averaged over the 1 m Fence compared to ratios predicted by the ESM.	368
6-55.	Measured PCE/TCE ratios versus NAPL remaining for concentrations averaged over the 1 m Fence compared to ratios predicted by the ESM.	369
6-56.	Measured TCE/TCM ratios versus NAPL remaining for averaged concentrations at monitoring location ES-2 compared to ratios predicted by the ESM.	370
6-57.	Measured PCE/TCM ratios versus NAPL remaining for averaged concentrations at monitoring location ES-2 compared to ratios predicted by the ESM.	371
6-58.	Measured PCE/TCE ratios versus NAPL remaining for averaged concentrations at monitoring location ES-2 compared to ratios predicted by the ESM.	372
6-59.	Measured TCE/TCM ratios versus NAPL remaining for averaged concentrations at monitoring location ES-1 compared to ratios predicted by the ESM.	373
6-60.	Measured PCE/TCM ratios versus NAPL remaining for averaged concentrations at monitoring location ES-1 compared to ratios predicted by the ESM.	374
6-61.	Measured PCE/TCE ratios versus NAPL remaining for averaged concentrations at monitoring location ES-1 compared to ratios predicted by the ESM.	375
6-62.	Measured TCE/TCM ratios versus NAPL remaining for monitoring point ES-2-8 compared to ratios predicted by the ESM.	376
6-63.	Measured PCE/TCM ratios versus NAPL remaining for monitoring point ES-2-8 compared to ratios predicted by the ESM.	377

Page

6-64. Measured PCE/TCE ratios versus NAPL remaining for monitoring point ES-2-8 compared to ratios predicted by the ESM. 378

Chapter 7

7-1. Location of the Free-Release experimental site at the Canadian Forces Base Borden. 399

7-2. Plan map of test cell for the Free-Release Experiment. 400

7-3. Section diagram of monitoring points located downgradient of the NAPL source zone. 401

7-4. Hydraulic conductivity profiles for the aquifer inside the test cell. 402

7-5. Temporal variation in water levels in the extraction wells and injection wells. 403

7-6. Slope of the water table along the test cell. 404

7-7. Vertical profiles of linear groundwater velocity determined from the arrival of chloride tracer at the monitoring points. 405

7-8. Section diagram showing configuration of the NAPL source zone. 406

7-9. Plan map showing lateral extent of NAPL zone. 407

7-10. Aqueous phase plumes in the monitoring arrays. 408

7-11. Temporal variation in aqueous concentrations at monitoring point FR-5-7. 409

7-12. Temporal variation in aqueous concentrations at monitoring point FR-5-5. 410

7-13. Temporal variation in aqueous concentrations at monitoring point FR-5-9. 411

7-14. Temporal variation in aqueous concentrations averaged for monitoring location FR-6. 412

7-15. Temporal variation in aqueous concentrations averaged for monitoring location FR-5. 413

7-16. Temporal variation in aqueous concentrations averaged for monitoring location FR-4. 414

7-17. Temporal variation in aqueous concentrations averaged for monitoring location FR-7. 415

7-18. Temporal variation in aqueous concentrations averaged for monitoring location FR-3. 416

7-19. Temporal variation in aqueous concentrations in the effluent of the test cell. 417

7-20. Temporal variation in chemical mass flux for the effluent from the test cell. 418

7-21. Temporal change in NAPL mass remaining based on mass removed in cell effluent. 419

7-22. Temporal variation in aqueous concentration ratios for the effluent from the test cell. 420

7-23. Change in aqueous concentration ratios versus NAPL remaining for the effluent from the test cell. 421

List of Figures

		Page
7-24.	Temporal variation in aqueous concentration ratios averaged for monitoring location FR-6.	422
7-25.	Change in aqueous concentration ratios versus NAPL remaining averaged for monitoring location FR-6.	423
7-26.	Temporal variation in aqueous concentration ratios averaged for monitoring location FR-5.	424
7-27.	Change in aqueous concentration ratios versus NAPL remaining averaged for monitoring location FR-5.	425
7-28.	Temporal variation in aqueous concentration ratios averaged for monitoring location FR-4.	426
7-29.	Change in aqueous concentration ratios versus NAPL remaining averaged for monitoring location FR-4.	427
7-30.	Temporal variation of aqueous concentration ratios at monitoring point FR-5-7.	428
7-31.	Change in aqueous concentration ratios versus NAPL remaining for monitoring point FR-5-7.	429
7-32.	Temporal variation of aqueous concentration ratios at monitoring point FR-5-5.	430
7-33.	Change in aqueous concentration ratios versus NAPL remaining for monitoring point FR-5-5.	431
7-34.	Temporal variation of aqueous concentration ratios at monitoring point FR-5-9.	432
7-35.	Change in aqueous concentration ratios versus NAPL remaining for monitoring point FR-5-9.	433
7-36.	Temporal variation in aqueous concentration ratios averaged for monitoring location FR-7.	434
7-37.	Change in aqueous concentration ratios versus NAPL remaining averaged for monitoring location FR-7.	435
7-38.	Temporal variation in aqueous concentration ratios averaged for monitoring location FR-3.	436
7-39.	Change in aqueous concentration ratios versus NAPL remaining averaged for monitoring location FR-3.	437
7-40.	Change in TCE/TCM ratio versus NAPL remaining predicted by ESM.	438
7-41.	Change in PCE/TCM ratio versus NAPL remaining predicted by ESM.	439
7-42.	Change in PCE/TCE ratio versus NAPL remaining predicted by ESM.	440
7-43.	Measured TCE/TCM ratios versus NAPL remaining for average concentrations in the cell effluent compared to ratios predicted by ESM.	441
7-44.	Measured PCE/TCM ratios versus NAPL remaining for average concentrations in the cell effluent compared to ratios predicted by ESM.	442
7-45.	Measured PCE/TCE ratios versus NAPL remaining for average concentrations in the cell effluent compared to ratios predicted by ESM.	443
7-46.	Measured TCE/TCM ratios versus NAPL remaining for average concentrations at monitoring location FR-6 compared to ratios predicted by ESM.	444

List of Figures

		Page
7-47.	Measured PCE/TCM ratios versus NAPL remaining for average concentrations at monitoring location FR-6 compared to ratios predicted by ESM.	445
7-48.	Measured PCE/TCE ratios versus NAPL remaining for average concentrations at monitoring location FR-6 compared to ratios predicted by ESM.	446
7-49.	Measured TCE/TCM ratios versus NAPL remaining for average concentrations at monitoring location FR-5 compared to ratios predicted by ESM.	447
7-50.	Measured PCE/TCM ratios versus NAPL remaining for average concentrations at monitoring location FR-5 compared to ratios predicted by ESM.	448
7-51.	Measured PCE/TCE ratios versus NAPL remaining for average concentrations at monitoring location FR-5 compared to ratios predicted by ESM.	449
7-52.	Measured TCE/TCM ratios versus NAPL remaining for average concentrations at monitoring location FR-4 compared to ratios predicted by ESM.	450
7-53.	Measured PCE/TCM ratios versus NAPL remaining for average concentrations at monitoring location FR-4 compared to ratios predicted by ESM.	451
7-54.	Measured PCE/TCE ratios versus NAPL remaining for average concentrations at monitoring location FR-4 compared to ratios predicted by ESM.	452
7-55.	Measured TCE/TCM ratios versus NAPL remaining for concentrations at monitoring point FR-5-7 compared to ratios predicted by ESM.	453
7-56.	Measured PCE/TCM ratios versus NAPL remaining for concentrations at monitoring point FR-5-7 compared to ratios predicted by ESM.	454
7-57.	Measured PCE/TCE ratios versus NAPL remaining for concentrations at monitoring point FR-5-7 compared to ratios predicted by ESM.	455

Chapter 8

8-1.	Change in aqueous concentration ratios versus time at the pumping well PW-2.	482
8-2.	Change in aqueous concentration ratios versus chemical mass removed at the pumping well PW-2.	483
8-3.	Measured TCE/TCM ratios for a 17,000 g NAPL source compared to the ratios predicted by ESM.	484
8-4.	Measured PCE/TCM ratios for a 17,000 g NAPL source compared to the ratios predicted by ESM.	485
8-5.	Measured PCE/TCE ratios for a 17,000 g NAPL source compared to the ratios predicted by ESM.	486
8-6.	Measured TCE/TCM ratios for a 12,000 g NAPL source compared to the ratios predicted by ESM.	487
8-7.	Measured TCE/TCM ratios for a 22,000 g NAPL source compared to the ratios predicted by ESM.	488
8-8.	Location of the Dayton, New Jersey site.	489
8-9.	Aqueous-phase plumes at the Dayton site in April 1978 before the start of pumping.	490

List of Figures

		Page
8-10.	Aqueous-phase plumes at the Dayton site in September 1984 after the end of pumping.	491
8-11.	Aqueous-phase plumes at the Dayton site in May 1989.	492
8-12.	PCE aqueous concentrations in multi-level monitoring installation adjacent to the source area.	493
8-13.	Temporal variation in aqueous concentrations measured in pumping well GW-32.	494
8-14.	Variation in PCE/TCA ratio versus time for pumping well GW-32.	495
8-15.	Variation in PCE/TCA ratio versus mass removed for pumping well GW-32.	496
8-16.	Change in aqueous concentration ratios versus NAPL remaining predicted for the Dayton site by ESM for 1-cell, 2-cell and 5-cell configurations.	497
8-17.	Measured PCE/TCA ratio versus NAPL mass remaining for extraction well GW-32, for a 5,000 kg source, compared to ratios predicted by ESM.	498
8-18.	Measured PCE/TCA ratio versus NAPL mass remaining for extraction well GW-32, for a 6,000 kg source, compared to ratios predicted by ESM.	499
8-19.	Measured PCE/TCA ratio versus NAPL mass remaining for extraction well GW-32, for a 4,000 kg source, compared to ratios predicted by ESM.	500

1. Introduction

1.1 Background

The predominant cause of groundwater contamination at many waste disposal and industrial facilities is the presence of NAPL (non-aqueous phase liquid) organic chemicals in the subsurface. NAPLs can be either LNAPL (light non-aqueous phase liquid) chemicals such as petroleum fuels which are less dense than water, or can be DNAPL (dense non-aqueous phase liquids) such as chlorinated solvents, PCBs and coal tar which are more dense than water. At many sites, the plumes of dissolved organic contaminants that are found in the groundwater zone are derived from the dissolution of NAPL chemicals residing below the water table (Feenstra et al., 1996).

The longevity of NAPL source zones and the persistence of the resulting groundwater contamination will be determined by the rate of NAPL dissolution and the mass of chemicals contained in the NAPL source zone. Estimates of the rate of dissolution may be obtained from groundwater monitoring data, but estimates of the chemical mass are more elusive. Knowledge of the chemical mass contained in NAPL source zones is necessary in order to evaluate the performance of remedial technologies directed at cleanup of the source zones.

1.2 Existing Methods for Estimation of NAPL Mass

At waste disposal sites and industrial facilities where NAPL has been released to the subsurface, there are seldom records or accounts of eye witnesses to allow determination of the quantities released. For example, at the Dayton, New Jersey industrial site described in Chapter 8, there was no record of any chemical spill or leakage yet more than 5,000 kg of chlorinated solvents have been removed from the aquifer and a NAPL source zone continues to emit aqueous-phase contaminants to the groundwater.

Direct sampling and analysis of soil samples are part of almost all investigations of subsurface contamination. Soil analyses can be used to calculate chemical mass in NAPL source zones if the volumes and chemical concentrations of the NAPL-contaminated soil can be determined. However, spatial variability in the distribution of NAPL will seriously impair the use of sampling and analysis of soils for calculation of chemical mass. At many sites, it may difficult to simply identify the presence of NAPL below the water table and determine the general location of NAPL zones (Feenstra and Cherry, 1996). Based on insights provided by experimental releases (Poulsen and Kueper, 1992; Kueper et al., 1993; Brewster et al., 1995) and computer modeling (Kueper and Frind, 1991a and 1991b; Kueper and Gerhard, 1995) of chlorinated solvent DNAPL in sandy aquifers, it is evident that the distribution of the NAPL residual and pools may vary on a scale of millimetres to centimetres vertically, and centimetres to a few metres, laterally. The physical scale of this spatial variability is much smaller than can be characterized by site investigations at real sites of groundwater contamination where soil samples are commonly separated by metres, vertically, and tens of metres, laterally.

Partitioning interwell tracer tests (PITTs) have been proposed as a method for identifying the presence of NAPL and quantifying the NAPL mass in source zones (Jin et al., 1995; Wilson and Mackay, 1995; Nelson and Brusseau, 1996). PITTs involve the injection of chemical tracers into the subsurface in the area of a suspected NAPL source zone. One or more of the tracers, referred to as partitioning tracers, will partition into the NAPL encountered by the injected fluids. One or more of the tracers are non-partitioning tracers which do not interact with the NAPL. Delay in the arrival times of the partitioning tracer(s) compared to the non-partitioning tracer(s) at the extraction well indicates the presence of NAPL which slowed the rate of migration of the partitioning tracer(s). The degree of delay in arrival times between the partitioning and non-partitioning tracers should be

proportional to the mass of the NAPL encountered by the injected fluids. The promise of PITTs for estimation of NAPL mass has been illustrated by means of laboratory column tests and computer modeling. Field-scale trials for estimation of NAPL mass have been conducted but have not yet been reported in the peer-reviewed literature.

A key potential limitation of PITTs in the quantification of NAPL mass is the requirement that chemical equilibrium be achieved between the injected tracer and the NAPL. It is not known whether this condition occurs reliably in real aquifers. In any case, the application of PITTs to estimate the mass contained in large NAPL zones may be a relatively costly site investigation method.

At the present time, estimates of the chemical mass contained in NAPL zones remain limited to "order-of-magnitude" accuracy. Methods which allow estimates of NAPL mass within an accuracy of a factor of two times or better would be valuable in the design and evaluation of remedial measures.

1.3 Aqueous Concentration Ratios for Estimation of NAPL Mass

Petroleum fuels, coal tars, creosote and PCB liquids are all multi-component mixtures. In addition, the NAPL found at many waste disposal and industrial sites is commonly comprised of numerous different chemical components. In many circumstances, different NAPL components will have different solubilities in water and will dissolve into the groundwater at different rates. The preferential dissolution of the more soluble components from the NAPL will cause the aqueous concentration ratios of different components to change in response to the changes in NAPL composition as dissolution continues. Feenstra (1990) conducted a preliminary attempt to relate the changes in aqueous concentration ratios to the chemical mass contained in multi-component NAPL residual zones. This preliminary work described a simple 1-cell equilibration model referred to as the Effective

Solubility Model (ESM). The results of the 1-cell ESM compared well with the results of a published laboratory experiment. For this method, the temporal changes in aqueous concentration ratios from groundwater monitoring near a NAPL zone would be compared to the results of ESM simulations to estimate the chemical mass contained in the NAPL zone (see Figure 1-1). This preliminary work illustrated the potential for the use of the ESM method but its performance was tested against only one laboratory experiment.

The research in this thesis describes the further development and evaluation of this method to estimate the mass of chemicals contained in multi-component NAPL residual zones.

This research benefited from being able to utilize the findings of two controlled field experiments for dissolution of multi-component NAPL in a sandy aquifer conducted at the Borden experimental site. The first experiment, referred to as the "Emplaced-Source" experiment, involved the placement of a uniform block of soil within the sand aquifer. The block contained 14.8 L of DNAPL at residual saturation. The DNAPL was comprised of a mixture of chloroform, trichloroethylene, and tetrachloroethylene. Groundwater flow was permitted to pass through the source zone under natural conditions. The aqueous-phase contaminant plumes emitted from the source zone were monitored in detail for more than 1,000 days. The second experiment, referred to as the "Free-Release" experiment, involved the injection of 5 L of DNAPL into the sand aquifer inside a test cell. The DNAPL was a mixture similar to that used in the Emplaced Source. Groundwater flow was induced through the Free-Release source zone and the aqueous-phase plumes were monitored for 220 days. The results of these field experiments allowed further testing of the ESM method for estimating the chemical mass contained in NAPL residual zones.

The results of this research are provided in the following chapters:

Chapter 2- Determination of Effective Solubility

Chapter 3- Principles for Dissolution of Multi-Component NAPL Zones

Chapter 4- Description of Effective Solubility Model (ESM)

Chapter 5- Comparison to Results of Laboratory Studies to ESM

Chapter 6- Controlled Field Study: Emplaced-Source Experiment

Chapter 7- Controlled Field Study: Free-Release Experiment

Chapter 8- Application of the ESM Method for Evaluation of NAPL Sites

The following sections of this introductory chapter describe conceptual models for NAPL source zones and the chemical composition of NAPLs which cause groundwater problems, to provide a framework for the subsequent evaluation of dissolution of multi-component NAPL.

1.4 Conceptual Models for NAPL Source Zones

Contamination of the subsurface environment by NAPLs has been recognized, since the 1960s, as a potential threat to groundwater used for drinking supply. The earliest recognition arose from problems with taste, odour and explosive vapors derived from releases of petroleum fuels (LNAPL) such as gasoline, diesel fuel and heating oils. The principal focus of early studies was understanding the migration of the LNAPL in the vadose zone and its spreading at the water table. Later studies in the 1970s (van der Waarden et al., 1971; Bastien et al., 1977) demonstrated that a portion of most petroleum fuels is soluble in water and as a result, LNAPL in the subsurface can emit plumes of dissolved organic contaminants to the groundwater.

It was not widely recognized, until the 1980s, that DNAPLs such as chlorinated solvents could pose an even more serious threat to groundwater supplies than that posed by petroleum fuels. Because of their density, DNAPLs can penetrate through the vadose zone and below the water table into the groundwater zone. The DNAPL that penetrates into the groundwater zone represents a source that can emit significant concentrations of dissolved organic contaminants directly to the groundwater for time periods as long as decades to centuries.

Figure 1-2 shows a conceptual model for the groundwater contamination resulting from the release of an LNAPL, such as gasoline, to the subsurface. Depending on the volume of the release, rate of release, thickness of the vadose zone, and geological structure in the vadose zone, LNAPL can penetrate downward to the water table. As the LNAPL migrates through the vadose zone, a portion of the LNAPL volume is retained within the pores of the soil by capillary forces. This portion of the LNAPL is referred to a residual. Because it is less dense than water, the LNAPL cannot penetrate far below the water table. LNAPL may accumulate and spread laterally as a pool at the water table. The water-filled pores in the groundwater zone create a capillary resistance that the LNAPL cannot overcome. Fluctuations in the water table elevation will tend to smear the LNAPL pool up and down and create zones of residual LNAPL within the groundwater zone. Groundwater contamination will be caused by dissolution of LNAPL in the residual zones and pools.

Early representations of a conceptual model for LNAPL (Schwille, 1967) depicted a relatively uniform zone of residual LNAPL in the vadose zone and a discrete pool of LNAPL at the water table. Subsequent research and experience at field sites have shown that geological variability in the vadose zone and groundwater zone will cause significant spatial variability in the residual zones and pools, as reflected in Figure 1-2.

Figure 1-3 shows a conceptual model for the groundwater contamination resulting from the release of a DNAPL, such as chlorinated solvent, to the subsurface. Depending on the volume of the release, rate of release, thickness of the vadose zone, and geological structure in the vadose zone, DNAPL can penetrate downward to the water table. As the DNAPL migrates through the vadose zone, a portion of the DNAPL volume is retained as residual. However, because it is more dense than water, the DNAPL can penetrate below the water table. Where DNAPL encounters zones of lower permeability, DNAPL may accumulate and migrate laterally as a pool. The water-filled pores in zones of lower permeability in the vadose zone, or zones of lower permeability in the groundwater zone create capillary resistance that the DNAPL may not overcome. Groundwater contamination will be caused by dissolution of DNAPL in the residual zones and pools above and below the water table.

Early representations of a conceptual model for DNAPL (Schwille, 1981; Feenstra, 1986) depicted a relatively uniform zone of residual DNAPL in the vadose zone and discrete pool of DNAPL only at major aquitard layers. Subsequent research and experience at field sites have shown that geological variability in the vadose zone and groundwater zone will cause significant spatial variability in the residual zones and pools, as reflected in Figure 1-3.

Conceptual diagrams such as Figure 1-3 illustrate areas of vertical columns of residual NAPL, horizontal layers of residual NAPL, thin NAPL pools and thick NAPL pools. However, at real NAPL sites it is not known precisely how or where the NAPL occurs. The migration of NAPL along localized vertical pathways and formation of thin horizontal residual layers and pools is expected in stratified aquifers based on controlled field experiments and computer modeling (Kueper et al., 1993; Brewster et al., 1995; Kueper and Frind, 1991a and 1991b; Kueper and Gerhard, 1995). The accumulation of thick NAPL pools requires both sufficient volumes of NAPL and strata with the necessary configuration and capillary resistance to entrap

the NAPL. It is uncommon for thick NAPL pools to be found in aquifers except at sites such as manufactured gas plants or wood preserving facilities where very large quantities of coal tar or creosote NAPL have been released. At many sites of contamination by chlorinated solvents, it would expected that the majority of the NAPL would be distributed as residual and thin pools. However, specific details on NAPL distribution will require very intensive site investigations and such studies are rarely conducted.

1.5 Chemical Composition of NAPLs

The most important organic contaminants in groundwater are volatile organic compounds (VOCs) such as chlorinated solvents and BTEX (benzene, toluene, ethyl benzene and xylenes). These compounds have high solubilities compared to their respective drinking water standards and they are not strongly sorbed on geologic materials. As a result, VOCs have the potential to cause large plumes of dissolved contaminants in the groundwater. In addition, chlorinated solvents are not highly susceptible to biodegradation processes in the groundwater.

The NAPLs that cause significant groundwater contamination problems generally contain VOCs, but may exhibit also a wide variety of other organic compounds. In some cases, NAPLs found in the subsurface may be simple mixtures of organic liquids such as chlorinated solvents. In other cases, NAPLs may be very complex mixtures of organic liquids such as gasoline. In yet other cases, NAPLs may be complex mixtures of organic liquids and organic compounds which are normally solids. The dissolution behaviour of multi-component NAPLs will depend on the chemical composition of the NAPL and the properties of its components.

The following section provides examples of the chemical compositions of various NAPLs which represent common groundwater contamination problems. Some of these examples will be used in later sections to

demonstrate specific aspects of dissolution theory and practical application of the dissolution models.

Table 1-1 shows the chemical composition of DNAPL samples collected from two monitoring wells in a sandy aquifer located adjacent to a waste disposal basin at the United States Department of Energy Savannah River Plant, near Aiken, South Carolina. This DNAPL is a relatively simple mixture of PCE (tetrachloroethylene) and TCE (trichloroethylene), which were solvents used in the manufacture of nuclear fuels. PCE and TCE in the DNAPL occur in roughly the same proportions as the volumes of each solvent used at the facility. Simple mixtures of DNAPL such as this would be typical of waste materials at manufacturing facilities. Of particular note in this case, is the difference in composition between the two wells, and the change in composition in well MSB-3D-1 with time. Both effects are likely due to spatial variation in the DNAPL composition. Variation in composition such as this would be expected at waste disposal facilities where the components become mixed in the waste stream rather than in a manufacturing process.

Table 1-2 shows the chemical composition of DNAPL recovered from two monitoring wells (WN-3-I and WN-8-I) and an extraction well (EW-4) at the Tyson's Superfund site in King of Prussia, Pennsylvania. This site was an illegal dump of hazardous and sewage wastes. The principal components are VOCs including 1,2,3-trichloropropane and BTEX compounds. These samples exhibit an even greater spatial variability than the samples in Table 1-1. Of particular note in this case is the large proportion of the DNAPL that could not be characterized by the GC/MS (gas chromatography/mass spectrometry) methods used for the analysis. The uncharacterized portion ranges from 19% to 52% of the DNAPL. Qualitatively, the uncharacterized portion consists of aliphatic and aromatic hydrocarbons and large molecular weight organics believed to have been derived from sewage wastes. The occurrence of a large

portion of DNAPL that cannot be readily characterized is common at many waste disposal facilities.

Table 1-3 shows the average chemical composition of DNAPL recovered from nine monitoring wells at the S-Area Landfill in Niagara Falls, New York. This DNAPL is a mixture of waste products from the manufacture of halogenated hydrocarbon chemicals at the Occidental Chemical Company sites in Niagara Falls. The DNAPL is a very complex mixture of chlorinated solvents, chlorinated benzenes and other chlorinated hydrocarbons. The components of the DNAPL represent an extreme range in pure-phase solubility ranging from 1,400 mg/L for trichloroethylene to 0.003 mg/L for perchloropentacyclododecane (Mirex). Many of these compounds are solids in their pure form

Table 1-4 shows the major components of gasoline. The twenty components having concentrations greater than 1% by weight comprise about 62% of the gasoline. The BTEX compounds are the principal components that may cause plumes of dissolved contaminants. The other aliphatic and aromatic compounds are generally much less soluble than the BTEX compounds.

Table 1-5 shows the major components of coal tar. Coal tar is comprised principally of polycyclic aromatic hydrocarbons (PAHs) with lesser proportions of sulfur- and nitrogen-containing heterocyclic hydrocarbons, phenolic compounds and sometimes BTEX compounds. The majority of the PAH compounds are solids in their pure form. However, when the components are mixed at high temperature during the production of coal tar there is a mutual depression of the melting points of the components so that the resultant mixture remains as a liquid.

Table 1-6 shows the isomer compositions of various PCB (polychlorinated biphenyl) Aroclors. PCB Aroclors were commercial

products, which can be comprised of 100 or more individual PCB compounds. These compounds are commonly grouped according to the number of chlorine substitutions in each molecule, ranging from one to ten chlorines. There are substantial differences in solubility between the different PCB compounds, with solubility declining with increasing chlorine content. This table illustrates that there is a substantial difference in chemical composition between Aroclors 1242, 1254 and 1260. Although PCB compounds have generally low solubilities in water, subsurface contamination by PCB Aroclors has attracted much attention in recent years.

These preceding examples illustrate the range in chemical composition that may be encountered in NAPL in the subsurface, and set the chemical framework for the following discussions on dissolution behaviour of multi-component NAPL.

Table 1-1. Composition of waste solvent DNAPL recovered from monitoring wells at the Savannah River Plant, Aiken, South Carolina. PCE (tetrachloroethylene) and TCE (trichloroethylene). Data from Jackson and Mariner (1995).

Well and Sampling Date	PCE % by Weight	TCE % by Weight
MSB-3D-1		
April 1991	94.1	5.9
September 1991	90.9	9.1
February 1992	98.1	1.9
MSB-22-1		
December 1991	83.4	16.6
February 1992	93.8	6.2

Table 1-2. Composition of waste solvent DNAPL recovered from monitoring wells at the Tyson's Superfund site, King of Prussia, Pennsylvania. Data from ERM (1992).

Compound	Well WN-3-I % by Weight	Well WN-8-I % by Weight	Well EW-4 % by Weight
1,2,3-Trichloropropane	23.0	73.0	63.0
Total Xylenes	17.0	6.0	9.5
Toluene	4.0	1.0	1.9
Ethyl Benzene	4.0	1.0	1.4
Uncharacterized by GC/MS	52.0	19.0	24.0

Table 1-3. Average composition of DNAPL recovered from nine monitoring wells at the S-Area Landfill, Niagara Falls, New York. Data from Occidental Chemical Corporation (1988).

Compound	% by Weight
Trichloroethylene	0.4
Carbon Tetrachloride	0.9
Chlorobenzene	0.6
Toluene	0.1
Tetrachloroethylene	10.0
Chlorotoluenes	1.0
Dichlorobenzenes	0.5
Hexachloroethane	0.8
Trichlorobenzenes	0.3
Tetrachlorobenzenes	28.9
Hexachlorobutadiene	3.5
Hexachlorocyclopentadiene	9.5
Hexachlorocyclohexanes	0.2
Perchloropentacyclododecane	0.1
Pentachlorobenzene	5.5
Octachlorostyrene	10.8
Hexachlorobenzene	1.3
TOTAL	83.4

Table 1-4. Major components of gasoline. Typical analysis of API (American Petroleum Institute) PS-6 standard gasoline from Kreamer and Stetzenbach (1990).

Compound	% by Weight
BTEX Compounds	
Benzene	1.94
Toluene	4.73
Ethyl Benzene	2.00
m-Xylene	5.66
o-Xylene	2.27
p-Xylene	1.72
Total BTEX	18.32
2-Methylbutane	8.72
2,2,4-Trimethylpentane	5.22
2-Methylpentane	3.93
n-Butane	3.83
1,2,4-Trimethylbenzene	3.26
n-Pentane	3.11
2,3,4-Trimethylpentane	2.99
2,3,3-Trimethylpentane	2.85
3-Methylpentane	2.36
2,3-Dimethylbutane	1.66
n-Hexane	1.58
1-Methyl-3-Ethylbenzene	1.54
1-Methyl-4-Ethylbenzene	1.54
3-Methylhexane	1.3
Total Major Components	62.21

Table 1-5. Major components of coal tar. Data from Ripp et al. (1993).

Compound	Sample 1 % by Weight	Sample 4 % by Weight	Sample 5 % by Weight
Naphthalene	7.07	5.2	13.5
2-Methylnaphthalene	3.34	3.74	3.41
1-Methylnaphthalene	2.35	2.15	1.96
Acenaphthylene	0.061	1.21	1.78
Acenaphthene	1.19	0.09	0.165
Dibenzofuran	0.40	0.109	0.115
Fluorene	1.16	0.698	0.895
Phenanthrene	3.26	1.7	3.46
Anthracene	0.857	0.542	0.767
Fluoranthene	1.34	0.476	1.26
Pyrene	1.32	0.689	1.79
Benzo(a)anthracene	0.49	0.234	0.513
Chrysene	0.51	0.234	0.647
Benzo(b)fluoranthene	0.215	0.135	0.313
Benzo(k)fluoranthene	0.295	0.061	0.285
Benzo(a)pyrene	0.39	0.156	0.642
Indeno(1,2,3-cd)pyrene	0.261	0.108	0.489
Benzo(g,h,i)perylene	0.311	0.127	0.709
Carbazole	0.11	0.020	0.016
Dibenzothiophene	-	0.202	0.323
Benzene	0.055	0.0014	0.497
Toluene	0.212	0.0009	0.70
Ethylbenzene	0.186	0.0037	0.27
m-/p-Xylenes	0.337	0.0083	0.611
o-Xylene	0.175	0.0075	0.195
Total Quantified	25.895	17.9028	35.312

Table 1-6. Isomer composition of PCB Aroclors. Data from Webb and McCall (1973).

Isomer Group	Aroclor 1242 % by Weight	Aroclor 1254 % by Weight	Aroclor 1260 % by Weight
1-Chlorine isomers	1.1		
2-Chlorine isomers	17.0		
3-Chlorine isomers	39.0		
4-Chlorine isomers	32.0	14.0	
5-Chlorine isomers	9.6	62.0	12.0
6-Chlorine isomers	0.5	23.0	46.0
7-Chlorine isomers		1.0	35.0
8-Chlorine isomers			6.1

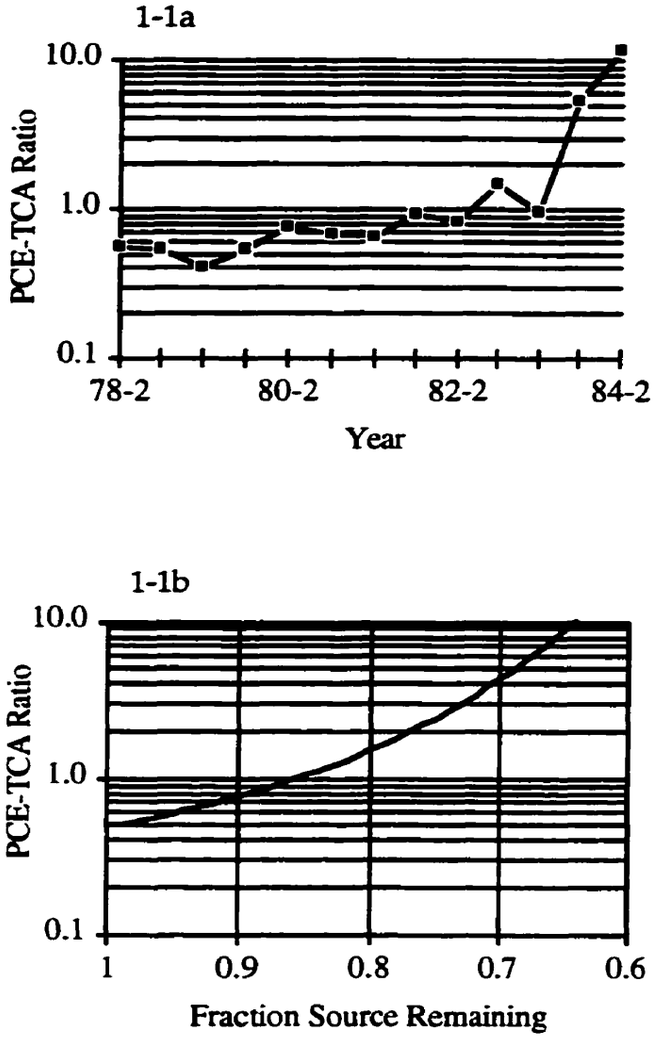

Figure 1-1. Example of changes in measured (1-1a) aqueous concentration ratios observed at the Dayton, New Jersey site, and aqueous concentration ratios (1-1b) predicted by a 1-cell ESM. From Feenstra (1990).

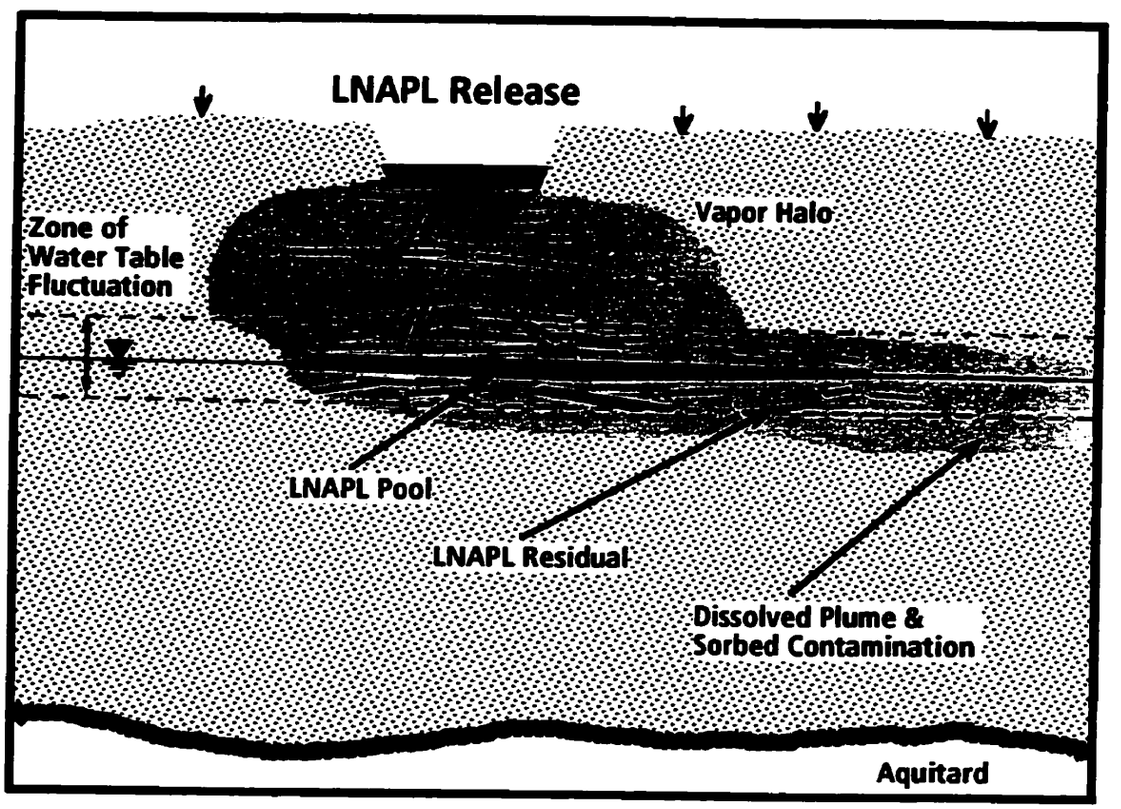

Figure 1-2. Conceptual model for LNAPL contamination in the subsurface.

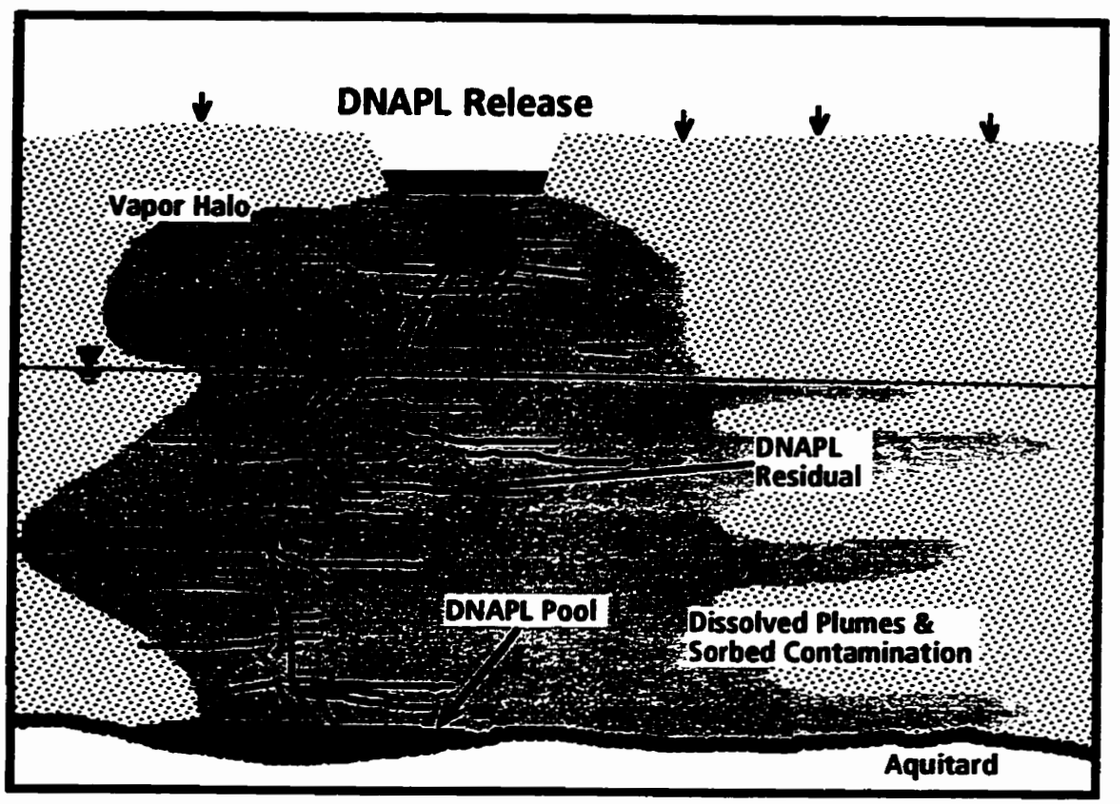

Figure 1-3. Conceptual model for DNAPL contamination in the subsurface.

2. Determination of Effective Solubility

2.1 Introduction

The ESM relies on the principle that the aqueous concentration, or effective solubility, of contaminants in groundwater at equilibrium with a multi-component NAPL can be determined from the chemical composition of the NAPL. Effective solubility of an organic compound can be defined as the maximum concentration that can be achieved in water which is in equilibrium with a multi-component NAPL of specified chemical composition. The effective solubility of an organic compound will be lower than the aqueous solubility of the pure-phase compound.

2.2 Solubility of a Single-Component NAPL

For a pure liquid organic compound in contact with water, the chemical activity of the compound in the organic phase is defined by (Mackay et al., 1991):

$$a_{org} = \chi_{org} \gamma_{org} \qquad [2\text{-}1]$$

where :

χ_{org} *is the mole fraction of the compound in the organic phase*

γ_{org} *is the activity coefficient of the compound in the organic phase*

The organic phase will consist of the organic compound and a small proportion of water dissolved in the organic phase. For organic compounds such as chlorinated solvents and petroleum hydrocarbons, the mole fraction solubility of water in the organic phase ranges from approximately 0.001 to 0.01. A compilation of values of water solubility in various chlorinated hydrocarbons is shown in Table 2-1. As a result, the mole fraction of the organic compound in the organic phase ranges from 0.999 to 0.99 and can be assumed to be unity.

The activity coefficient is a factor intended to account for molecular interactions within the organic phase and can be less than unity or greater than unity depending on the components of the organic phase. However, for a single component organic phase where molecules interact only with like molecules and it is assumed commonly that the activity coefficient is unity.

As a result of the two preceding assumptions, the chemical activity of a single component organic phase is also unity.

The chemical activity of the compound in the aqueous phase is defined by:

$$a_{aq} = \chi_{aq} \gamma_{aq} \qquad [2\text{-}2]$$

where :

χ_{aq} *is the mole fraction of the compound in the aqueous phase*

γ_{aq} *is the activity coefficient of the compound in the aqueous phase*

At equilibrium, the chemical activity in organic phase equals the chemical activity on the aqueous phase, and therefore:

$$\chi_{aq} \gamma_{aq} = \chi_{org} \gamma_{org} = 1 \qquad [2\text{-}3]$$

$$\chi_{aq} = \frac{1}{\gamma_{aq}} \qquad [2\text{-}4]$$

Equation 2-4 defines the mole fraction aqueous solubility of a single component NAPL or pure organic liquid compound. For use in subsequent formulations, equation 2-4 can be expressed as:

$$\chi_{aq}^{p} = \frac{1}{\gamma_{aq}^{p}} \qquad [2\text{-}5]$$

where :

χ^{p}_{aq} *is the mole fraction of the pure compound in the aqueous phase*

γ^{p}_{aq} *is the activity coefficient of the pure compound in the aqueous phase*

2.3 Effective Solubility of Multi-Component NAPLs

2.3.1 Ideal Behaviour

For a multi-component NAPL in equilibrium with water, the chemical activities of each component must be equal in both the NAPL and aqueous phases. Therefore:

$$\chi^{i}_{aq} \ \gamma^{i}_{aq} = \chi^{i}_{NAPL} \ \gamma^{i}_{NAPL} \qquad [2\text{-}6]$$

The mole fraction concentration of compound, i, in the water in equilibrium with the multi-component NAPL is expressed as:

$$\chi^{i}_{aq} = \frac{\chi^{i}_{NAPL} \ \gamma^{i}_{NAPL}}{\gamma^{i}_{aq}} \qquad [2\text{-}7]$$

The combination of equations 2-5 and 2-7 yields:

$$\frac{\chi^{i}_{aq}}{\chi^{p}_{aq}} = \frac{\chi^{i}_{NAPL} \ \gamma^{i}_{NAPL} \ \gamma^{p}_{aq}}{\gamma^{i}_{aq}} \qquad [2\text{-}8]$$

For a multi-component NAPL, there will be multiple components in the aqueous phase due to dissolution. As a result, γ^{i}_{aq} may differ from γ^{p}_{aq} if the aqueous-phase components interact with each other. However, hydrophobic organic compounds such as petroleum hydrocarbons and chlorinated solvents have only a relatively low solubility in water so that the opportunity for chemical interactions in the aqueous phase is low. It is assumed commonly that $\gamma^{i}_{aq} = \gamma^{p}_{aq}$. This assumption was validated

experimentally for mixtures of hydrocarbon compounds (Burris and MacIntyre, 1986a) but not for compounds that are commonly groundwater contaminants. However, calculations based on semi-empirical chemical structure modeling suggest that this assumption is reasonable when the aqueous concentrations of the various components are less than several thousand milligrams per litre. These calculations are described in Appendix A. With the preceding assumption, equation 2-8 simplifies to:

$$\frac{\chi^i_{aq}}{\chi^p_{NAPL}} = \chi^i_{NAPL} \ \gamma^i_{NAPL} \qquad [2\text{-}9]$$

If there are no chemical interactions between the components in the NAPL phase, then $\gamma^i_{NAPL} = 1$, and equation 2-9 simplifies to:

$$\frac{\chi^i_{aq}}{\chi^p_{aq}} = \chi^i_{NAPL} \qquad [2\text{-}10]$$

Although this assumption is made commonly in the evaluation of effective solubilities of multi-component NAPL, it is not clear that this assumption is generally applicable to groundwater contamination problems in the same way as the other assumptions made leading to equation 2-9.

Equation 2-9 and equation 2-10 can be expressed also in terms of concentrations rather than mole fractions in the aqueous phase by:

$$\frac{C^i}{S^i} = \chi^i_{NAPL} \ \gamma^i_{NAPL} \qquad [2\text{-}11]$$

Or if $\gamma^i_{NAPL} = 1$:

$$\frac{C^i}{S^i} = \chi^i_{NAPL} \qquad [2\text{-}12]$$

$$C^i = \chi^i_{NAPL}\, S^i \qquad [2\text{-}13]$$

where :

C^i *is the effective solubility*

S^i *is the pure −phase solubility*

Equation 2-13 expresses a relationship analogous to Raoult's Law for vapor and is commonly referred to as Raoult's Law for aqueous solutions also. Implicit in this relationship is the assumption that all components in the NAPL phase and aqueous phase exhibit ideal behaviour (i.e. no chemical interactions). In this form, Raoult's Law can be used to determine effective solubility for a particular component of a multi-component NAPL with knowledge of the mole fraction of the component in the NAPL and the pure-phase solubility of the component.

The mole fraction is a normalized molar concentration for the component in the NAPL. The mole fraction of a component can be calculated directly from a chemical analysis of the NAPL provided that all, i.e. 100%, of the NAPL components are identified and quantified. For a chemical analysis with the component concentrations expressed as weight per unit weight or volume, the component concentrations are divided by the molecular weight of each component to yield a molar concentration. The molar concentrations for all the components are summed, and the mole fractions of each component are calculated based on the individual molar concentrations and the summed molar concentration for the NAPL. For a chemical analysis with component concentrations expressed as volume per unit volume, component concentrations must first be multiplied by the density of the

component. In cases where not all components of the NAPL are characterized, measurements or estimates must be made of the molecular weight or density of the uncharacterized components. This difficulty is discussed in detail in Section 2.6.4.

2.3.2 Non-Ideal Behaviour

In the evaluation of groundwater contamination problems, it would be optimum to have measured values of effective solubility for all the components of the NAPLs in question over the range of NAPL composition expected. However, this is almost never the case, and effective solubility must be estimated based on the properties of the components and the NAPL composition. Raoult's Law provides a relatively simple means of estimating effective solubility.

The estimation of effective solubility of the multi-component NAPL using Raoult's Law requires several assumptions:

1) Mole fraction of water is the NAPL is low.

2) There are no chemical interactions between components in the aqueous phase such that: $\gamma_{aq}^{i} = \gamma_{aq}^{o}$

3) There are no chemical interactions between components in the NAPL phase such that: $\gamma_{NAPL}^{i} = 1$

If these conditions are not satisfied, the determination of effective solubility values using Raoult's Law can cause underestimation or overestimation relative to the true effective solubility. If the degree of error associated with the use of Raoult's Law is 10% to 30% or lower, the error can be considered acceptably small, relative to the magnitude of other errors and uncertainties associated with the evaluation of groundwater problems. With regard to the application of Raoult's Law, the largest potential error relates to

the assumption that there are no chemical interactions between components in the NAPL phase such that $\gamma^{i}_{NAPL} = 1$. In circumstances where measured effective solubility values are available, they can be compared to values predicted using Raoult's Law to determine whether Raoult's Law is applicable in a given situation.

2.4 Solubility of Solid-Phase Organic Compounds

The pure-phase solubility values referred to in preceding discussion relates to organic compounds that are liquids in their pure form. Liquid organic compounds include benzene, toluene, ethyl benzene and xylenes (BTEX), low molecular weight petroleum hydrocarbons, and chlorinated solvents. There are, however, circumstances in which a multi-component NAPL may contain components which are solids in their pure form at temperatures typical in the subsurface.

Some NAPLs may contain solid-phase components dissolved in other liquid components. An example would be PCB (polychlorinated biphenyl) compounds in trichlorobenzene liquid. The melting point of PCBs ranges from 34°C for monochlorobiphenyl to about 160°C for octachlorobiphenyls. Some NAPLs, such as coal tar, creosote and PCB Aroclors are chemical products comprised primarily of solid-phase compounds. The products are liquids because they are formed at high temperature and the mixture causes a mutual depression of the melting points of the components. Coal tar or creosote are comprised of primarily of PAH (polycyclic aromatic hydrocarbon) compounds whose melting points range from 80°C for naphthalene to 254°C for chrysene.

The pure-phase solubility values found in the published literature for solid-phase organic compounds represent the aqueous solubility of the compound in equilibrium with the solid-phase material. However, the aqueous solubility of the solid-phase compound will be lower than that of the

same compound that exists in a liquid state. A liquid-phase solubility or supercooled liquid solubility for compounds which are solids can be estimated (Miller et al., 1985) by :

$$S_{liquid} = S_{solid} \exp\left[\frac{\Delta S}{R}(T_M / T - 1)\right] \quad [2\text{-}14]$$

where :

S_{liquid} *is the supercooled liquid solubility*

S_{solid} *is the solid –phase solubility*

T_M *is the melting point in °K*

T *is the system temperature in °K*

ΔS *is the entropy of fusion in cal/mol K*

R *is the "Universal Gas Constant in cal/mol K*

ΔS values are available for some compounds which are potential contaminants in groundwater and values vary by a factor of two times. However, an average value of 13.4 cal/mol K is used commonly for PAH compounds (Yalkowsky and Banerjee, 1992) so that the ΔS/R term has a value of 6.8.

The supercooled liquid solubility is always higher than the solid-phase solubility and the difference increases as the melting point increases. Examples of the solid-phase solubility and supercooled liquid solubility for selected PAH compounds are shown in Table 2-2. The supercooled liquid solubility of naphthalene (melting point - 80°C) is 3.5 times higher than its solid-phase solubility. The supercooled liquid solubility of anthracene (melting point - 217°C) is 126 times higher than its solid-phase solubility. The relationship between solid-phase solubility and supercooled liquid solubility versus melting point is illustrated in Figure 2-1.

This property can lead to the circumstance where the effective solubility of a component in a NAPL mixture may be higher than the compound's solid-phase solubility. This circumstance occurs for perchloropentacyclododecane (Mirex) in the DNAPL shown in Table 1-3. Mirex comprises 0.1 % by weight of the DNAPL (mole fraction approximately 0.001). The solid-phase solubility of Mirex is 0.2 mg/L. However, because of its extremely high melting point (486°C), the calculated supercooled liquid solubility of Mirex is 7,200 mg/L, or 36,000 times higher than the solid-phase solubility. If it is assumed that Raoult's Law can be applied, the calculated effective solubility of Mirex in this DNAPL is 7.2 mg/L. This calculated value exceeds the solid-phase solubility by a factor of 36 times. In this case, the effective solubility of Mirex in water in contact with this DNAPL will be limited to the solid-phase solubility value.

2.5 Applicability of Raoult's Law for Simple NAPLs

There have been relatively few published studies which have evaluated the applicability of Raoult's Law to mixtures of organic compounds relevant to groundwater contamination problems. This section provides a compilation of the available information on the effective solubility of simple NAPL mixtures. For the purpose of this discussion, a simple NAPL mixture is comprised of a small number of components and all the components are identified and quantified. Contamination of the subsurface by spills, leaks and disposal at industrial facilities is caused frequently by relatively simple NAPL mixtures. The results of testing of more complex multi-component mixtures are described in Section 2.6.

2.5.1 Chlorinated Solvent Mixtures

Broholm and Feenstra (1995) determined the effective solubility of various chlorinated solvents in 2-component (binary) and 3-component (ternary) mixtures. The solvents tested included: chloroform (TCM), carbon

tetrachloride (PCM), 1,1,1-trichloroethane (TCA), trichloroethylene (TCE) and tetrachloroethylene (PCE). These compounds were selected because they are among the most common groundwater contaminants and because mixtures of TCM, TCE and PCE were used subsequently in both the Emplaced-Source and Free-Release field dissolution experiments. Effective solubility was determined by means of batch experiments conducted at 23°C to 24°C. The mixtures tested included:

TCE - TCM	TCE - PCM
TCE - TCA	TCE - PCE
PCE - TCM	PCE - PCM
PCE - TCA	TCM - TCE - PCE

For each test, a DNAPL mixture of solvents was equilibrated with organic-free distilled water for a period of at least 2 days. The water to DNAPL ratio was 4.97 to 1 so that the DNAPL was not depleted significantly in any component by dissolution into the water. For each binary and ternary system, the proportion of the solvent components in the DNAPL ranged from mole fractions of 0.03 to 0.97. An aliquot of the water was removed, extracted with hexane and analysed in triplicate by GC/ECD (gas chromatography/electron capture detection). The standard deviation of replicate analyses is about ±5%. The pure-phase solubilities determined for the chlorinated solvents are shown in Table 2-3.

The results of the effective solubility tests are summarized graphically in Figures 2-2 to 2-9. For each binary and ternary system, the measured aqueous concentrations are plotted versus the aqueous concentration predicted by Raoult's Law. If Raoult's Law is applicable, there should be a one-to-one correspondence between the measured and predicted concentrations, as shown by the straight line on each graph.

On each graph in Figures 2-2 to 2-9, the measured aqueous concentration is plotted versus the aqueous concentration predicted using three variations of Raoult's Law. Raoult's Law as shown in equation 2-13 relates the effective solubility of a component to the pure-phase solubility of the component and the mole fraction of the component in the NAPL. On practical grounds, the analysis of NAPL samples provides a weight-based or volume-based concentration. It may not always be possible to calculate the mole fraction of each component in complex NAPL mixtures because both the concentration and molecular weight of all components must be determined. It has been suggested by Shiu et al. (1988) that only a small potential error is imparted by the used of volume fraction in Raoult's Law calculations. For comparison purposes, the aqueous concentrations were predicted using weight fraction and volume fraction, in addition to mole fraction, to assess the degree of error that might result from direct use of volume or weight fraction.

For the binary and ternary systems of chlorinated solvents tested, the aqueous concentrations predicted by Raoult's Law compare favourably to the measured aqueous concentrations. This represents ideal behaviour. The average deviation and maximum deviation of the predicted concentrations from ideal behaviour in each binary and ternary system are shown in Table 2-4.

In general, the predicted aqueous concentrations based on mole fraction provided the best estimate of effective solubility with an average deviation of 7.0% and a maximum deviation of -40.4%, averaged over the eight binary and ternary systems. The average deviation is only slightly larger than the variability of about 5% in measurement of the aqueous concentrations. The predicted aqueous concentrations based on weight fraction and volume fraction exhibited larger deviations from ideal behaviour, though not appreciably larger. The average and maximum deviations for predictions based on weight fraction were 12.4% and 63.9%,

respectively. The average and maximum deviations for predictions based on volume fraction were 9.0% and 50.5%, respectively. For NAPL compositions which ranged from mole fractions of 0.03 to 0.97, the magnitude of deviation from ideal behaviour did not vary systematically with NAPL composition.

These laboratory experiments suggest Raoult's Law provides a reasonable means for determining the effective solubility of mixtures of chlorinated solvents.

2.5.2 Chlorinated Benzene Mixtures

Banerjee (1984) determined the effective solubility of various chlorinated benzenes in binary and ternary mixtures. The compounds tested included: chlorobenzene (CBz), 1,3-dichlorobenzene (13-DCBz), 1,2,4-trichlorobenzene (124-TCBz) and 1,2,4,5-tetrachlorobenzene (1245-TeCBz). The effective solubility was determined by means of batch experiments conducted at 25°C. For each test, the chlorinated benzene mixtures were equilibrated with distilled water for a period of 3 days. The water to organic compound ratio ranged from as high as 300 to 1, to as low as 7.5 to 1. For each binary and ternary system, the proportion of components in the NAPL ranged from mole fractions of 0.0059 to 0.9941. An aliquot of water was removed and analysed by HPLC (high pressure liquid chromatography). The standard deviation of replicate analyses was about 5%. The pure-phase solubilities of the chlorinated benzenes are shown in Table 2-5.

The results of these effective solubility tests are summarized graphically in Figures 2-10, 2-11 and 2-12. For these systems, the aqueous concentrations predicted by Raoult's Law compare favourably to the measured aqueous concentrations. The average and maximum deviation of the predicted concentrations from ideal behaviour in each system are shown in Table 2-6.

The predicted aqueous concentrations based on mole fraction provided the best estimate of effective solubility with an average deviation of 10.6% and a maximum deviation of 88.3%, averaged over the three binary and ternary systems. The predicted aqueous concentrations based on volume fraction are comparable to predictions based on mole fraction. The predicted aqueous concentrations based on weight fraction exhibit somewhat larger deviations from ideal behaviour. These laboratory experiments suggest that Raoult's Law provides a reasonable means for determining the effective solubility of mixtures of chlorinated benzenes.

All of the laboratory experiments performed by Broholm and Feenstra (1995) and those by Banerjee (1984) considered thus far, involved mixtures of liquid organics. Another experiment by Banerjee illustrates the principles described in Section 2.4 for mixtures of organic liquids and organic solids. This experiment involved mixtures of chlorobenzene (CBz), which is a liquid, and 1,2,4,5-tetrachlorobenzene (1245-TeCBz), which is a solid. If the mole fraction of 1245-TeCBz in the mixture is less than 0.1, the two components form a homogeneous organic liquid. If the mole fraction of 1245-TeCBz exceeds 0.1, crystals of 1245-TeCBz are present in the CBz liquid. The tests by Banerjee considered mixtures having less than 0.1 mole fraction 1245-TeCBz and greater than 0.1 mole fraction 1245-TeCBz.

The results of these tests are shown in Figure 2-13. The CBz and 1245-TeCBz system did not exhibit ideal behaviour over the range of NAPL composition tested. There is, however, consistency with the principles described in Sections 2.2 and 2.4. At low 1245-TeCBz mole fractions, corresponding to high aqueous concentrations of CBz and low aqueous concentrations of 1245-TeCBz, the predicted concentrations for CBz compare well to the measured concentration (Figure 2-13a). The predicted concentrations for 1245-TeCBz compare well to the measured concentration only if the supercooled liquid solubility is used in the calculation of Raoult's Law (Figure 2-13b). If the solid-phase solubility for 1245-TeCBz is used, the

predicted aqueous concentrations are about 25 times lower than those measured (Figure 2-13c). These tests clearly illustrate that the liquid-phase solubility of solid organic compounds must be used in Raoult's Law calculations.

At high 1245-TeCBz mole fractions where crystals of 1245-TeCBz are present, the measured aqueous concentration of CBz was much higher than predicted, although somewhat lower than the pure-phase solubility. The measured aqueous concentration of 1245-TeCBz was much lower than predicted, being close to the solid-phase solubility value of 0.465 mg/L. These results indicate that Raoult's Law is applicable when the organic components form a homogeneous NAPL, but is not applicable in heterogeneous mixtures of liquids and solids. In heterogeneous mixtures, the solubilities of the components may reflect their pure-phase solubility values.

2.5.3 Petroleum Hydrocarbon Mixtures

Leinonen and Mackay (1973) and Burris and MacIntyre (1986a, 1986b, 1986c) determined the effective solubility of various petroleum hydrocarbons in various mixtures. Aside from the obvious difference of using different organic compounds, these studies differed in an important manner from those by Broholm and Feenstra (1995) and Banerjee (1984). The chlorinated solvents considered by Broholm and Feenstra were all chlorinated methanes, alkanes and alkenes. Banerjee considered only chlorinated monoaromatics. In contrast, Leinonen and Mackay, and Burris and MacIntyre considered mixtures of structurally dissimilar aliphatic and aromatic compounds.

Leinonen and Mackay examined mixtures of benzene (Bz) and 2-methyl pentane (2-MP) by means of batch experiments. For each test, a mixture of hydrocarbons was equilibrated with water at 25°C for at least 18 hours. The water to NAPL ratio was 40 to 1. An aliquot of water was removed, extracted with heptane, and analysed by GC/FID (gas

chromatography/flame ionization detection). The standard deviation of replicate analyses was <10%. The pure-phase solubility of Bz and 2-MP were 1,765 mg/L and 14.2 mg/L, respectively. The results of the effective solubility tests are summarized graphically in Figure 2-14.

Burris and MacIntyre examined binary mixtures of n-octane, 1-methyl naphthalene (1-MP), tetralin, methylcyclohexane (MCH), and ethyl benzene (EBz) by means of batch experiments. For each test, a mixture of hydrocarbons was equilibrated with organic-free distilled water at 20°C for at least 3 days. The water to NAPL ratio ranged from as high as 800 to 1 to as low as 133 to 1. An aliquot of water was removed, extracted with pentane, and analysed by GC/FID. The standard deviation of replicate analyses was <5%. The pure-phase solubilities of the hydrocarbons are shown in Table 2-7. The results of the effective solubility tests are summarized graphically in Figures 2-15, 2-16 and 2-17.

For the binary systems of hydrocarbons tested, the aqueous concentrations predicted by Raoult's Law exhibited greater deviation from the measured concentrations than the chlorinated solvent and chlorinated benzene mixtures. In almost all cases, the predicted aqueous concentrations were lower than the measured concentrations. The average and maximum deviation of the predicted concentrations from ideal behaviour in each system are shown in Tables 2-8 and 2-9. For the Leinonen and Mackay experiments, the average deviation and maximum deviation of predicted concentrations based on mole fraction were 29.8% and -58%, respectively. For the Burris and MacIntyre experiments, the average deviation and maximum deviation of predicted concentrations based on mole fraction were 20.9% and -75.3%, respectively. Comparable average and maximum deviation from measured aqueous concentrations were shown for predicted concentrations based on weight fraction and volume fraction.

Burris and MacIntyre (1986b) and (1986c) also examined a quaternary hydrocarbon mixture and a simulated JP-4 jet fuel mixture. These mixtures were tested using the same procedures as the binary mixtures described in the preceding paragraphs, but only one formulation of each mixture was tested. The quaternary mixture was comprised of ethyl benzene, tetralin, 1-methyl naphthalene and methylcyclohexane. The simulated JP-4 jet fuel was comprised of 12 hydrocarbon components. The results of the effective solubility tests for the quaternary mixture and simulated JP-4 jet fuel are shown graphically in Figures 2-18 and 2-19, respectively. As with the binary systems, the predicted aqueous concentrations are lower than the measured concentrations.

For the quaternary system, the average deviation and maximum deviation of predicted concentrations based on mole fraction were 29.0% and -54.6%, respectively. Deviations were comparable for predicted concentrations based on volume fraction, and lower for predicted concentrations based on weight fraction.

For the simulated JP-4 jet fuel, the average deviation and maximum deviation of predicted concentrations based on mole fraction were 24.6% and -55.3%, respectively. Deviations for predicted concentrations based on weight fraction and volume fraction were slightly higher.

2.5.4 Conclusions on Raoult's Law for Simple NAPLs

Based on the laboratory experiments performed for this study and information in the published literature, it is apparent that Raoult's Law provides a relatively accurate means for the estimation of effective solubility for simple NAPL mixtures. Simple NAPL mixtures are those comprised of relatively few components, and for which all components have been characterized. The following specific conclusions can be made:

- For NAPL mixtures comprised of structurally similar compounds, such as the mixtures of chlorinated solvents considered by Broholm and Feenstra (1995) and the mixtures of chlorinated benzenes considered by Banerjee (1984), effective solubilities predicted by Raoult's Law deviate from measured concentrations by about 10% to 30%, or less.

- For NAPL comprised of structurally dissimilar compounds such as mixtures of aliphatics and aromatic compounds, such as the mixtures considered by Leinonen and Mackay (1973) and Burris and MacIntyre (1986a, 1986b, 1986c), effective solubilities predicted by Raoult's Law deviate from measured concentrations by about 25% to 50%, or less.

- Calculation of effective solubility using Raoult's Law is most accurate when based on mole fraction. However, use of weight fraction or volume fraction will decrease accuracy only slightly.

- Calculations of effective solubility using Raoult's Law must utilize the supercooled liquid solubility values for compounds that are solids in their pure form at ambient temperature.

- Calculations of effective solubility using Raoult's Law are not applicable if the NAPL is a heterogeneous mixture of liquid and solids.

2.6 Applicability of Raoult's Law for Complex NAPLs

Complex NAPL mixtures may be the cause of subsurface contamination at many sites. For the purpose of this discussion, a complex NAPL mixture is one comprised of many components and contains components which have not been identified and/or quantified. Complex NAPLs include most petroleum fuels, creosote and coal tar, and many of the

NAPLs found at hazardous waste disposal sites. This section provides a compilation of the available information on the effective solubility of complex NAPL mixtures.

2.6.1 Gasoline

Gasoline is a mixture of 100 or more low molecular weight aliphatic and aromatic hydrocarbon compounds. A typical analysis of PS-6 standard gasoline showing the concentrations of the 20 major components is found in Table 1-4. Almost all of the components in gasoline are liquids in their pure form. Benzene, toluene, ethyl benzene, and xylenes (BTEX) are the components of gasoline having the highest solubilities and are those of greatest concern with regard to groundwater contamination. The effective solubilities of various components of gasoline have been determined by TRC (1985), Poulsen et al. (1992) and Cline et al. (1991).

TRC (1985) determined the effective solubility of 12 components of a sample of PS-6 standard gasoline by means of a batch experiment. The 12 components considered in this test comprised 38 weight percent of the gasoline. Gasoline was equilibrated with organic-free distilled water for a period of 2 hours. The water to NAPL ratio was 10 to 1. An aliquot of water was removed and analysed by GC/FID. The results of the effective solubility tests are summarized graphically in Figure 2-20.

Poulsen et al. (1992) determined the effective solubility of 6 components of a sample of PS-6 standard gasoline by means of a batch experiment. The 6 components considered in this test comprised 15.4 weight percent of the gasoline. Gasoline was equilibrated with natural low TDS (total dissolved solids) groundwater from the Borden site for a period of 4 hours. The water to NAPL ratio was 10 to 1. An aliquot of water was removed, extracted with hexane, and analysed by GC/FID. The results of the effective solubility tests are summarized graphically in Figure 2-21.

Cline et al. (1991) determined the effective solubility of 8 components in 31 samples of gasoline by means of a batch experiments. The average measured effective solubility and average gasoline composition were reported. The 8 components considered in these tests comprised an average of 24.7 weight percent of the gasoline. Gasoline was equilibrated with organic-free distilled water for a period of 90 minutes. The water to NAPL ratio was 20 to 1. An aliquot of water was removed and analysed by GC/FID. The results of the effective solubility tests are summarized graphically in Figure 2-22.

For complex NAPL such as gasoline, the mole fraction and volume fraction of the various components cannot be calculated directly because not all the NAPL components were identified and quantified. The weight fraction can be calculated directly from the analysis of the NAPL. In order to calculate the mole fraction of the characterized components, a value must be assumed for the average molecular mass of the compounds comprising the uncharacterized portion of the NAPL. In order to calculate the volume fraction of the characterized components, a value must be assumed for the average density of the compounds comprising the uncharacterized portion of the NAPL. Although the uncharacterized portion of the NAPL in these tests ranged from 62 to 85 weight percent, the average molecular mass and density for gasoline are well known. For the predicted aqueous concentrations shown in Figures 2-20, 2-21 and 2-22, the uncharacterized portion of the gasoline was assigned an average molecular mass of 100 g/mole and a density of 0.75 g/cm^3 (Cline et al., 1991).

These laboratory experiments suggest Raoult's Law provides a reasonable means for determining the effective solubility of gasoline components. The average deviation and maximum deviation in predicted aqueous concentrations from measured concentrations are shown in Table 2-10. The average deviation in predicted concentrations ranged from

19.2% to 39.4%. The maximum deviation ranged from 36.1% to 68.2%. These values are comparable to the deviations in predicted concentrations for the simple hydrocarbon mixtures described in Section 2.5. Predicted aqueous concentrations based on weight fraction or volume fraction generally yield larger deviations from the measured concentrations than predicted concentrations based on mole fraction.

2.6.2 Diesel Fuel

Diesel fuel is mixture of 100 or more intermediate molecular weight aliphatic and aromatic hydrocarbon compounds. Diesel fuel is comprised of about 40% normal alkanes, 40% iso- and cycloalkanes, and 20% aromatics. Although polycyclic aromatic hydrocarbons (PAH) comprise only a few weight percent of diesel fuel, they are some of the compounds of greatest concern with regard to groundwater contamination. The effective solubilities of various components of diesel have been determined by Lee et al. (1992a).

Lee et al. (1992a) determined the effective solubility of 8 PAH compounds in 4 samples of diesel fuel by means of batch experiments. The 8 components considered in these tests comprised about 1 weight percent of the diesel fuel. Diesel was equilibrated with organic-free deionized water for a period of 24 hours. The water to NAPL ratio was 10 to 1. An aliquot of water was removed, extracted with dichloromethane and analysed by GC/ITD (gas chromatography/ion trap detection). The results of the effective solubility tests are summarized graphically in Figure 2-23, 2-24, 2-25 and 2-26.

The average molecular masses of the diesel fuel samples were estimated by Lee et al. from the chromatograms. The density of each sample was measured directly. The mole fractions of the PAH compounds in each sample were calculated using the estimated average molecular masses, which ranged from 225 g/mole to 232 g/mole. The volume fractions of the PAH

compounds in each sample were calculated using the NAPL density, which ranged from 0.851 g/cm^3 to 0.869 g/cm^3.

The average deviation and maximum deviation in predicted aqueous concentrations from measured concentrations are shown in Table 2-11. The average deviation in predicted concentrations ranged from 40.4% to 68.4%. The maximum deviation ranged from 76.0% to 133%. Predicted aqueous concentrations based on weight fraction or volume fraction generally yield comparable or slightly larger deviations from the measured concentrations than predicted concentrations based on mole fraction. These laboratory experiments suggest Raoult's Law provides a reasonable means for determining the effective solubility of diesel fuel components, although the deviation from measured values is greater than for simple NAPL mixtures and gasoline.

2.6.3 Creosote and Coal Tar

Creosote and coal tars are mixtures of several hundred or more hydrocarbon compounds. Creosote and coal tars are comprised primarily of PAH compounds with lesser proportions of sulfur- and nitrogen-containing heterocyclic compounds, phenolic compounds, and sometimes BTEX compounds. The effective solubilities of various components of creosote and coal tars have been determined by Priddle and MacQuarrie (1994) and Lee et al. (1992b), respectively.

Priddle and MacQuarrie (1994) determined the effective solubility of 6 PAH compounds in a sample of creosote by means of a static generator column experiment. The 6 components considered in this test comprised about 52.3 weight percent of the creosote. Creosote was equilibrated with organic-free deionized water for a period of 10 days. The water to NAPL ratio was approximately 10 to 1. An aliquot of water was removed, extracted with dichloromethane and analysed by GC/MSD (gas chromatography/mass

selective detection). The results of the effective solubility tests are summarized graphically in Figure 2-27.

The average molecular mass of the creosote sample was by Priddle and MacQuarrie from the chromatograms. The density of the sample was measured directly. The mole fractions of the PAH compounds in the sample were calculated using the estimated average molecular mass of 180 g/mole. The volume fractions of the PAH compounds in the sample were calculated using the NAPL density of 1.10 g/cm^3.

Lee et al. (1992b) determined the effective solubility of 12 PAH compounds in 3 samples of low-viscosity liquid coal tar by means of batch experiments. The 12 components considered in these tests comprised about 17.0 to 30.1 weight percent of the coal tar. The chemical compositions of these coal tars are shown in Table 1-5. Coal tar was equilibrated with 0.01 mole/L calcium chloride solution for a period of 7 days. The water to NAPL ratio was approximately 80 to 1. An aliquot of water was removed, extracted with dichloromethane and analysed by GC/ITD (gas chromatography/ion trap detection). The results of the effective solubility tests are summarized graphically in Figure 2-28, 2-29 and 2-30.

The average molecular masses of the coal tar samples were estimated based on vapour pressure osmometry. The density of each sample was measured directly. The mole fractions of the PAH compounds in each sample were calculated using the estimated average molecular weights, which ranged from 230 g/mole to 250 g/mole. The volume fractions of the PAH compounds in each sample were calculated using the NAPL density, which ranged from 1.064 g/cm^3 to 1.133 g/cm^3.

The average deviation and maximum deviation in predicted aqueous concentrations from measured concentrations are shown in Table 2-12. For the creosote sample and coal tars #4 and #5, the average deviation in

predicted concentrations ranged from 39.6% to 83.2%. Predicted aqueous concentrations based on weight fraction or volume fraction generally yield similar or slightly smaller deviations from the measured concentrations compared to predicted concentrations based on mole fraction.

The deviations in predicted aqueous concentration for coal tar #1, and the maximum deviations for all the coal tar samples are much larger than those exhibited for simple NAPL mixtures, gasoline or diesel fuel. In almost all cases, the predicted aqueous concentrations are higher than the measured concentrations. For fluoranthene in coal tar #1, the predicted concentration was 12.2 times higher than the measured concentration. In general, the largest deviations occur for the compounds with the lowest effective solubility.

The reasons for the large deviations in predicted aqueous concentrations for the coal tar samples are not clear. All of the measured aqueous concentrations are less than the solid-phase solubility of the PAH compounds. As a result, the measured effective solubilities of the components are not controlled by the presence of crystalline compounds in the coal tar.

For the higher molecular weight PAH compounds such as fluoranthene, pyrene and benzo(a)anthracene which exhibit the largest deviations, the measured aqueous concentrations are 0.02 mg/L or less. The analytical error at low concentrations is likely larger than at higher concentrations and could account for deviations of about ±50% to a factor of 2. However, analytical errors could not likely account for deviations a high a factor of 12.2 times.

There will also be error imparted to the predicted aqueous concentrations because of inaccuracies in the supercooled liquid solubilities used in the Raoult's Law calculations. The supercooled liquid solubilities are

calculated using published solid-phase solubility values and equation 2-14. There may be inaccuracy in the published solid-phase solubility values. Supercooled liquid solubility values were estimated using equation 2-14 with the assumption that the entropy of fusion is a constant for all the PAH compounds considered because specific entropy of fusion values are not available for all the PAH compounds. Inaccuracy in the calculation of the supercooled liquid solubilities is consistent with the trend in the deviations of the predicted aqueous concentrations. The PAH compounds having the lowest solid-phase solubility have also the highest melting point, and as a result, their calculated supercooled liquid solubility will be most influenced by errors associated with equation 2-14.

These laboratory experiments suggest Raoult's Law must be used with caution in determining the effective solubility of coal tar components. Raoult's Law may provide reasonable estimates of effective solubility for the compounds having the higher effective solubility, but may be inaccurate by as much as a factor of ten times for other compounds.

2.6.4 Effect of Uncharacterized Portion of NAPL

For each of the examples of complex NAPLs described in the preceding sections, significant proportions of the NAPLs were not characterized specifically. Although the concentration of the uncharacterized (UC) portion was known, the compounds present were not identified. As a result, the mole fractions of the characterized components could not be calculated until a molecular mass was assigned to the UC portion of the NAPL. For the examples of gasoline, diesel fuel, creosote and coal tar, the average molecular mass of the NAPL components was estimated by gas chromatography or vapour pressure osmometry. This average molecular mass value was assigned to the uncharacterized portion of the NAPL. The average molecular masses for specific chemical products are known sufficiently well, in general, to allow their use in the calculation of effective solubilities of the important

components. The average molecular mass for gasoline ranges from 100 g/mole to 105 g/mole (Cline et al., 1991). The average molecular mass for diesel fuel ranges from 225 g/mole to 232 g/mole (Lee et al, 1992a). The average molecular mass for coal tar ranges from 230 g/mole to 250 g/mole (Lee et al., 1992b).

However, at many sites of groundwater contamination, the average molecular mass of NAPL has not been measured specifically nor can be selected reliably from the published literature. As a result, the application of Raoult's Law requires the estimation of the molecular mass of the UC portion of the NAPL. The value of molecular mass assigned to the UC portion, together with the concentration of the UC portion, will influence the mole fractions calculated for all the characterized components.

Table 2-13 shows an example of the effect of different assumed molecular masses for the UC portion on the effective solubilities of a sample of NAPL from the Tyson's Superfund site (shown also in Table 1-2). The best estimate of the molecular mass of the UC fraction was 200 g/mole determined from gas chromatograms of the hydrocarbons present in the NAPL sample. This value is regarded as the true value for this example. The effective solubilities of trichloropropane, toluene, xylenes and ethyl benzene were calculated using this value, and values of 150 g/mole and 250 g/mole, representing the possible range in molecular mass for the UC portion. A lower value for the assumed molecular mass results in a higher mole fraction for the UC portion and consequently lower effective solubility values for the characterized components. The effective solubility for each of the characterized components is reduced by the same factor. As a result, the ratios of the effective solubilities of the characterized components does not change. A higher value for the assumed molecular mass results in a lower mole fraction for the UC portion and consequently higher effective solubility values for the characterized components.

For this particular NAPL sample, the potential uncertainty imparted to the calculated effective solubilities of characterized components (i.e. a factor of 0.88 to 1.09) is smaller than any uncertainty associated with the molecular mass of the UC portion (i.e. a factor of 0.75 to 1.25). However, the uncertainty imparted to the calculated effective solubilities will approach the uncertainty associated with the molecular mass for NAPL samples in which the UC portion has a higher concentration. The uncertainty imparted to the calculated effective solubilities will be higher also if the molecular mass of the UC portion is less than the average molecular mass of the characterized components. The general sensitivity of calculated effective solubility to different values of the molecular mass of the UC portion is shown in Figures 2-31, 2-32 and 2-33. In all cases the uncertainty imparted to the calculated effective solubility of the characterized components is less than the uncertainty in the assumed molecular mass of the UC portion. In the cases where the UC portion comprises a lower concentration in the NAPL, uncertainties imparted to the calculated effective solubilities of the characterized components will be very small (i.e. 0.95 to 1.05).

2.6.5 Conclusions on Raoult's Law for Complex NAPLs

Based on information in the published literature, it is apparent that Raoult's Law provides a reasonable means for the estimation of effective solubility for complex NAPL mixtures, although deviations between estimated and measured values are greater generally than for simple NAPL mixtures. The following specific conclusions can be made:

- For gasoline, effective solubilities predicted by Raoult's Law deviate from measured concentrations by only 20% to 40%, or less. This is comparable to many simple NAPL mixtures.

- For diesel fuel, effective solubilities predicted by Raoult's Law deviate from measured concentrations by 40% to 70%, or less.

- For coal tar and creosote NAPL, effective solubilities predicted by Raoult's Law deviate from measured concentrations by 40% to 80% for most compounds in most samples. However, for low solubility components in some sample, predicted effective solubilities may deviate from measured values by factors up to 12 times. As a result, Raoult's Law should be used with caution for complex NAPL mixtures similar to coal tar and creosote.

2.7 Prediction of Effective Solubility using UNIFAC

The most significant fundamental assumption invoked in the application of Raoult's Law to predict effective solubility is that there is no chemical interaction between the various components of a multi-component NAPL. Specifically, it is assumed that the activity coefficients for the NAPL components equal unity, $\gamma^{i}_{NAPL} = 1$.

UNIFAC (Universal Quasi-chemical Functional Group Activity Coefficients) is a calculation method which can be used to predict the activity coefficients of individual organic compounds in liquid mixtures. The chemical interaction between molecules in a liquid mixture depends on the size and shape of the molecules, and the energy interactions between the chemical functional groups comprising the molecules. The fundamental basis for UNIFAC calculations is that organic compounds can be expressed as combinations of chemical functional groups, and that the interactions between the molecules can be characterized by the summation of the chemical interactions between the functional groups. The principles for UNIFAC were described by Fredenslund et al. (1977) and its potential applicability has grown as appropriate parameters have been measured or developed for the interactions of a greater number of functional groups. Because of the number of possible interactions, UNIFAC calculations are commonly performed using a computer model. Lyman et al. (1982) provide a description of the procedures for UNIFAC calculations.

For the purpose of this evaluation, the results of laboratory experiments and Raoult's Law predictions of effective solubility described in Sections 2.5 and 2.6 were compared to effective solubility values predicted using UNIFAC. The computer code PC-UNIFAC Version 4.0[1] was used to calculate the activity coefficients (γ^i_{NAPL}) of the components in each of the NAPL mixtures. The value of the activity coefficient was then substituted into equation 2-11 to determine the effective solubility.

2.7.1 Chlorinated Solvent Mixtures

The effective solubility values calculated by UNIFAC for the laboratory experiments of Broholm and Feenstra (1995) are shown in Figures 2-35 through 2-41. The average and maximum deviation of the Raoult's Law and UNIFAC predictions from measured effective solubility values are shown in Table 2-14. For these mixtures of chlorinated solvents, Raoult's Law provided reasonably accurate estimates of effective solubility. UNIFAC predictions were slightly worse than Raoult's Law predictions. This is likely due to inadequacies in the UNIFAC database of functional group interaction parameters. The average deviation of the UNIFAC predictions from measured values was 13.3% compared to 7.0% for Raoult's Law predictions. The maximum deviation of the UNIFAC predictions from measured values was -53.0% compared to -40.4% for Raoult's Law predictions.

2.7.2 Chlorinated Benzene Mixtures

The effective solubility values calculated by UNIFAC for the laboratory experiments of Banerjee (1984) are shown in Figures 2-42 through 2-44. The average and maximum deviation of the Raoult's Law and UNIFAC predictions from measured effective solubility values are shown in Table 2-15. For these mixtures of chlorinated benzenes, Raoult's Law

[1] PC-UNIFAC Version 4.0 (1993). Available commercially from bri, inc., P. O. Box 7834, Atlanta, Georgia 30357-0834.

provided reasonably accurate estimates of effective solubility and UNIFAC predictions were comparable.

2.7.3 Petroleum Hydrocarbon Mixtures

The effective solubility values calculated by UNIFAC for the laboratory experiments of Leinonen and Mackay (1973) are shown in Figure 2-45. The average and maximum deviation of the Raoult's Law and UNIFAC predictions from measured effective solubility values are shown in Table 2-16.

The effective solubility values calculated by UNIFAC for the laboratory experiments of Burris and MacIntyre (1986a, 1986b and 1986c) are shown in Figures 2-46 through 2-50. The average and maximum deviation of the Raoult's Law and UNIFAC predictions from measured effective solubility values are shown in Table 2-17. For these mixtures of petroleum hydrocarbons, Raoult's Law provided reasonably accurate estimates of effective solubility but UNIFAC predictions deviate slightly less from measured values. For the Burris and MacIntyre experiments, the average and maximum deviations for the UNIFAC predictions were 10.9% and -52.8%, respectively, compared to 20.9% and -75.3% for the Raoult's Law predictions.

2.7.4 Gasoline

The effective solubility values calculated by UNIFAC for the laboratory experiments of TRC (1985), Poulsen et al. (1992) and Cline et al. (1991) are shown in Figures 2-51 through 2-53. The average and maximum deviation of the Raoult's Law and UNIFAC predictions from measured effective solubility values are shown in Table 2-18. For each set of experiments, UNIFAC and Raoult's Law predictions were comparable.

2.7.5 Diesel Fuel

The effective solubility values calculated by UNIFAC for the laboratory experiments of Lee et al. (1992a) are shown in Figures 2-54 through 2-57. The average and maximum deviation of the Raoult's Law and UNIFAC predictions from measured effective solubility values are shown in Table 2-19. For these diesel fuels, UNIFAC predictions exhibited much larger deviations from measured values than Raoult's Law predictions.

2.7.6 Creosote and Coal Tar

The effective solubility values calculated by UNIFAC for the laboratory experiments of Priddle and MacQuarrie (1994) are shown in Figure 2-58 and those of Lee et al. (1992b) are shown in Figures 2-59 through 2-61. The average and maximum deviation of the Raoult's Law and UNIFAC predictions from measured effective solubility values are shown in Table 2-20. For these creosote and coal tar mixtures, UNIFAC and Raoult's Law predictions were comparable to measured values.

2.7.7 Conclusions on UNIFAC for NAPL Mixtures

Based on the preceding exercise, it is apparent that UNIFAC predictions of effective solubility are not substantially more accurate than Raoult's Law predictions for most simple or complex NAPL mixtures. The only exception appears to be relatively simple mixtures of structurally dissimilar hydrocarbon compounds. For the mixtures of aliphatic and aromatic hydrocarbons tested by Burris and MacIntyre (1986a, 1986b and 1986c), the deviation from measured values of effective solubility exhibited by the UNIFAC predictions was about half that of the Raoult's Law predictions. However, UNIFAC does not provide more accurate predictions than Raoult's Law for more complex mixture of hydrocarbons such as gasoline, diesel fuel, creosote or coal tar.

2.8 Other Factors Influencing Solubility

2.8.1 Temperature

For the range in temperature found in the subsurface environment, the aqueous solubilities of organic compounds vary only by a small amount. Over the temperature range of 0°C to 25°C, pure-phase solubility increases for some compounds, decreases for some compounds, and remains essentially constant for other compounds. Most compounds exhibit changes in solubility of 20% to 30% or less. The pure-phase solubility values of selected compounds at 0°C and 25°C are shown in Table 2-21. Because of the small changes in solubility with temperature over this temperature range, laboratory measured values at 25°C are not corrected commonly for the lower temperature in the subsurface.

2.8.2 pH

In general, the solubility of organic compounds is not influenced by the pH of the aqueous phase. However, pH will influence the solubility of organic acids and bases such as phenolics, carboxylic acids and amines can form non-ionic and ionic species in water at the range of pH (i.e. about 5 to 8) found in groundwater. Organic compounds in their non-ionic form will have lower solubility than when in their ionic form.

The dissociation of an organic acid into ionic and non-ionic forms can be expressed by:

$$HA_{aq} = H^{+} + A^{-} \qquad [2\text{-}15]$$

where :

HA_{aq} *is the non −ionic organic compound*

H^+ *is hydrogen ion*

A^- *is the ionic organic compound*

The partitioning between ionic and non-ionic forms of the organic compound is expressed by:

$$K_a = \frac{[H^+][A^-]}{[HA_{aq}]} \qquad [2\text{-}16]$$

where :

K_a *is the dissociation constant*

$[HA_{aq}]$ *is the chemical activity of the non −ionic organic compound*

$[H^+]$ *is the chemical activity of hydrogen ion*

$[A^-]$ *is the chemical activity of the ionic organic compound*

When the pH of the aqueous phase equals the negative log of the K_a (i.e. pK_a), the chemical activity of the ionic and non-ionic forms are equal. For the organic acids, when the pH of the aqueous phase is less than the pK_a, the non-ionic form is predominant. When the pH of the aqueous phase is greater than the pK_a, the ionic form is predominant.

Similarly, the dissociation of an organic base into ionic and non-ionic forms can be expressed by:

$$BH^+ = B_{aq} + H^+ \qquad [2\text{-}17]$$

where :

BH^+ *is the ionic organic compound*

B_{aq} *is the non −ionic organic compound*

H^+ *is hydrogen ion*

The partitioning between ionic and non-ionic forms of the organic compound is expressed by:

$$K_a = \frac{[H^+][B_{aq}]}{[HB^+]} \qquad [2\text{-}18]$$

where :

K_a *is the dissociation constant*

$[B_{aq}]$ *is the chemical activity of the non −ionic organic compound*

$[H^+]$ *is the chemical activity of hydrogen ion*

$[BH^+]$ *is the chemical activity of the ionic organic compound*

When the pH of the aqueous phase equals the negative log of the K_a (i.e. pK_a), the chemical activity of the ionic and non-ionic forms are equal. For organic bases, when the pH of the aqueous phase is less than the pK_a, the ionic form is predominant. When the pH of the aqueous phase is greater than the pK_a, the non-ionic form is predominant.

For organic acids, the proportion of the compound in non-ionic form at a specified pH is given by:

$$\alpha^{acid}_{non-ionic} = \frac{1}{1 + 10^{(pH-pKa)}} \qquad [2\text{-}19]$$

For organic bases, the proportion of the compound in non-ionic form at a specified pH is given by:

$$\alpha_{non-ionic}^{base} = 1 - \frac{1}{1 + 10^{(pH-pKa)}} \quad [2\text{-}20]$$

Table 2-22 provides a listing of the pK_a values of selected organic acids and bases which are found commonly as groundwater contaminants. For compounds with pK_a values far beyond the pH range of groundwater (i.e <4 and >9), only the non-ionic or ionic forms will be present. This includes phenol and methylated phenols (cresols). This simplifies the determination of solubility.

However, there are numerous compounds with pK_a values comparable to the pH range found in groundwater. In particular, dichloro-, trichloro-, tetrachloro- and pentachlorophenols have pK_a values that range from about 5 to 8. For these compounds, varying proportions of the non-ionic and ionic forms of each molecule may be present in the aqueous phase depending on the pH. Because the solubilities of the non-ionic and ionic forms will be very different, the total solubility of such compounds in water will be highly dependent on pH.

Figure 2-62 illustrates this case for pentachlorophenol (PCP), a compound that is used widely as a wood preservative chemical. The pK_a of PCP is 4.75. At pH values less than the pK_a, the non-ionic form is predominant (Figure 2-62a). At higher pH values, the ionic form is predominant. The pure-phase solubility of PCP reported in the literature ranges from about 10 mg/L to 20 mg/L with the most commonly used value being 14 mg/L.

Although it is seldom specified in the literature, these solubility values represent the solubility of PCP at low pH when the dissolved PCP in the non-ionic form. The solubility of PCP at neutral to high pH has not been reported specifically in the literature. However, Lee et al. (1990) measured the change

in the K_{OC} value for PCP with pH and found that K_{OC} decreases by a factor of 50 times from pH 3 to pH 7. K_{OC} is the organic carbon - water partition coefficient which reflects the degree to which PCP may sorb on soil organic carbon. K_{OC} has been shown to be inversely correlated to solubility (Lyman et al., 1990).

As a result, it is expected that the solubility of PCP would increase by about 50 times from pH 3 to pH 7. This yields an estimated solubility of 700 mg/L for PCP when present in the ionic form. The total solubility of PCP at a given pH is given by:

$$S_{total} = \alpha_{non-ionic} S_{non-ionic} + (1-\alpha_{non-ionic}) S_{ionic} \qquad [2\text{-}21]$$

where :

S_{total} *is the total solubility*

$\alpha_{non-ionic}$ *is the fraction non −ionic form*

$S_{non-ionic}$ *is the solubility of non −ionic form*

S_{ionic} *is the solubility of ionic form*

This relationship is shown in Figure 2-62b. This illustrates that pH will have a significant effect on the solubility of compounds such as pentachlorophenol and is a factor that must be considered in the determination of effective solubility NAPLs comprised of such compounds.

2.8.3 Dissolved Inorganics

High concentrations of dissolved inorganic salts in the aqueous phase will decrease the solubility of organic compounds. This effect is referred to as "salting out". It is believed to be caused by the extensive hydration of inorganic ions in solution which binds a substantial proportion of the water molecules. This bound water is unavailable for the organics to dissolve into, and as a result, the solubility of organic compounds is reduced. However, the

dissolved salt concentrations must be very high before the effect becomes significant. Experimental data are available for some organic compounds. Table 2-23 shows the solubility of several organic compounds in both distilled water and seawater. For these compounds, the solubility in seawater is 23% to 43% lower than in distilled water. The total salt concentration in seawater is about 35,000 mg/L and is considerably higher than encountered commonly in groundwater, even groundwater contaminated by landfill leachates.

The decrease in solubility due to salting out can be estimated for other organic compounds and related to salt concentration. The salting out effect was established empirically by Setchenow (1889) by:

$$\frac{S_{water}}{S_{salt\ solution}} = 10^{Ks\ [\ salt\ ]} \qquad [2\text{-}22]$$

where :

S_{water} *is the solubility of the organic in water*

$S_{salt\ solution}$ *is the solubility of the organic in salt solution*

Ks *is the Salting Constant*

$[\ salt\ ]$ *is the molar concentration of salt in water*

Although Salting Constant values are not available for all organic compounds of relevance in groundwater, available data suggest that the Salting Constant varies only from about 0.1 to 0.4 L/mole (see Table 2-24). This small range in Salting Constant appears to apply to both non-ionic and ionic compounds. The Salting Constant for phenol is comparable to the other compounds in Table 2-24.

Figure 2-63 shows the solubility of organic compounds in salt solutions relative to distilled water versus salt concentration. This graph illustrates that solubility is decreased by 10% to 40% at seawater concentrations, equivalent to about 35,000 mg/L dissolved salts. The decrease in solubility is

probably less than 10% at salt concentrations of 5,000 mg/L or less. As a result, in most circumstances of groundwater contamination by organic compounds, there should be no significant effect on solubility as a result of presence of dissolved inorganics in water.

2.8.4 Miscible Co-solvents

The solubility of organic compounds in groundwater may be enhanced by the presence of other miscible co-solvents in the groundwater. Industrial chemicals commonly released to the subsurface environment which may act as co-solvents include: acetone, methyl ethyl ketone (MEK), methanol and isopropanol (IPA). These compounds have either a very high solubility in water, or are completely miscible in water, such that these compounds can occur at very high concentrations (>10,000 mg/L) in groundwater if released in sufficient quantity.

As was previously indicated in Section 2.3.1, when the concentrations of dissolved organic compounds are less than a few hundred to a few thousand milligrams per litre, there are no significant chemical interactions between the dissolved organic compounds. Hence, the presence of low to moderate concentrations of other organic compounds does not influence the solubility of a specific organic compound. However, if the concentrations of other organics (co-solvents) are sufficiently high, the solubility of specific organic compounds is enhanced. This enhancement occurs because the co-solvents replace water as the molecules surrounding the specific compound.

Rao et al. (1985) describe the theoretical basis for estimating the solubility of an organic compound in a mixture of water and co-solvent. This relationship is given as:

$$\ln\left[\frac{C^i}{S^i}\right] = f_c\left[\frac{(\Delta\gamma^c)(HSA)}{(k_B)(T)}\right] \qquad [2\text{-}23]$$

where :

$\frac{C^i}{S^i}$ *is the effective solubility relative to the pure - phase solubility*

f_c *is the volume fraction of co −solvent in the water*

$\Delta\gamma^c$ *is the difference in interfacial energy for an organic/water and an organic/co −solvent system (kJ/nm ^{2})*

HSA is the hydrophobic surface area of the organic compound (nm ^{2})

k_B *is Boltzman' s Constant (kJ/K)*

T is the temperature (K)

The difference in interfacial energy is fixed for a given organic compound in a given water/co-solvent system. This parameter may be estimated from macroscopic interfacial tensions (Schwarzenbach et al., 1992). For hydrophobic organic compounds such as chlorinated solvents and BTEX compounds, the hydrophobic surface area is equivalent to the total molecular surface area (TSA) of the compound. TSA values for selected organic compounds are shown in Table 2-25.

From equation 2-23, it is evident that the increase in effective solubility of the organic will be greater for higher co-solvent concentrations. For a given co-solvent system and co-solvent concentration, the increase in effective solubility will be greater for organic compounds having higher HSA values. In general, high molecular-weight, low-solubility organic compounds have higher HSA so that the presence of co-solvents will influence the effective solubility of low-solubility compounds to a greater degree than high-solubility organic compounds.

The theoretical relationship shown in equation 2-23 has been validated experimentally by Nkedi-Kizza et al. (1985) for anthracene in methanol-water and acetone-water systems. The results of theoretical calculations for TCE, 1,2,4-trichlorobenzene (124-TCBz) and pyrene in a methanol-water system are

shown in Figure 2-64. The results of calculations for TCE, 124-TCBz and pyrene in an acetone-water system are shown in Figure 2-65. TSA values used for TCE, 124-TCBz and pyrene were 1.1 nm^2, 1.6 nm^2 and 2.12 nm^2, respectively. Values for the difference in interfacial energy used were 2.36×10^{-23} kJ/nm^2 for the methanol-water system, and 3.65×10^{-23} kJ/nm^2 for the acetone-water system. The value of Boltzman's Constant was 1.38×10^{-26} kJ/K, and the temperature was 293 K.

The results of these calculations indicate that a methanol concentration of at least 40,000 mg/L is required to increase the effective solubility of pyrene by a factor of 2 times. The increase in effective solubility for TCE is a factor of 1.5 times at the same methanol concentration. Acetone has a slightly greater influence on effective solubility. An acetone concentration of 30,000 mg/L is required to increase the effective solubility of pyrene by a factor of 2 times. The increase in effective solubility of most organic compounds will be less than about 30% for co-solvent concentrations of 10,000 mg/L, or lower.

2.8.5 Surfactants

Surfactants are a particular class of organic chemicals which have the potential to increase the solubility of other organic compounds to a much greater degree than miscible co-solvents. Surfactants are used widely in industry for cleaning and in commercial applications for cleaning, in food products and in pharmaceutical products.

Surfactants are molecules which have two distinct structural characteristics. One end of the surfactant molecule has an affinity for water (hydrophilic), while the other end has an affinity for other organic compounds (lipophilic, or conversely, hydrophobic). The hydrophobic ends of surfactant molecules are comprised commonly of long hydrocarbon chains, or tails. Surfactants may be cationic, anionic or nonionic in character when dissolved in water.

Surfactants are highly soluble in water, commonly thousands of milligrams per litre, or greater. When dissolved in water at low concentrations, surfactants have only a small effect on increasing the solubility of other organic compounds. At low concentrations, surfactant molecules are present as individual monomers. At higher concentrations, the surfactant molecules begin to form clusters, or aggregates, referred to as micelles. Within the micelles, the hydrophobic tails of the surfactant molecules are arranged to point to the centre of the micelle, thus forming a pseudophase of hydrocarbon liquid at the centre of the micelle. The hydrophobic core of the micelles provides the site within which other organic compounds can partition, or sorb, from the water. If the degree of partitioning of the organic compound into the micelle is appreciable, the total concentration of the organic in the water may exceed the solubility of the compound because of the additional chemical mass held within the micelles.

The effect of surfactants on the solubility of organics will be greatest for those organic compounds that partition strongly into other hydrophobic organics. The octanol-water partition coefficient (K_{ow}), which has been measured for most organic compounds, provides a measure of a compound's tendency to partition into hydrophobic organic liquid or solid phase. The higher the K_{ow}, the greater the partitioning of an organic compound from water into a hydrophobic organic phase. The K_{ow} of an organic compound is correlated inversely its solubility in water. Compounds with high K_{ow} have a low solubility. As a result, organic compounds with a low solubility in water will be influenced more by the presence of surfactants than organic compounds with a high solubility.

The surfactant concentrations at which micelles begin to form is referred to as the critical micelle concentration, or CMC. The CMC for different surfactants may range from a few milligrams per litre to more than a

hundred thousand milligrams per litre. For a specific surfactant, CMC will also vary with temperature, pH and general water chemistry.

The effect of surfactants on the solubility of important groundwater contaminants have been studied by various investigators. The typical effect of surfactant concentrations on contaminant solubility is shown for the surfactant, sodium dodecyl sulfate, on 1,2,3-trichlorobenzene (123-TCBz) in Figure 2-66. In this example, for surfactant concentrations less than the CMC, there is only a slight increase in 123-TCBz solubility with increasing surfactant concentration. However, at concentrations greater than the CMC, there is a substantial increase in 123-TCBz solubility with further increases in surfactant concentration. The slope of this portion of the curve is referred to as the molar solubilization ratio, or MSR. Specific MSR values can be determined experimentally for different organic compounds in the presence of different surfactants.

With knowledge of the CMC of a surfactant, and the MSR for a organic compound-surfactant combination, the potential increase in solubility of the organic compounds can be estimated by (Edwards et al., 1991):

$$C = S + MSR\,(C_{surf} - CMC) \qquad [2\text{-}24]$$

where :
C is the aqueous concentration of the organic compound
S is the solubility of the organic compound
MSR is the molar solubilization ratio
C_{surf} is the concentration of surfactant
CMC is the critical micelle concentration for the surfactant
All concentrations in mol/L

This relationship was used to illustrate the effect of surfactant concentrations on the solubility of several common groundwater

contaminants. Measured values for MSR and CMC were used in these calculations.

Figure 2-67 shows the increase in solubility for 1,2-dichloroethylene (12-DCE), trichloroethylene (TCE) and tetrachloroethylene (PCE) in the presence of two different surfactants. CMC and MSR values were taken from Shiau et al. (1994). Of these three compounds, 12-DCE has the highest solubility and is affected the least by the surfactant. Surfactant concentrations much greater than the CMC are necessary to increase the solubility of 12-DCE and TCE by a factor of 2 times. In contrast, lower surfactant concentrations are necessary to increase the solubility of PCE by a factor of 2 times.

Figure 2-68 shows the increase in solubility for naphthalene, phenanthrene and pyrene in the presence of four different surfactants. CMC and MSR values were taken from Edwards et al. (1991). Of these three compounds, naphthalene has the highest solubility and is affected least by the surfactant. Lower surfactant concentrations are necessary to cause a substantial increase in the solubility of phenanthrene and pyrene.

Figure 2-69 shows the increase in solubility for 1,2,3-trichorobenzene (123-TCBz) and the pesticide, DDT, in the presence of six different surfactants. CMC and MSR values were taken from Kile and Chiou (1989). Of these two compounds, DDT has a very low solubility and very substantial increases in solubility are caused by surfactant concentrations above the CMC.

Of the surfactant compounds illustrated in the preceding figures, the MSR (slope of the lines) is generally greater for surfactants having lower CMC values. As a result, the surfactants most likely to increase the solubility of groundwater contaminants are those with the lowest CMC. Rosen (1989) compiled CMC values for 125 common surfactants at a temperature of 15°C to 25°C. These data are summarized in Figure 2-70. The median CMC value is about 600 mg/L, but the CMC values span a range from 1 mg/L to greater than

100,000 mg/L. In the context of groundwater contamination, there are few circumstances where the concentrations of surfactants could be expected to occur in hundreds or thousands of milligrams per litre.

However, of the 125 surfactants considered by Milton, 10% had CMC values ranging from 1 mg/L to 10 mg/L and 30% had CMC values ranging from 1 mg/L to 100 mg/L. Surfactants released with other organic chemicals to landfills, lagoons or sewer systems could have surfactant concentrations in this range. If certain types of surfactants occur in groundwater at these concentrations, the solubility of normally low-solubility organic compounds could be increased.

2.8.6 Dissolved Organic Matter

The presence of dissolved organic matter in groundwater may also increase the solubility of organic contaminants. Dissolved organic matter in groundwater may include dissolved humic substances and other natural material. Comparable high molecular weight organic compounds may be associated also with sewage and industrial wastewater discharges and landfill leachate. Specific organic contaminants may associate or partition with such organic macromolecules in much the same manner as they may partition into surfactant micelles. If the macromolecules occur at sufficient concentration in groundwater, the solubility of organic contaminants may be increased.

Based on the relationships developed by Enfield et al. (1989), it is possible to estimate the increase in solubility of a specific organic contaminant in the presence of dissolved organic matter by:

$$\frac{C}{S} = \left[1 + K_p^{DOM} \; f_{oc}^{DOM} \; C^{DOM}\right] \qquad [2\text{-}25]$$

and

$$\log K_p^{DOM} = -0.923 \log S + 3.294 \quad [2\text{-}26]$$

where :

$\frac{C}{S}$ *is the aqueous concentration relative to the solubility of the organic compound*

K_p^{DOM} *is the water –dissolved organic matter partition coefficient*

f_{oc}^{DOM} *is the fraction organic carbon in the dissolved organic matter*

C^{DOM} *is the concentration of dissolved organic matter*

S *is the solubility of the organic compound in mg/L*

These relationships were used to calculate the increase in solubility for organic contaminants for a specified dissolved organic matter concentration. The results of these calculations are shown in Figure 2-71. These calculations indicate that the solubility of organic contaminants such as chlorinated solvents and BTEX compounds with normally high solubility (i.e. >100 mg/L) will not be increased significantly by the presence of even high concentrations of dissolved organic matter. The solubility of contaminants having normally moderate solubility (i.e. 1 mg/L to 100 mg/L) will be increased only by the presence of dissolved organic matter at concentrations of several thousand milligrams per litre or higher. The solubility of contaminants having normally low solubility (<1 mg/L) may be increased significantly for dissolved organic matter concentrations above several tens of milligrams per litre.

2.9 Overall Conclusions Regarding Effective Solubility

Based on the data, calculations and discussion in the preceding section, the following specific conclusions are made:

<u>Predictions of Effective Solubility by Raoult's Law</u>

- For NAPL mixtures comprised of structurally similar compounds, such as the mixtures of chlorinated solvents considered by Broholm

and Feenstra (1995) and the mixtures of chlorinated benzenes considered by Banerjee (1984), effective solubilities predicted by Raoult's Law should deviate from measured concentrations by only 10% to 30%, or less.

- For NAPL comprised of structurally dissimilar compounds such as mixtures of aliphatics and aromatic hydrocarbons, such as the mixtures considered by Leinonen and Mackay (1973) and Burris and MacIntyre (1986a, 1986b, 1986c), effective solubilities predicted by Raoult's Law should deviate from measured concentrations by only 25% to 50%, or less.

- For gasoline, effective solubilities predicted by Raoult's Law deviate from measured concentrations by only 20% to 40%, or less. This is comparable to many simple NAPL mixtures.

- For diesel fuel, effective solubilities predicted by Raoult's Law deviate from measured concentrations by 40% to 70%, or less.

- The potential error in effective solubility values predicted by Raoult's Law is comparable to, or smaller than the uncertainty associated with the chemical analysis of groundwater samples. The uncertainty in chemical analyses from commercial laboratories ranges typically from ±30% to ±60% for the organic contaminants found commonly in groundwater (see Table 2-26).

- For coal tar and creosote NAPL, effective solubilities predicted by Raoult's Law deviate from measured concentrations by 40% to 80% for most compounds in most samples. However, for low solubility components in some samples, predicted effective solubilities may deviate from measured values by factors up to 12 times. As a result, Raoult's Law should be used with caution for complex NAPL mixtures similar to coal tar and creosote.

- Calculation of effective solubility using Raoult's Law is most accurate when based on mole fraction. However, use of weight fraction or volume fraction will decrease accuracy only slightly.

- Calculations of effective solubility using Raoult's Law must utilize the supercooled liquid solubility values for compounds that are solids in their pure form at ambient temperature.

- Calculations of effective solubility using Raoult's Law are not applicable if the NAPL is a heterogeneous mixture of liquid and solids.

Predictions of Effective Solubility using UNIFAC

- Predictions of effective solubility using activity coefficients calculated by UNIFAC are not substantially more accurate than Raoult's Law predictions for most simple or complex NAPL mixtures. The only exception appears to be relatively simple mixtures of structurally dissimilar compounds. For the mixtures of aliphatic and aromatic hydrocarbons tested by Burris and MacIntyre (1986a, 1986b and 1986c), the deviation from measured values of effective solubility exhibited by the UNIFAC predictions was about half that of the Raoult's Law predictions.

Effect of Temperature

- Over the temperature range of 0°C to 25°C, the solubility of the majority of organic compounds varies by 20% to 30% or less. The solubility of some compounds increases with increasing temperature while the solubility of other compounds decreases.

Effect of pH

- The solubility of ionic organic compounds may vary significantly with pH for compounds having pK_a values ranging from 5 to 8, the normal range of groundwater pH. Such compounds include most chlorophenols and nitrophenols. The solubility of these compounds will be higher at higher pH.

Effect of Salinity

- The solubility of organic compounds will be reduced by very high concentrations of dissolved salts. The reduction in solubility will be only about 10% to 40% for most organic compounds at dissolved salt concentrations equivalent to those in seawater (i.e. 35,000 mg/L).

Effect of Miscible Co-Solvents

- The solubility of organic compounds will be increased by the presence of very high concentrations of miscible co-solvents such as acetone or methanol. The increase in solubility will be greater than about 30% only for co-solvent concentrations greater than 10,000 mg/L.

Effect of Surfactants

- The solubility of organic compounds will be increased by the presence of surfactants. The increase in solubility will be greatest for organic compounds with normally low solubility. The increase in solubility will depend also on the nature of the surfactant.

- Many common industrial and commercial surfactants at concentrations of several tens of milligrams per litre may increase

the solubility of organic contaminants by a factor of two times, or more.

Effect of Dissolved Organic Matter

- The solubility of organic compounds will be increased by high concentrations of dissolved organic matter. The increase in solubility will be greatest for organic compounds with normally low solubility.

- For normally moderate-solubility contaminants, dissolved organic matter at concentrations of several thousand milligrams per litre may increase their solubility by a factor of two times, or more.

- For normally low-solubility contaminants, dissolved organic matter at concentrations of several hundred milligrams per litre may increase their solubility by a factor of two times, or more.

In summary, Raoult's Law is the most reliable method for the prediction of effective solubility of organic contaminants derived from the dissolution of multi-component NAPL, in the majority of circumstances in groundwater. However, it must be recognized that Raoult's Law will not be directly applicable in the following circumstances:

- NAPL is a heterogeneous mixture of liquid and solids. This might be the case for weathered NAPL in which very low solubility compounds have crystallized due to the loss of more volatile or soluble components.

- Contaminants are ionic compounds with pK_a ranging from 5 to 8. This would include most chlorophenols and nitrophenols.

- Groundwater is a brine having a salinity exceeding about 35,000 mg/L. This might be the case for NAPL released to deep

sedimentary basins via deep well injection or NAPL associated with some liquid industrial discharges.

- Groundwater contains miscible co-solvents such as acetone or methanol at concentrations exceeding 10,000 mg/L. This may be the case in some industrial waste disposal landfills or lagoons.

- Groundwater contains surfactants at concentrations exceeding tens to hundreds of milligrams per litre. This may be the case in some industrial waste disposal landfills or lagoons.

- Groundwater contains dissolved organic matter at concentrations exceeding several hundred to several thousand milligrams per litre. This may be the case at some domestic waste or industrial waste landfills or lagoons.

Table 2-1. Solubility of water in selected liquid organic compounds. Data from Horvath (1982).

Compound	Mole Fraction of Water in Organic Phase	Mole Fraction of Organic in Organic Phase
Dichloromethane	0.0086	0.9914
Chloroform	0.0055	0.9945
Carbon Tetrachloride	0.0010	0.999
1,2-Dichloroethane	0.011	0.989
1,1,1-Trichloroethane	0.0026	0.9975
1,1,2-Trichloroethane	0.0088	0.9912
Trichlorotrifluoroethane	0.0011	0.9989
Trichloroethylene	0.0023	0.9977
Tetrachloroethylene	0.00088	0.99912
Chlorobenzene	0.0025	0.9975
1,2-Dichlorobenzene	0.011	0.989
1,2,4-Trichlorobenzene	0.0020	0.998
Hexachlorobutadiene	0.00079	0.99921

Table 2-2. Solid-phase solubility and supercooled liquid solubility values for selected PAH compounds. Melting point and solid-phase solubility data from Miller et al. (1985). Supercooled liquid solubility calculated using equation 2-14.

Compound	Melting Pt. (°C)	Melting Pt. (K)	Solid-phase Solubility (mg/L)	Supercooled Liquid Solubility (mg/L)
Naphthalene	80	353	31	110
2-Methylnaphthalene	35	308	25	32
Acenaphthene	96	369	3.9	20
Acenaphthylene	92	365	3.9	18
Fluorene	117	390	1.9	16
Phenanthrene	100	373	1.2	6.6
Anthracene	216	489	0.73	9.2
Pyrene	156	429	0.13	2.6
Fluoranthene	111	384	0.26	1.9
Benzo(a)fluorene	187	460	0.045	1.8
Benzo(b)fluorene	209	482	0.002	0.13
Chrysene	255	528	0.002	0.38
Benz(a)anthracene	160	433	0.014	0.30
Benz(b)fluoranthene	357	630	0.00057	1.1
Perylene	277	550	0.0004	0.13
Benzo(a)pyrene	179	452	0.0038	0.13

Table 2-3. Pure-phase solubility of chlorinated solvents at 23°C to 24°C determined by Broholm and Feenstra (1995).

Compound	Solubility (mg/L)	Number of Tests	Standard Deviation (%)
Chloroform (TCM)	8,700	13	5.4
Carbon Tetrachloride (PCM)	780	6	3.4
1,1,1,-Trichloroethane (TCA)	1,250	6	2.8
Trichloroethylene (TCE)	1,400	22	4.0
Tetrachloroethylene (PCE)	240	19	3.7

Table 2-4. Deviation of aqueous concentrations predicted by Raoult's Law from measured aqueous concentrations for laboratory experiments of Broholm and Feenstra (1995).

System	Component	Predicted by Mole Fraction		Predicted by Weight Fraction		Predicted by Volume Fraction	
		Average Deviation (%)	Maximum Deviation (%)	Average Deviation (%)	Maximum Deviation (%)	Average Deviation (%)	Maximum Deviation (%)
TCE - TCM	TCE	7.9	-15.0	6.3	14.2	6.4	14.5
	TCM	7.7	16.3	6.2	9.7	6.1	9.6
TCE - PCM	TCE	3.0	-6.4	9.0	-13.6	5.3	-10.0
	PCM	5.9	-12.9	2.2	5.9	3.2	-6.9
TCE - TCA	TCE	7.7	12.7	7.6	12.2	9.1	-12.2
	TCA	4.3	-8.9	3.8	-7.7	3.2	6.4
TCE - PCE	TCE	8.0	-15.0	14.7	-28.0	11.5	-21.7
	PCE	7.8	19.6	20.1	46.2	13.5	33.8
PCE - TCM	PCE	7.4	19.7	20.6	63.9	14.1	50.5
	TCM	6.4	-18.3	12.6	-40.0	10.6	-34.7
PCE - PCM	PCE	7.1	10.9	9.7	17.8	8.8	15.5
	PCM	4.2	-8.0	7.1	-13.6	6.1	-11.8
PCE - TCA	PCE	5.3	-12.2	12.7	23.4	5.5	-11.8
	TCA	8.5	-19.7	13.9	-33.2	8.6	-20.6
TCM- TCE - PCE	TCM	11.4	-27.5	28.7	-51.7	16.8	-39.1
	TCE	5.0	10.6	11.0	27.8	6.6	-13.4
	PCE	12.0	-40.4	23.8	44.3	17.9	-30.7
Overall Average		7.0		12.4		9.0	

Key:
TCE - Trichloroethylene PCM - Carbon Tetrachloride PCE - Tetrachloroethylene
TCM - Chloroform TCA - 1,1,1-Trichloroethane
Deviations calculated as [(Measured-Predicted)/Measured] x 100
Average Deviation - Average of absolute deviations for all the samples tested in each system.
Maximum Deviation - Largest deviation determined for an individual sample.

File:Broholm Deviation from Ideal/Sheet1

Table 2-5. Pure-phase solubility of chlorinated benzenes at 25°C determined by Banerjee (1984).

NR - Data not reported.

Compound	Solubility (mg/L)	Number of Tests	Standard Error (%)
Chlorobenzene (CBz)	502	5	5.4
1,3-Dichlorobenzene (13-DCBz)	143	NR	NR
1,2,4-Trichlorobenzene (124-TCBz)	31.3	NR	NR
1,2,4,5-Tetrachlorobenzene (1245-TeCBz) Measured Solid-phase	0.465	NR	NR
1,2,4,5-Tetrachlorobenzene (1245-TeCBz) Calculated liquid-phase	11.6	NR	NR

Table 2-6. Deviation of aqueous concentrations predicted by Raoult's Law from the measured aqueous concentrations for the laboratory experiments of Banerjee (1984).

System	Component	Predicted by Mole Fraction		Predicted by Weight Fraction		Predicted by Volume Fraction	
		Average Deviation (%)	Maximum Deviation (%)	Average Deviation (%)	Maximum Deviation (%)	Average Deviation (%)	Maximum Deviation (%)
CBz - 13-DCBz	CBz	1.3	-8.0	13.7	-27.5	5.9	-15.9
	13-DCBz	0.7	1.7	13.3	27.8	4.8	11.0
CBz - 124-TCBz	CBz	12.5	25.2	22.1	-46.2	12.0	-34.4
	124-TCBz	19.2	-42.0	10.7	33.3	14.6	-32.8
CBz - 13-DCBz -124-TCBz	CBz	20.8	88.3	24.8	40.5	20.6	67.8
	13-DCBz	7.0	17.1	13.4	36.3	8.4	24.0
	124-TCBz	12.4	-16.9	12.7	33.0	5.5	-8.6
Averages		10.6		15.8		10.3	

Key:
CBz - Chlorobenzene
13-DCBz - 1,3-Dichlorobenzene
124-TCBz - 1,2,4-Trichlorobenzene
Deviations calculated as [(Measured-Predicted)/Measured] x 100
Average Deviation - Average of absolute deviations for all the samples tested in each system.
Maximum Deviation - Largest deviation determined for an individual sample.

File:Banerjee Deviation from Ideal/Sheet1

Table 2-7. Pure-phase solubility of selected hydrocarbons at 20°C determined by Burris and MacIntyre (1986b).

Compound	Solubility (mg/L)
n-Octane	0.88
1-Methyl Naphthalene	87.9
Tetralin	42.7
Methylcyclohexane	15.2
Ethyl Benzene	181

Table 2-8. Deviation of aqueous concentrations predicted by Raoult's Law from the measured aqueous concentrations for the laboratory experiments by Leinonen and Mackay (1973).

System	Component	Predicted by Mole Fraction		Predicted by Weight Fraction		Predicted by Volume Fraction	
		Average Deviation (%)	Maximum Deviation (%)	Average Deviation (%)	Maximum Deviation (%)	Average Deviation (%)	Maximum Deviation (%)
Bz - 2-MPent	Bz	27.2	-49.9	36.1	-58.6	45.4	-67.1
	2-MPent	32.3	-58.0	24.8	-49.1	16.5	-37.8
Averages		29.8		30.5		31.0	

Key:
Bz - Benzene
2-MPent - 2-Methyl Pentane
Deviations calculated as [(Measured-Predicted)/Measured] x 100
Average Deviation - Average of absolute deviations for all the samples tested in each system.
Maximum Deviation - Largest deviation determined for an individual sample.

File:Leinonen Deviation from Ideal/Sheet1

Table 2-9. Deviation of aqueous concentrations predicted by Raoult's Law from the measured aqueous concentrations from the laboratory experiments by Burris and MacIntyre.

System	Reference	Component	Predicted by Mole Fraction		Predicted by Weight Fraction		Predicted by Volume Fraction	
			Average Deviation (%)	Maximum Deviation (%)	Average Deviation (%)	Maximum Deviation (%)	Average Deviation (%)	Maximum Deviation (%)
Octane - 1-MNaph	Burris and MacIntyre (1986a)	n-Oct	21.2	-60.9	26.3	-68.0	17.2	-54.6
		1-MNAph	30.7	-75.3	27.2	-70.0	33.7	-78.7
Tetralin- MCH	Burris and MacIntyre (1986a)	Tetralin	11.8	-34.4	3.9	-14.5	9.8	-30.4
		MCH	24.9	-62.0	31.3	-71.0	26.3	-64.2
EBz - n-Oct	Burris and MacIntyre (1986a)	EBz	10.2	-25.2	12.4	-29.7	18.9	-42.0
		n-Oct	22.8	-61.6	21.0	-59.0	15.8	-50.5
Four-Component Mixture	Burris and MacIntyre (1986b)	EBz	-	-12.2		-12.5		-16.8
		Tetralin		-24.9		-6.8		-20.8
		1-MNaph		-54.6		-39.4		-51.5
		MCH		24.1		14.4		22.5
Simulated JP-4 Fuel	Burris and MacIntyre (1986c)	8-Total	24.6	-55.3	31.9	-51.2	38.8	-63.5
Averages			20.9		22.0		22.9	

Key:
n-Oct - n-Octane
1-MNaph - 1-Methyl Naphthalene
MCH - Methylcyclohexane
EBz - Ethyl Benzene
Deviations calculated as [(Measured-Predicted)/Measured] x 100
Average Deviation - Average of absolute deviations for all the samples tested in each system.
Maximum Deviation - Largest deviation determined for an individual sample.

File:Burris Deviation from Ideal/Sheet1

Table 2-10. Deviation of aqueous concentrations predicted by Raoult's Law from measured aqueous concentrations for laboratory experiments on gasoline.

System	Predicted based on:	Average Deviation	Maximum Deviation	Reference
PS-6 Gasoline (12 components)	Mole Fraction	39.2%	64.3%	TRC (1985)
	Weight Fraction	33.6%	-70.9%	TRC (1985)
	Volume Fraction	41.0%	-62.1%	TRC (1985)
PS-6 Gasoline (6 components)	Mole Fraction	28.9%	-41.2%	Poulsen et al. (1992)
	Weight Fraction	32.0%	-37.3%	Poulsen et al. (1992)
	Volume Fraction	33.6%	-47.8%	Poulsen et al. (1992)
Average of 31 Gasolines (8 components)	Mole Fraction	18.3%	-36.1%	Cline et al. (1991)
	Weight Fraction	20.5%	-32.1%	Cline et al. (1991)
	Volume Fraction	24.9%	-42.8%	Cline et al. (1991)

Key:

Deviations calculated as [(Measured-Predicted)/Measured] x 100

Average Deviation - Average of absolute deviations for all the components tested in each system.

Maximum Deviation - Largest deviation determined for an individual component.

Table 2-11. Deviation of aqueous concentrations predicted by Raoult's Law from measured aqueous concentrations for laboratory experiments on diesel fuels.

System	Predicted based on:	Average Deviation	Maximum Deviation	Reference
Diesel Fuel #1	Mole Fraction	37.2%	-70.9%	Lee et al. (1992a)
	Weight Fraction	47.0%	-77.6%	Lee et al. (1992a)
	Volume Fraction	59.0%	-81.2%	Lee et al. (1992a)
Diesel Fuel #2	Mole Fraction	57.7%	-94.1%	Lee et al. (1992a)
	Weight Fraction	67.3%	-94.7%	Lee et al. (1992a)
	Volume Fraction	66.7%	-96.4%	Lee et al. (1992a)
Diesel Fuel #3	Mole Fraction	38.0%	-56.7%	Lee et al. (1992a)
	Weight Fraction	43.7%	-65.3%	Lee et al. (1992a)
	Volume Fraction	48.5%	-70.7%	Lee et al. (1992a)
Diesel Fuel #4	Mole Fraction	41.9%	-95.6%	Lee et al. (1992a)
	Weight Fraction	49.0%	-95.6%	Lee et al. (1992a)
	Volume Fraction	52.8%	-97.1%	Lee et al. (1992a)

Key:

Deviations calculated as [(Measured-Predicted)/Measured] x 100

Average Deviation - Average of absolute deviations for all the components tested.

Maximum Deviation - Largest deviation determined for an individual component.

Table 2-12. Deviation of aqueous concentrations predicted by Raoult's Law from measured aqueous concentrations for laboratory experiments on creosote and coal tars.

System	Predicted based on:	Average Deviation	Maximum Deviation	Reference
Creosote	Mole Fraction	145%	410%	Priddle and MacQuarrie (1994)
	Weight Fraction	130%	430%	Priddle and MacQuarrie (1994)
	Volume Fraction	110%	360%	Priddle and MacQuarrie (1994)
Coal Tar #1	Mole Fraction	305%	850%	Lee et al. (1992b)
	Weight Fraction	220%	780%	Lee et al. (1992b)
	Volume Fraction	215%	665%	Lee et al. (1992b)
Coal Tar #4	Mole Fraction	64.2%	305%	Lee et al. (1992b)
	Weight Fraction	57.0%	245%	Lee et al. (1992b)
	Volume Fraction	50.0%	195%	Lee et al. (1992b)
Coal Tar #5	Mole Fraction	59.1%	275%	Lee et al. (1992b)
	Weight Fraction	56.5%	225%	Lee et al. (1992b)
	Volume Fraction	49.9%	195%	Lee et al. (1992b)

Key:

Deviations calculated as [(Measured-Predicted)/Measured] x 100

Average Deviation - Average of absolute deviations for all the components tested in each system.

Maximum Deviation - Largest deviation determined for an individual component.

Table 2-13. Example of the uncertainty imparted to the calculated effective solubilities of the characterized components of NAPL for different values of the molecular mass of the UC (uncharacterized) portion. NAPL sample is from the Tyson's Superfund site (see Table 1-2).

Component	Weight%	Molecular Mass (moles/g)	Mole Fraction	Solubility (mg/L)	Effective Solubility (mg/L)	Effective Solubility Relative to Case 1
CASE 1						
Trichloropropane	23	146	0.239	1,900	454	-
Toluene	4.2	92	0.069	580	40.2	-
Xylenes	17	106	0.243	200	48.6	-
Ethyl benzene	3.8	106	0.054	190	10.3	-
UC Portion	52	200	0.394	-	-	-
CASE 2						
Trichloropropane	23	146	0.211	1,900	401	0.88
Toluene	4.2	92	0.061	580	35.5	0.88
Xylenes	17	106	0.215	200	43.0	0.88
Ethyl benzene	3.8	106	0.048	190	9.1	0.88
UC Portion	52	150	0.465	-	-	-
CASE 3						
Trichloropropane	23	146	0.259	1,900	493	1.09
Toluene	4.2	92	0.075	580	43.6	1.09
Xylenes	17	106	0.264	200	52.8	1.09
Ethyl benzene	3.8	106	0.059	190	11.2	1.09
UC Portion	52	250	0.342	-	-	-

Table 2-14. Deviation in aqueous concentrations predicted by Raoult's Law and UNIFAC from measured aqueous concentrations for laboratory experiments of Broholm and Feenstra (1995).

System	Component	Predicted by Raoult's Law		Predicted by UNIFAC	
		Average Deviation (%)	Maximum Deviation (%)	Average Deviation (%)	Maximum Deviation (%)
TCE - TCM	TCE	7.9	-15.0	24.2	-50.8
	TCM	7.7	16.3	9.2	-32.4
TCE - PCM	TCE	3.0	-6.4	3.6	-6.8
	PCM	5.9	-12.9	3.5	-6.7
TCE - TCA	TCE	7.7	12.7	15.4	-23.9
	TCA	4.3	-8.9	16.1	-33.3
TCE - PCE	TCE	8.0	-15.0	8.1	-15.2
	PCE	7.8	19.6	7.6	19.0
PCE - TCM	PCE	7.4	19.7	27.4	-51.7
	TCM	6.4	-18.3	14.2	-47.2
PCE - PCM	PCE	7.1	10.9	8.1	14.7
	PCM	4.2	-8.0	3.3	-6.3
PCE - TCA	PCE	5.3	-12.2	14.1	-32.9
	TCA	8.5	-19.7	18.4	-42.4
TCM- TCE - PCE	TCM	11.4	-27.5	31.3	-51.4
	TCE	5.0	10.6	7.0	-15.8
	PCE	12.0	-40.4	14.2	-53.0
Averages		7.0		13.3	

Key:
TCE - Trichloroethylene PCM - Carbon Tetrachloride PCE - Tetrachloroethylene
TCM - Chloroform TCA - 1,1,1-Trichloroethane
Deviations calculated as [(Measured-Predicted)/Measured] x 100
Average Deviation - Average of absolute deviations for all the samples tested in each system.
Maximum Deviation - Largest deviation determined for an individual sample.

File:UNIFAC Broholm Deviation/Sheet1

Table 2-15. Deviation of aqueous concentrations predicted by Raoult's Law and UNIFAC from measured aqueous concentrations for laboratory experiments of Banerjee (1984).

System	Component	Predicted by Raoult's Law		Predicted by UNIFAC	
		Average Deviation (%)	Maximum Deviation (%)	Average Deviation (%)	Maximum Deviation (%)
CBz - 13-DCBz	CBz	1.3	-8.0	1.4	-6.9
	13-DCBz	0.7	1.7	0.7	3.1
CBz - 124-TCBz	CBz	12.5	25.2	13.1	28.2
	124-TCBz	19.2	-42.0	18.8	-40.8
CBz - 13-DCBz -124-TCBz	CBz	20.8	88.3	21.0	91.3
	13-DCBz	7.0	17.1	6.9	17.7
	124-TCBz	12.4	-16.9	11.1	-16.5
Averages		10.6		10.4	

Key:
CBz - Chlorobenzene 124-TCBz - 1,2,4-Trichlorobenzene
13-DCBz - 1,3-Dichlorobenzene
Deviations calculated as [(Measured-Predicted)/Measured] x 100
Average Deviation - Average of absolute deviations for all the samples tested in each system.
Maximum Deviation - Largest deviation determined for an individual sample.

File:UNIFAC Banerjee Deviation/Sheet1

Table 2-16. Deviation of aqueous concentrations predicted by Raoult's Law and UNIFAC from the measured aqueous concentrations for the laboratory experiments by Leinonen and Mackay (1973).

System	Component	Predicted by Raoult's Law		Predicted by UNIFAC	
		Average Deviation (%)	Maximum Deviation (%)	Average Deviation (%)	Maximum Deviation (%)
Bz - 2-MPent	Bz	27.1	-49.9	14.1	-32.4
	2-MPent	22.2	-58.0	24.9	-49.1
Averages		24.7		19.5	

Key:
Bz - Benzene
2-MPent - 2-Methyl Pentane
Deviations calculated as [(Measured-Predicted)/Measured] x 100
Average Deviation - Average of absolute deviations for all the samples tested in each system.
Maximum Deviation - Largest deviation determined for an individual sample.

File:UNIFAC Leinonen Deviation/Sheet1

Table 2-17. Deviation of aqueous concentrations predicted by Raoult's Law and UNIFAC from the measured aqueous concentrations from the laboratory experiments by Burris and MacIntyre.

System	Reference	Component	Predicted by Raoult's Law		Predicted by UNIFAC	
			Average Deviation (%)	Maximum Deviation (%)	Average Deviation (%)	Maximum Deviation (%)
n-Oct - 1-MNaph	Burris and MacIntyre (1986a)	n-Oct	21.2	-60.9	4.9	-19.0
		1-MNaph	30.7	-75.3	18.8	-48.4
Tetralin- MCH	Burris and MacIntyre (1986a)	Tetralin	11.8	-34.4	5.6	-14.4
		MCH	24.9	-62.0	20.5	-52.8
EBz - n-Oct	Burris and MacIntyre (1986a)	EBz	10.2	-25.2	2.3	-9.5
		n-Oct	22.8	-61.6	16.8	-46.8
Four-Component Mixture	Burris and MacIntyre (1986b)	EBz	-	-12.2	-	0.2
		Tetralin	-	-24.9	-	-13.8
		1-MNaph	-	-54.6	-	-32.8
		MCH	-	24.1	-	28.4
Simulated JP-4 Fuel	Burris and MacIntyre (1986c)	8 -Total	24.6	-55.3	7.7	-19.9
Averages			20.9		10.9	

Key:

n-Oct - n-Octane

1-MNaph - 1-Methyl Naphthalene

MCH - Methylcyclohexane

EBz - Ethyl Benzene

Deviations calculated as [(Measured-Predicted)/Measured] x 100

Average Deviation - Average of absolute deviations for all the samples tested in each system.

Maximum Deviation - Largest deviation determined for an individual sample.

File:UNIFAC Burris Deviation/Sheet1

Table 2-18. Deviation of aqueous concentrations predicted by Raoult's Law and UNIFAC from measured aqueous concentrations for laboratory experiments on gasolines.

System	Predicted based on:	Average Deviation	Maximum Deviation	Reference
PS-6 Gasoline (12 components)	Mole Fraction	39.2%	64.3%	TRC (1985)
	UNIFAC	32.5%	66.0%	TRC (1985)
PS-6 Gasoline (6 components)	Mole Fraction	28.9%	41.2%	Poulsen et al. (1992)
	UNIFAC	20.5%	67.2%	Poulsen et al. (1992)
Average of 31 Gasolines (8 components)	Mole Fraction	18.3%	36.1%	Cline et al. (1991)
	UNIFAC	18.8%	33.9%	Cline et al. (1991)

Key:

Deviations calculated as [(Measured-Predicted)/Measured] x 100

Average Deviation - Average of absolute deviations for all the components tested in each system.

Maximum Deviation - Largest deviation determined for an individual component.

Table 2-19. Deviation of aqueous concentrations predicted by Raoult's Law and UNIFAC from measured aqueous concentrations for laboratory experiments on diesel fuels.

System	Predicted based on:	Average Deviation	Maximum Deviation	Reference
Diesel Fuel #1	Mole Fraction	37.2%	70.9%	Lee et al. (1992a)
	UNIFAC	110%	340%	Lee et al. (1992a)
Diesel Fuel #2	Mole Fraction	57.7%	-94.1%	Lee et al. (1992a)
	UNIFAC	120%	665%	Lee et al. (1992a)
Diesel Fuel #3	Mole Fraction	38.0%	130%	Lee et al. (1992a)
	UNIFAC	205%	660%	Lee et al. (1992a)
Diesel Fuel #4	Mole Fraction	41.9%	-95.6%	Lee et al. (1992a)
	UNIFAC	49.0%	-95.6%	Lee et al. (1992a)

Key:

Deviations calculated as [(Measured-Predicted)/Measured] x 100

Average Deviation - Average of absolute deviations for all the components tested in each system.

Maximum Deviation - Largest deviation determined for an individual component.

Table 2-20. Deviation of aqueous concentrations predicted by Raoult's Law and UNIFAC from measured aqueous concentrations for laboratory experiments on creosote and coal tars.

System	Predicted based on:	Average Deviation	Maximum Deviation	Reference
Creosote	Mole Fraction	145%	410%	Priddle and MacQuarrie (1994)
	UNIFAC	145%	420%	Priddle and MacQuarrie (1994)
Coal Tar #1	Mole Fraction	305%	850%	Lee et al. (1992b)
	UNIFAC	285%	860%	Lee et al. (1992b)
Coal Tar #4	Mole Fraction	64.2%	305%	Lee et al. (1992b)
	UNIFAC	60.1%	280%	Lee et al. (1992b)
Coal Tar #5	Mole Fraction	59.1%	275%	Lee et al. (1992b)
	UNIFAC	57.7%	260%	Lee et al. (1992b)

Key:

Deviations calculated as [(Measured-Predicted)/Measured] x 100

Average Deviation - Average of absolute deviations for all the components tested in each system.

Maximum Deviation - Largest deviation determined for an individual component.

Table 2-21. Pure-phase solubility values of selected organic compounds at 0°C and 25°C.

Compound	Solubility at 0°C (mg/L)	Solubility at 25°C (mg/L)	Reference
Toluene	724	573	Polak and Lu (1973)
Ethyl Benzene	197	177	Polak and Lu (1973)
m-Xylene	196	162	Polak and Lu (1973)
o-Xylene	142	213	Polak and Lu (1973)
Dichloromethane	19,610	13,030	Horvath (1982)
Chloroform	9,950	7,920	Horvath (1982)
Carbon Tetrachloride	978	793	Horvath (1982)
1,2-Dichloroethane	8,880	8,608	Horvath (1982)
1,1,1-Trichloroethane	1,910	1,495	Horvath (1982)
Trichloroethylene	1,049	1,099	Horvath (1982)
Tetrachloroethylene	150	150	Horvath (1982)
Freon-113	106	166	Horvath (1982)
1,2-Dichlorobenzene	45	93	Horvath (1982)

Table 2-22. Organics acid and bases which can be important groundwater contaminants.

Compound	Dissociation Constant pKa	Reference
ORGANIC ACIDS		
Phenol	9.99	Dean (1985)
2-Methyl Phenol	10.26	Dean (1985)
3-Methyl Phenol	10.00	Dean (1985)
4-Methyl Phenol	10.26	Dean (1985)
2-Chlorophenol	8.55	Dean (1985)
3-Chlorophenol	9.10	Dean (1985)
4-Chlorophenol	9.43	Dean (1985)
2,4-Dichlorophenol	7.85	Dean (1985)
2,6-Dichlorophenol	6.78	Dean (1985)
3,4-Dichlorophenol	8.63	Dean (1985)
2,3,4-Trichlorophenol	6.97	Dean (1985)
2,4,5-Trichlorophenol	6.72	Dean (1985)
2,4,6-Trichlorophenol	5.99	Dean (1985)
2,3,4,5-Tetrachlorophenol	5.64	Dean (1985)
2,3,4,6-Tetrachlorophenol	5.22	Dean (1985)
Pentachlorophenol	4.74	Dean (1985)
2-Nitrophenol	7.22	Dean (1985)
3-Nitrophenol	8.36	Dean (1985)
4-Nitrophenol	7.15	Dean (1985)
ORGANIC BASES		
Aniline	4.60	Perrin (1972)
2-Chloroaniline	2.66	Perrin (1972)
3-Chloroaniline	3.51	Perrin (1972)
4-Chloroaniline	3.98	Perrin (1972)

Table 2-23. Comparison of solubility of various organic compounds in distilled water and seawater at 25°C.
Data from Sutton and Calder (1975).

Compound	Solubility in Distilled Water (mg/L)	Solubility in Seawater (mg/L)
Toluene	534	379
Ethyl Benzene	161	111
m-Xylene	146	106
o-Xylene	170	130
p-Xylene	156	111
Isopropyl Benzene	65	43
1,2,4-Trimethylbenzene	59	40
1,2,3-Trimethylbenzene	75	49
1,3,5-Trimethylbenzene	48	31
n-Butylbenzene	12	7.1
s-Butylbenzene	18	12
t-Butylbenzene	30	21

Table 2-24. Salting Constants for various organic compounds in seawater and sodium chloride solutions.
Data from Schwarzenbach et al. (1992).

Compound	Salting Constant (L/mole) for Seawater	Salting Constant (L/mole) for Sodium Chloride Solutions
Benzene	-	0.18, 0.19
Toluene	0.17	-
Naphthalene	0.25, 0.28	0.21, 0.19
Phenanthrene	0.25, 0.23	0.27, 0.29
Anthracene	0.26, 0.35	0.24, 0.25
Pyrene	0.31, 0.32	0.29, 0.29
Chrysene	-	0.34
Biphenyl	0.41	0.26
4-Aminotoluene	0.19	0.17
4-Nitrotoluene	0.11	0.14
2,4'-Dichlorobiphenyl	0.3	-
2,4,4'-Trichlorobiphenyl	0.4	-
2,3',4',5-Tetrachlorobiphenyl	0.2	-
2,2',3,4,5'-Pentachlorobiphenyl	0.3	-
2,2',3,4,4',5-Hexachlorobiphenyl	0.3	-

Table 2-25. Total molecular surface area (TSA) for various organic compounds.

Compound	TSA (nm^2)	Reference
Benzene	1.10	Yalkowsky and Valvani (1979)
Toluene	1.27	Yalkowsky and Valvani (1979)
Ethyl Benzene	1.45	Yalkowsky and Valvani (1979)
Xylenes	1.50	Yalkowsky and Valvani (1979)
Dichloromethane	0.82	Mackay et al. (1982)
Chloroform	0.99	Mackay et al. (1982)
Carbon Tetrachloride	1.19	Mackay et al. (1982)
1,2-Dichloroethane	0.96	Yalkowsky and Valvani (1979)
1,1,1-Trichloroethane	1.12	Yalkowsky and Valvani (1979)
Trichloroethylene	1.10	Okouchi et al. (1992)
Tetrachloroethylene	1.28	Okouchi et al. (1992)
Chlorobenzene	1.27	Yalkowsky and Valvani (1979)
1,4-Dichlorobenzene	1.45	Yalkowsky and Valvani (1979)
1,2,4-Trichlorobenzene	1.60	Yalkowsky and Valvani (1979)
Naphthalene	1.56	Yalkowsky and Valvani (1979)
Phenanthrene	1.98	Yalkowsky and Valvani (1979)
Anthracene	2.02	Yalkowsky and Valvani (1979)
Pyrene	2.12	Yalkowsky and Valvani (1979)

Table 2-26. Examples of the uncertainty associated with the chemical analysis of organic contaminants in groundwater by commercial analytical laboratories.

Compound	Acceptable Range (%) for Lab Spikes [1] US EPA Methods 624/625	Acceptable Range (%) for QC Samples [2] NYS DOH 1982	Acceptable Range (%) for QC Samples [3] NYS DOH 1988
Benzene	37 - 151	-	-
Toluene	47 - 150	-	-
Ethyl Benzene	37 - 162	-	-
Chloroform	51 - 138	-	-
Carbon Tetrachloride	70 - 140	42 - 158	-
1,1,1-Trichloroethane	52 - 162	62 - 138	-
Trichloroethylene	71 - 157	67 - 133	-
Tetrachloroethylene	64 - 148	53 - 147	-
Acenaphthylene	33 - 145	-	69 - 150
Benzo(a)anthracene	33 - 143	-	69 -192
Benzo(a)pyrene	17 - 163	-	78 - 258
1,4-Dichlorobenzene	20 - 124	-	-
Hexachlorobutadiene	24 - 116	-	25 - 147
Pyrene	52 - 115	-	63 - 183
1,2,4-Trichlorobenzene	44 - 144	-	46 - 151

Key:

[1] Acceptable range, expressed as a percent, in measured concentration for laboratory spiked samples. Data from United States Federal Register 40 CFR Part 136.

[2] [3] Acceptable range, expressed as a percent, in measured concentration for blind spiked samples tested for the laboratory certification program of the New York State Department of Health (NYS DOH).

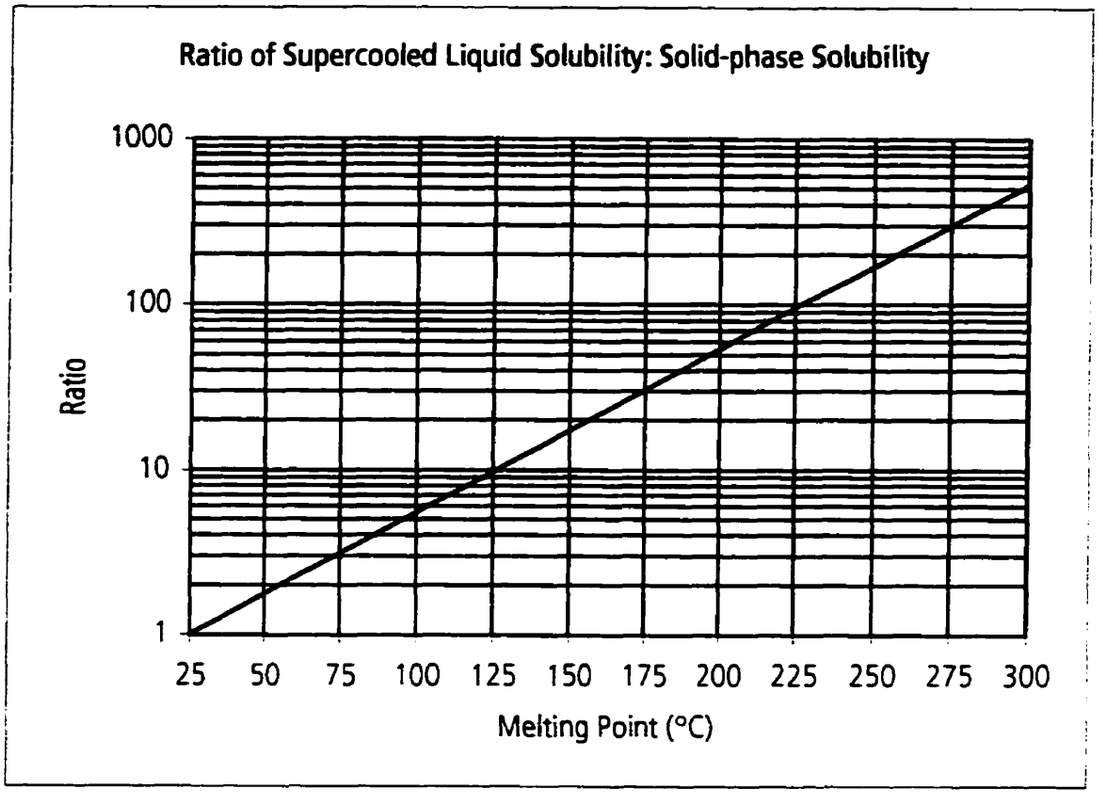

Figure 2-1. Relationship between supercooled liquid solubility and solid-phase solubility versus melting point.

Calculated from equation 2-13.

2-2a

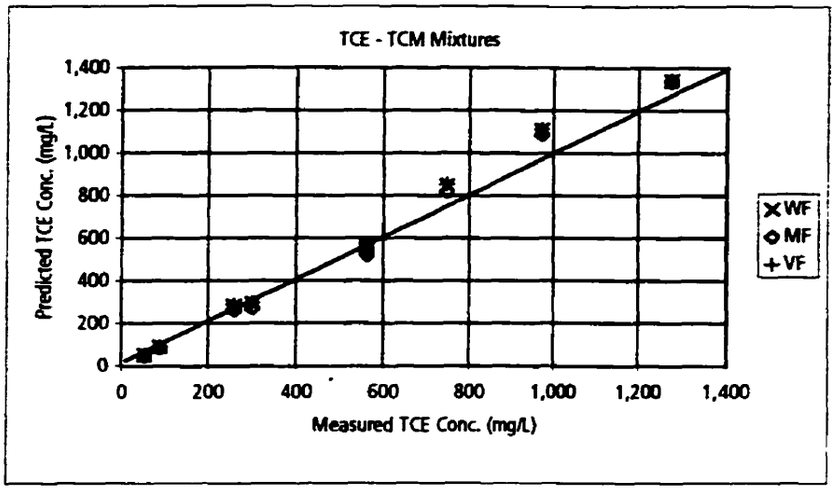

2-2b

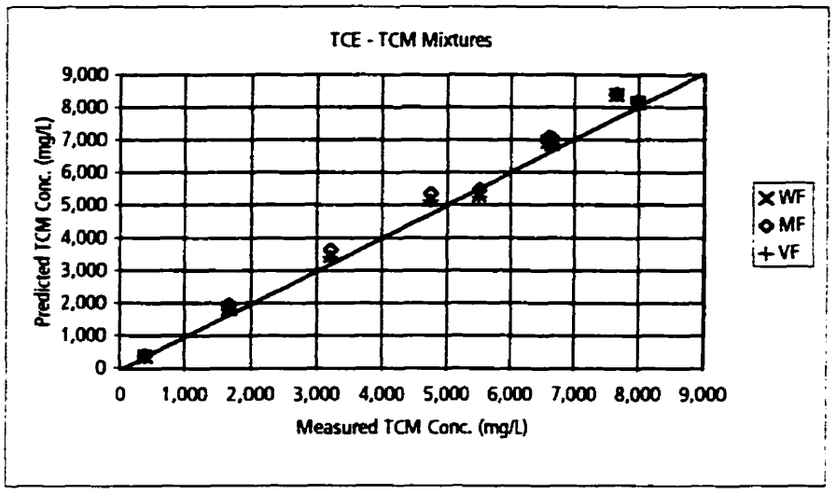

Key:
TCE - Trichloroethylene
TCM - Chloroform
WF - Concentrations calculated by Raoult's Law using weight fraction in NAPL.
MF - Concentrations calculated by Raoult's Law using mole fraction in NAPL.
VF - Concentrations calculated by Raoult's Law using volume fraction in NAPL.

Figure 2-2. Comparison of measured aqueous concentrations to aqueous concentrations calculated by Raoult's Law for trichloroethyene - chloroform mixtures.

Data from Broholm and Feenstra (1995).

File:Broholm TCE-TCM Data/Sheet1

2-3a

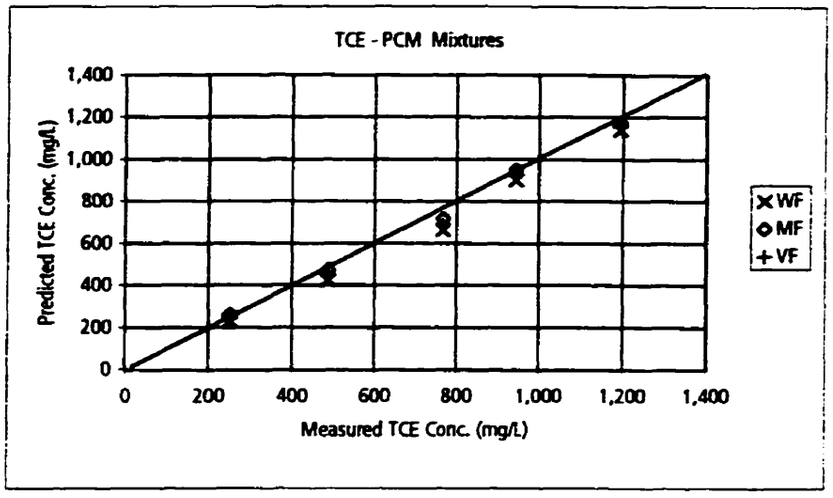

2-3b

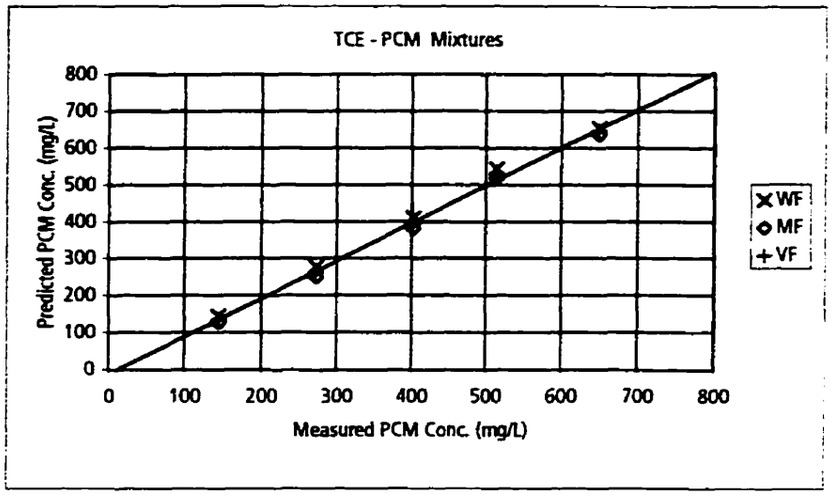

Key:
TCE - Trichloroethylene
PCM - Carbon Tetrachloride
WF - Concentrations calculated by Raoult's Law using weight fraction in NAPL.
MF - Concentrations calculated by Raoult's Law using mole fraction in NAPL.
VF - Concentrations calculated by Raoult's Law using volume fraction in NAPL.

Figure 2-3. Comparison of measured aqueous concentrations to aqueous concentrations calculated by Raoult's Law for trichloroethyene - carbon tetrachloride mixtures.

Data from Broholm and Feenstra (1995).

2-4a

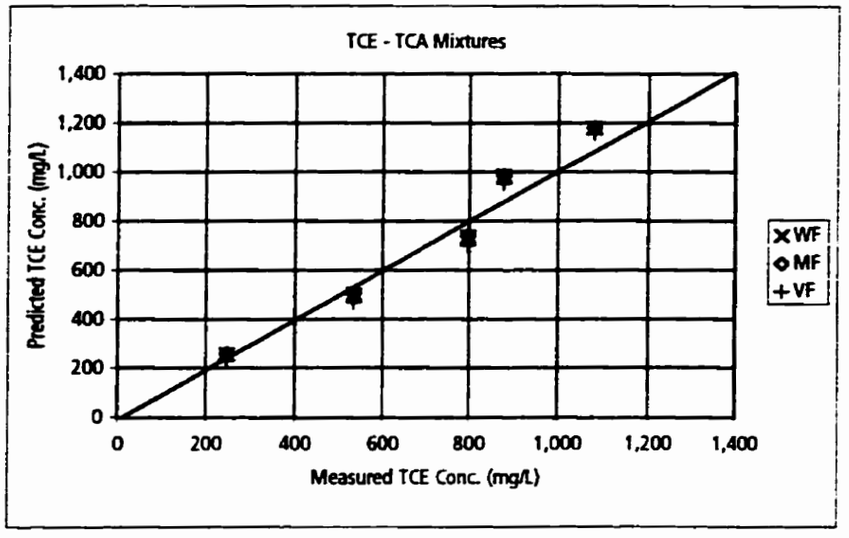

2-4b

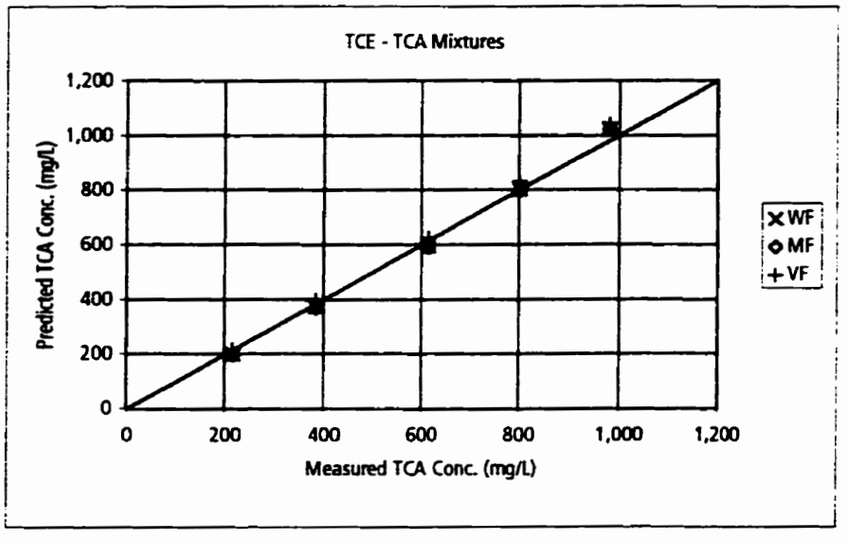

Key:
TCE - Trichloroethylene
TCA - 1,1,1-Trichloroethane
WF - Concentrations calculated by Raoult's Law using weight fraction in NAPL.
MF - Concentrations calculated by Raoult's Law using mole fraction in NAPL.
VF - Concentrations calculated by Raoult's Law using volume fraction in NAPL.

Figure 2-4. Comparison of measured aqueous concentrations to aqueous concentrations calculated by Raoult's Law for trichloroethyene - 1,1,1-trichloroethane mixtures.

Data from Broholm and Feenstra (1995).

2-5a

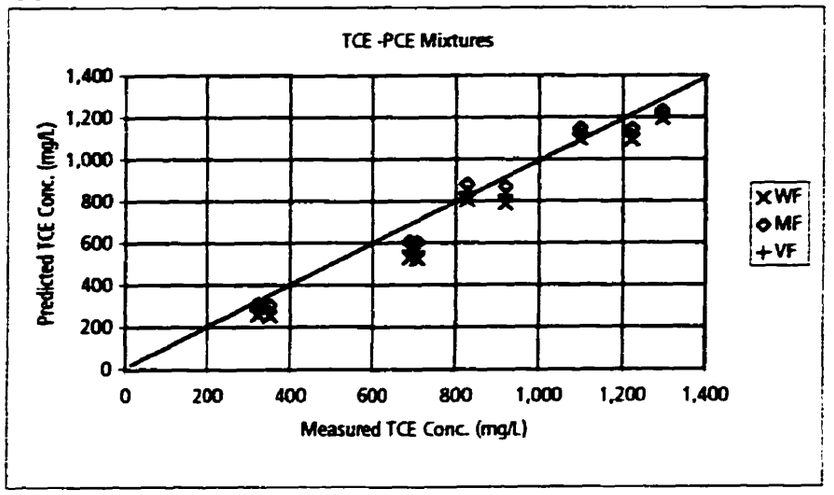

2-5b

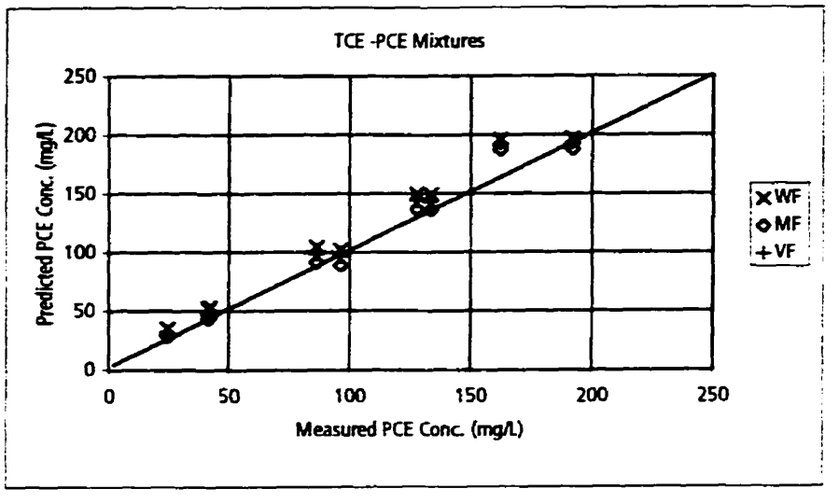

Key:
TCE - Trichloroethylene
PCE - Tetrachloroethylene
WF - Concentrations calculated by Raoult's Law using weight fraction in NAPL.
MF - Concentrations calculated by Raoult's Law using mole fraction in NAPL.
VF - Concentrations calculated by Raoult's Law using volume fraction in NAPL.

Figure 2-5. Comparison of measured aqueous concentrations to aqueous concentrations calculated by Raoult's Law for trichloroethyene - tetrachloroethylene mixtures.

Data from Broholm and Feenstra (1995).

2-6a

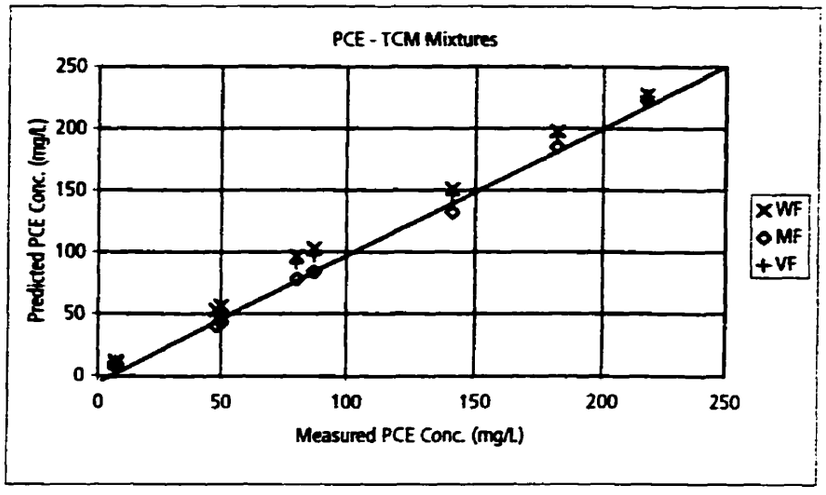

2-6b

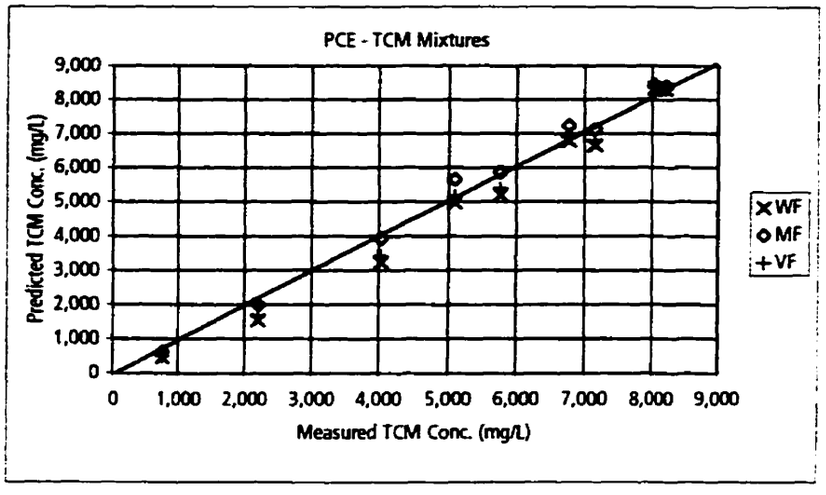

Key:
PCE - Tetrachloroethylene
TCM - Chloroform
WF - Concentrations calculated by Raoult's Law using weight fraction in NAPL.
MF - Concentrations calculated by Raoult's Law using mole fraction in NAPL.
VF - Concentrations calculated by Raoult's Law using volume fraction in NAPL.

Figure 2-6. Comparison of measured aqueous concentrations to aqueous concentrations calculated by Raoult's Law for tetrachloroethyene - chloroform mixtures.

Data from Broholm and Feenstra (1995).

2-7a

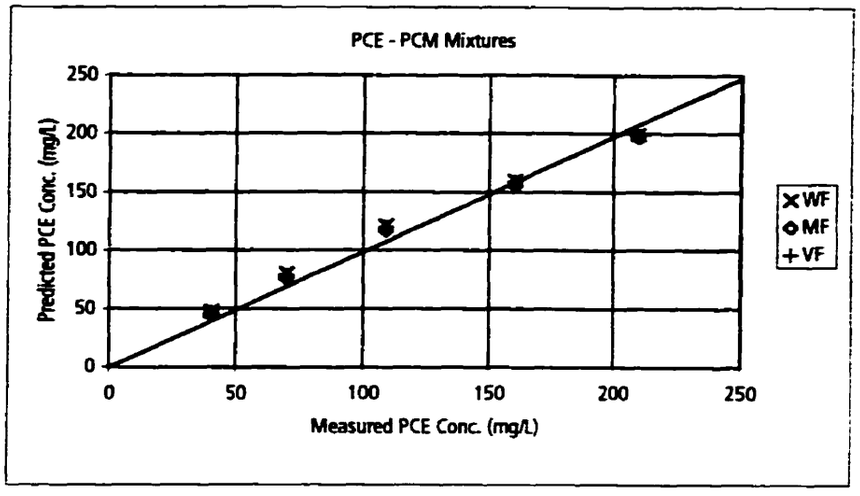

2-7b

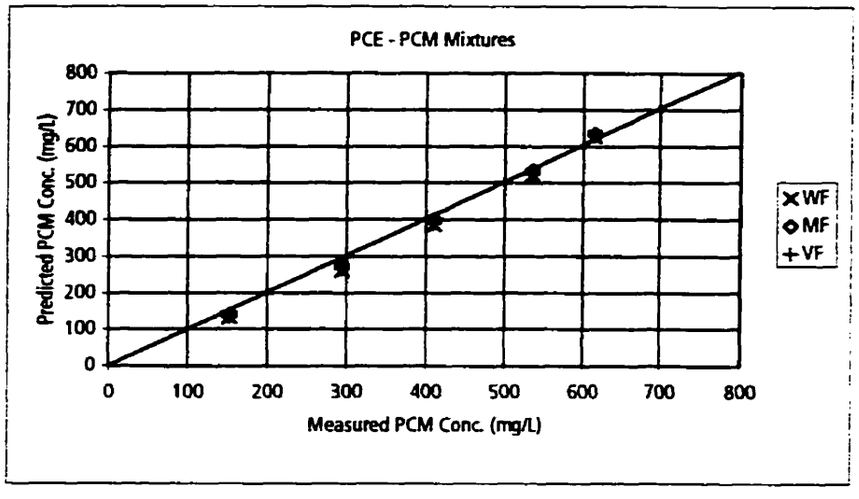

Key:
PCE - Tetrachloroethylene
PCM - Carbon Tetrachloride
WF - Concentrations calculated by Raoult's Law using weight fraction in NAPL.
MF - Concentrations calculated by Raoult's Law using mole fraction in NAPL.
VF - Concentrations calculated by Raoult's Law using volume fraction in NAPL.

Figure 2-7. Comparison of measured aqueous concentrations to aqueous concentrations calculated by Raoult's Law for tetrachloroethyene - carbon tetrachloride mixtures.

Data from Broholm and Feenstra (1995).

2-8a

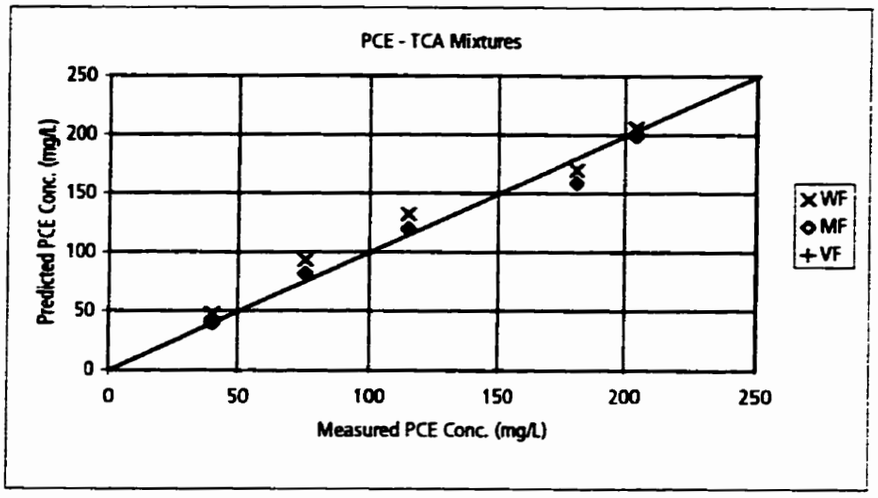

2-8a

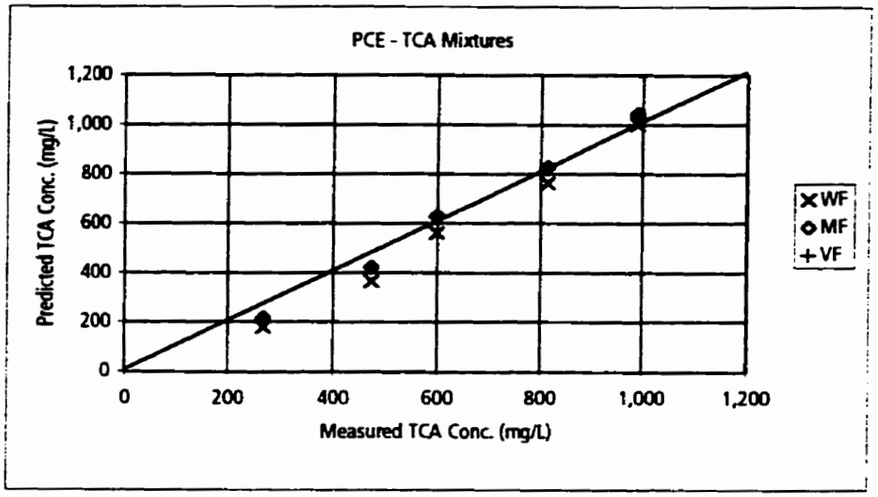

Key:
PCE - Tetrachloroethylene
TCA - 1,1,1-Trichloroethane
WF - Concentrations calculated by Raoult's Law using weight fraction in NAPL.
MF - Concentrations calculated by Raoult's Law using mole fraction in NAPL.
VF - Concentrations calculated by Raoult's Law using volume fraction in NAPL.

Figure 2-8. Comparison of measured aqueous concentrations to aqueous concentrations calculated by Raoult's Law for tetrachloroethyene - 1,1,1-trichloroethane mixtures.

Data from Broholm and Feenstra (1995).

2-9a

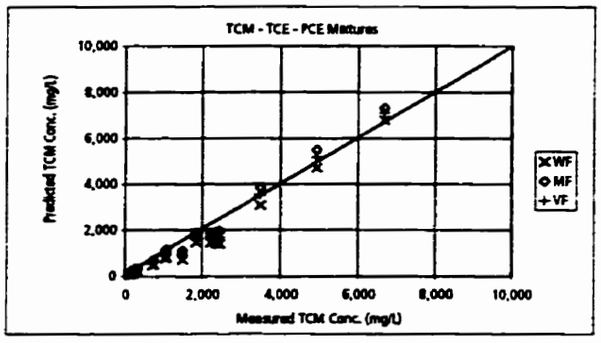

2-9b

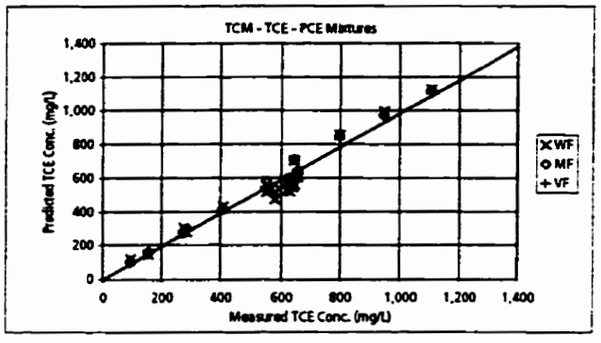

2-9c

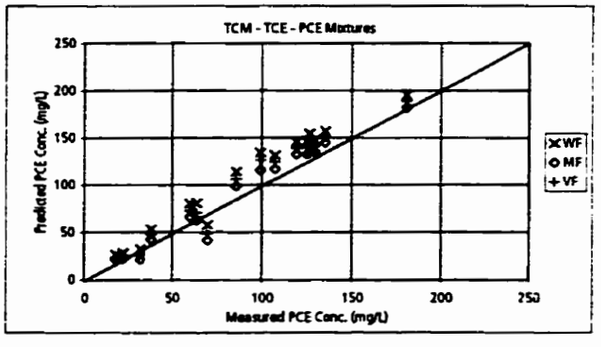

Key:
TCM - Chloroform PCE - Tetrachloroethylene
TCE - Trichloroethylene
WF - Concentrations calculated by Raoult's Law using weight fraction in NAPL.
MF - Concentrations calculated by Raoult's Law using mole fraction in NAPL.
VF - Concentrations calculated by Raoult's Law using volume fraction in NAPL.

Figure 2-9. Comparison of measured aqueous concentrations to aqueous concentrations calculated by Raoult's Law for chloroform - trichloroethylene - tetrachloroethylene mixtures.

Data from Broholm and Feenstra (1995).

2-10a

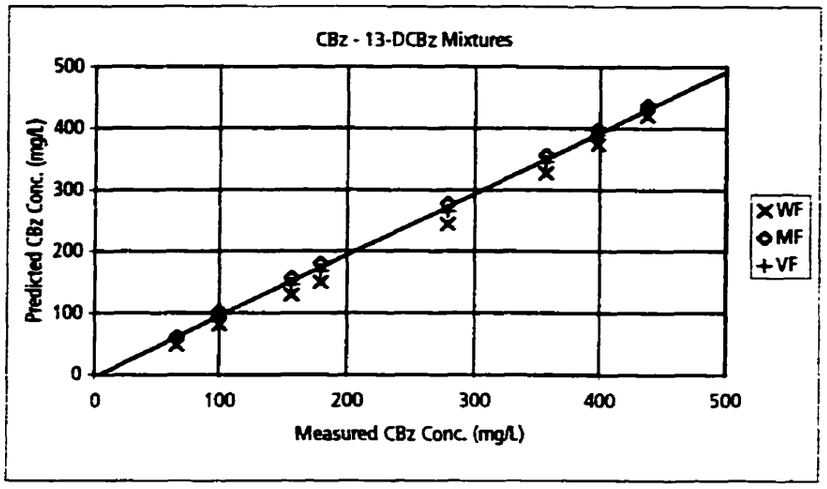

2-10b

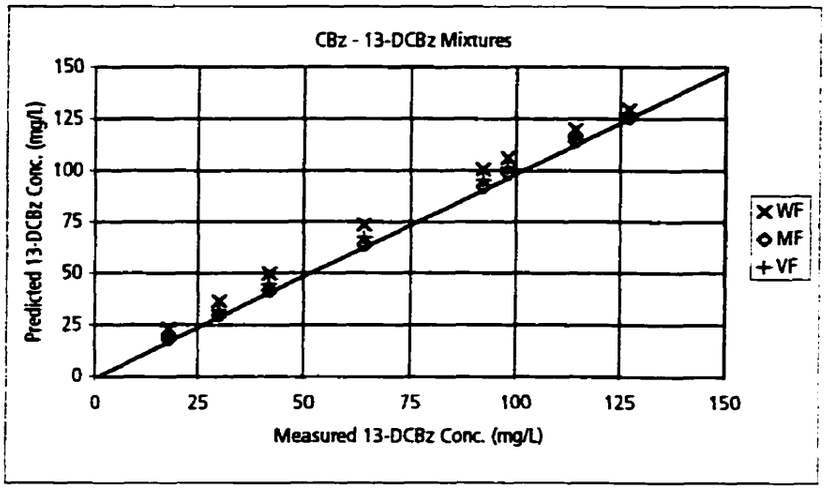

Key:
CBz - Chlorobenzene
13-DCBz - 1,3-Dichlorobenzene
WF - Concentrations calculated by Raoult's Law using weight fraction in NAPL.
MF - Concentrations calculated by Raoult's Law using mole fraction in NAPL.
VF - Concentrations calculated by Raoult's Law using volume fraction in NAPL.

Figure 2-10. Comparison of measured aqueous concentrations to aqueous concentrations calculated by Raoult's Law for chlorobenzene - 1,3-dichlorobenzene mixtures.

Data from Banerjee (1984).

2-11a

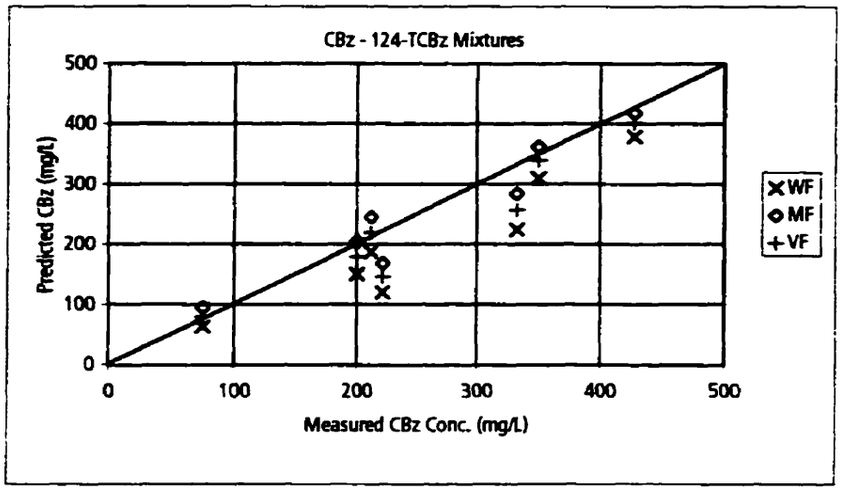

2-11a

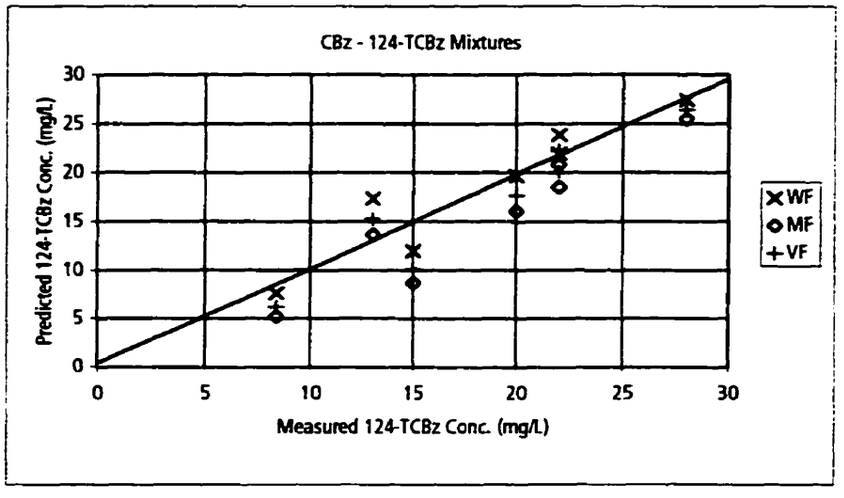

Key:
CBz - Chlorobenzene
124-TCBz - 1,2,4-Trichlorobenzene
WF - Concentrations calculated by Raoult's Law using weight fraction in NAPL.
MF - Concentrations calculated by Raoult's Law using mole fraction in NAPL.
VF - Concentrations calculated by Raoult's Law using volume fraction in NAPL.

Figure 2-11. Comparison of measured aqueous concentrations to aqueous concentrations calculated by Raoult's Law for chlorobenzene - 1,2,4-trichlorobenzene mixtures.

Data from Banerjee (1984).

2-12a

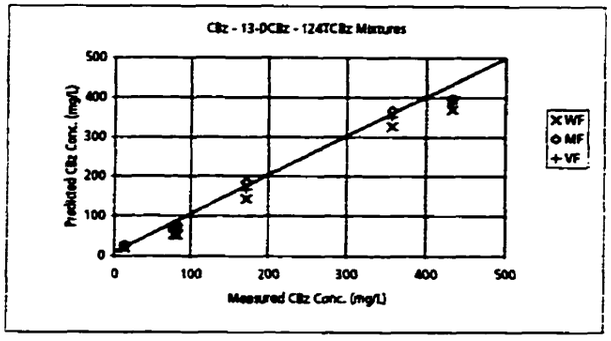

2-12b

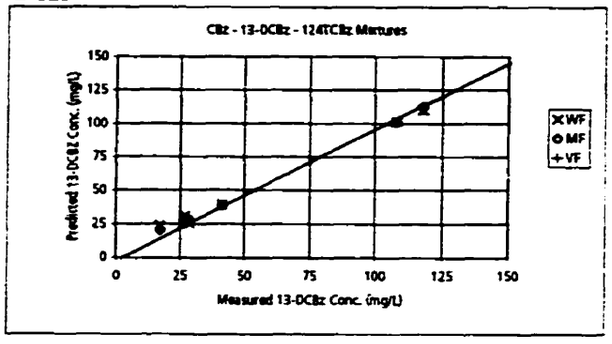

2-12c

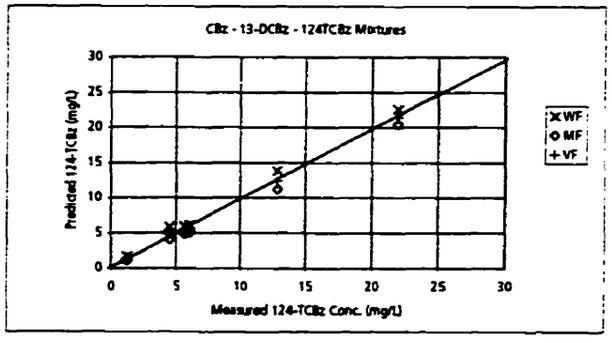

Key:
CBz - Chlorobenzene
13-DCBz - 1,3-Dichlorobenzene
124-TCBz - 1,2,4-Trichlorobenzene
WF - Concentrations calculated by Raoult's Law using weight fraction in NAPL
MF - Concentrations calculated by Raoult's Law using mole fraction in NAPL
VF - Concentrations calculated by Raoult's Law using volume fraction in NAPL

Figure 2-12. Comparison of measured aqueous concentrations to aqueous concentrations calculated by Raoult's Law for chlorobenzene - 1,3-dichlorobenzene - 1,2,4-trichlorobenzene mixtures.

Data from Banerjee (1984).

2-13a

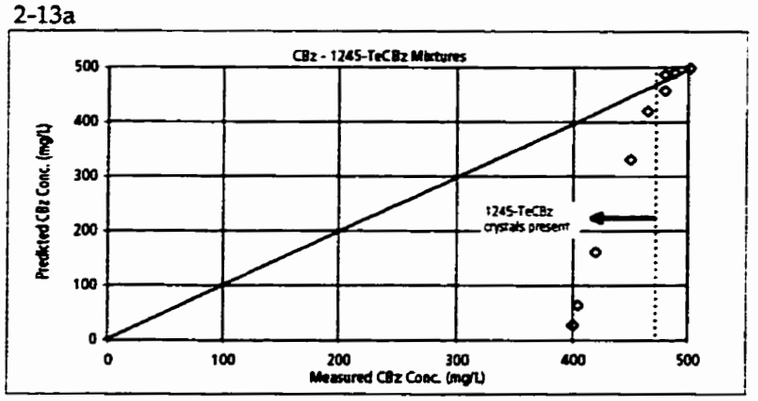

2-13b

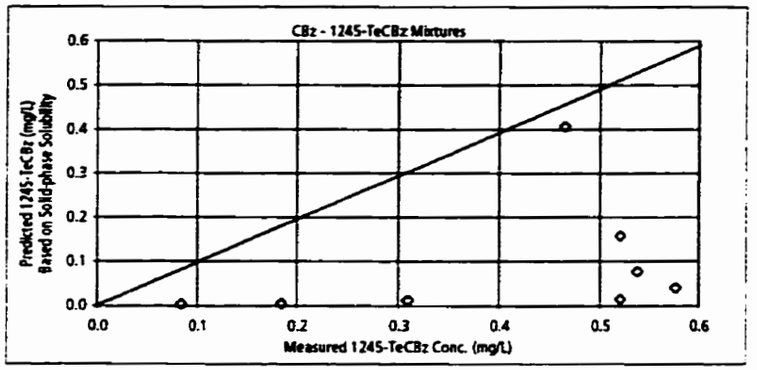

2-13c

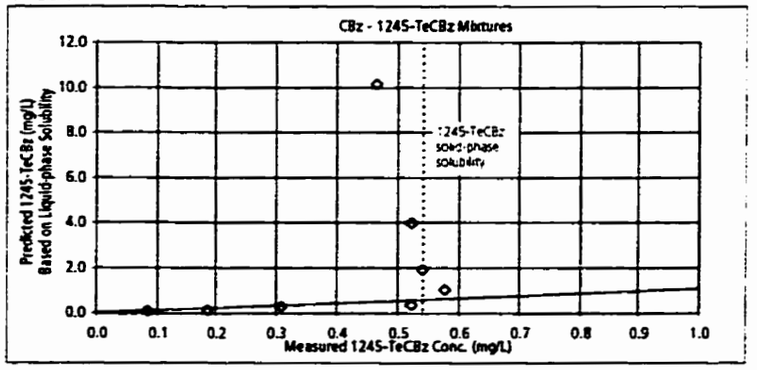

Key:
CBz - Chlorobenzene
1245-TeCBz - 1,2,4,5-Tetrachlorobenzene
Concentrations calculated by Raoult's Law using mole fraction in NAPL

Figure 2-13. Comparison of measured aqueous concentrations to aqueous concentrations calculated by Raoult's Law for chlorobenzene - 1,2,4,5-tetrachlorobenzene mixtures.

Data from Banerjee (1984).

2-14a

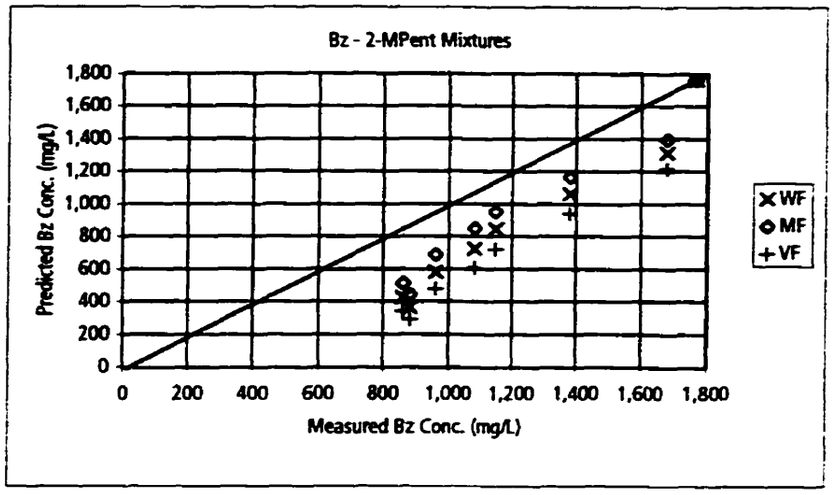

2-14b

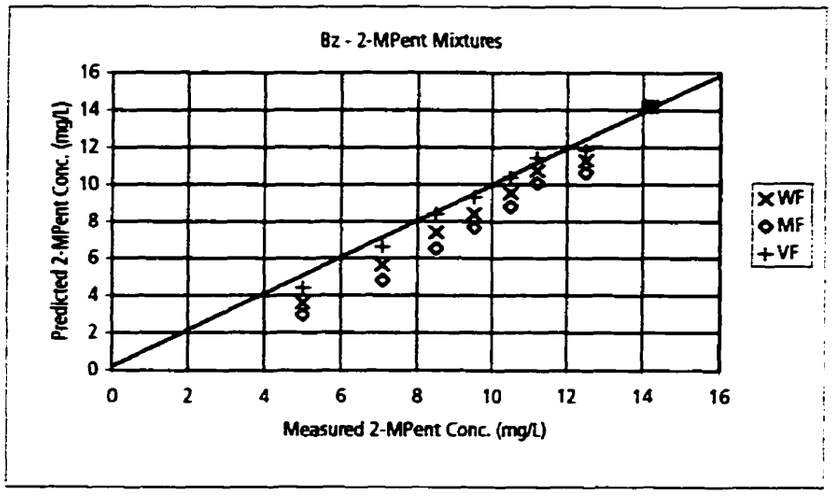

Key:
Bz - Benzene
2-MPent - 2-Methyl Pentane
WF - Concentrations calculated by Raoult's Law using weight fraction in NAPL.
MF - Concentrations calculated by Raoult's Law using mole fraction in NAPL.
VF - Concentrations calculated by Raoult's Law using volume fraction in NAPL.

Figure 2-14. Comparison of measured aqueous concentrations to aqueous concentrations calculated by Raoult's Law for benzene - 2-methyl pentane mixtures.

Data from Leinonen and Mackay (1973).

File:Leinonen Bz-MP Data1:Sheet1

2-15a

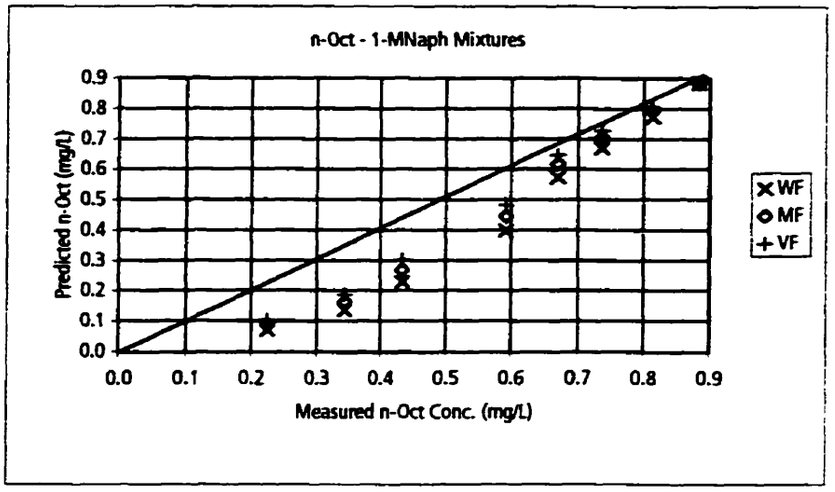

2-15b

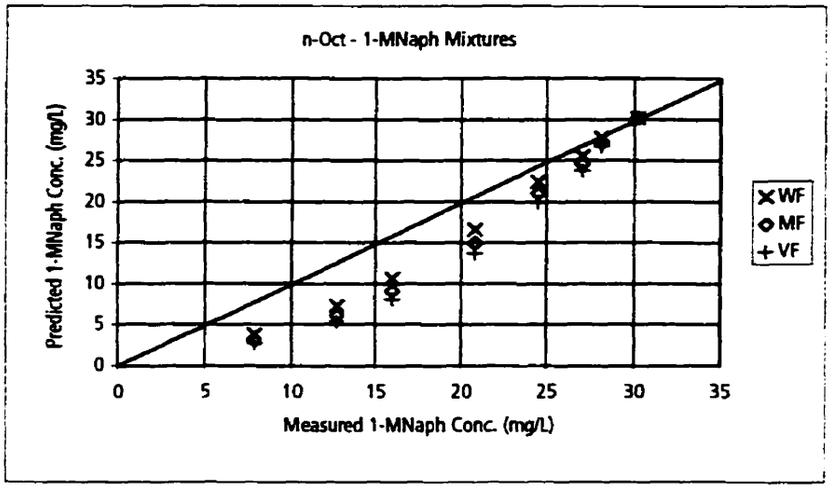

Key:
n-Oct - n-Octane
1-MNaph - 1-Methyl Naphthalene
WF - Concentrations calculated by Raoult's Law using weight fraction in NAPL.
MF - Concentrations calculated by Raoult's Law using mole fraction in NAPL.
VF - Concentrations calculated by Raoult's Law using volume fraction in NAPL.

Figure 2-15. Comparison of measured aqueous concentrations to aqueous concentrations calculated by Raoult's Law for n-octane - 1-methyl naphthalene mixtures.

Data from Burris and MacIntyre (1986a).

2-16a

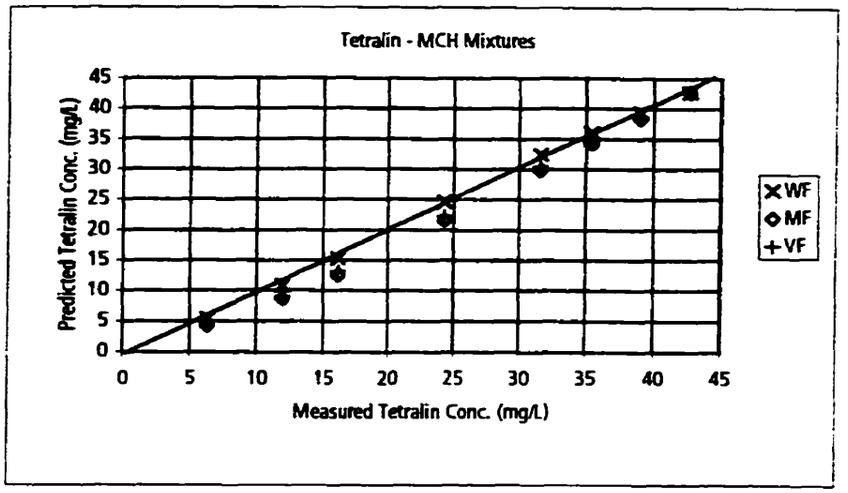

2-16b

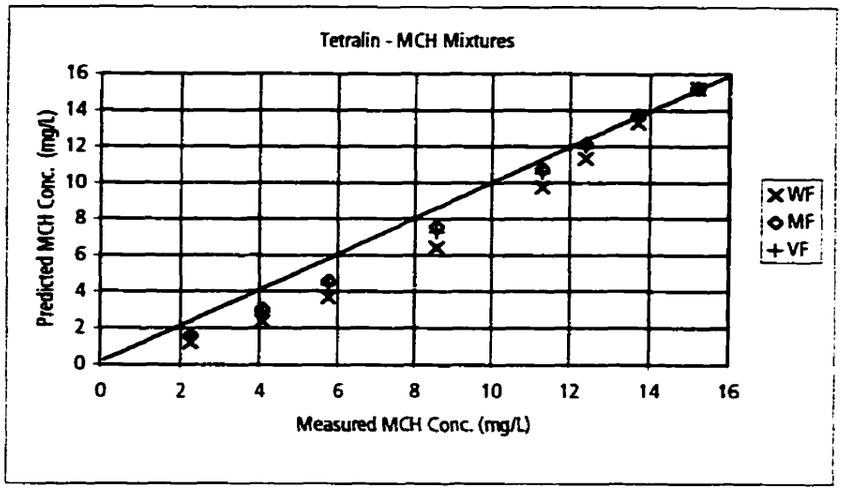

Key:
MCH - Methylcyclohexane
WF - Concentrations calculated by Raoult's Law using weight fraction in NAPL.
MF - Concentrations calculated by Raoult's Law using mole fraction in NAPL.
VF - Concentrations calculated by Raoult's Law using volume fraction in NAPL.

Figure 2-16. Comparison of measured aqueous concentrations to aqueous concentrations calculated by Raoult's Law for tetralin - methylcyclohexane mixtures.

Data from Burris and MacIntyre (1986a).

2-17a

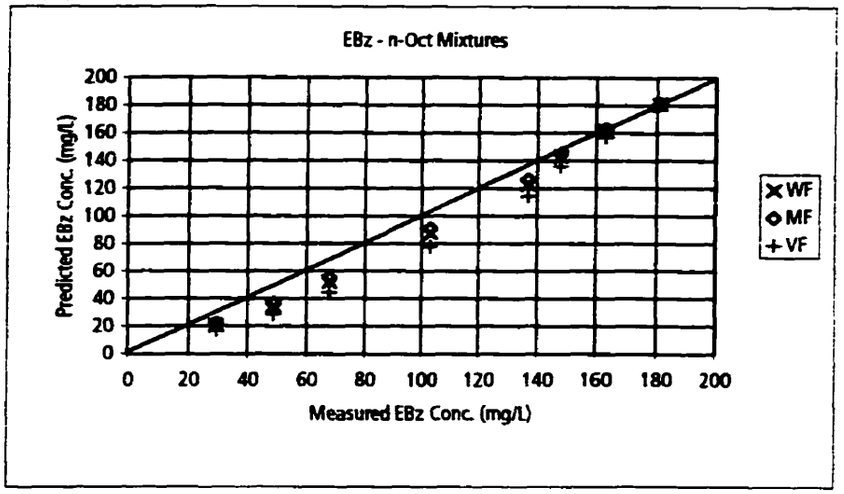

2-17b

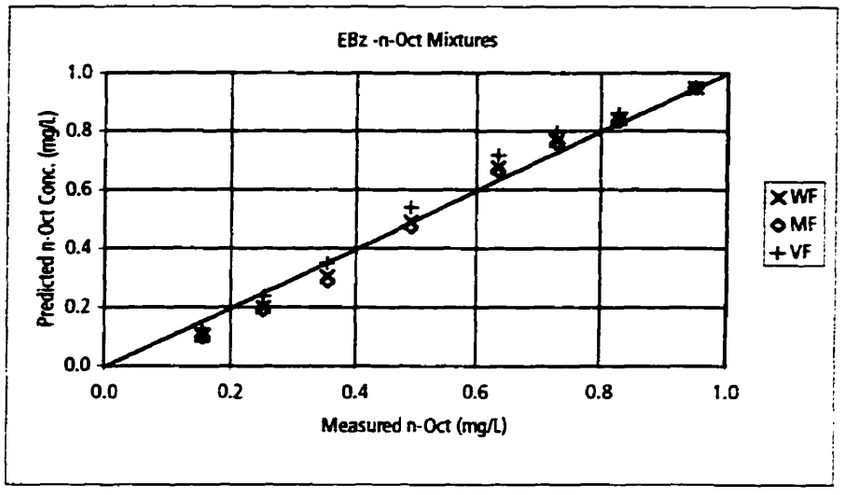

Key:
EBz - Ethyl Benzene
n-Oct - n-Octane
WF - Concentrations calculated by Raoult's Law using weight fraction in NAPL.
MF - Concentrations calculated by Raoult's Law using mole fraction in NAPL.
VF - Concentrations calculated by Raoult's Law using volume fraction in NAPL.

Figure 2-17. Comparison of measured aqueous concentrations to aqueous concentrations calculated by Raoult's Law for ethyl benzene - n-octane mixtures.

Data from Burris and MacIntyre (1986a).

File:Burns EBz-nOct Data/Sheet1

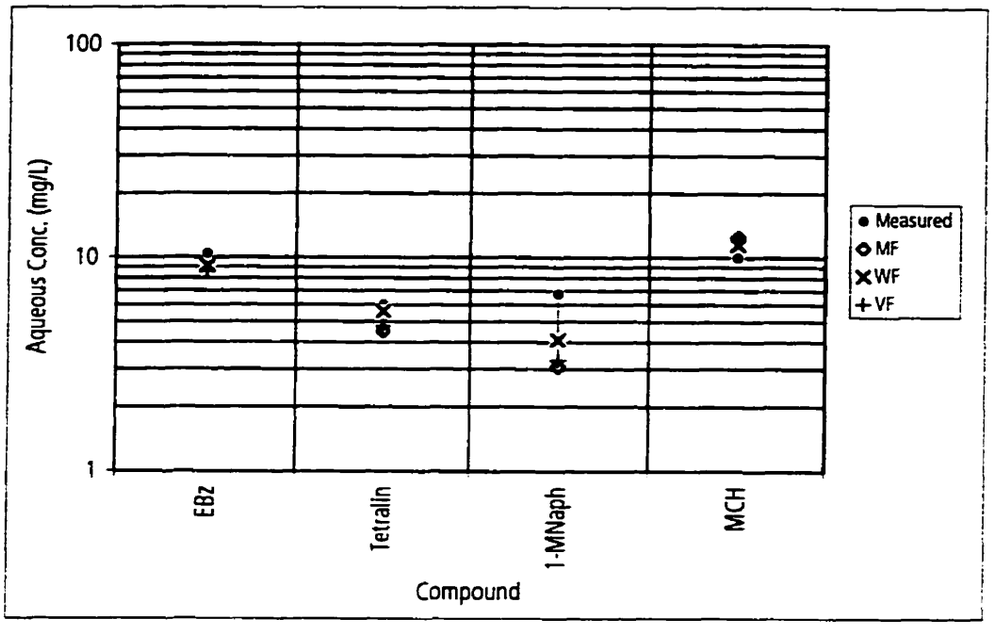

Key:
EBz - Ethyl Benzene MCH - Methylcyclohexane
1-MNaph - 1-Methyl Naphthalene
WF - Concentrations calculated by Raoult's Law using weight fraction in NAPL.
MF - Concentrations calculated by Raoult's Law using mole fraction in NAPL.
VF - Concentrations calculated by Raoult's Law using volume fraction in NAPL.

Figure 2-18. Comparison of measured aqueous concentrations to aqueous concentrations calculated by Raoult's Law for a 4-component hydrocarbon mixture.

Data from Burris and MacIntyre (1986b)

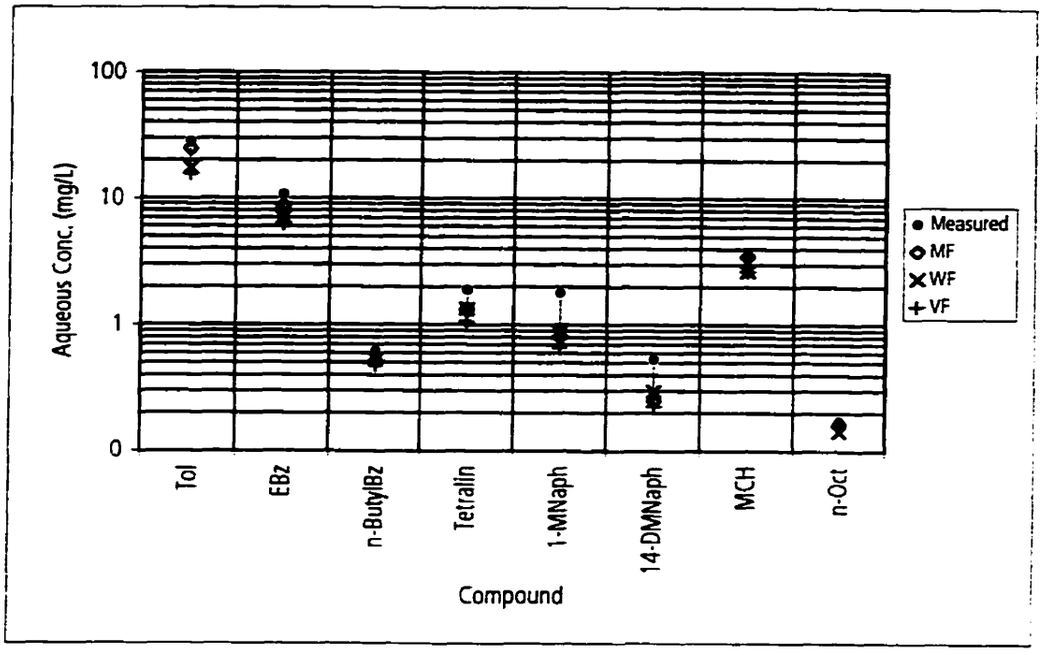

Key:

Tol - Toluene
EBz - Ethyl Benzene
N-ButylBz - n-Butyl Benzene
1-MNaph - 1-Methyl Naphthalene
14-DMNaph - 1,4-Dimethyl Naphthalene
MCH - Methylcyclohexane
n-Oct - n-Octane

WF - Concentrations calculated by Raoult's Law using weight fraction in NAPL.
MF - Concentrations calculated by Raoult's Law using mole fraction in NAPL.
VF - Concentrations calculated by Raoult's Law using volume fraction in NAPL.

Figure 2-19. Comparison of measured aqueous concentrations to aqueous concentrations calculated by Raoult's Law for a simulated JP-4 jet fuel mixture.

Data from Burris and MacIntyre (1986c)

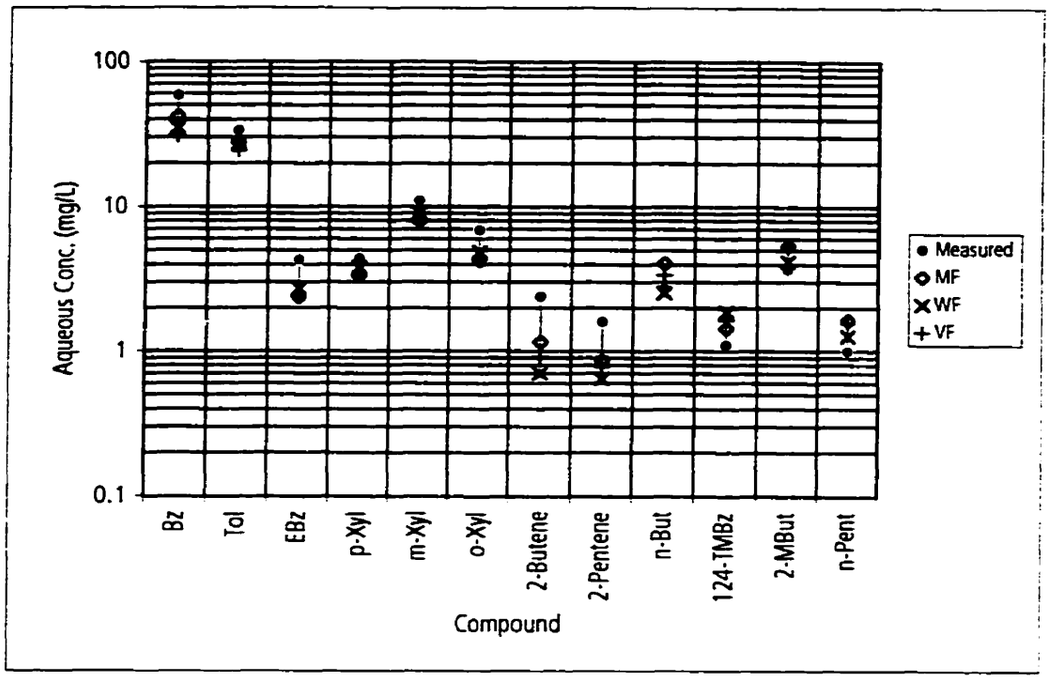

Key:

Bz - Benzene	o-Xyl - o-Xylene
Tol - Toluene	n-But - n-Butane
EBz - Ethyl Benzene	124-TMBz - 1,2,4-Trimethyl Benzene
p-Xyl - p-Xylene	2-MBut - 2-Methyl Butane
m-Xyl - m-Xylene	n-Pent - n-Petane

WF - Concentrations calculated by Raoult's Law using weight fraction in NAPL.
MF - Concentrations calculated by Raoult's Law using mole fraction in NAPL.
VF - Concentrations calculated by Raoult's Law using volume fraction in NAPL.

Figure 2-20. Comparison of measured aqueous concentrations to aqueous concentrations calculated by Raoult's Law for a PS-6 gasoline.

Data from TRC (1985).

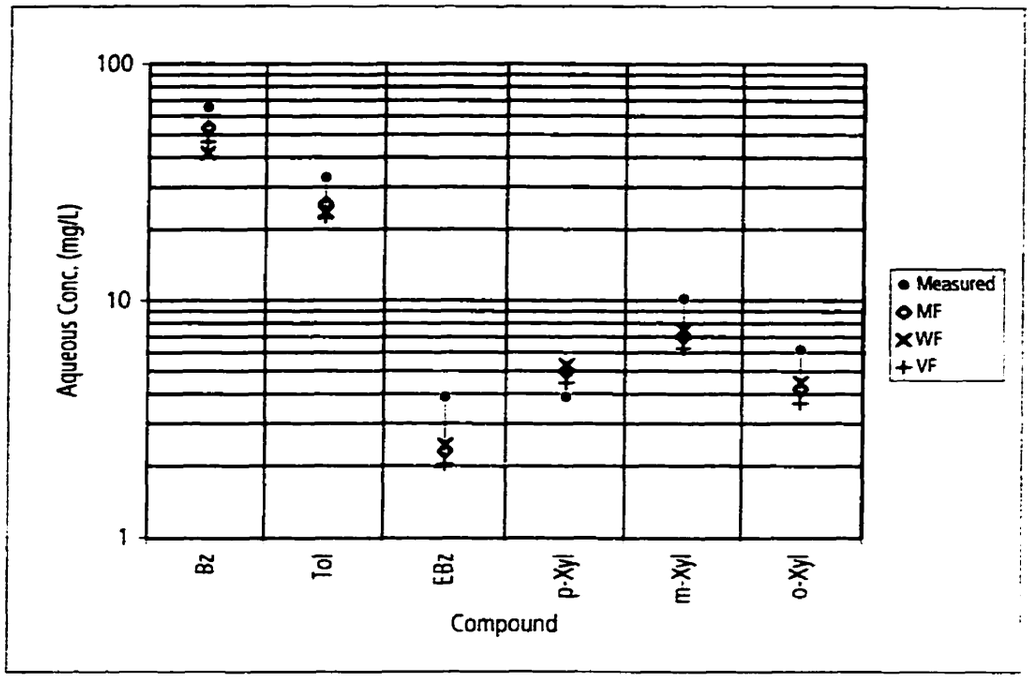

Key:

Bz - Benzene	p-Xyl - p-Xylene
Tol - Toluene	m-Xyl - m-Xylene
EBz - Ethyl Benzene	o-Xyl - o-Xylene

WF - Concentrations calculated by Raoult's Law using weight fraction in NAPL.
MF - Concentrations calculated by Raoult's Law using mole fraction in NAPL.
VF - Concentrations calculated by Raoult's Law using volume fraction in NAPL.

Figure 2-21. Comparison of measured aqueous concentrations to aqueous concentrations calculated by Raoult's Law for a PS-6 gasoline.

Data from Poulsen et al. (1992).

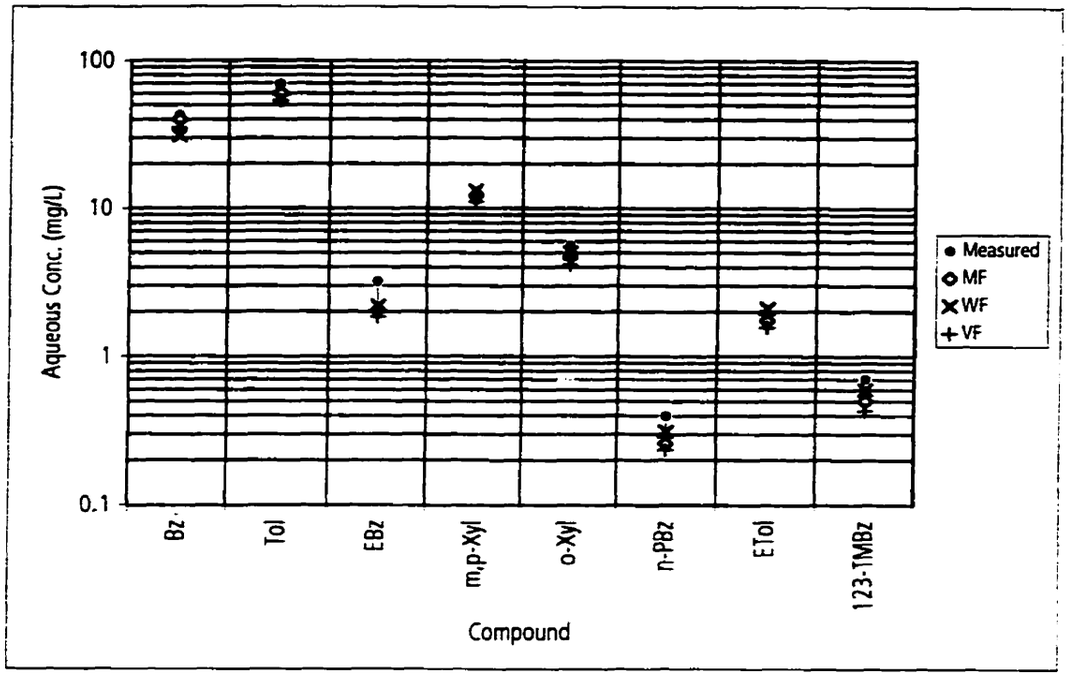

Key:

Bz - Benzene	o-Xyl - o-Xylene
Tol - Toluene	n-PBz - n-Propyl Benzene
EBz - Ethyl Benzene	ETol - 3-Ethyl Toluene + 4-Ethyl Toluene
m-,p-Xyl - m-Xylene + p-Xylene	123-TMBz - 1,2,3-Trimethyl Benzene

WF - Concentrations calculated by Raoult's Law using weight fraction in NAPL.
MF - Concentrations calculated by Raoult's Law using mole fraction in NAPL.
VF - Concentrations calculated by Raoult's Law using volume fraction in NAPL.

Figure 2-22. Comparison of measured aqueous concentrations to aqueous concentrations calculated by Raoult's Law for the average composition of 31 gasolines.

Data from Cline et al. (1991).

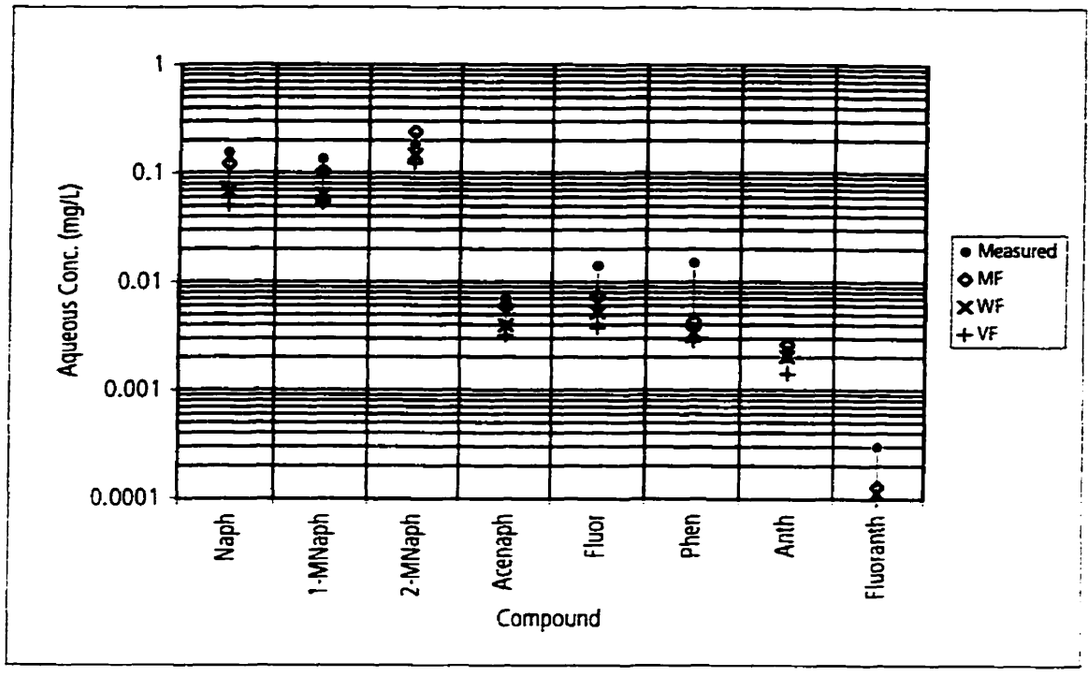

Key:

Naph - Naphthalene	Fluor - Fluorene
1-MNaph - 1-Methyl Naphthalene	Phen - Phenanthrene
2-MNaph - 2-Methyl Naphthalene	Anth - Anthracene
Acenaph - Acenaphthene	Fluoranth - Fluoranthene

WF - Concentrations calculated by Raoult's Law using weight fraction in NAPL.
MF - Concentrations calculated by Raoult's Law using mole fraction in NAPL.
VF - Concentrations calculated by Raoult's Law using volume fraction in NAPL.

Figure 2-23. Comparison of measured aqueous concentrations to aqueous concentrations calculated by Raoult's Law for a sample of diesel fuel (#1).

Data from Lee et al. (1992b).

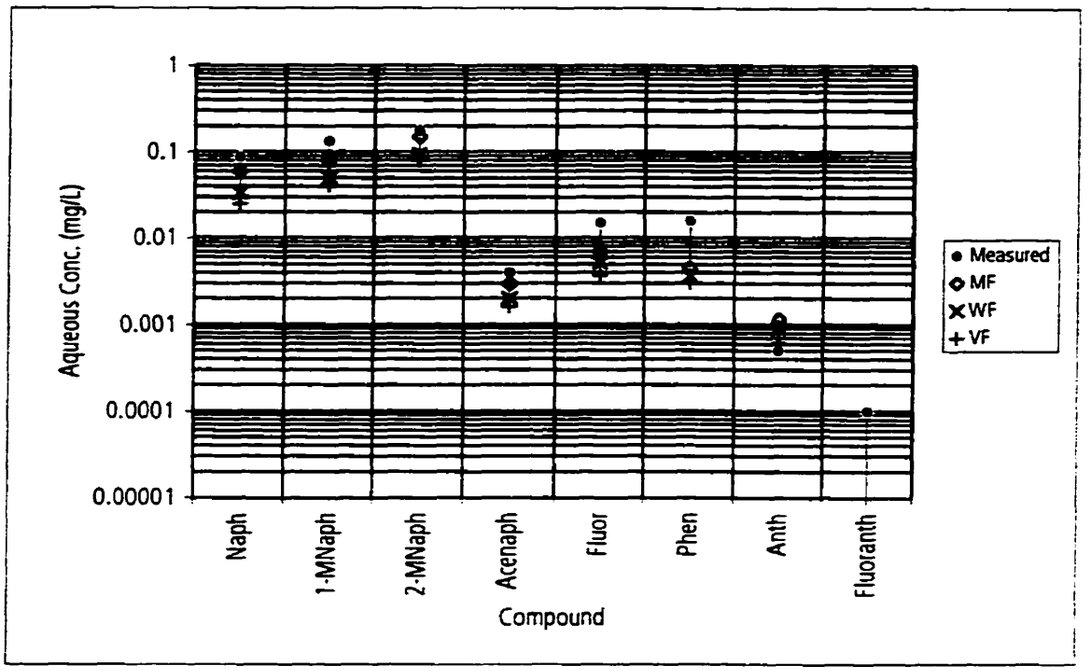

Key:

Naph - Naphthalene	Fluor - Fluorene
1-MNaph - 1-Methyl Naphthalene	Phen - Phenanthrene
2-MNaph - 2-Methyl Naphthalene	Anth - Anthracene
Acenaph - Acenaphthene	Fluoranth - Fluoranthene

WF - Concentrations calculated by Raoult's Law using weight fraction in NAPL.
MF - Concentrations calculated by Raoult's Law using mole fraction in NAPL.
VF - Concentrations calculated by Raoult's Law using volume fraction in NAPL.

Figure 2-24. Comparison of measured aqueous concentrations to aqueous concentrations calculated by Raoult's Law for a sample of diesel fuel (#2).

Data from Lee et al. (1992b).

File:Lee Diesel #2 Data/Sheet1

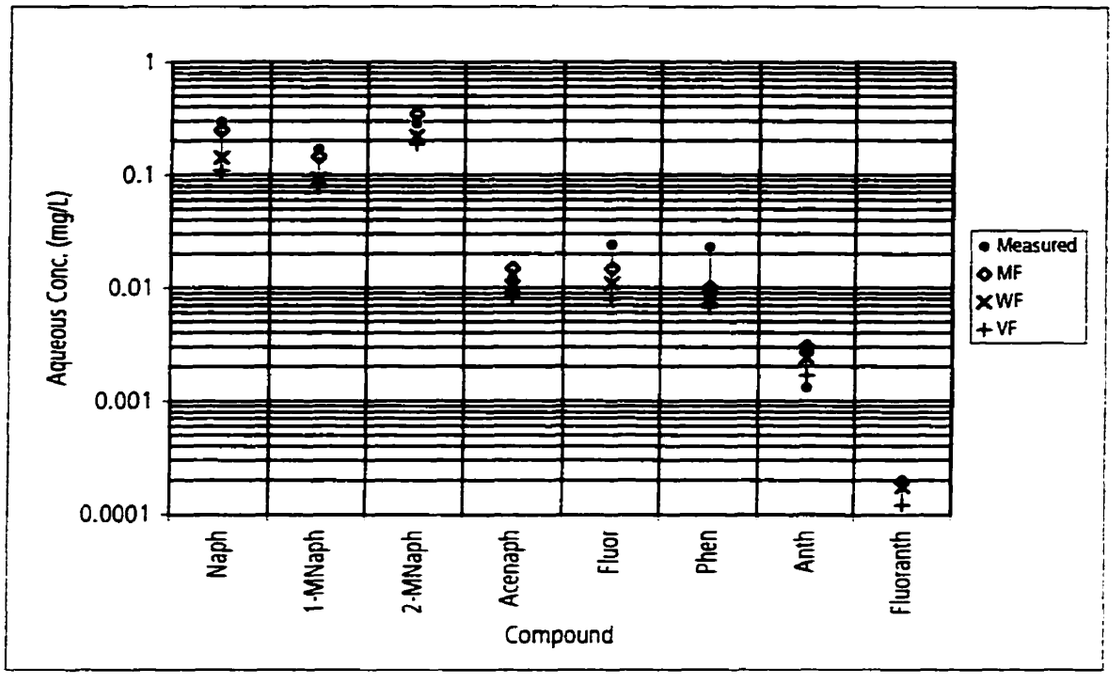

Key:

Naph - Naphthalene	Fluor - Fluorene
1-MNaph - 1-Methyl Naphthalene	Phen - Phenanthrene
2-MNaph - 2-Methyl Naphthalene	Anth - Anthracene
Acenaph - Acenaphthene	Fluoranth - Fluoranthene

WF - Concentrations calculated by Raoult's Law using weight fraction in NAPL.
MF - Concentrations calculated by Raoult's Law using mole fraction in NAPL.
VF - Concentrations calculated by Raoult's Law using volume fraction in NAPL.

Figure 2-25. Comparison of measured aqueous concentrations to aqueous concentrations calculated by Raoult's Law for a sample of diesel fuel (#3).

Data from Lee et al. (1992b).

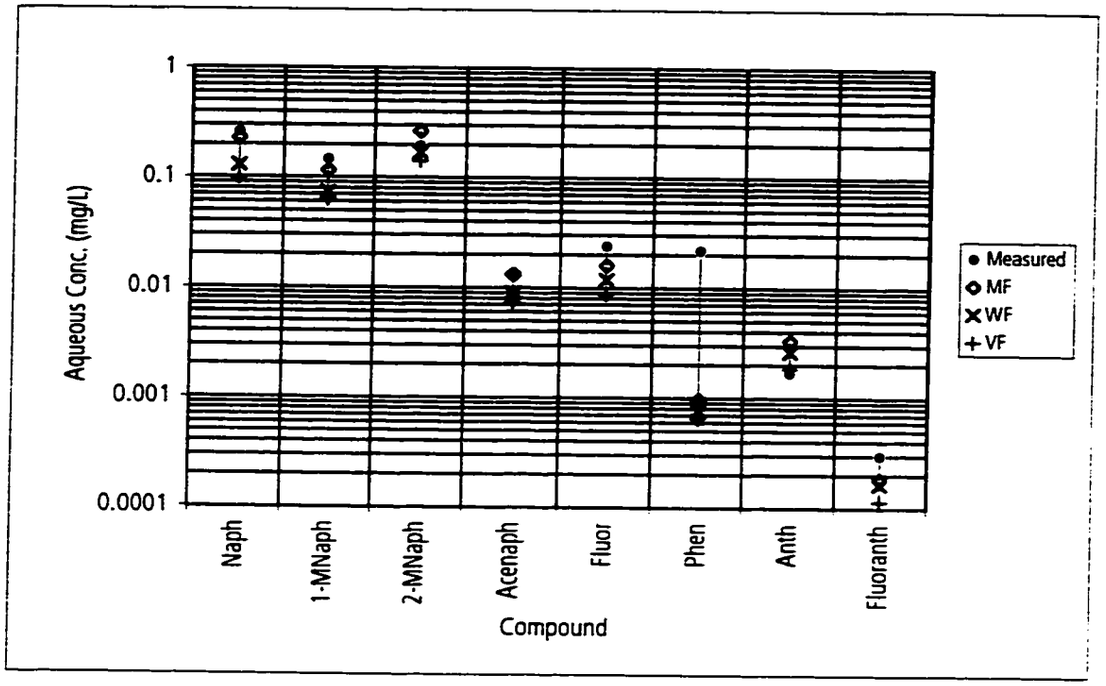

Key:

Naph - Naphthalene	Fluor - Fluorene
1-MNaph - 1-Methyl Naphthalene	Phen - Phenanthrene
2-MNaph - 2-Methyl Naphthalene	Anth - Anthracene
Acenaph - Acenaphthene	Fluoranth - Fluoranthene

WF - Concentrations calculated by Raoult's Law using weight fraction in NAPL.
MF - Concentrations calculated by Raoult's Law using mole fraction in NAPL.
VF - Concentrations calculated by Raoult's Law using volume fraction in NAPL.

Figure 2-26. Comparison of measured aqueous concentrations to aqueous concentrations calculated by Raoult's Law for a sample of diesel fuel (#4).

Data from Lee et al. (1992b).

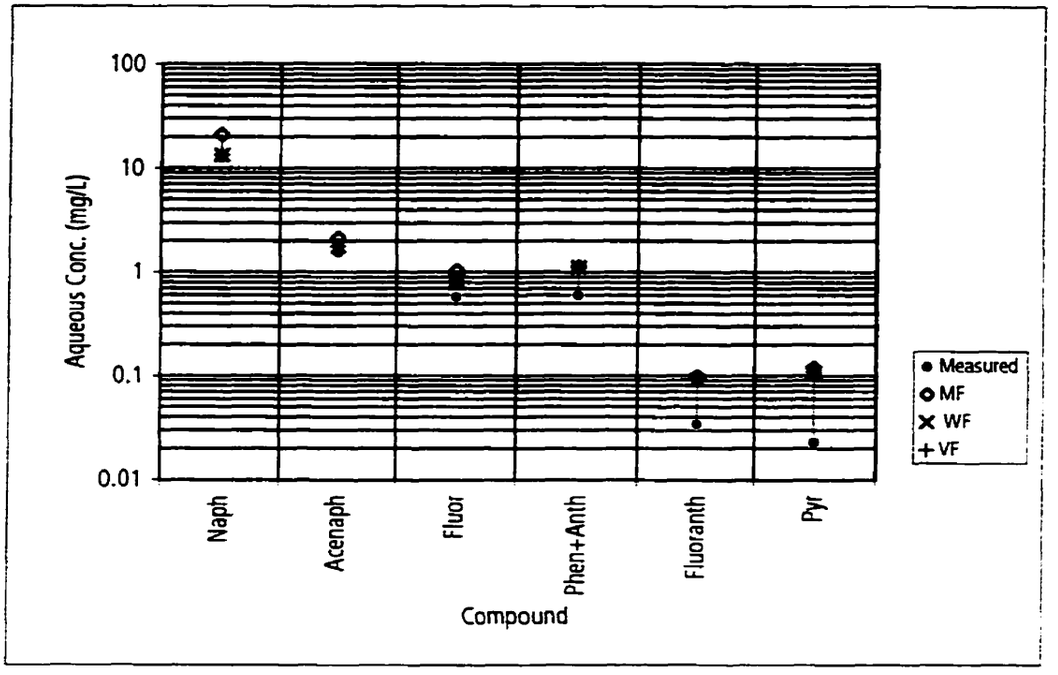

Key:

Naph - Naphthalene	Phen+Anth - Phenanthrene + Anthracene
Acenaph - Acenaphthene	Fluoranth - Fluoranthene
Fluor - Fluorene	Pyr - Pyrene

WF - Concentrations calculated by Raoult's Law using weight fraction in NAPL.
MF - Concentrations calculated by Raoult's Law using mole fraction in NAPL.
VF - Concentrations calculated by Raoult's Law using volume fraction in NAPL.

Figure 2-27. Comparison of measured aqueous concentrations to aqueous concentrations calculated by Raoult's Law for a sample of creosote.

Data from Priddle and MacQuarrie (1994).

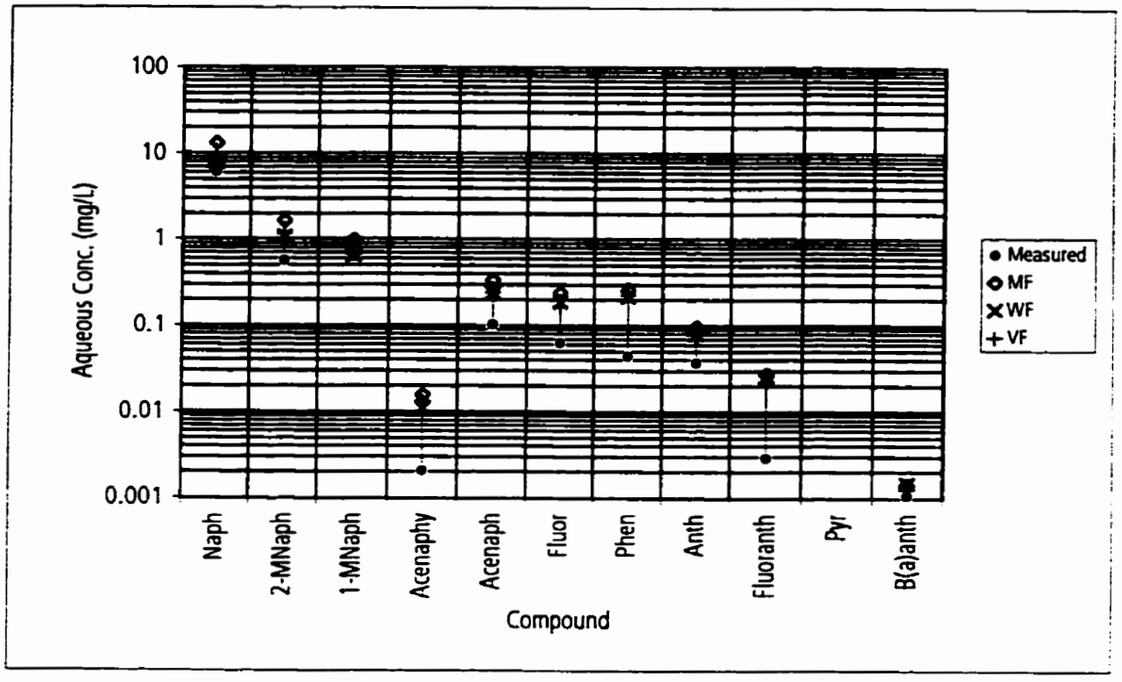

Key:

Naph - Naphthalene	Phen - Phenanthrene
2-MNaph - 2-Methyl Naphthalene	Anth - Anthracene
1-MNaph - 1-Methyl Naphthalene	Fluoranth - Fluoranthene
Acenaph - Acenaphthene	Pyr - Pyrene
Acenaphy - Acenaphthylene	B(a)anth - Benzo(a)anthracene
Fluor - Fluorene	

WF - Concentrations calculated by Raoult's Law using weight fraction in NAPL.
MF - Concentrations calculated by Raoult's Law using mole fraction in NAPL.
VF - Concentrations calculated by Raoult's Law using volume fraction in NAPL.

Figure 2-28. Comparison of measured aqueous concentrations to aqueous concentrations calculated by Raoult's Law for a sample of coal tar (#1).

Data from Lee et al. (1992a).

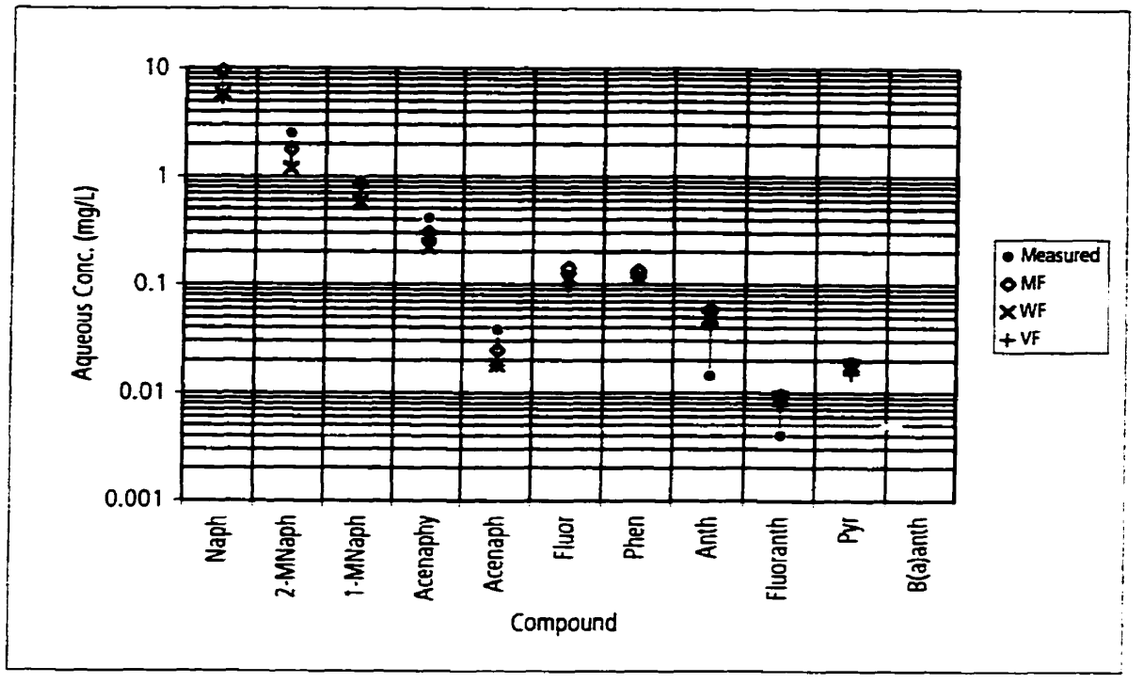

Key:

Naph - Naphthalene
2-MNaph - 2-Methyl Naphthalene
1-MNaph - 1-Methyl Naphthalene
Acenaph - Acenaphthene
Acenaphy - Acenaphthylene
Fluor - Fluorene
Phen - Phenanthrene
Anth - Anthracene
Fluoranth - Fluoranthene
Pyr - Pyrene
B(a)anth - Benzo(a)anthracene

WF - Concentrations calculated by Raoult's Law using weight fraction in NAPL.
MF - Concentrations calculated by Raoult's Law using mole fraction in NAPL.
VF - Concentrations calculated by Raoult's Law using volume fraction in NAPL.

Figure 2-29. Comparison of measured aqueous concentrations to aqueous concentrations calculated by Raoult's Law for a sample of coal tar (#4).

Data from Lee et al. (1992a).

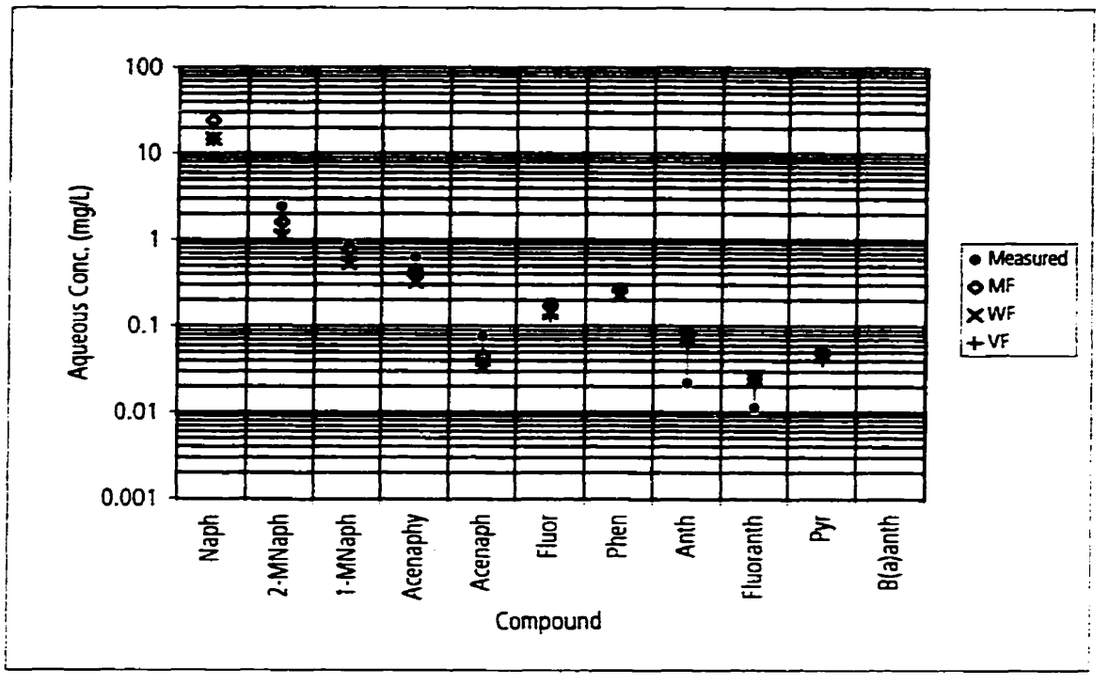

Key:

Naph - Naphthalene	Phen - Phenanthrene
2-MNaph - 2-Methyl Naphthalene	Anth - Anthracene
1-MNaph - 1-Methyl Naphthalene	Fluoranth - Fluoranthene
Acenaph - Acenaphthene	Pyr - Pyrene
Acenaphy - Acenaphthylene	B(a)anth - Benzo(a)anthracene
Fluor - Fluorene	

WF - Concentrations calculated by Raoult's Law using weight fraction in NAPL.
MF - Concentrations calculated by Raoult's Law using mole fraction in NAPL.
VF - Concentrations calculated by Raoult's Law using volume fraction in NAPL.

Figure 2-30. Comparison of measured aqueous concentrations to aqueous concentrations calculated by Raoult's Law for a sample of coal tar (#5).

Data from Lee et al. (1992a).

File:Lee Coal Tar Data #5/Sheet1

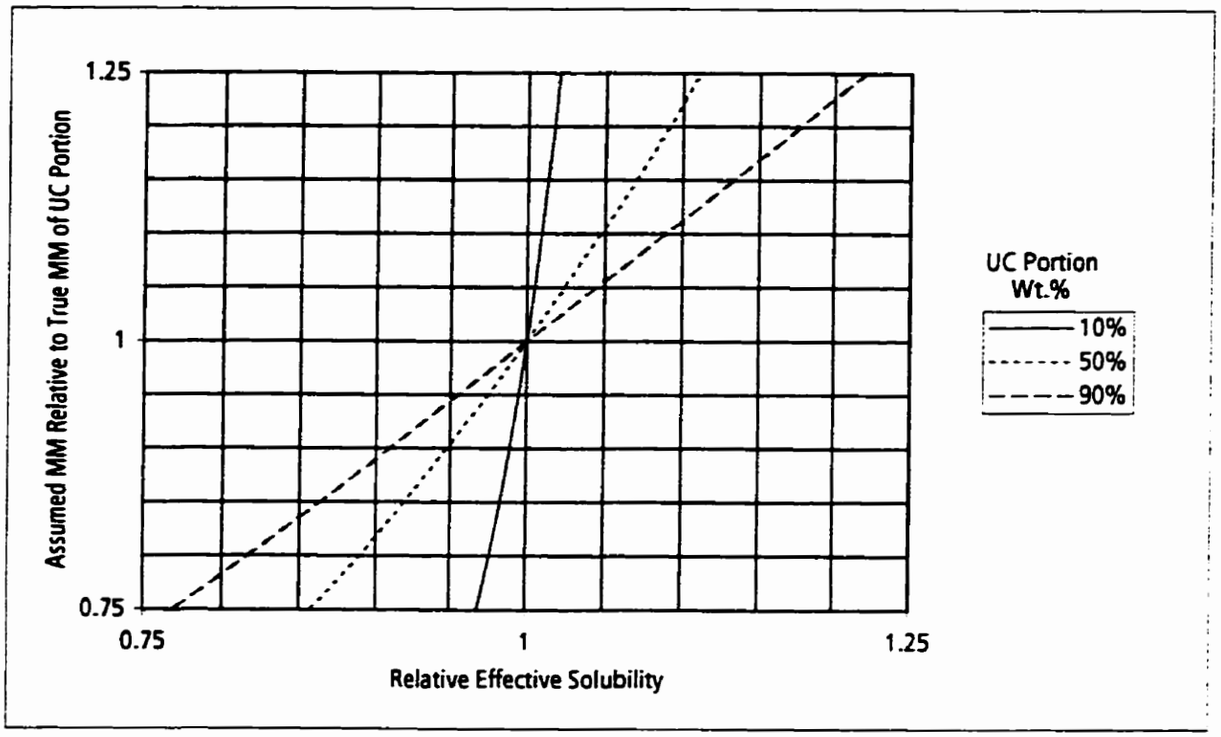

Figure 2-31. Illustration of the sensitivity of the calculated effective solubility to the assumed molecular mass (MM) of the uncharacterized (UC) portion of a multi-component NAPL. For ratio of MM of UC portion to average MM of characterized portion equal to 1.

Relative effective solubility is the ratio of the effective solubility calculated using the assumed MM for the UC portion to the effective solubility calculated using the true MM for the UC portion.

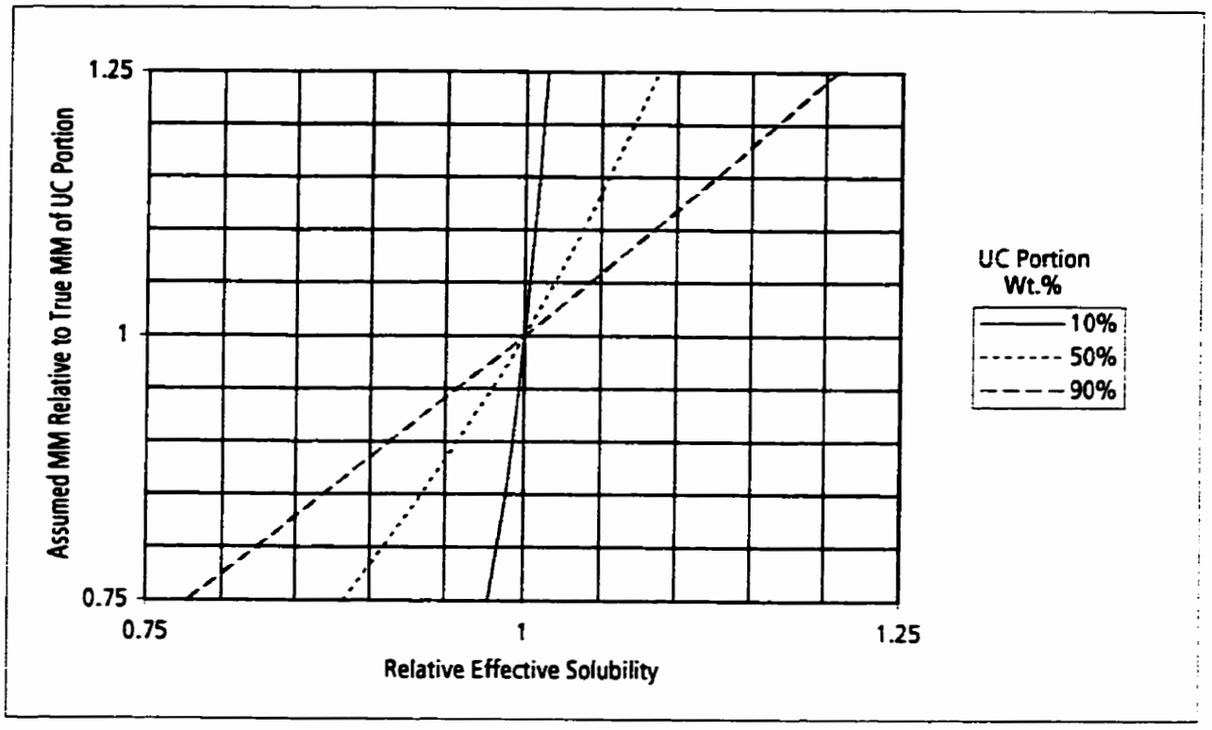

Figure 2-32. Illustration of the sensitivity of the calculated effective solubility to the assumed molecular mass (MM) of the uncharacterized (UC) portion of a multi-component NAPL. For ratio of MM of UC portion to average MM of characterized portion equal to 1.5.

Relative effective solubility is the ratio of the effective solubility calculated using the assumed MM for the UC portion to the effective solubility calculated using the true MM for the UC portion.

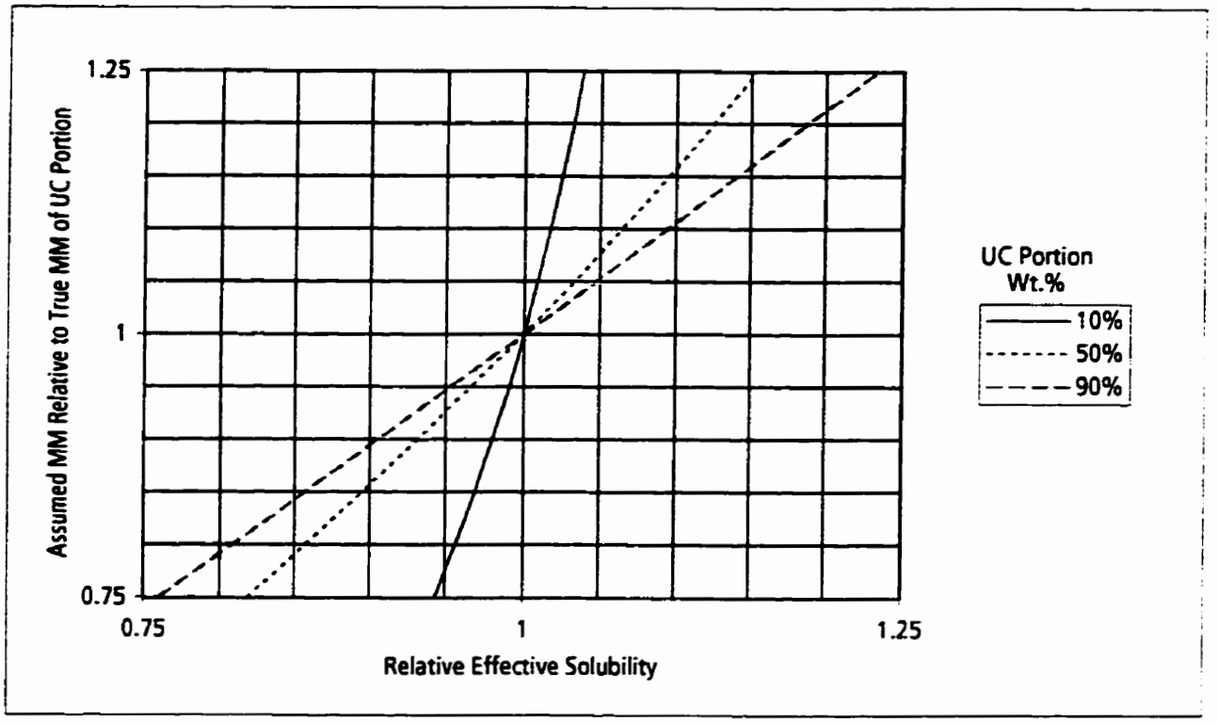

Figure 2-33. Illustration of the sensitivity of the calculated effective solubility to the assumed molecular mass (MM) of the uncharacterized (UC) portion of a multi-component NAPL. For ratio of MM of UC portion to average MM of characterized portion equal to 0.5.

Relative effective solubility is the ratio of the effective solubility calculated using the assumed MM for the UC portion to the effective solubility calculated using the true MM for the UC portion.

2-34a

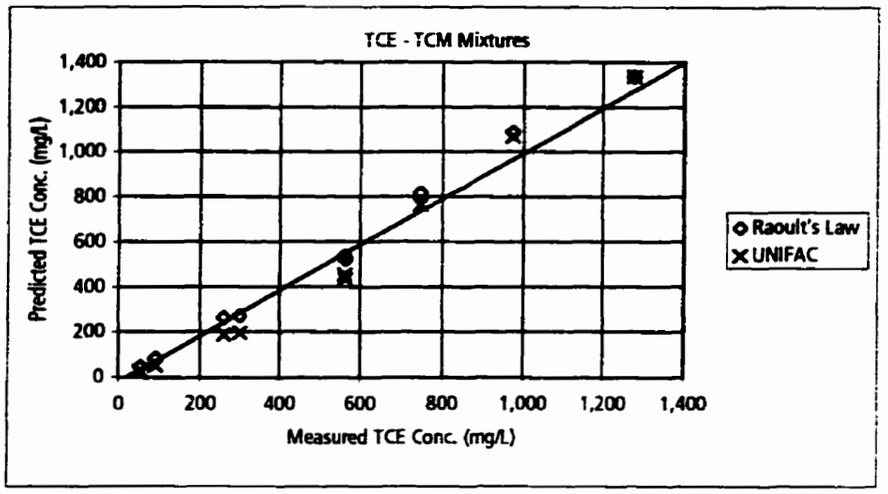

2-34b

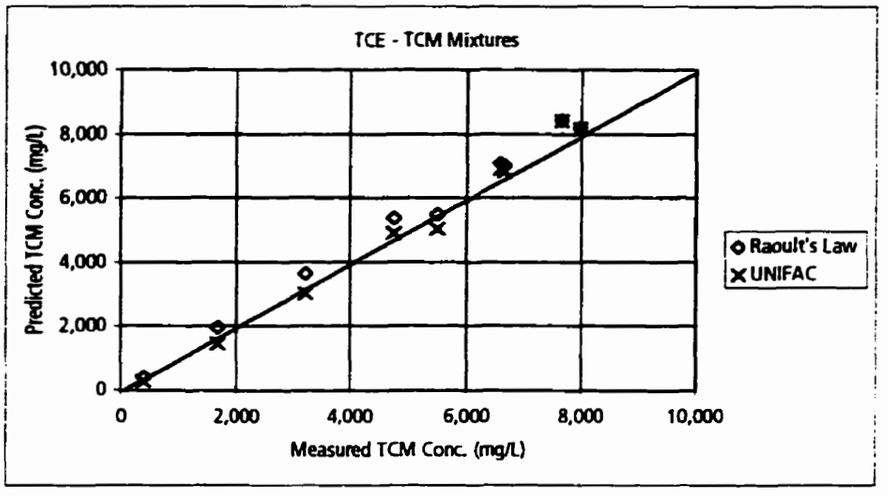

Key:
TCE - Trichloroethylene
TCM - Chloroform
Raoult's Law - Concentration calculated by Raoult's Law using mole fraction in NAPL.
UNIFAC - Concentration calculated by equation 2-11 using activity coefficients calculated by UNIFAC.

Figure 2-34. Comparison of measured aqueous concentrations to aqueous concentrations calculated by Raoult's Law and UNIFAC for trichloroethylene - chloroform mixtures.

Data from Broholm and Feenstra (1995).

2-35a

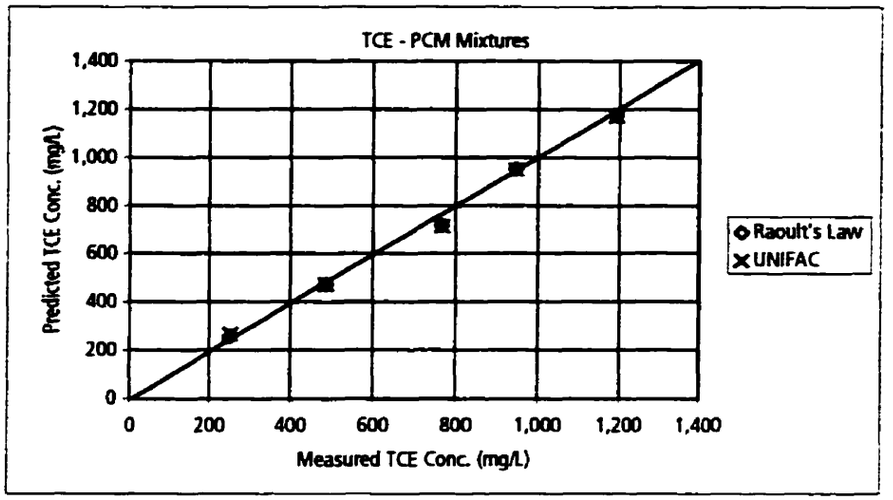

2-35b

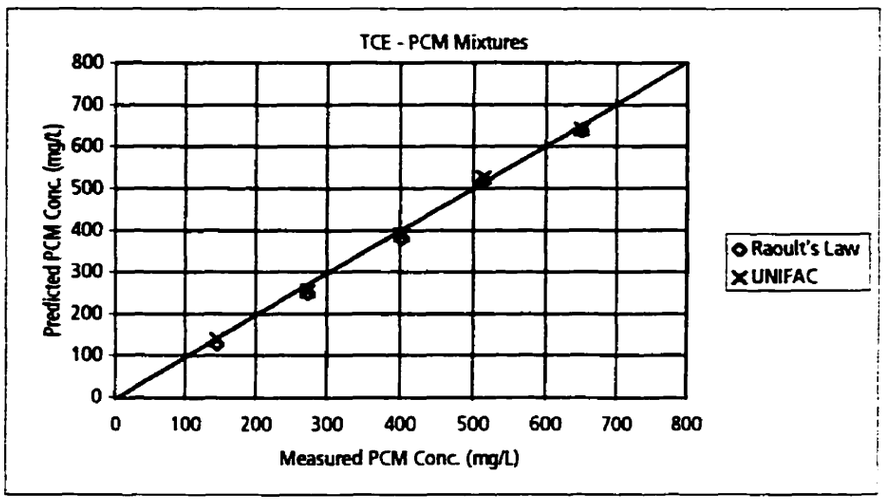

Key:
TCE - Trichloroethylene
PCM - Carbon Tetrachloride
Raoult's Law - Concentration calculated by Raoult's Law using mole fraction in NAPL.
UNIFAC - Concentration calculated by equation 2-11 using activity coefficients calculated by UNIFAC.

Figure 2-35. Comparison of measured aqueous concentrations to aqueous concentrations calculated by Raoult's Law and UNIFAC for trichloroethylene - carbon tetrachloride mixtures.

Data from Broholm and Feenstra (1995).

2-36a

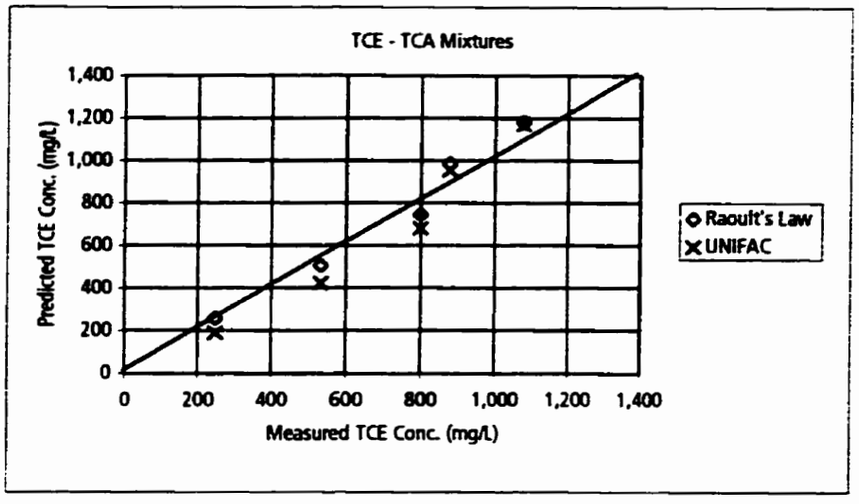

2-36b

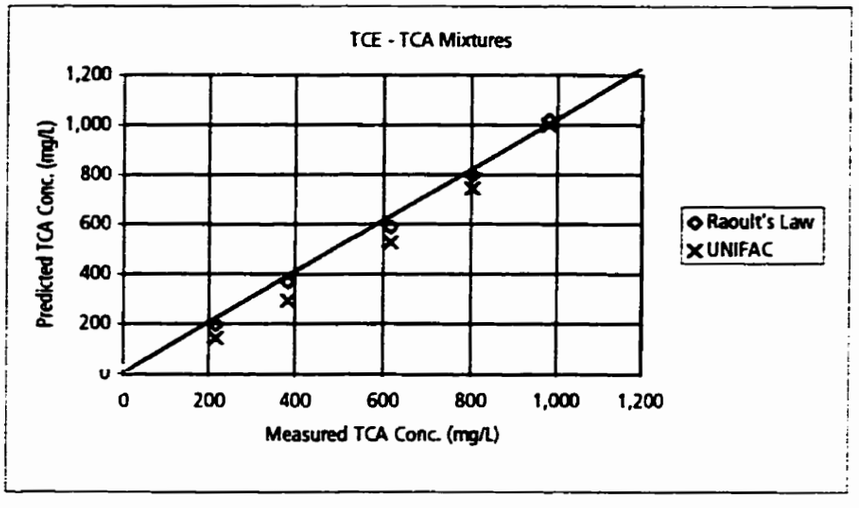

Key:
TCE - Trichloroethylene
TCA - 1,1,1-Trichloroethane
Raoult's Law - Concentration calculated by Raoult's Law using mole fraction in NAPL.
UNIFAC - Concentration calculated by equation 2-11 using activity coefficients calculated by UNIFAC.

Figure 2-36. Comparison of measured aqueous concentrations to aqueous concentrations calculated by Raoult's Law and UNIFAC for trichloroethylene - 1,1,1-trichloroethane mixtures.

Data from Broholm and Feenstra (1995).

2-37a

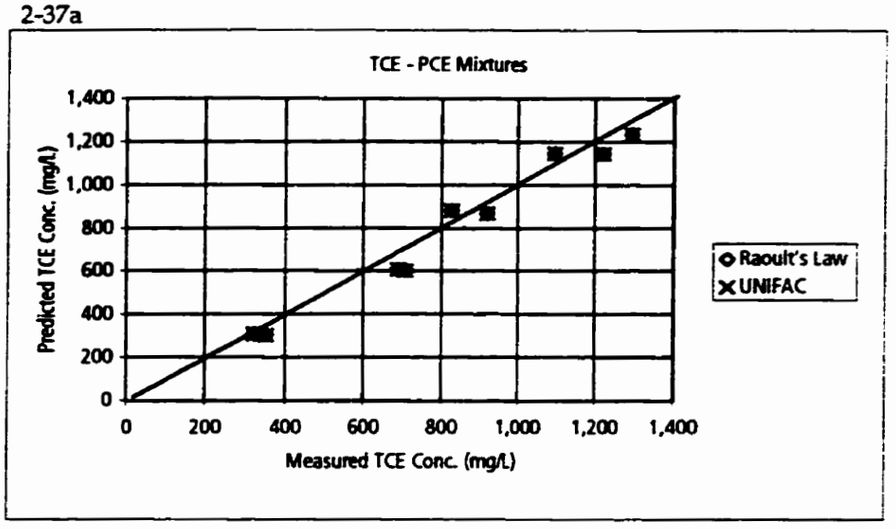

2-37b

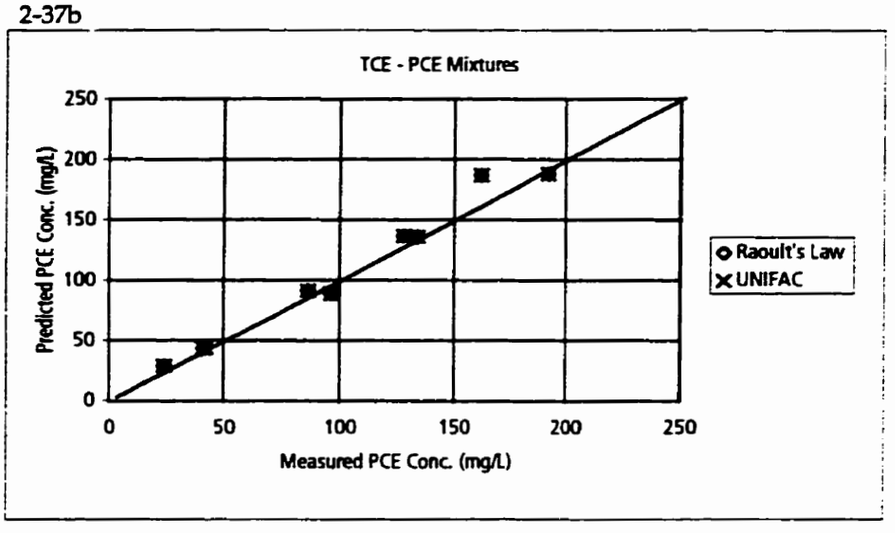

Key:
TCE - Trichloroethylene
PCE - Tetrachloroethylene
Raoult's Law - Concentration calculated by Raoult's Law using mole fraction in NAPL.
UNIFAC - Concentration calculated by equation 2-11 using activity coefficients calculated by UNIFAC.

Figure 2-37. Comparison of measured aqueous concentrations to aqueous concentrations calculated by Raoult's Law and UNIFAC for trichloroethylene - tetrachloroethylene mixtures.

Data from Broholm and Feenstra (1995).

2-38a

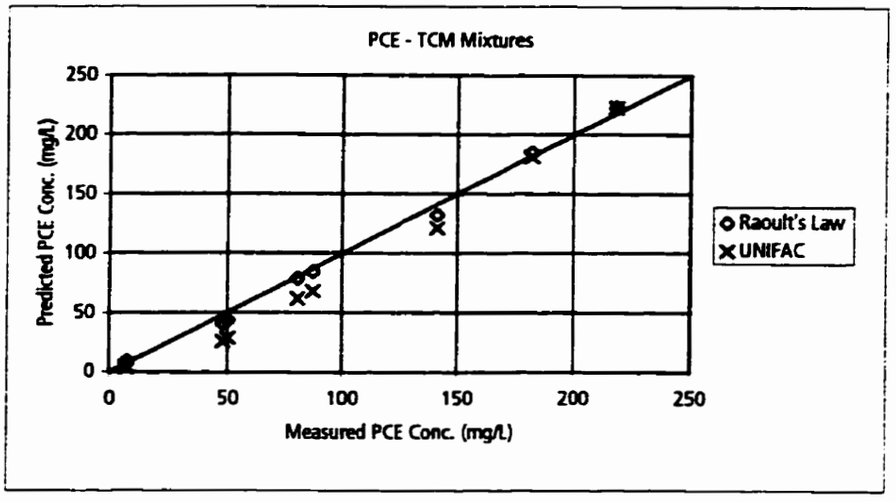

2-38b

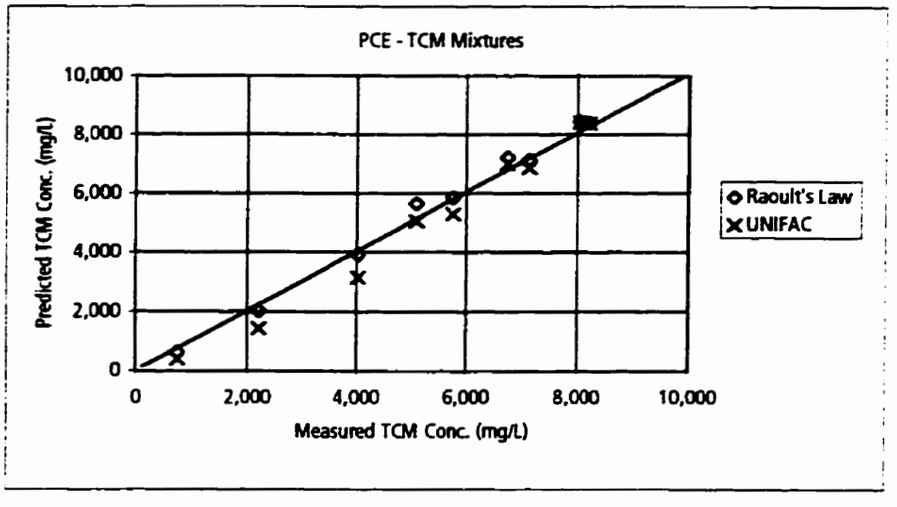

Key:
PCE - Tetrachloroethylene
TCM - Chloroform
Raoult's Law - Concentration calculated by Raoult's Law using mole fraction in NAPL.
UNIFAC - Concentration calculated by equation 2-11 using activity coefficients calculated by UNIFAC.

Figure 2-38. Comparison of measured aqueous concentrations to aqueous concentrations calculated by Raoult's Law and UNIFAC for tetrachloroethylene - chloroform mixtures.

Data from Broholm and Feenstra (1995).

2-39a

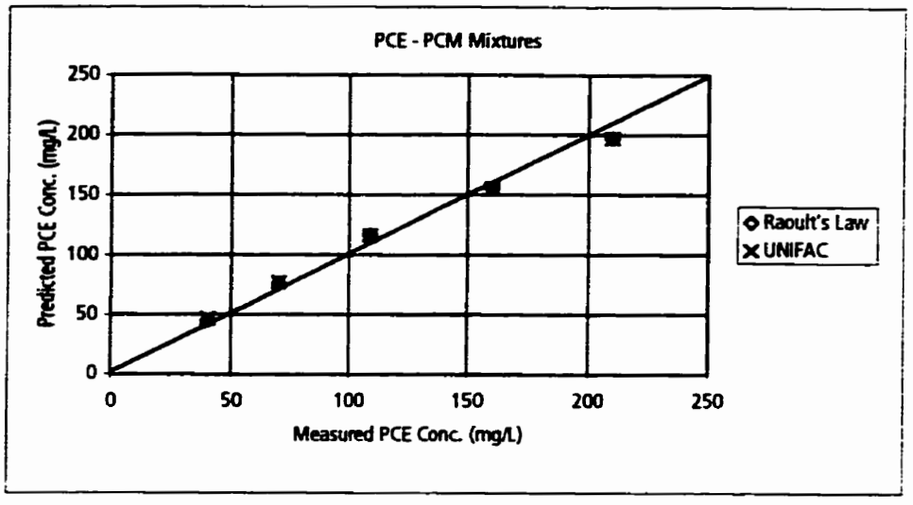

2-39b

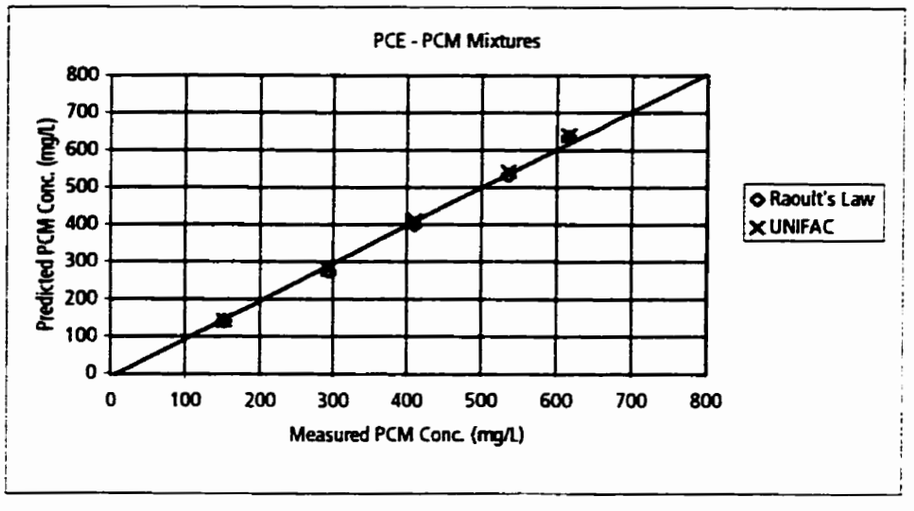

Key:
PCE - Tetrachloroethylene
PCM - Carbon Tetrachloride
Raoult's Law - Concentration calculated by Raoult's Law using mole fraction in NAPL.
UNIFAC - Concentration calculated by equation 2-11 using activity coefficients calculated by UNIFAC.

Figure 2-39. Comparison of measured aqueous concentrations to aqueous concentrations calculated by Raoult's Law and UNIFAC for tetrachloroethylene - carbon tetrachloride mixtures.

Data from Broholm and Feenstra (1995).

2-40a

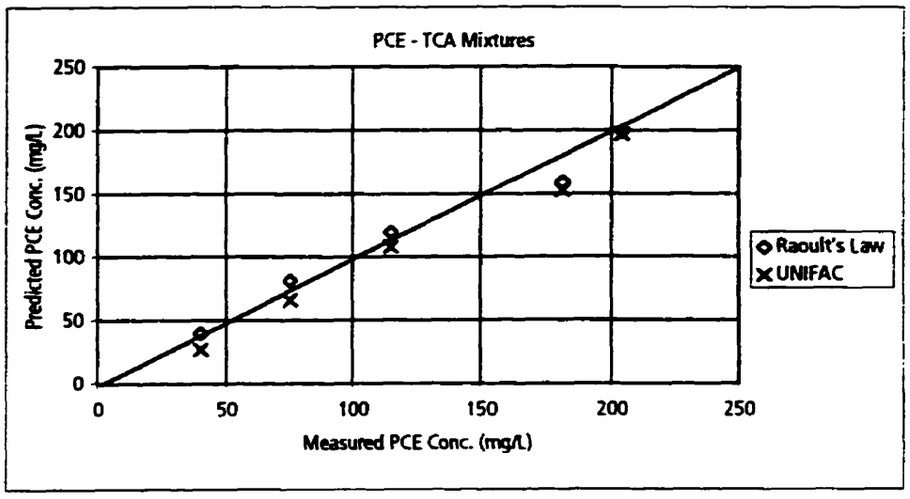

2-40b

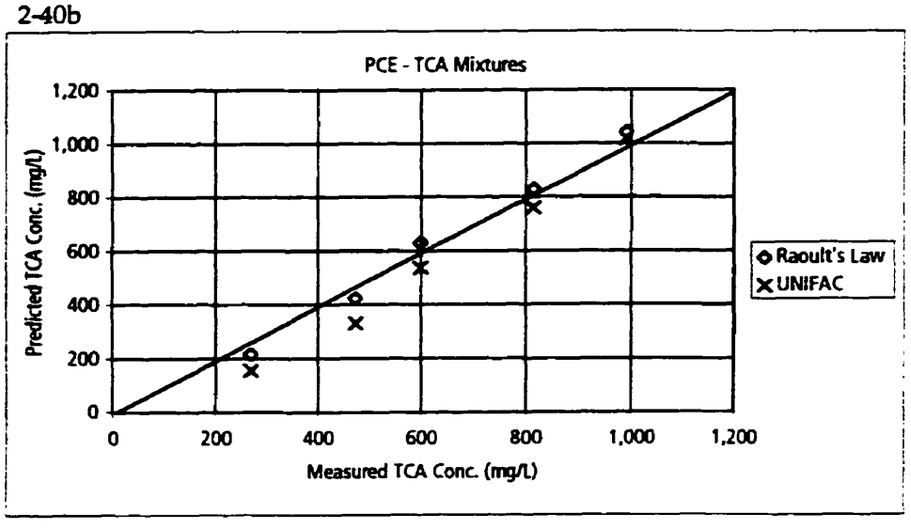

Key:
PCE - Tetrachloroethylene
TCA - 1,1,1-Trichloroethane
Raoult's Law - Concentration calculated by Raoult's Law using mole fraction in NAPL.
UNIFAC - Concentration calculated by equation 2-11 using activity coefficients calculated by UNIFAC.

Figure 2-40. Comparison of measured aqueous concentrations to aqueous concentrations calculated by Raoult's Law and UNIFAC for tetrachloroethylene - 1,1,1-trichloroethane mixtures.

Data from Broholm and Feenstra (1995).

2-41a

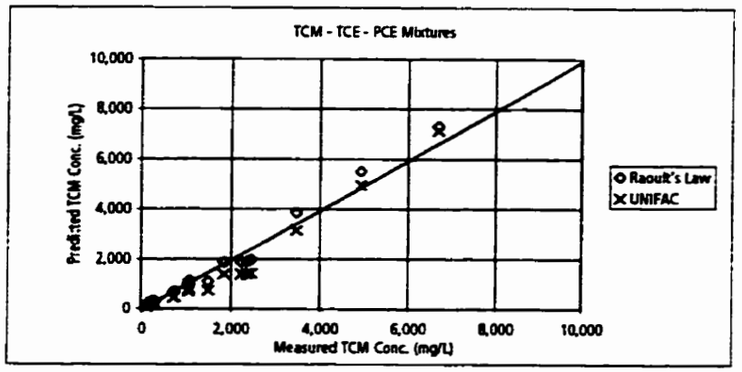

2-41b

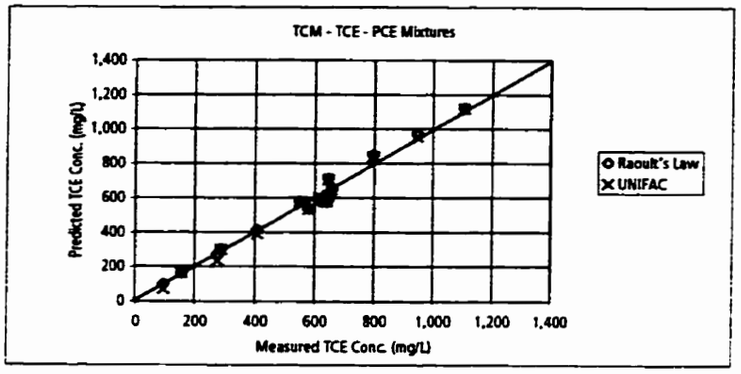

2-41c

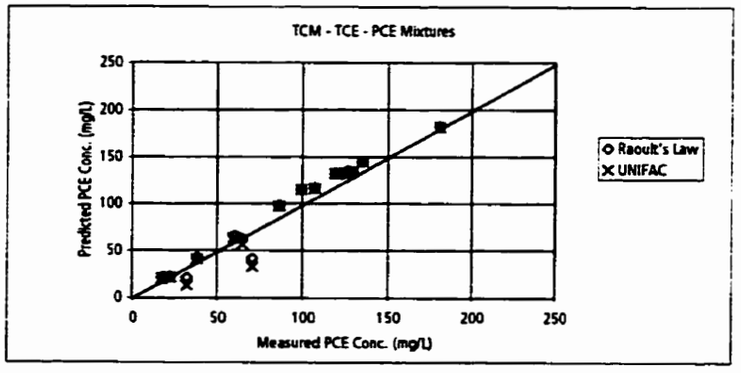

Key:
TCM - Chloroform PCE - Tetrachloroethylene
TCE - Trichloroethylene
Raoult's Law - Concentration calculated by Raoult's Law using mole fraction in NAPL.
UNIFAC - Concentration calculated by equation 2-11 using activity coefficients calculated by UNIFAC.

Figure 2-41. Comparison of measured aqueous concentrations to aqueous concentrations calculated by Raoult's Law and UNIFAC for chloroform - trichloroethylene - tetrachloroethylene mixtures. Data from Broholm and Feenstra (1995).

2-42a

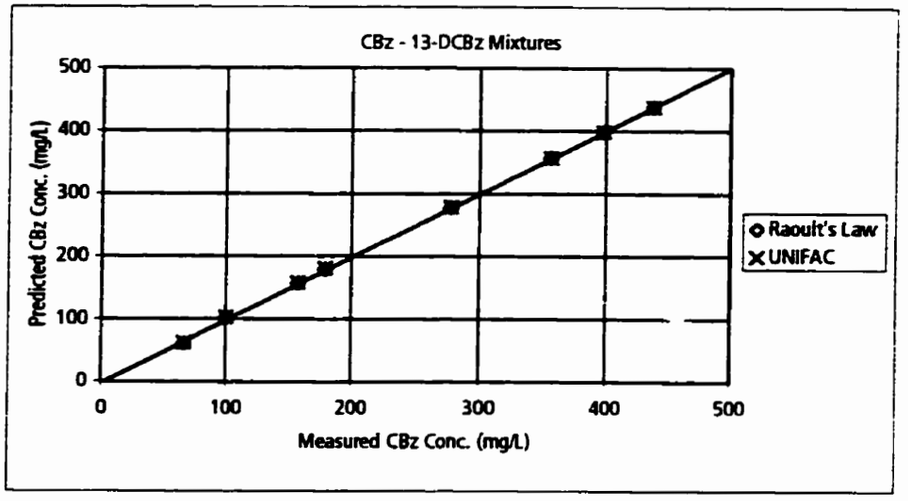

2-42b

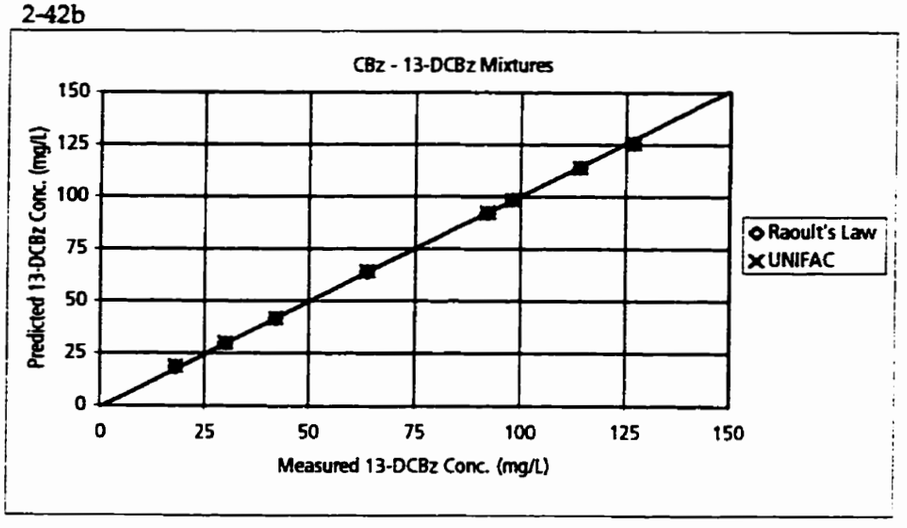

Key:
CBz - Chlorobenzene
13-DCBz - 1,3-Dichlorobenzene
Raoult's Law - Concentration calculated by Raoult's Law using mole fraction in NAPL.
UNIFAC - Concentration calculated by equation 2-11 using activity coefficients calculated by UNIFAC.

Figure 2-42. Comparison of measured aqueous concentrations to aqueous concentrations calculated by Raoult's Law and UNIFAC for chlorobenzene - 1,3-dichlorobenzene mixtures.

Data from Banerjee (1984).

2-43a

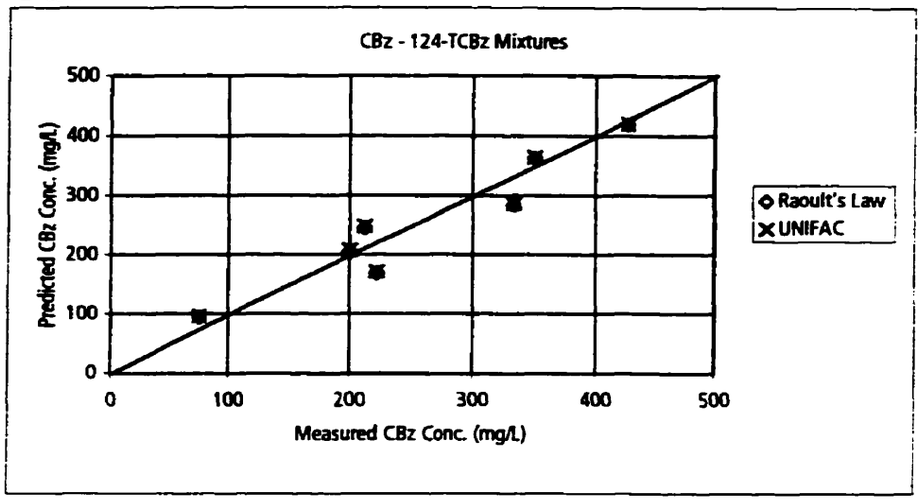

2-43a

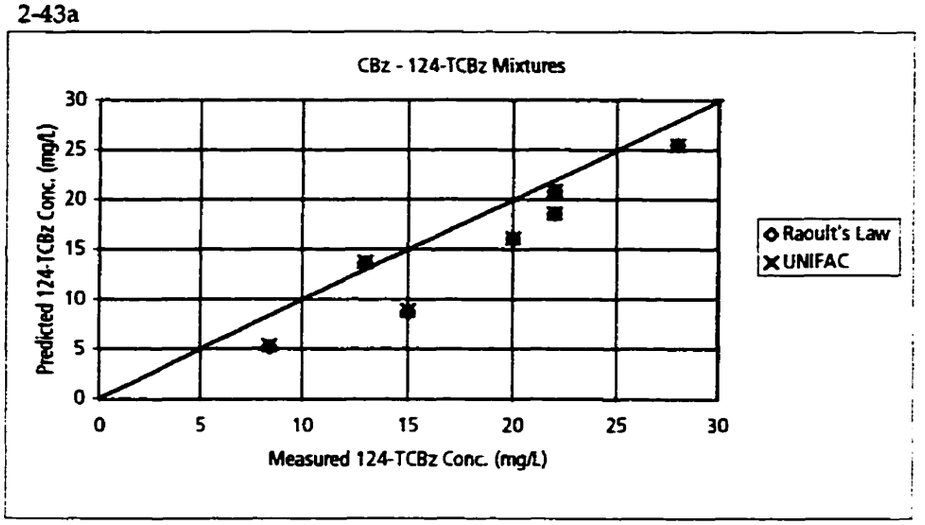

Key:
CBz - Chlorobenzene
124-TCBz - 1,2,4-Trichlorobenzene
Raoult's Law - Concentration calculated by Raoult's Law using mole fraction in NAPL.
UNIFAC - Concentration calculated by equation 2-11 using activity coefficients calculated by UNIFAC.

Figure 2-43. Comparison of measured aqueous concentrations to aqueous concentrations calculated by Raoult's Law and UNIFAC for chlorobenzene - 1,2,4-trichlorobenzene mixtures.

Data from Banerjee (1984).

2-44a

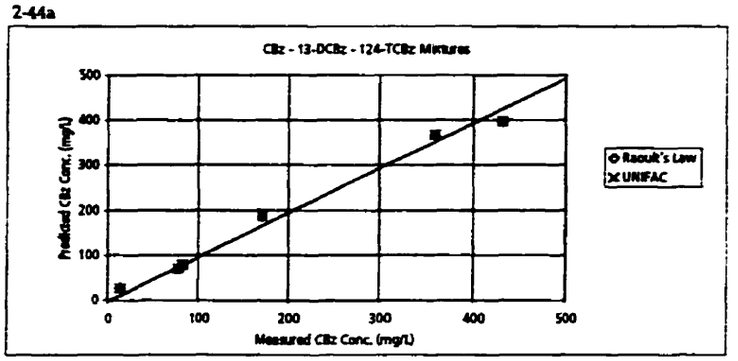

2-44b

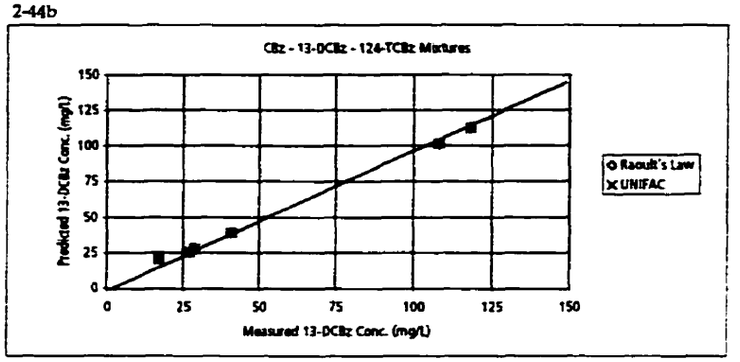

2-44c

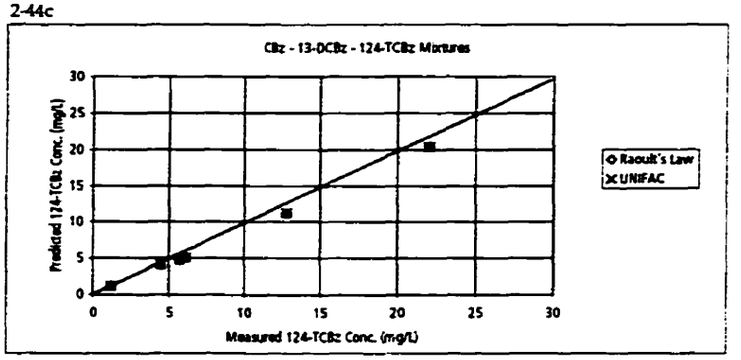

Key:
CBz - Chlorobenzene
13-DCBz - 1,3-Dichlorobenzene
124-TCBz - 1,2,4-Trichlorobenzene
Raoult's Law - Concentration calculated by Raoult's Law using mole fraction in NAPL.
UNIFAC - Concentration calculated by equation 2-11 using activity coefficients calculated by UNIFAC.

Figure 2-44. Comparison of measured aqueous concentrations to aqueous concentrations calculated by Raoult's Law and UNIFAC for chlorobenzene - 1,3-dichlorobenzene - 1,2,4-trichlorobenzene mixtures.

Data from Banerjee (1984).

2-45a

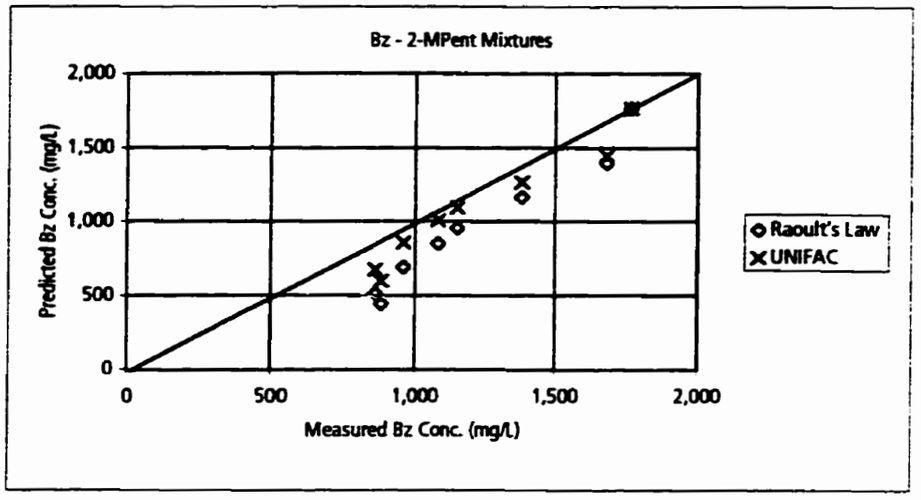

2-45b

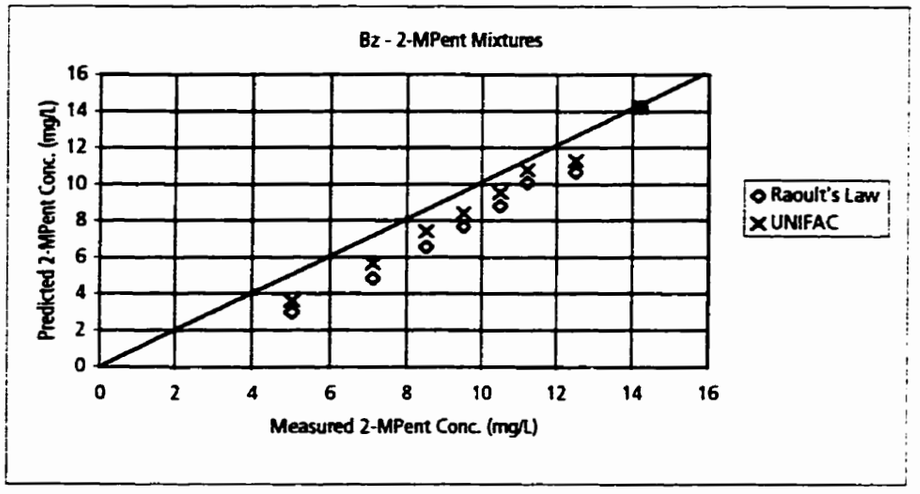

Key:
Bz - Benzene
2-MPent - 2-Methyl Pentane
Raoult's Law - Concentration calculated by Raoult's Law using mole fraction in NAPL.
UNIFAC - Concentration calculated by equation 2-11 using activity coefficients calculated by UNIFAC.

Figure 2-45. Comparison of measured aqueous concentrations to aqueous concentrations calculated by Raoult's Law and UNIFAC for benzene - 2-methyl pentane mixtures.

Data from Leinonen and Mackay (1973).

2-46a

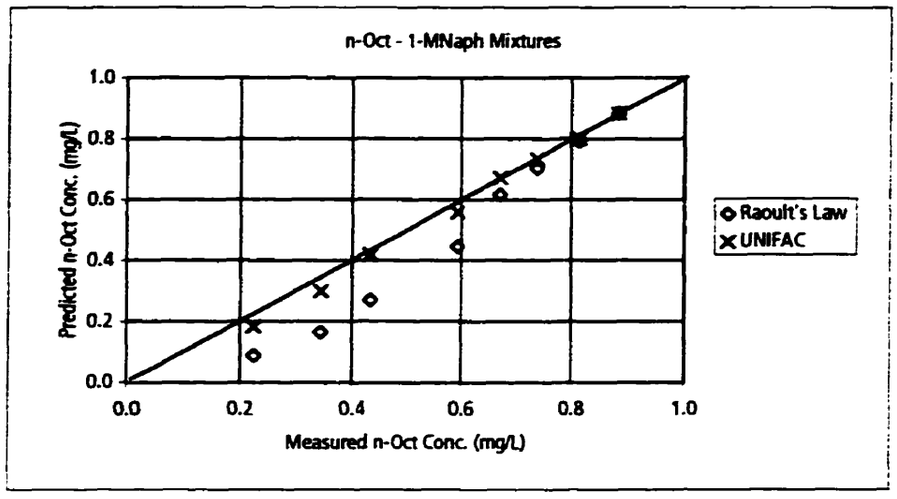

2-46b

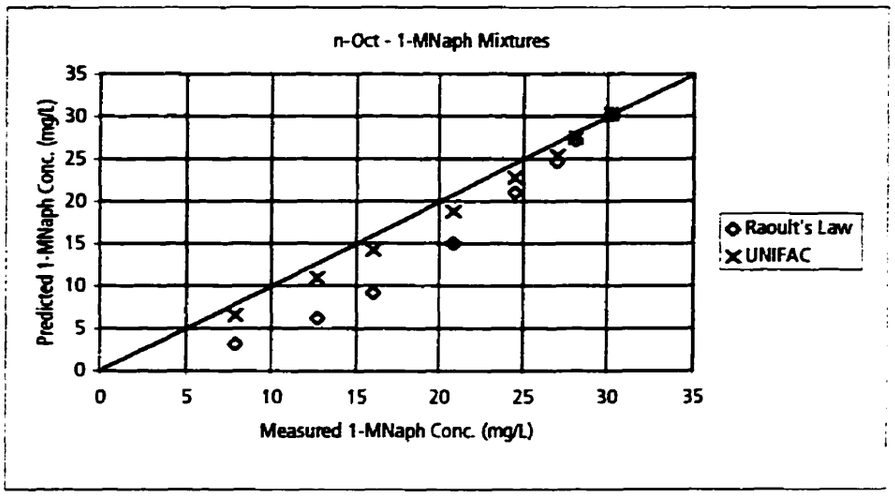

Key:
n-Oct - n-Octane
1-MNaph - 1-Methyl Naphthalene
Raoult's Law - Concentration calculated by Raoult's Law using mole fraction in NAPL.
UNIFAC - Concentration calculated by equation 2-11 using activity coefficients calculated by UNIFAC.

Figure 2-46. Comparison of measured aqueous concentrations to aqueous concentrations calculated by Raoult's Law and UNIFAC for n-octane - 1-methyl naphthalene mixtures.

Data from Burris and MacIntyre (1986a).

2-47a

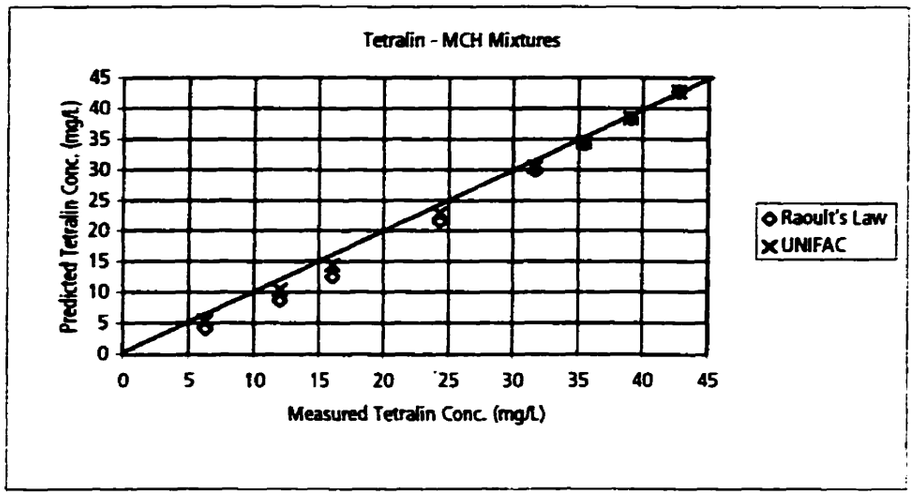

2-47b

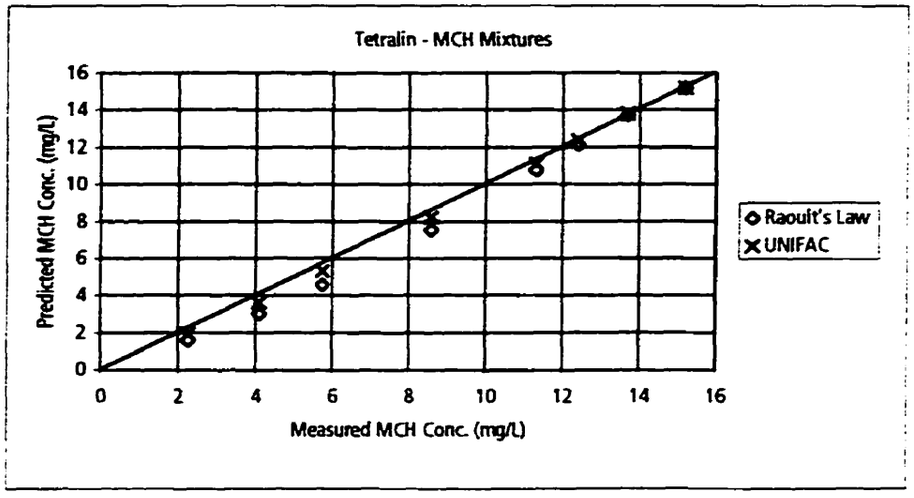

Key:
MCH - Methylcyclohexane
Raoult's Law - Concentration calculated by Raoult's Law using mole fraction in NAPL.
UNIFAC - Concentration calculated by equation 2-11 using activity coefficients calculated by UNIFAC.

Figure 2-47. Comparison of measured aqueous concentrations to aqueous concentrations calculated by Raoult's Law and UNIFAC for tetralin - methylcyclohexane mixtures.

Data from Burris and MacIntyre (1986a).

2-48a

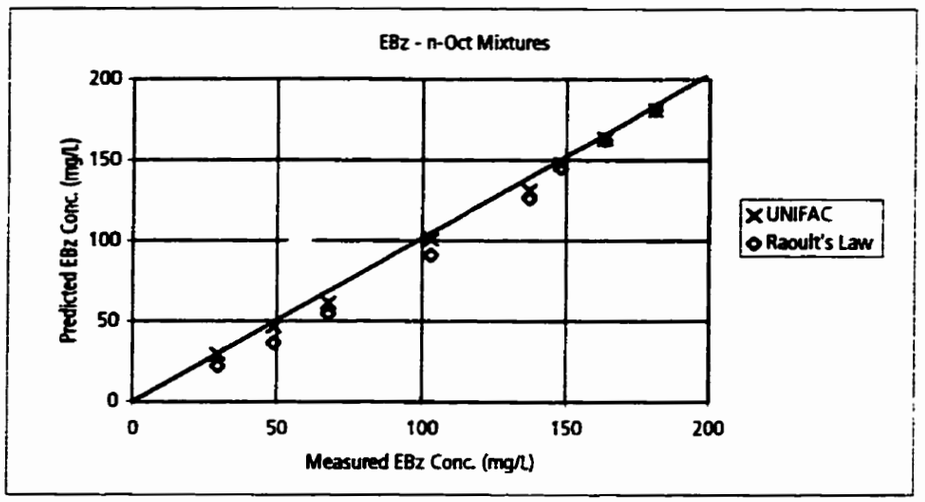

2-48b

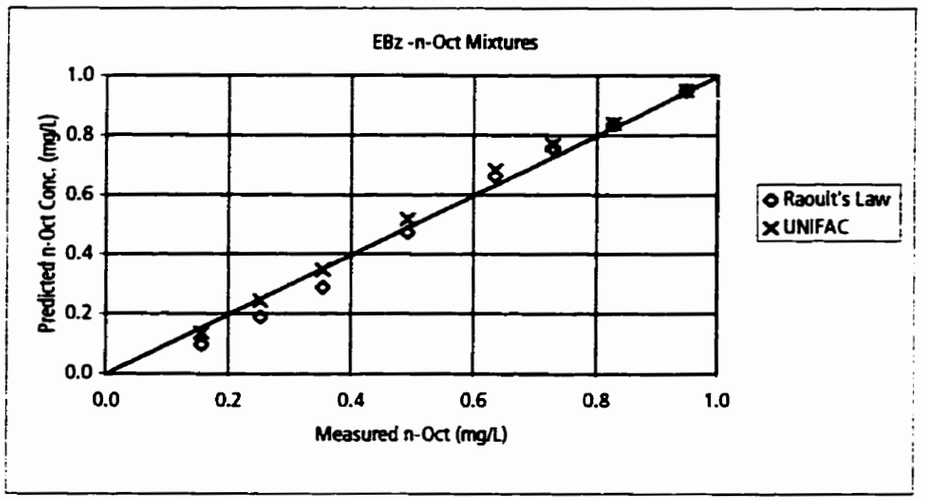

Key:
EBz - Ethyl Benzene
n-Oct - n-Octane
Raoult's Law - Concentration calculated by Raoult's Law using mole fraction in NAPL.
UNIFAC - Concentration calculated by equation 2-11 using activity coefficients calculated by UNIFAC.

Figure 2-48. Comparison of measured aqueous concentrations to aqueous concentrations calculated by Raoult's Law and UNIFAC for ethyl benzene - n-octane mixtures.

Data from Burris and MacIntyre (1986a).

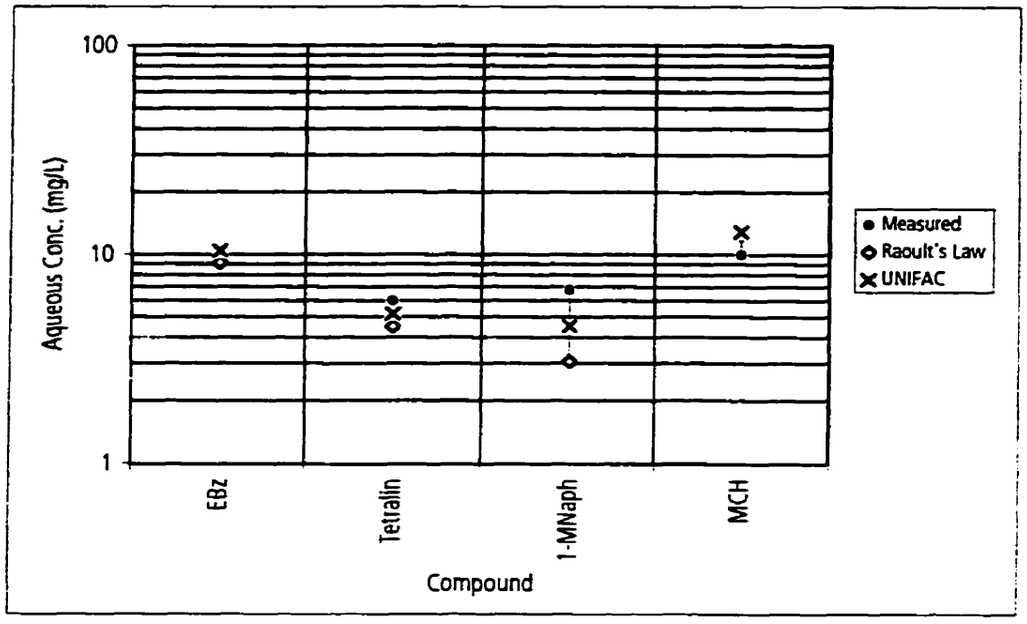

Key:
EBz - Ethyl Benzene MCH - Methylcyclohexane
1-MNaph - 1-Methyl Naphthalene
Raoult's Law - Concentration calculated by Raoult's Law using mole fraction in NAPL.
UNIFAC - Concentration calculated by equation 2-11 using activity coefficients calculated by UNIFAC.

Figure 2-49. Comparison of measured aqueous concentrations to aqueous concentrations calculated by Raoult's Law and UNIFAC for a 4-component hydrocarbon mixture.

Data from Burris and MacIntyre (1986b).

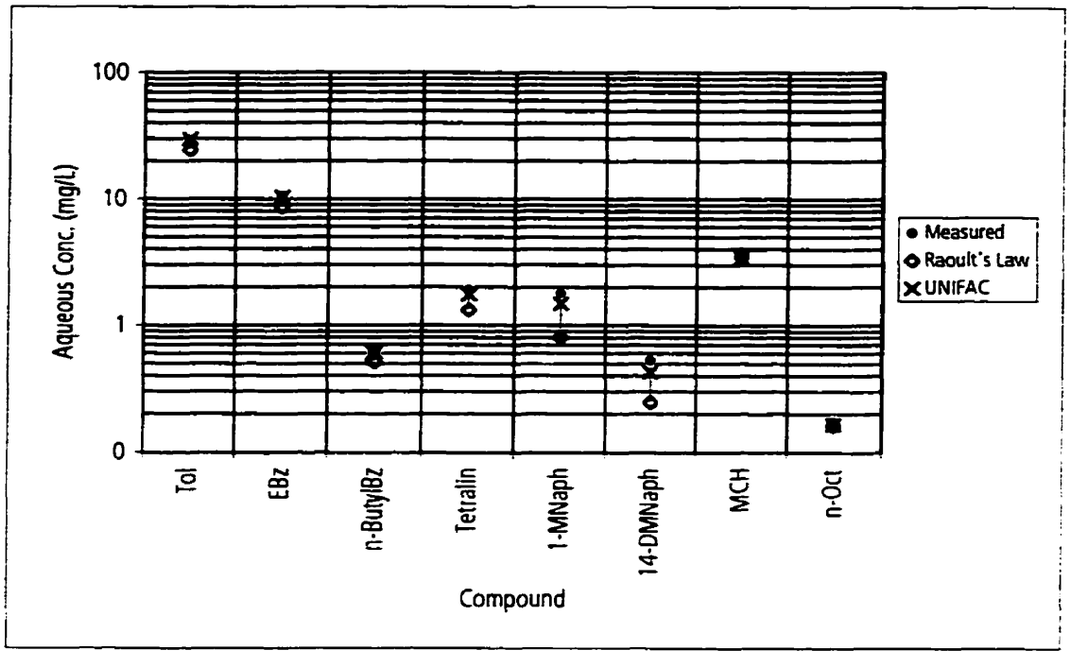

Key:
Tol - Toluene
EBz - Ethyl Benzene
n-ButylBz - n-Butyl Benzene
1-MNaph - 1-Methyl Naphthalene
14-DMNaph - 1,4-Dimethyl Naphthalene
MCH - Methylcyclohexane
n-Oct - n-Octane
Raoult's Law - Concentration calculated by Raoult's Law using mole fraction in NAPL.
UNIFAC - Concentration calculated by equation 2-11 using activity coefficients calculated by UNIFAC.

Figure 2-50. Comparison of measured aqueous concentrations to aqueous concentrations calculated by Raoult's Law and UNIFAC for a simulated JP-4 jet fuel mixture.

Data from Burris and MacIntyre (1986c).

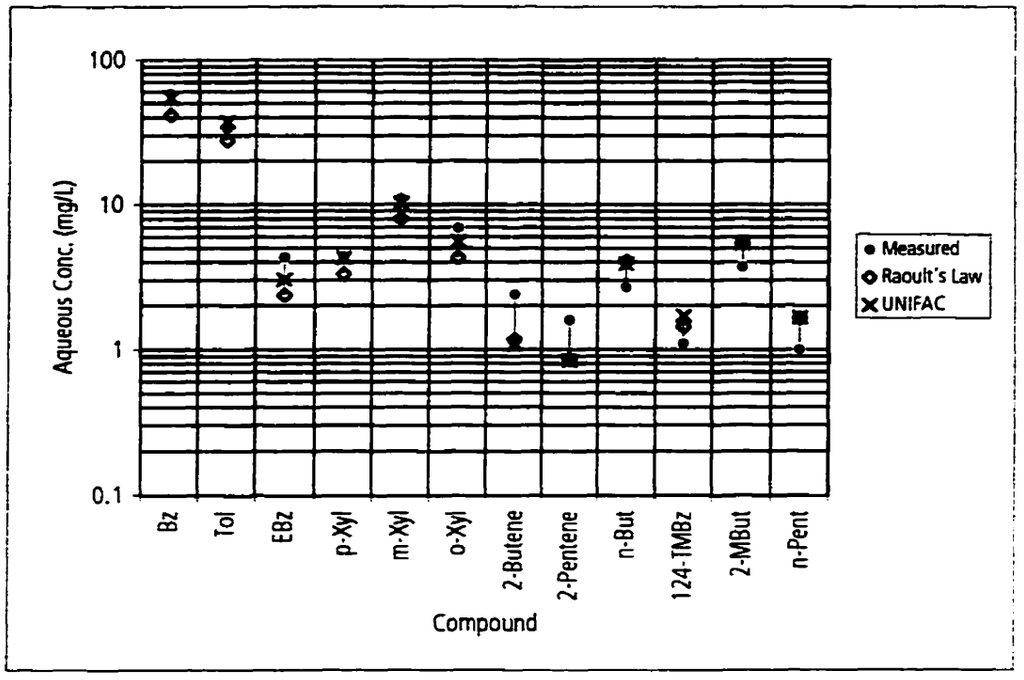

Key:

Bz - Benzene	o-Xyl - o-Xylene
Tol - Toluene	n-But - n-Butane
EBz - Ethyl Benzene	124-TMBz - 1,2,4-Trimethyl Benzene
p-Xyl - p-Xylene	2-MBut - 2-Methyl Butane
m-Xyl - m-Xylene	n-Pent- n-Pentane

Raoult's Law - Concentration calculated by Raoult's Law using mole fraction in NAPL.
UNIFAC - Concentration calculated by equation 2-11 using activity coefficients calculated by UNIFAC.

Figure 2-51. Comparison of measured aqueous concentrations to aqueous concentrations calculated by Raoult's Law and UNIFAC for a PS-6 gasoline.

Data from TRC (1985).

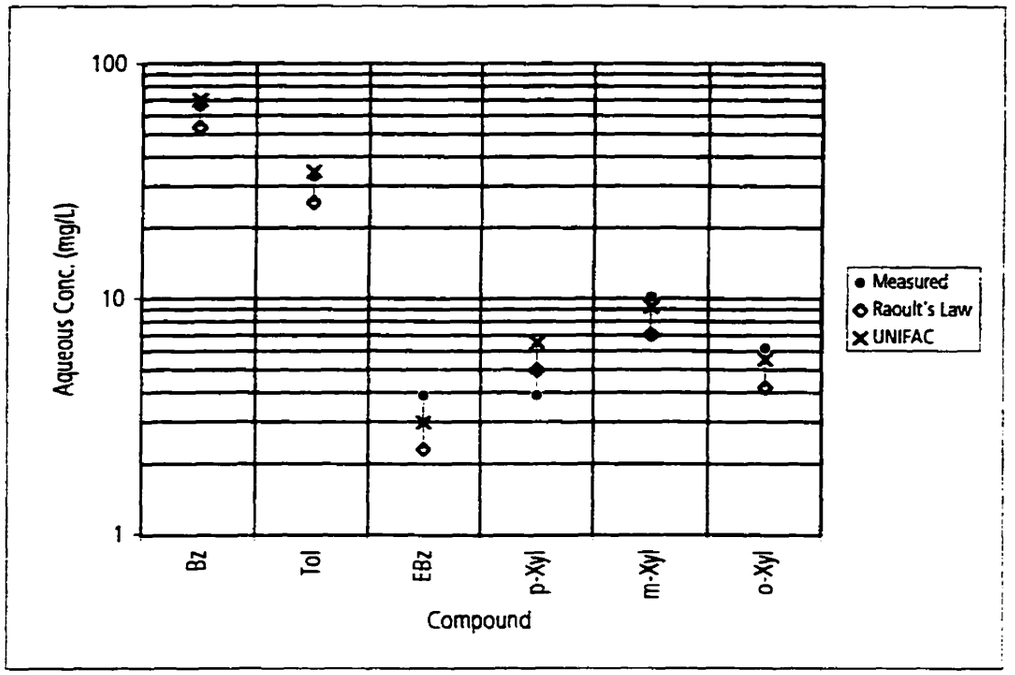

Key:
Bz - Benzene
Tol - Toluene
EBz - Ethyl Benzene
p-Xyl - p-Xylene
m-Xyl - m-Xylene
o-Xyl - o-Xylene
Raoult's Law - Concentration calculated by Raoult's Law using mole fraction in NAPL.
UNIFAC - Concentration calculated by equation 2-11 using activity coefficients calculated by UNIFAC.

Figure 2-52. Comparison of measured aqueous concentrations to aqueous concentrations calculated by Raoult's Law and UNIFAC for a PS-6 gasoline.

Data from Poulsen et al. (1992).

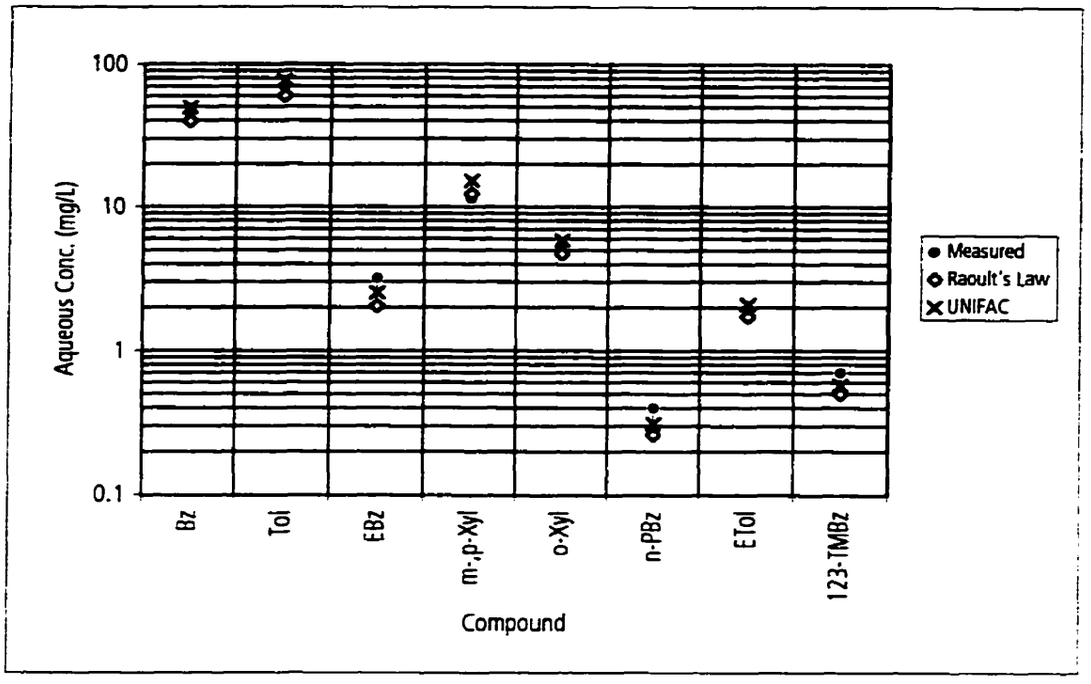

Key:

Bz - Benzene	o-Xyl - o-Xylene
Tol - Toluene	n-PBz - n-Propyl Benzene
EBz Ethyl Benzene	ETol - 3-, 4-Ethyl Toluene
m-,p-Xyl - m-Xylene + p-Xylene	123-TMBz - 1,2,3-Trimethyl Benzene

Raoult's Law - Concentration calculated by Raoult's Law using mole fraction in NAPL.
UNIFAC - Concentration calculated by equation 2-11 using activity coefficients calculated by UNIFAC.

Figure 2-53. Comparison of measured aqueous concentrations to aqueous concentrations calculated by Raoult's Law and UNIFAC for the average composition of 31 gasolines.

Data from Cline et al. (1991).

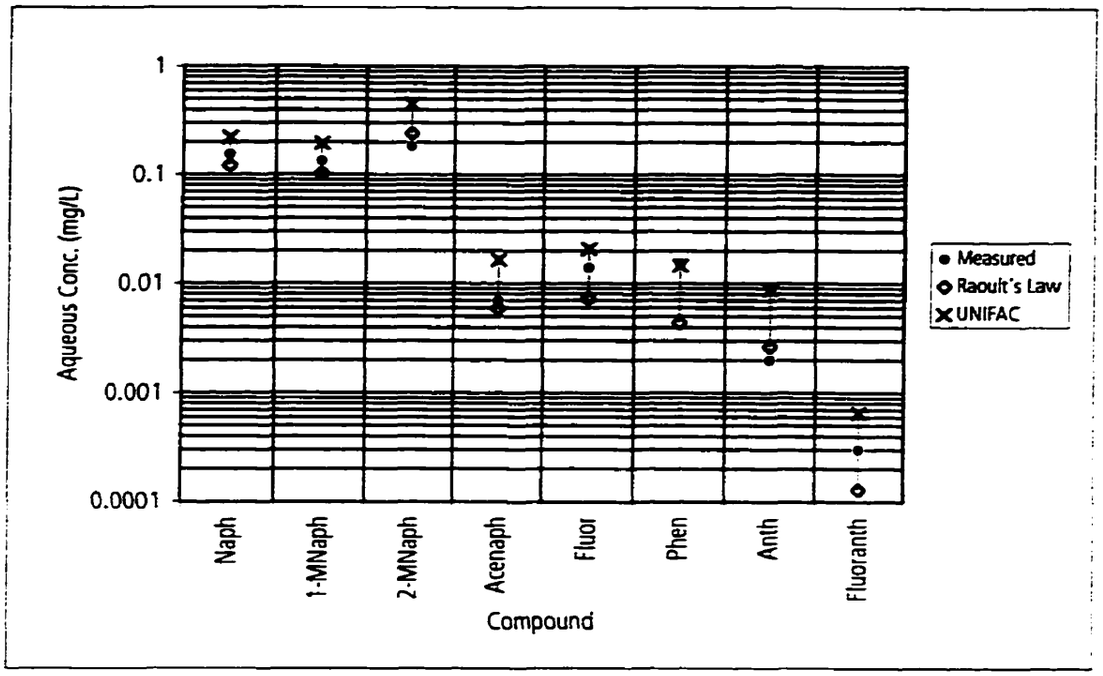

Key:

Naph - Naphthalene	Fluor - Fluorene
1-MNaph - 1-Methyl Naphthalene	Phen - Phenanthrene
2-MNaph - 2-Methyl Naphthalene	Anth - Anthracene
Acenaph - Acenaphthene	Fluoranth - Fluoranthene

Raoult's Law - Concentration calculated by Raoult's Law using mole fraction in NAPL.
UNIFAC - Concentration calculated by equation 2-11 using activity coefficients calculated by UNIFAC.

Figure 2-54. Comparison of measured aqueous concentrations to aqueous concentrations calculated by Raoult's Law and UNIFAC for a sample of diesel fuel (#1).

Data from Lee et al. (1992b).

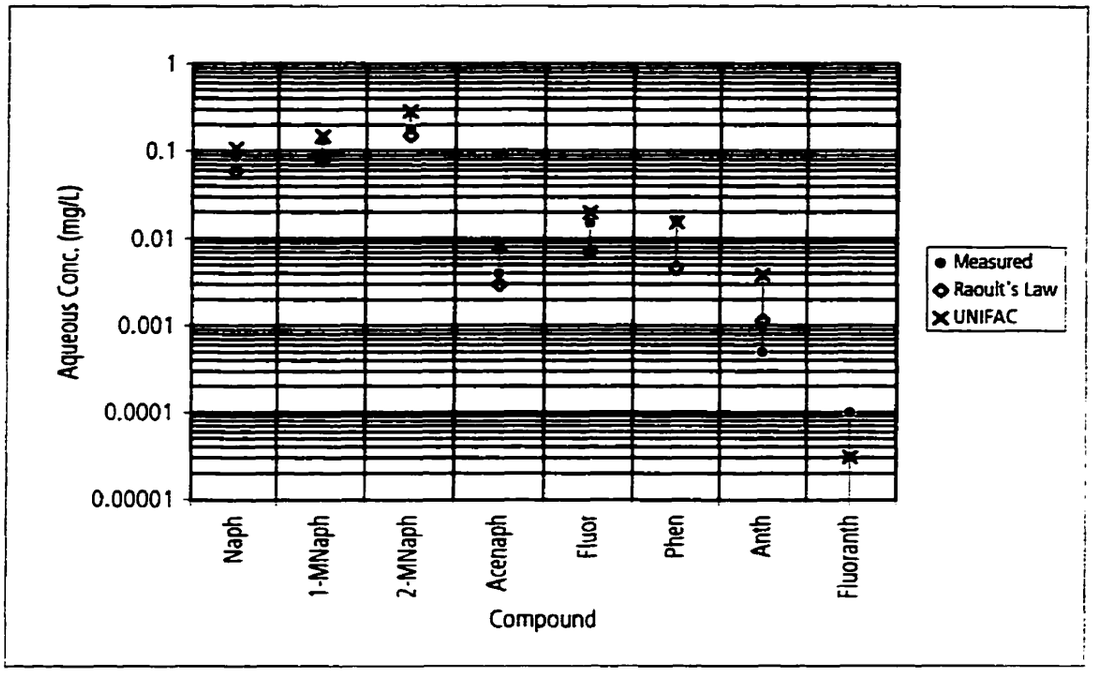

Key:

Naph - Naphthalene	Fluor - Fluorene
1-MNaph - 1-Methyl Naphthalene	Phen - Phenanthrene
2-MNaph - 2-Methyl Naphthalene	Anth - Anthracene
Acenaph - Acenaphthene	Fluoranth - Fluoranthene

Raoult's Law - Concentration calculated by Raoult's Law using mole fraction in NAPL.
UNIFAC - Concentration calculated by equation 2-11 using activity coefficients calculated by UNIFAC.

Figure 2-55. Comparison of measured aqueous concentrations to aqueous concentrations calculated by Raoult's Law and UNIFAC for a sample of diesel fuel (#2).

Data from Lee et al. (1992b).

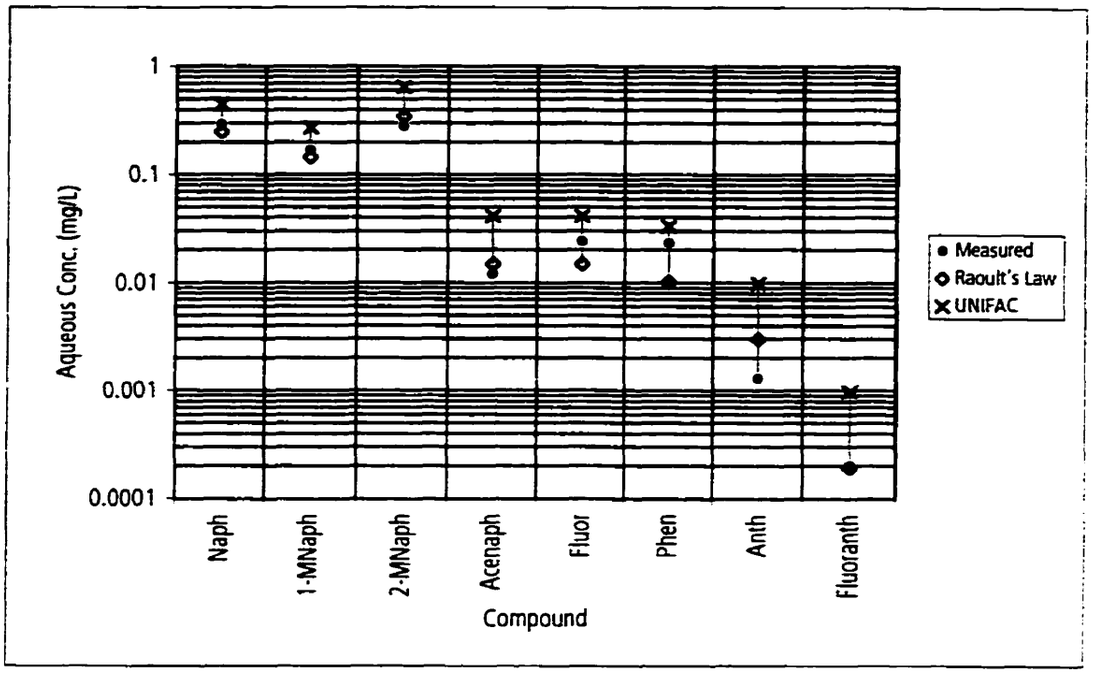

Key:

Naph - Naphthalene	Fluor - Fluorene
1-MNaph - 1-Methyl Naphthalene	Phen - Phenanthrene
2-MNaph - 2-Methyl Naphthalene	Anth - Anthracene
Acenaph - Acenaphthene	Fluoranth - Fluoranthene

Raoult's Law - Concentration calculated by Raoult's Law using mole fraction in NAPL.
UNIFAC - Concentration calculated by equation 2-11 using activity coefficients calculated by UNIFAC.

Figure 2-56. Comparison of measured aqueous concentrations to aqueous concentrations calculated by Raoult's Law and UNIFAC for a sample of diesel fuel (#3).

Data from Lee et al. (1992b).

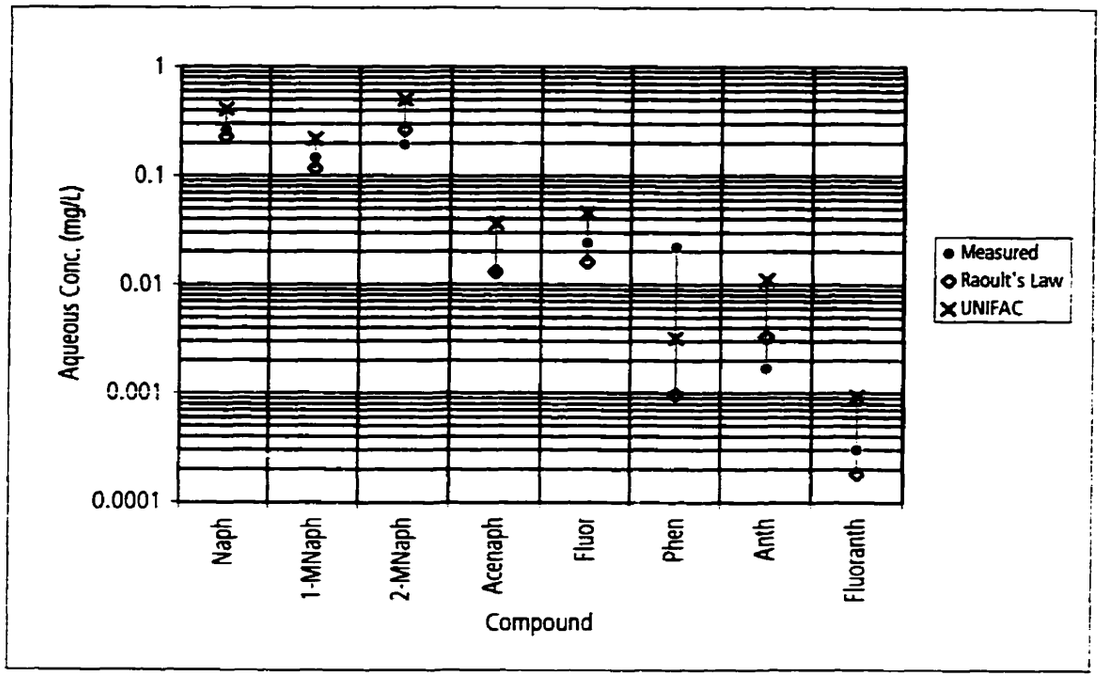

Key:

Naph - Naphthalene	Fluor - Fluorene
1-MNaph - 1-Methyl Naphthalene	Phen - Phenanthrene
2-MNaph - 2-Methyl Naphthalene	Anth - Anthracene
Acenaph - Acenaphthene	Fluoranth - Fluoranthene

Raoult's Law - Concentration calculated by Raoult's Law using mole fraction in NAPL.
UNIFAC - Concentration calculated by equation 2-11 using activity coefficients calculated by UNIFAC.

Figure 2-57. Comparison of measured aqueous concentrations to aqueous concentrations calculated by Raoult's Law and UNIFAC for a sample of diesel fuel (#4).

Data from Lee et al. (1992b).

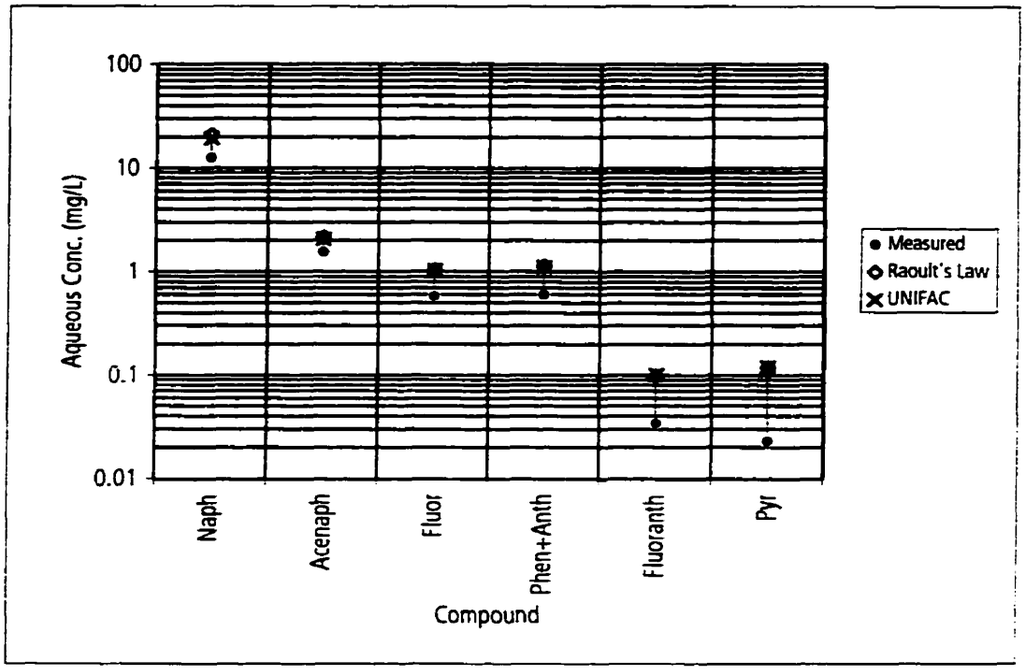

Key:

Naph - Naphthalene
Acenaph - Acenaphthene
Fluor - Fluorene
Phen+Anth - Phenanthrene + Anthracene
Fluoranth - Fluoranthene
Pyr - Pyrene

Raoult's Law - Concentration calculated by Raoult's Law using mole fraction in NAPL.
UNIFAC - Concentration calculated by equation 2-11 using activity coefficients calculated by UNIFAC.

Figure 2-58. Comparison of measured aqueous concentrations to aqueous concentrations calculated by Raoult's Law and UNIFAC for a sample of creosote.

Data from Priddle and MacQuarrie (1994).

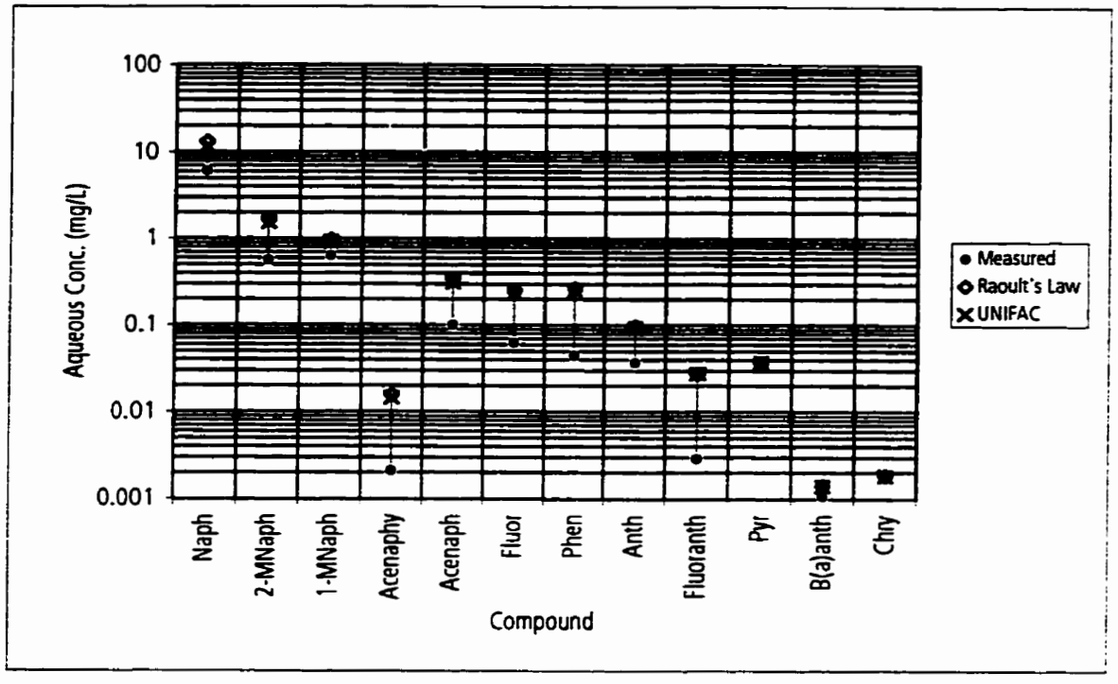

Key:

Naph - Naphthalene	Phen - Phenanthrene
2-MNaph - 2-Methyl Naphthalene	Anth - Anthracene
1-MNaph - 1-Methyl Naphthalene	Fluoranth - Fluoranthene
Acenaph - Acenaphthene	Pyr - Pyrene
Acenaphy - Acenaphthylene	B(a)anth - Benzo(a)anthracene
Fluor - Fluorene	Chry - Chrysene

Raoult's Law - Concentration calculated by Raoult's Law using mole fraction in NAPL.
UNIFAC - Concentration calculated by equation 2-11 using activity coefficients calculated by UNIFAC.

Figure 2-59. Comparison of measured aqueous concentrations to aqueous concentrations calculated by Raoult's Law and UNIFAC for a sample of coal tar (#1).

Data from Lee et al. (1992a).

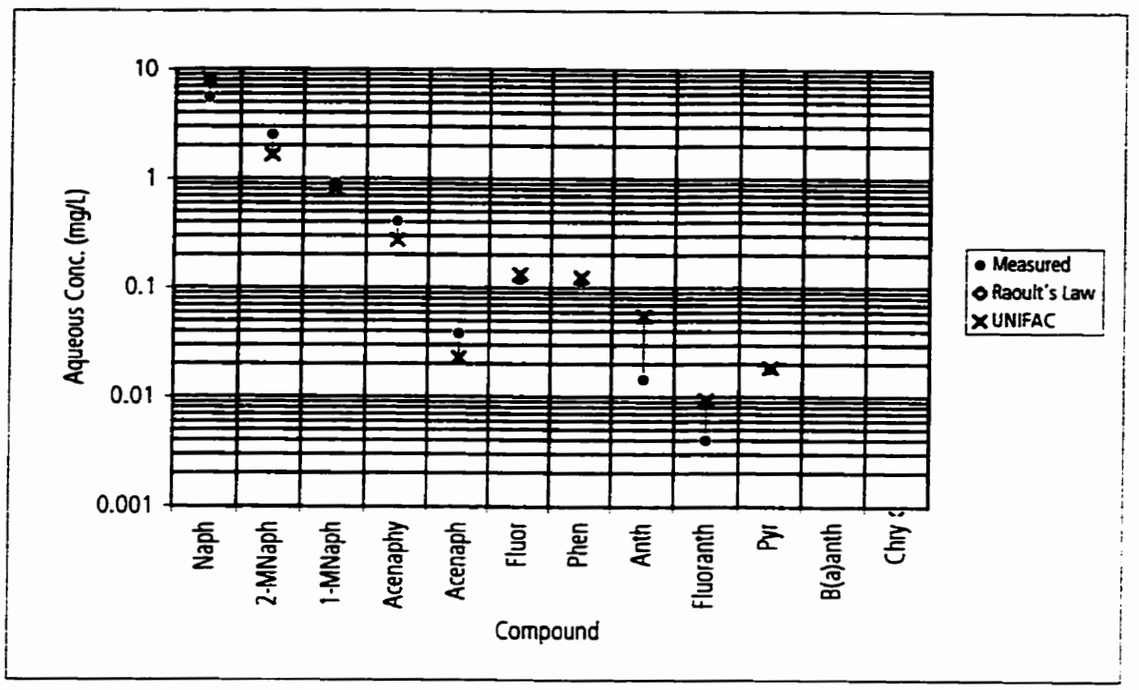

Key:

Naph - Naphthalene	Phen - Phenanthrene
2-MNaph - 2-Methyl Naphthalene	Anth - Anthracene
1-MNaph - 1-Methyl Naphthalene	Fluoranth - Fluoranthene
Acenaph - Acenaphthene	Pyr - Pyrene
Acenaphy - Acenaphthylene	B(a)anth - Benzo(a)anthracene
Fluor - Fluorene	Chry - Chrysene

Raoult's Law - Concentration calculated by Raoult's Law using mole fraction in NAPL.
UNIFAC - Concentration calculated by equation 2-11 using activity coefficients calculated by UNIFAC.

Figure 2-60. Comparison of measured aqueous concentrations to aqueous concentrations calculated by Raoult's Law and UNIFAC for a sample of coal tar (#4).

Data from Lee et al. (1992a).

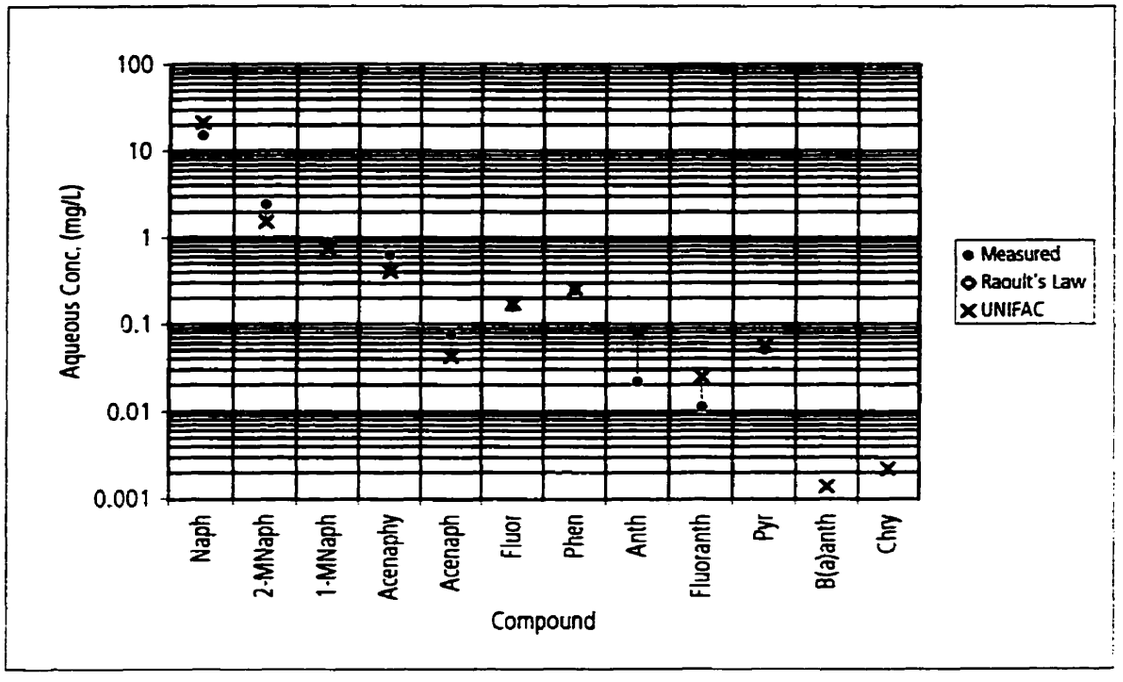

Key:

Naph - Naphthalene	Phen - Phenanthrene
2-MNaph - 2-Methyl Naphthalene	Anth - Anthracene
1-MNaph - 1-Methyl Naphthalene	Fluoranth - Fluoranthene
Acenaph - Acenaphthene	Pyr - Pyrene
Acenaphy - Acenaphthylene	B(a)anth - Benzo(a)anthracene
Fluor - Fluorene	Chry - Chrysene

Raoult's Law - Concentration calculated by Raoult's Law using mole fraction in NAPL.
UNIFAC - Concentration calculated by equation 2-11 using activity coefficients calculated by UNIFAC.

Figure 2-61. Comparison of measured aqueous concentrations to aqueous concentrations calculated by Raoult's Law and UNIFAC for a sample of coal tar (#5).

Data from Lee et al. (1992a).

2-62a

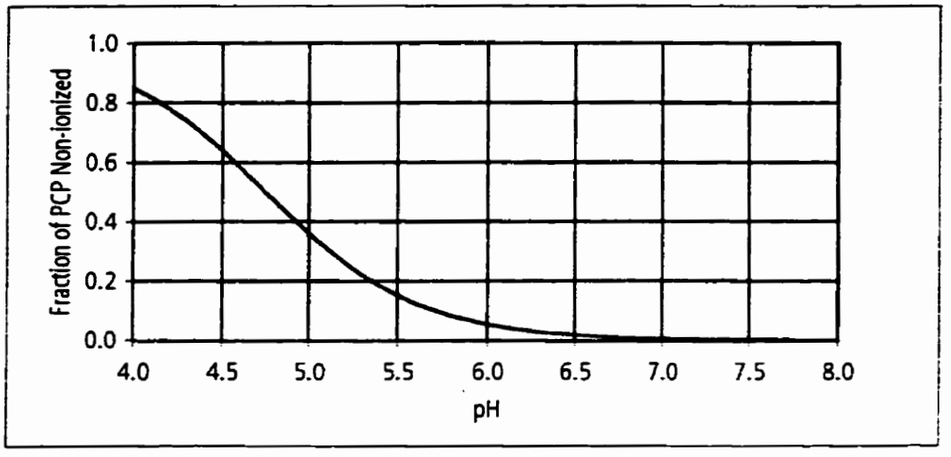

2-62b

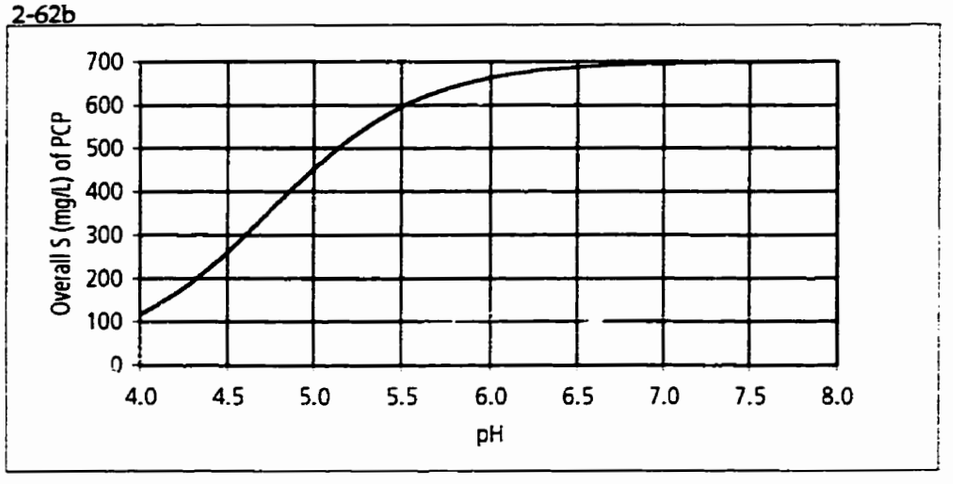

Solubility of non-ionized form	14	mg/L
Solubility of ionized form	700	mg/L
pKa	4.75	

Solubility of non-ionized form from Benvenue and Beckman (1963).
Solubility of ionized form estimated from Lee et al., (1990).

Figure 2-62. Solid-phase solubility of pentachlorophenol (PCP) versus pH.

File:PCP Solubility vs. pH/Sheet1

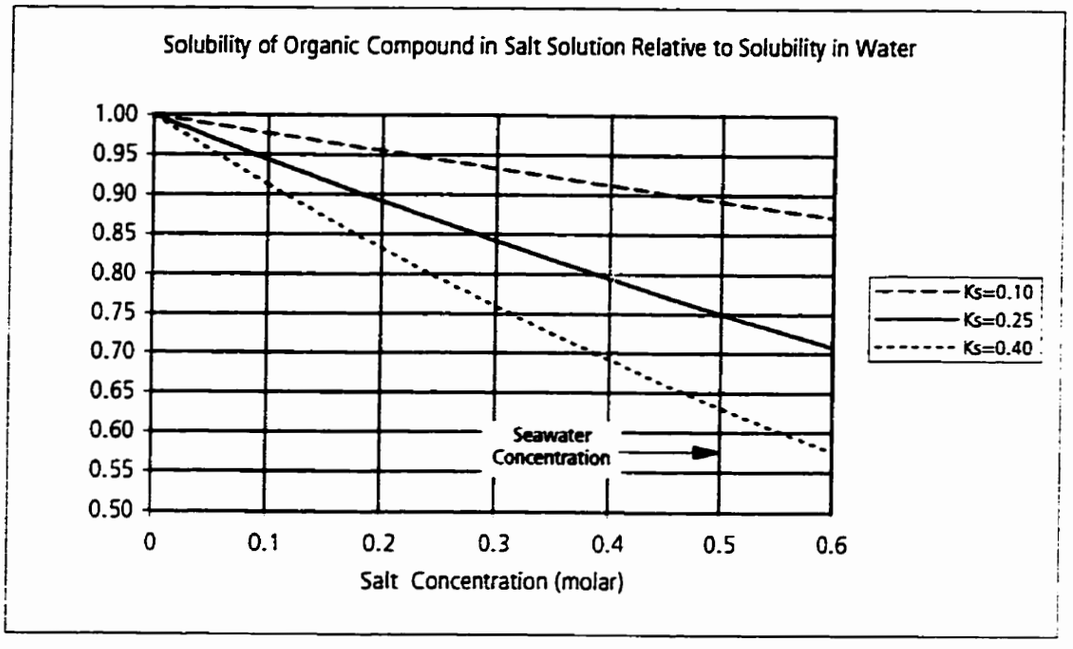

Figure 2-63. Solubility of organic compounds with increasing concentration of dissolved salts.

Seawater concentration 0.5 molar ~ 35,000 mg/L dissolved solids. Calculated from equation 2-21.

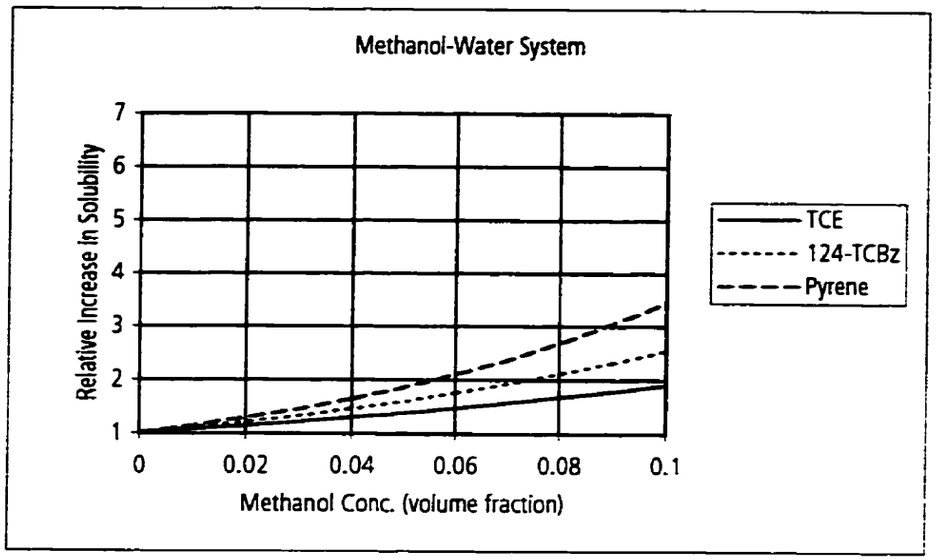

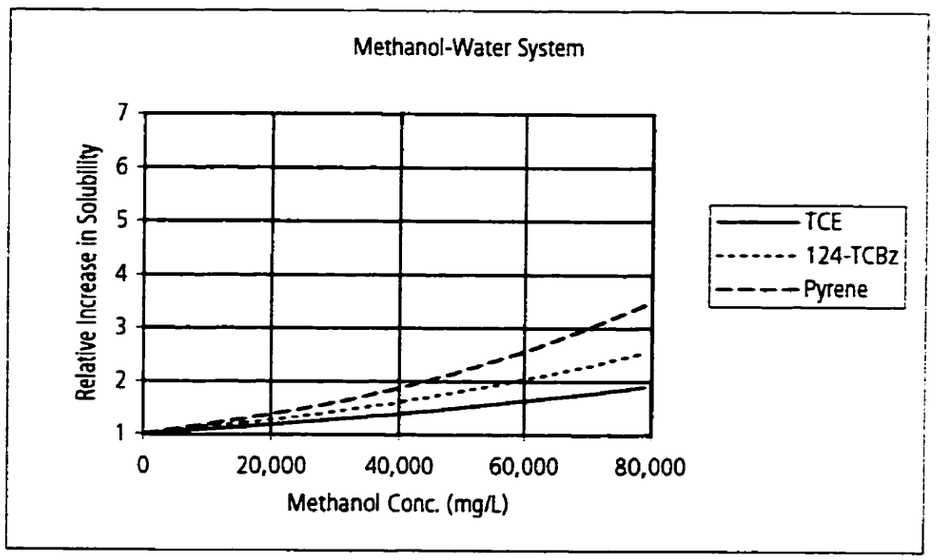

Figure 2-64. Increase in solubility of trichloroethylene (TCE), 1,2,4-trichlorobenzene (124-TCBz) and pyrene in a methanol-water system.

Solubility calculated based on method of Rao et al. (1985).

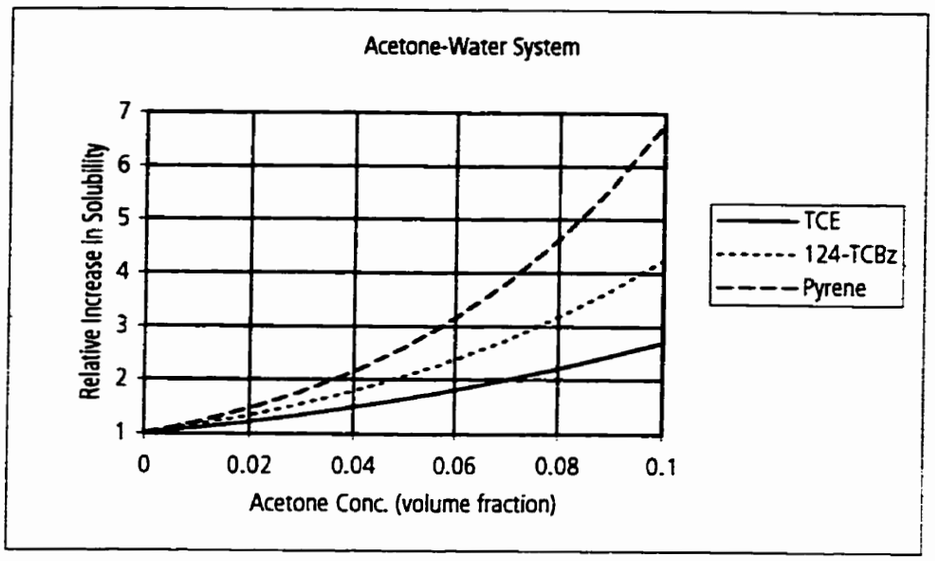

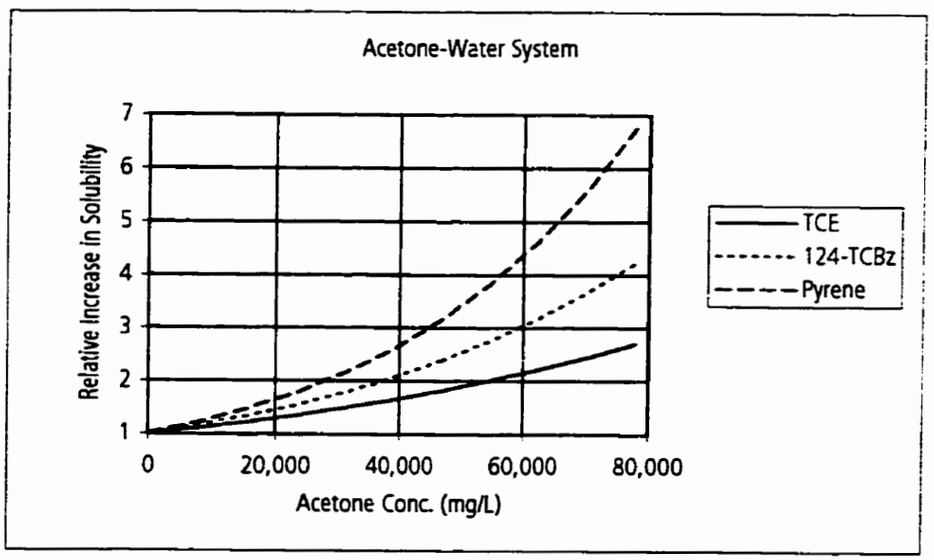

Figure 2-65. Increase in solubility of trichloroethylene (TCE), 1,2,4-trichlorobenzene (124-TCBz) and pyrene in an acetone-water system.

Solubility calculated based on method of Rao et al. (1985).

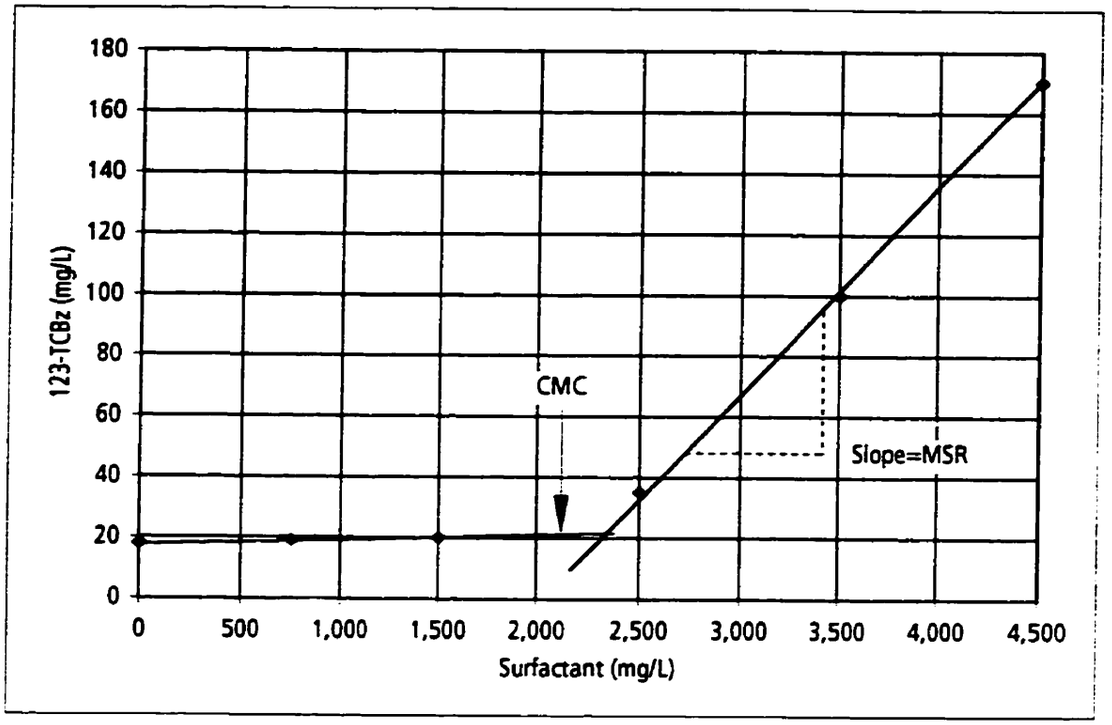

Key:
123-TCBz - 1,2,3-Trichlorobenzene
CMC - Critical micelle concentration = 2,100 mg/L for sodium dodecyl sulfate
MSR - Molar solubilization ratio

Figure 2-66. Example of the effect of the surfactant, sodium dodecyl sulfate, on the solubility of 1,2,3-trichlorobenzene.

Data from Kile and Chiou (1989).

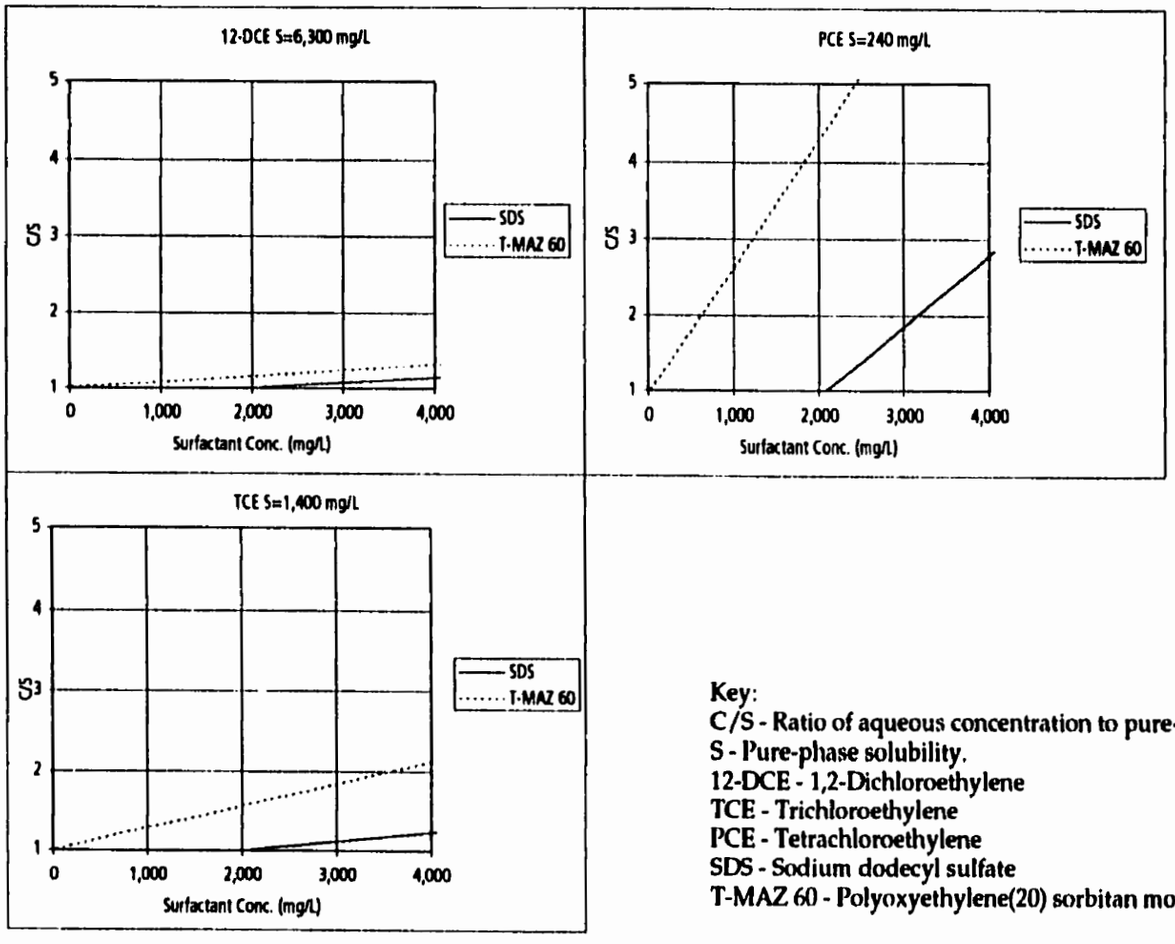

Key:
C/S - Ratio of aqueous concentration to pure-phase solubility.
S - Pure-phase solubility.
12-DCE - 1,2-Dichloroethylene
TCE - Trichloroethylene
PCE - Tetrachloroethylene
SDS - Sodium dodecyl sulfate
T-MAZ 60 - Polyoxyethylene(20) sorbitan monostearate

Figure 2-67. Increase in solubility of 1,2-dichloroethylene, trichloroethylene and tetrachloroethylene in the presence of various surfactants.

CMC for SDS = 2,100 mg/L, CMC for T-MAZ 60 = 28 mg/L
Curves calculated from Shiau et al. (1994).

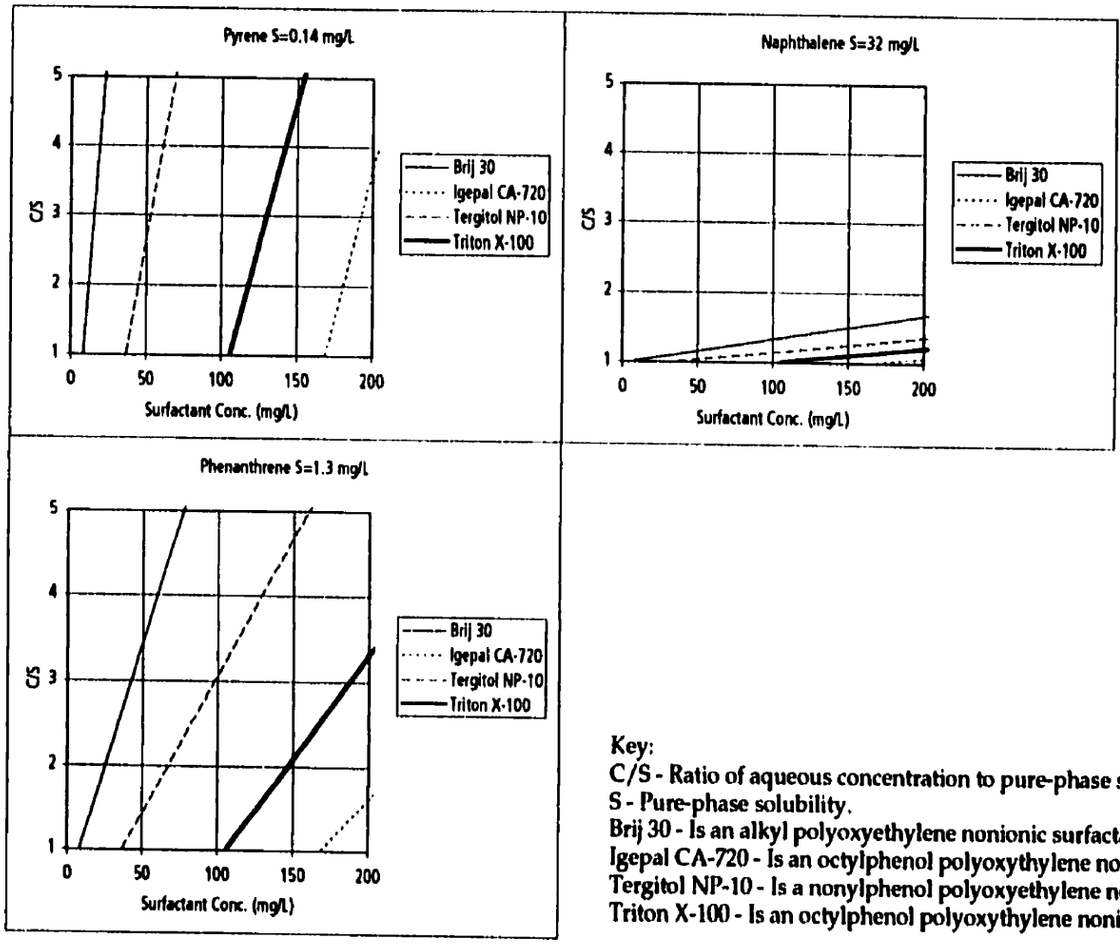

Key:
C/S - Ratio of aqueous concentration to pure-phase solubility.
S - Pure-phase solubility.
Brij 30 - Is an alkyl polyoxyethylene nonionic surfactant
Igepal CA-720 - Is an octylphenol polyoxythylene nonionic surfactant
Tergitol NP-10 - Is a nonylphenol polyoxyethylene nonionic surfactant
Triton X-100 - Is an octylphenol polyoxythylene nonionic surfactant

Figure 2-68. Increase in solubility of naphthalene, phenanthrene and pyrene in the presence of various surfactants.

CMC of Brij 30 = 8.3 mg/L, of Igepal CA-720 = 169 mg/L, of Tergitol NP-10 = 37 mg/L, of Triton X-100 = 106 mg/L
Curves calculated from Edwards et al. (1991).

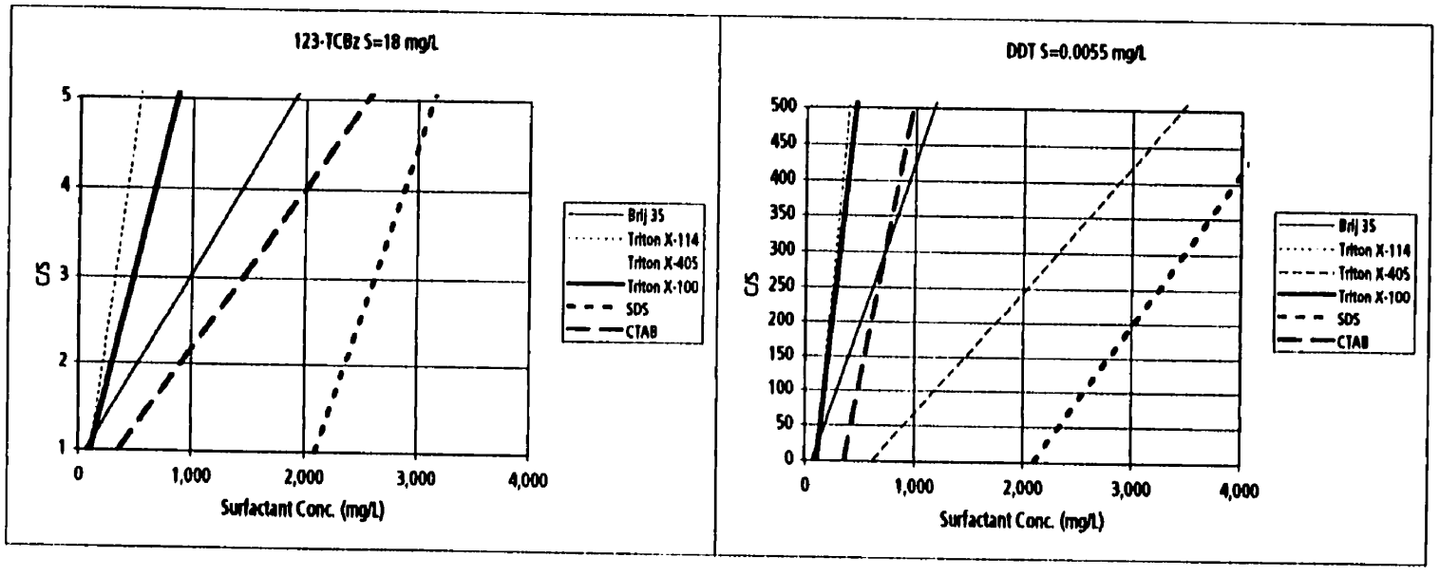

Key:
C/S - Ratio of aqueous concentration to pure-phase solubility
S - Pure-phase solubility
123-TCBz - 1,2,3-Trichlorobenzene
Brij 35 - Is an alkyl polyoxyethylene nonionic surfactant
Triton X-114 - Is a phenol polyoxythylene nonionic surfactant
Triton X-405 - Is a phenol polyoxythylene nonionic surfactant
Triton X-100 - Is an octylphenol polyoxythylene nonionic surfactant
SDS - Sodium dodecyl sulfate
CTAB - Cetyltrimethylammonium bromide

Figure 2-69. Increase in solubility of 1,2,3-trichlorobenzene and DDT in the presence of various surfactants.

CMC of Brij 35 = 74 mg/L, of Triton X-114 = 110 mg/L, of Triton X-405 = 620 mg/L, Triton X-100 = 130 mg/L, of SDS = 2,100 mg/L, of CTAB = 361 mg/L.

Curves calculated from Kile and Chiou (1989).

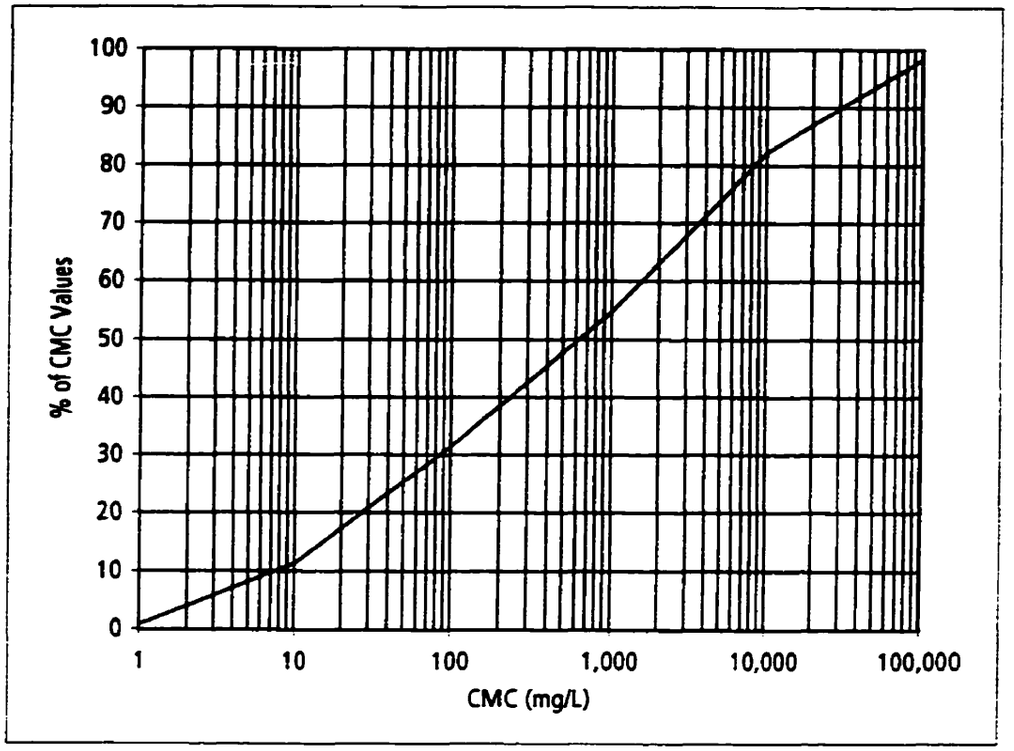

Key:
CMC - Critical micelle concentration

Figure 2-70. Values of CMC for a set of 125 typical surfactant compounds.

Data from Milton (1989).

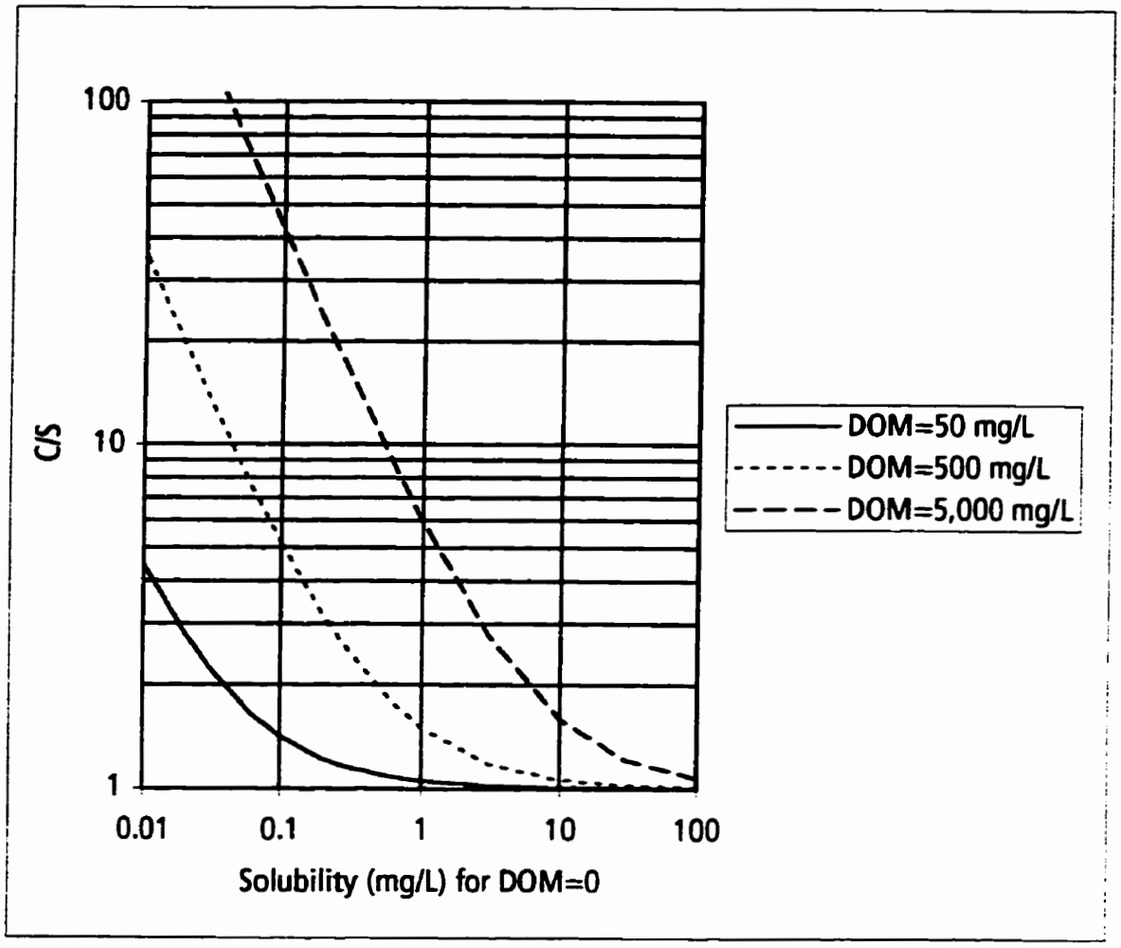

Key:
C/S - Ratio of aqueous concentration to pure-phase solubility
S - Pure-phase solubility
DOM - Dissolved organic matter

Figure 2-71. Increase in solubility of organic contaminants due to the presence of dissolved organic matter.

3. Principles for Dissolution of Multi-Component NAPL

3.1 Introduction

The dissolution of NAPL in groundwater involves the transfer of chemical mass from the NAPL into the surrounding groundwater. The rate of dissolution, or mass transfer, will influence the magnitude of aqueous chemical concentrations in the groundwater emitted from a NAPL source zone, as well as the length of time that a NAPL source zone will continue to contribute dissolved contaminants to the groundwater. As a result, NAPL dissolution has been the subject of considerable research in recent years. The following section describes the aspects of NAPL dissolution which are relevant to this examination of using aqueous concentrations ratios to estimate the chemical mass contained in NAPL zones.

3.2 Dissolution of NAPL Residual

In zones of residual NAPL, the NAPL occupies 5% to 20% or less of the total porosity. At these residual saturation values, the NAPL reduces but does not prevent the flow of groundwater through the NAPL zone. In sandy aquifers the permeability of the zone of NAPL residual to groundwater may be reduced, at most, by a factor of 2 to 3 times compared to the aquifer outside the NAPL zone (McWhorter and Kueper, 1996). As groundwater flows through the NAPL residual, a portion of the NAPL will be dissolved into the groundwater.

3.2.1 Pore-Scale Mass Transfer Models

Mass transfer across phase boundaries, such as NAPL-groundwater, has been a subject of study in the fields of fluid mechanics, chemical process engineering, surface water hydrology, heat transfer and, most recently, groundwater contamination. The rate of mass transfer across a NAPL-water interface is expressed typically as a function of a mass transfer coefficient, a

driving force, and an interfacial contact area between the NAPL and water, such as:

$$J = K_c \ \Delta C \ A_{NAPL} \qquad [3\text{-}1]$$

where :

J is the mass flux (in units of (M/T)

K_c is the mass transfer coefficient (L/T)

ΔC is the concentration difference (M/L^3)

A_{NAPL} is the interfacial area (L^2)

The driving force for mass transfer is the concentration difference across the interface and is usually expressed as the difference between the effective solubility of a NAPL component and the dissolved concentration in the bulk water flowing past the NAPL. The interfacial area of the NAPL residual is a function of the volume of NAPL contained in the pores and the geometric configuration of the NAPL globules and ganglia. The mass transfer coefficient is a function of the water flow conditions.

The mass transfer rate can be expressed also as the mass flux per unit area by:

$$N = K_c \ \Delta C \qquad [3\text{-}2]$$

where :

N is the mass flux per unit area ($M/T/L^2$)

K_c is the mass transfer coefficient (L/T)

ΔC is the concentration difference (M/L^3)

Several models have been described in the literature which attempt to describe this pore-scale mass transfer. These models include: the Stagnant Film Model (Nernst, 1904), the Penetration Model (Higbie, 1935) and the

Random Surface Renewal Model (Dankwerts, 1951). Each of these models assume that there is a resistance to mass transfer caused by the presence of a stagnant or partially mixed boundary layer between the NAPL and the flowing water.

In the case of the Stagnant Film Model, mass transfer from the NAPL to the flowing water occurs by aqueous-phase diffusion across a stagnant boundary layer according to:

$$N = D \frac{(C_i - Cw)}{\delta} \qquad [3\text{-}3]$$

so that:

$$K_c = \frac{D}{\delta} \qquad [3\text{-}4]$$

where :

N *is the mass flux per unit area* $(M/T/L^2)$

D *is the diffusion coefficient* (L^2/T)

K_c *is the mass transfer coefficient* (L/T)

C_w *is the concentration in the flowing water* (M/L^3)

C_i *is the effective solubility* (M/L^3)

δ *is the thickness of the boundary layer* (L)

For this model, the boundary layer thickness is an empirical parameter that accounts for water flow conditions such as fluid viscosity and velocity. The boundary layer thickness must be calculated for a specific set of conditions from experimental data.

The Penetration Model assumes that there is some degree of mixing within the boundary layer. In this case, an imaginary element of water moves from the flowing water through the boundary layer to the NAPL

interface. For some time period, the water element remains in contact with the NAPL allowing diffusive mass transfer from the NAPL to the element. This model is described by:

$$K_c = 2\sqrt{\frac{D}{\pi\ t}} \qquad [3\text{-}5]$$

where :

D is the diffusion coefficient (L^2 /T)

t is the contact time (T)

For this model, the contact time is an empirical parameter that accounts for water flow conditions. The contact time must be calculated for a specific set of conditions from experimental data.

The Random Surface Renewal Model assumes also that there is some degree of mixing within the boundary layer. In this case, imaginary elements of water move from the flowing water through the boundary layer to the NAPL interface. The water elements remain in contact with the NAPL for a range of times, allowing diffusive mass transfer from the NAPL to the element. This model is described by:

$$K_c = \sqrt{s\ D} \qquad [3\text{-}6]$$

where :

D is the diffusion coefficient (L^2 /T)

s is the rate of surface renewal (1/T)

For this model, the rate of surface renewal is an empirical parameter that accounts for water flow conditions. The rate of surface renewal must be calculated for a specific set of conditions from experimental data.

Although these three models provide different formulations for mass transfer, in all cases, the mass transfer coefficient is related directly to, or related to the square root of, the diffusion coefficient.

The scientific literature reports relatively few measurements of aqueous-phase diffusion coefficients for common organic contaminants in groundwater. However, there are a variety of empirical relationships that can be used to estimate diffusion coefficients of solutes in water. A relationship used widely in the field of chemical engineering (Perry's Chemical Engineering Handbook, 1984) is:

$$D = 7.4x10^{-8} \left[\frac{\sqrt{\phi \ MM_w} \ T}{\mu \ MV^{0.6}} \right] \qquad [3\text{-}7]$$

where :

D is the diffusion coefficient (cm^2/s)

ϕ is an association constant for water = 2.6

MM_w is the molecular mass of water (g/mol)

T is the temperature (K)

μ is the viscosity of water (cP)

MV is the molar volume of the solute (cm^3/mol)

Using this relationship, the aqueous-phase diffusion coefficient was calculated for a selection of organic contaminants common in groundwater. These values are shown in Table 3-1. The calculated value of 9.6×10^{-6} cm^2/s for benzene compares closely with the value of 1.0×10^{-5} cm^2/s measured by Bonolli and Witherspoon (1968). Diffusion coefficients are higher for lower molecular weight compounds and lower for higher molecular weight compounds, but the differences between compounds are only about 10% to 20%. Because there are only small differences between the aqueous-phase

diffusion coefficients, the mass transfer coefficients for different components in a multi-component NAPL will be similar.

Because the diffusion coefficients of most common groundwater contaminants are similar, the mass transfer coefficients for different components of many multi-component NAPL should be similar also. Based on these simple mass transfer models, the overall rates of mass transfer of different components of a NAPL and their aqueous concentrations should be determined primarily by the effective solubility of each component (see equation 3-1). The effective solubility of the NAPL components is determined by the NAPL composition.

In this way, the aqueous contaminant concentrations emitted from a multi-component NAPL will reflect the composition of the NAPL. Changes in the NAPL composition due to preferential dissolution of higher-solubility components will, in turn, be reflected in the aqueous concentrations emitted from the NAPL source.

3.2.2 Laboratory-Scale Mass Transfer Models

For a given volume of porous medium containing NAPL, it may be possible to determine the overall rates of mass transfer experimentally. However, it is extremely difficult to determine the NAPL-water interfacial area to allow calculation of the mass transfer coefficient according to equation 3-1. As a result, it is common practice to define the overall mass transfer rate is terms of a lumped mass transfer coefficient which incorporates the interfacial area as:

$$\lambda = K_c \frac{A_{NAPL}}{V} \qquad [3\text{-}8]$$

so that:

$$J = \lambda (C_i - C_w) \qquad [3\text{-}9]$$

where :

λ *is the lumped mass transfer coefficient (1/T)*

K_c *is the mass transfer coefficient (L/T)*

A_{NAPL} *is the interfacial area* (L^2)

V *is a representative volume of porous medium* (L^3)

J *is the mass flux (M/T)*

C_w *is the concentration in the flowing water* (M/L^3)

C_i *is the effective solubility* (M/L^3)

In recent years, numerous researchers have performed laboratory dissolution experiments and mathematical analyses to attempt to develop models that can predict the rate of mass transfer, and the resulting groundwater concentrations, for single-component NAPL residual in porous media. From the results of a laboratory experiment, a lumped mass transfer coefficient is determined. However, the value for the lumped mass transfer coefficient will be specific to the particular soil, NAPL residual saturation and water flow condition. The lumped mass transfer coefficient will vary depending on the pore structure of the soil, the volume and geometric configuration of NAPL residual and the water velocity. The lumped mass transfer coefficient will decline also as dissolution proceeds and NAPL residual is depleted.

In most cases, researchers have attempted to describe the results of laboratory experiments by means of correlation equations of dimensionless parameters. These empirical equations relate the observed mass transfer coefficients to parameters describing characteristics of the soil and water flow conditions. One such correlation equation developed by Miller et al., 1990, related the Sherwood Number (a dimensionless measure of the mass transfer rate), to the Reynolds Number (a dimensionless measure of the water flow

conditions), the NAPL saturation, and Schmidt Number (a dimensionless ratio of advective to diffusive mass transport).

$$Sh = \frac{\lambda (d_{50})^2}{D} = 12\, Re^{0.75} (\theta_{NAPL})^{0.6} Sc^{0.5} \qquad [3\text{-}10]$$

where :

Sh is the Sherwood Number

λ is the lumped mass transfer coefficient

d_{50} is the median grain diameter

D is the diffusion coefficient

Re is the Reynolds Number $= \frac{d_{50} q \rho}{\mu}$

q is the Darcy velocity

ρ is the water density

μ is the water viscosity

θ_{NAPL} is the NAPL saturation expressed as a fraction of the pore space

Sc is the Schmidt Number $= \frac{\mu}{\rho D}$

Although this correlation equation described adequately the toluene dissolution experiments by Miller et al. (1990), it could not describe subsequent experiments with styrene and TCE (Powers et al., 1992; Geller and Hunt, 1993), with hydrocarbon mixtures (Parker et al., 1991) or with TCE (Imhoff et al., 1993) in different soil materials. Similarly, none of the comparable correlation equations developed for these other studies could describe dissolution adequately beyond their specific experimental conditions.

However, the formulations of all these correlation models suggest that, for a given NAPL residual and water flow condition, the mass transfer coefficients for different NAPL compounds should be similar provided the diffusion coefficient values are similar. Powers et al., (1992) examined

dissolution of TCE and styrene in different experiments for the same sand under similar water flow conditions. Diffusion coefficients for TCE and styrene differ by only 10% and the mass transfer coefficients determined experimentally for TCE and styrene were similar.

Recent laboratory experiments conducted by Mukherji et al. (1997) determined the mass transfer coefficients for toluene and eight different PAH compounds during dissolution of coal tar NAPL. This study found that mass transfer coefficients for individual compounds ranged from 1.2×10^{-3} cm/s to 1.9×10^{-3} cm/s but there was no statistically significant difference between the compounds (see Table 3-2). The diffusion coefficients for the individual compounds differed from each other by 25% or less so that mass transfer coefficients would be expected to be similar.

The results of both pore-scale mass transfer models and laboratory-scale dissolution models suggest that mass transfer coefficients for different components of a multi-component NAPL should be similar. As a result, the aqueous contaminant concentrations emitted from the NAPL residual zone should be determined primarily by the effective solubility of the components, for a given NAPL zone and set of water flow conditions.

3.3 Non-Equilibrium Mass Transfer for Multi-Component NAPL

Despite the fact that dissolution models developed from specific laboratory experiments are not yet capable of general predictions of the rate of mass transfer under differing conditions, these experiments have provided general insights on the relationship between water velocity and the magnitude of dissolved concentrations emitted from a zone of NAPL residual. For initial NAPL saturations of 5% to 20% of the pore space, used typically in these experiments, aqueous concentrations increase to their solubility limit rapidly. A useful measure of the speed of equilibration is the

residence time for water in the NAPL zone. The residence time is a function of the length of the NAPL zone and the water velocity.

In laboratory column experiments for the dissolution of iso-octane, Fried et al. (1979) found that water reached the solubility limit after a residence time of about 15 minutes. For dissolution of toluene (Miller et al., 1990), the solubility limit was reached after residence times of 30 to 40 minutes. For dissolution of TCE and styrene (Powers et al., 1992; Powers et al., 1994), the solubility limits were reached after residence times 5 to 10 minutes. For dissolution of TCE (Imhoff et al., 1993), the solubility limit was reached after residence times of about 15 minutes. Aqueous concentrations decline from solubility limits as the residence time decreases in response to depletion of the NAPL.

These studies indicate that aqueous concentrations would be expected at the solubility limit in groundwater exiting NAPL zones which are more than a few centimetres in length, at typical groundwater velocities of a metre per day, or less. The fact that concentrations of dissolved contaminants at the solubility limit are infrequently observed in field settings is likely a reflection of dilution effects from spatial variability in NAPL distributions, long monitoring well intakes, and dispersion in aquifers.

These same dilution effects will make the detailed study of NAPL dissolution and mass transfer very difficult in field settings. Because of uncertainty in the exact size and geometry of NAPL residual zones, and the unknown degree of dilution reflected in the contaminant concentrations found in monitoring wells, it will not be possible to relate the magnitude of aqueous concentrations in the groundwater to the composition of the NAPL source zone. However, because dilution affects all dissolved contaminants to the same degree, information about the composition of the NAPL source reflected in the ratios of aqueous concentrations should be preserved despite dilution processes.

Laboratory dissolution experiments have indicated also that the rates of mass transfer may be limited under conditions of high groundwater velocity or low NAPL residual saturation. In such circumstances, the aqueous concentrations emitted from a NAPL residual zone will be lower than their effective solubility limits. However, based on pore-scale and laboratory-scale dissolution models, such non-equilibrium mass transfer effects should influence the magnitude of the aqueous concentrations of different NAPL components to the same degree. As a result, the aqueous concentration ratios emitted during non-equilibrium mass transfer should still reflect the composition of the NAPL.

Burris and MacIntyre reported a series of shake-flask dissolution experiments which can be used to illustrate that aqueous concentration ratios remain constant for different NAPL components during dissolution under non-equilibrium conditions. Burris and MacIntyre (1985) evaluated the time to achieve the solubility limits for a NAPL mixture of methylcyclohexane (MCH) and 1-methyl naphthalene (1-MNaph). These data are shown in Figure 3-1. Burris and MacIntyre (1986b) evaluated the time to achieve the solubility limits for a NAPL mixture of methylcyclohexane, ethyl benzene (EBz), tetralin (THN) and 1-methyl naphthalene. These data are shown in Figure 3-2. Burris and MacIntyre (1986c) evaluated the time to achieve the solubility limits for a NAPL mixture of methylcyclohexane and 1-methyl naphthalene. These data are shown in Figure 3-3.

The results of each of these experiments illustrate that the aqueous concentrations ratios (relative concentration) of the components are constant during the approach to the solubility limit at equilibrium. For example, as shown in Figure 3-1, the relative concentrations of methycyclohexane and 1-methyl naphthalene remain at about 53% and 47%, respectively (or expressed as a methylcyclohexane: 1-methyl naphthalene ratio of 1.1). The relative concentration of the components remains the same, as determined by their respective effective solubilities, despite the fact that the total dissolved

concentrations increase from 4% of their solubility limits to 100% during the dissolution experiment.

3.4 Chromatographic Effect in Multi-Component NAPL Residual Zones

For dissolution of multi-component NAPL in short-length laboratory column experiments or shake-flask experiments, the composition of the NAPL may change with time but is relatively homogeneous at any point in time. However, at real sites of NAPL contamination, the flow path of groundwater through the NAPL residual zone may be sufficiently long that the aqueous concentrations and NAPL composition in the upgradient portion of the NAPL zone may differ from those in the downgradient portion of the NAPL zone. Aqueous concentrations emitted from the upgradient portion of the NAPL residual may be modified by chemical exchange with NAPL of different composition in the downgradient portion of the NAPL zone. If the aqueous concentration of a component entering the downgradient portion of the NAPL is lower than the effective solubility of that component for the NAPL at that location, further dissolution of that component will occur in the downgradient portion of the NAPL. If the aqueous concentration of a component entering the downgradient portion of the NAPL is higher than the effective solubility of the component for the downgradient NAPL, a portion of the aqueous-phase contaminant will partition or dissolve into the downgradient NAPL. In this way, the temporal changes in aqueous concentrations that would be expected in response to changes in NAPL composition are delayed until changes in NAPL composition occur in the downgradient portion of the NAPL zone. This potential effect was recognized by Mackay et al. (1991) and referred to as a "chromatographic effect". This term derives from the fact that the process by which aqueous concentrations are altered due to exchange with downgradient NAPL is similar to that in chromatographic columns in which chemicals are separated with increasing effectiveness by columns of increasing length.

3-5 Dissolution of NAPL Pools

In NAPL pools, NAPL exceeds residual saturation values and is potentially mobile. Depending on the capillary pressures exerting during NAPL infiltration and the capillary properties of the aquifer, NAPL saturation values in pools range typically from 40% to 70% of the porosity (Feenstra et al., 1996). At these high NAPL saturations, the permeability of the pool to groundwater flow may reduced by a factor of 10 times or more (McWhorter and Kueper, 1996). As a result, there will generally be little horizontal groundwater flow through NAPL pools. Dissolution of a pool will occur predominantly along the upper margin of the pool where groundwater flow in the aquifer contacts the pool. Because pools form on strata having lower permeability, there is likely to be little groundwater flow along the bottom margin of the pool.

Hunt et al. (1988) described an analytical model for dissolution from along the surface of a DNAPL pool in an aquifer. This model allows calculation of the aqueous concentrations in groundwater above a pool, measured at the downgradient edge of the pool according to:

$$C(z) = S_{eff}\ erfc\left[\frac{z}{2\sqrt{\frac{D_z L}{V}}}\right] \qquad [3\text{-}11]$$

where :

C(z) is the aqueous concentration at z, above the pool (M/L^3)

z is the distance above the pool (L)

S_{eff} is the effective solubility of the contaminant (M/L^3)

erfc is the complementary error function

D_z is the vertical dispersion coefficient (L/T)

L is the length of the pool (L)

V is the linear groundwater velocity (L/T)

and by:

$$D_z = D\tau + \alpha_z V \qquad [3\text{-}12]$$

where :

D is the diffusion coefficient (L^2 /T)

τ is the tortuosity

α_z is the vertical dispersivity (L)

According to this model, equilibrium mass transfer occurs at the upper surface of the pool such that the aqueous concentration at the top of the pool is determined by the effective solubility of the compound. Aqueous-phase contaminants migrate upward into the aquifer as a result of vertical dispersion. The magnitude of the vertical dispersion coefficient is determined by the aqueous-phase diffusion coefficient, the vertical dispersivity and the groundwater velocity. The aqueous concentrations of contaminants measured in groundwater downgradient of a NAPL pool will be lower than the effective solubility limit. The magnitude of the aqueous concentration will be determined largely by the vertical distance over which groundwater samples are collected. Samples collected from monitoring wells will long intakes will yield lower concentrations than wells with short intakes. Aqueous concentrations will be lower also for short NAPL pools.

Simulations from this model compare well with laboratory experiments of single-component NAPL pool dissolution reported by Johnson and Pankow (1992) for TCA and TCE, Pearce et al. (1994) for TCA and TCE, and Voudrias and Yeh (1994) for toluene. There are no laboratory studies available that have compared this model to results for dissolution of multi-component NAPL pools.

Based on equations 3-11 and 3-12, dissolution of the individual components of a multi-component NAPL will depend principally on the effective solubility of the components. The only model parameter, other than effective solubility, that reflects a characteristic of an individual component is the aqueous-phase diffusion coefficient in equation 3-12. However, the diffusion coefficients are similar for most organic compounds that are common groundwater contaminants. All of the other model parameters are physical properties of the NAPL pool, the groundwater flow condition, or the aquifer. As a result of these relationships, the aqueous concentrations at the top of a multi-component NAPL pool will be determined by the effective solubility of the individual components. The effective solubility is determined by the NAPL composition at the top of the pool. Although vertical dispersion causes a reduction in aqueous concentrations with distance above the pool, dispersion is essentially a dilution process which will affect the aqueous concentrations of all the components to the same degree. Consequently, the aqueous concentration ratios in the groundwater should be determined by the NAPL composition at the top of the pool.

This effect is illustrated in Figure 3-4 by the results of dissolution simulations for a multi-component NAPL pool consisting of an equimolar mixture of chloroform (TCM) and tetrachloroethylene (PCE) in a typical sandy aquifer. Figure 3-4a shows vertical profiles of relative aqueous concentrations at the downgradient edge of pools measuring 1 m and 10 m in length. Other model input parameters are shown in the key for the figure. Values for tortuosity and vertical dispersivity are taken from laboratory tests of pool

dissolution. The aqueous concentrations are highest at the top of the pool and decline with distance above the pool. The aqueous concentrations extend a greater distance upward from the pool for the 10 m pool due to the longer contact time and greater opportunity for upward dispersion. The concentration profiles for TCM and PCE differ slightly because of slightly different diffusion coefficients. For the vertical dispersivity and groundwater velocity values selected here, the molecular diffusion coefficient is an important parameter in determining vertical dispersion. For higher values of vertical dispersivity or groundwater velocity, the degree of vertical dispersion will not be influenced by differences in molecular diffusion coefficients for different components.

Profiles of PCE/TCM ratios are shown in Figure 3-4b. The ratio at the top of the pool is 0.0276 reflecting the NAPL composition. The PCE/TCM ratio declines with distance above the pool reflecting that the rate of TCM diffusion is slightly greater than that of PCE. However, the PCE/TCM ratios calculated from the average aqueous concentrations in the plumes above the pools were 0.0261 for the 1 m pool and 0.0259 for the 10 m pool. These average ratios compare closely to the ratio at the top of the pool. This is the case because the aqueous concentrations are highest close to the pool and the highest concentrations determine the value of the average ratio.

The pool dissolution simulations suggest that the aqueous concentration ratios emitted by dissolution of a multi-component NAPL pool may reflect the NAPL composition in the same way as for dissolution of multi-component NAPL residual. Laboratory experiments by Whelan et al. (1994) for dissolution of an equimolar mixture of TCE and 112-TCA found that the aqueous concentration ratio close to the top of the pool fluctuated from 0.29 to 0.33 during the early stages of the experiment and compared closely to the ratio of 0.31 predicted for the TCE + 112-TCA mixture.

As dissolution of a multi-component NAPL pool proceeds, the NAPL composition at the top of the pool will change as the more soluble components are dissolved preferentially. Depending on the rate of dissolution along the top of the pool, the NAPL composition at the top of the pool may differ from the NAPL composition deeper in the pool. If this is the case, the aqueous concentration ratios measured in the plume will not reflect the overall NAPL composition. If NAPL pools are thin (i.e. a few centimetres of less), diffusive replenishment of the soluble components to the groundwater-NAPL pool interface may be sufficiently rapid to maintain a uniform chemical composition vertically within the NAPL pool. This is not likely to be the case for thick NAPL pools. The rate of molecular diffusion within NAPL should be roughly similar to aqueous-phase diffusion if the viscosity of the NAPL is similar to that of water (Perry's Handbook of Chemical Engineering, 1984). The rate of diffusion through high viscosity NAPL will be slower than that through water.

As groundwater passes along the top of a NAPL pool it is likely that there will be some opportunity for the aqueous-phase contaminants dissolved from the upgradient portion of the pool to interact with the NAPL in the downgradient portion of the NAPL. This exchange could cause a chromatographic effect similar to that possible in NAPL residual zones.

No laboratory studies are presently available to evaluate how aqueous concentration ratios would change during dissolution of multi-component NAPL pools. Consequently, there is little potential at this time for using aqueous concentration ratios to estimate NAPL mass contained in pools.

3.6 Conceptual Models for Dissolution of Multi-Component NAPL

Theoretical pore-scale models and empirical laboratory models of NAPL dissolution suggest that the rate of mass transfer and resultant aqueous concentrations emitted by dissolution of multi-component NAPL residual

will be determined primarily by the effective solubility of the NAPL components, for a given NAPL source and set of water flow conditions. The effective solubilities of NAPL components are determined by the NAPL composition. Changes in the NAPL composition due to preferential dissolution of higher-solubility components will, in turn, be reflected in the aqueous concentrations emitted from the NAPL residual at later times. However, in a field setting it will not be possible to relate the magnitude of aqueous concentrations in the groundwater to the characteristics of the NAPL residual zone because of uncertainty in the exact size and geometry of NAPL residual zones, and the unknown degree of dilution reflected in the contaminant concentrations found in monitoring wells. In addition, non-equilibrium mass transfer may occur under conditions of low NAPL residual saturation or high groundwater velocity. However, because dilution and non-equilibrium mass transfer should affect all dissolved contaminants to the same degree, information about the composition of NAPL residual reflected in the ratios of aqueous concentrations may be preserved. The preliminary study by Feenstra (1990) suggested that estimates of the chemical mass in NAPL residual zones may be possible using measured changes in aqueous concentration ratios in groundwater, together with predicted changes derived from a 1-cell Effective Solubility Model (ESM).

Figure 3-5 illustrates several different conceptual conditions for further evaluation of dissolution of multi-component NAPL in the subsurface. Case 1 represents the condition where groundwater flow occurs directly through a short zone of NAPL residual. In this case, the aqueous concentration ratios measured in the groundwater reflect the NAPL composition but the length of the flow path through the NAPL is sufficiently short that the aqueous concentrations emitted from the upgradient portion of the NAPL are not altered by exchange with NAPL in the downgradient portion of the NAPL zone. There is no chromatographic effect on the

aqueous concentrations. The condition represented by Case 1 can be simulated using the 1-cell configuration of the ESM.

Case 2 represents the condition where groundwater flow occurs directly through a long zone of NAPL residual. In this case, the aqueous concentration ratios also reflect the NAPL composition initially but may be altered by the chromatographic effect. The condition represented by Case 2 requires that the ESM be extended to account for the chromatographic effect.

Case 3 represents the condition where groundwater flow occurs through, but predominantly around, a thin layer of NAPL residual. In this case, the aqueous concentrations emitted from groundwater flow directly through the NAPL zone may be influenced by the chromatographic effect in the same way as Case 2. However, for thin zones of NAPL residual such as this, there may be significant migration of aqueous-phase contaminants away from the layer due to vertical dispersion. As a result, some of the groundwater which by-passes the NAPL layer may acquire aqueous-phase contamination. Because this vertical dispersion should be essentially a dilution effect (see Section 3.5), the aqueous concentration ratios in the groundwater by-passing the NAPL layer may reflect the NAPL composition within the NAPL layer. However, because of the two-dimensional nature of flow through the layer and dispersion out of the layer, this condition cannot be represented specifically with the ESM.

Case 4 represents the condition where groundwater flow occurs along the top of a thin NAPL pool. Aqueous-phase contaminants are emitted to the groundwater by dissolution along the top of the pool. Aqueous concentrations extend upward into the aquifer as a result of vertical dispersion. Because this vertical dispersion should be essentially a dilution effect (see Section 3.5), the aqueous concentration ratios in the groundwater flowing over the NAPL pool may reflect the NAPL composition within the NAPL layer provided that the pool has a uniform chemical composition

throughout its thickness. This may occur for thin pools where the diffusion within the NAPL is sufficiently rapid to replenish the more soluble contaminants dissolved from the top of the pool. For thick pools as represented in Case 5, the aqueous concentrations in groundwater at the top of the pool will not reflect the overall chemical composition of the pool. The conditions in Cases 4 and 5 cannot be represented specifically with the ESM.

The following chapter describes the extension of the Effective Solubility Model (ESM) to account for the chromatographic effect on aqueous concentrations expected in long NAPL residual zones. Subsequent chapters describe comparisons of the predictions from the ESM to the results of laboratory experiments for dissolution of multi-component NAPL residual, and to two controlled field experiments at Borden where zones of residual NAPL and thin NAPL pools were created in a sandy aquifer.

Table 3-1. Calculated values for aqueous-phase diffusion coefficients for selected organic contaminants common in groundwater.

Calculated using the method of Wilke and Chang (1955) as described in Perry's Handbook of Chemical Engineering (1984). Values of molar volume from Mackay et al. (1992a, 1992b, 1993).

Compound	Molar Volume (cm^3/mol)	Diffusion Coefficient (cm^2/s) at 20°C	Diffusion Coefficient Relative to that of Tetrachloroethylene
Benzene	96.0	9.6×10^{-6}	1.19
Toluene	118.0	8.5×10^{-6}	1.05
Ethyl Benzene	140.4	7.6×10^{-6}	0.95
Xylenes	140.4	7.6×10^{-6}	0.95
Dichloromethane	71.0	1.1×10^{-5}	1.42
Chloroform	92.0	9.8×10^{-6}	1.22
Carbon Tetrachloride	113.0	8.7×10^{-6}	1.08
1,2-Dichloroethane	94.0	9.7×10^{-6}	1.20
1,1,1-Trichloroethane	115.0	8.6×10^{-6}	1.07
Trichloroethylene	107.0	9.0×10^{-6}	1.11
Tetrachloroethylene	128.0	8.1×10^{-6}	1.00
Chlorobenzene	116.9	8.5×10^{-6}	1.06
1,4-Dichlorobenzene	137.8	7.7×10^{-6}	0.96
1,2,4-Trichlorobenzene	158.7	7.1×10^{-6}	0.88
Naphthalene	148.0	7.4×10^{-6}	0.92
Phenanthrene	199.0	6.2×10^{-6}	0.77
Anthracene	197.0	6.2×10^{-6}	0.77
Pyrene	214.0	5.9×10^{-6}	0.73

Table 3-2. Measured values for mass transfer coefficients determined for the dissolution of coal tars.

From Mukherji et al. (1997).

Compound	Reported Diffusion Coefficient (cm^2/s)	Measured Mass Transfer Coefficient (cm/s)	Number of Tests
Toluene	9.6×10^{-6}	1.2×10^{-3}	9
Naphthalene	8.0×10^{-6}	1.2×10^{-3}	6
2-Methyl Naphthalene	7.4×10^{-6}	1.3×10^{-3}	9
Ethyl Naphthalene	6.8×10^{-6}	1.5×10^{-3}	8
Acenaphthylene	7.3×10^{-6}	1.4×10^{-3}	9
Fluorene	6.9×10^{-6}	1.4×10^{-3}	9
Phenanthrene	6.7×10^{-6}	1.5×10^{-3}	9
Fluoranthene	6.4×10^{-6}	1.9×10^{-3}	7
Pyrene	6.4×10^{-6}	1.8×10^{-3}	7

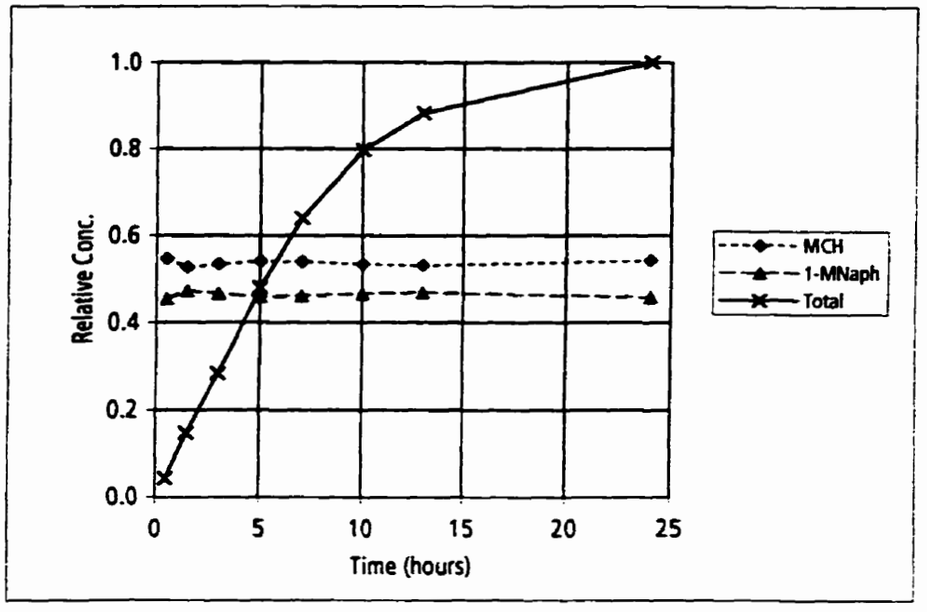

Key:
Relative Conc. - Concentration relative to the total dissolved concentration.
MCH - Methylcyclohexane
1-MNaph - 1-Methyl naphthalene

Figure 3-1. Consistency in relative aqueous concentrations during approach to solubility limits for dissolution of mixture of methylcylcohexane and 1-methyl naphthalene.

Data from Burris and MacIntyre (1985).

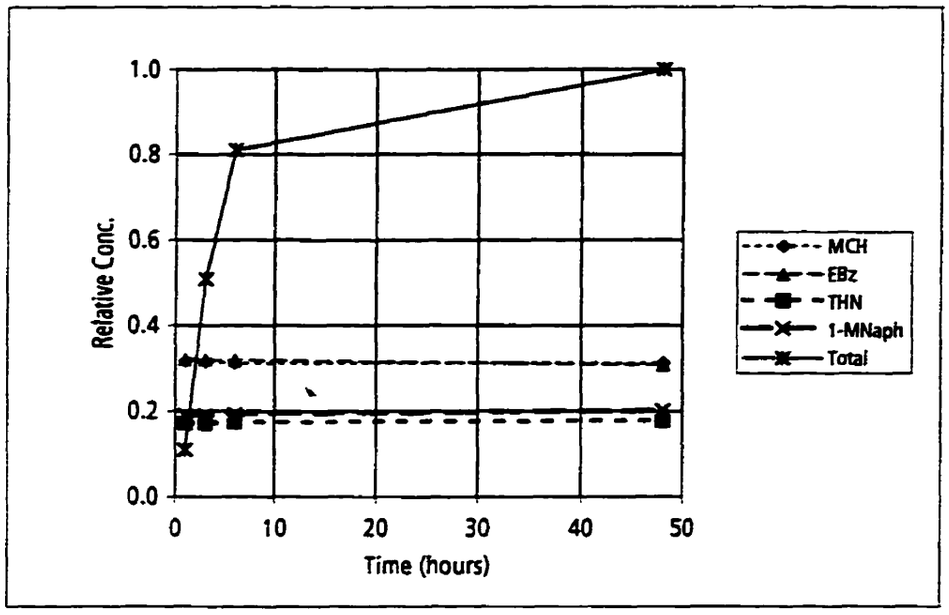

Key:
Relative Conc. - Concentration relative to the total dissolved concentration.
MCH - Methylcyclohexane
EBz - Ethyl benzene
THN - tetralin
1-MNaph - 1-Methyl naphthalene

Figure 3-2. Consistency in relative aqueous concentrations during approach to solubility limits for dissolution of mixture of methylcyclohexane, ethyl benzene, tetralin, and 1-methyl naphthalene.

Data from Burris and MacIntyre (1986b).

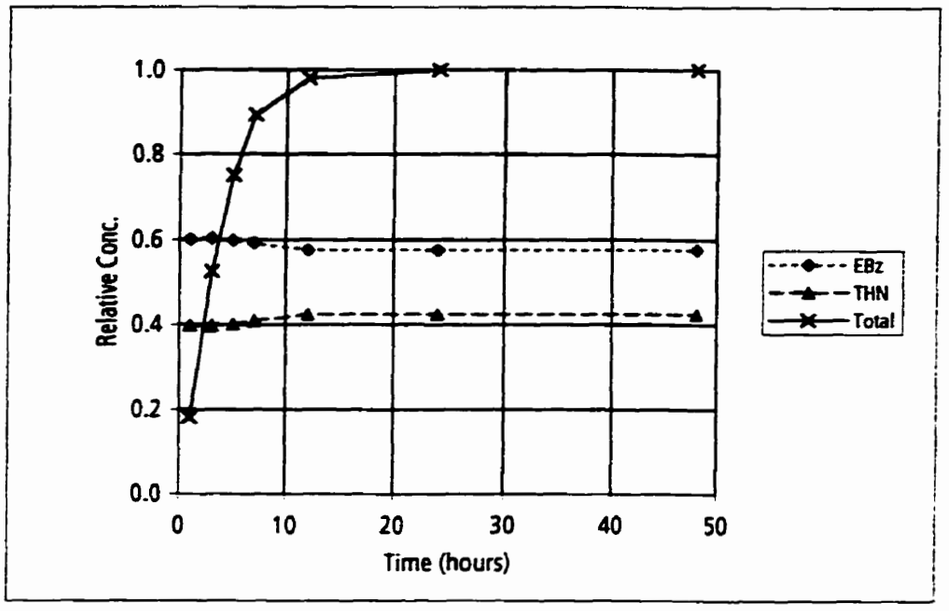

Key:
Relative Conc. - Concentration relative to the total dissolved concentration.
EBz - Ethyl benzene
THN - Tetralin

Figure 3-3. Consistency in relative aqueous concentrations during approach to solubility limits for dissolution of mixture of ethyl benzene and tetralin.

Data from Burris and MacIntyre (1986c).

3-4a

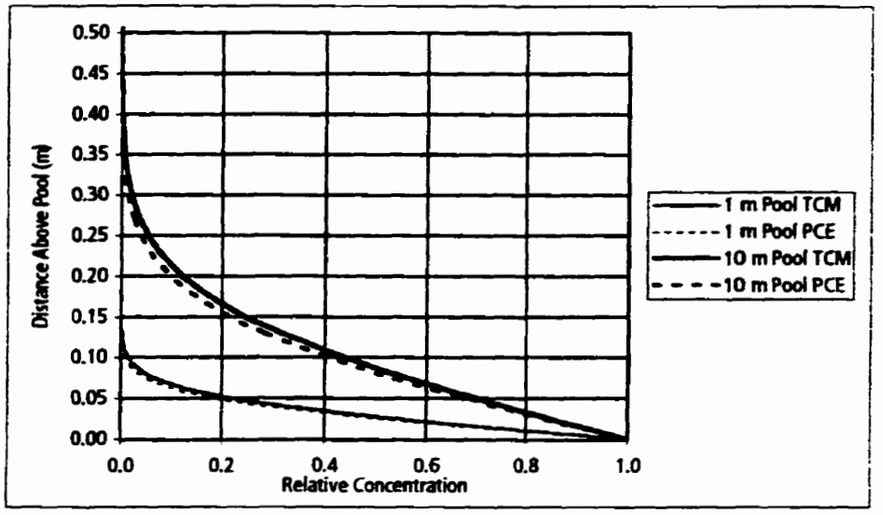

3-4b

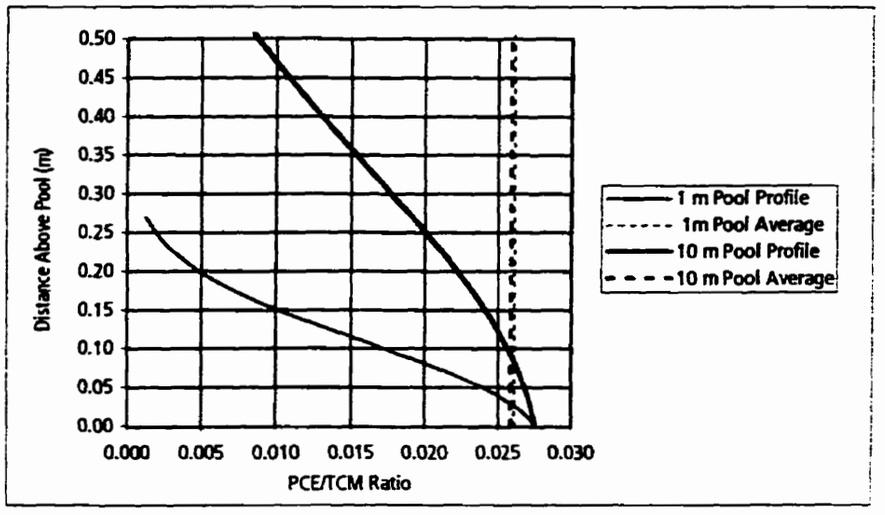

Key:
TCM - Chloroform
PCE - Tetrachloroethylene
Groundwater velocity = 0.1 m/day
Tortuosity= 0.7 (Voudrias and Yeh, 1994)
Dispersivity= 0.00023 m (Johnson and Pankow, 1992)
Diffusion coefficient for TCM= 9.8×10^{-6} cm²/s (Table 3-1)
Diffusion coefficient for PCE= 8.1×10^{-6} cm²/s (Table 3-1)

Figure 3-4. Aqueous concentrations and concentration ratios above a multi-component NAPL pool of TCM and PCE.

Concentrations calculated using equations 3-10 and 3-11.

Average ratios are calculated from the average aqueous concentrations of the full concentration profile.

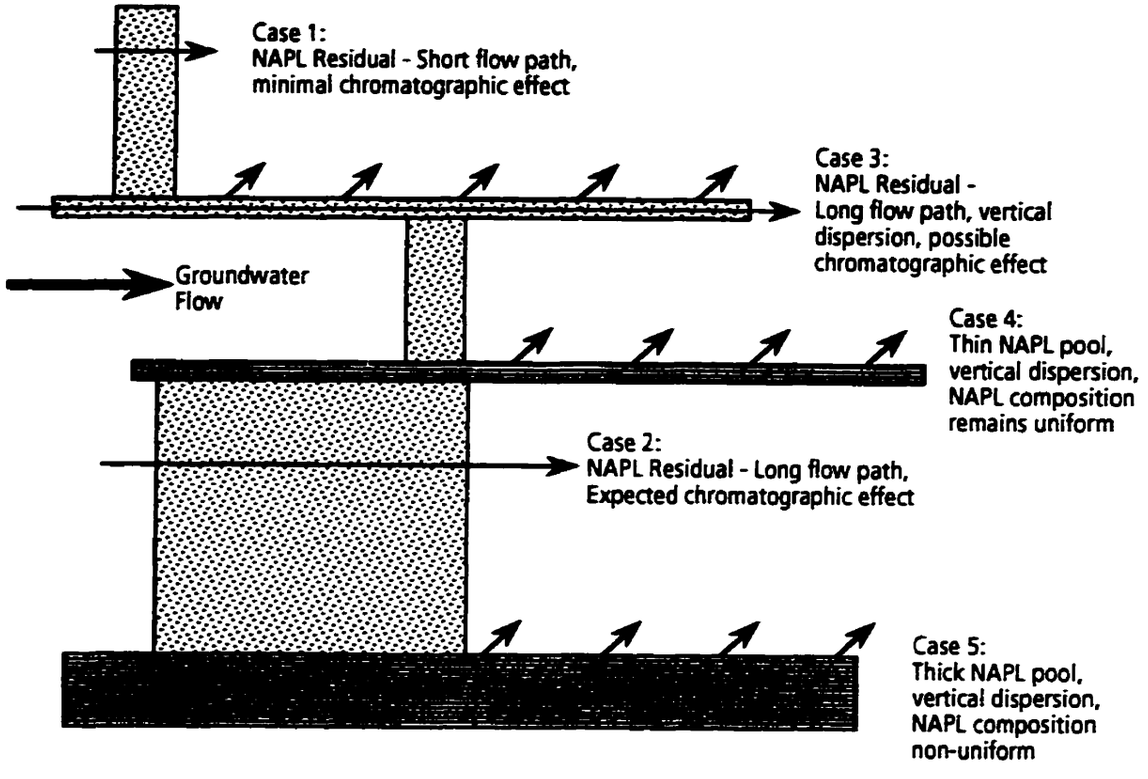

Figure 3-5. Schematic diagram of conceptual conditions for dissolution of multi-component NAPL.

4. Description of Effective Solubility Model (ESM)

4.1 Principles

The Effective Solubility Model (ESM) was developed to provide a method of describing the changes in aqueous concentrations of organic contaminants emitted from the dissolution of a multi-component zone of NAPL residual. The ESM relies on the principle that the aqueous concentrations can be determined from the NAPL composition. As described in Chapter 2, Raoult's Law provides reasonable prediction of effective solubility in most circumstances. Using Raoult's Law, aqueous concentrations are calculated using the mole fractions of the components in the NAPL and the pure-phase solubilities of the components.

In its simplest form, the ESM represents a single cell, of unit volume, into which clean water enters the cell and equilibrates with NAPL. Aqueous concentrations are calculated according to Raoult's Law and the NAPL composition. The water leaves the cell, the masses of the components removed by the water from the NAPL are calculated, and a new NAPL composition is determined based on the chemical mass removed.

Shiu et al. (1988) used a model similar to this simple ESM to simulate the results of laboratory dissolution experiments. They related the equilibrium aqueous concentrations to total volumetric flow of water through the columns. Feenstra (1990) used the 1-cell ESM to simulate the results of a laboratory dissolution experiment and the changes in aqueous concentrations ratios observed in pump-and-treat system at a site of NAPL contamination. He related the changes in aqueous concentration ratios to the degree of mass depletion of the NAPL. Shiu et al. (1988) and Feenstra (1990) showed that the results of these simple dissolution models compared well to laboratory dissolution experiments. However, it must be recognized that

these laboratory experiments represented NAPL zones only a few centimetres in length.

Because water moving through NAPL residual zones will equilibrate rapidly with the NAPL, aqueous concentration emitted from the upgradient portion of a NAPL zone may exchange with NAPL of differing composition at the downgradient portion of the NAPL zone and change in concentration. This potential effect cannot be simulated by a single equilibration cell. To account for this chromatographic effect, the ESM was extended to simulate a series of equilibration cells linked sequentially. The equilibration calculations within each cell take the total chemical mass and allocate appropriate proportions to the NAPL, sorbed and aqueous-phases according Raoult's Law and linear partitioning relationships. For each equilibration step for each cell, the calculated sorbed-phase and NAPL-phase chemical mass is retained within the cell and the calculated aqueous-phase chemical mass is passed to the next downgradient cell for the next equilibration step.

4.2 Calculation Method

4.2.1 Input Parameters

The ESM allows the calculation of the aqueous concentrations and concentration ratios for the dissolution of NAPL residual, based on the physical and chemical characteristics of the NAPL, and the physical characteristics of the porous medium.

Fixed-value parameters for the ESM include:

For NAPL Components-

- Pure-phase solubility
- Molecular mass
- Soil organic carbon-water partition coefficient
- Density

For Porous Medium-

- Dry bulk density
- Total porosity
- Fraction organic carbon

Initial-value parameters for the ESM include:

- Initial NAPL volume
- Initial NAPL component concentrations

There are also several calculated fixed parameters. For illustrating relationships, the following equations do not include conversion factors to provide consistent dimensional units. For simplicity, NAPL-filled and water-filled porosity, and total porosity values are expressed here in volume units because a unit volume of porous medium is considered in each cell.

For sorption of aqueous contaminants on the aquifer solids-

$$K_d = K_{oc} \; f_{oc} \qquad [4\text{-}1]$$

where :

K_d *is the sorption coefficient for the porous medium* (L^3/M)

K_{oc} *is the organic carbon –water partition coefficient* (L^3/M)

f_{oc} *is the weight fraction organic carbon in the porous medium*

Calculated initial parameters include:

For initial water-filled porosity-

$$\theta^o_{water} = \theta_{total} - \theta^o_{NAPL} \qquad [4\text{-}2]$$

where :

θ^{o}_{water} *is the initial water –filled porosity* (L^3)

θ_{total} *is the total porosity* (L^3)

θ^{o}_{NAPL} *is the initial NAPL –filled porosity* (L^3)

For initial NAPL density-

$$\rho^{o}_{NAPL} = \left(\sum \left[\frac{c^{i,o}}{\rho^{i}} \right] \right)^{-1} \qquad [4\text{-}3]$$

where :

ρ^{o}_{NAPL} *is the initial NAPL density* (M/L^3)

$c^{i,o}$ *is the concentration of component, i, in the NAPL (M/M)*

ρ^{i} *is the density of component, i, in the NAPL* (M/L^3)

For initial mass of each NAPL component-

$$M^{i,o} = c^{i,o} \; \theta^{o}_{NAPL} \; \rho^{o}_{NAPL} \qquad [4\text{-}4]$$

where :

$M^{i,o}$ *is the initial mass of component, i, in the NAPL (M)*

θ^{o}_{NAPL} *is the initial NAPL –filled porosity* (L^3)

ρ^{o}_{NAPL} *is the initial NAPL density* (M/L^3)

The preceding parameters and calculated parameters define the initial conditions for the ESM simulations. The initial conditions are the same in all cells. The following section describes the calculations for each

equilibration step in each cell. The chemical mass partitioning calculations are solved iteratively.

4.2.2 Iterative Calculations

For each equilibration step in each cell, the sequence of calculations begins with the calculation of the total chemical mass in the cell. For the first equilibration step, the total mass of each component in the cell is determined by equation 4-4. For subsequent steps, the total chemical mass of each component in the cell is determined by the NAPL-phase and sorbed-phase chemical mass remaining in the cell from the previous equilibration step, plus the aqueous-phase chemical mass imported to the cell from the previous equilibration step from the upgradient cell.

At the start of each equilibration step, the total chemical mass of each component is assumed to reside in the NAPL phase. The mole fractions of each component in the NAPL are calculated, and aqueous concentrations are determined by Raoult's Law. The sorbed-phase concentrations of each component are calculated based on the aqueous concentrations. The aqueous-phase chemical mass and the sorbed-phase chemical mass are then calculated based on their respective concentrations. However, the sum of the NAPL-phase mass, sorbed-phase mass and aqueous-phase mass then exceeds the total mass.

A revised value of the NAPL-phase chemical mass of each component is calculated as the total chemical mass minus the aqueous-phase mass and sorbed-phase mass. This revised NAPL-phase mass is then cycled back through the same sequence of calculations until the calculated aqueous-phase concentration no longer change significantly between iterations, and equilibration of chemical mass between the NAPL phase, sorbed phase and aqueous phase is achieved.

For each equilibration step, one cell volume of water moves through each of the cells. There is no time period associated with an equilibration step. It is assumed that chemical equilibrium is achieved in each cell.

A flow chart describing the calculation sequence is shown in Figure 4-1. The following paragraphs describe the equations employed in the calculation sequence.

1. Determine the total chemical mass of each component in the cell and assign to the NAPL phase.

   This calculation employs values from the upgradient cell and previous equilibration step so that superscripts, c and e, are specified in the following equation.

$$M_{NAPL}^{i,c,e} = M_{NAPL}^{i,c,e-1} + M_{sorbed}^{i,c,e-1} + M_{aqueous}^{i,c-1,e-1} \qquad [4\text{-}5]$$

where:

$M_{NAPL}^{i,c,e}$ *is the mass of component, i, in cell, c, at step, e*

$M_{NAPL}^{i,c,e-1}$ *is the NAPL mass of component, i, in cell, c, at previous step, e−1*

$M_{sorbed}^{i,c,e-1}$ *is the sorbed mass of component, i, in cell, c, at previous step, e−1*

$M_{aqueous}^{i,c-1,e-1}$ *is the aqueous mass of component, i, in upgradient cell, c−1, at previous step, e−1*

2. Calculate molar concentration of each component in the NAPL.

   This calculation does not employ values from other cells or equilibration steps so the superscripts, c and e, used in equation 4-5 are omitted.

$$X^i = \frac{M^i_{NAPL}}{MM^i} \qquad [4\text{-}6]$$

where :

X^i_{NAPL} *is the molar concentration of component, i, in the NAPL (mol)*

M^i_{NAPL} *is the NAPL mass of component, i (M)*

MM^i *is the molecular mass of component, i (M/mol)*

3. Calculate mole fraction of each component in the NAPL.

   This calculation does not employ values from other cells or equilibration steps so the superscripts, c and e, used in equation 4-5 are omitted.

$$\chi^i_{NAPL} = \frac{X^i_{NAPL}}{\sum X^i_{NAPL}} \qquad [4\text{-}7]$$

where :

χ^i_{NAPL} *is the mole fraction of component, i, in the NAPL*

4. Calculate aqueous concentration of each component based on Raoult's Law.

   This calculation does not employ values from other cells or equilibration steps so the superscripts, c and e, used in equation 4-5 are omitted.

$$C^i = \chi^i_{NAPL} \; S^i \qquad [4\text{-}8]$$

where :

C^i *is the aqueous concentration of component, i* (M/L^3)

S^i *is the pure – phase solubility of component, i* (M/L^3)

In the circumstance where $\chi^{i}_{NAPL} = 0$, calculate aqueous concentration by:

$$C^{i} = \frac{M^{i}_{NAPL}}{\theta_{water} + (\rho_b \ K^{i}_{d})} \qquad [4\text{-}9]$$

where :

M^{i}_{NAPL} *is the mass of component, i, in cell, c, at step e*

θ_{water} *is the water –filled porosity* (L^3)

ρ_b *is the dry bulk density of the porous medium* (M/L^3)

K^{i}_{d} *is sorption coefficient for component, i* (L^3/M)

5. Calculate aqueous-phase chemical mass for each component.

This calculation does not employ values from other cells or equilibration steps so the superscripts, c and e, used in equation 4-5 are omitted.

$$M^{i}_{aqueous} = C^{i} \ \theta_{water} \qquad [4\text{-}10]$$

where :

$M^{i}_{aqueous}$ *is the aqueous mass of component, i*

6. Calculate sorbed-phase chemical mass for each component.

This calculation does not employ values from other cells or equilibration steps so the superscripts, c and e, used in equation 4-5 are omitted.

$$M^{i}_{sorbed} = C^{i} \ \rho_b \ K^{i}_{d} \qquad [4\text{-}11]$$

where :

M^{i}_{sorbed} *is the sorbed mass of component, i*

7. **Calculate revised NAPL-phase chemical mass for each component.**

   This calculation does not employ values from other cells or equilibration steps so the superscripts, c and e, used in equation 4-5 are omitted.

$$(M^{i}_{NAPL})' = M^{i}_{NAPL} - M^{i}_{aqueous} - M^{i}_{sorbed} \qquad [4\text{-}12]$$

where :

$(M^{i}_{NAPL})'$ *is the revised NAPL mass of component, i*

M^{i}_{NAPL} *is the NAPL mass of component, i,*

8. **Calculate NAPL-filled porosity.**

   This calculation does not employ values from other cells or equilibration steps so the superscripts, c and e, used in equation 4-5 are omitted.

$$\theta_{NAPL} = \sum \frac{(M^{i}_{NAPL})'}{\rho^{i}} \qquad [4\text{-}13]$$

where :

θ_{NAPL} *is the NAPL –filled porosity* (L^3)

ρ^{i} *is the density of component, i, in the NAPL* (M/L^3)

9. Calculate revised water-filled porosity.

   This calculation does not employ values from other cells or equilibration steps so the superscripts, c and e, used in equation 4-5 are omitted.

$$\theta_{water} = \theta_{total} - \theta_{NAPL} \qquad [4\text{-}14]$$

where :

θ_{water} *is the water –filled porosity* (L^3)

θ_{total} *is the total porosity* (L^3)

θ_{NAPL} *is the NAPL –filled porosity* (L^3)

10. Using revised NAPL-phase chemical mass for each component and water-filled porosity, repeat calculations until the change in aqueous concentrations between iterations is suitably small. The tolerance used is this work was 10^{-6}.

The ESM was implemented as an executable macro (programmed in Visual Basic) in Microsoft Excel v. 5.0. The fixed-value parameters and initial-value parameters described in Section 4.2.1 are specific input parameters to the ESM. In addition, the number of cells and number of equilibration steps are specified. A listing of the macro program is found in Appendix B.

4.2.3 Output

The ESM calculates the aqueous concentrations of each NAPL component emitted from the last model cell for each equilibration step. The aqueous concentration ratios are calculated from these values. The ratio (referred to as Q) of the volume of water passed through the NAPL zone to the total NAPL volume in the series of cells, and the relative NAPL mass

remaining are calculated for each equilibration step. The key relationship to be examined is the change in aqueous concentration ratios relative to the NAPL mass remaining.

4.3 Sensitivity Analyses

4.3.1 Overview

A series of model simulations were performed to illustrate the effect of varying input parameter values on the calculated aqueous concentrations ratios. Of the fixed-value and initial-value parameters, not all will have a significant effect on the calculated aqueous concentration ratios. For example, the molecular mass and density of individual NAPL components vary over a relatively small range in comparison to parameters such as pure-phase solubility and K_{OC} of the components, or f_{OC} of the porous medium. Some parameters are correlated with other parameters. Pure-phase solubility of the components is inversely related to K_{OC}, and total porosity is inversely related to dry bulk density of the porous medium. For these reasons, pure-phase solubility of the components, initial NAPL residual content, f_{OC} and total porosity of the porous medium were considered principal parameters for the sensitivity analyses.

All sensitivity analyses considered hypothetical binary NAPL mixtures comprised of 50% by weight of each component. For simplicity, each component has a molecular mass of 100 g/mole and a density of 1,000 kg/m^3. Sensitivity analyses considered combinations of pure-phase solubility values including:

Component A=1,000 mg/L - Component B=500 mg/L

Component A=1,000 mg/L - Component B=100 mg/L

Component A=1,000 mg/L - Component B=10 mg/L

Component A=1,000 mg/L - Component B=1 mg/L

Component A=100 mg/L - Component B=10 mg/L

This range in pure-phase solubility for these combinations reflects the range in values for the most important organic contaminants in groundwater.

Sensitivity analyses considered initial NAPL residual content values including:

$1\ L/m^3$ $5\ L/m^3$ $15\ L/m^3$ $50\ L/m^3$

These values represent residual saturations of 0.3%, 1.7%, 5% and 17% of pore space, respectively, in a porous medium with total porosity of 0.3. Initial NAPL residual saturations in most laboratory dissolution experiments range from about 5% to 15%.

Sensitivity analyses considered f_{oc} values for the porous medium including:

0.01 0.001 0.0001

These values represent organic carbon contents of 1.0%, 0.1% and 0.01% by weight, respectively. This reflects the range expected in natural porous media.

Sensitivity analyses considered porosity values for the porous medium including:

0.2 0.3 0.4

These values reflect the range in porosity expected in natural porous media.

In addition to varying the fixed-value and initial-value parameters, sensitivity analyses considered the effect of increasing the number of cells

linked in the ESM. The following sections describe the results of the sensitivity analyses.

4.3.2 Effect of Solubility of Components

A series of model simulations were performed to illustrate the effect of the solubility of the NAPL components on the aqueous concentration ratios. Four binary NAPL mixtures were considered with component pure-phase solubilities of 1,000 mg/L and 500 mg/L (Mix 1); 1,000 mg/L and 100 mg/L (Mix 2); 1,000 mg/L and 10 mg/L (Mix 3); and, 1,000 mg/L and 1 mg/L (Mix 4), respectively. The results of these simulations are shown in Figure 4-2.

Because of the different pure-phase solubilities of the components of each mixture, the initial aqueous concentration ratio (component B/ component A) is different for each mixture. The initial aqueous concentration ratios are 0.5, 0.1, 0.01 and 0.001, respectively, for Mix 1, Mix 2, Mix 3 and Mix 4. These ratios depend on both the NAPL composition and the pure-phase solubilities of the NAPL components.

The shape of each of the curves is different for each mixture. For Mix 1, the pure-phase solubility of component A and component B differ only by a factor of 2 times. As a result, dissolution removes an appreciable proportion of both components and the aqueous concentration ratio B/A increases slowly as NAPL mass is depleted. In contrast, for Mix 4, the pure-phase solubility of component A and component B differ by a factor of 1,000 times. Consequently, dissolution removes component A much more rapidly than component B and the ratio B/A increases rapidly as NAPL mass is depleted. For Mix 4, almost all of component A is depleted before a significant proportion of component B is removed.

4-3.3 Effect of Number of Cells

A series of model simulations were performed to illustrate the effect of number of equilibration cells on the change in aqueous concentration ratio relative to the NAPL mass remaining. Four binary NAPL mixtures were considered with component pure-phase solubilities of 1,000 mg/L and 500 mg/L; 1,000 mg/L and 100 mg/L; 1,000 mg/L and 10 mg/L; and, 1,000 mg/L and 1 mg/L, respectively. For each NAPL mixture, simulations were performed for 1-cell, 10-cell and 100-cell configurations. The greater the number of cells, the greater the chromatographic effect of chemical exchange between the aqueous-phase contaminants emitted from the upgradient cells and the NAPL in the downgradient cells. The numbers of cells can be viewed as representing the generic length of the NAPL residual zone. The results of these simulations are shown in Figures 4-3, 4-4, 4-5 and 4-6.

The effect of a greater number of cells on the change in aqueous concentration ratios is similar for each of the NAPL mixtures. During the early stage of NAPL dissolution for multiple-cell configurations, the aqueous concentration ratio remains constant for some period as the aqueous concentrations emitted from the NAPL zone are controlled predominantly by the NAPL contained in downgradient cells which have undergone less dissolution. At later stages of dissolution, the aqueous concentration ratios increase rapidly in response to the eventual changes in NAPL composition in the downgradient cells. For greater numbers of cells, the period of early constant ratios is greater and the eventual rate of increase in ratios is more abrupt.

For NAPL mixtures having a high contrast in the pure-phase solubility of the components (see Figures 4-5 and 4-6), the eventual increase in ratios is extremely abrupt. This effect is comparable to the enhanced separation of solute peaks observed in chromatographic columns of increasing length.

The effect of the number of cells is most significant at early and late stages of dissolution with regard to the ability to predict the NAPL remaining based on the aqueous concentration ratio. For example, in Figure 4-4, a B/A ratio of 0.2 could relate to a value of NAPL remaining of 0.7 or 0.45 depending on the number of cells specified. A greater number of cells yields a lower prediction of NAPL mass remaining. Similarly, a B/A ratio of 20 could relate to a value of NAPL remaining of 0.45 or 0.28 depending on the number of cells specified. In this case, a greater number of cells yields a higher prediction of NAPL mass remaining.

4.3.4 Effect of Soil Organic Carbon

A series of model simulations were performed to illustrate the effect of different organic carbon contents on the change in aqueous concentration ratios relative to the NAPL mass remaining. The organic carbon content will determine the proportion of the chemical mass sorbed on the porous medium solids. Five binary NAPL mixtures were considered with component pure-phase solubilities of 1,000 mg/L and 500 mg/L; 1,000 mg/L and 100 mg/L; 1,000 mg/L and 10 mg/L; 1,000 mg/L and 1 mg/L; and, 100 mg/L and 10 mg/L, respectively. For each NAPL mixture, simulations were performed for f_{OC} values of 0.0001, 0.001 and 0.01. The results of these simulations are shown in Figures 4-7, 4-8, 4-9, 4-10 and 4-11.

The effect of higher values of f_{OC} on the change in aqueous concentration ratios is similar for each of the NAPL mixtures. During early stages of dissolution, there is no difference in B/A ratio regardless of the f_{OC} value. This is the case because the chemical mass which can be sorbed on the porous medium solids is small in comparison to the chemical mass contained in the NAPL remaining. During later stages of dissolution, the B/A ratios for f_{OC} values of 0.0001 and 0.001 differ from those for an f_{OC} value of 0.01. For high f_{OC} values, the mass of soil organic carbon may be

comparable to the NAPL mass and act to buffer the changes aqueous concentrations emitted from the NAPL zone.

For the examples shown in Figures 4-9 and 4-10, a B/A ratio of 1 could relate to a value of NAPL remaining of 0.5 or 0.47 depending on the f_{OC} value specified. Consequently, this effect is relatively minor.

4.3.5 Effect of Porosity

A series of model simulations were performed to illustrate the effect of different porosity values on the change in aqueous concentration ratios relative to the NAPL mass remaining. Five binary NAPL mixtures were considered with component pure-phase solubilities of 1,000 mg/L and 500 mg/L; 1,000 mg/L and 100 mg/L; 1,000 mg/L and 10 mg/L; 1,000 mg/L and 1 mg/L; and, 100 mg/L and 10 mg/L, respectively. For each NAPL mixture, simulations were performed for porosity values of 0.2, 0.3 and 0.4. The results of these simulations are shown in Figures 4-12, 4-13, 4-14, 4-15 and 4-16. There is essentially no effect of differing porosity on the aqueous concentration ratios calculated by the ESM.

4.3.6 Effect of Initial NAPL Content

A series of model simulations were performed to illustrate the effect of initial NAPL content on the change in aqueous concentration ratios relative to the NAPL mass remaining. Five binary NAPL mixtures were considered with component pure-phase solubilities of 1,000 mg/L and 500 mg/L; 1,000 mg/L and 100 mg/L; 1,000 mg/L and 10 mg/L; 1,000 mg/L and 1 mg/L; and, 100 mg/L and 10 mg/L, respectively. For the first four NAPL mixtures, simulations were performed for initial NAPL contents of 5 L/m^3, 15 L/m^3 and 50 L/m^3. For the final NAPL mixture, initial NAPL contents of 1 L/m^3, 5 L/m^3 and 15 L/m^3 were used. The results of these simulations are shown in Figures 4-17, 4-18, 4-19, 4-20 and 4-21.

The effect of higher values of porosity on the change in aqueous concentration ratios is similar for each of the NAPL mixtures. For the NAPL mixtures where component A has a pure-phase solubility of 1,000 mg/L, B/A ratios are slightly higher for lower values of initial NAPL content. This is the case because each equilibration step removes an appreciable proportion of the NAPL when initial NAPL contents are low. This effect is not observed for the NAPL mixture where component A has a pure-phase solubility of 100 mg/L (see Figure 4-21). For the examples shown in Figures 4-19 and 4-20, a B/A ratio of 0.1 could relate to a value of NAPL remaining of 0.52 or 0.50 depending on the value of the initial NAPL content specified. Consequently, the effect of initial NAPL content is relatively minor.

4.4 Error Analyses

As illustrated in the preceding sections, the aqueous concentration ratios calculated by the ESM are affected to only a minor degree, by values of f_{OC}, porosity and initial NAPL content which vary over the range of values expected at actual field sites.

The aqueous concentration ratios calculated by the ESM are determined principally by the effective solubility of the NAPL components. The effective solubility is defined by the NAPL composition and pure-phase solubilities of the components according to Raoult's Law. The potential error in effective solubility calculated by Raoult's Law may be less than 10% for simple mixtures to 50% of more for complex mixture of organic compounds. A series of simulations were performed to evaluate the effect of errors in effective solubility on the aqueous concentration ratios calculated by the ESM.

Four binary NAPL mixtures were considered with component pure-phase solubilities of 1,000 mg/L and 500 mg/L; 1,000 mg/L and 100 mg/L; 1,000 mg/L and 10 mg/L; and, 1,000 mg/L and 1 mg/L, respectively. For each NAPL mixture, simulations were performed assuming that the effective

solubility values of the components were in error by +15% and -15%. The initial NAPL composition of each mixture was adjusted for the error analyses so that the initial aqueous concentration ratios of the different simulations were equal. The results of these simulations are shown in Figures 4-22 through 4-29.

These simulations illustrate that relatively small errors in the effective solubility of the NAPL components may have a significant effect on the aqueous concentration ratios calculated by the ESM for the later stages of dissolution. The effect on the aqueous concentration ratios is similar in magnitude, but opposite in direction, for a given error in the effective solubility of component A or component B. For example, in Figures 4-24 and 4-25, a B/A ratio of 1.0 could relate to a value of NAPL remaining of 0.45 for no error in solubility, or 0.48 for an error in +15% in the solubility of component A. Similarly, a B/A ratio of 1.0 could relate to a value of NAPL remaining of 0.45 for no error in solubility or 0.40 for an error of +15% in the solubility of component B.

When applying ESM simulations to cases of groundwater contamination in which the NAPL composition is known, the initial aqueous concentrations ratios can be compared to the predicted initial ratios to provide an indication of potential errors in the effective solubility of the components. However, at actual field sites where the NAPL composition is not known and the examination of initial aqueous concentration ratios is not possible, some form of generic error analysis may be warranted due to the potential effect of errors in effective solubility on the aqueous concentration ratios calculated by the ESM.

Another source of potential error in the aqueous concentration ratios predicted by the ESM is the case where the actual NAPL consists of other components not accounted for in the calculations. This might be the case at sites of contamination by complex multi-component NAPL, especially when

not all components of the NAPL cause measurable aqueous-phase contamination of the groundwater. In most cases the "unknown" components are low-solubility hydrocarbons.

The presence of unknown components will affect the aqueous concentrations predicted for the known components because the unknown component will alter the mole fraction of the known components in the NAPL. The presence of unknown components should not alter the ratios of the known components.

Figure 4-30 shows the results of ESM simulations for a binary NAPL mixture having component solubilities of 1,000 mg/L and 100 mg/L. In one case, there is no unknown component, while in the other cases there is an unknown component that comprises 50 wt.% of the NAPL. For the cases where the unknown component is present, the NAPL remaining is expressed in terms of the mass of the known components remaining. For the 1-cell configuration there is no difference in predicted aqueous concentration ratios when there is an unknown component present. Figure 4-31 shows a similar comparison for a 10-cell configuration. In this case, the presence of an unknown component appears to have a slight effect on the predicted ratios, presumably because the unknown component influences the chromatographic effect of the greater number of cells. The overall effect on the predicted ratios is small.

4.5 Conclusions Regarding the ESM

The Effective Solubility Model (ESM) has the potential to be a useful tool in evaluating in the dissolution of multi-component NAPL. Predictions of the changes in aqueous concentration ratios versus NAPL mass remaining can be made without specific assumptions regarding the geometry of the NAPL source zone, groundwater flow rates or mass transfer coefficients. The results of ESM simulations are most sensitive to the NAPL composition, the

pure-phase solubilities of the NAPL components, and the number of equilibration cells specified in the model. The results of the ESM simulations are insensitive to the other model input parameters: fraction organic carbon in the aquifer, porosity or initial NAPL content.

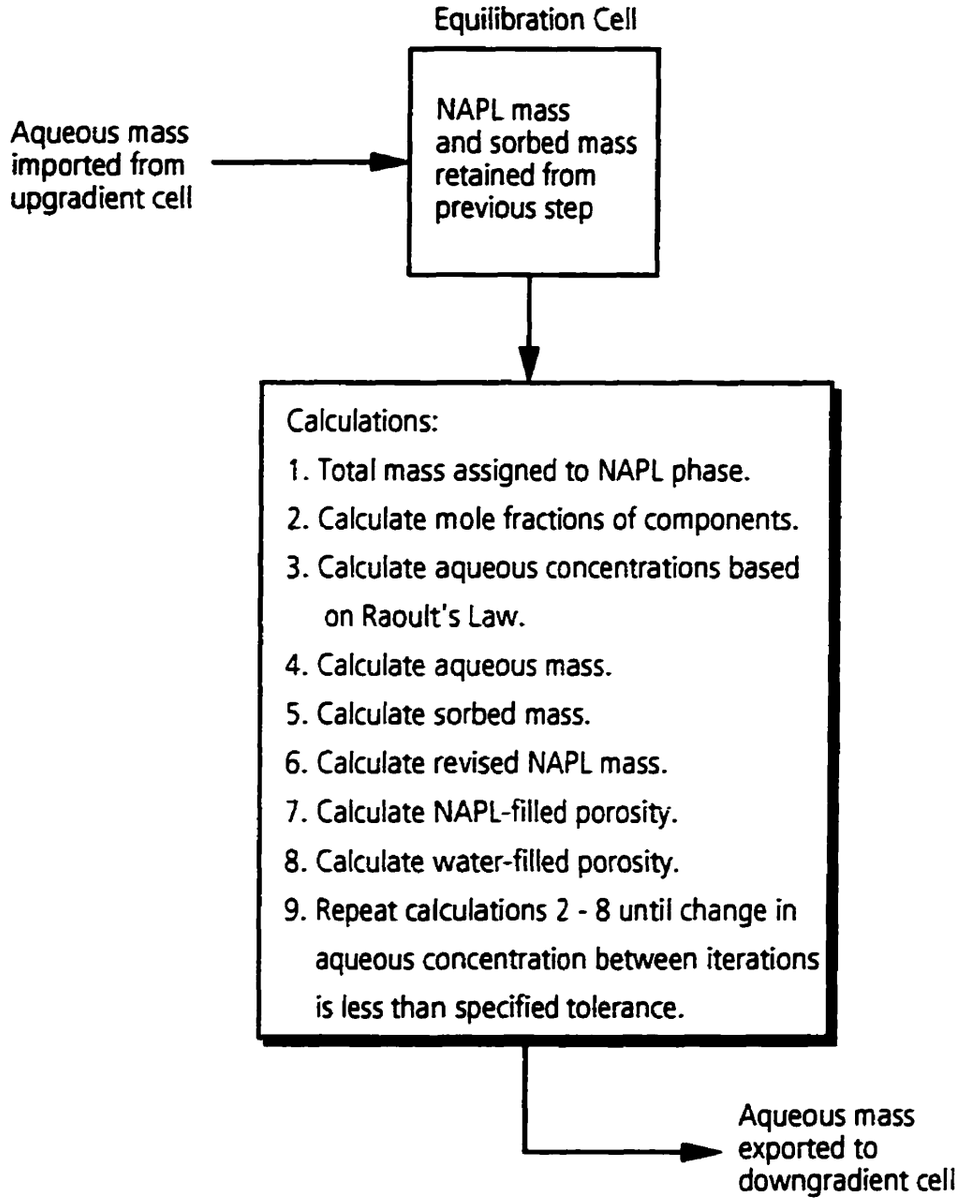

Figure 4-1. Schematic of calculation sequence for the Effective Solubility Model.

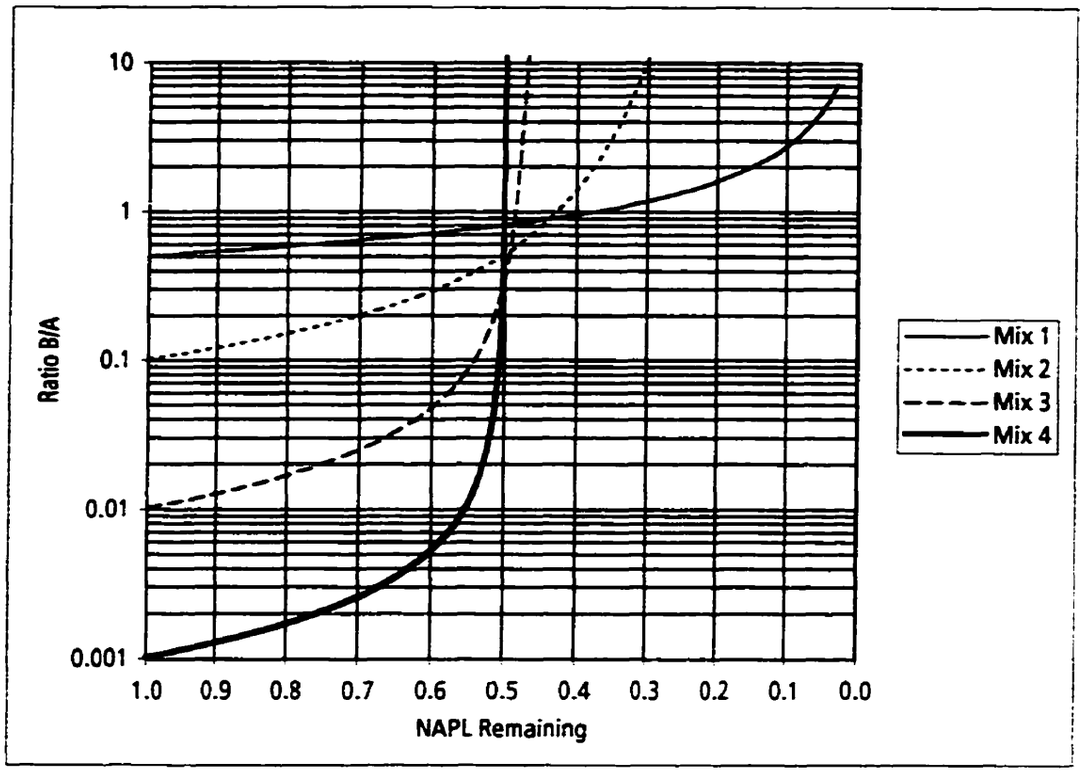

	Pure-Phase Solubility	
	Component A	Component B
Mix 1 -	1,000 mg/L	500 mg/L
Mix 2 -	1,000 mg/L	100 mg/L
Mix 3 -	1,000 mg/L	10 mg/L
Mix 4 -	1,000 mg/L	1 mg/L

Additional Input Parameters:
Total Porosity - 0.3
f_{oc} - 0.0001
NAPL Content - 15 L/m³

Figure 4-2. Aqueous concentration ratios predicted by ESM for binary NAPL mixtures with differing pure-phase solubility, for 1-cell configuration.

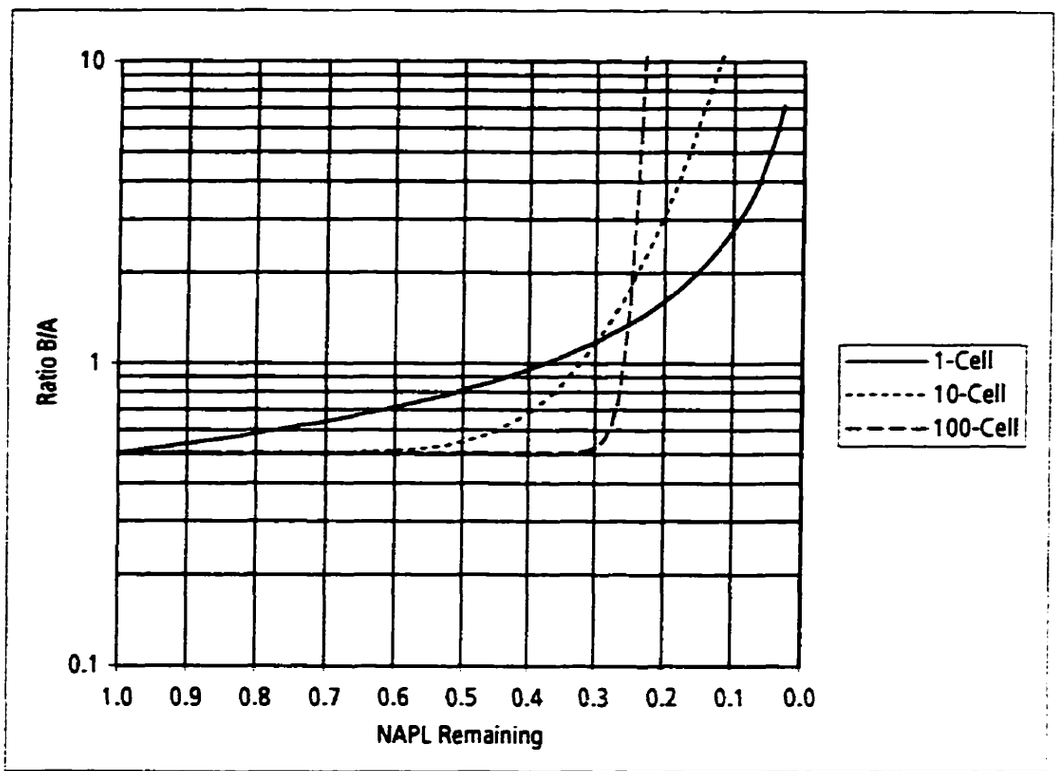

Additional Input Parameters:
Total Porosity - 0.3
f_{oc} - 0.0001
NAPL Content - 15 L/m³
K_{oc} - 50 mL/g (component A)
K_{oc} - 100 mL/g (component B)

Figure 4-3. Aqueous concentration ratios predicted by ESM for binary NAPL mixture with pure-phase solubilities of 1,000 mg/L (component A) and 500 mg/L (component B) for 1-cell, 10-cell and 100-cell configurations.

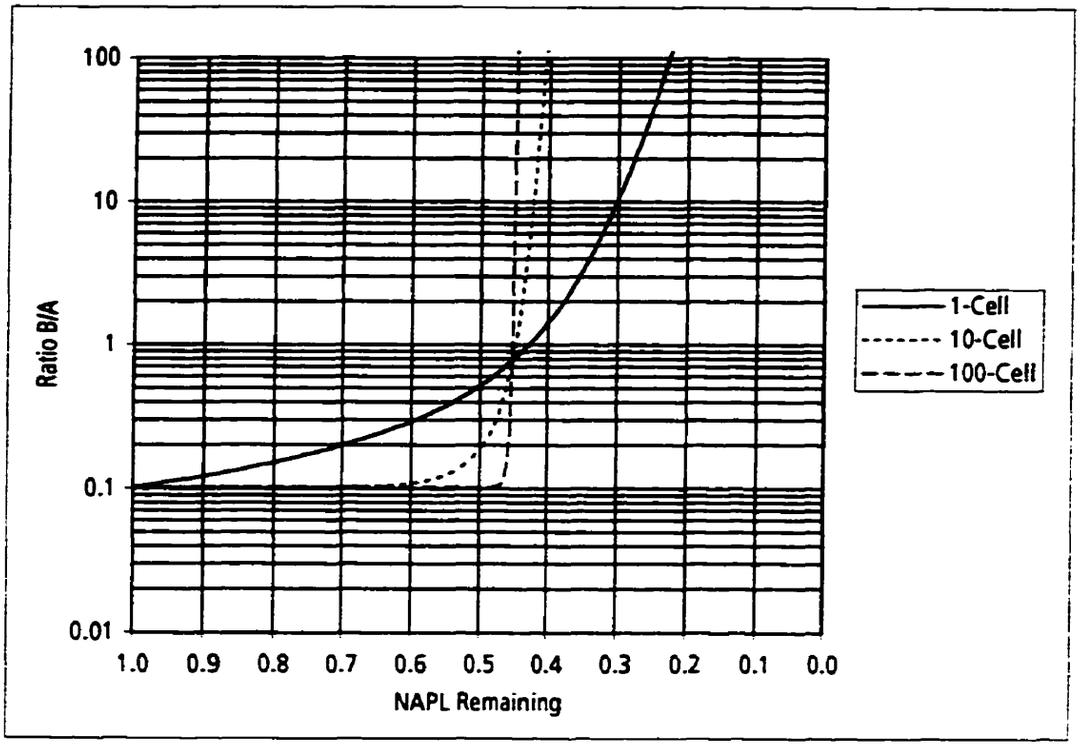

Additional Input Parameters:
Total Porosity - 0.3
f_{oc} - 0.0001
NAPL Content - 15 L/m³
K_{oc} - 50 mL/g (component A)
K_{oc} - 500 mL/g (component B)

Figure 4-4. Aqueous concentration ratios predicted by ESM for binary NAPL mixture with pure-phase solubilities of 1,000 mg/L (component A) and 100 mg/L (component B) for 1-cell, 10-cell and 100-cell configurations.

File:(Fig4-4) No. Cells #2/Plots

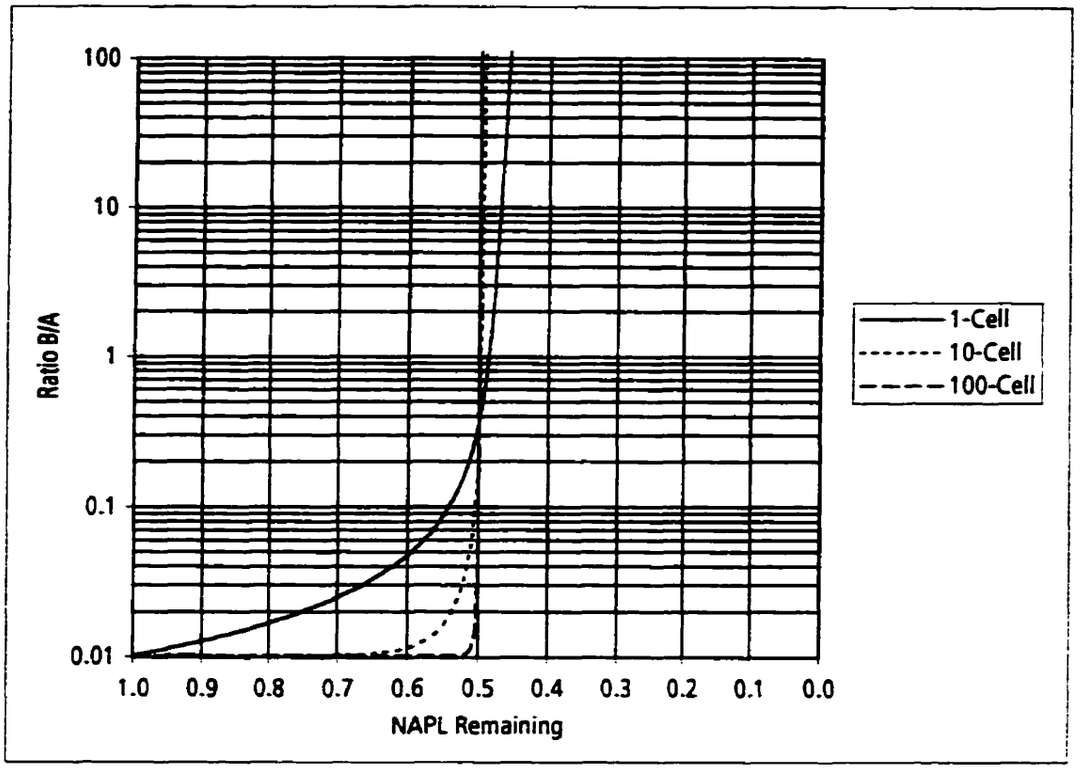

Additional Input Parameters:
Total Porosity - 0.3
f_{oc} - 0.0001
NAPL Content - 15 L/m³

K_{oc} - 50 mL/g (component A)
K_{oc} - 5,000 mL/g (component B)

Figure 4-5. Aqueous concentration ratios predicted by ESM for binary NAPL mixture with pure-phase solubilities of 1,000 mg/L (component A) and 10 mg/L (component B) for 1-cell, 10-cell and 100-cell configurations.

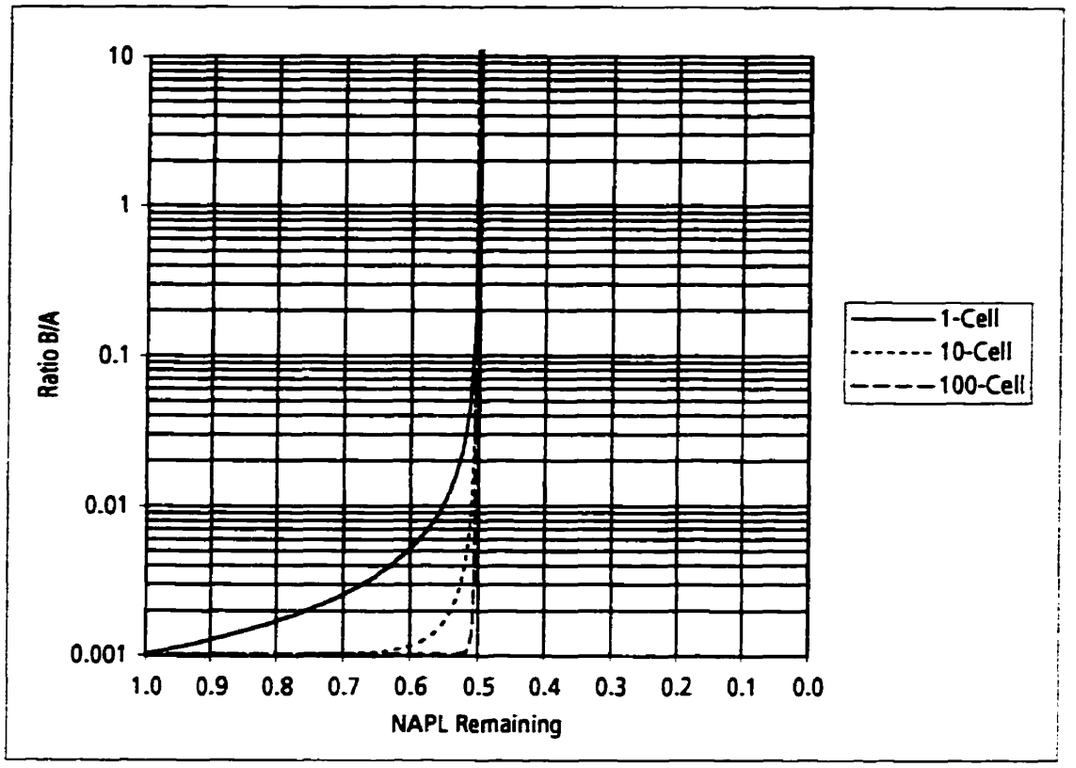

Additional Input Parameters:
Total Porosity - 0.3
f_{oc} - 0.0001
NAPL Content - 15 L/m³

K_{oc} - 50 mL/g (component A)
K_{oc} - 50,000 mL/g (component B)

Figure 4-6. Aqueous concentration ratios predicted by ESM for binary NAPL mixture with pure-phase solubilities of 1,000 mg/L (component A) and 1 mg/L (component B) for 1-cell, 10-cell and 100-cell configurations.

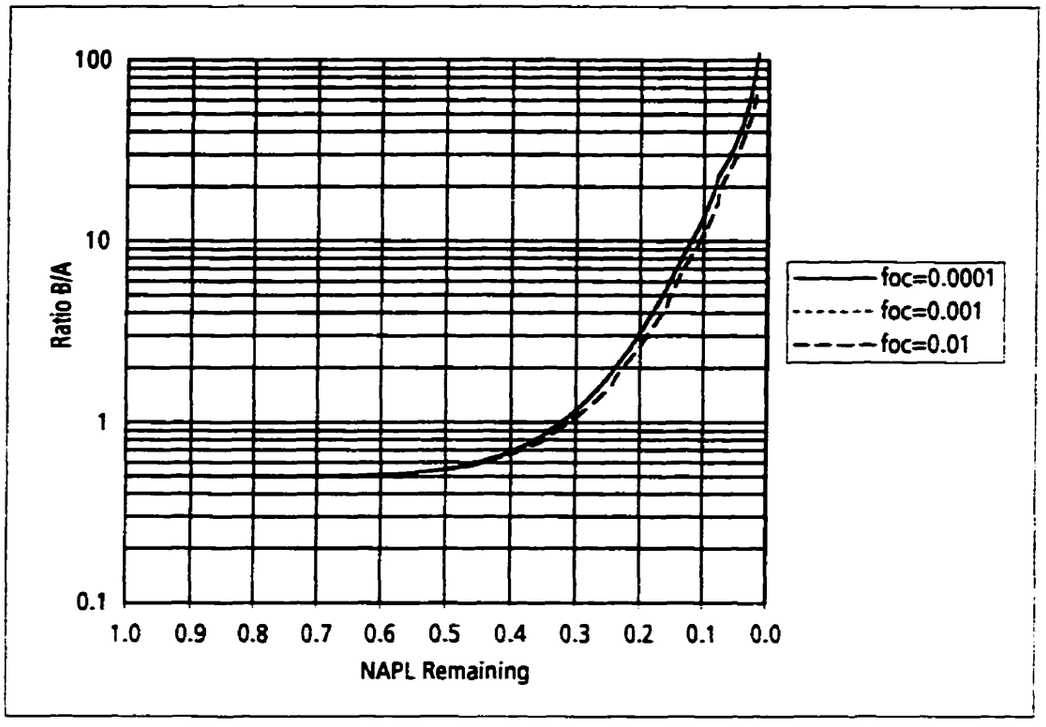

Additional Input Parmeters:
10-Cell Configuration
Total Porosity - 0.3
NAPL Residual Content - 15 L/m³
K_{oc} - 50 mL/g (component A)
K_{oc} - 100 mL/g (component B)

Figure 4-7. Aqueous concentration ratios predicted by ESM for binary NAPL mixture with pure-phase solubilities of 1,000 mg/L (component A) and 500 mg/L (component B) for f_{oc} values of 0.0001, 0.001 and 0.01.

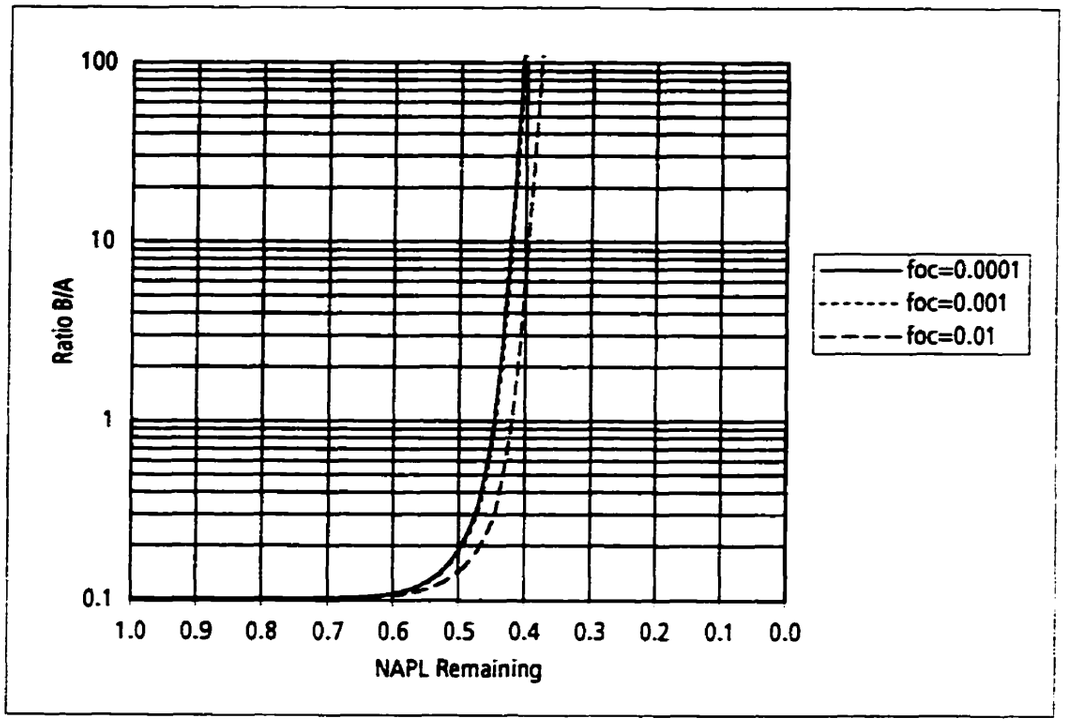

Additional Input Parmeters:
10-Cell Configuration
Total Porosity - 0.3
NAPL Residual Content - 15 L/m³

K_{oc} - 50 mL/g (component A)
K_{oc} - 500 mL/g (component B)

Figure 4-8. Aqueous concentration ratios predicted by ESM for binary NAPL mixture with pure-phase solubilities of 1,000 mg/L (component A) and 100 mg/L (component B) for f_{oc} values of 0.0001, 0.001 and 0.01.

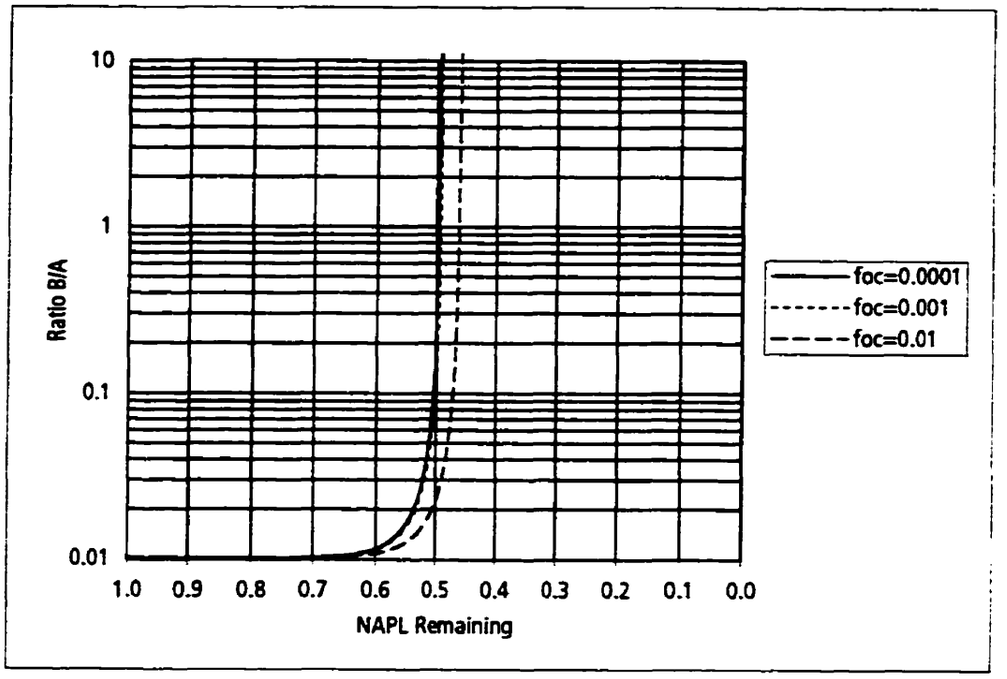

Additional Input Parmeters:
10-Cell Configuration
Total Porosity - 0.3
NAPL Residual Content - 15 L/m³

K_{oc} - 50 mL/g (component A)
K_{oc} - 5,000 mL/g (component B)

Figure 4-9. Aqueous concentration ratios predicted by ESM for binary NAPL mixture with pure-phase solubilities of 1,000 mg/L (component A) and 10 mg/L (component B) for f_{oc} values of 0.0001, 0.001 and 0.01.

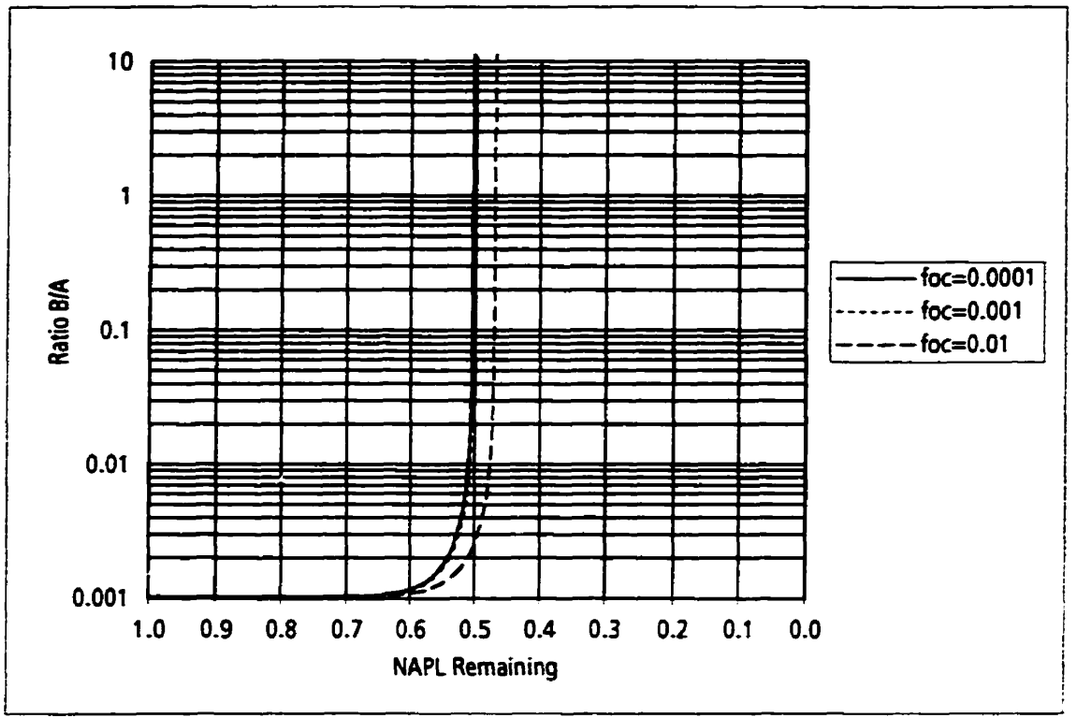

Additional Input Parmeters:
10-Cell Configuration
Total Porosity - 0.3
NAPL Residual Content - 15 L/m³

K_{oc} - 50 mL/g (component A)
K_{oc} - 50,000 mL/g (component B)

Figure 4-10. Aqueous concentration ratios predicted by ESM for binary NAPL mixture with pure-phase solubilities of 1,000 mg/L (component A) and 1 mg/L (component B) for f_{oc} values of 0.0001, 0.001 and 0.01.

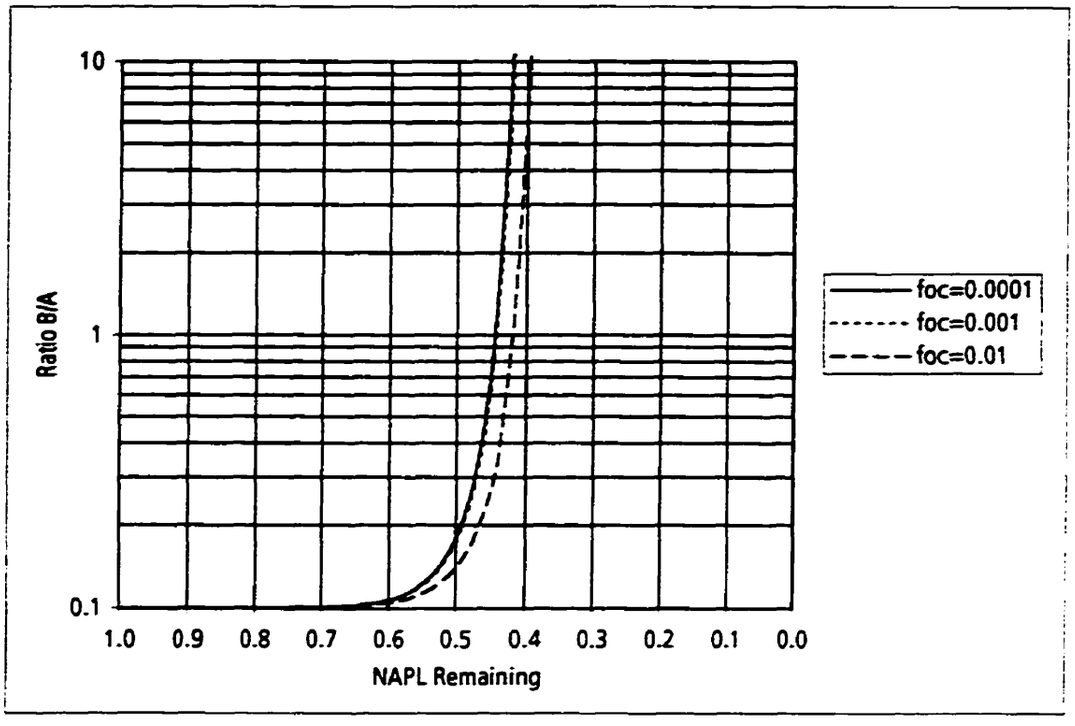

Additional Input Parmeters:
10-Cell Configuration
Total Porosity - 0.3
NAPL Residual Content - 15 L/m³

K_{oc} - 500 mL/g (component A)
K_{oc} - 5,000 mL/g (component B)

Figure 4-11. Aqueous concentration ratios predicted by ESM for binary NAPL mixture with pure-phase solubilities of 100 mg/L (component A) and 10 mg/L (component B) for f_{oc} values of 0.0001, 0.001 and 0.01.

File:foc 10-Cell #5 Equil.EXCL/Plot

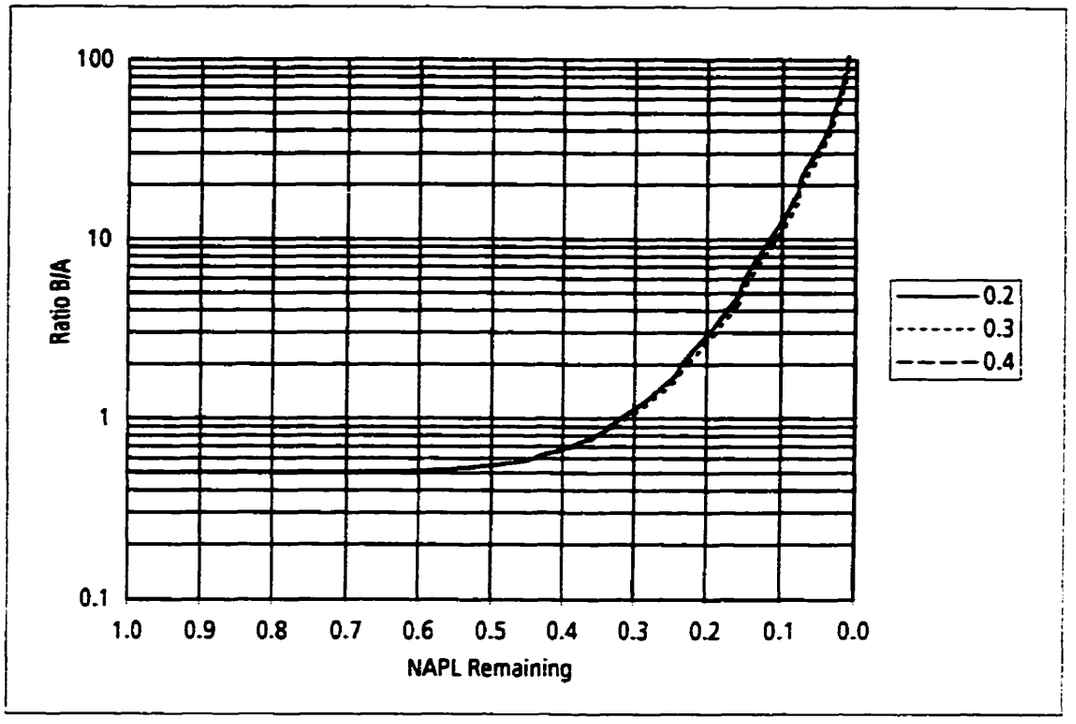

Additional Input Parmeters:
10-Cell Configuration
f_{oc} - 0.0001
NAPL Residual Content - 15 L/m³
K_{oc} - 50 mL/g (component A)
K_{oc} - 100 mL/g (component B)

Figure 4-12. Aqueous concentration ratios predicted by ESM for binary NAPL mixture with pure-phase solubilities of 1,000 mg/L (component A) and 500 mg/L (component B) for porosity values of 0.2, 0.3 and 0.4.

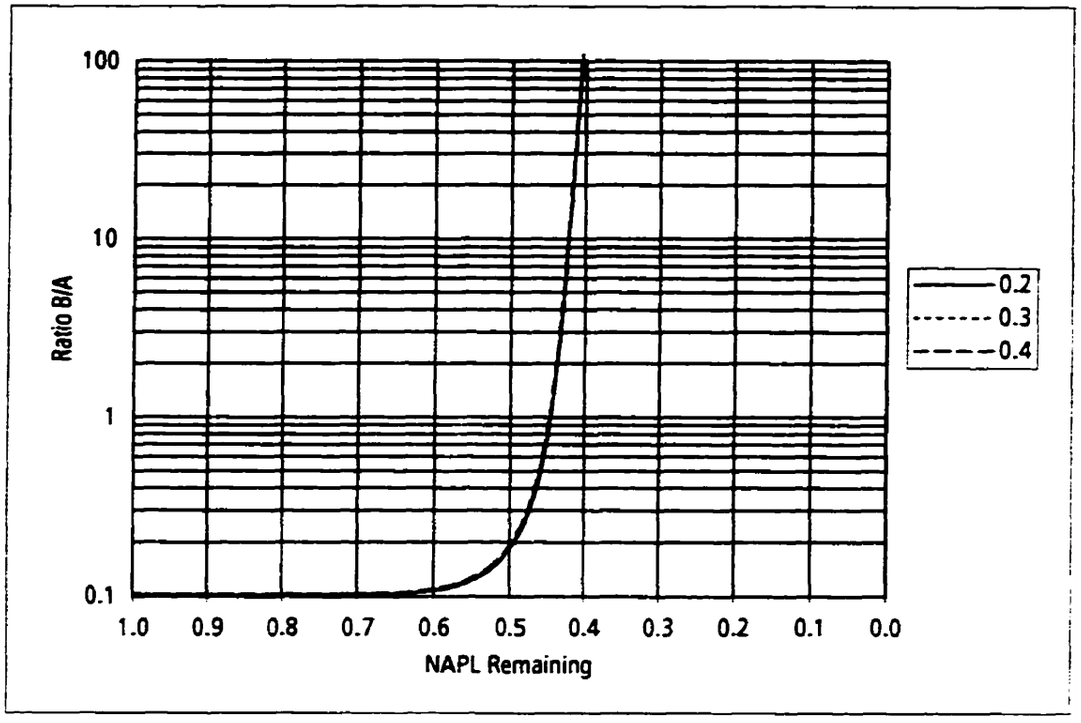

Additional Input Parmeters:
10-Cell Configuration
f_{oc} - 0.0001
NAPL Residual Content - 15 L/m³
K_{oc} - 50 mL/g (component A)
K_{oc} - 500 mL/g (component B)

Figure 4-13. Aqueous concentration ratios predicted by ESM for binary NAPL mixture with pure-phase solubilities of 1,000 mg/L (component A) and 100 mg/L (component B) for porosity values of 0.2, 0.3 and 0.4.

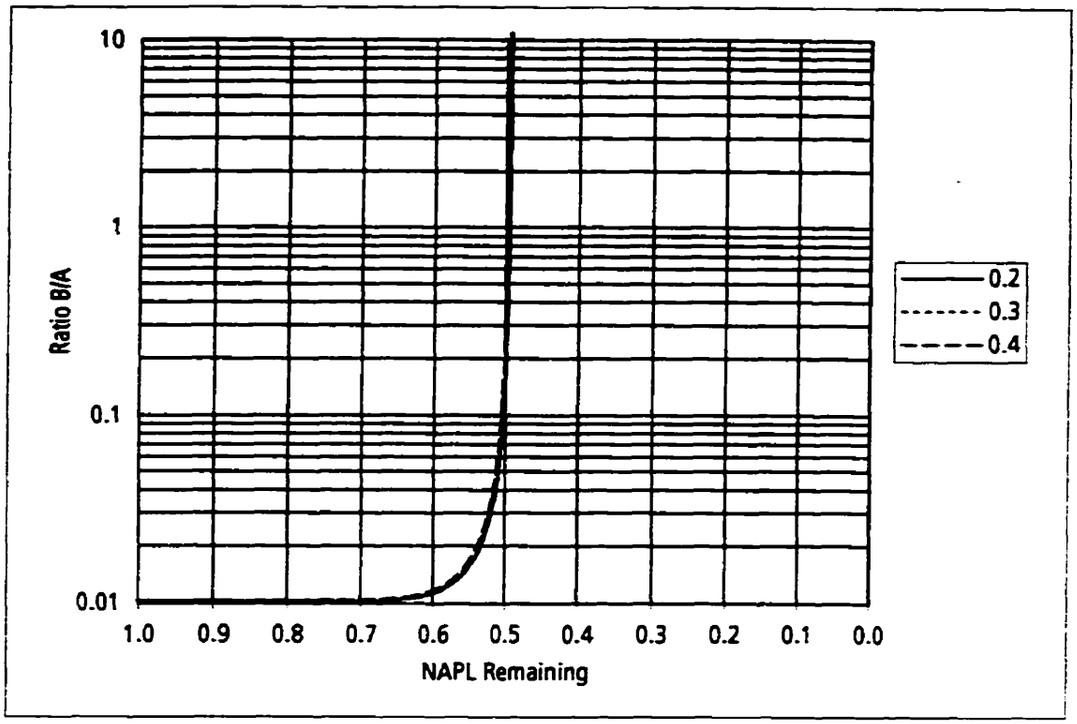

Additional Input Parmeters:
10-Cell Configuration
f_{oc} - 0.0001
NAPL Residual Content - 15 L/m³
K_{oc} - 50 mL/g (component A)
K_{oc} - 5,000 mL/g (component B)

Figure 4-14. Aqueous concentration ratios predicted by ESM for binary NAPL mixture with pure-phase solubilities of 1,000 mg/L (component A) and 10 mg/L (component B) for porosity values of 0.2, 0.3 and 0.4.

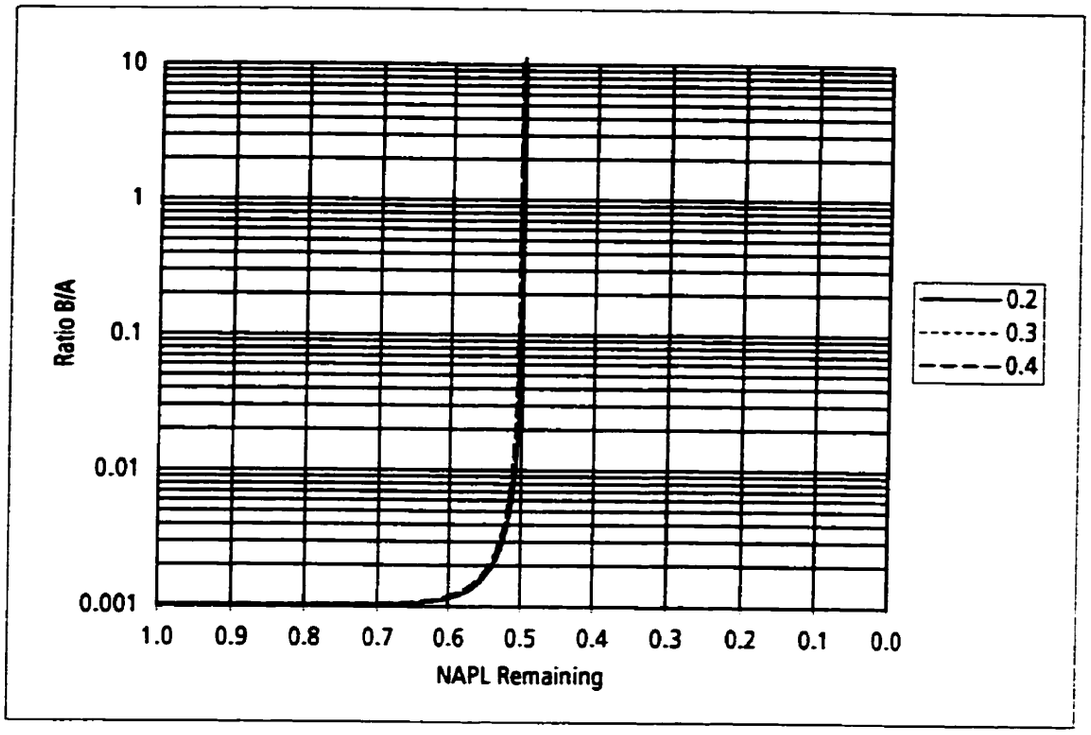

Additional Input Parmeters:
10-Cell Configuration
f_{oc} - 0.0001
NAPL Residual Content - 15 L/m³

K_{oc} - 50 mL/g (component A)
K_{oc} - 50,000 mL/g (component B)

Figure 4-15. Aqueous concentration ratios predicted by ESM for binary NAPL mixture with pure-phase solubilities of 1,000 mg/L (component A) and 1 mg/L (component B) for porosity values of 0.2, 0.3 and 0.4.

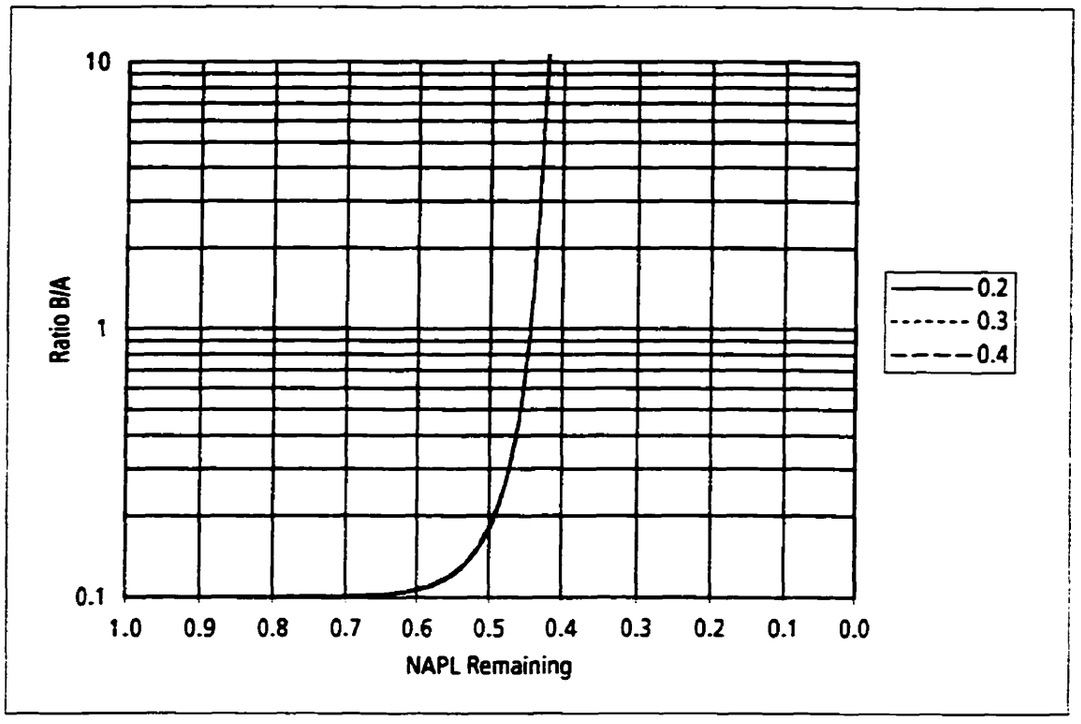

Additional Input Parmeters:
10-Cell Configuration
f_{oc} - 0.0001
NAPL Residual Content - 15 L/m³
K_{oc} - 500 mL/g (component A)
K_{oc} - 5,000 mL/g (component B)

Figure 4-16. Aqueous concentration ratios predicted by ESM for binary NAPL mixture with pure-phase solubilities of 100 mg/L (component A) and 10 mg/L (component B) for porosity values of 0.2, 0.3 and 0.4.

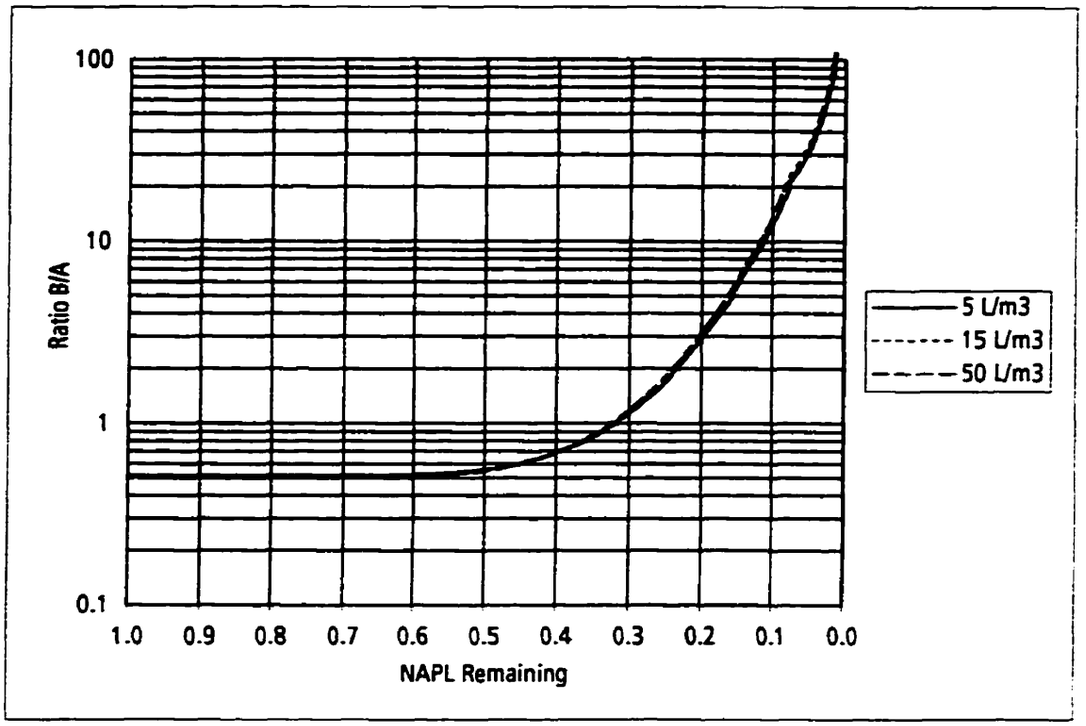

Additional Input Parmeters:
10-Cell Configuration
Total Porosity - 0.3
f_{oc} - 0.001

K_{oc} - 50 mL/g (component A)
K_{oc} - 100 mL/g (component B)

Figure 4-17. Aqueous concentration ratios predicted by ESM for binary NAPL mixture with pure-phase solubilities of 1,000 mg/L (component A) and 500 mg/L (component B) for NAPL residual contents of 5 L/m^3, 15 L/m^3, and 50 L/m^3.

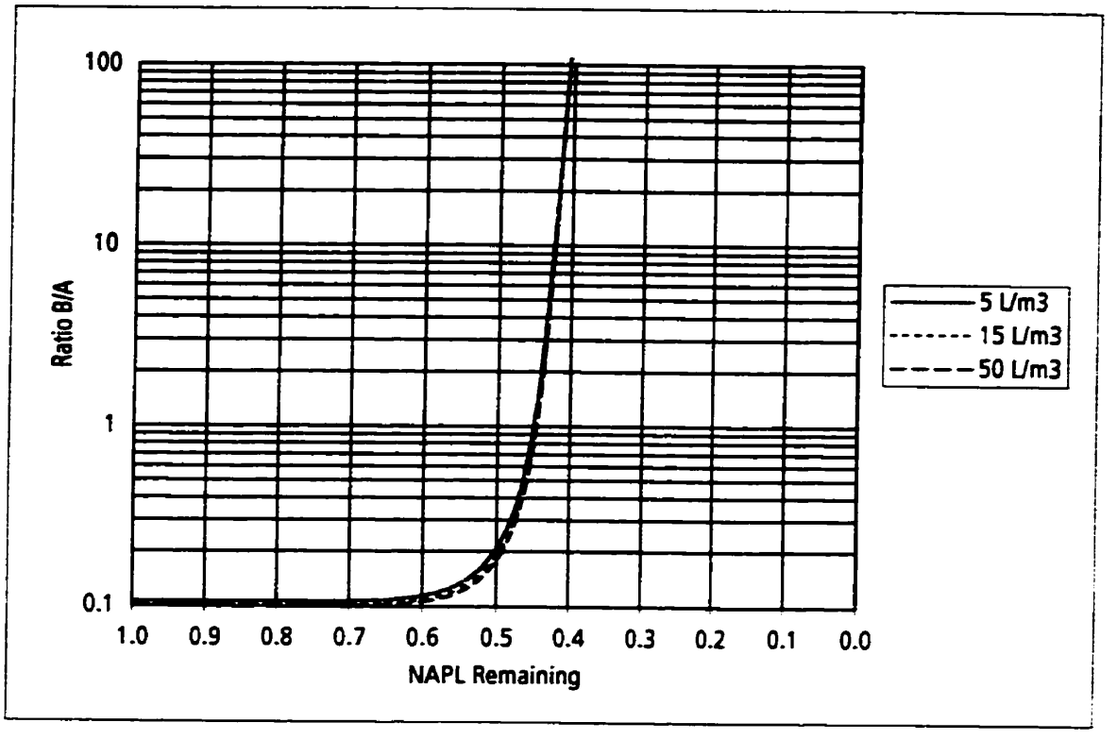

Additional Input Parmeters:
10-Cell Configuration
Total Porosity - 0.3
f_{oc} - 0.001

K_{oc} - 50 mL/g (component A)
K_{oc} - 500 mL/g (component B)

Figure 4-18. Aqueous concentration ratios predicted by ESM for binary NAPL mixture with pure-phase solubilities of 1,000 mg/L (component A) and 100 mg/L (component B) for NAPL residual contents of 5 L/m^3, 15 L/m^3, and 50 L/m^3.

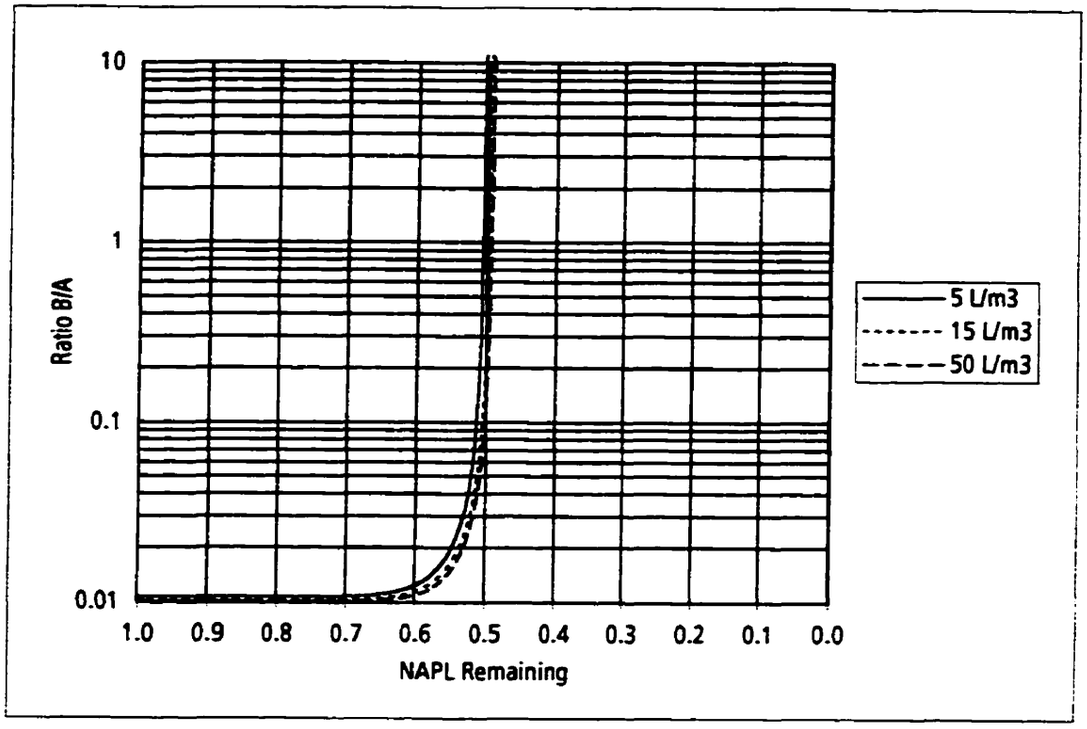

Additional Input Parmeters:
10-Cell Configuration
Total Porosity - 0.3
f_{oc} - 0.001

K_{oc} - 50 mL/g (component A)
K_{oc} - 5,000 mL/g (component B)

Figure 4-19. Aqueous concentration ratios predicted by ESM for binary NAPL mixture with pure-phase solubilities of 1,000 mg/L (component A) and 10 mg/L (component B) for NAPL residual contents of 5 L/m^3, 15 L/m^3, and 50 L/m^3.

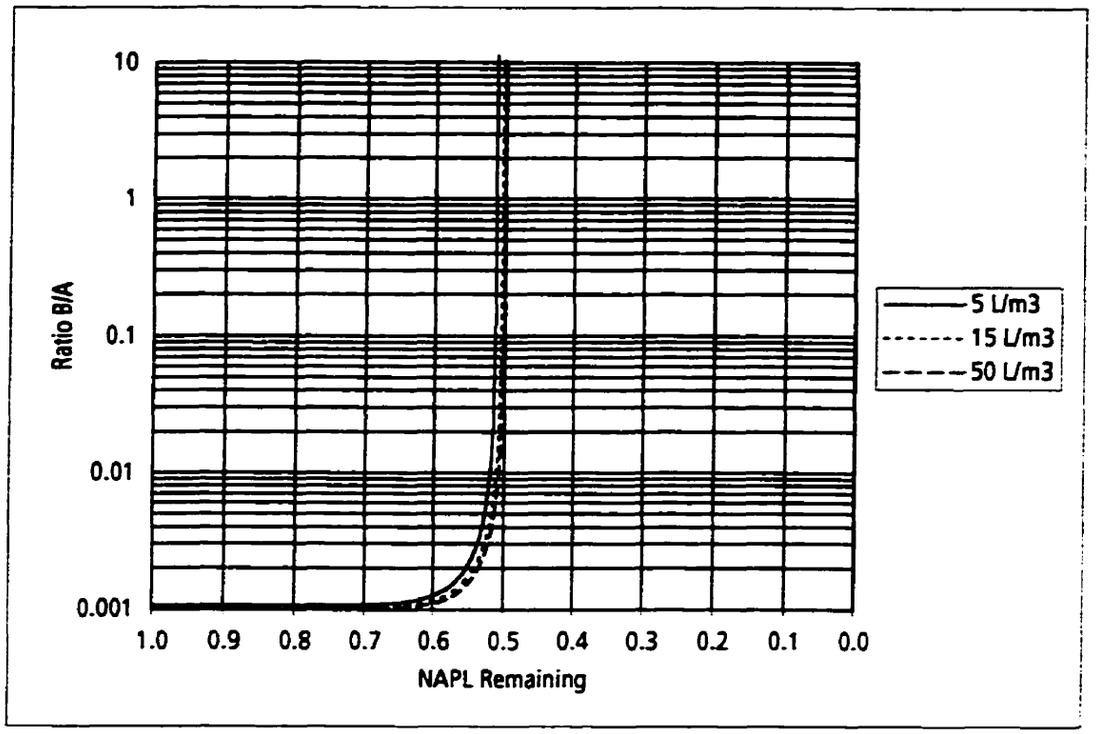

Additional Input Parmeters:
10-Cell Configuration
Total Porosity - 0.3
f_{oc} - 0.001

K_{oc} - 50 mL/g (component A)
K_{oc} - 50,000 mL/g (component B)

Figure 4-20. Aqueous concentration ratios predicted by ESM for binary NAPL mixture with pure-phase solubilities of 1,000 mg/L (component A) and 1 mg/L (component B) for NAPL residual contents of 5 L/m³, 15 L/m³, and 50 L/m³.

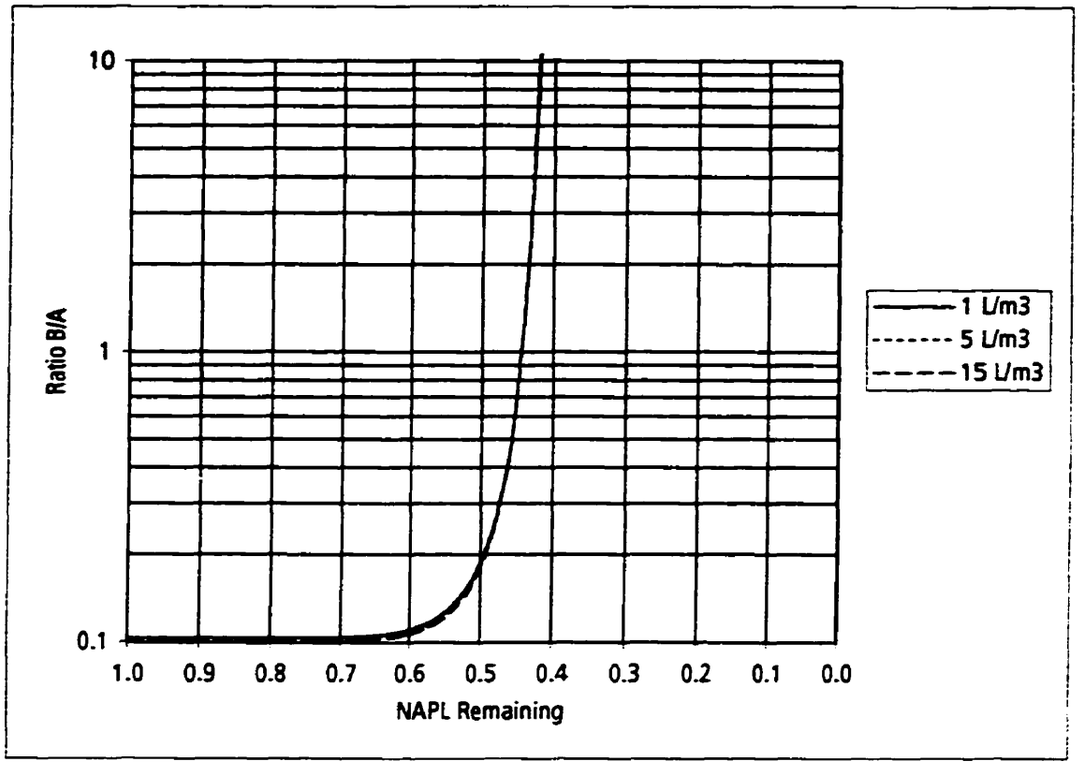

Additional Input Parmeters:
10-Cell Configuration
Total Porosity - 0.3
f_{oc} - 0.001

K_{oc} - 500 mL/g (component A)
K_{oc} - 5,000 mL/g (component B)

Figure 4-21. Aqueous concentration ratios predicted by ESM for binary NAPL mixture with pure-phase solubilities of 100 mg/L (component A) and 10 mg/L (component B) for NAPL residual contents of 1 L/m^3, 5 L/m^3, and 15 L/m^3.

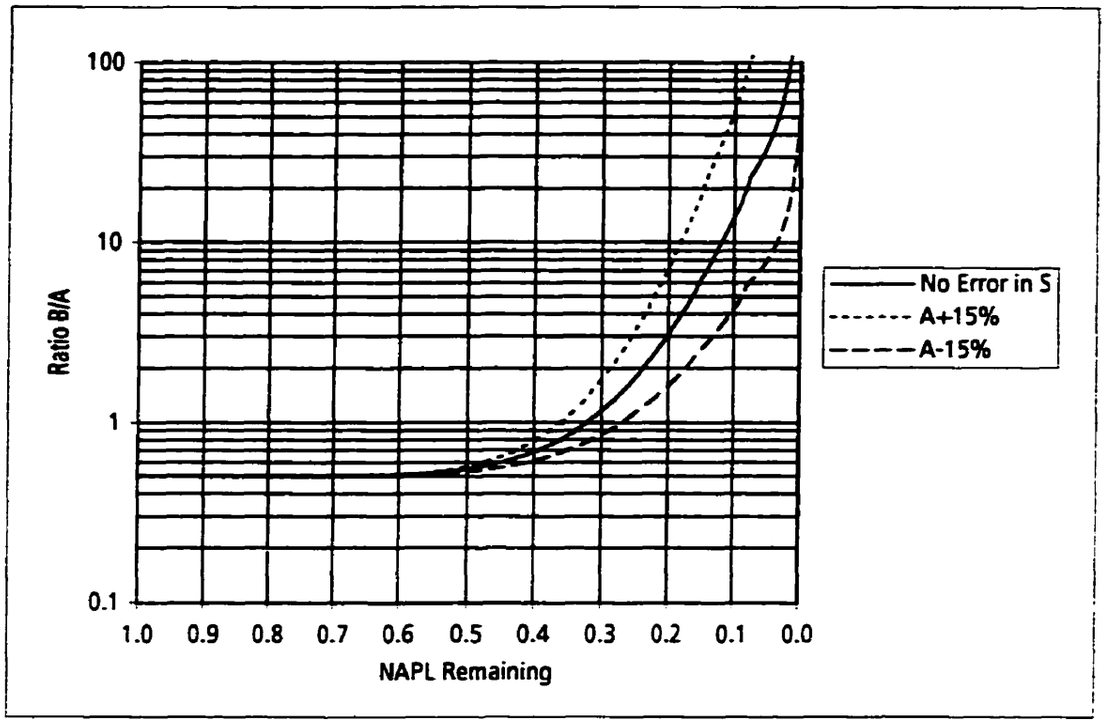

Additional Input Parameters:
10-Cell Configuration
Total Porosity - 0.3
f_{oc} - 0.0001
K_{oc} - 50 mL/g (component A)
K_{oc} - 100 mL/g (component B)

NAPL Residual Content - 15 L/m³
Solubility A+15% - 1,150 mg/L
Solubility A-15% - 850 mg/L

Figure 4-22. Aqueous concentration ratios predicted by ESM for binary NAPL mixture with pure-phase solubilities of 1,000 mg/L (component A) and 500 mg/L (component B) for +15% and -15% error in the solubility of component A.

File:10-Cell #1 Equil.EXCL/Plot

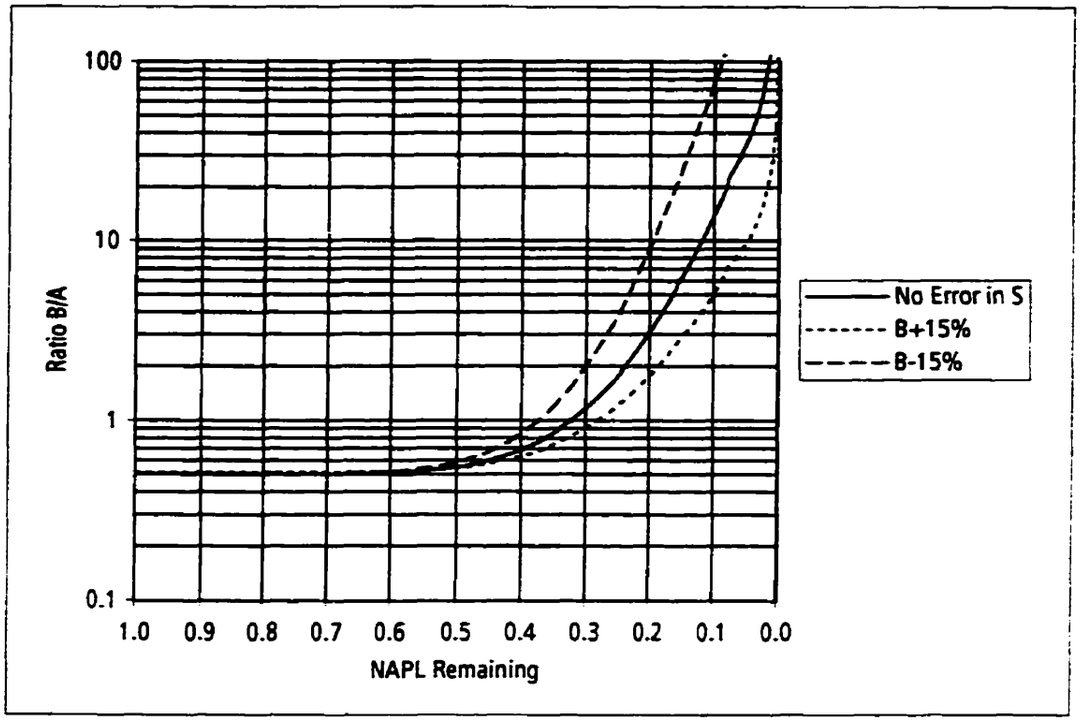

Additional Input Parameters:
10-Cell Configuration
Total Porosity - 0.3
f_{oc} - 0.0001
K_{oc} - 50 mL/g (component A)
K_{oc} - 100 mL/g (component B)

NAPL Residual Content - 15 L/m³
Solubility B+15% - 575 mg/L
Solubility B-15% - 425 mg/L

Figure 4-23. Aqueous concentration ratios predicted by ESM for binary NAPL mixture with pure-phase solubilities of 1,000 mg/L (component A) and 500 mg/L (component B) for +15% and -15% error in the solubility of component B.

File:10-Cell #1 Equil.EXCL/Plot

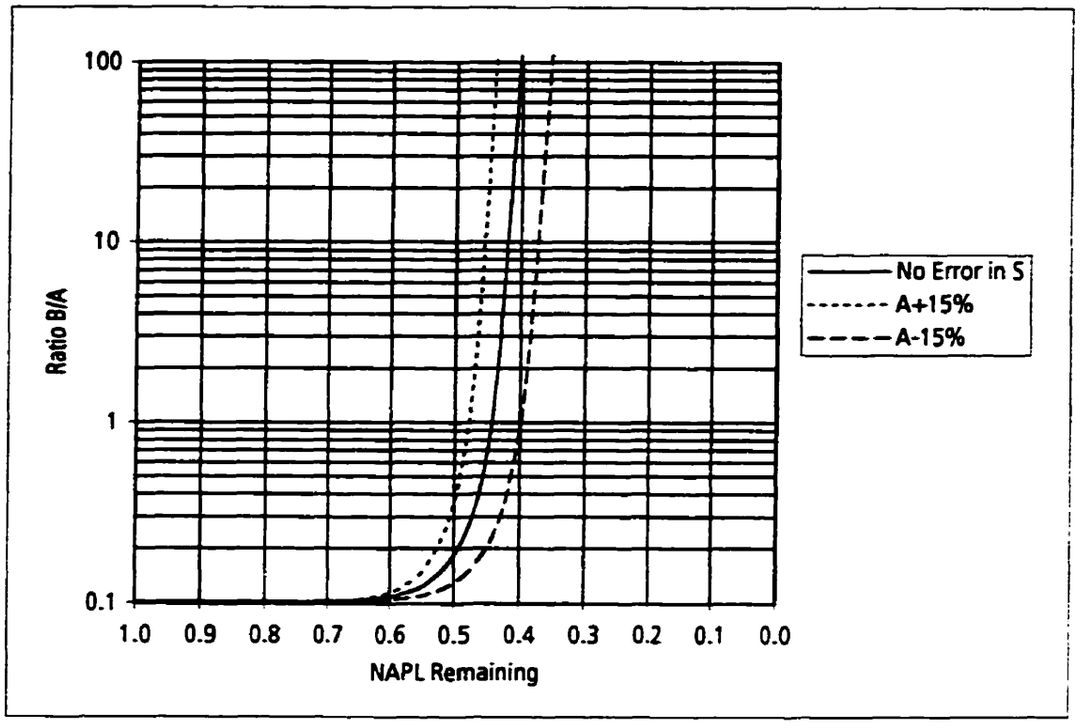

Additional Input Parameters:
10-Cell Configuration
Total Porosity - 0.3
f_{oc} - 0.0001
K_{oc} - 50 mL/g (component A)
K_{oc} - 500 mL/g (component B)
NAPL Residual Content - 15 L/m³
Solubility A+15% - 1,150 mg/L
Solubility A-15% - 850 mg/L

Figure 4-24. Aqueous concentration ratios predicted by ESM for binary NAPL mixture with pure-phase solubilities of 1,000 mg/L (component A) and 100 mg/L (component B) for +15% and -15% error in the solubility of component A.

File:10-Cell #2 Equil.EXCL/Plot

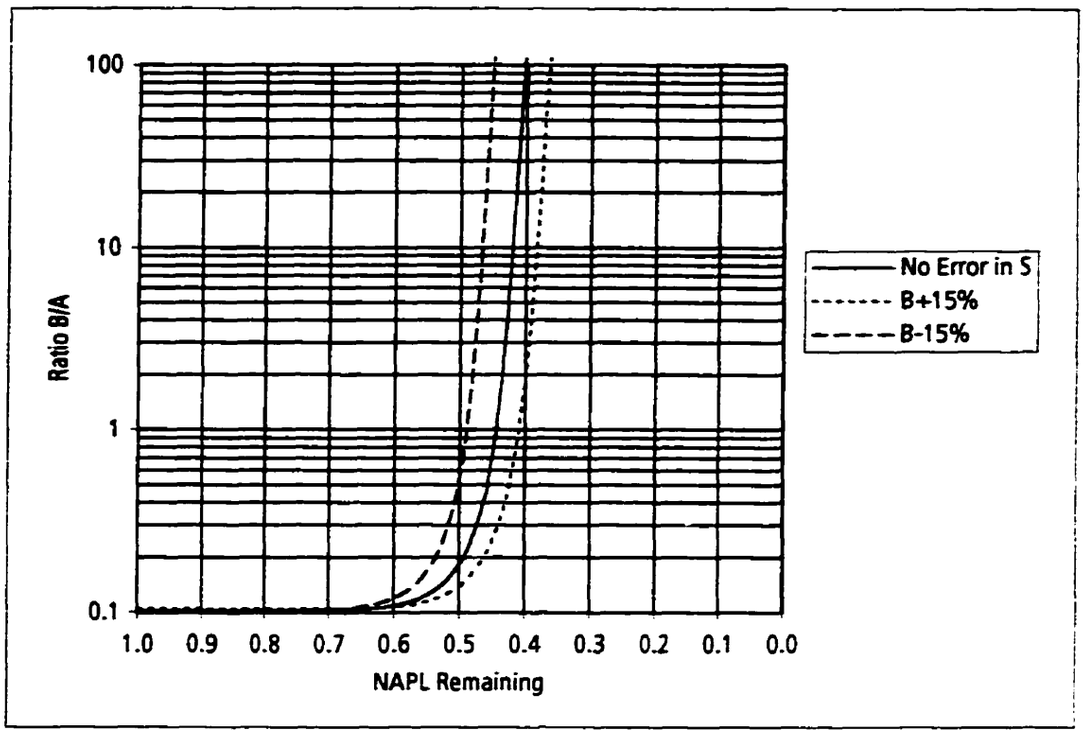

Additional Input Parameters:
10-Cell Configuration
Total Porosity - 0.3
f_{oc} - 0.0001
K_{oc} - 50 mL/g (component A)
K_{oc} - 500 mL/g (component B)
NAPL Residual Content - 15 L/m³
Solubility B+15% - 115 mg/L
Solubility B-15% - 85 mg/L

Figure 4-25. Aqueous concentration ratios predicted by ESM for binary NAPL mixture with pure-phase solubilities of 1,000 mg/L (component A) and 100 mg/L (component B) for +15% and -15% error in the solubility of component B.

File:10-Cell #2 Equil.EXCL/Plot

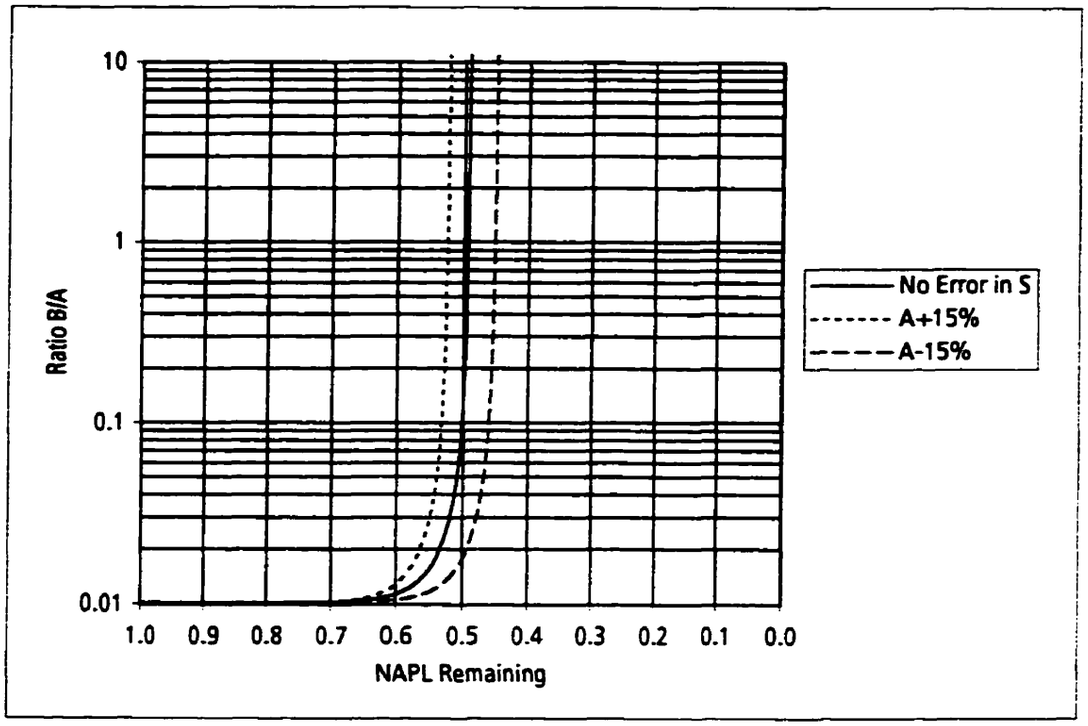

Additional Input Parameters:
10-Cell Configuration
Total Porosity - 0.3
f_{oc} - 0.0001
K_{oc} - 50 mL/g (component A)
K_{oc} - 5,000 mL/g (component B)
NAPL Residual Content - 15 L/m³
Solubility A+15% - 1,150 mg/L
Solubility A-15% - 850 mg/L

Figure 4-26. Aqueous concentration ratios predicted by ESM for binary NAPL mixture with pure-phase solubilities of 1,000 mg/L (component A) and 10 mg/L (component B) for +15% and -15% error in the solubility of component A.

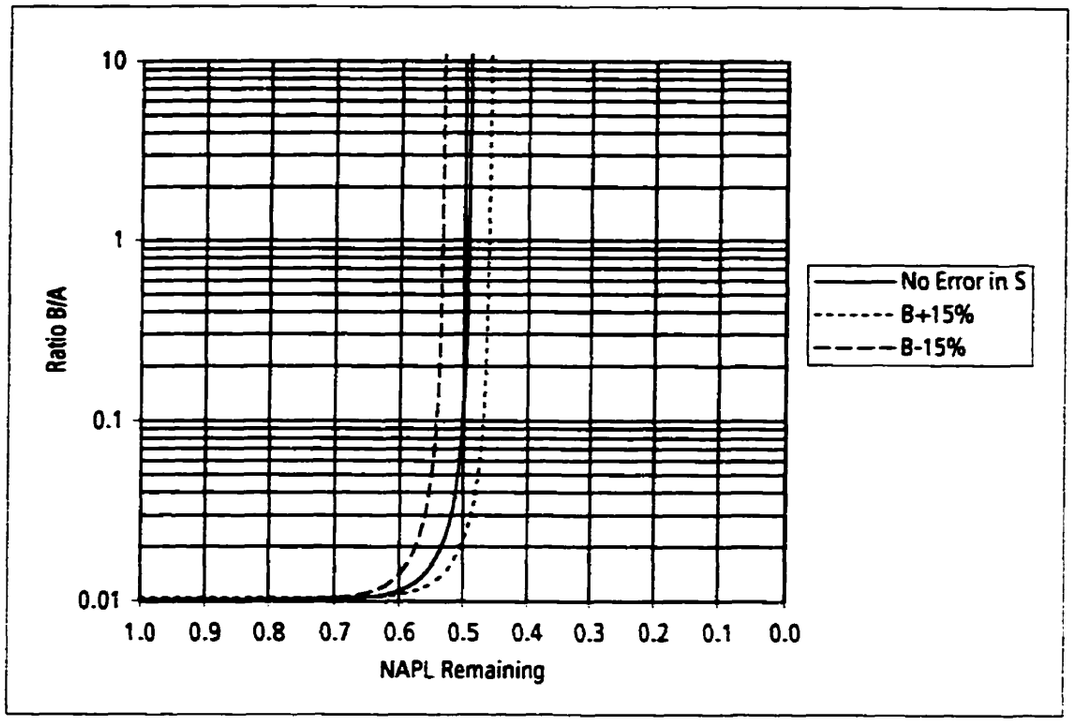

Additional Input Parameters:
10-Cell Configuration
Total Porosity - 0.3
f_{oc} - 0.0001
K_{oc} - 50 mL/g (component A)
K_{oc} - 5,000 mL/g (component B)
NAPL Residual Content - 15 L/m³
Solubility B+15% - 11.5 mg/L
Solubility B-15% - 8.5 mg/L

Figure 4-27. Aqueous concentration ratios predicted by ESM for binary NAPL mixture with pure-phase solubilities of 1,000 mg/L (component A) and 10 mg/L (component B) for +15% and -15% error in the solubility of component B.

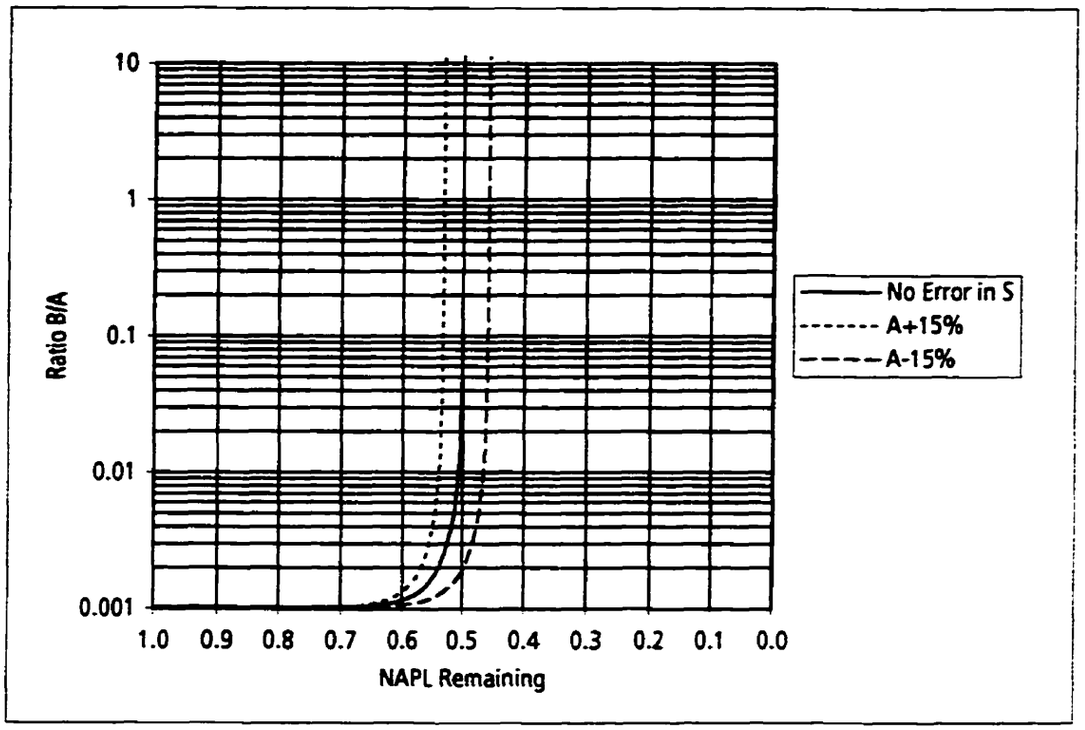

Additional Input Parameters:
10-Cell Configuration
Total Porosity - 0.3
f_{oc} - 0.0001
K_{oc} - 50 mL/g (component A)
K_{oc} - 50,000 mL/g (component B)
NAPL Residual Content - 15 L/m³
Solubility A+15% - 1,150 mg/L
Solubility A-15% - 850 mg/L

Figure 4-28. Aqueous concentration ratios predicted by ESM for binary NAPL mixture with pure-phase solubilities of 1,000 mg/L (component A) and 1 mg/L (component B) for +15% and -15% error in the solubility of component A.

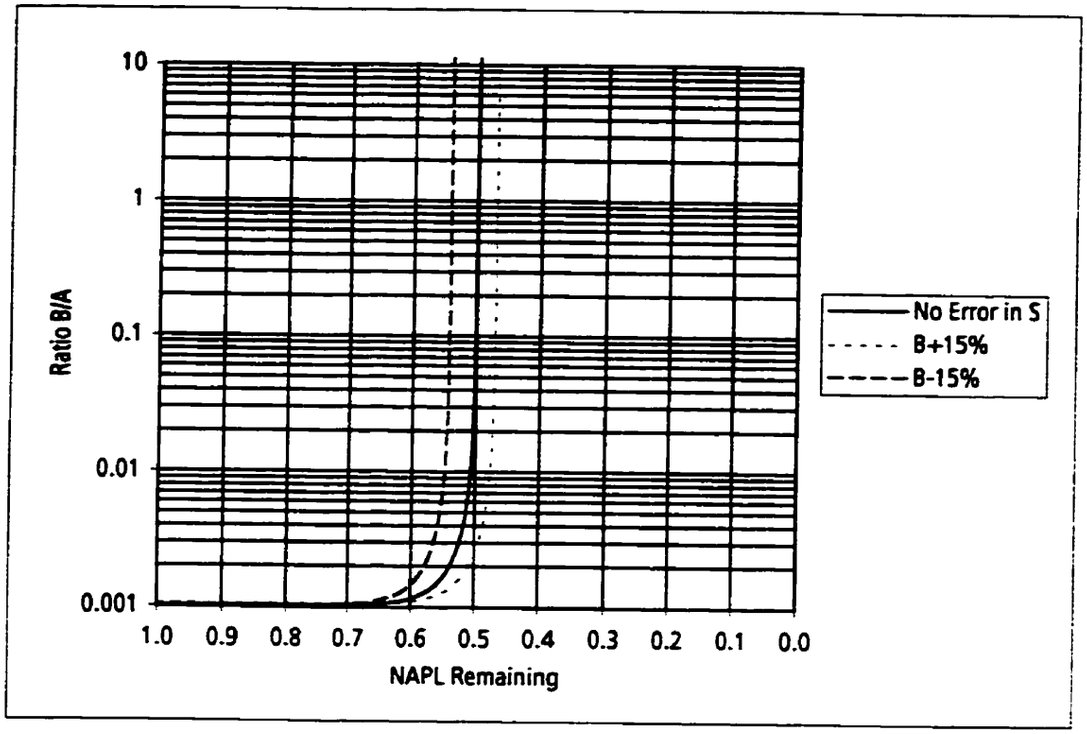

Additional Input Parameters:
10-Cell Configuration
Total Porosity - 0.3
f_{oc} - 0.0001
K_{oc} - 50 mL/g (component A)
K_{oc} - 50,000 mL/g (component B)

NAPL Residual Content - 15 L/m³
Solubility B+15% - 1.15 mg/L
Solubility B-15% - 0.85 mg/L

Figure 4-29. Aqueous concentration ratios predicted by ESM for binary NAPL mixture with pure-phase solubilities of 1,000 mg/L (component A) and 1 mg/L (component B) for +15% and -15% error in the solubility of component B.

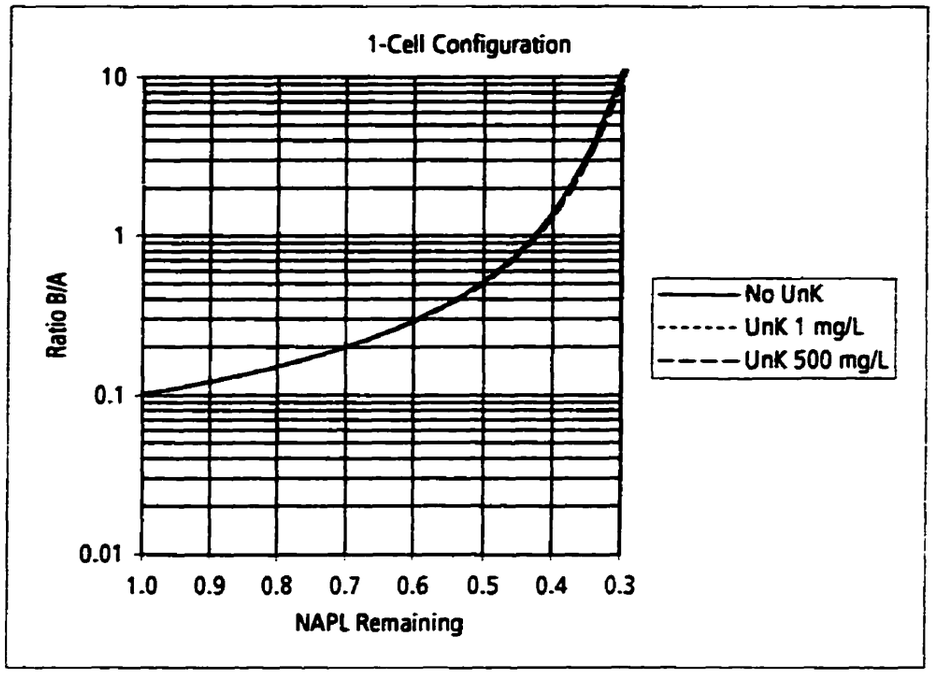

Additional Input Parameters:

Total Porosity - 0.3
f_{oc} - 0.0001
NAPL Residual Content - 20 L/m³
Solubility - 1,000 mg/L (component A)
Solubility - 100 mg/L (component B)
Component A - 25 wt.%
Component B - 25 wt.%
Unknown Component - 50 wt.%

Figure 4-30. Aqueous concentration ratios predicted by 1-cell ESM for NAPL mixtures having an unknown (UnK) component with different pure-phase solubility values.

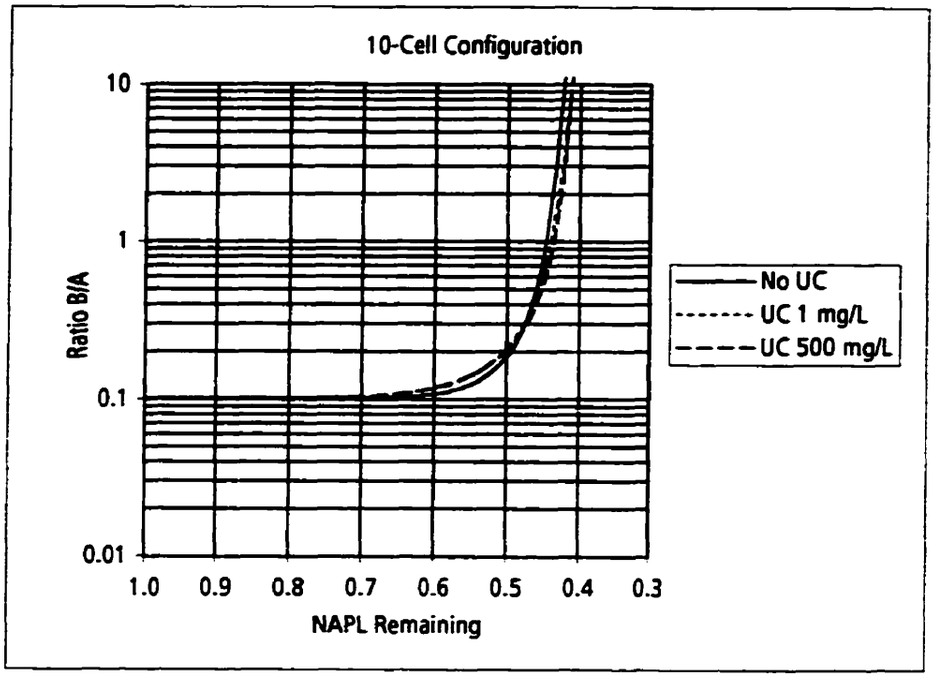

Additional Input Parameters:
Total Porosity - 0.3
f_{oc} - 0.0001
NAPL Residual Content - 20 L/m³
Solubility - 1,000 mg/L (component A)
Solubility - 100 mg/L (component B)
Component A - 25 wt.%
Component B - 25 wt.%
Unknown Component - 50 wt.%

Figure 4-31. Aqueous concentration ratios predicted by 10-cell ESM for NAPL mixtures having an unknown (UnK) component with different pure-phase solubility values.

5. Comparison of Results of Laboratory Studies to ESM

ESM simulations were compared to the results of three published laboratory column dissolution experiments. In each experiment, the NAPL composition and mass of NAPL placed in the column was known, and the aqueous concentrations emitted from the column were measured. Aqueous concentration ratios and the NAPL mass remaining were determined from the experimental data. This allowed direct comparison to ESM simulations.

5.1 Chlorinated Benzene Mixture

5.1.1 Experimental Conditions

Mackay et al. (1991) performed a laboratory column dissolution experiment using a mixture of monochloro-, trichloro-, tetrachloro-, pentachloro- and hexachlorobenzene. The chemical composition of this NAPL mixture and the properties of its components are shown in Table 5-1. This experiment used a "generator column" rather than a column packed with natural porous medium. The generator column method for the evaluation of NAPL dissolution was described by Shiu et al. (1988). The generator column consisted of a 30-cm long, 0.64-cm diameter, stainless steel tubing packed with chromasorb W (30/60 mesh or 0.59 mm to 0.25 mm diameter). Chromasorb is comprised of porous polymer beads and is used in chromatography applications. The chromasorb beads were coated with 0.3 mL of the NAPL mixture prior to placement in the column. Water was passed through the column at a rate of 1 to 5 mL/minute and the column effluent was analysed by high-performance liquid chromatography (HPLC).

The measured aqueous concentrations are shown in Figure 5-1 plotted versus the ratio, Q, of the cumulative volume of water passed through the column relative to the initial volume of NAPL in the column. Mackay et al. (1991) expressed the results of their experiments in terms of Q, rather than

time or column pore volumes, so that the experiments results are plotted here also versus Q. The aqueous concentrations of pentachlorobenzene and hexachlorobenzene are not shown because they occurred at concentrations close to the detection limit of the analytical method and did not vary significantly during the experiment. Chlorobenzene (CBz) has the highest effective solubility and was dissolved preferentially from the NAPL. Chlorobenzene concentrations declined rapidly with increasing Q, and almost disappeared as Q approached a value of 10,000. As chlorobenzene concentrations declined, 1,2,4-trichlorobenzene (124-TCBz) concentrations increased and then remained relatively constant until Q approached at value of about 22,000. At this point, 1,2,4-trichlorobenzene concentrations declined. The concentrations of 1,2,3,5-tetrachlorobenzene (1235-TeCBz) remained constant during the experiments at a value just above the analytical detection limit.

The measured aqueous concentration ratios of 124-TCBz/CBz, 1235-TeCBz/CBz and 1235-TeCBz/124-TCBz are shown in Figures 5-2, 5-3 and 5-4, respectively, plotted versus Q. The measured aqueous concentration ratios of 124-TCBz/CBz, 1235-TeCBz/CBz and 1235-TeCBz/124-TCBz are shown in Figures 5-5, 5-6 and 5-7, respectively, plotted versus the mass of NAPL remaining. The ratios of 124-TCBz/CBz and 1235-TeCBz/CBz increased rapidly as chlorobenzene dissolved from the NAPL. The ratio of 1235-TeCBz/124-TCBz increased only at the later stages of dissolution.

5.1.2 Comparison to ESM

The ESM was used to simulate the changes in aqueous concentrations and concentration ratios for dissolution of the chlorinated benzene mixture. The properties of the components listed in Table 5-1 were used as input data. The column packing was assumed to have a dry bulk density of 1,458 kg/m^3, a total porosity of 0.45 and negligible potential for sorption (i.e. very low f_{OC}). The initial NAPL content was assumed to be 15 L/m^3. Using these parameter

values, simulations were performed for 1-cell, 2-cell and 4-cell configurations. The number of cells used is the only parameter not defined by the NAPL or porous medium properties.

The measured aqueous concentrations versus Q are compared to the aqueous concentrations predicted by the ESM in Figures 5-8, 5-9 and 5-10 for the 1-cell, 2-cell and 4-cell configurations, respectively. For all three configurations, the measured initial aqueous concentrations compared very well to the effective solubility values calculated by Raoult's Law. These values are shown in Table 5-2. This indicates that chemical equilibrium is attained between the water and NAPL as water flows through the column. It indicates also that Raoult's Law is an appropriate method for the calculation of effective solubility. The aqueous concentrations calculated by the ESM compare reasonably well with the measured concentrations for all three cell configurations. The results of the 2-cell configuration provide the best match to the measured chlorobenzene concentrations and the 3-cell configuration provides the best match for the 1,2,4-trichlorobenzene concentrations.

The measured aqueous concentration ratios versus NAPL remaining are compared to the aqueous concentration ratios calculated by the ESM in Figures 5-11, 5-12 and 5-13 for the 124-TCBz/CBz, 1235-TeCBz/CBz and 1235-TeCBz/124-TCBz ratios, respectively. For the 124-TCBz/CBz ratio, the results of the 2-cell configuration provide the best match to the measured ratios. A small number of cells would be consist with a short NAPL zone which does not cause an appreciable chromatographic effect. For the 1235-TeCBz/CBz ratio, the results of the 4-cell configuration provide the best match to the measured ratios but the match is still relatively poor. None of the simulations compare well to the measured 1235-TeCBz/124-TCBz ratios. The discrepancy in the number of cells required for a match between the 124-TCBz/CBz ratio (i.e. 2-cell) and the 1235-TeCBz/CBz ratio (i.e. 4-cell), and the lack of match for the 1235-TeCBz/124-TCBz ratio may be due to the fact the

aqueous concentrations of 1235-TeCBz were close to the analytical detection limit and did not reflect the aqueous concentrations accurately.

5.2 Petroleum Hydrocarbon Mixture

5.2.1 Experimental Conditions

Ramanantsoa et al. (1986) performed a laboratory column dissolution experiment using a mixture of petroleum hydrocarbons including: cyclohexane, 2,3-dimethyl butane and hexane. The chemical composition and properties of this mixture are shown in Table 5-3. This experiment used a sand-filled column containing NAPL at residual saturation. Water was passed through the column and the aqueous concentrations in the column effluent were measured by infrared spectrometry.

The measured aqueous concentrations are shown in Figure 5-14 plotted versus the ratio, Q. Ramanantsoa et al., (1986) expressed the results of their experiments in terms of Q rather than time or column pore volumes of water, so the experimental results are plotted here also as Q. Cyclohexane (CHex) has the highest effective solubility and is removed preferentially from the NAPL. Cyclohexane concentrations declined rapidly with increasing Q, and almost disappeared as Q approached a value of 1,000. As cyclohexane concentrations declined, 2,3-dimethyl butane (DMB) and hexane (Hex) concentrations increased until each, in turn began to decline as NAPL was depleted. Dimethyl butane disappeared at a value of Q of 1,700 and hexane disappeared at 2,000.

The measured aqueous concentration ratios of Hex/CHex, Hex/DMB and DMB/CHex are shown in Figures 5-15, 5-16 and 5-17, respectively, plotted versus Q. The measured aqueous concentration ratios of Hex/CHex, Hex/DMB and DMB/CHex are shown in Figures 5-18, 5-19 and 5-20, respectively, plotted versus the mass of NAPL remaining. All the measured

concentration ratios increased rapidly as components were dissolved sequentially from the NAPL according to their effective solubility.

5.2.2 Comparison to ESM

The ESM was used to simulate the changes in aqueous concentrations and concentration ratios for dissolution of the petroleum hydrocarbon mixture. The properties of the components listed in Table 5-3 were used as input data. The column packing was assumed to have a dry bulk density of 1,458 kg/m^3, a total porosity of 0.45 and negligible potential for sorption (i.e. very low f_{OC}). The initial NAPL content was assumed to be 15 L/m^3. Using these parameter values, simulations were performed for 1-cell, 5-cell and 10-cell configurations. The number of cells used is the only parameter not defined by the NAPL or porous medium properties.

The measured aqueous concentration ratios versus NAPL remaining are compared to the ratios predicted by the ESM in Figures 5-21, 5-22 and 5-23 for Hex/CHex, Hex/DMB, and DMB/Hex, respectively, each for 1-cell, 5-cell and 10-cell configurations. With the exception of CHex, the measured initial aqueous concentrations compared reasonably well to the effective solubility values calculated by Raoult's Law. These values are shown in Table 5-4. The measured aqueous concentration for CHex was 26.5 mg/L compared to a value of 21 mg/L predicted by Raoult's Law. The aqueous concentration ratios calculated by the ESM do not compare well with the measured concentration ratios for the 1-cell configuration. This indicates that the chromatographic effect alters the aqueous concentrations emitted from the NAPL residual. The results of the 10-cell configuration provide the best match to the measured ratios, but the quality of the match is much better for the Hex/DMB ratio than the Hex/CHex or DMB/CHex ratios. This is may be due to the fact that the aqueous concentrations for CHex predicted by Raoult's Law were lower than the measured concentrations.

5.3 Benzene-Toluene Mixture

5.3.1 Experimental Conditions

Geller and Hunt (1993) performed a laboratory column dissolution experiment using a mixture of benzene and toluene. The chemical composition of this NAPL mixture and properties of its components are shown in Table 5-5. The column consisted of 5-cm diameter, 15-cm long glass tubing packed with 40-45 mesh (0.42 mm to 0.35 mm diameter) silica glass beads. A volume of 1.39 mL of NAPL mixture was injected into the centre of the column via a needle and syringe. Water was passed through the column at a rate equivalent to a Darcy velocity of 5 m/day. The column effluent was analysed by gas chromatography.

The measured aqueous concentrations are shown in Figure 5-24 plotted versus the number of column pore volumes of water. Geller and Hunt expressed the results of their experiments in terms of column pore volumes, rather than time or water:NAPL ratio, Q, so the experimental results are plotted here also versus column pore volumes. Benzene (Bz) has the highest effective solubility and was removed preferentially from the NAPL. Benzene concentrations declined rapidly with increasing pore volumes, and almost disappeared as the number of pore volumes approached a value of 100.

The measured aqueous concentration ratios of Tol/Bz are shown in Figures 5-25, plotted versus the number of column pore volumes. The measured aqueous concentration ratios of Tol/Bz are shown in Figures 5-26, plotted versus the mass of NAPL remaining.

5.3.2 Comparison to ESM

The ESM was used to simulate the changes in aqueous concentrations and concentration ratios for dissolution of the benzene-toluene mixture. The properties of the components listed in Table 5-5 were used as input data. The column packing was assumed to have a dry bulk density of 1,647 kg/m^3, a total porosity of 0.39 and negligible potential for sorption (i.e. very low f_{OC}). The initial NAPL content was assumed to be 15 L/m^3. Using these parameter values, simulations were performed for 1-cell, 2-cell and 3-cell configurations.

The measured aqueous concentration ratios versus NAPL mass remaining are compared to the ratios predicted by the ESM in Figure 5-27 for 1-cell, 2-cell and 3-cell configurations. For all three configurations, the measured initial aqueous concentrations were far less than the effective solubility values calculated by Raoult's Law. These values are shown in Table 5-6. This indicates that chemical equilibrium was not attained between the water and NAPL as water flows through the column. This is likely due to the high water velocity and NAPL zone geometry in the column. However, despite the fact that the magnitude of the aqueous concentrations was far less than effective solubility, the measured initial aqueous concentration ratio was identical to the predicted initial ratio. This indicates that dilution effects caused the lowering of aqueous concentration, but Raoult's Law and the ESM are still appropriate method for the calculation of aqueous concentration ratios. The results of the 2-cell configuration provide the best overall match to the measured ratios.

5.4 Conclusions Regarding Comparison to Laboratory Studies

For the three laboratory experiments considered here, the aqueous concentration ratios calculated by the ESM compare favourably with the measured concentration ratios as the ratios change during NAPL dissolution.

For the experiments using the chlorinated benzene mixture and the benzene-toluene mixture, the ratios calculated by the 1-cell configuration of the ESM compare reasonably well with the measured ratios. Slightly better matches between the calculated and measured ratios were obtained by 2-cell or 4-cell configurations. For the experiment using the petroleum hydrocarbon mixture, a reasonable match between the calculated and measured ratios required a 10-cell configuration of the ESM.

For application to an actual field site, ESM simulations would be used to calculate the expected change in aqueous concentration ratios versus the NAPL mass remaining. The change in aqueous concentration ratios observed at the site during some period of routine groundwater monitoring, or during groundwater extraction, would be then compared to the ESM calculations to allow prediction of the NAPL mass remaining at the site.

In its simplest 1-cell configuration, the ESM requires no "fitting parameters". The results of ESM simulations are dependent principally on the NAPL composition and the solubilities of the NAPL components. Information on the properties of the porous medium are required for the ESM, but the results of the simulations are insensitive to these parameters. No specific information is required on the groundwater flow rates, chemical mass transfer coefficients or dilution effects.

If the 1-cell configuration of the ESM were used to evaluate the changes in aqueous concentration ratios in the three laboratory experiments without knowledge of the actual NAPL mass remaining, reasonable predictions of the NAPL remaining could be made for the chlorinated benzene and benzene-toluene mixtures. For example, as shown in Figure 5-11, at the point where the measured 124-TCBz/CBz ratio reached 0.25, the ESM predicted the NAPL mass remaining to be 0.7 whereas the true NAPL mass remaining was 0.64. Similarly, at the point where the measured 124-TCBz/CBz ratios reached 20, the ESM predicted the NAPL mass remaining to be 0.47 whereas the true

NAPL remaining was 0.53. In comparison to the large uncertainty in estimating the mass contained in NAPL source zones by direct soil sampling and analysis, errors in prediction of NAPL remaining equivalent of 0.06, or 6% of the NAPL mass, are very small.

Predictions of NAPL mass remaining by the 1-cell configuration of the ESM would not be as reliable for the experiment using petroleum hydrocarbons. For example, as shown in Figure 5-21, at the point where the measured Hex/CHex ratio reached 0.3, the ESM predicted the NAPL mass remaining to be 0.73 whereas the true NAPL mass remaining was 0.49. Similarly, at the point where the measured Hex/CHex ratios reached 10, the ESM predicted the NAPL mass remaining to be 0.16 whereas the true NAPL remaining was 0.30. The error in the prediction of NAPL mass remaining is considerably larger in this experiment than in the other two experiments.

It must be recognized that the number of cells used in the ESM is a generic representation of the length of the NAPL residual zone. It is possible, or even likely, that the results of small-scale laboratory experiments measured in centimetres can be represented by 1-cell configurations of the ESM whereas larger-scale NAPL zones at field sites cannot. The following chapter describes the results of two field-scale dissolution experiments for comparison to the ESM.

Table 5-1. Composition and properties of chlorinated benzene mixture.

Property	CBz	124-TCBz	1235-TeCBz	PCBz	HCBz	Ref.
Molecular Mass (g/mol)	112.6	181.5	215.9	250.3	284.8	[1]
Density (kg/m^3)	1106	1570	1570	1609	2044	[2]
Liquid-Phase Solubility (mg/L)	470	46.1	5.6	4.0	0.48	[1]
K_{OC} (mL/g)	479	10,470	17,780	30,900	17,780	[2]
Composition (wt.%)	37.0	49.0	6.75	3.4	3.4	[1]

Key:
CBz - Chlorobenzene
124-TCBz - 1,2,4-Trichlorobenzene
1235-TeCBz - 1,2,3,5-Tetrachlorobenzene
PCBz - Pentachlorobenzene
HCBz - Hexachlorobenzene
[1] Mackay et al. (1991)
[2] Mackay et al. (1993)

Table 5-2. Comparison of measured initial aqueous concentrations to effective solubility values calculated by Raoult's Law for the chlorinated benzene mixture.

	Chlorobenzene	1,2,4-Trichlorobenzene	1,2,3,5-Tetrachlorobenzene
Measured Initial Aqueous Concentration (mg/L)	235	21	0.25
Effective Solubility calculated by Raoult's Law	234	19	0.27

Table 5-3. Composition and properties of petroleum hydrocarbon mixture.

Property	CHex	DMB	Hex	Ref.
Molecular Mass (g/mol)	84.2	86.2	86.2	[1]
Density (kg/m^3)	779	649	660	[2]
Liquid-Phase Solubility (mg/L)	56.2	20.2	12.3	[1]
K_{OC} (mL/g)	2,750	6,600	12,900	[2]
Composition (wt.%)	37.0	31.0	32.0	[1]

Key:
CHex - Cyclohexane
DMB - 2,3-Dimethyl butane
Hex - Hexane
[1] Ramanantsoa et al. (1986)
[2] Mackay et al. (1993)

Table 5-4. Comparison of measured initial aqueous concentrations to effective solubility values calculated by Raoult's Law for the petroleum hydrocarbon mixture.

	Cyclohexane	2,3-Dimethyl Butane	Hexane
Measured Initial Aqueous Concentration (mg/L)	26.5	7.5	4.0
Effective Solubility calculated by Raoult's Law	21	6.2	3.9

Table 5-5. Composition and properties of benzene - toluene mixture.

Property	Benzene	Toluene	Ref.
Molecular Mass (g/mol)	78.0	92.0	[1]
Density (kg/m^3)	876.5	866.9	[2]
Liquid-Phase Solubility (mg/L)	1,780	580	[1]
K_{OC} (mL/g)	49	55	[2]
Composition (wt.%)	50.0	50.0	[1]

Key:
[1] Geller and Hunt (1993)
[2] Mackay et al. (1993)

Table 5-6. Comparison of measured initial aqueous concentrations to effective solubility values calculated by Raoult's Law for the benzene - toluene mixture.

	Benzene	Toluene	Toluene/Benzene Ratio
Measured Initial Aqueous Concentration (mg/L)	56	16	0.29
Effective Solubility calculated by Raoult's Law	948	271	0.29

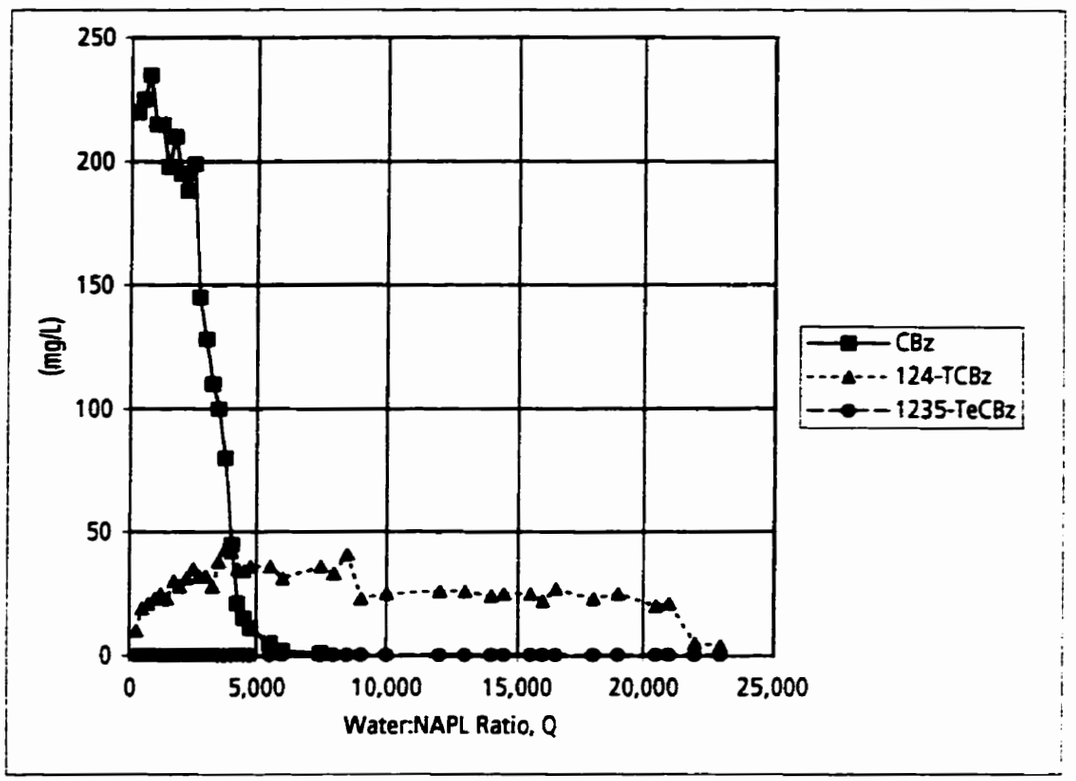

Key:
CBz - Chlorobenzene
124-TCBz - 1,2,4-Trichlorobenzene
1235-TeCBz - 1,2,3,5-Tetrachlorobenzene

Figure 5-1. Measured aqueous concentrations for mixture of chlorobenzenes in a laboratory column experiment.

Data from Mackay et al. (1991).

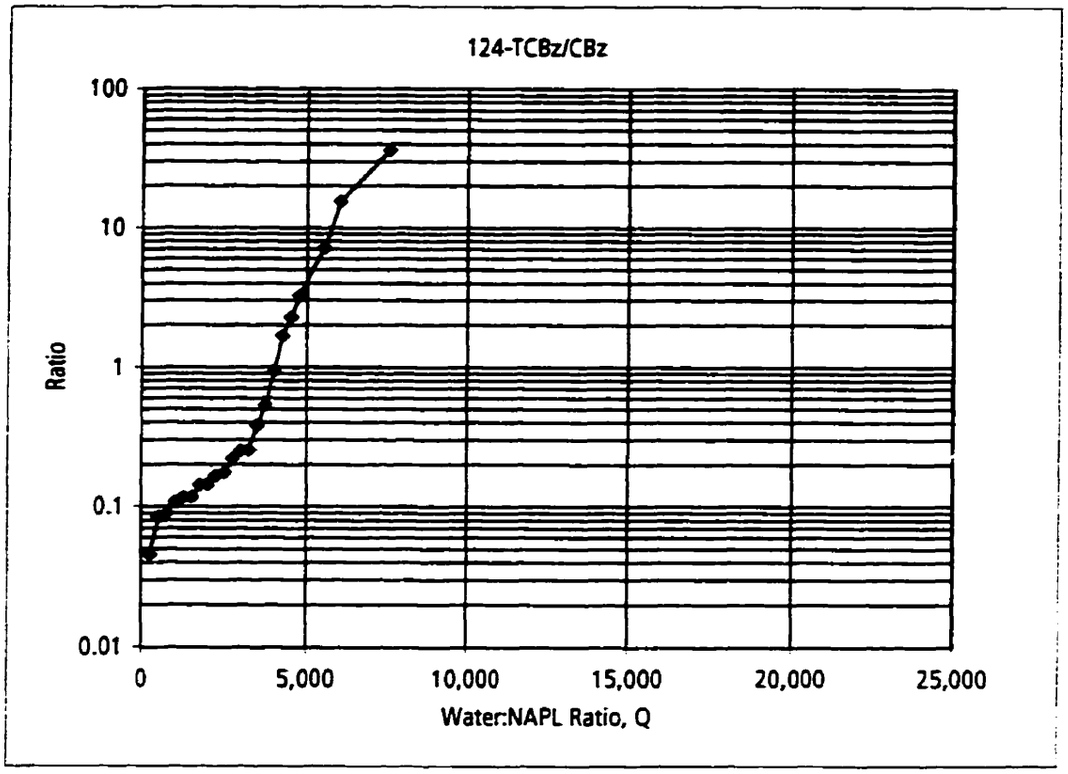

Key:
CBz - Chlorobenzene
124-TCBz - 1,2,4-Trichlorobenzene

Figure 5-2. Measured trichlorobenzene/chlorobenzene ratios for dissolution of a mixture of chlorobenzenes.

Data from Mackay et al. (1991).

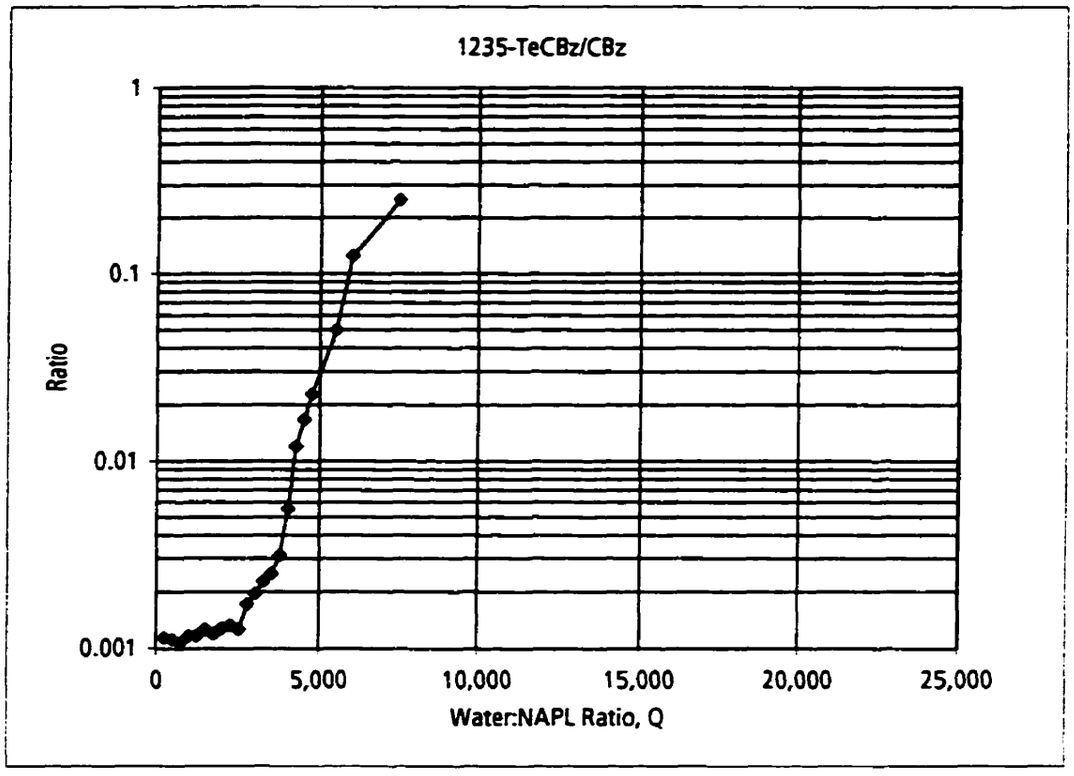

Key:
CBz - Chlorobenzene
1235-TeCBz - 1,2,3,5-Tetrachlorobenzene

Figure 5-3. Measured tetrachlorobenzene/chlorobenzene ratios for dissolution of a mixture of chlorobenzenes.

Data from Mackay et al. (1991).

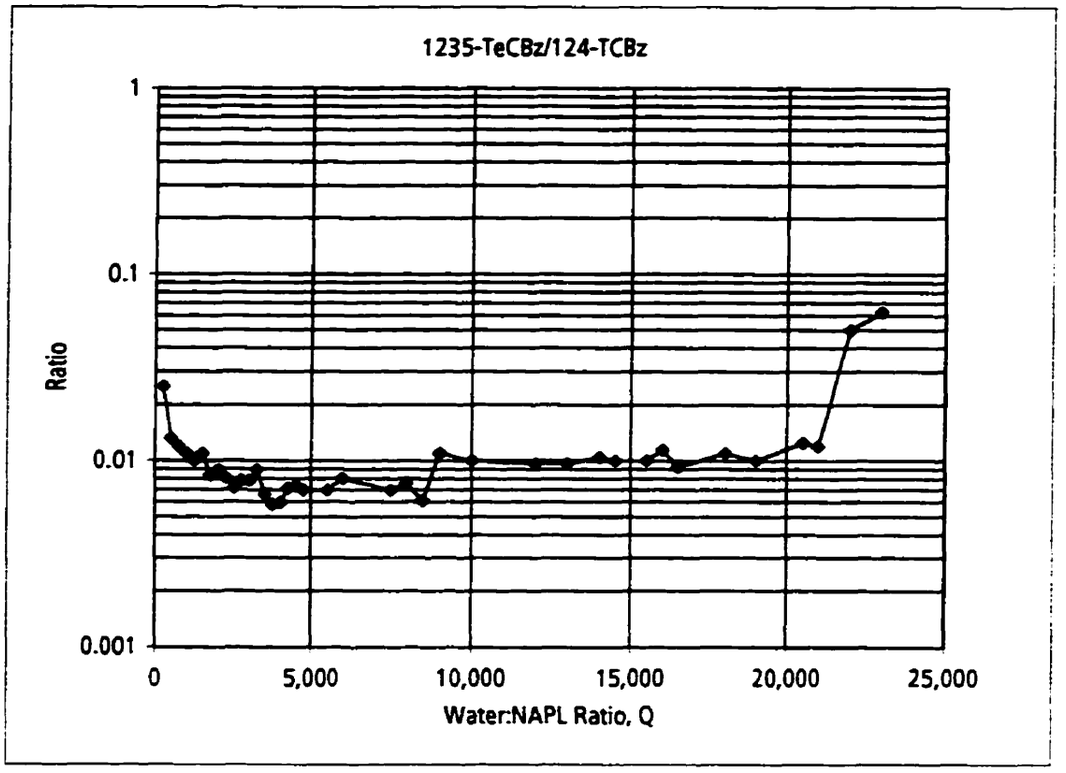

Key:
124-TCBz - 1,2,4-Trichlorobenzene
1235-TeCBz - 1,2,3,5-Tetrachlorobenzene

Figure 5-4. Measured tetrachlorobenzene/trichlorobenzene ratios for dissolution of a mixture of chlorobenzenes.

Data from Mackay et al. (1991).

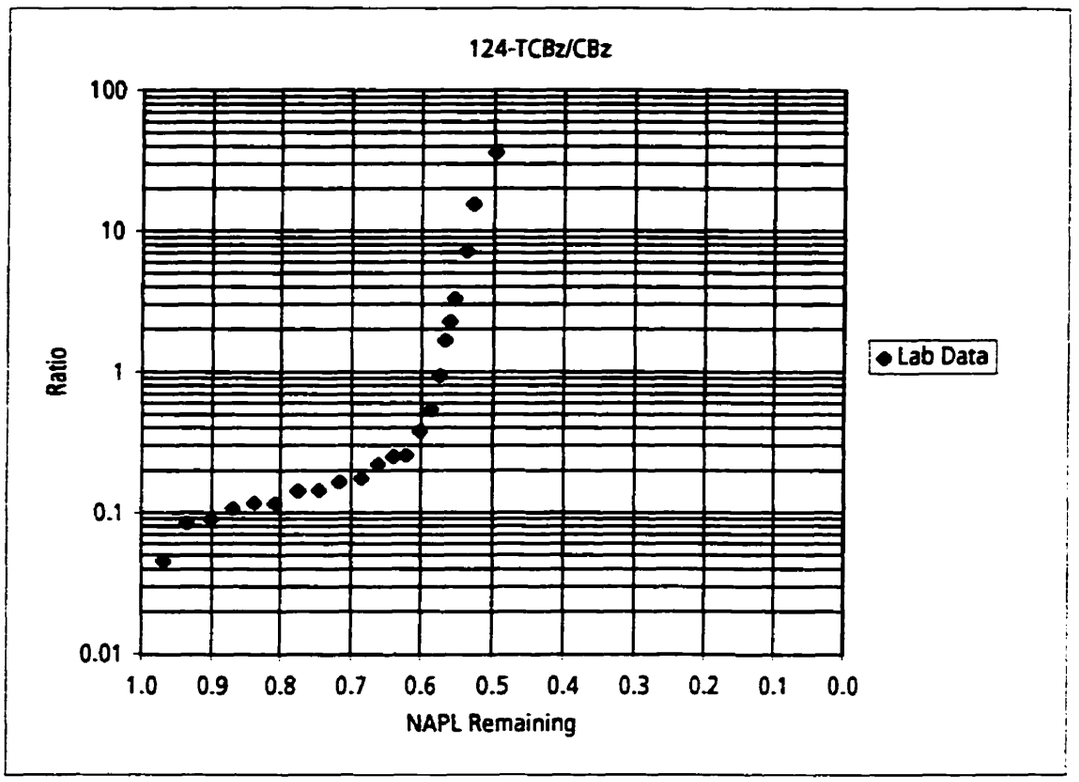

Key:
CBz - Chlorobenzene
124-TCBz - 1,2,4-Trichlorobenzene

Figure 5-5. Measured trichlorobenzene/chlorobenzene ratios versus NAPL remaining for dissolution of a mixture of chlorobenzenes.

Data from Mackay et al. (1991).

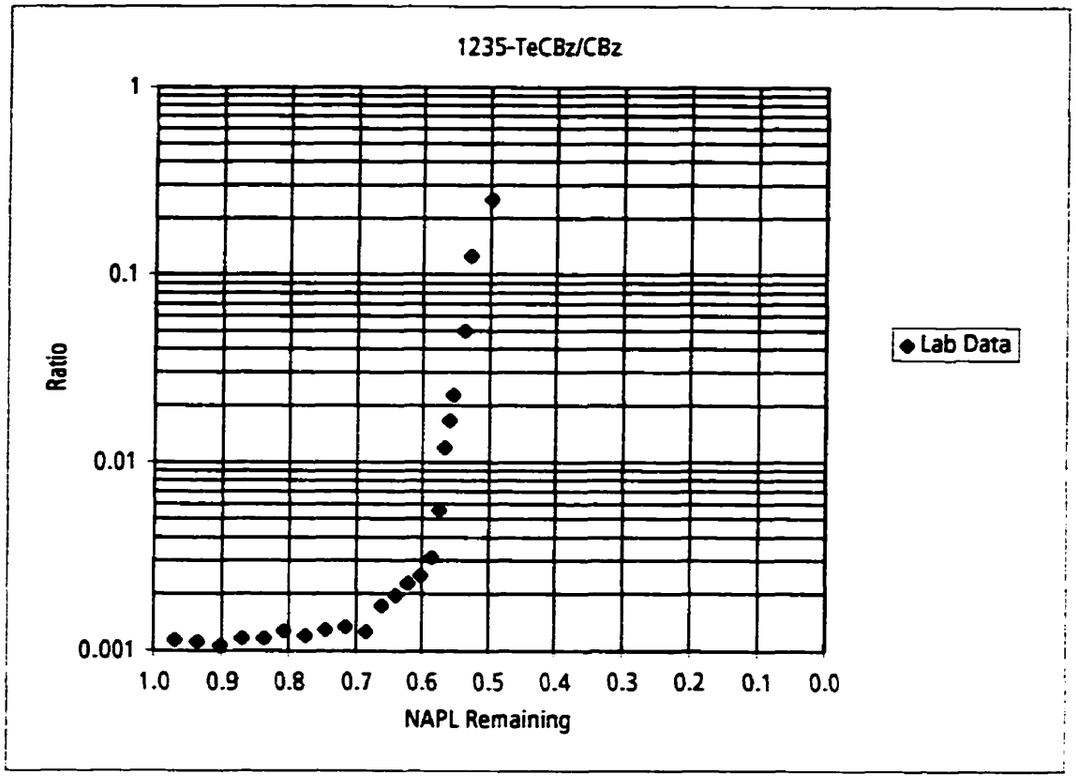

Key:
CBz - Chlorobenzene
1235-TeCBz - 1,2,3,5-Tetrachlorobenzene

Figure 5-6. Measured tetrachlorobenzene/chlorobenzene ratios versus NAPL remaining for dissolution of a mixture of chlorobenzenes

Data from Mackay et al. (1991).

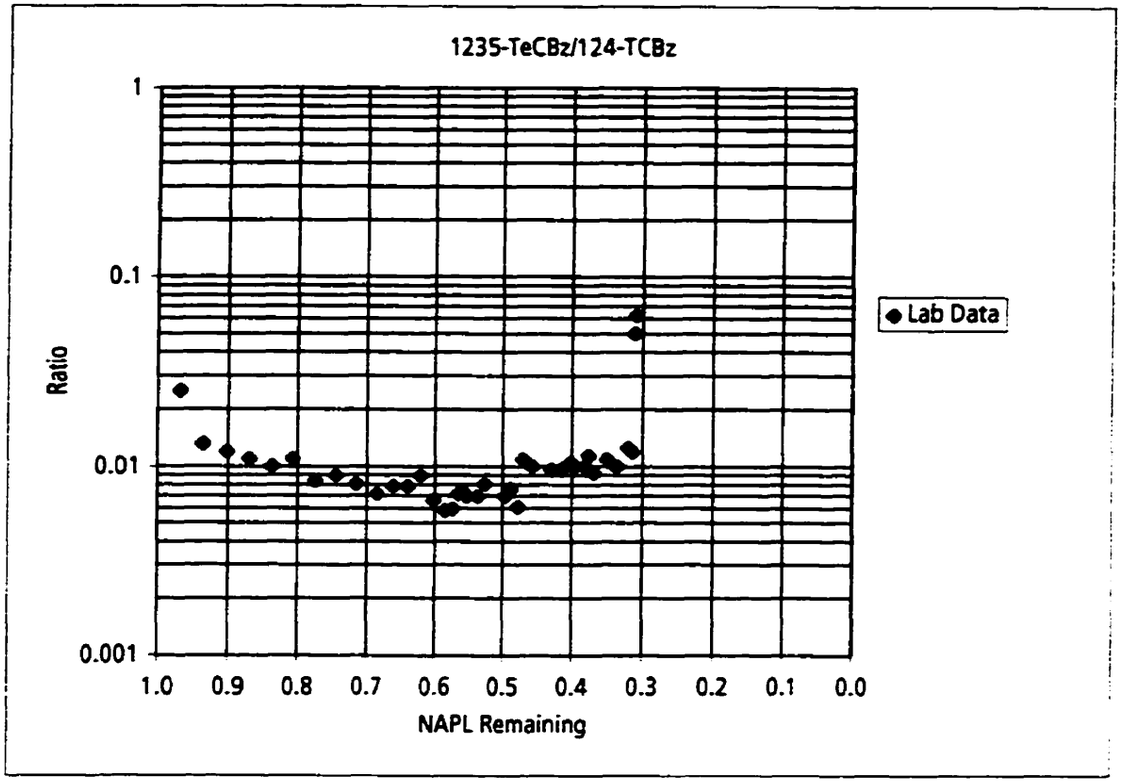

Key:
124-TCBz - 1,2,4-Trichlorobenzene
1235-TeCBz - 1,2,3,5-Tetrachlorobenzene

Figure 5-7. Measured tetrachlorobenzene/trichlorobenzene ratios versus NAPL remaining for dissolution of a mixture of chlorobenzenes.

Data from Mackay et al. (1991).

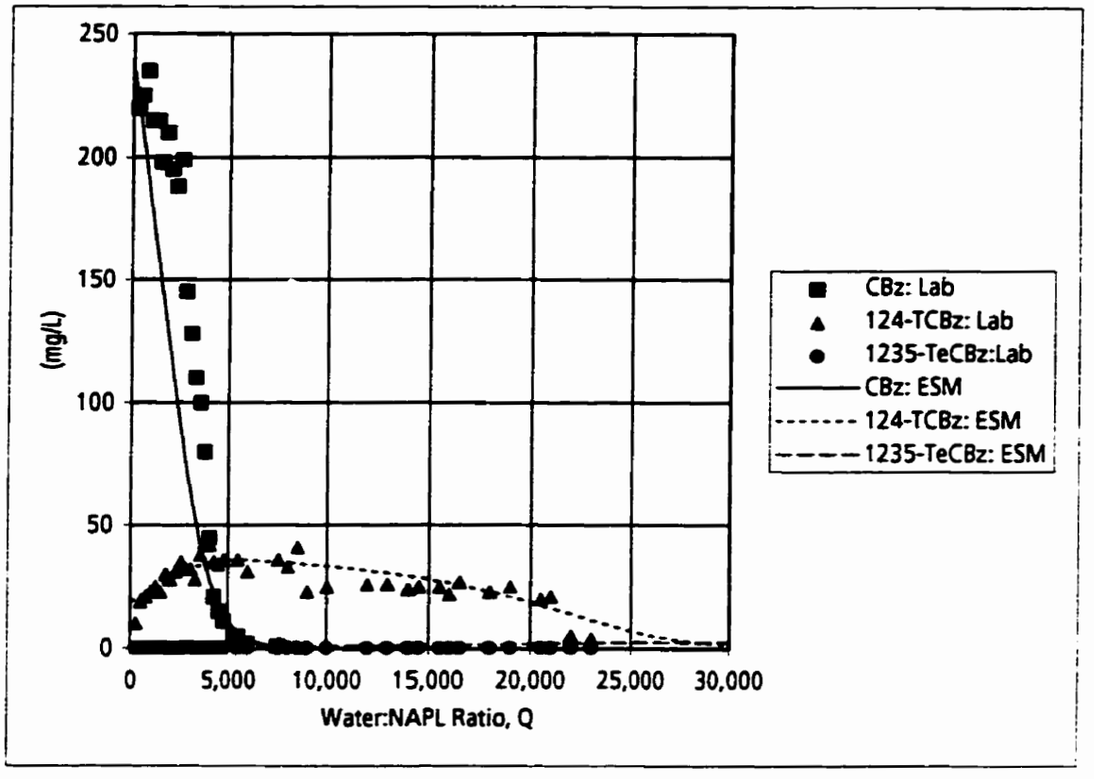

Key:
CBz - Chlorobenzene
124-TCBz - 1,2,4-Trichlorobenzene
1235-TeCBz - 1,2,3,5-Tetrachlorobenzene

Figure 5-8. Comparison of measured aqueous concentrations to aqueous concentrations predicted using the ESM for 1-cell configuration.

Data from Mackay et al. (1991).

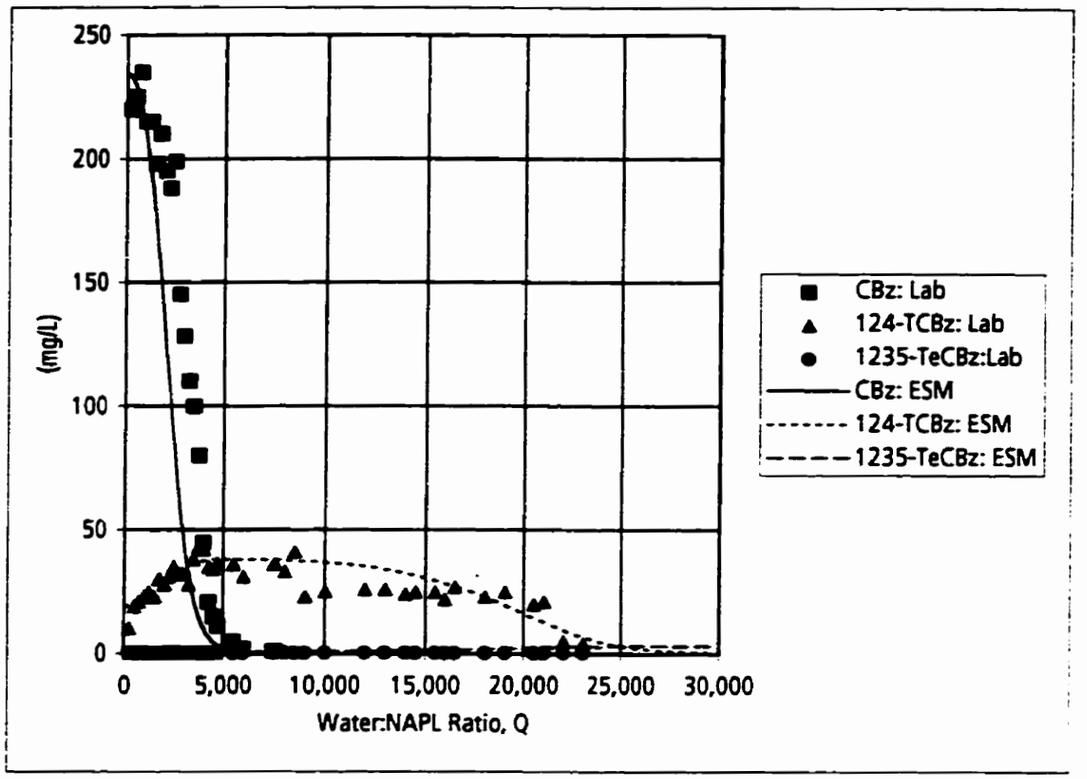

Key:
CBz - Chlorobenzene
124-TCBz - 1,2,4-Trichlorobenzene
1235-TeCBz - 1,2,3,5-Tetrachlorobenzene

Figure 5-9. Comparison of measured aqueous concentrations to aqueous concentrations predicted using the ESM for 2-cell configuration.

Data from Mackay et al. (1991).

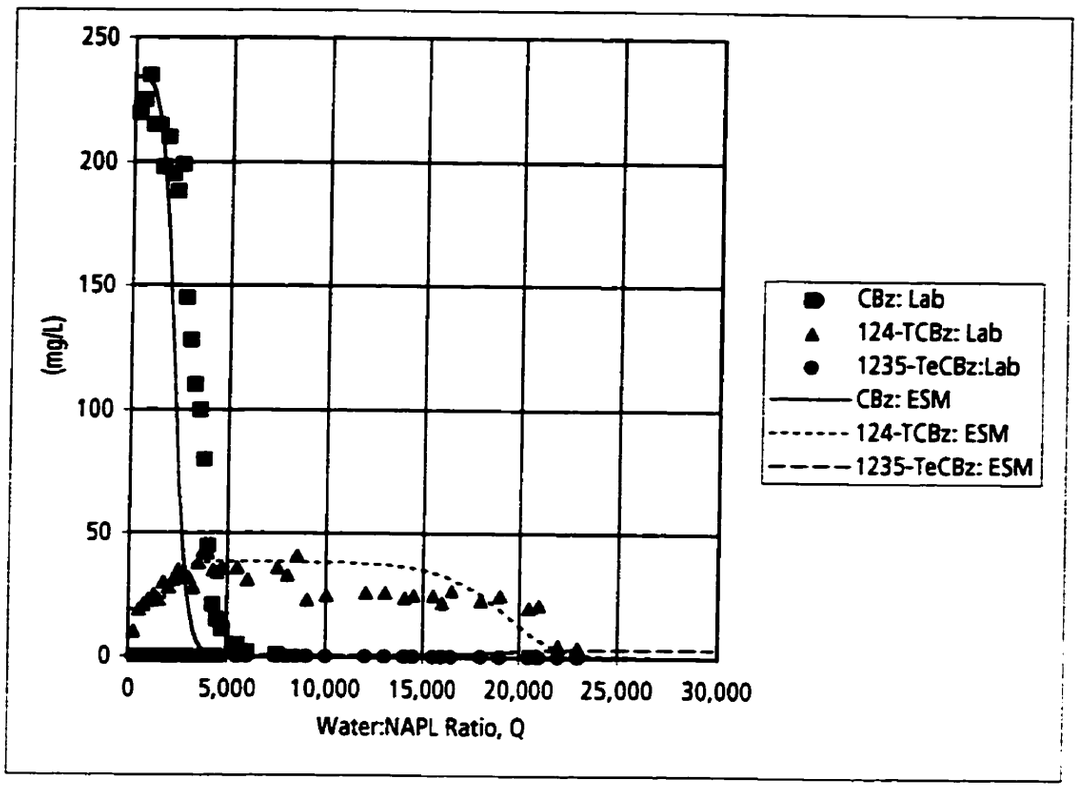

Key:
CBz - Chlorobenzene
124-TCBz - 1,2,4-Trichlorobenzene
1235-TeCBz - 1,2,3,5-Tetrachlorobenzene

Figure 5-10. Comparison of measured aqueous concentrations to aqueous concentrations predicted using the ESM for 4-cell configuration.

Data from Mackay et al. (1991).

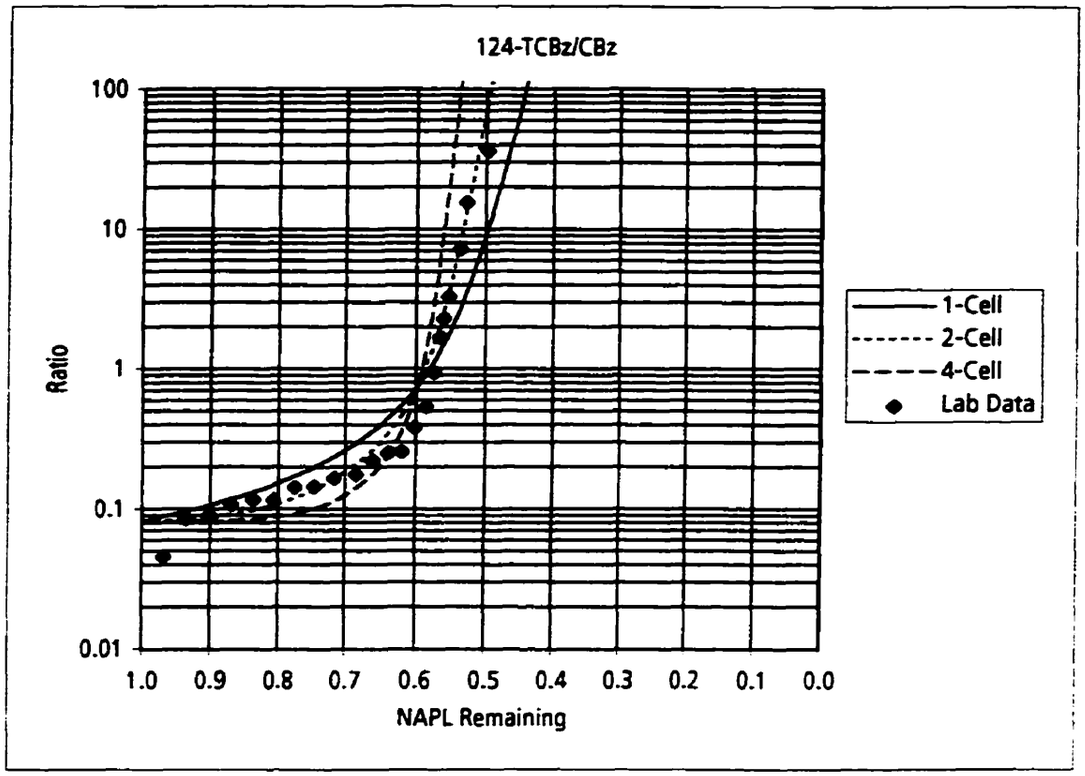

Key:
CBz - Chlorobenzene
124-TCBz - 1,2,4-Trichlorobenzene

Figure 5-11. Comparison of measured trichlorobenzene/chlorobenzene ratios to ratios predicted using the ESM for 1-cell, 2-cell and 4-cell configurations.

Data from Mackay et al. (1991).

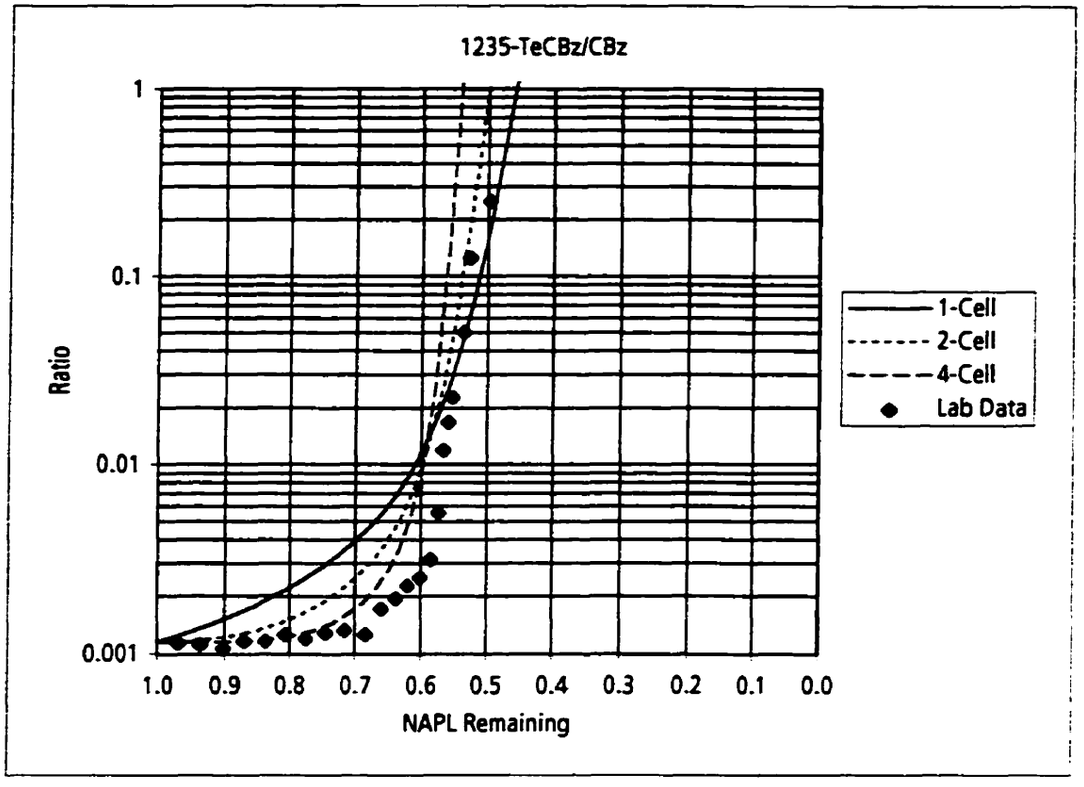

Key:
CBz - Chlorobenzene
1235-TeCBz - 1,2,3,5-Tetrachlorobenzene

Figure 5-12. Comparison of measured tetrachlorobenzene/chlorobenzene ratio to ratios predicted using the ESM for 1-cell, 2-cell and 4-cell configurations.

Data from Mackay et al. (1991).

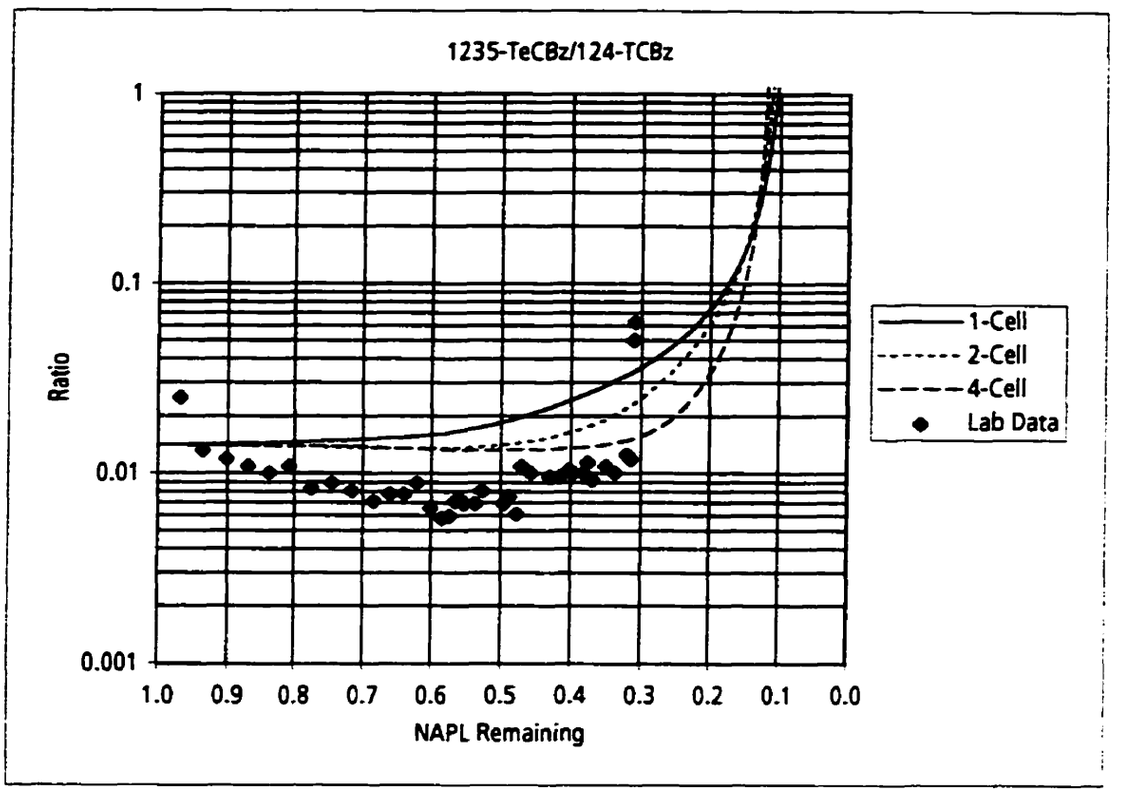

Key:
124-TCBz - 1,2,4-Trichlorobenzene
1235-TeCBz - 1,2,3,5-Tetrachlorobenzene

Figure 5-13. Comparison of measured tetrachlorobenzene/trichlorobenzene ratios to ratios predicted using the ESM for 1-cell, 2-cell and 4-cell configurations.

Data from Mackay et al. (1991).

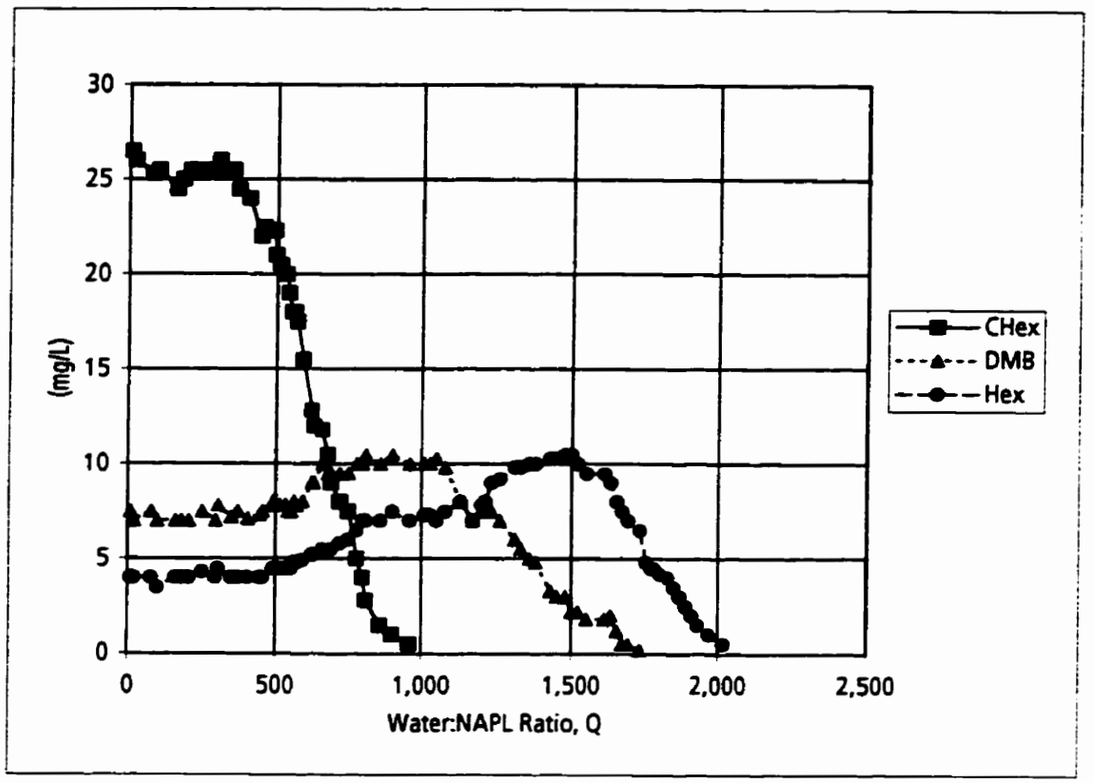

Key:
CHex - Cyclohexane
DMB - 2,3-Dimethyl butane
Hex - Hexane

Figure 5-14. Measured aqueous concentrations for mixture of hydrocarbons in a laboratory column dissolution experiment.

Data from Ramanantsoa et al. (1986).

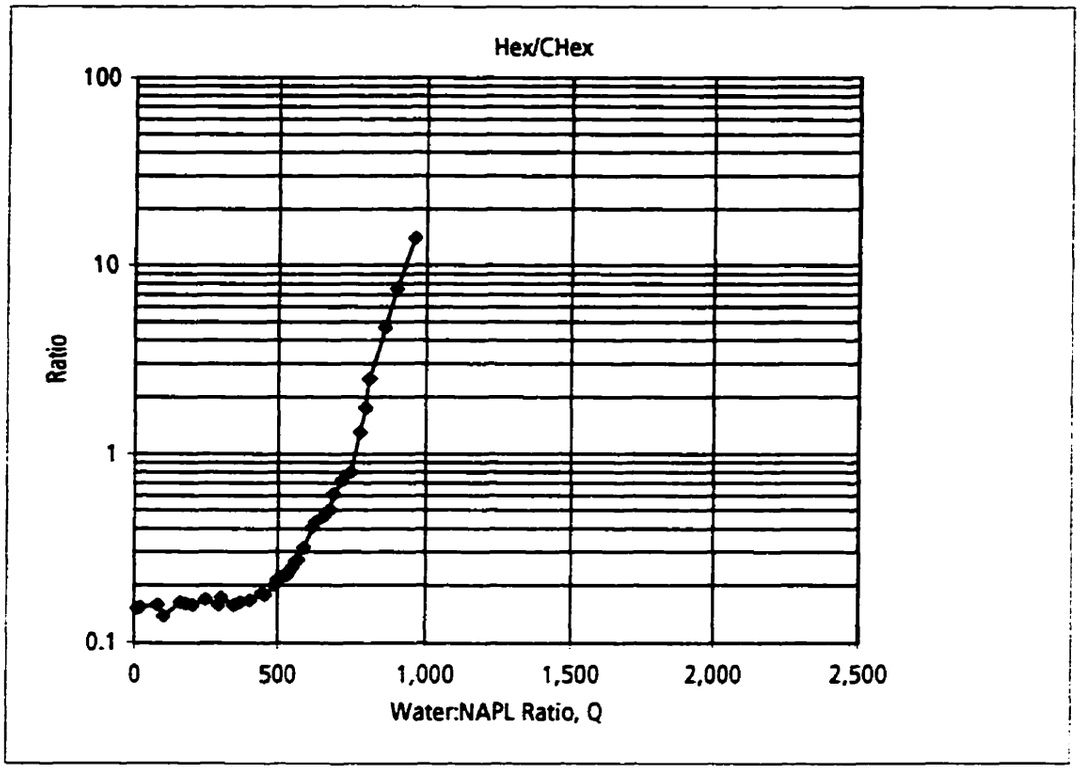

Key:
CHex - Cyclohexane
Hex - Hexane

Figure 5-15. Measured hexane/cyclohexane ratios for dissolution of a mixture of hydrocarbons.

Data from Ramanantsoa et al. (1986).

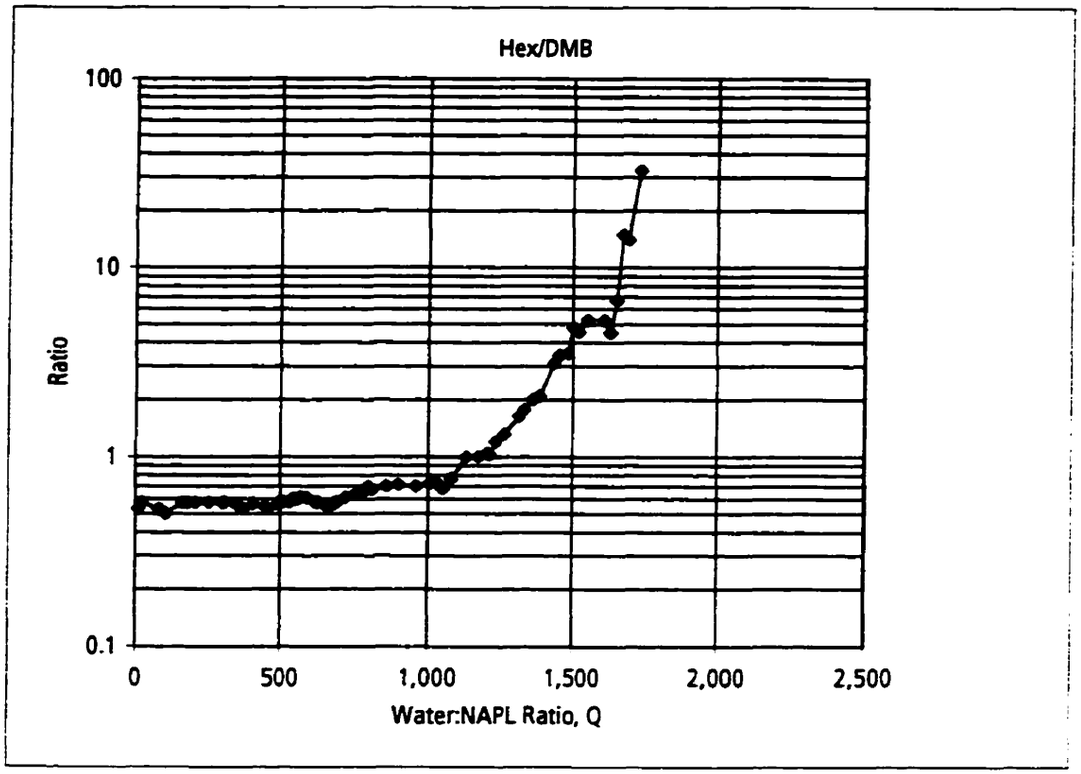

Key:
DMB - 2,3-Dimethyl butane
Hex - Hexane

Figure 5-16. Measured hexane/dimethyl butane ratios for dissolution of a mixture of hydrocarbons.

Data from Ramanantsoa et al. (1986).

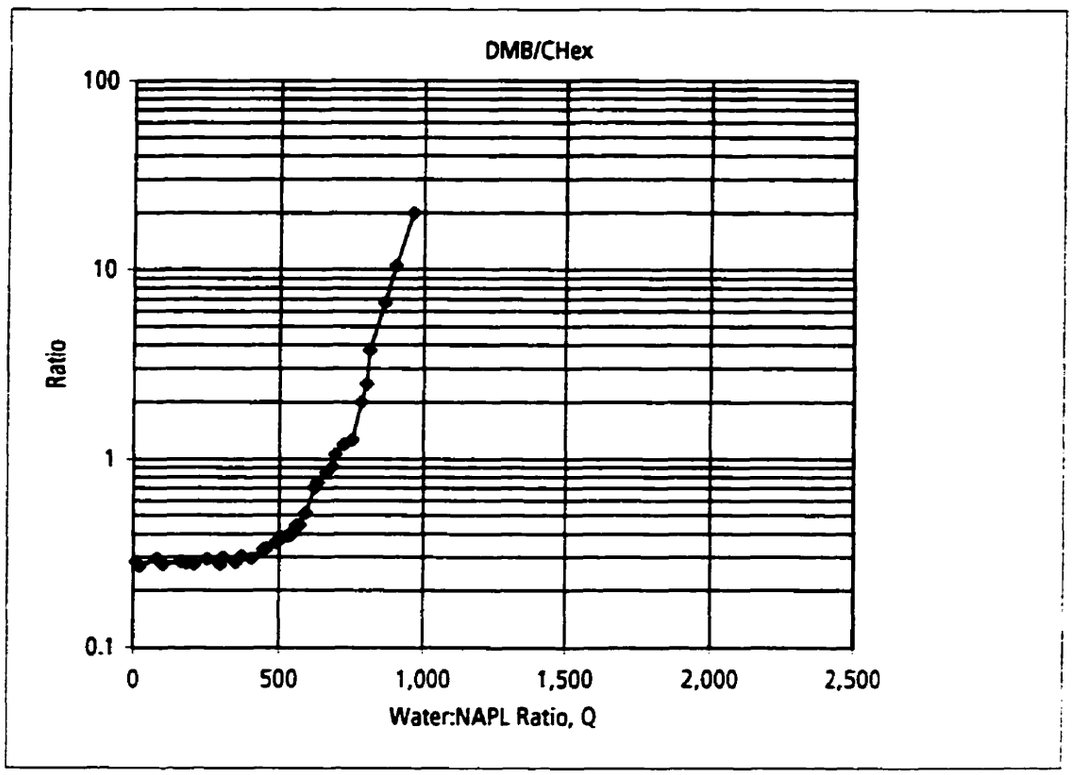

Key:
CHex - Cyclohexane
DMB - 2,3-Dimethyl butane

Figure 5-17. Measured dimethyl butane/cyclohexane ratios for dissolution of a mixture of hydrocarbons.

Data from Ramanantsoa et al. (1986).

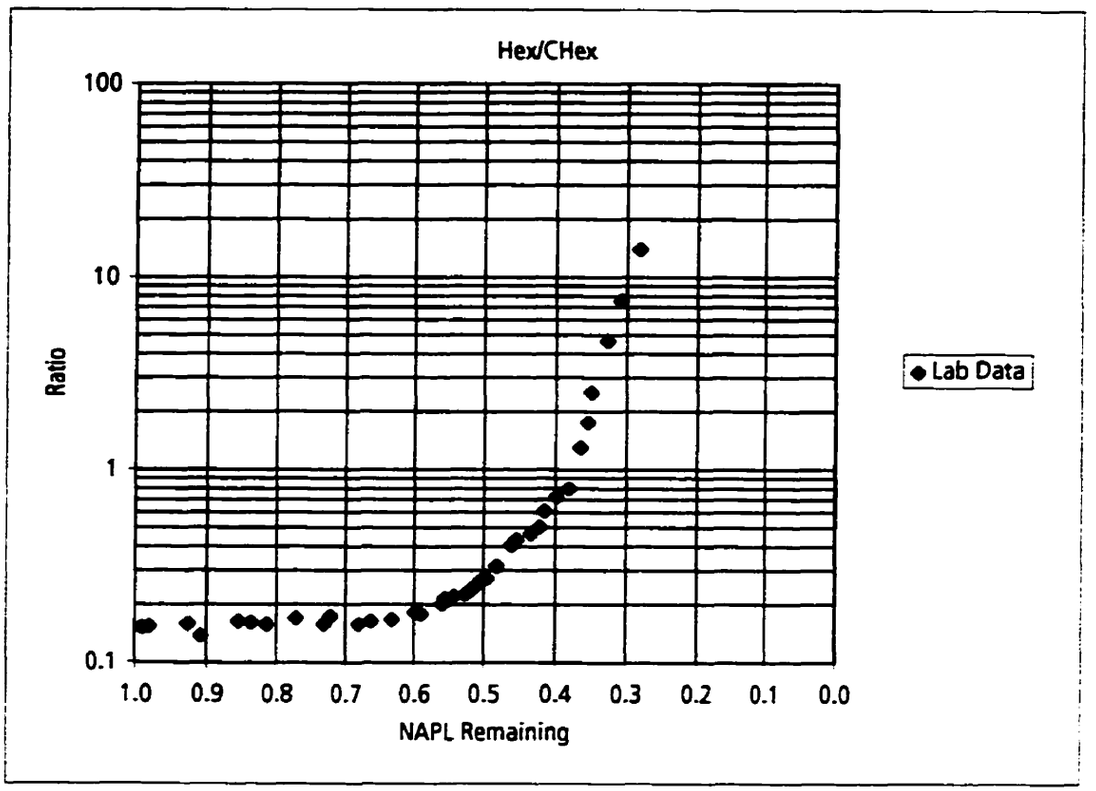

Key:
CHex - Cyclohexane
Hex - Hexane

Figure 5-18. Measured hexane/cyclohexane ratios versus NAPL remaining for dissolution of a mixture of hydrocarbons.

Data from Ramanantsoa et al. (1986).

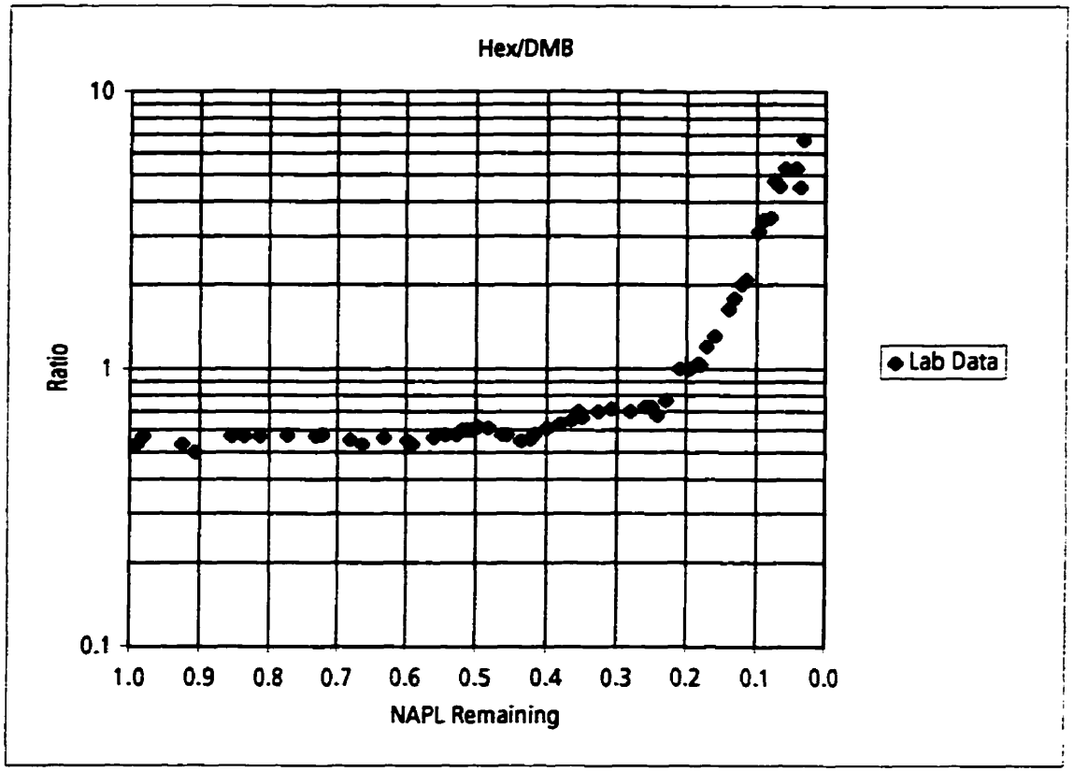

Key:
DMB - 2,3-Dimethyl butane
Hex - Hexane

Figure 5-19. Measured hexane/dimethyl butane ratios versus NAPL remaining for dissolution of a mixture of hydrocarbons.

Data from Ramanantsoa et al. (1986).

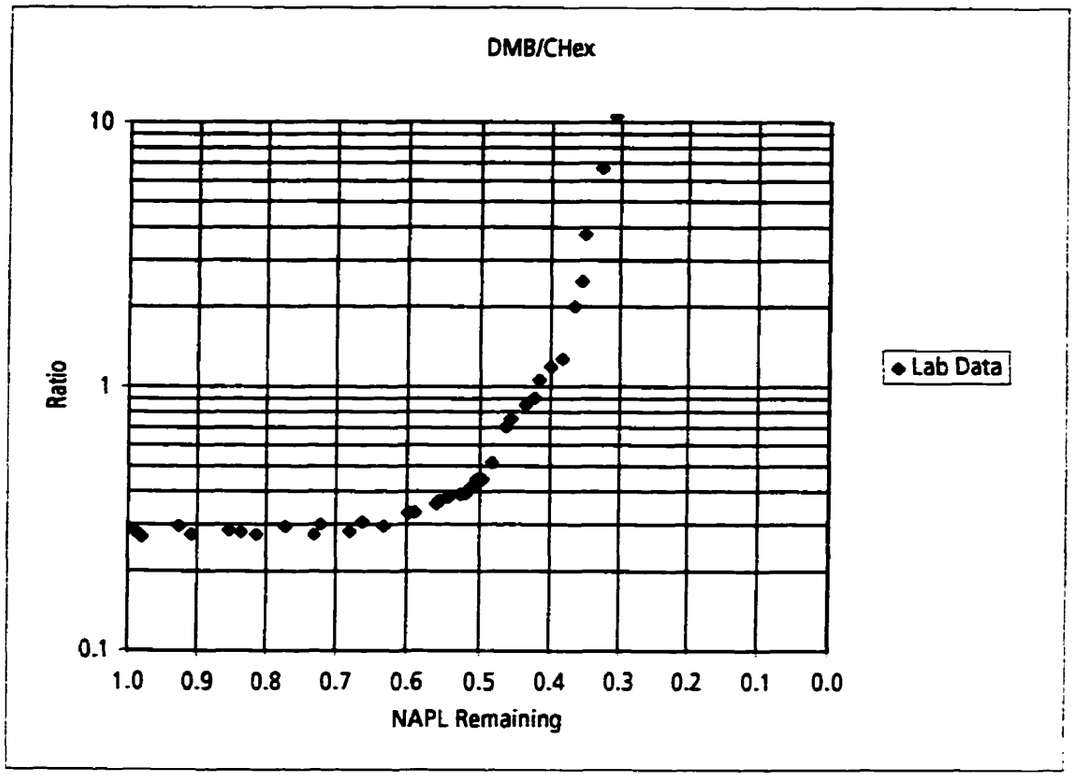

Key:
CHex - Cyclohexane
DMB - 2,3-Dimethyl butane

Figure 5-20. Measured dimethyl butane/cyclohexane ratios versus NAPL remaining for dissolution of a mixture of hydrocarbons.

Data from Ramanantsoa et al. (1986).

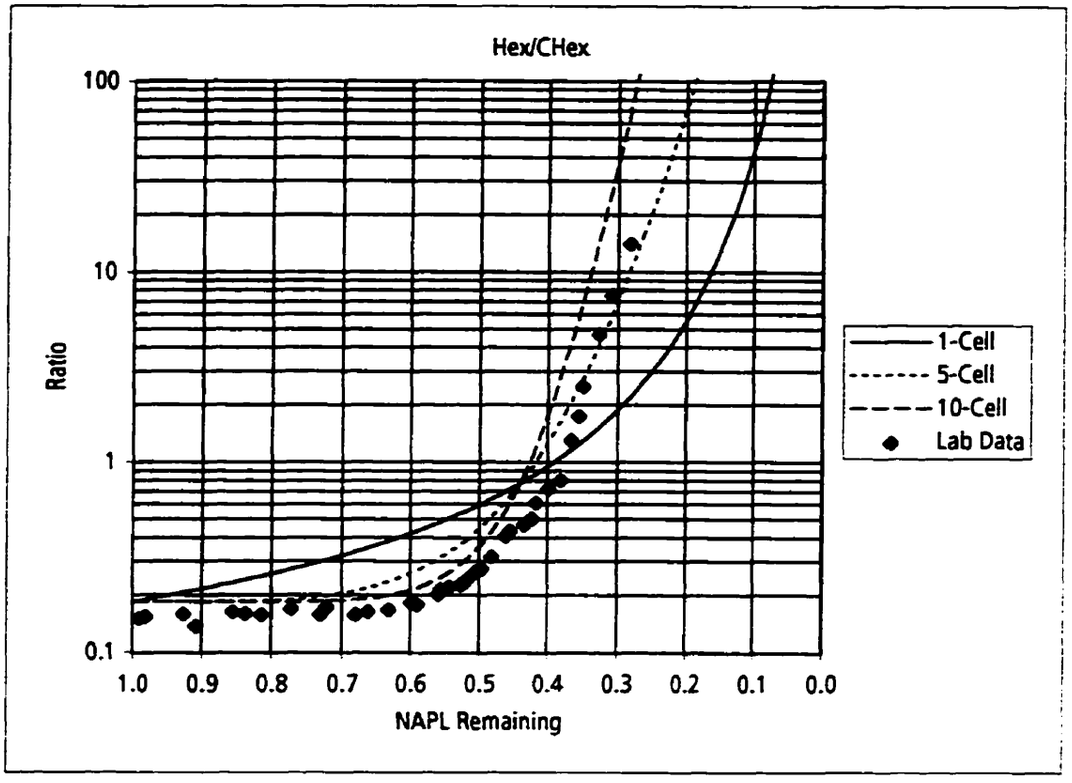

Key:
CHex - Cyclohexane
Hex - Hexane

Figure 5-21. Comparison of measured hexane/cyclohexane ratios to ratios predicted using ESM for 1-cell, 5-cell and 10-cell configurations.

Data from Ramanantsoa et al. (1986).

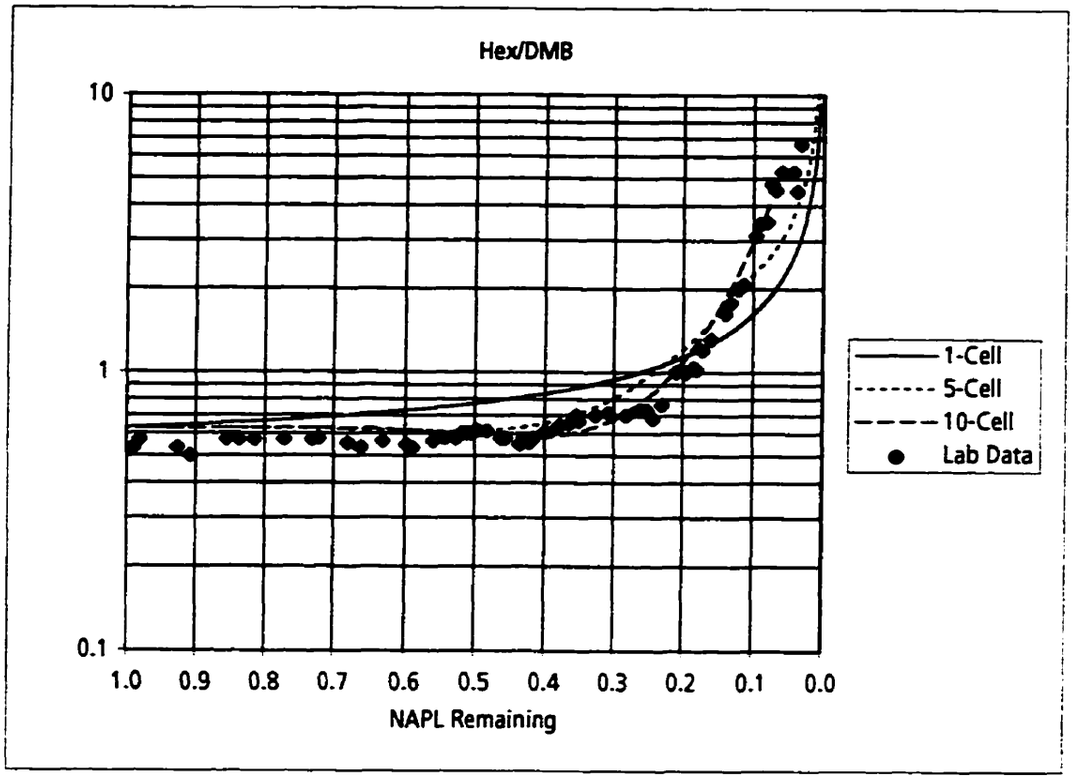

Key:
DMB - 2,3-Dimethyl butane
Hex - Hexane

Figure 5-22. Comparison of measured hexane/dimethyl butane ratios to ratios predicted using ESM for 1-cell, 5-cell and 10-cell configurations.

Data from Ramanantsoa et al. (1986).

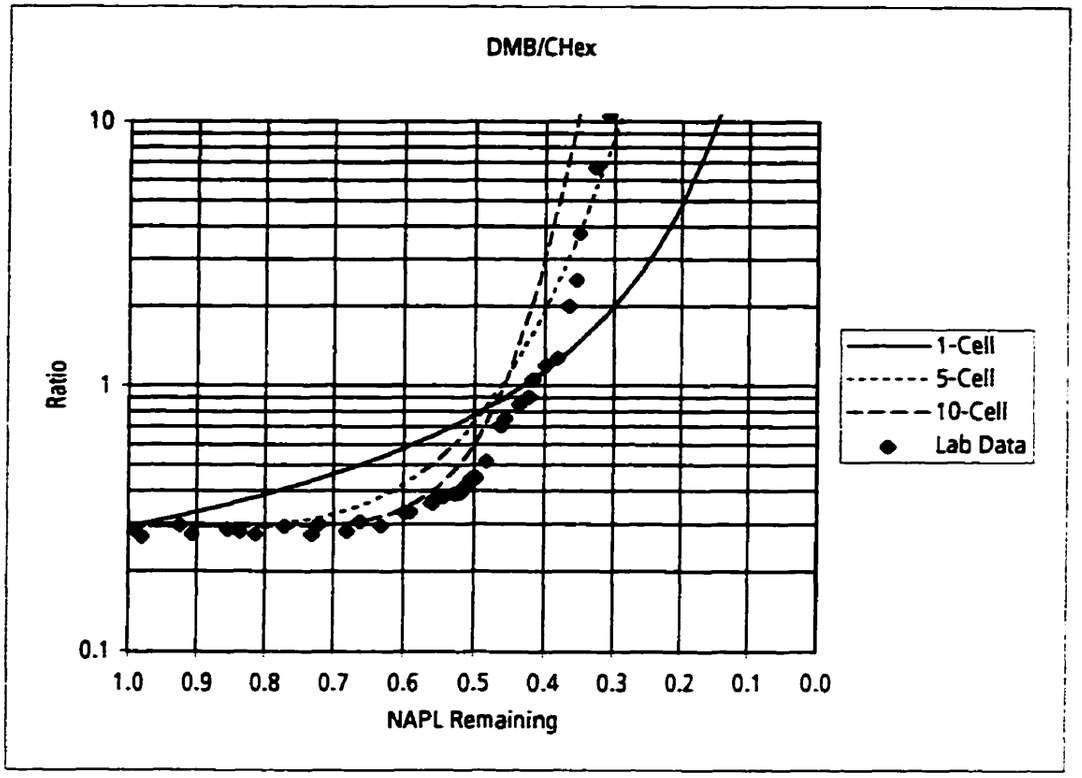

Key:
CHex - Cyclohexane
DMB - 2,3-Dimethyl butane
Hex - Hexane

Figure 5-23. Comparison of measured dimethyl butane/cyclohexane ratios to ratios predicted using ESM for 1-cell, 5-cell and 10-cell configurations.

Data from Ramanantsoa et al. (1986).

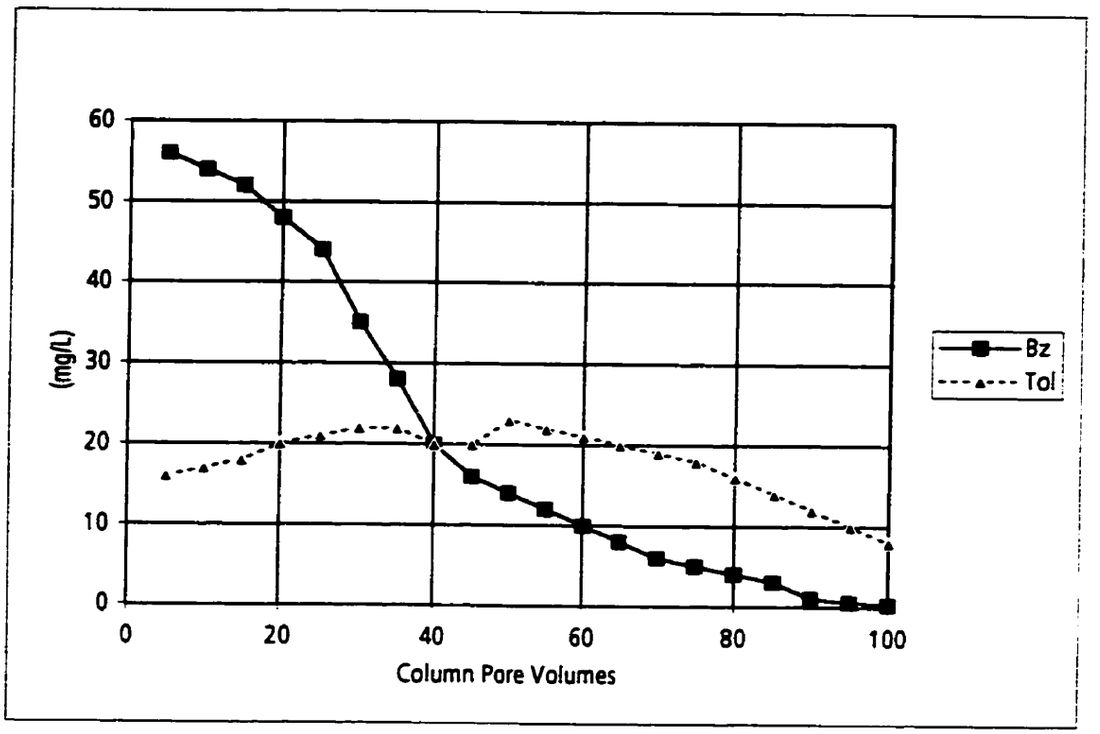

Key:
Bz - Benzene
Tol - Toluene

Figure 5-24. Measured aqueous concentrations for a benzene-toluene mixture in a laboratory column dissolution experiment.

Data from Geller and Hunt (1993).

File:Geller Equil.EXCL/Plots

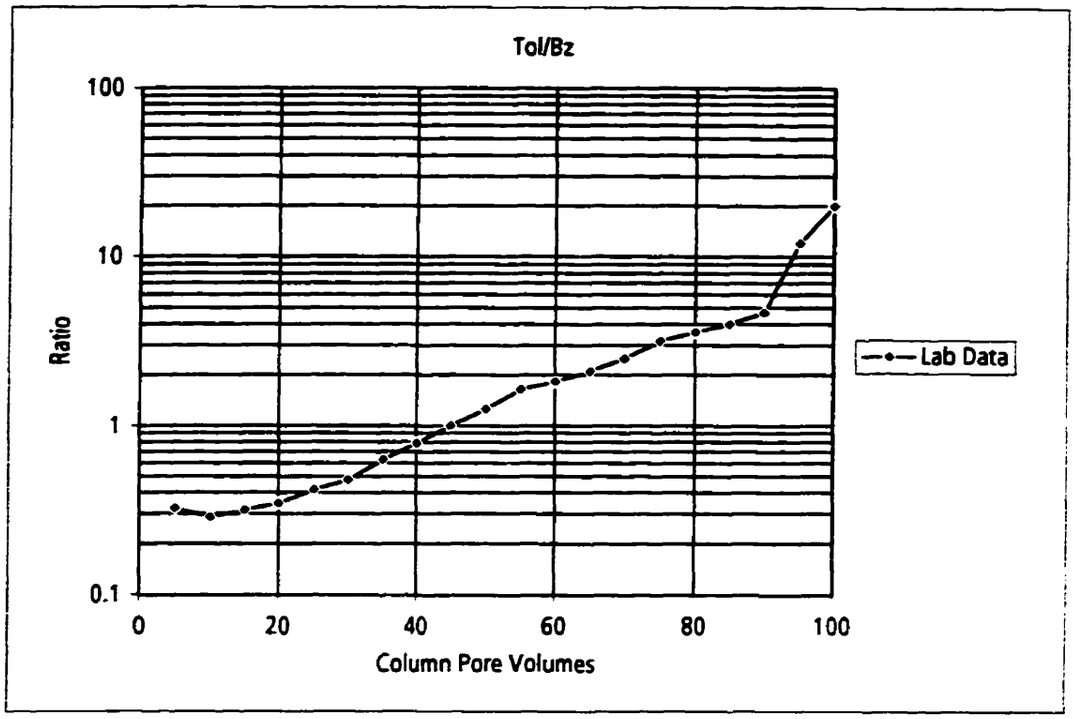

Key:
Bz - Benzene
Tol - Toluene

Figure 5-25. Measured toluene/benzene ratios for dissolution of a benzene-toluene mixture.

Data from Geller and Hunt (1993).

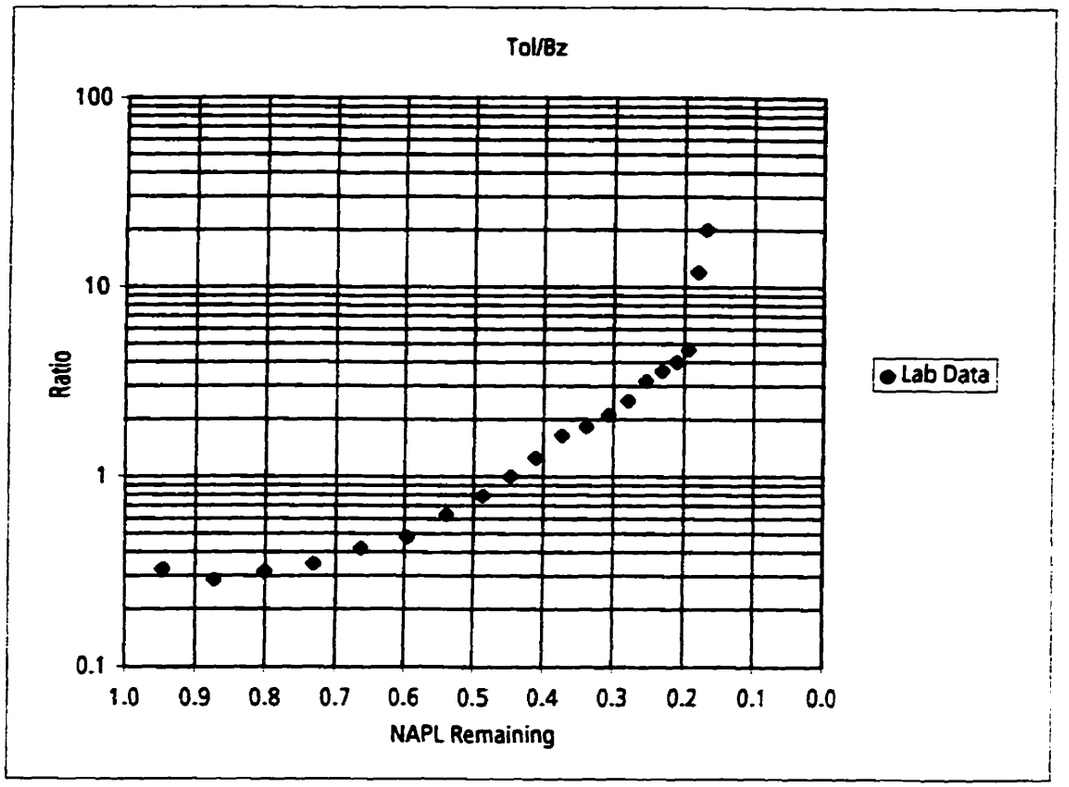

Key:
Bz - Benzene
Tol - Toluene

Figure 5-26. Measured toluene/benzene ratios versus NAPL remaining for dissolution of a benzene-toluene mixture.

Data from Geller and Hunt (1993).

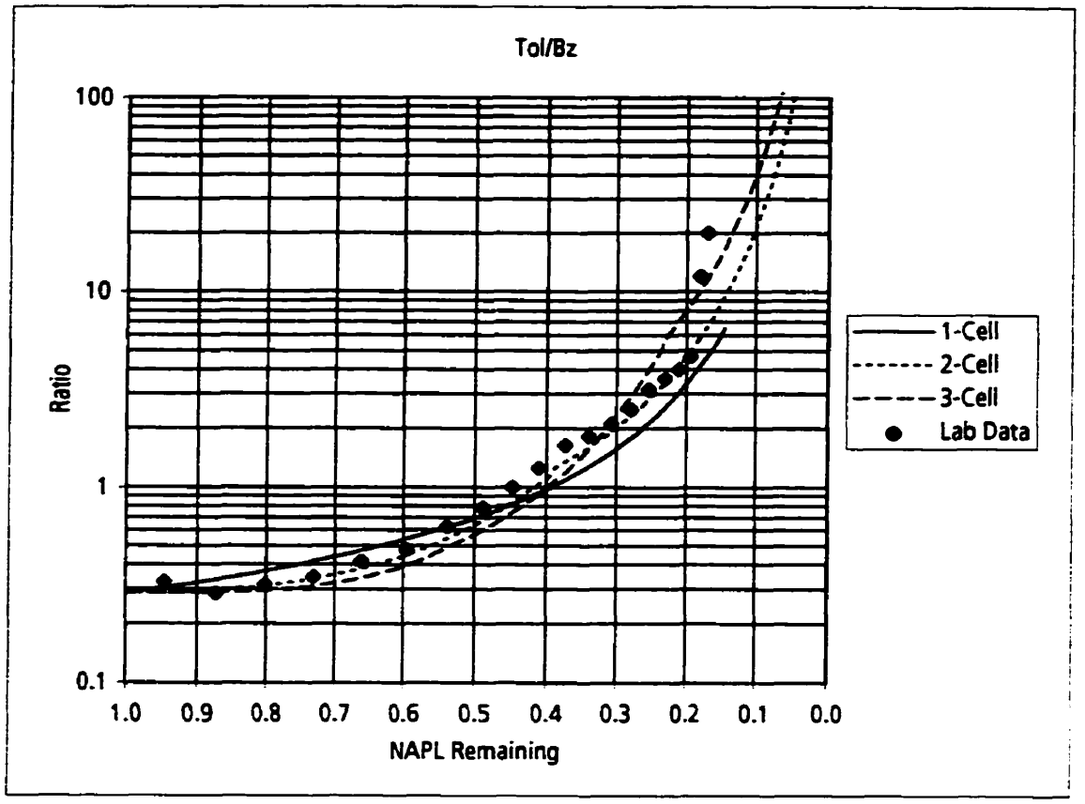

Key:
Bz - Benzene
Tol - Toluene

Figure 5-27. Comparison of measured toluene/benzene ratios to ratios predicted using ESM for 1-cell, 2-cell and 3-cell configurations.

Data from Geller and Hunt (1993).

File:Geller Equil.EXCL/Plots

6. Controlled Field Study: Emplaced-Source Experiment

6.1 Overview

A controlled field-scale dissolution experiment, referred to here as the Emplaced-Source Experiment, was conducted to examine the dissolution of a residual NAPL source of chlorinated solvents in a sandy aquifer. This experiment was performed at the University of Waterloo Borden field experimental site beginning in the fall of 1989. This experiment allowed examination of the dissolution of a NAPL residual zone larger than those represented in laboratory experiments. A residual NAPL source zone of known mass, composition and geometry was emplaced directly in the groundwater zone, and the aqueous concentrations emitted from the NAPL zone were measured. Aqueous concentration ratios and the NAPL mass remaining were determined from the experimental data. This allowed direct comparison of the experimental results to ESM simulations of NAPL dissolution.

The Borden experimental site is located in an unconfined sandy aquifer at the Canadian Forces Base Borden, Ontario (see Figure 6-1). The Borden aquifer is comprised of unconsolidated glaciolacustrine sand. The Emplaced-Source (ES) site is situated in an area where the aquifer is approximately 10 m thick. The ES experiment takes place in the upper portion of the aquifer. The lower portion of the aquifer has been contaminated by a former domestic waste landfill (see Figure 6-2).

During the past two decades, the area around the ES site has been host to numerous natural-gradient tracer tests which have studied the physical and chemical processes controlling the transport of inorganic and organic contaminants in groundwater. The location of these previous experiments and references to their results are shown in Figure 6-2. These experiments involved the injection of a finite pulse of aqueous-phase contaminant into

the aquifer, followed by detailed three-dimensional monitoring of the aqueous-phase plume as it migrated away from the injection location. The ES experiment differs from these previous experiments in that a zone of residual NAPL contamination was emplaced directed in the aquifer below the water table to act as an on-going source of aqueous-phase contaminants.

The ES experiment was designed to examine various aspects of the dissolution of the NAPL source zone and the resultant migration of the aqueous-phase plumes. A specific objective of the ES experiment was to examine the dissolution of a multi-component NAPL mixture under field conditions, and evaluate whether temporal changes in aqueous concentration ratios may be used to determine the mass of contaminants contained in NAPL residual zones. This is the work described in this chapter.

Other objectives of the ES experiment included: evaluation of the retardation of the aqueous-phase plumes; modeling of dispersion of plumes emitted from continuous sources; and, evaluation of the performance of groundwater pump-and-treat for plume remediation. Other studies have included: modeling of dispersion of plumes affected by fluctuating groundwater flow direction; and, the evaluation of soil-gas surveys for delineation of aqueous-phase plumes situated below the water table. An overview of the Emplaced-Source Experiment was provided by Rivett, Feenstra and Cherry (1991). Evaluations of retardation and dispersion of the aqueous-phase plumes are provided by Rivett, Feenstra and Cherry (1992, 1994a and 1994b). The evaluation of soil-gas surveys is provided by Rivett (1995) and a preliminary evaluation of groundwater pump-and-treat performance is provided by Rivett (1993).

6.2 Experimental Conditions

6.2.1 Source Installation

The ES experiment is located in an area where the sand aquifer is about 10 m to 12 m in thickness. The water table occurs at 2.5 m to 3.0 m below ground surface. The leachate plume created by the nearby landfill occurs about 8 m below ground surface. The ES experiment was performed in the uncontaminated zone of groundwater above the leachate plume.

A schematic diagram of the source zone is shown in Figure 6-3. The source zone is a rectangular block measuring 1.5 m in length, 1.0 m in height, and 0.5 m in thickness. The top of the source zone was placed approximately 0.9 m below the seasonal low water table elevation. The long dimension of the source zone was oriented to be perpendicular to the direction of groundwater measured in the late summer. Subsequent monitoring determined that the groundwater flow direction varies seasonally over an arc of about 30°.

The source consists of native sand excavated from the source zone, mixed with 18 L of NAPL. This volume of NAPL represented a saturation of 2.5% of the bulk source volume, or about 6.3% of the pore space in the source zone. At this saturation value, the NAPL would be immobile and represent a residual NAPL source.

The NAPL consisted of 9.7% by weight TCM (chloroform), 42.5% TCE (trichloroethylene) and 47.6% PCE (tetrachloroethylene). These compounds were selected to provide a wide range in pure-phase solubility: 8,700,000 µg/L, 1,400,000 µg/L and 240,000 µg/L, for TCM, TCE and PCE, respectively. The source material also contained 72 kg of gypsum powder added to provide sulfate as an inorganic tracer for studies of retardation of the aqueous-phase plumes.

In order to place the source zone, a backhoe was used to excavate 2.5 m through the vadose zone down to the water table. At the base of the excavation, a 2.0 m long by 1.0 m wide cell was constructed using interlocking steel sheet piling. The sheet piling extended to a depth of 3.0 m below the water table, to a total depth of 5.5 m below ground surface. The area within and around the sheet piling cell was dewatered using a system of five 5-cm diameter wells pumped at a total rate of 120 L/min. After about 12 hours, the water table inside the cell declined sufficiently and the sand inside the cell was excavated to a depth of 5.0 m below ground surface. Sand removed from the source zone was mixed in 40 L batches with the solvent mixture and gypsum powder for about 3 minutes, in a gasoline-powered mortar mixer. After mixing, the batches where placed and compacted inside a removable steel form with the final dimensions of the source zone. A total of 720 L of source material was placed in the source zone. Source mixing and placement took about 3 hours. Native sand was placed and compacted in annular space between the source form and the sheet piling, and the source form was removed. Native sand was then placed and compacted above the source zone to the level of the former water table.

The source zone and aquifer material within the sheet piling cell was allowed to resaturate over a period of 2 hours by gradually reducing the groundwater pumping rate. Some clean water was also introduced to the top of the cell to minimize the movement of aqueous-phase contaminants up through the source zone as the zone resaturated with water. After recovery of the water table, the sheet pilings were removed to permit horizontal groundwater flow through the NAPL source zone. The vadose zone excavation was backfilled to ground surface using native sand materials.

The source zone was exposed to groundwater flow on October 18, 1989. Monitoring of the dissolution of the source zone continued for more than 1,000 days. Growth of the aqueous-phase plumes occurred under natural gradient conditions for the first 475 days. After that time, a groundwater

pump-and-treat system was installed to intercept the aqueous-phase plumes emitted from the source zone. The pump-and-treat system did not influence the dissolution of the source.

6.2.2 Site Layout and Study Program

The hydrogeological conditions, dissolution of the source zone, and the migration of the aqueous-phase plumes were studied using an extensive array of monitoring wells, multi-level groundwater samplers and aquifer cores. The layout of the ES site is shown in Figure 6-4. The overall site is about 100 m in length and 65 m in width.

Groundwater flow directions and hydraulic gradients were determined from a network of 50 water table monitoring wells. Water table measurements were performed every 7 to 14 days during the first 450 days of the experiment.

The dissolution of the source zone and migration of the aqueous-phase plumes were determined from a network of 173 multi-level groundwater samplers consisting of over 2,300 individual sampling points. At each sampler location, up to 14 groundwater samples could be collected from different depths in the aquifer. A section diagram of the vertical locations of groundwater monitoring points along the centre line of the aqueous plumes is shown in Figure 6-5. During the course of the experiment, more than 8,200 groundwater samples were collected and analysed.

The principal groundwater monitoring data to be considered in this chapter were collected from the array of 8 multi-level groundwater samplers located closest to the source zone. This array is located 1 m downgradient of the source zone and is referred to as, the 1-m Fence. A section diagram showing the locations of the 106 monitoring points along the 1-m Fence is shown in Figure 6-6. Groundwater samples were collected most frequently

from the 1-m Fence to evaluate source zone dissolution and less frequently in downgradient areas to evaluate plume migration.

A total of 16 cores of aquifer material were collected also from the ES site for the determination of hydraulic conductivity. Cores were collected from the source zone on three occasions to determine the chemical composition of the source zone.

6.3 Investigation and Monitoring Methods

6.3.1 Water Table Monitoring

Water table monitoring installations consisted of 3.75-cm or 5-cm diameter PVC drive-point wells. Each well had a 1.5-m long slotted screen and was installed to a depth suitable to intersect water table through its range of seasonal variation. Water levels were measured using an electric water level finder tape.

6.3.2 Groundwater Sampling

The multi-level groundwater samplers consisted of a bundle of 3.2-mm diameter Teflon sampling tubes attached to a central 2-cm diameter rigid PVC pipe. Each tube was open at the end with the opening covered by nylon screening. Most samplers had 14 monitoring points installed at different depths within the aquifer. The vertical spacing between monitoring points was 20 cm to 30 cm. The lateral spacing between monitoring locations ranged from 0.5 m to 4.0 m. The majority of multi-level samplers were installed inside a temporary casing driven to the desired depth using a pneumatic hammer. The end of the temporary casing was plugged during driving with a disposable steel drivepoint. At the desired depth, the prefabricated sampler bundle was inserted and the drivepoint knocked out. The sampler was held in place while the temporary casing was removed. The aquifer sand is cohesionless and collapses around the sampler bundle. This method of

sampler installation has been used successfully in the Borden aquifer since the work of Sudicky et al. (1983) with no evidence of "short-circuiting" between monitoring points. Some samplers were installed through a temporary casing used first to collect aquifer cores.

A 14-place manifold system was used to collect groundwater samples simultaneously from all monitoring points in a sampler bundle. This sampling system was described by Mackay et al. (1986). The manifold system is constructed of stainless steel tubing and fittings. Groundwater was drawn by vacuum from the monitoring point tubes into the manifold, where it passed into an 18-mL glass sample vial and then a 20-mL polyethylene vial prior to entering a 125-mL glass vacuum flask. At least 100 mL of groundwater was purged from each point and flushed through the sample vial prior to collection of the sample. This water volume represents about 9 tubing volumes for a monitoring point of average depth. This volume of water represents the groundwater drawn from a sphere with a radius of 4 cm around the monitoring point. After purging the required water volume, the flow-through heads on the glass and polyethylene vials were removed. The glass vials were sealed immediately with a Teflon-lined rubber septa and crimp-on caps, and used for the analysis of chlorinated solvents The polyethylene vials were sealed with polyethylene-lined caps, and used for the analysis of sulfate. Between multi-level sampler locations, the tubing and fittings of the manifold were blown out with air and wiped dry to prevent cross contamination of samples. In addition, whenever possible, the sequence of sampling proceeded from areas of low aqueous concentrations to areas of higher concentrations.

The analysis of chlorinated solvents in groundwater was performed using a pentane extraction method similar to that described by Glaze et al. (1983). Samples with low aqueous concentrations were extracted using a pentane:water ratio of 1:6. Samples with higher aqueous concentrations required pentane:water ratios up to 1,000:1. Aliquots of pentane extracts were

analysed by direct injection to a Varian 3300 gas chromatograph with electron capture detector. The detection limits were 5 μg/L for TCM and 1 μg/L for both TCE and PCE. Replicates of field samples and laboratory quality control standards indicated a standard error (standard deviation/mean) of 5% to 15% in the chlorinated solvent analyses. This analytical error is small in comparison to that which would be expected in results from commercial analytical laboratories (see Table 2-26).

6.3.3 Aquifer Cores

Aquifer cores and source zone cores were collected using the piston-coring method of Starr and Ingleton (1992). Aquifer cores downgradient of the source zone were continuous 5-cm diameter cores ranging from 4.0 m to 6.0 m in length. The cores were divided into 5-cm long segments for the laboratory determination of hydraulic conductivity using the falling head permeameter method of Sudicky (1986). Hydraulic conductivity values were corrected to the ambient groundwater temperature of 10°C.

Cores were collected from the centre of the source zone for the analysis of solvent concentrations. The cores were divided into 5-cm long segments from which 2 cm^3 of sand was transferred immediately into a glass vial containing 20 mL of methanol. Aliquots of methanol extract were diluted, as required, and analysed by direct injection to a Varian 3300 gas chromatograph with electron capture detector. Duplicates of field samples indicated a standard error (standard deviation/mean) of about 7% in the chlorinated solvent analyses.

6.4 Hydrogeological Conditions

6.4.1 Hydraulic Conductivity

The Borden aquifer at the ES site is comprised of medium-grained to fine-grained glaciolacustrine sand, with occasional beds of coarse sand & gravel or silt, and exhibits distinct laminations or bedding features. Individual beds range from several millimetres to several centimetres in thickness. Bedding is primarily horizontal but cross-bedding and convolute bedding features also occur commonly. Although the Borden aquifer exhibits a notable degree of textural variability, it is relatively homogeneous when compared to many other sandy aquifers.

The hydraulic conductivity of the Borden aquifer at the ES site was found to range from 1.6×10^{-5} cm/s to 3.1×10^{-2} cm/s based on the results of 764 permeameter tests from 16 cores. The geometric average hydraulic conductivity was 6.3×10^{-3} cm/s. This geometric average value compares well with the geometric average value of 7.2×10^{-3} cm/s obtained by Sudicky (1986). Of particular interest for this study are the results of Core 3 collected at location ES-3 (see Figure 6-6), situated 1 m directly downgradient of the source zone. These data are shown in Figure 6-7. Values ranged from 1.6×10^{-3} cm/s to 1.7×10^{-2} cm/s, with a geometric average of value of 6.6×10^{-3} cm/s. These values compare well with the general site conditions. There is a zone of lower hydraulic conductivity values at elevations 95.3 m to 95.8 m corresponding to the central portion of the source zone which extends from 95.1 m to 96.1 m. Higher hydraulic conductivity values occurred adjacent to the upper and lower portions of the source zone. The arithmetic average hydraulic conductivity for Core 3 was 7.7×10^{-3} cm/s. This value is used in Section 6.7.1 to calculate the chemical mass flux across the 1 m Fence.

One core was collected from the source zone immediately following installation. The hydraulic conductivity of the source zone material is lower than the aquifer material by a factor of 2.5 times because of the presence of the residual NAPL and gypsum powder in the source zone. Hydraulic conductivity of the source material ranged from 1.7×10^{-3} cm /s to 5.8×10^{-3} cm/s with a geometric average of 2.8×10^{-3} cm/s and an arithmetic average of 3.0×10^{-3} cm/s. The source core shows the same trend as Core 3 with the lowest hydraulic conductivity in the central portion of the source zone and higher values in the upper and lower portion of the source zone.

6.4.2 Groundwater Flow Direction

The source zone was oriented with its long dimension perpendicular to the direction of groundwater measured in the late summer of 1989 when the ES experiment was designed. However, monitoring has shown that the average direction of flow differed slightly from the assumed direction, and there was a substantial seasonal fluctuation in flow direction.

Figure 6-8 shows the fluctuation in water table elevation in a typical well, and the change in interpreted groundwater flow direction during the first 450 days of the ES experiment. The elevation of the water table fluctuated seasonally by about 0.8 m, with the highest levels occurring from 150 days to 250 days (spring and early summer) and lowest levels occurring from 0 days to 150 days and 250 days to 400 days (fall and winter).

The direction of groundwater flow fluctuated over an arc of about 30°. A negative flow angle shown in Figure 6-8 is directed to the left, relative to a line pointing downgradient of the source and perpendicular to the source. The direction of flow was generally between -5° and -10° (i.e. close to perpendicular to the source), with the flow angle increasing during periods of low water level. Large deviations in flow direction from -25° to -35° appear to occur in response to rapid declines or increases in water table elevation. The

fluctuations in the direction of flow influenced the position of the aqueous-phase plumes monitored at the 1 m Fence.

6.4.3 Hydraulic Gradient

The hydraulic gradient determined by the slope of the water table fluctuated seasonally, in concert with the elevation of the water table. The hydraulic gradient was highest (0.0064 m/m) when the water table was high and lowest (0.0034 m/m) when the water table was low (see Figure 6-9). The average hydraulic gradient was 0.0051 m/m.

Based on the geometric average hydraulic conductivity, hydraulic gradient and a porosity value of 0.33, the average linear groundwater velocity is calculated to be 8.4 cm/day.

6.4.4 Source Zone Composition

Despite attempts to minimize the handling of source material and the time required for placement in the subsurface, it was expected that some loss of solvents would occur as a result of volatilization to the atmosphere. As a result, a core was collected from the centre of the source zone for chemical analysis immediately following installation of the source. The solvent concentrations expressed as weight % of the NAPL are shown in Figure 6-10 together with the original solvent concentrations in the NAPL. Although the solvent concentrations in the source core were relatively uniform within the source zone, 46% of the TCM and 24% of TCE was lost during placement. Only 5% of the PCE was lost during placement. The relative degree of loss of the different solvents is proportional to their vapor pressures. The composition and chemical masses of the NAPL source zone are summarized in Table 6-1.

Groundwater monitoring and soil-gas surveys conducted following installation of the source determined that some very small quantities of

source material were spilled at the ground surface where the source mixing took place, in the vadose zone at the wall of the excavation, and about 0.4 m to 1.4 m above the source zone. The groundwater plumes and soil-gas plumes created by this material differs in composition and location from those created by the source zone. The spilled material remained at the ground surface for 2 days before the excavation was backfilled and almost all of the TCM and most of the TCE was lost. Groundwater monitoring points affected by this extraneous material are not included in the following evaluation of source zone dissolution. A more complete description of the interpretation of the effects of the spilled material is provided by Rivett (1995).

6.5 Overall Plume Migration

The aqueous-phase solvent plumes downgradient of the source zone were sampled in detail on five occasions at 56 days, 90 days, 125 days, 194 days and 322 days following emplacement of the source. The arrival or "breakthrough" of aqueous-phase solvents was monitored more frequently at selected monitoring points. The extents of the aqueous-phase plumes at 322 days are shown in Figure 6-11. The concentration contours shown in this figure are based on concentrations at each multi-level sampler location, averaged vertically over the thickness of the plume. The TCM plume was about 50 m long and 6 m wide. A longitudinal vertical section of the TCM plume at 322 days is shown in Figure 6-12. The concentrations in this figure represent the concentrations at individual monitoring points. Concentrations in the core of the plume exceeded 100,000 µg/L. The plume had a thickness of up to 3 m. The TCE plume was slightly smaller than the TCM plume, about 45 m in length. The PCE plume was about 30 m in length.

The extents of the aqueous-phase plumes reflect the different degree of retardation of the three solvents. Based on comparison to the migration of the sulfate from the source zone and preliminary transport modeling, the

retardation factors are estimated to be 1.0, 1.1 and 1.6 for TCM, TCE and PCE, respectively (Rivett, Feenstra and Cherry, 1992).

In February of 1991, 475 days after emplacement of the source zone, a groundwater pump-and-treat system was commenced in order to prevent further expansion of the aqueous-phase plumes. Three pumping wells were situated along the centre line of the aqueous-phase plume at distances of 25 m, 37 m and 45 m from the source zone (see Figure 6-13). The wells were constructed of 5-cm diameter PVC casing with 3-m long slotted screens open over the vertical extent of the plumes. Each well pumped at 3.5 L/min. to 8 L/min. The extracted water was treated on granular activated carbon to remove the solvents and was re-injected to the aquifer about 150 m away from the ES site.

The operation of the pump-and-treat system accomplished relatively rapid remediation of the aquifer in the area between the pumping wells. The shrinkage of the plumes is illustrated in Figure 6-14. The area upgradient of PW-2 was not remediated because of the continued dissolution of the source zone. A more detailed description of the pump-and-treat remediation is provided in Rivett (1993).

In June of 1991, 600 days after emplacement of the source and while the pump-and-treat system was in operation, an experimental *in situ* treatment wall was installed 5 m downgradient of the source zone to intercept the aqueous-phase plume. The treatment wall was comprised of sand and elemental iron and relied on reductive dehalogenation reactions to degrade the chlorinated solvents. The wall designed to provide treatment of TCE and PCE to less than 5 µg/L from influent concentrations of approximately 250,000 µg/L and 43,000 µg/L, respectively. However, the treatment efficiency was found to be only 90% to 95% so that concentrations of 5,000 µg/L to 10,000 µg/L continued to migrate beyond the wall toward pumping well

PW-2. A more detailed description of the *in situ* treatment wall is provided by Gillham (1996).

6.6 Source Zone Dissolution

6.6.1 Overview

The principal data considered in evaluation of dissolution of the NAPL source zone were the results of groundwater sampling from the 1 m Fence. Samples were collected from the 1 m Fence on 32 occasions following emplacement of the source. The final complete set of samples was collected at 1,029 days. These data were used to calculate the chemical mass flux from the NAPL source zone and the rate of source depletion. The monitoring data were used also to calculate the temporal changes in aqueous concentrations and concentration ratios during dissolution of the source. These results were then compared to the results of the ESM.

6.6.2 Magnitude of Aqueous Concentrations

The initial effective solubilities of TCM, TCE and PCE are 680,000 µg/L, 610,000 µg/L and 120,000 µg/L, respectively, based on the initial NAPL source composition and Raoult's Law. These calculations are shown also in Table 6-2. Aqueous concentrations as high as the initial effective solubility values were observed only in a small number of monitoring points directly downgradient from the central portion of the source zone. Concentrations are lower around the margin of the source zone. Figure 6-15 shows the aqueous concentrations at monitoring point ES-2-8 in the centre of the plume. Peak concentrations of TCM, TCE and PCE were 680,000 µg/L, 690,000 µg/L and 120,000 µg/L, respectively, and compare well with the calculated initial effective solubilities. This observation supports further the applicability of Raoult's Law for mixtures of chlorinated solvents.

6.6.3 Temporal Changes in Aqueous Concentrations

Aqueous concentrations measured along the 1 m Fence vary in response to preferential dissolution of the more soluble components from the NAPL source, and in response to seasonal fluctuations in groundwater flow direction. At monitoring point ES-2-8 (see Figure 6-15), TCM begins to decline after about 200 days as a result of depletion of the source. Concentrations fluctuate also in response to seasonal changes in groundwater flow direction.

The seasonal changes in groundwater flow direction caused the plumes to vary in location. The forms of the aqueous-phase plumes along the 1 m Fence are shown in Figure 6-16 on 6 occasions at 90 days, 173 days, 230 days, 322 days, 630 days and 922 days. These occasions were selected to illustrate the principal changes which occurred in the plumes. The concentration contours were drawn in Spyglass® Transform Version 3.0 using a 0.01 m grid with kernel smoothing.

At times of 90 days, 173 days, and 922 days, groundwater flow was oblique to the source and the plumes was shifted to the right of the source zone. For example, at these times only low aqueous concentrations were observed at monitoring location ES-3. Higher concentrations were observed in ES-3 at 230 days and 630 days because the groundwater flow direction had shifted to be more perpendicular to the source zone. At 322 days, monitoring location ES-3 was in the high-concentration cores of the plumes. The shifts in position of the plumes makes it difficult to evaluate the monitoring results of individual monitoring points. Figure 6-17 shows the temporal variation in aqueous concentrations at monitoring point ES-3-9. Concentrations were high at 200 days to 400 days, and again at about 600 days when groundwater flow shifted the plumes to the right of the source zone. These shifts make it difficult to identify the temporal trend in concentrations or concentration ratios.

At later times, the size of the TCM plume and magnitude of the TCM concentrations declined as TCM was dissolved preferentially from the NAPL source zone (see Figure 6-16). The size of the plumes and magnitude of concentrations for TCE and PCE did not change notably during the 1,029 days of monitoring.

Although the overall sizes of the plumes are similar to the size of the source zone, the high-concentration centres of the plumes are much smaller than the source. This condition is likely the result the nature of groundwater flow through and around the source. The hydraulic conductivity of the source zone is about 0.4 of the hydraulic conductivity of the surrounding aquifer material. This difference in hydraulic conductivity results in a divergence of groundwater upgradient of the source zone and convergence of flow downgradient of the source zone. Based on three-dimensional groundwater flow modeling performed by Guiguer (1993), the divergence and convergence of flow takes place within about 0.5 m of the source zone.

The convergence of flow downgradient of the source zone resulted in dilution of the margins of plumes. Figure 6-18 shows the temporal variation in aqueous concentrations at monitoring point ES-2-12 situated at the lower margin of the plume. This point is only 0.8 m below ES-2-8 but concentrations were only generally less than 1,000 µg/L compared to values of 100,000 µg/L of more in ES-2-8.

The vertical profiles of hydraulic conductivity in the source zone and aquifer (see Figure 6-7) show zones of higher hydraulic conductivity at the upper and lower portions of the source zone. This would cause higher rates of groundwater in these zones compared to that in the central portion of the source zone and further accentuate the dilution effect of divergent-convergent groundwater flow.

6.6.4 Averaged Aqueous Concentrations

Further evaluation of the temporal variation in aqueous concentrations and ratios caused by dissolution was performed on values averaged over multiple monitoring points. The primary purpose of the averaging was to minimize the effect of temporal variations in aqueous concentrations caused by changes in groundwater flow direction. In addition, aqueous concentrations averaged vertically over all the monitoring points in a sampler bundle is likely a reasonable approximation of the results that would be obtained from a conventional monitoring well with an intake of moderate length (i.e. several metres). Aqueous concentrations averaged over the full area of the 1 m Fence is likely a reasonable approximation of the results of a groundwater extraction well which intercepted flow over a large area.

The temporal variations in aqueous concentrations for monitoring locations ES-4, ES-3, ES-2, ES-1 and ES-28 are shown in Figures 6-19, 6-20, 6-21, 6-22 and 6-23, respectively. Locations ES-4 and ES-28 were located at the lateral margins of the plumes and exhibited elevated concentrations only sporadically. Location ES-3 and ES-1 intersected the central portion of the plumes for short periods of time. Locations ES-2 intersected the central portion of the plumes consistently.

Area-averaged aqueous concentrations can be determined by a variety of methods. The simplest method is the Thiessen polygon method in which the concentration measured at each monitoring point is weighted according to the lateral and vertical spacing between adjacent monitoring points. Other methods involve different numerical schemes for interpolating the concentrations between the values measured at the monitoring points. Such methods include inverse distance interpolation and kriging. Guiguer (1993) calculated area-averaged concentrations using the Thiessen method, inverse

distance and kriging. The Thiessen method yielded the highest area-averaged values, but all the other methods were within 5% to 20% of the Thiessen method values. The inverse distance and kriging methods tend to smooth concentration gradients between points and cutoff peak values. In the case of the 1 m Fence, the value of the area-averaged concentration is determined largely by the results from only 4 to 6 monitoring points of the total of 106. As a result, the Thiessen polygon method was selected as the preferred method here, to preserve the influence of the peak concentration values.

The temporal variation in the area-averaged aqueous concentrations is shown in Figure 6-24. TCM concentrations peaked at about 100 days and exhibited a steady decline until concentrations reached very low levels at about 600 days. This trend reflects the preferential dissolution of TCM from the NAPL source zone. Concentrations of TCE and PCE remained relatively steady during the experiment despite the continued dissolution of the source. This is an illustration of how a NAPL source zone can provide an on-going source of aqueous-phase contaminants to the groundwater. These area-averaged concentration values will be used in the following section to calculate the degree of mass depletion of the source zone.

6.7 Determination of NAPL Mass Remaining

The quantity of NAPL mass remaining in the source zone was determined primarily by the difference between the initial mass and the cumulative chemical mass crossing the 1 m Fence. The quantity of NAPL mass remaining in the source was estimated also based on the analysis of source cores collected at 399 days and 1,128 days after emplacement of the source. The mass flux from the source was provided also by the monitoring of pumping well PW-2 in the pump-and-treat system.

6.7.1 Mass Flux Crossing the 1 m Fence

The chemical mass flux across the 1 m Fence at different times during the experiment was calculated using the time-varying area-averaged aqueous concentrations, the average hydraulic conductivity of the aquifer, and the time-varying hydraulic gradient. The time-varying area-averaged concentrations are shown in Figure 6-24. The average hydraulic conductivity of the aquifer at the 1 m Fence was 7.7×10^{-3} cm/s (see Figure 6-7). The hydraulic gradient at the ES site was measured only during the first 450 days of the experiment. For the purpose of these mass flux calculations, the same seasonal fluctuation in gradient observed in the first year was extrapolated to the second and third years of the experiment. The measured and extrapolated values for the hydraulic gradient are shown in Figure 6-25.

During the first year of the experiment, aqueous concentrations were measured on 23 occasions and hydraulic gradient determined on 40 occasions. For this period, mass flux calculations were based on the measured value of the hydraulic gradient which occurred closest to the time of groundwater sampling. In contrast, aqueous concentrations were measured on only 9 occasions during the second and third years of the experiment. For this reason, mass flux calculations for the second and third years were based on the average hydraulic gradient for the time period between sampling events. These average hydraulic gradient values are shown also in Figure 6-25.

The temporal variation in calculated chemical mass flux crossing the 1 m Fence is shown in Figure 6-26. The mass flux of TCM reached about 5 g/day at about 200 days and then declined to very low levels after 600 days in response to preferential dissolution from the source zone. The mass flux of TCE reached about 8 g/day for the first 300 days and then dropped to about 4 g/day. The mass flux of PCE remained at 1 g/day to 2 g/day during the entire experiment.

The change in NAPL mass with time was calculated from the initial chemical mass in the source zone and the cumulative mass crossing the 1 m Fence. These calculations are shown in Figure 6-27. The rate of source dissolution was greatest as TCM was removed from the NAPL source and slowed between 300 days and 600 days as TCM reached low concentrations. By the end of the experiment at 1,029 days, the NAPL mass remaining was 0.7 of the initial mass. The plot of NAPL mass remaining versus time is used Sections 6.8 and 6.9 to evaluate the relationship between aqueous concentration ratios and the NAPL mass remaining.

6.7.2 Source Cores

Estimates of the chemical mass remaining in the source zone were determined also from the analysis of source cores collected at 399 days and 1,128 days. The results of these analyses are shown for TCM, TCE and PCE in Figure 6-28, 6-29 and 6-30, respectively. The chemical concentrations in these figures are expressed as a percentage relative to the initial core concentration. At 399 days, the average TCM concentration in the source zone was 14% of the initial value. By 1,128 days, the source zone was devoid of TCM. The average TCE concentration in the source core was 88% of the initial value at 399 days and 28% of the initial value at 1,128 days. Because of its lower solubility and high proportion in the NAPL, there was no measurable decline in PCE in the source core at 399 days and only a slight decline to 96% of the initial concentration at 1,128 days.

It is also evident in the results of the TCE analyses of the source cores that dissolution of the source zone is not uniform. At 1,128 days there had been preferential removal of TCE from the upper portion and lower portion of the source zone. Preferential removal from these zones may have been the result of higher hydraulic conductivity in the aquifer and source (see Figure 6-7). However, there was also preferential dissolution of TCE from a 0.1 m thick zone in the central portion of the source. Based on the analyses of

the source cores, the NAPL mass remaining in the source was 0.90 at 399 days and 0.63 at 1,128 days. These estimates are shown in Figure 6-31 and compare favourably with those calculated from the mass crossing the 1 m Fence.

6.7.3 Pump-and-Treat System

From 475 days until 700 days, pumping well PW-2 intercepted the total chemical mass emitted from the source zone. Unfortunately, it is not possible to relate the mass removal from PW-2 to the mass remaining in the source zone at a specific time because there is a delay of 200 to 300 days for aqueous-phase solvents to migrate from the source to PW-2, and because the *in situ* treatment wall was installed between the source and PW-2 at 600 days. However, the monitoring results of PW-2 can provide an estimate of the chemical mass flux from the source during the period from about 500 days to 700 days.

The aqueous-phase concentrations in PW-2 are shown in Figure 6-32. TCM concentrations declined steadily as TCM was depleted from the source. TCE and PCE concentrations declined initially, but leveled off during the period from 600 days to 700 days. These steady concentrations reflect the mass flux from dissolution of the source zone. After 700 days, the concentrations declined in response to the removal of solvents by the *in situ* treatment wall.

The chemical mass flux from PW-2 is shown in Figure 6-33. For the period of steady aqueous concentrations from 600 days to 700 days, the TCE mass flux was 3 g/day to 4 g/day and the PCE mass flux was 1 g/day to 2 g/day. These values compare closely to the mass flux values calculated crossing the 1 m Fence (see Figure 6-26).

6.8 Temporal Variation in Aqueous Concentration Ratios

The seasonal fluctuations in groundwater flow direction and shifts in position of the aqueous-phase plumes make it difficult to evaluate trends in

aqueous concentrations and concentrations ratios at individual monitoring points and at sampler bundles that do not intersect the plumes continually. The most consistent aqueous concentration-time data are derived from the area-averaged concentrations for the 1 m Fence and from monitoring locations ES-2 and ES-1.

The temporal variation in aqueous concentration ratios for the area-averaged concentration for the 1 m Fence is shown in Figure 6-34. The TCE/TCM and PCE/TCM ratios increased gradually to 400 days as TCM was dissolved preferentially. During the late stages of TCM dissolution, TCE/TCM and PCE/TCM ratios increased markedly. PCE/TCE ratios increased gradually during the experiment. These trends in aqueous concentration ratios are those expected for the preferential dissolution of TCM and then TCE from the NAPL source zone. In this controlled field experiment, the change in NAPL mass remaining is known and aqueous concentration ratios can be plotted versus NAPL remaining in the manner shown in Chapters 4 and 5. These data are shown in Figure 6-35. In this case, the rate of dissolution of the NAPL source is relatively constant (see Figure 6-31) so that the plot of ratios versus NAPL remaining is similar to the plot of ratios versus time.

Similar plots of aqueous concentration ratios at monitoring locations ES-2 and ES-1 are shown in Figures 6-36, 6-37, 6-38 and 6-39. These figures show the same consistent increases in TCE/TCM and PCE/TCM ratios as those for the area-averaged concentrations for the 1 m Fence. Similar trends are observed in small number of individual monitoring points. Plots of aqueous concentration ratios at monitoring point ES-2-8 are shown in Figures 6-40 and 6-41. The consistency of the trends in these data are favourable for comparison to predictions by the ESM.

At sampler bundles which did not intersect the plumes continually, and at most individual monitoring points, the temporal variation in aqueous

concentrations ratios is erratic. Plots of aqueous concentration ratios at monitoring location ES-3 and monitoring point ES-3-9 are shown in Figures 6-42, 6-43, 6-44 and 6-45. Although these figures show a general increase in TCE/TCM and PCE/TCM ratios, the magnitude of the fluctuations is sufficiently large to preclude comparison of these curves to the predictions of the ESM. Plots of aqueous concentration ratios at monitoring locations ES-4 and ES-28 are shown in Figures 6-46, 6-47, 6-48 and 6-49. These locations were at the margins of the plumes and concentration ratios show no discernible trends.

6.9 Comparison of Measured Ratios to ESM

The ESM was used to simulate the changes in aqueous concentration ratios for the dissolution of the NAPL in the ES source zone. The composition of the NAPL and the properties of the components used as input parameters to the ESM are shown in Table 6-3. The aquifer was specified to have a dry bulk density of 1,809 kg/m^3, at total porosity of 0.33 and a fraction organic carbon (f_{OC}) of 0.0002. The initial NAPL content was specified to be 20 L/m^3. Using these parameters values, simulations were performed for 1-cell, 2-cell and 5-cell configurations. The number of cells is the only model input parameter not defined explicitly by the NAPL and aquifer properties.

TCE/TCM, PCE/TCM and PCE/TCE ratios versus NAPL mass remaining predicted by the ESM are shown in Figures 6-50, 6-51 and 6-52, respectively. The predicted ratios were compared to those site monitoring data that exhibited discernible trends in aqueous concentrations with time. The predicted ratios are compared to the measured ratios for the area-averaged concentrations crossing the 1 m Fence in Figures 6-53, 6-54 and 6-55; for monitoring location ES-2 in Figures 6-56, 6-57 and 6-58; for monitoring location ES-1 in Figures 6-59, 6-60 and 6-61; and, for monitoring point ES-2-8 in Figures 6-62, 6-63 and 6-64.

The changes in TCE/TCM and PCE/TCM ratios predicted by the ESM compare well with the measured ratios for the area-averaged 1 m Fence, monitoring location ES-2 and monitoring point ES-2-8. In each of these cases the best match between the predicted and measured ratios is provided by the 5-cell configuration of the ESM. This indicates that the size and character of the NAPL zone is sufficient to cause a chromatographic effect as aqueous-phase solvents dissolved from the upgradient portion of the source zone exchange with the NAPL present in the downgradient portion of the source zone.

There is a larger degree of scatter in the TCE/TCM and PCE/TCM ratio data from monitoring location ES-1 and although trends are comparable to the 1 m Fence, ES-2 and ES-2-8, it is not possible to match the measured data well with the results of a particular ESM configuration.

It is difficult also to compare the measured PCE/TCE ratios to those predicted by the ESM simulations because the PCE/TCE ratios change by only a factor of 10 times or less during the experiment. The degree of scatter in the PCE/TCE ratios due to analytical variations and fluctuations in groundwater flow is sufficiently large to mask any trends. In contrast, the measured TCE/TCM and PCE/TCM ratios change during the experiment by a factor of 1,000 times or more and this change is much larger than the scatter in ratio data from analytical and hydrogeologic variations.

6.10 Conclusions Regarding Emplaced-Source Experiment

The results of the Emplaced-Source experiment indicate that the changes in aqueous concentration ratios measured during dissolution of the NAPL source can be predicted with reasonable accuracy using the ESM.

Despite the fact that NAPL source zone in the field experiment was larger in dimensions than the NAPL zones in the laboratory experiments described in Chapter 5, measured ratios compared well with ratios calculated

by a 5-cell configuration of the ESM. The results of the laboratory experiments could be matched using from 1-cell, up to 10-cell configurations of the ESM. This suggests that the length of the NAPL zone is not the only factor which will determine the number of cells required by the ESM to obtain a suitable match. Other factors such as the pore-scale distribution of NAPL and pattern of groundwater flow also likely determine whether a chromatographic effect occurs within the source zone.

The 1-cell configuration of the ESM can be used to evaluate the changes in aqueous concentration ratios in the ES experiment and estimate NAPL mass remaining. For example, as shown in Figure 6-53, at the point where the measured TCE/TCM ratio reached 1,000, the ESM predicted the NAPL mass remaining to be about 0.55. In comparison, the true NAPL mass remaining was 0.70. Simple predictions of this type using a 1-cell configuration of the ESM may still be useful given the much larger uncertainty in estimating the mass contained in NAPL source zones by other methods such as direct soil sampling and analysis.

More accurate estimates of NAPL mass remaining can be made using multiple-cell configurations of the ESM. However, at sites of NAPL contamination there will be no *a priori* knowledge of the cell configuration most suitable for comparison to the groundwater monitoring data. A method for the comparison of field data to ESM simulations in order to select the most appropriate ESM configuration at a particular site is described in Chapter 8.

Table 6-1. Summary of initial source composition based on source core analyses.

Measurement	TCM	TCE	PCE	Total
Volume (L) mixed into Source Zone	1.8	8.1	8.1	18.0
Mass (g) mixed into Source Zone	2,682	11,826	13,203	27,711
NAPL Composition (weight %) mixed into Source Zone	9.7	42.7	47.6	100
Volume (L) determined from Source Core	0.97	6.16	7.70	14.8
Mass (g) determined from Source Core	1,448	8,988	12,543	22,979
NAPL Composition (weight %) determined from Source Core	6.3	39.1	54.6	100

Key:
TCM - Chloroform
TCE - Trichloroethylene
PCE - Tetrachloroethylene

Table 6-2. Calculation of initial effective solubilities of solvents based on initial NAPL source composition and Raoult's Law.

Measurement	TCM	TCE	PCE	Total
Pure-phase Solubility (µg/L)	8,700,000	1,400,000	240,000	
Weight % in NAPL	6.3	39.1	54.6	100
Mole Fraction in NAPL	0.078	0.438	0.484	1.00
Initial Effective Solubility (µg/L)	680,000	610,000	120,000	

Key:
TCM - Chloroform
TCE - Trichloroethylene
PCE - Tetrachloroethylene

Table 6-3. Composition and properties of the components in the NAPL in the source zone used as input parameters in the ESM simulations.

Parameter	TCM	TCE	PCE
Molecular Mass (g/mol)	119.4	131.5	165.8
Density (kg/m^3)	1,490	1,470	1,630
Pure-phase Solubility (µg/L)	8,700,000	1,400,000	240,000
K_{OC} (mL/g)	56	93	302
Composition (wt.%)	6.3	39.1	54.6

Key:
TCM - Chloroform
TCE - Trichloroethylene
PCE - Tetrachloroethylene

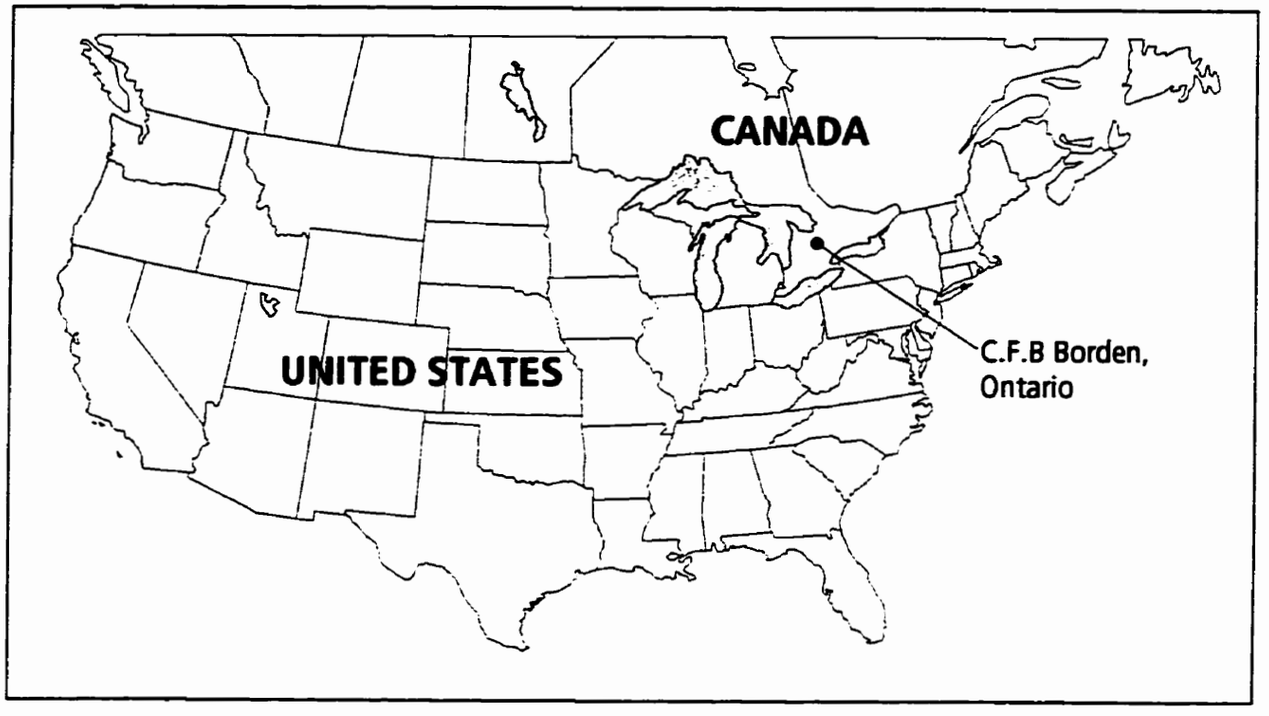

Figure 6-1. Location of Canadian Forces Base Borden, Ontario.

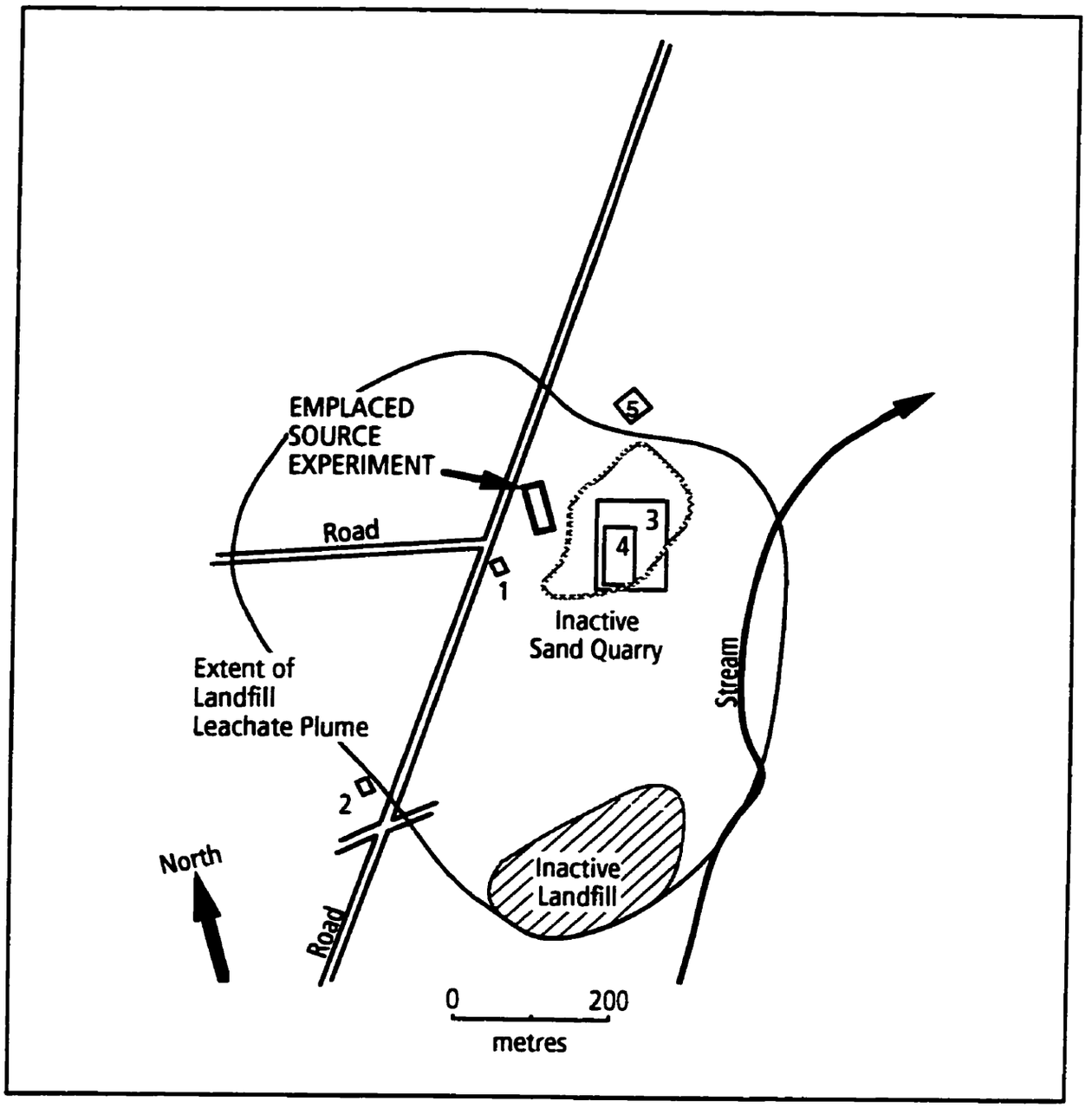

Figure 6-2. Location of the Emplaced-Source experimental site at the Canadian Forces Base Borden.

Other experimental sites shown are:
1. Chloride transport - Sudicky et al., (1983)
2. Organics transport - Sutton and Barker, (1985)
3. Chlorinated solvents transport- Mackay et al., (1986)
4. BTEX transport - Patrick et al., (1986)
5. Vapor transport- Hughes et al. (1990)

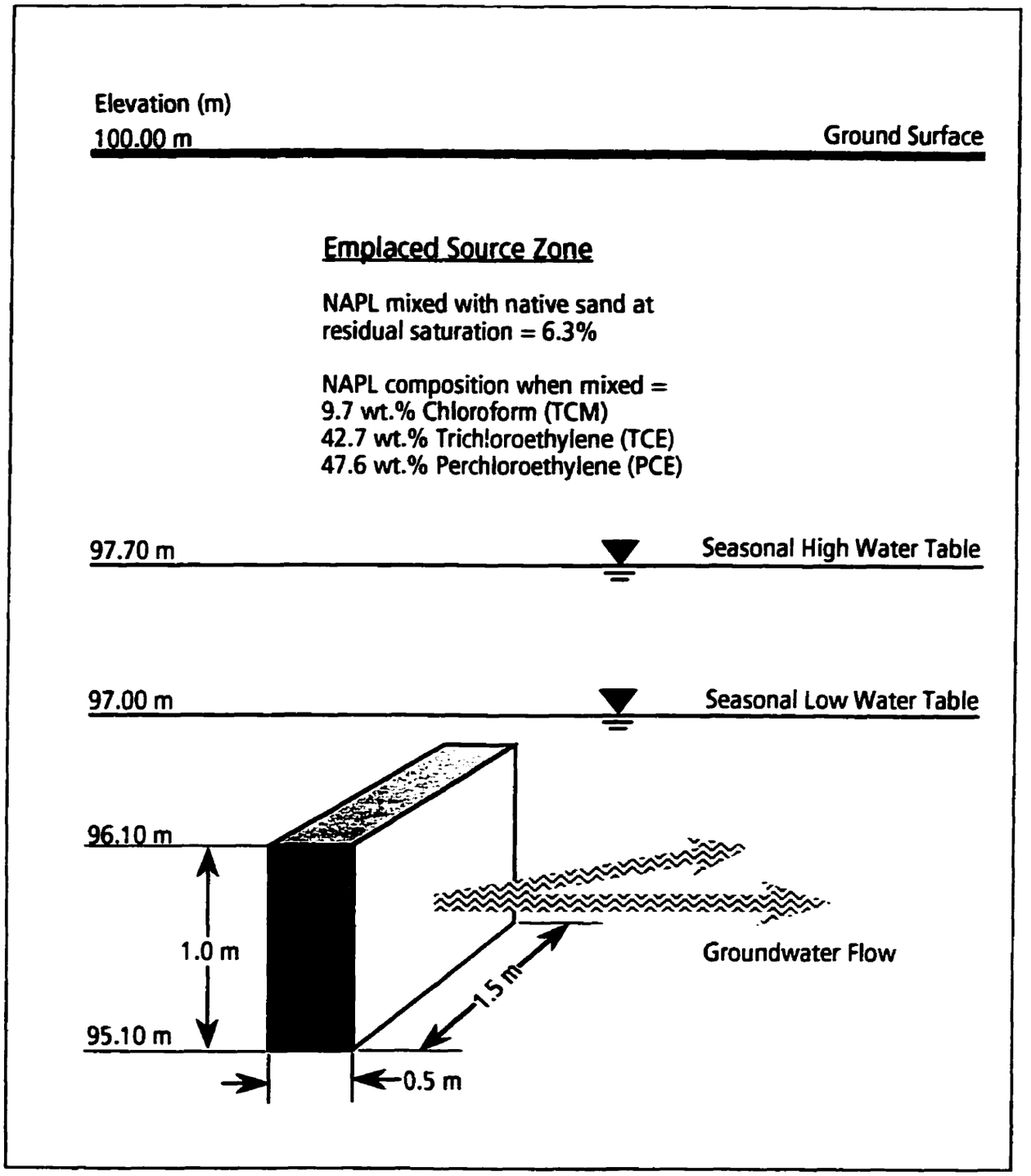

Figure 6-3. Schematic diagram of source zone configuration for the Emplaced-Source Experiment.

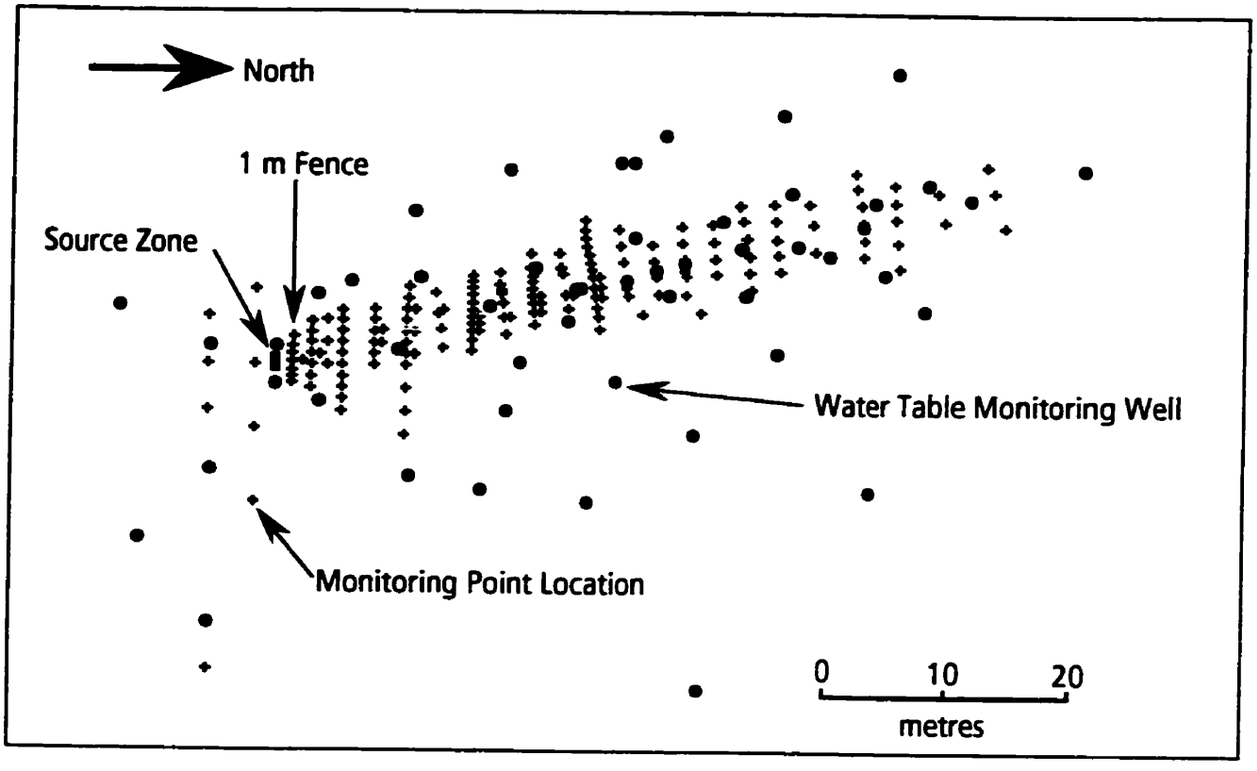

Figure 6-4. Layout of groundwater monitoring points and water table monitoring wells for the Emplaced-Source Experiment.

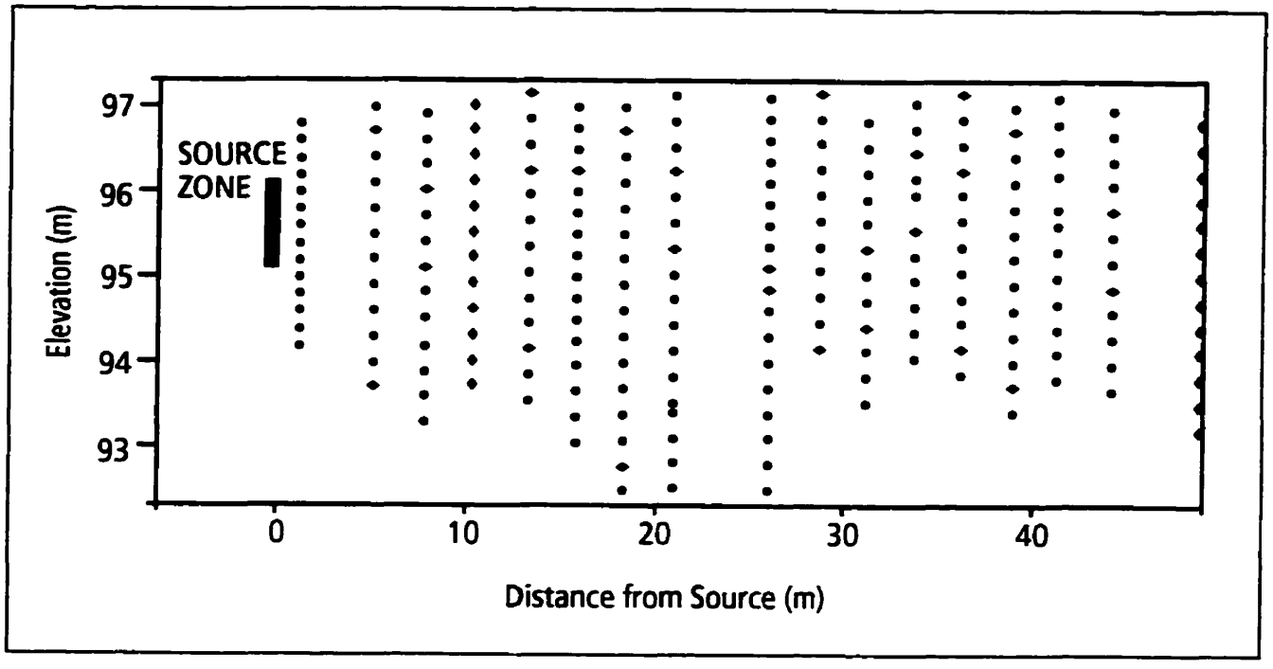

Figure 6-5. Locations of groundwater monitoring points along the centre line of the aqueous-phase plumes.

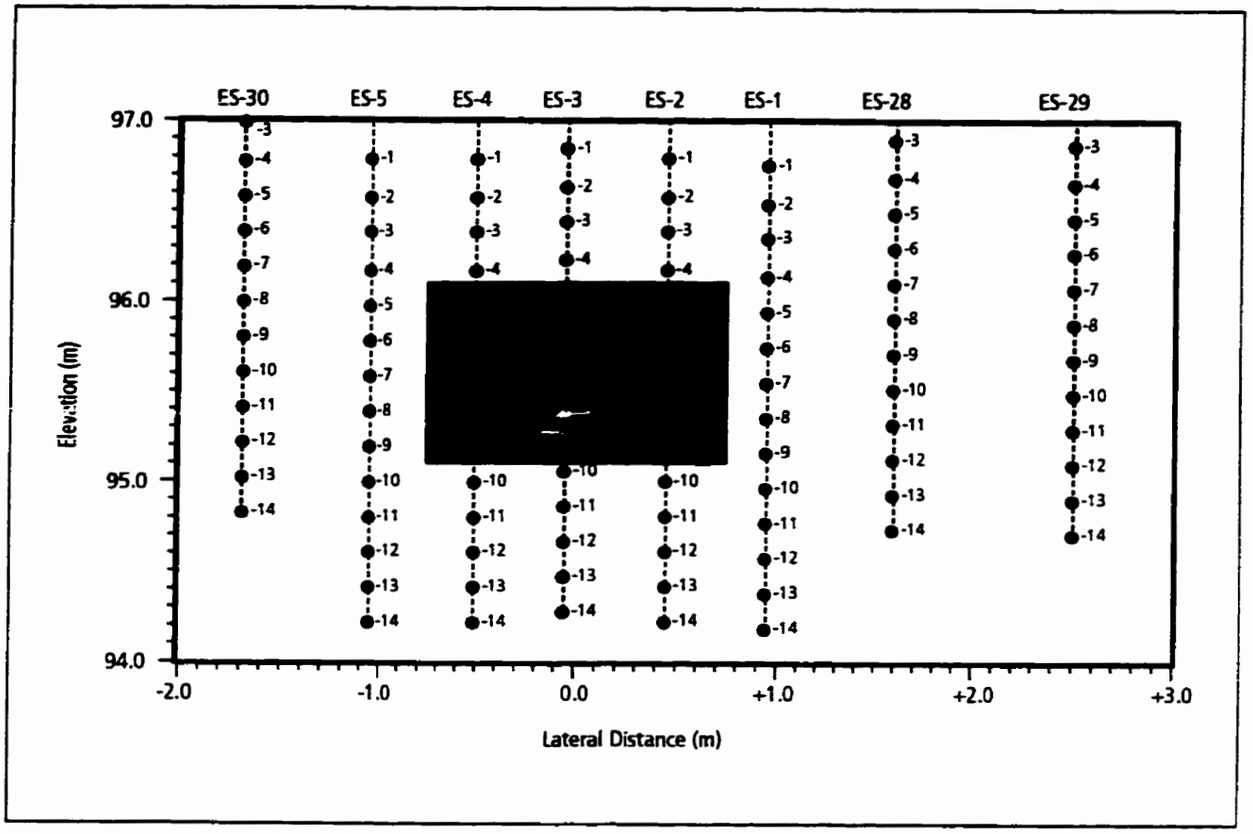

Figure 6-6. Section diagram of monitoring points located along the 1 m Fence, viewed looking upgradient toward the source.

Relative location of source zone shown as shaded area.

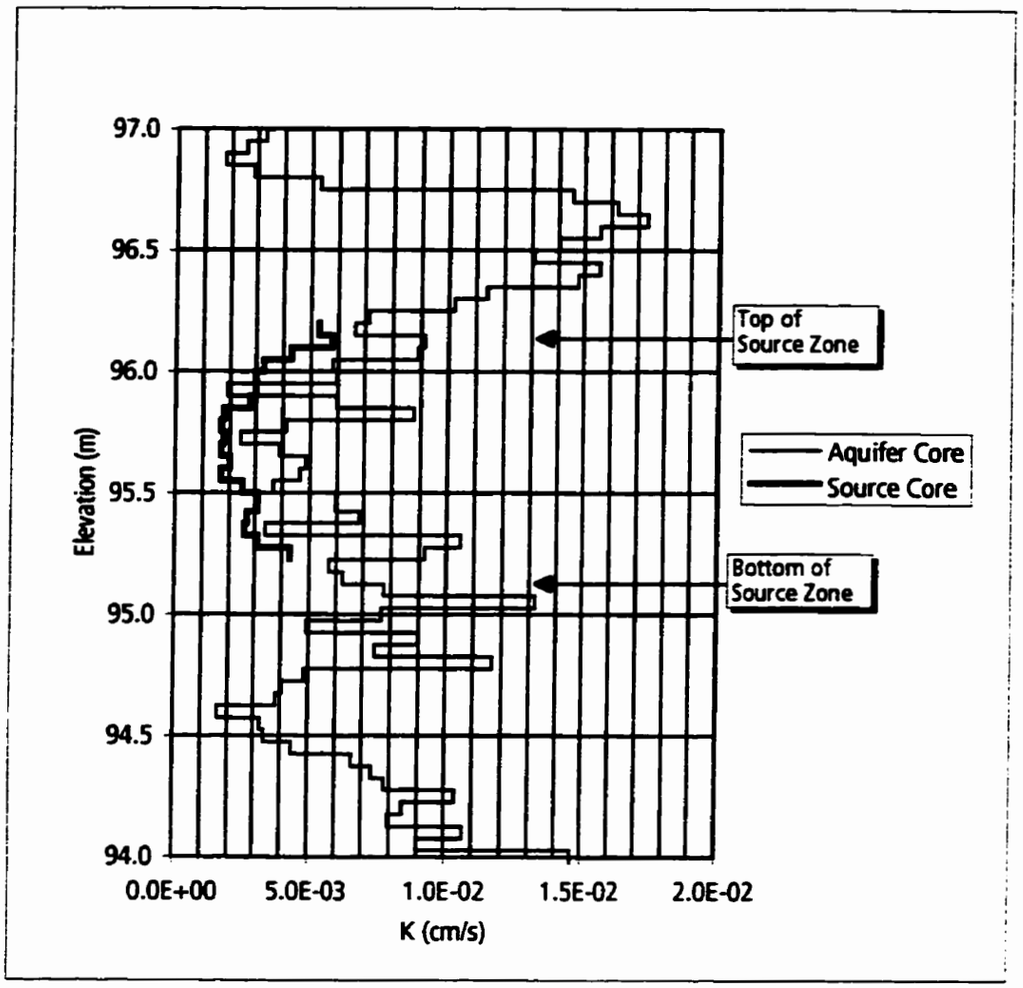

Figure 6-7. Hydraulic conductivity profiles for the aquifer at the 1 m Fence and in the source zone.

Hydraulic conductivity determined in the laboratory by falling-head permeameter.
Aquifer Core -Average K= 7.7E-3 cm/s
Source Core -Average K= 3.0E-3 cm/s

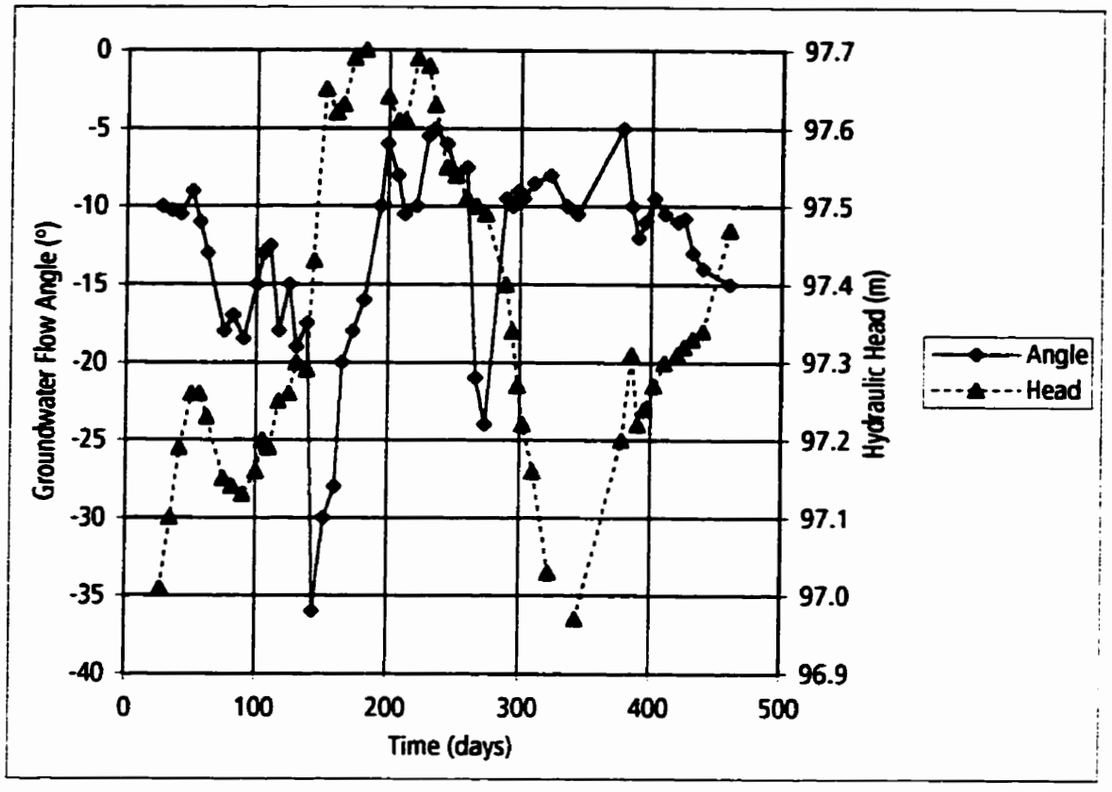

Figure 6-8. Temporal change in hydraulic head and groundwater flow direction.

Groundwater flow angle is measured relative to groundwater flow downgradient, perpendicular to the source zone.
Positive flow angle is directed to the right, negative angle is directed to the left.
Time is measured relative to emplacement of source.

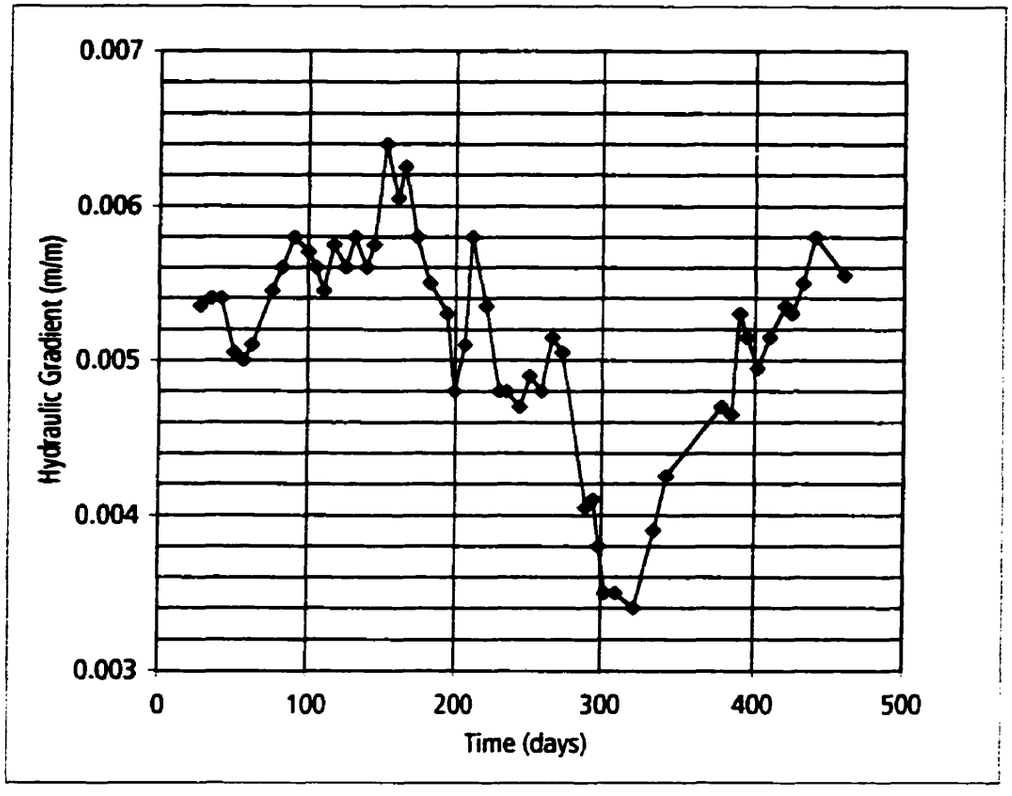

Figure 6-9. Temporal change in horizontal hydraulic gradient.

Time is measured relative to emplacement of source zone.

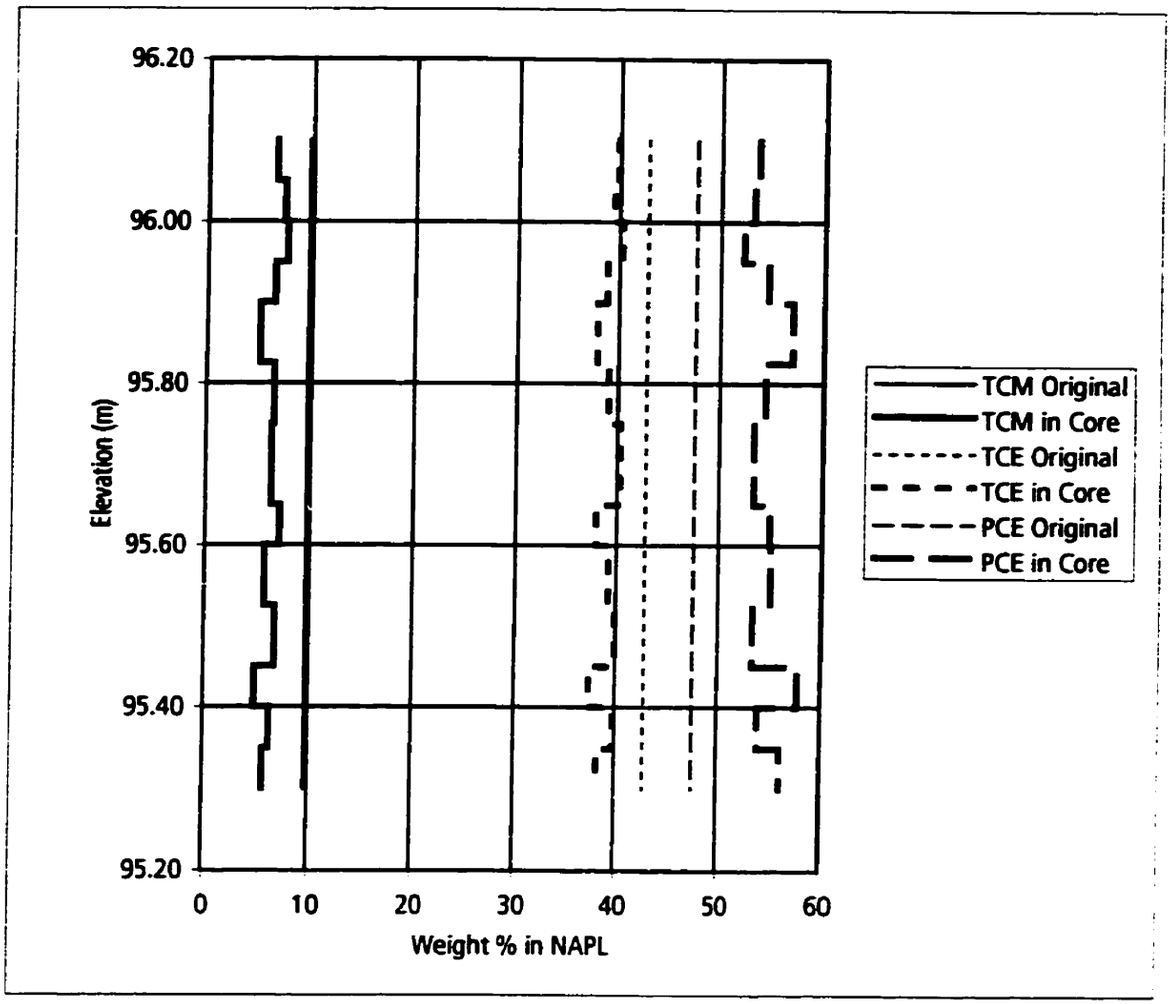

Key:
TCM - Chloroform
TCE - Trichloroethylene
PCE - Tetrachloroethylene

Figure 6-10. Initial composition of emplaced source based on the results of a soil core taken immediately after source emplacement.

Average Composition: TCM - 6.3 wt.%
TCE - 39.1 wt.%
PCE - 54.6 wt.%

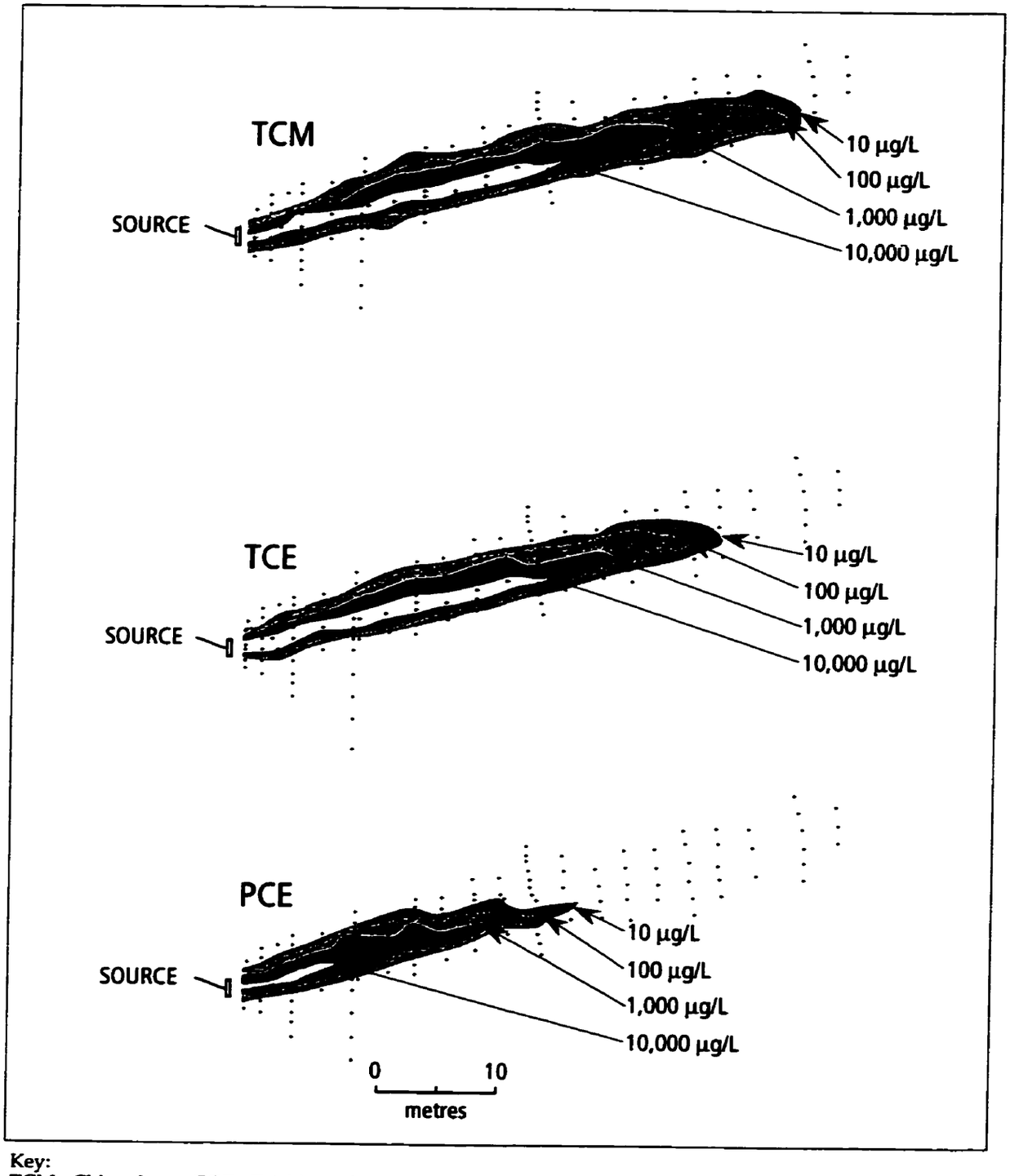

Key:
TCM - Chloroform; TCE - Trichloroethylene; PCE - Tetrachloroethylene

Figure 6-11. Extents of aqueous-phase plumes emitted from the source zone at 322 days after emplacement.

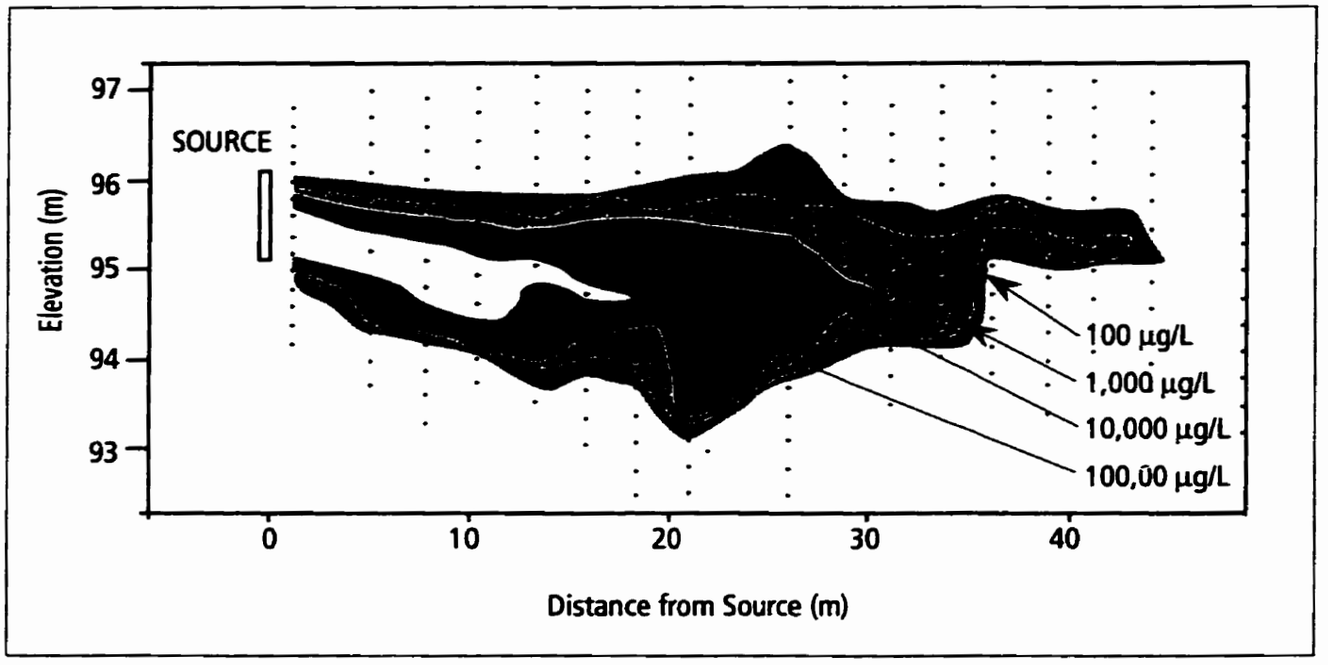

Figure 6-12. Longitudinal section of chloroform (TCM) aqueous-phase plume at 322 days.

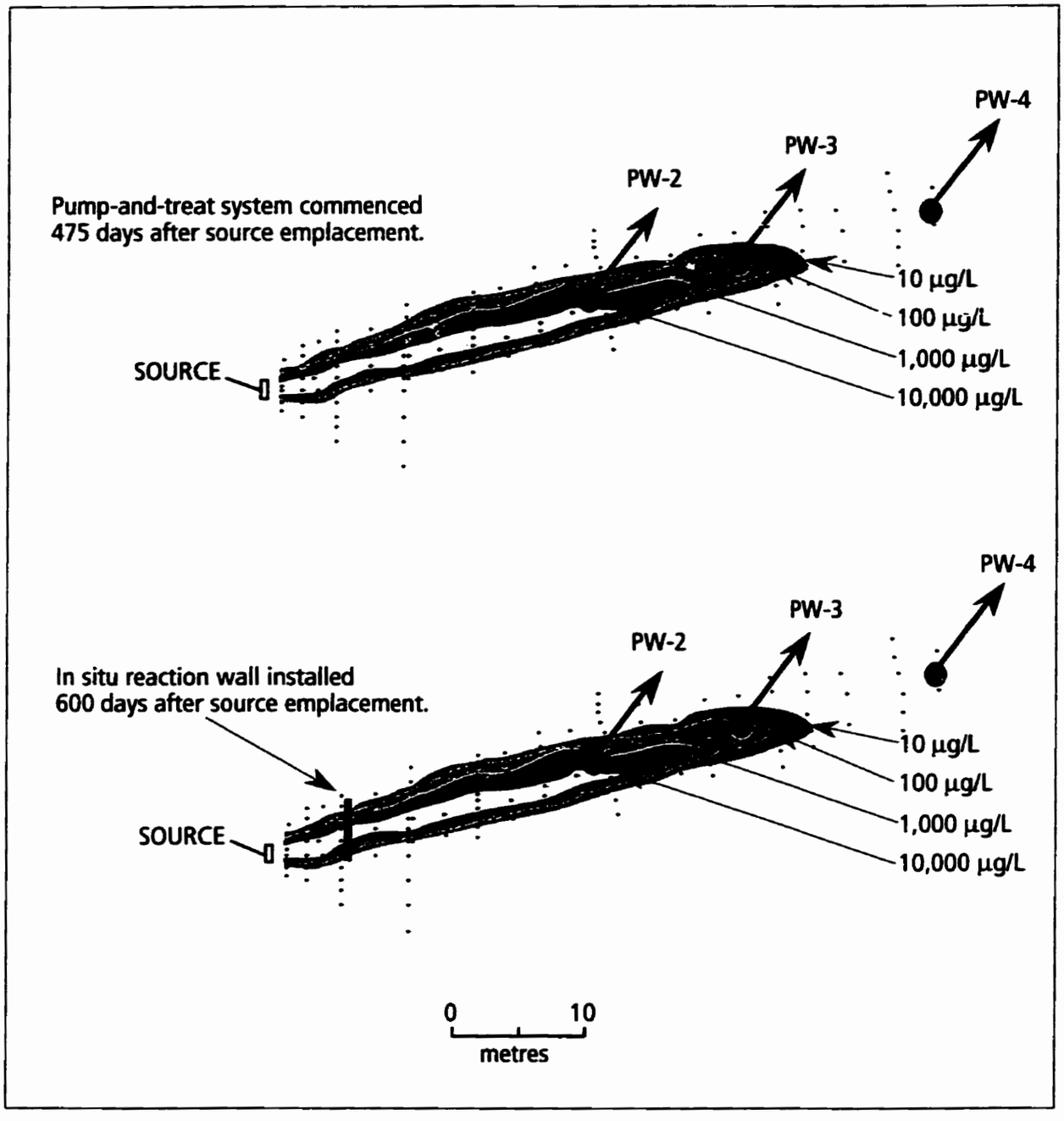

Figure 6-13. Layout of groundwater pump-and-treat system and *in situ* treatment wall installed to control the aqueous-phase plumes emitted from the source zone.

Systems are shown relative to the location of the TCE (trichloroethylene) plume at 322 days.

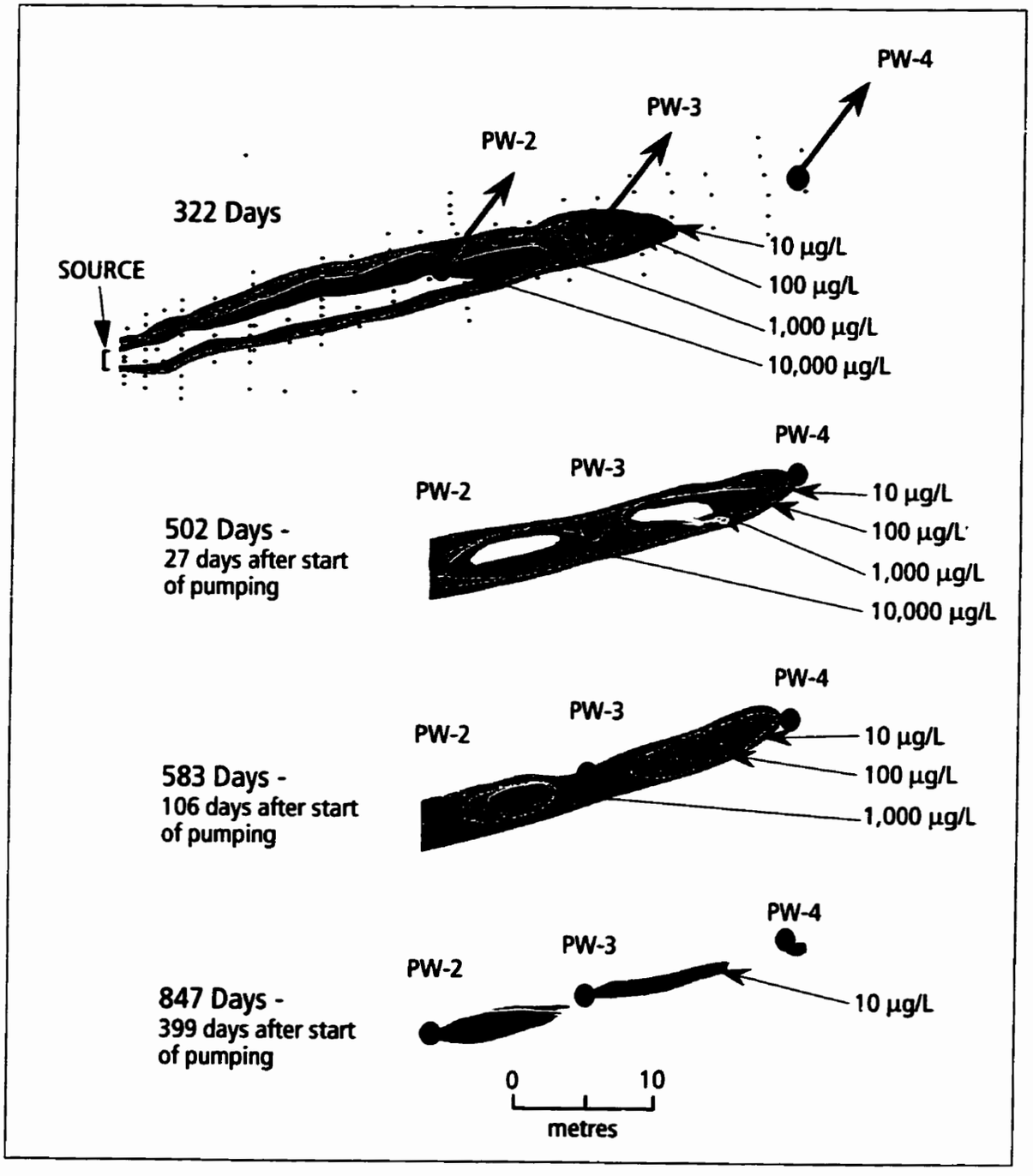

Figure 6-14 Shrinkage of TCE (trichloroethylene) plume downgradient of PW-2 in response to operation of pump-and-treat system.

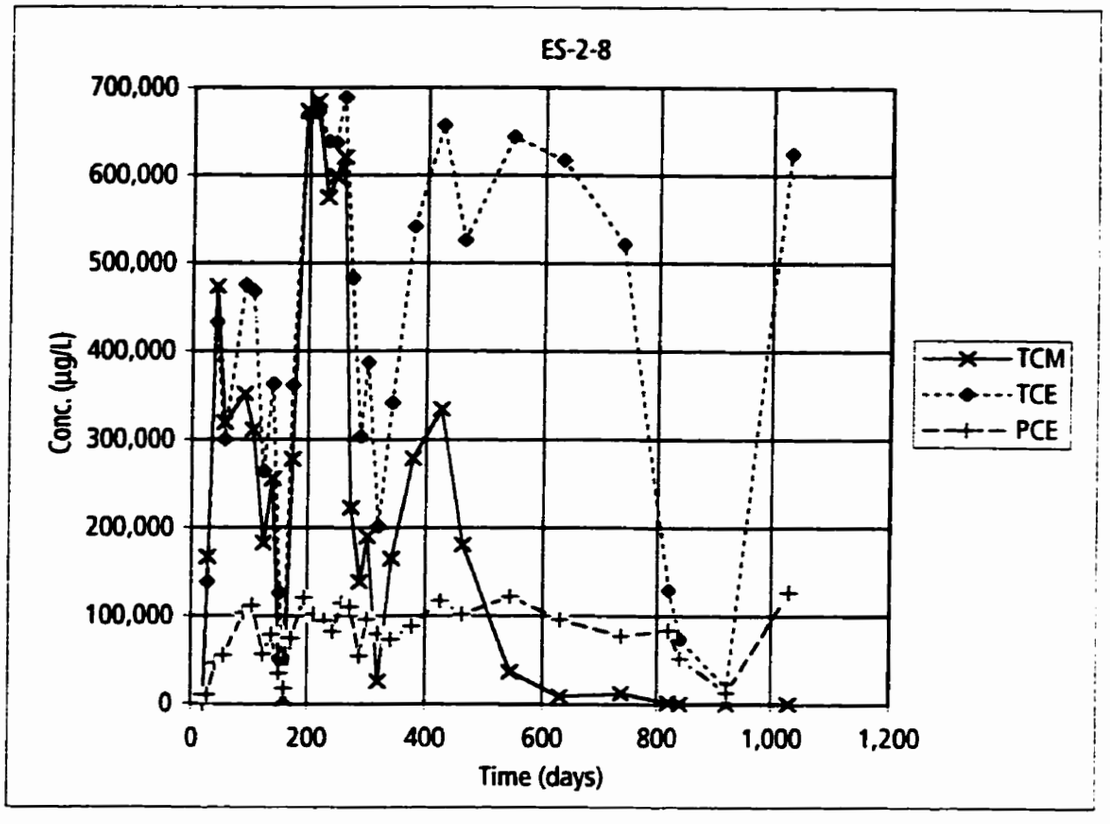

Key:
TCM - Chloroform
TCE - Trichloroethylene
PCE - Tetrachloroethylene

Figure 6-15. Temporal variation in aqueous concentrations at monitoring point ES-2-8.

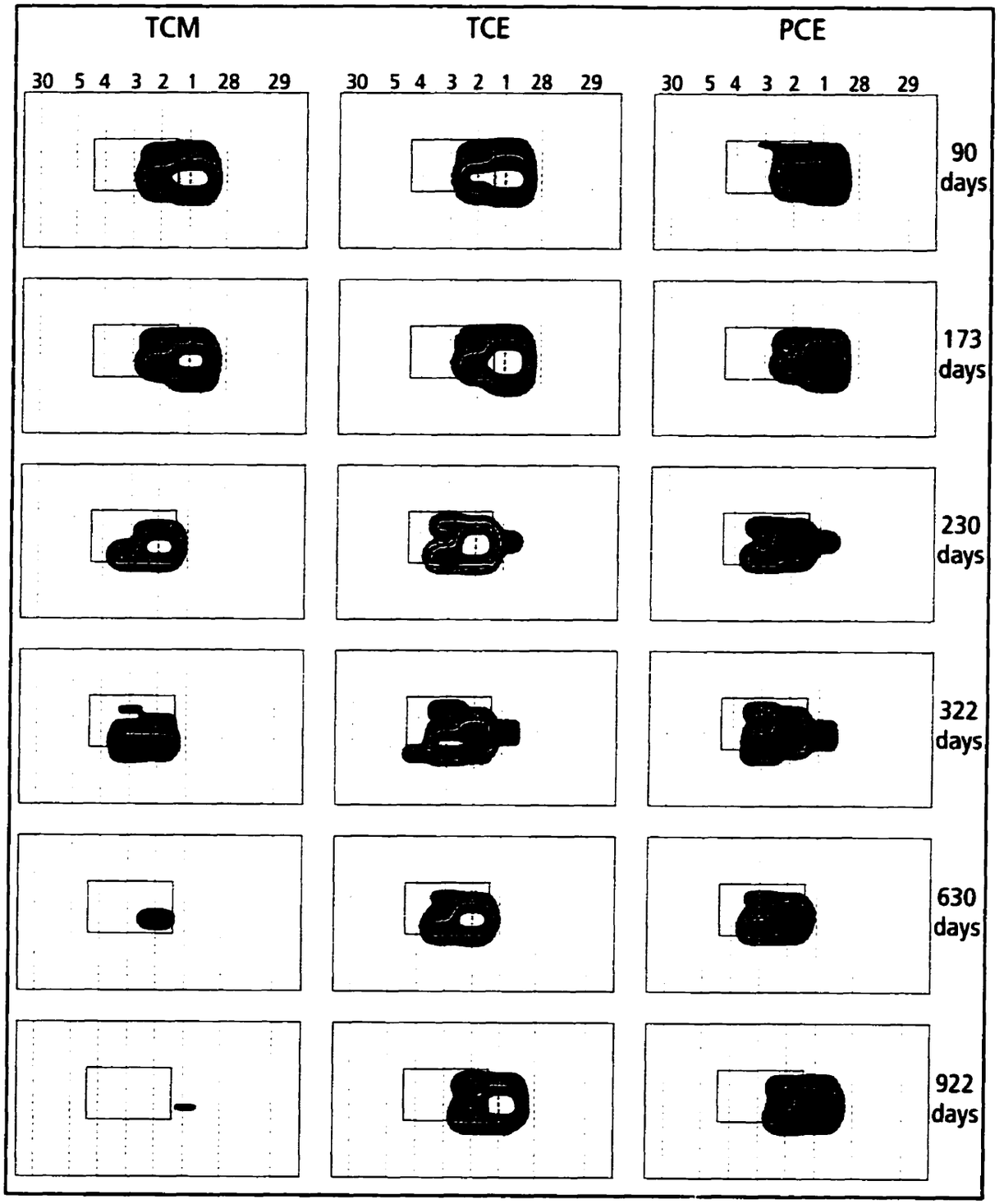

Figure 6-16. Aqueous-phase plumes along the 1 m Fence.

Rectangle indicates position of source zone: 1.5 m long and 1.0 m wide. Concentration contours are 1,000 µg/L, 10,000 µg/L, 100,000 µg/L and 300,000 µg/L for chloroform (TCM) and trichloroethylene (TCE); 1,000 µg/L, 10,000 µg/L and 30,000 µg/L for tetrachloroethylene (PCE).

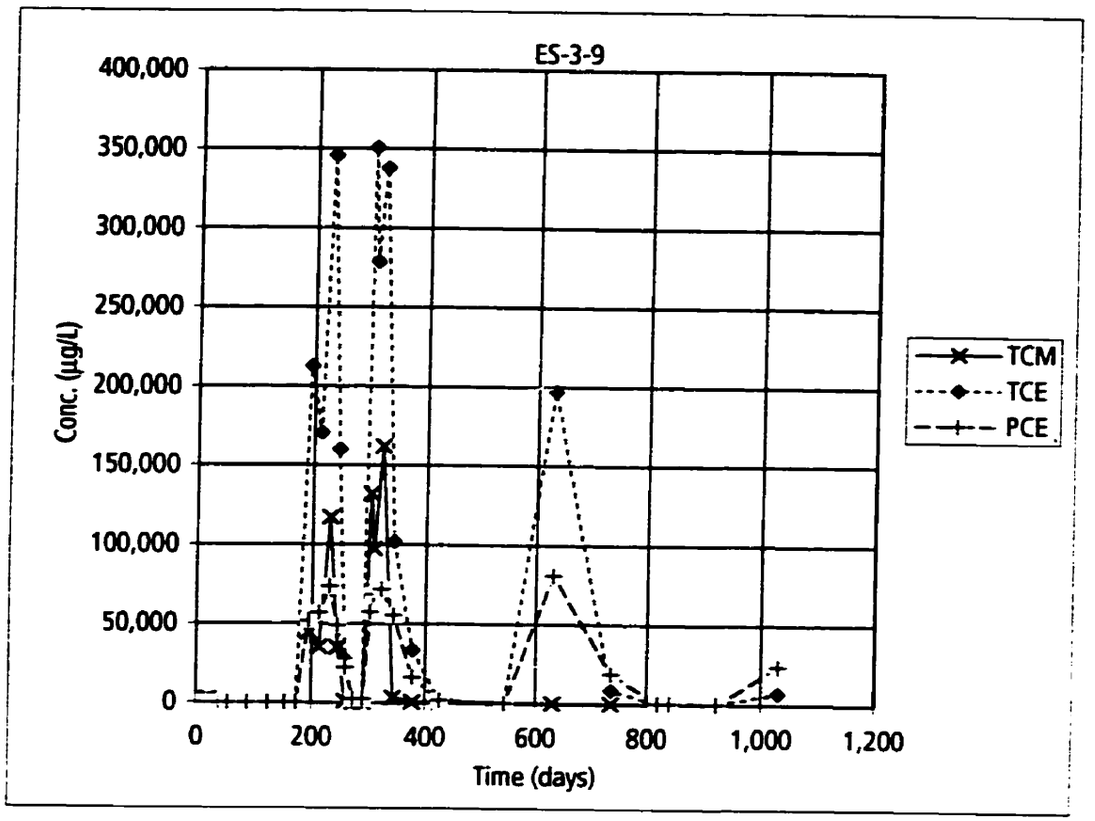

Key:
TCM - Chloroform
TCE - Trichloroethylene
PCE - Tetrachloroethylene

Figure 6-17. Temporal variation in aqueous concentrations at monitoring point ES-3-9.

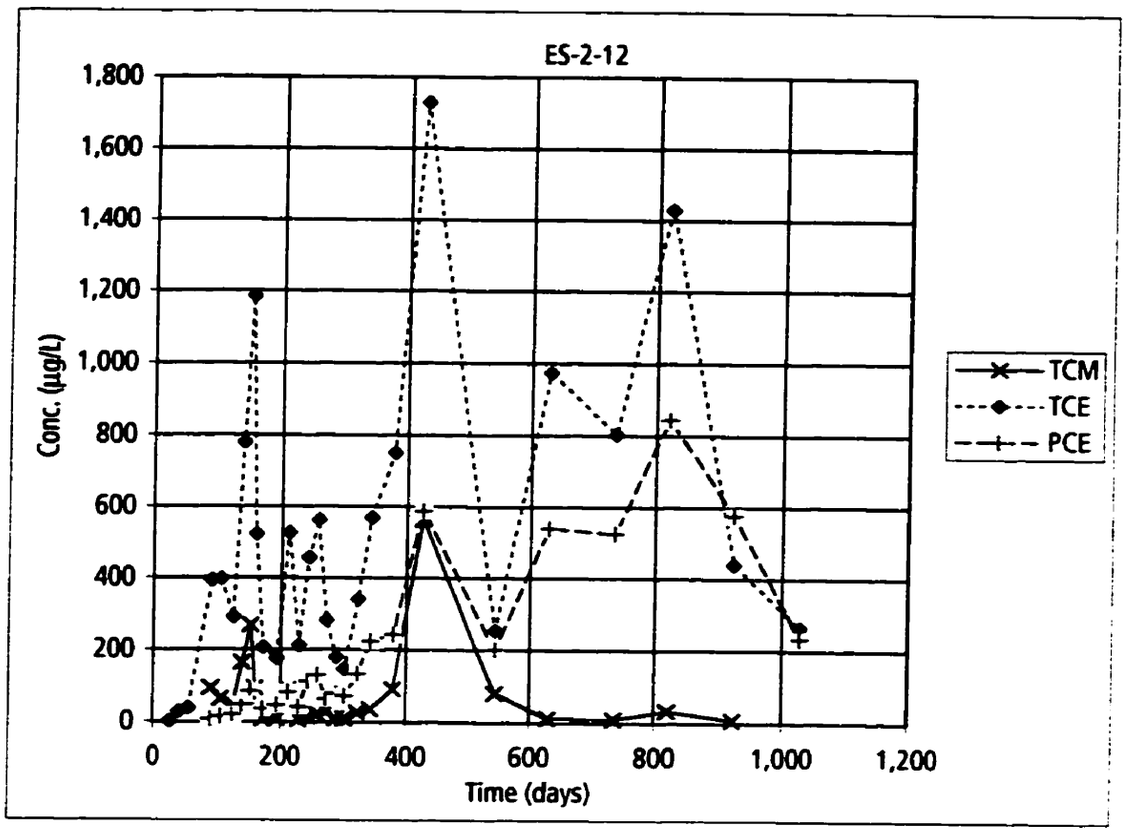

Key:
TCM - Chloroform
TCE - Trichloroethylene
PCE - Tetrachloroethylene

Figure 6-18. Temporal variation in aqueous concentrations at monitoring point ES-2-12.

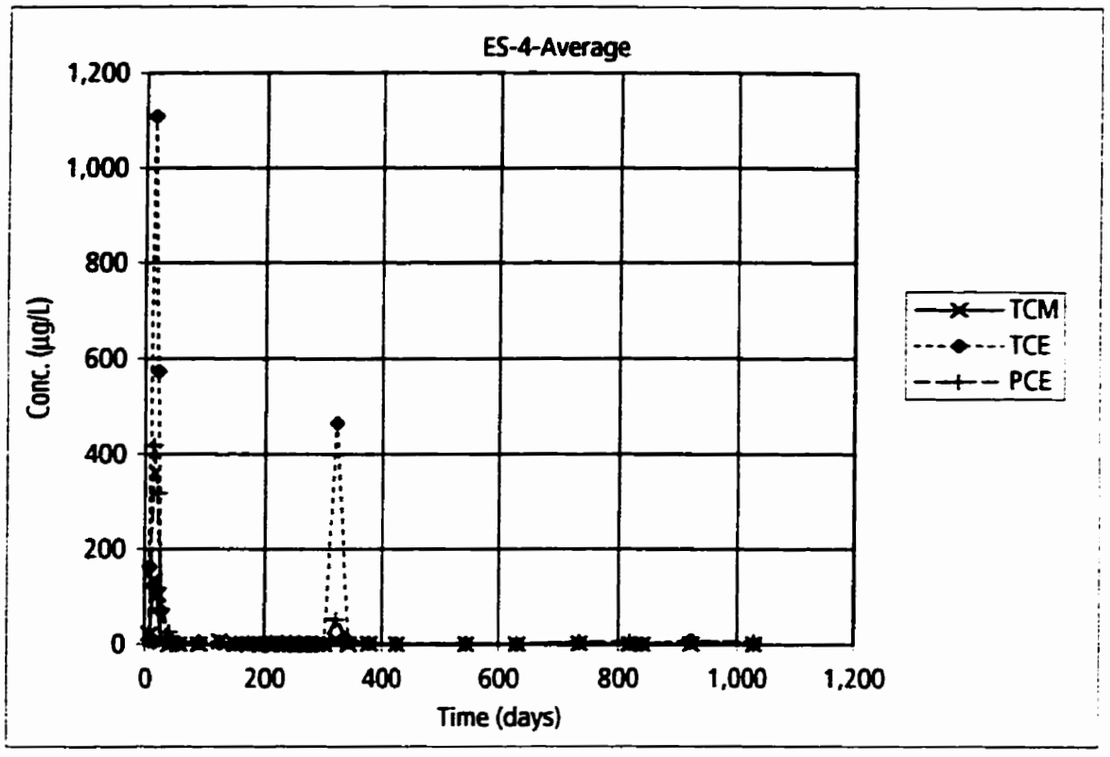

Key:
TCM - Chloroform
TCE - Trichloroethylene
PCE - Tetrachloroethylene

Figure 6-19. Temporal variation in aqueous concentrations averaged for monitoring location ES-4.

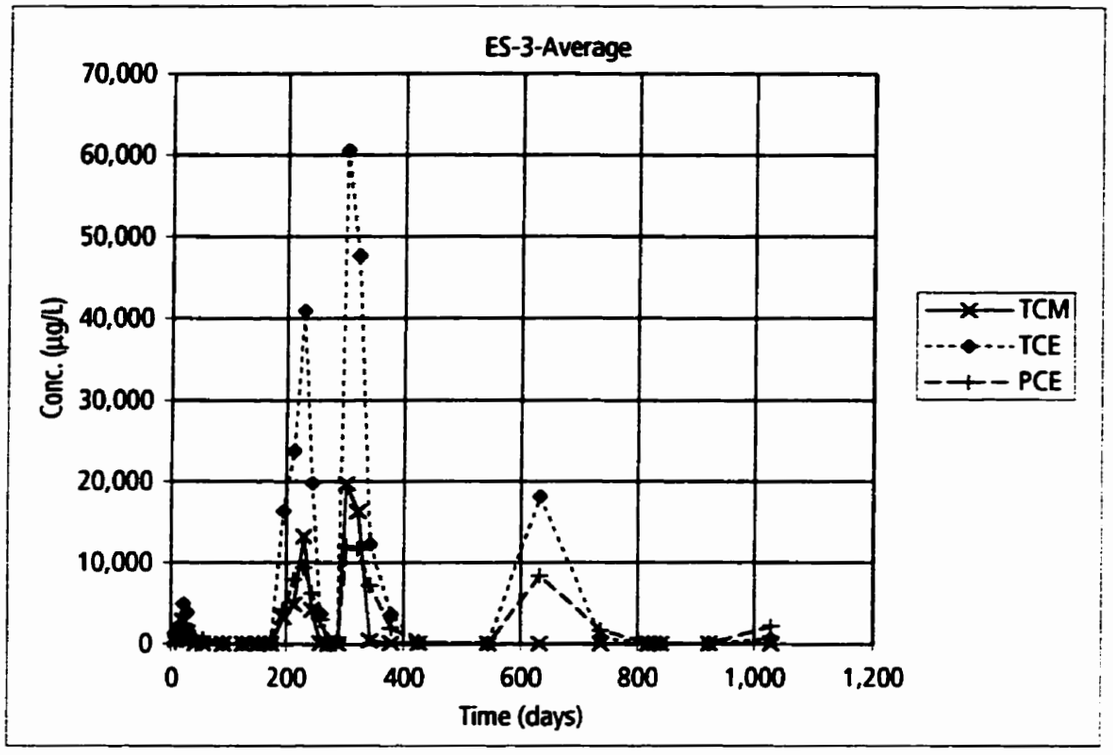

Key:
TCM - Chloroform
TCE - Trichloroethylene
PCE - Tetrachloroethylene

Figure 6-20. Temporal variation in aqueous concentrations averaged for monitoring location ES-3.

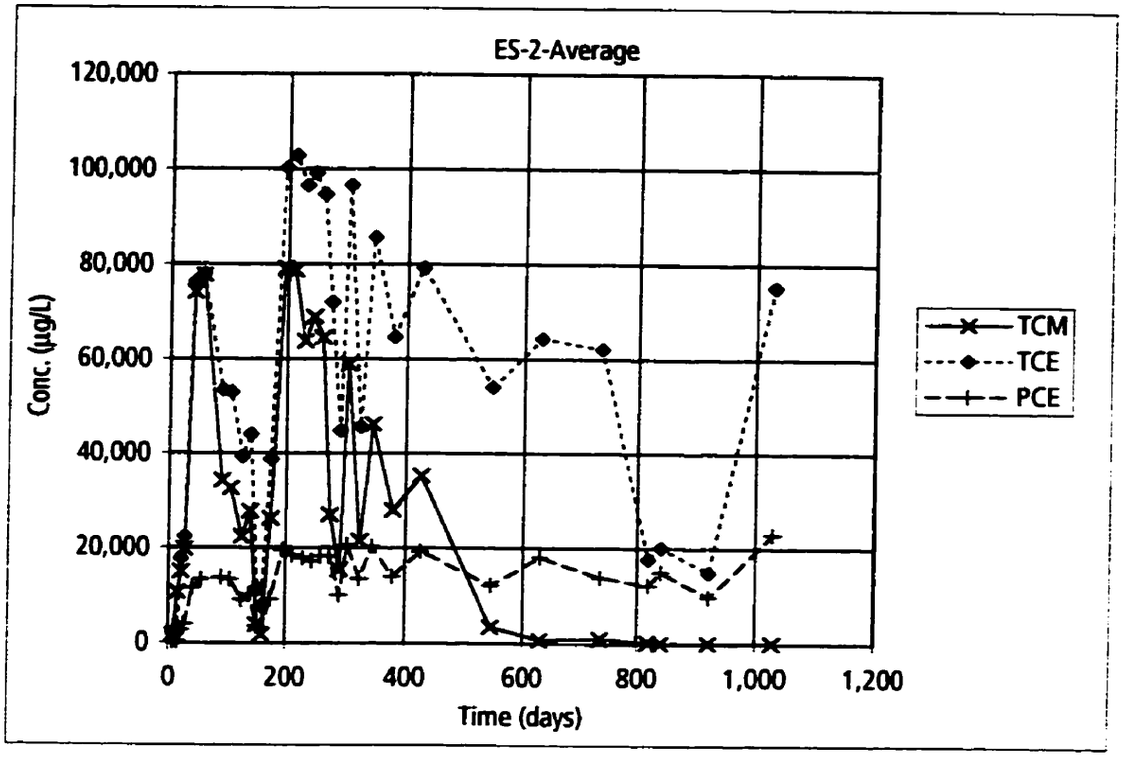

Key:
TCM - Chloroform
TCE - Trichloroethylene
PCE - Tetrachloroethylene

Figure 6-21. Temporal variation in aqueous concentrations averaged for monitoring location ES-2.

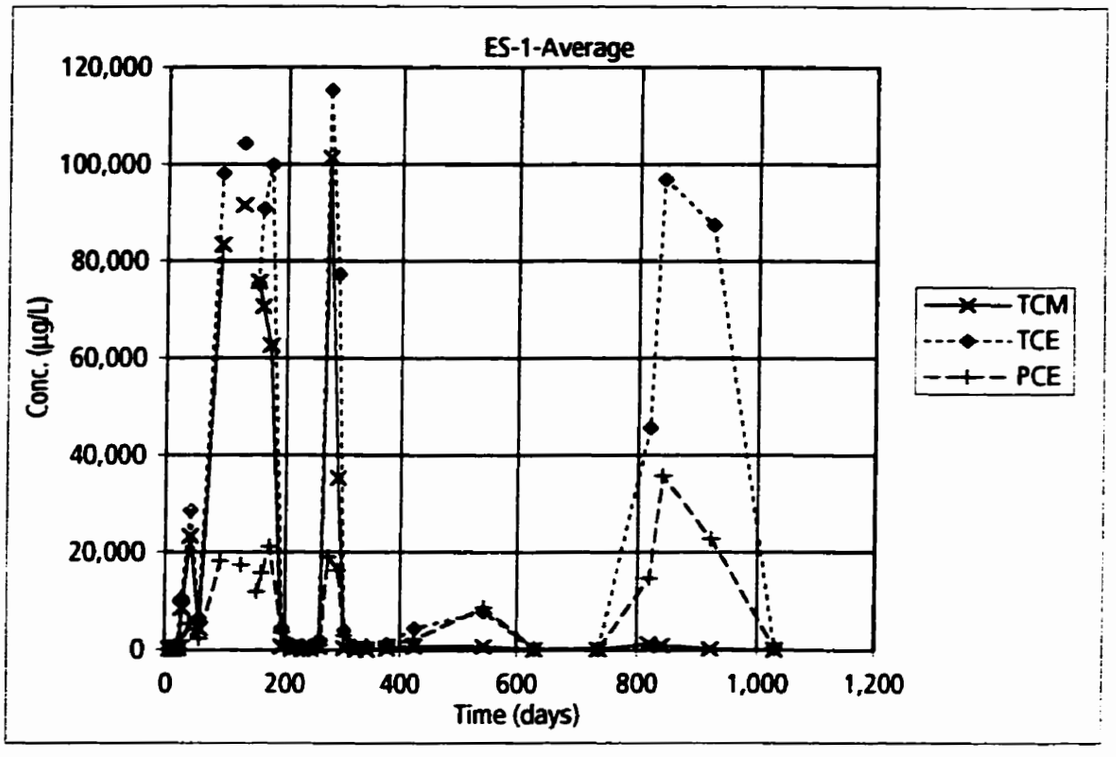

Key:
TCM - Chloroform
TCE - Trichloroethylene
PCE - Tetrachloroethylene

Figure 6-22. Temporal variation in aqueous concentrations averaged for monitoring location ES-1.

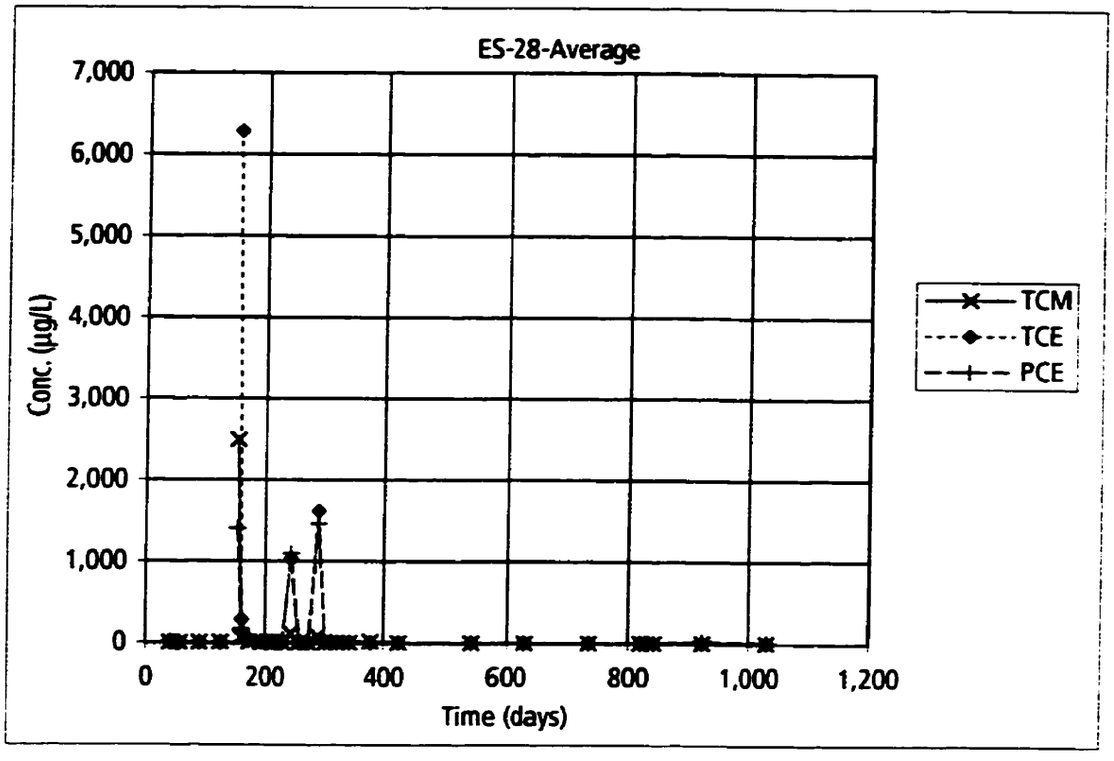

Key:
TCM - Chloroform
TCE - Trichloroethylene
PCE - Tetrachloroethylene

Figure 6-23. Temporal variation in aqueous concentrations averaged for monitoring location ES-28.

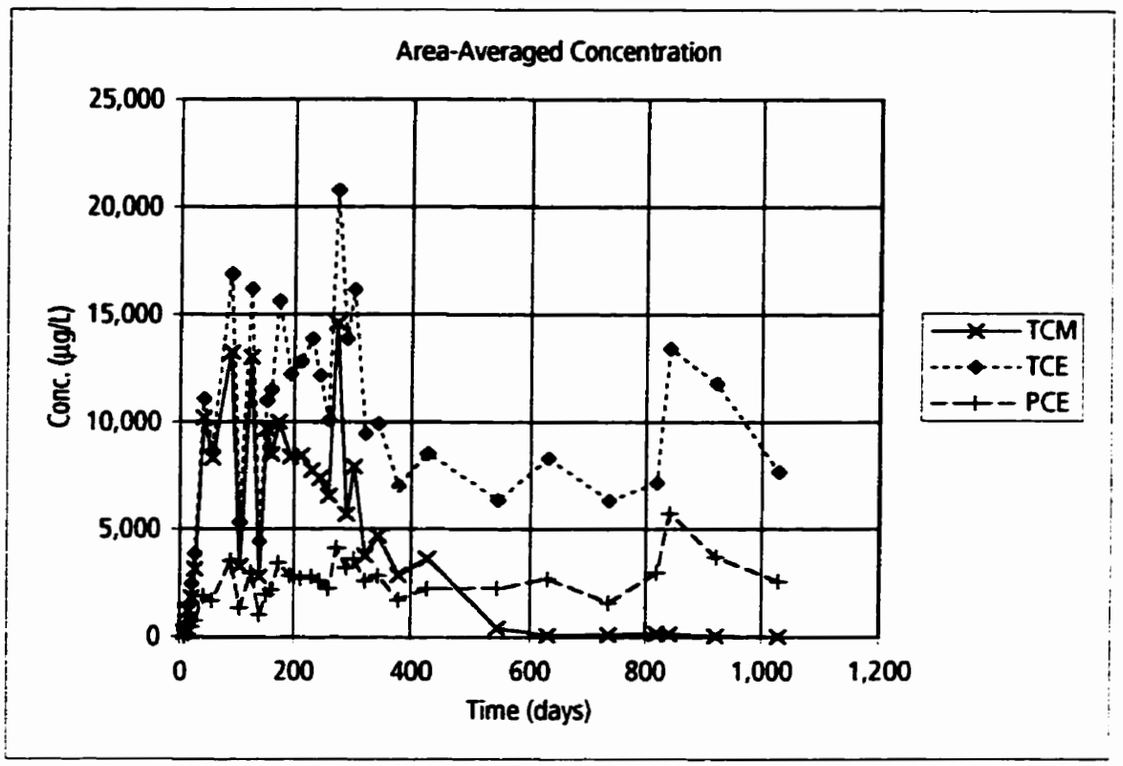

Key:
TCM - Chloroform
TCE - Trichloroethylene
PCE - Tetrachloroethylene

Figure 6-24. Temporal variation in aqueous concentrations averaged for all monitoring locations along the 1 m Fence.

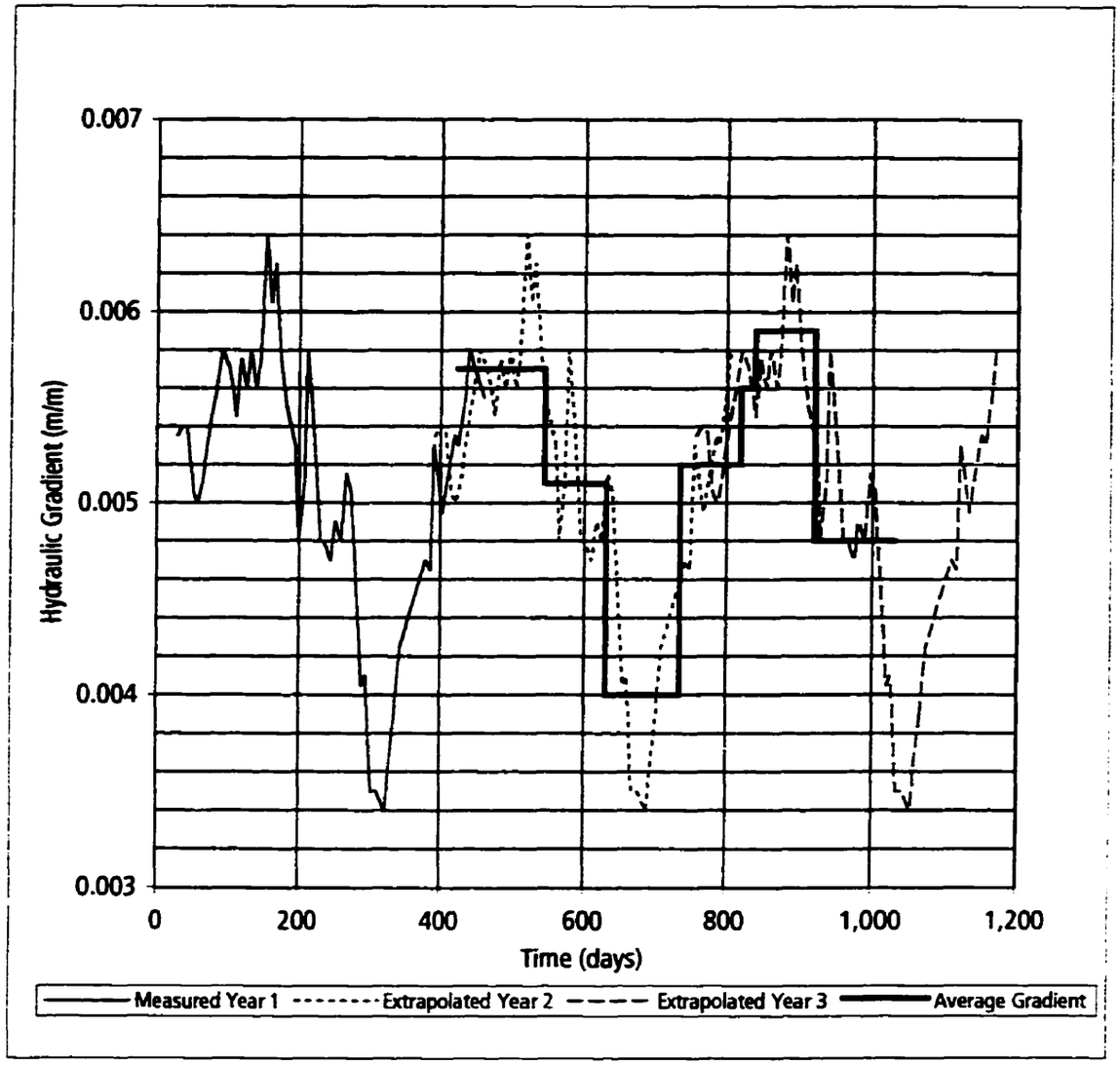

Figure 6-25. Hydraulic gradient values used for calculation of chemical mass flux crossing the 1 m Fence.

Gradient of Year 1 based on measured values. Gradient for Years 2 and 3 based on average of extrapolated values.

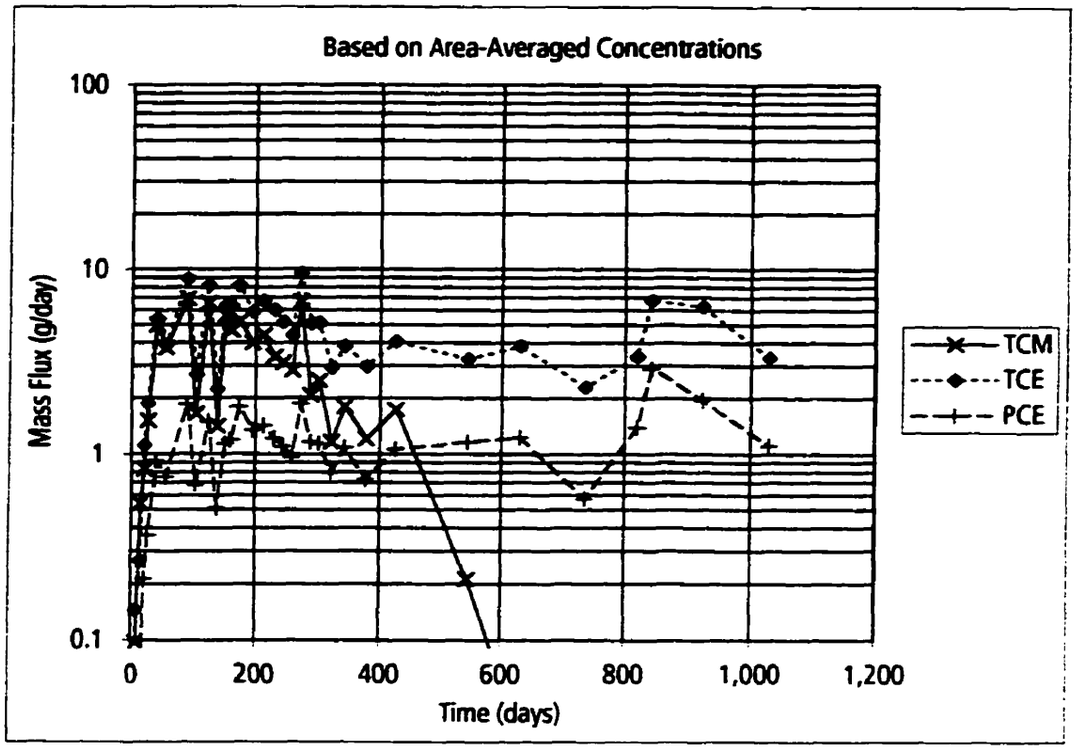

Key:
TCM - Chloroform
TCE - Trichloroethylene
PCE - Tetrachloroethylene

Figure 6-26. Temporal variation in chemical mass flux crossing the 1 m Fence.

Mass flux calculated from area-averaged aqueous concentrations, average hydraulic conductivity, and time-varying hydraulic gradient.

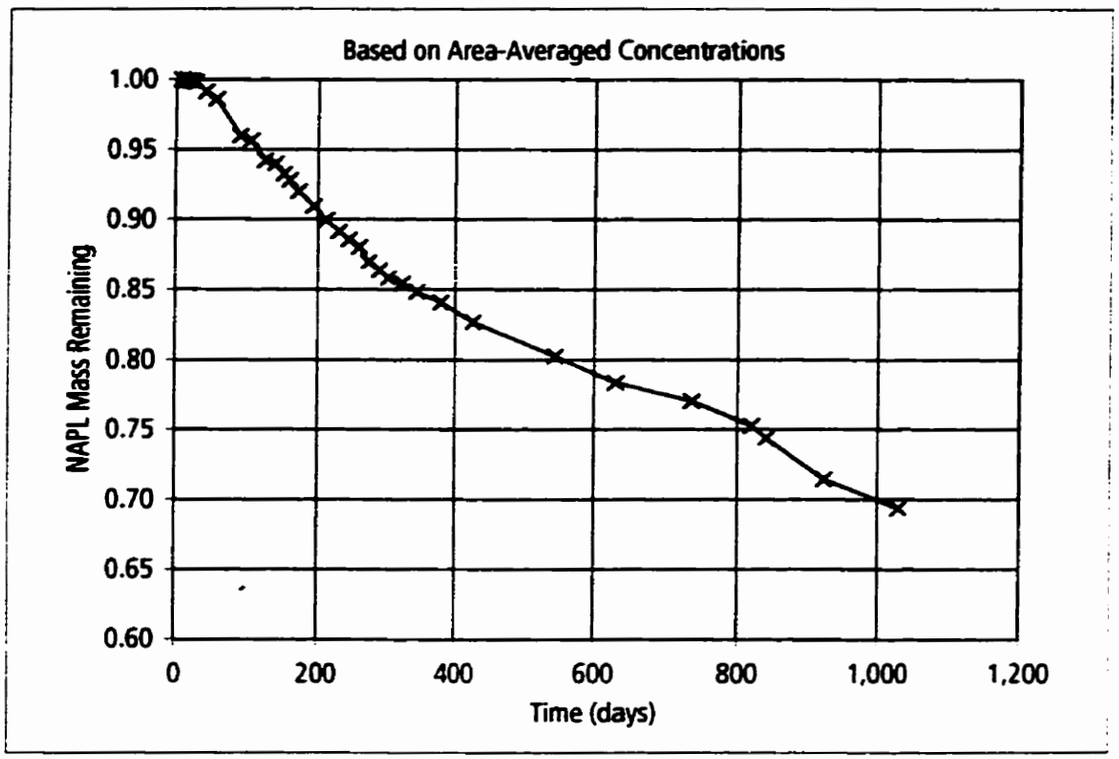

Figure 6-27. Change in NAPL mass remaining versus time based on calculated cumulative mass crossing the 1 m Fence.

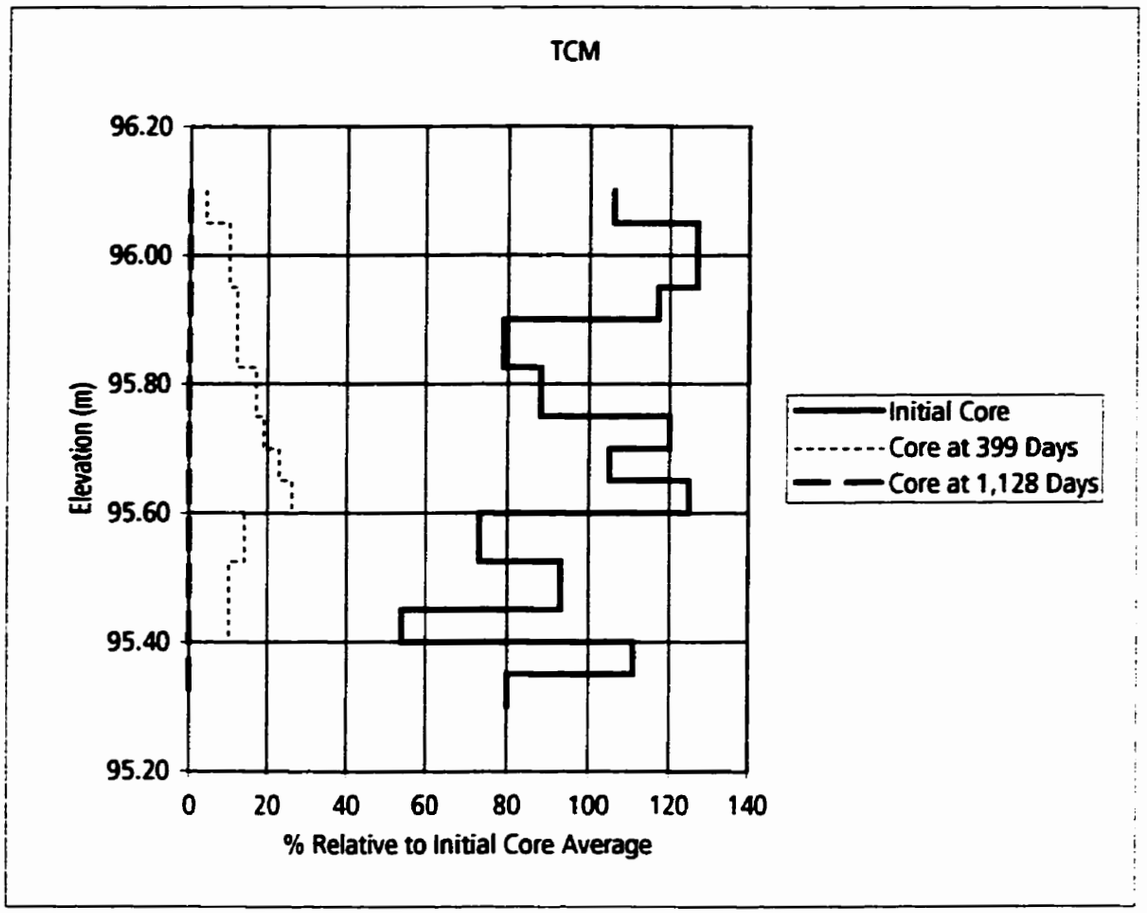

Figure 6-28. Change in chloroform (TCM) concentrations in source zone based on analysis of core samples.

Average 399 days - 14% of initial core concentration.
Average 1,128 days - 0% of initial core concentration.

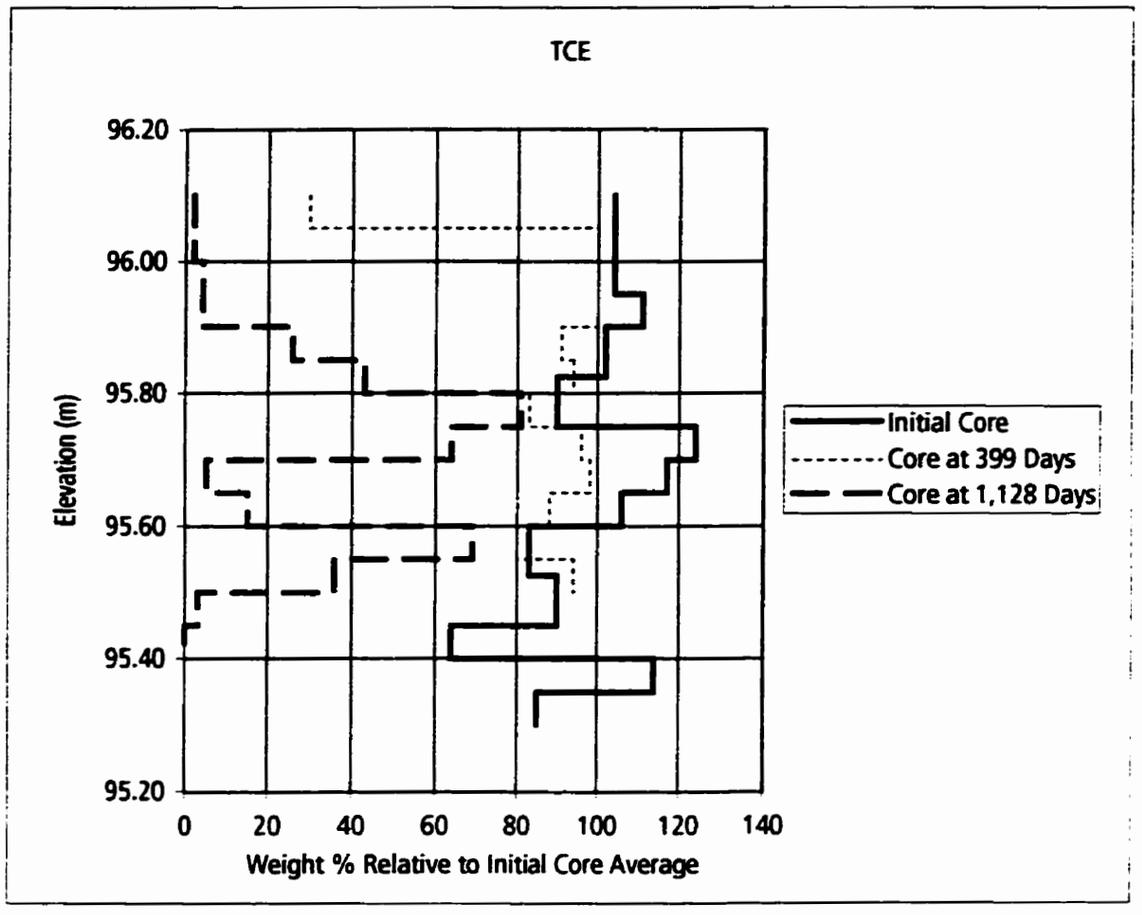

Figure 6-29. Change in trichloroethylene (TCE) concentrations in source zone based on analysis of core samples

Average 399 days - 88% of initial core concentration.
Average 1,128 days - 28% of initial core concentration.

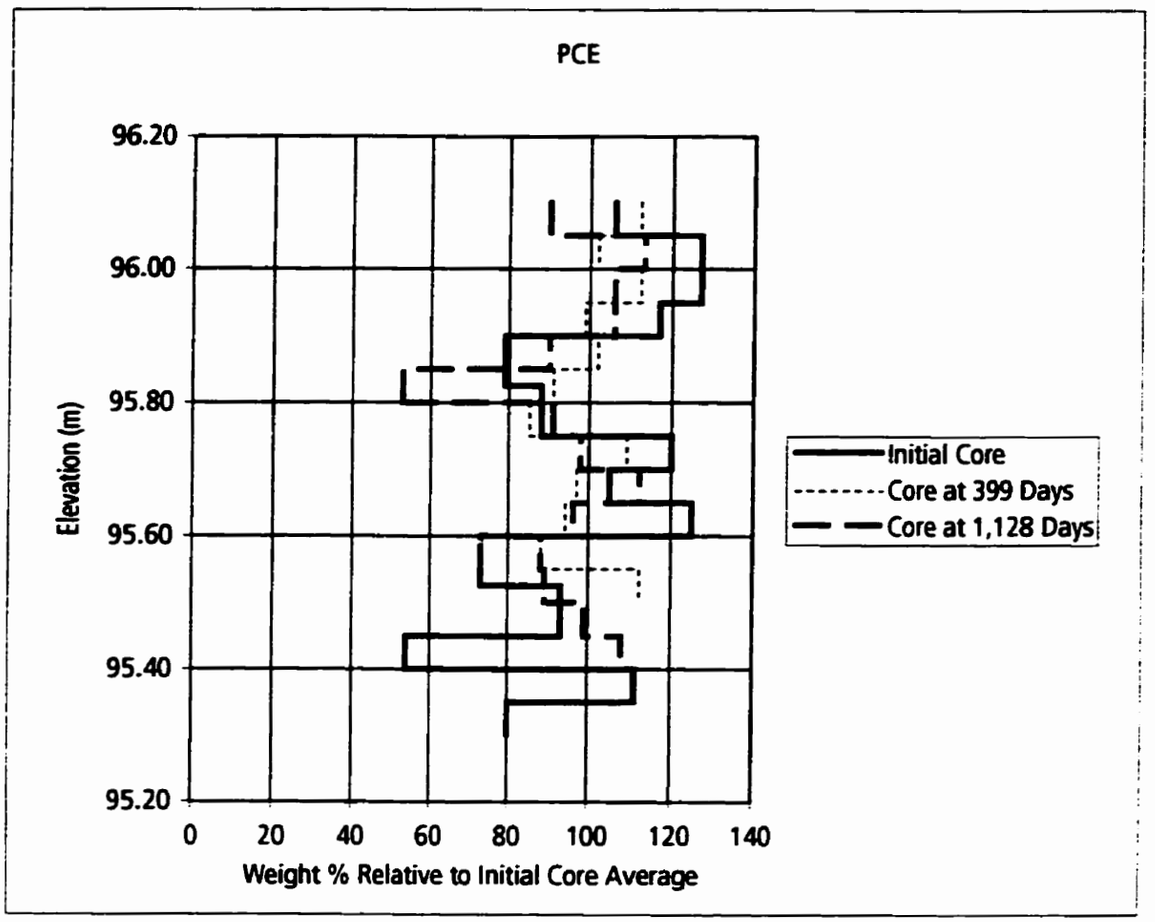

Figure 6-30. Change in tetrachloroethylene (PCE) concentrations in source zone based on analysis of core samples

Average 399 days - 100% of initial core concentration.
Average 1,128 days - 96% of initial core concentration.

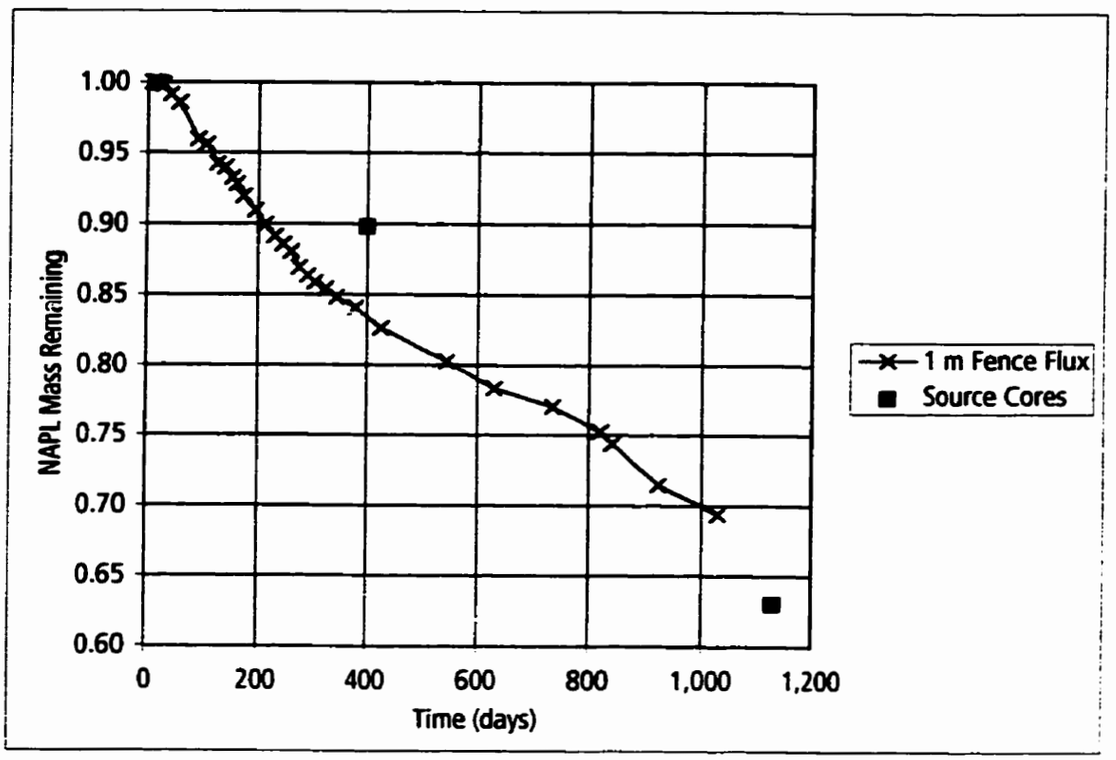

Figure 6-31. Change in NAPL mass remaining versus time based on calculated chemical mass crossing the 1 m Fence, compared to source cores.

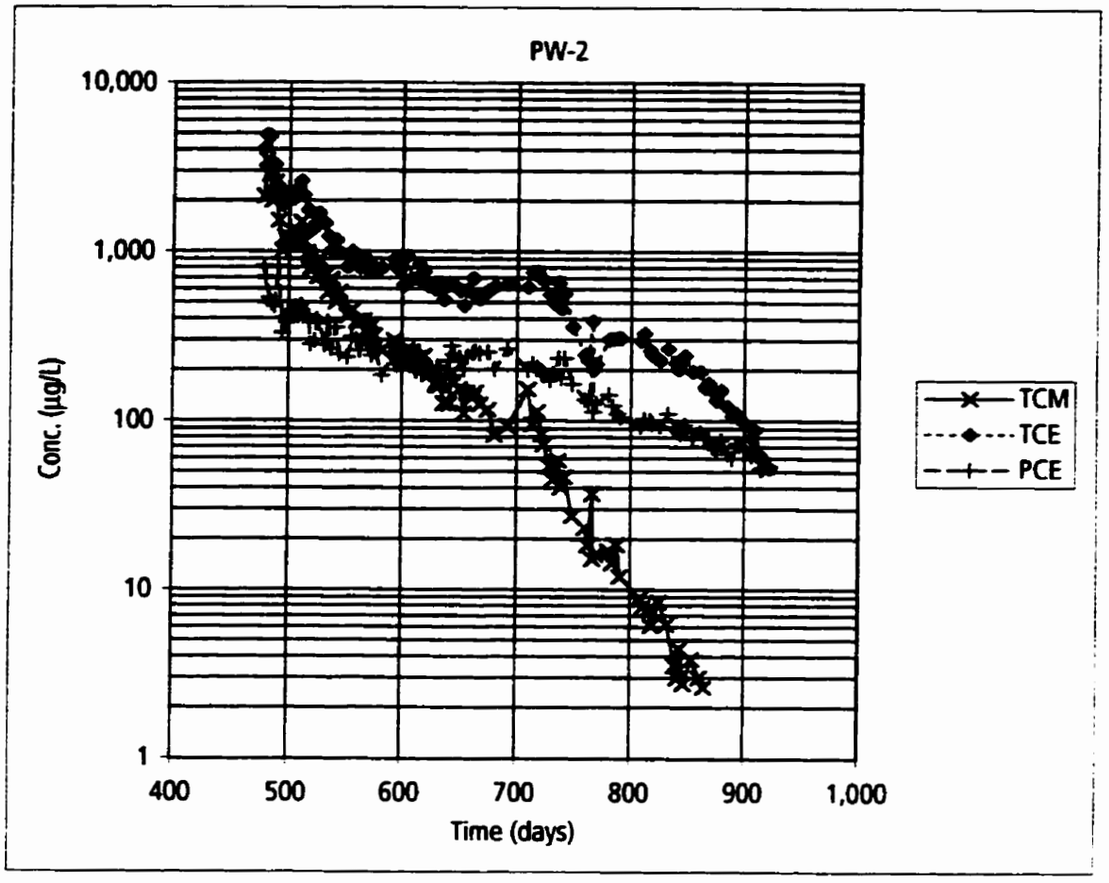

Key:
TCM - Chloroform
TCE - Trichloroethylene
PCE - Tetrachloroethylene

Figure 6-32. Aqueous-phase concentrations in PW-2 during operation of the pump-and treat system.

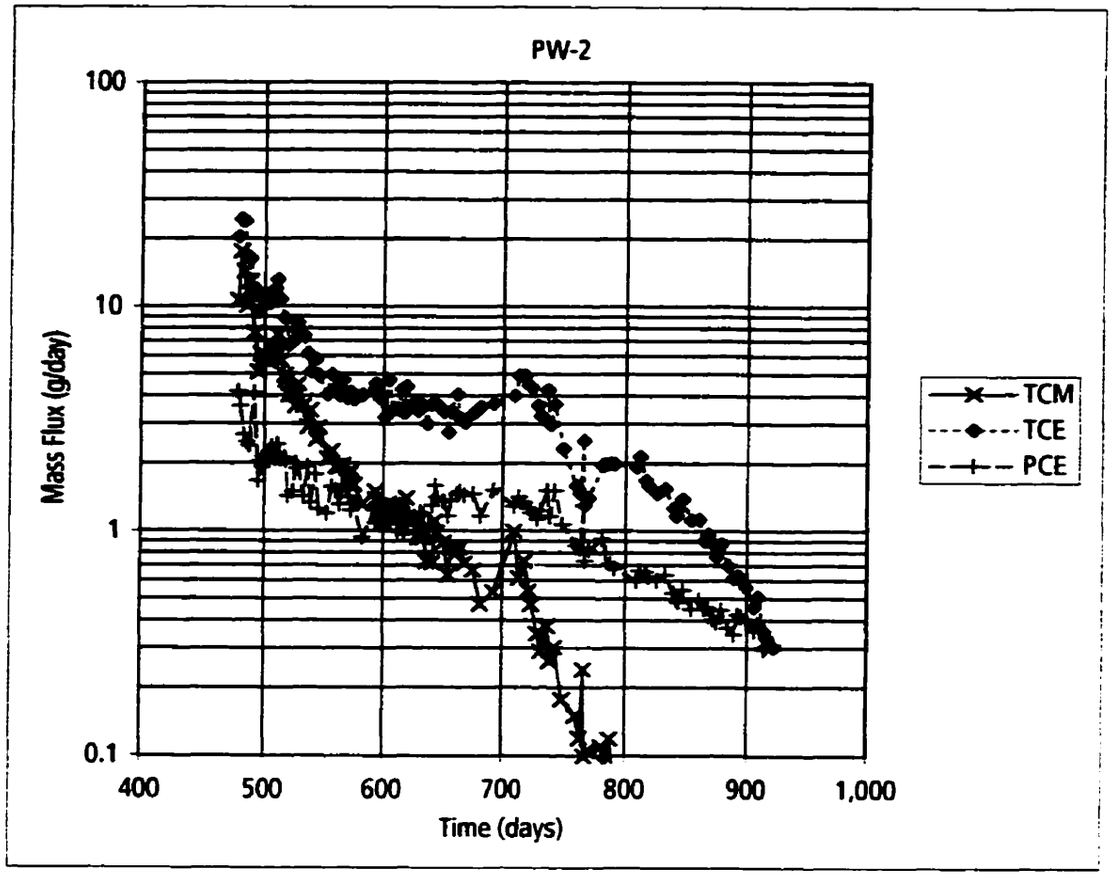

Key:
TCM - Chloroform
TCE - Trichloroethylene
PCE - Tetrachloroethylene

Figure 6-33. Calculated chemical mass flux from PW-2 during operation of the pump-and treat system.

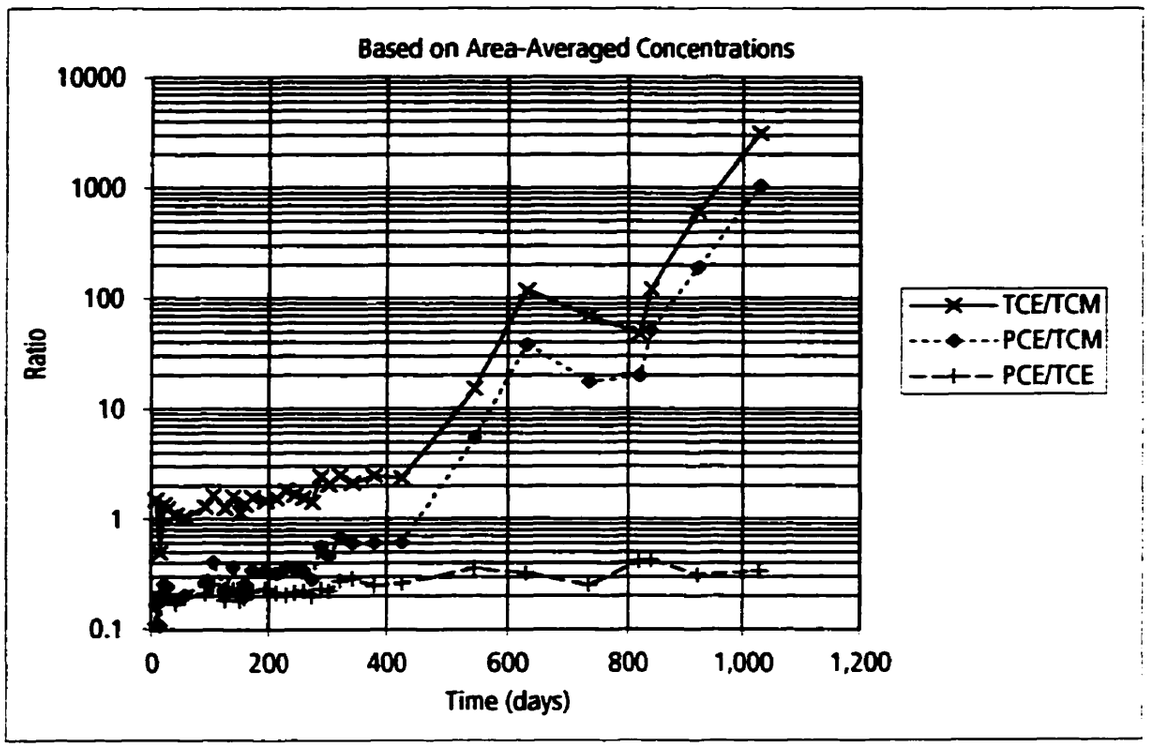

Key:
TCM - Chloroform
TCE - Trichloroethylene
PCE - Tetrachloroethylene

Figure 6-34. Temporal variation in aqueous concentration ratios for concentrations averaged for the 1 m Fence.

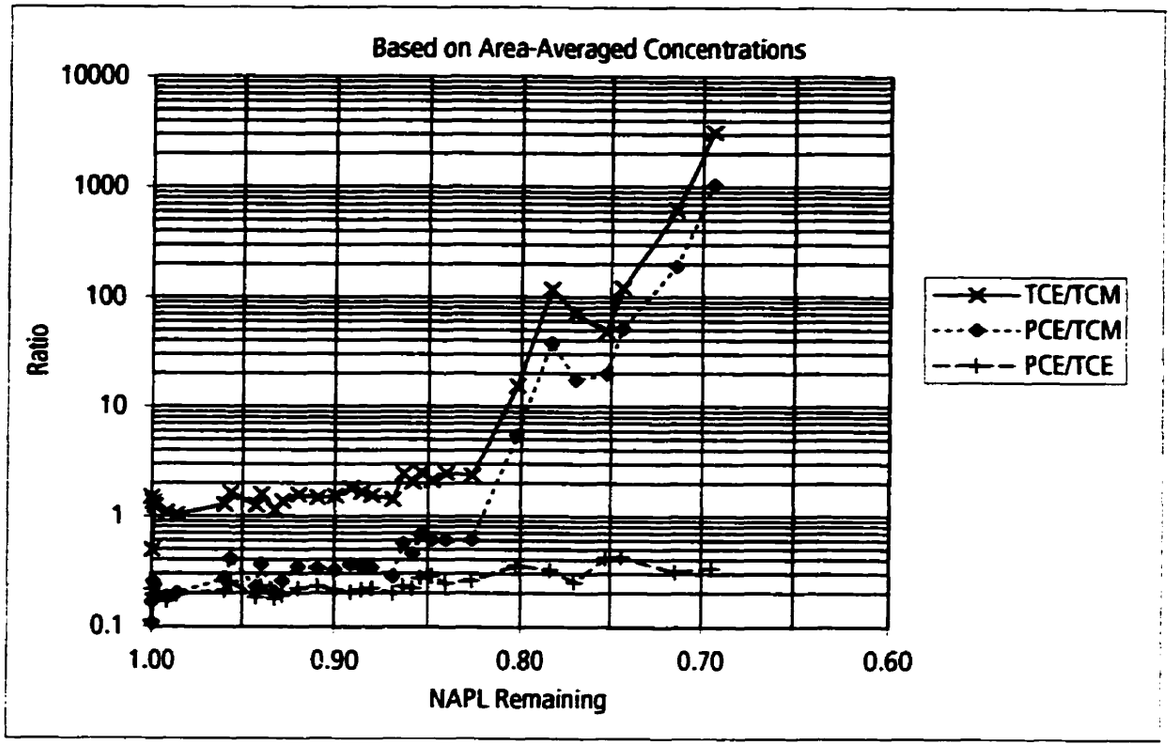

Key:
TCM - Chloroform
TCE - Trichloroethylene
PCE - Tetrachloroethylene

Figure 6-35. Change in aqueous concentration ratios versus NAPL mass remaining for concentrations averaged for the 1 m Fence.

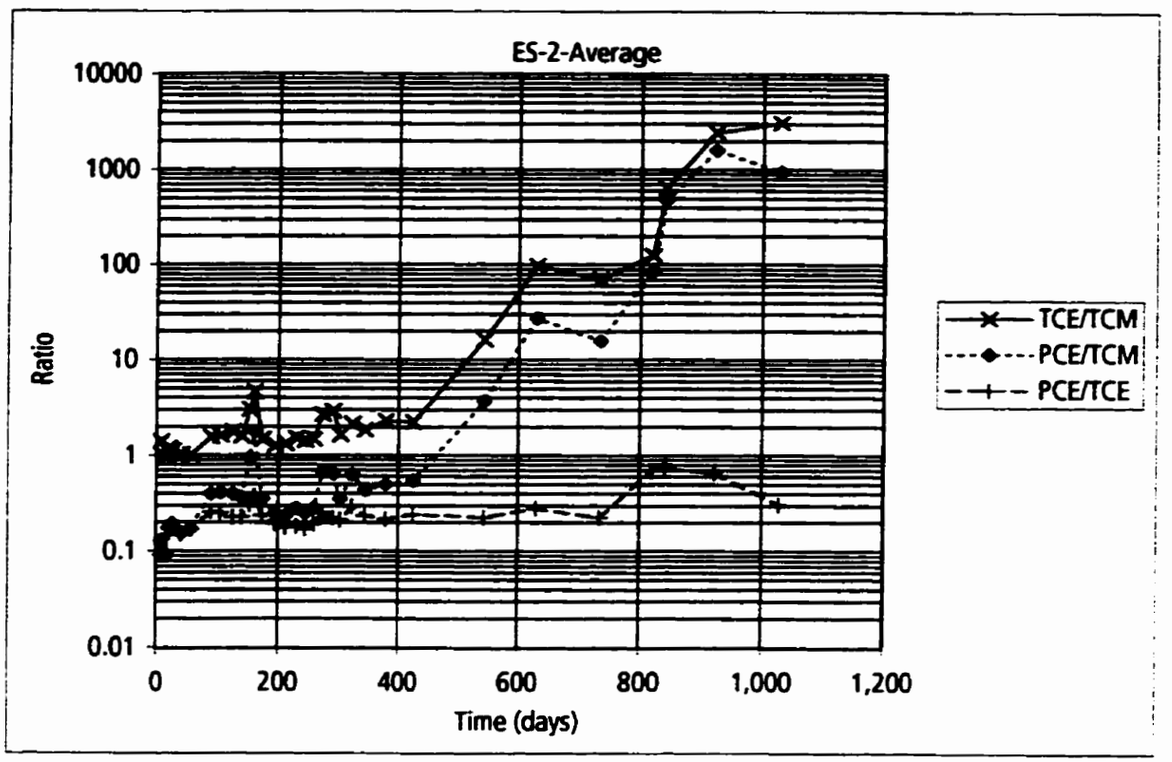

Key:
TCM - Chloroform
TCE - Trichloroethylene
PCE - Tetrachloroethylene

Figure 6-36. Temporal variation in aqueous concentration ratios for concentrations averaged for monitoring location ES-2.

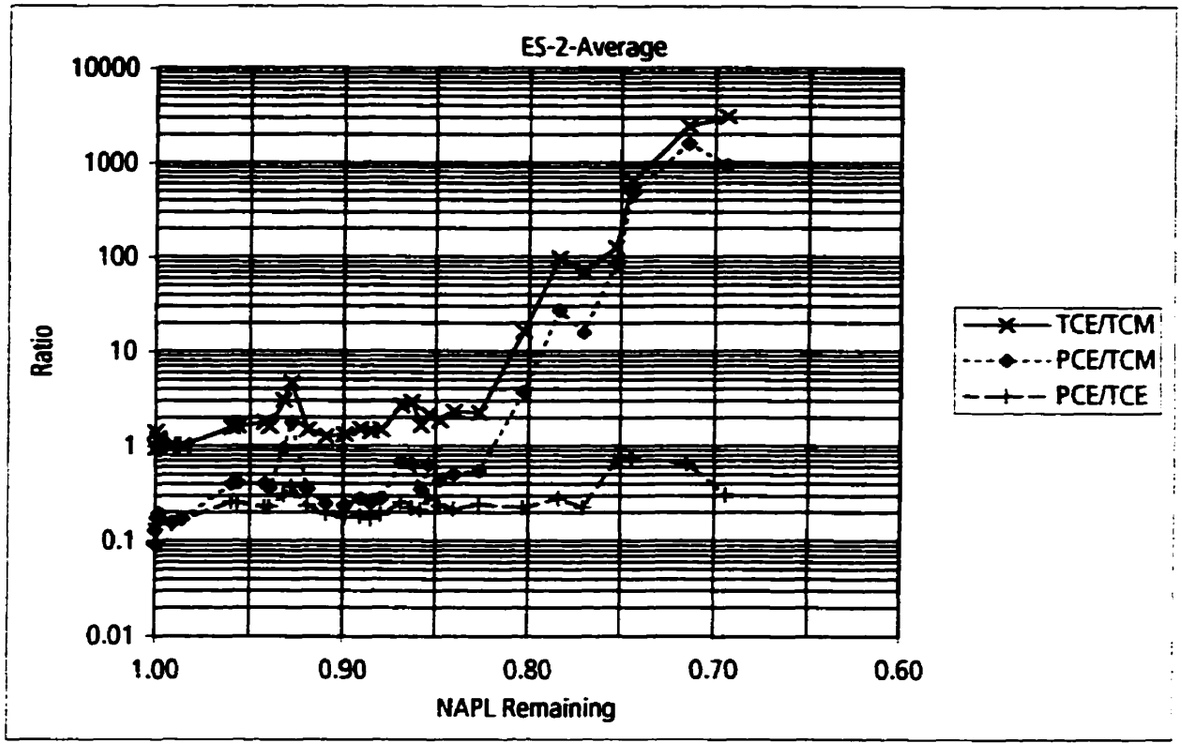

Key:
TCM - Chloroform
TCE - Trichloroethylene
PCE - Tetrachloroethylene

Figure 6-37. Change in aqueous concentration ratios versus NAPL mass remaining for concentrations averaged for monitoring location ES-2.

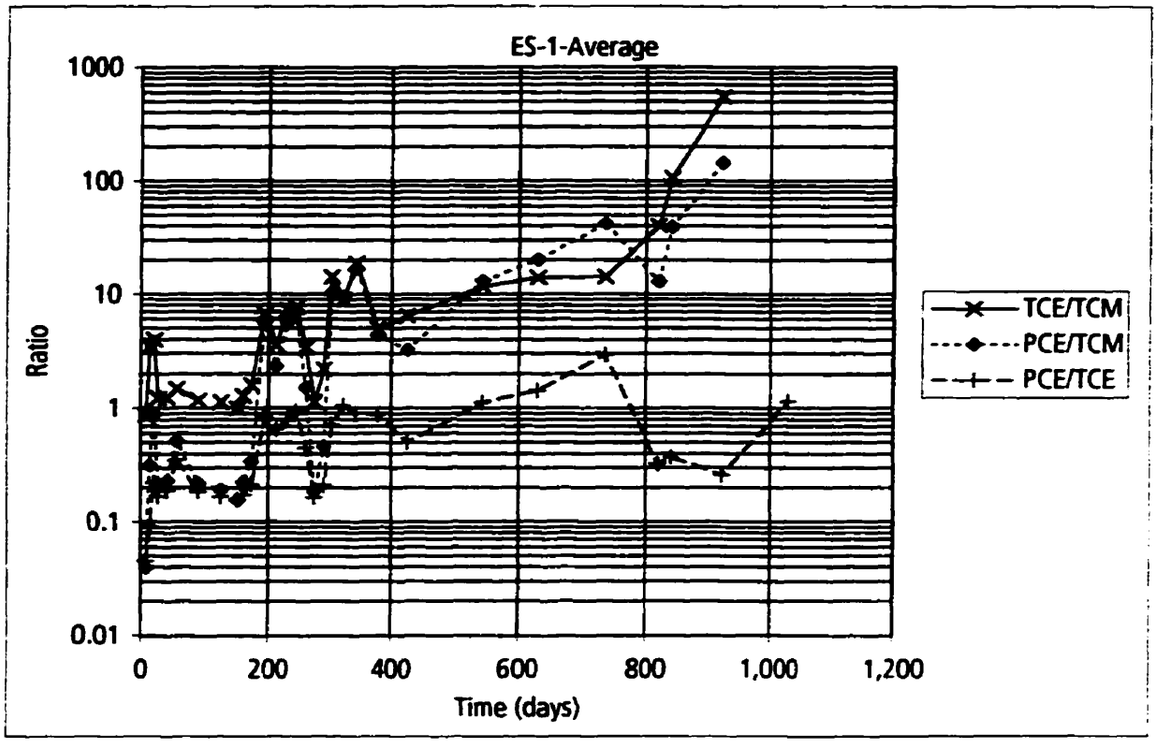

Key:
TCM - Chloroform
TCE - Trichloroethylene
PCE - Tetrachloroethylene

Figure 6-38. Temporal variation in aqueous concentration ratios for concentrations averaged for monitoring location ES-1.

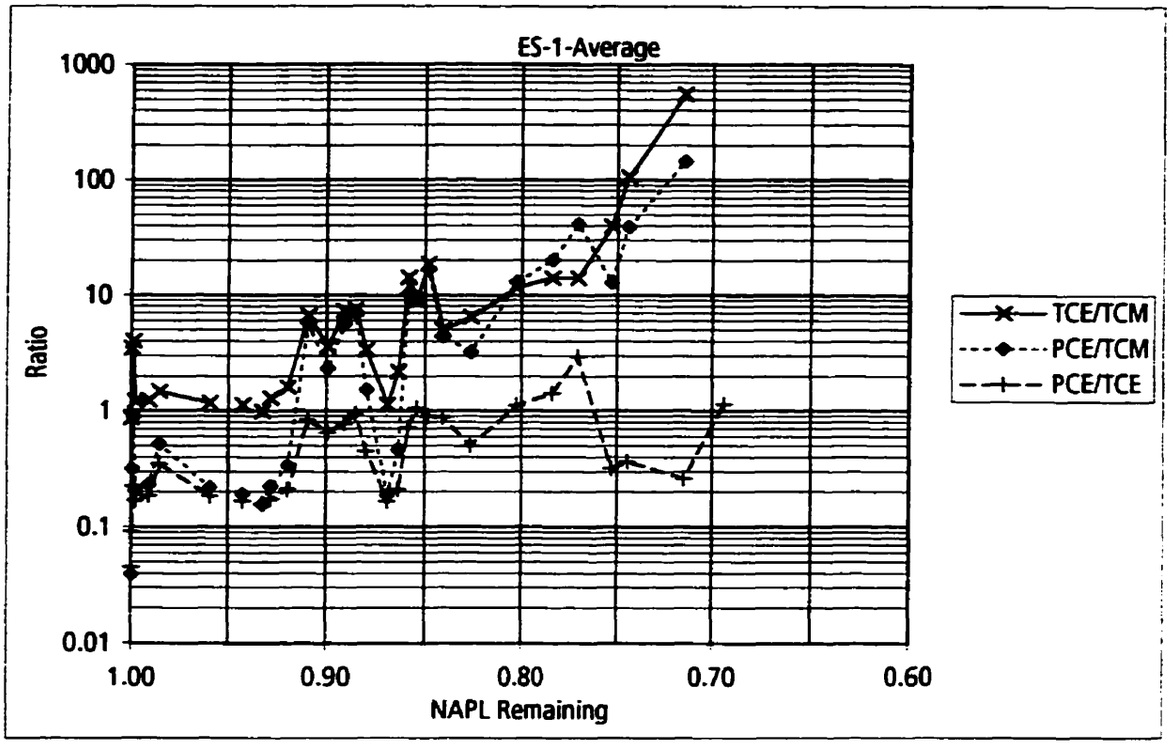

Key:
TCM - Chloroform
TCE - Trichloroethylene
PCE - Tetrachloroethylene

Figure 6-39. Change in aqueous concentration ratios versus NAPL remaining for concentrations averaged for monitoring location ES-1.

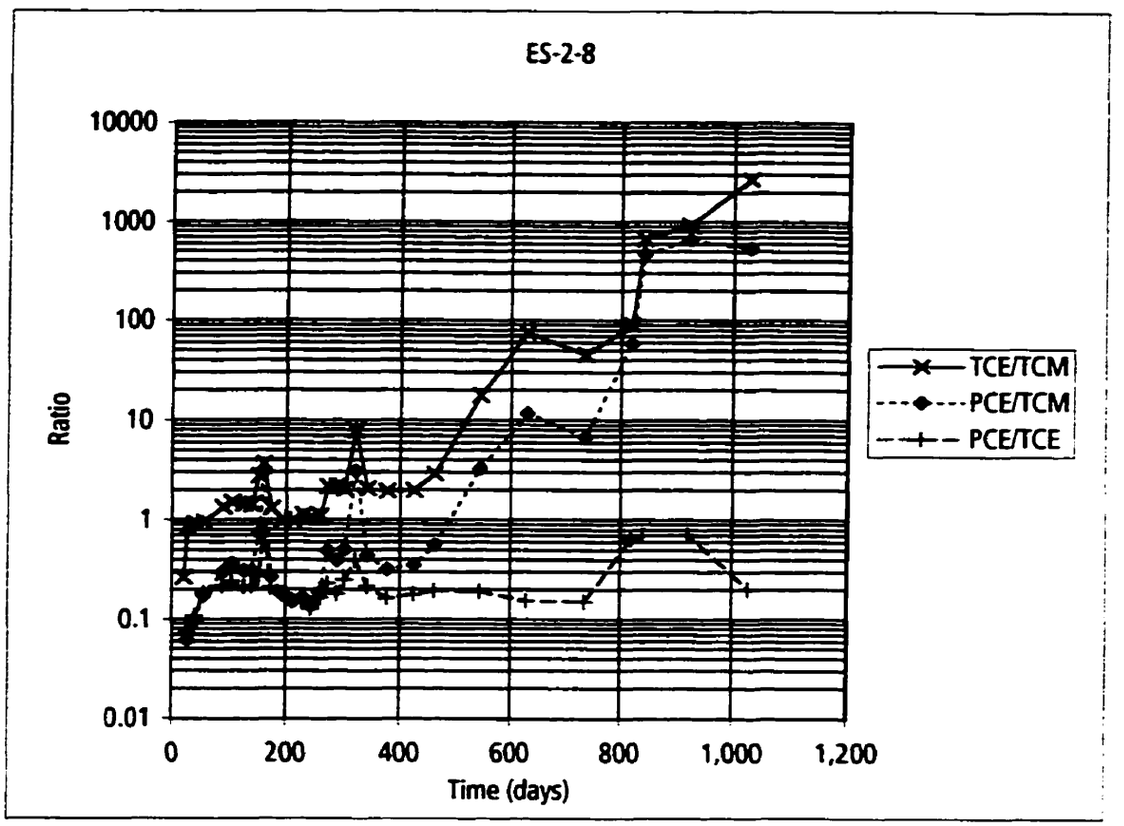

Key:
TCM - Chloroform
TCE - Trichloroethylene
PCE - Tetrachloroethylene

Figure 6-40. Temporal variation in aqueous concentration ratios at monitoring point ES-2-8.

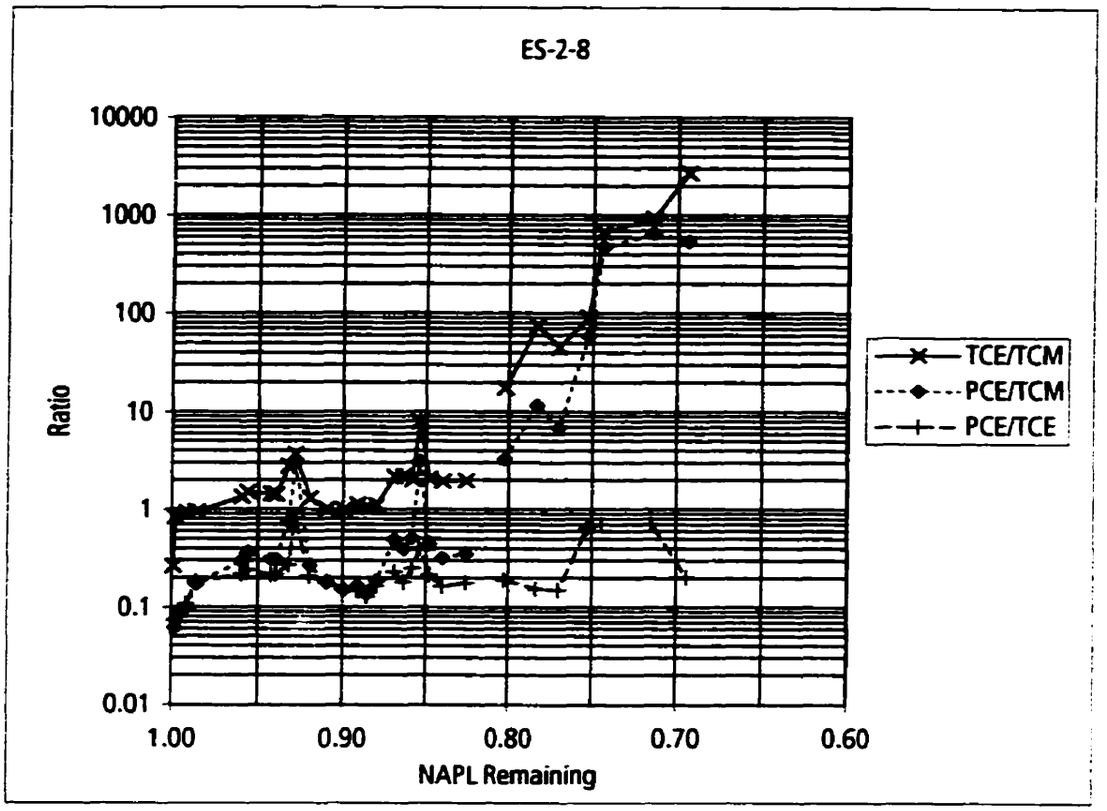

Key:
TCM - Chloroform
TCE - Trichloroethylene
PCE - Tetrachloroethylene

Figure 6-41. Change in aqueous concentration ratios versus NAPL mass remaining at monitoring point ES-2-8.

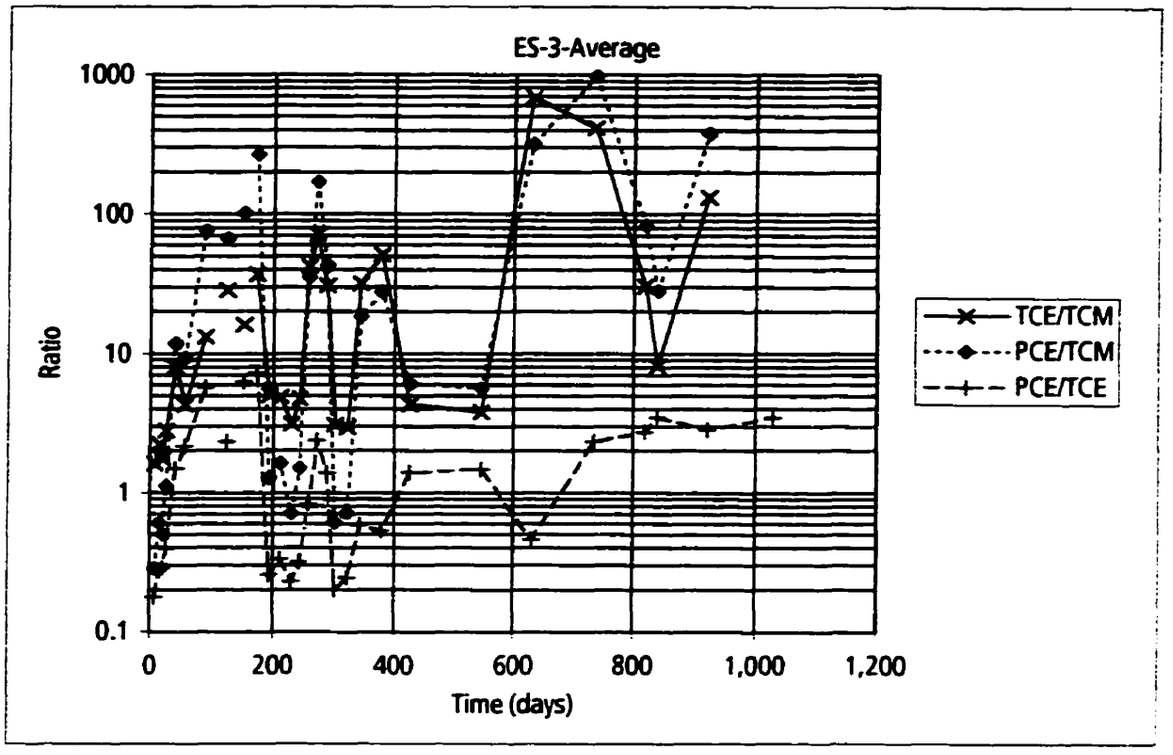

Key:
TCM - Chloroform
TCE - Trichloroethylene
PCE - Tetrachloroethylene

Figure 6-42. Temporal variation in aqueous concentration ratios for concentrations averaged for monitoring location ES-3.

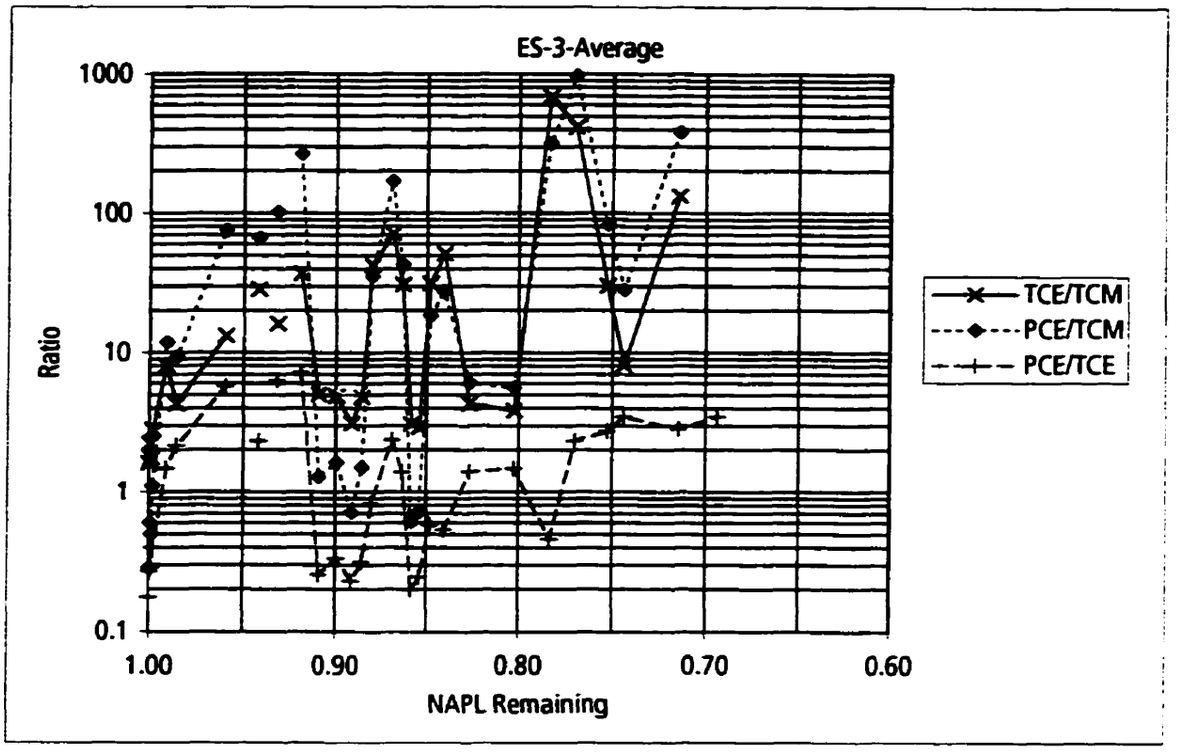

Key:
TCM - Chloroform
TCE - Trichloroethylene
PCE - Tetrachloroethylene

Figure 6-43. Change in aqueous concentration ratios versus NAPL mass remaining for concentrations averaged for monitoring location ES-3.

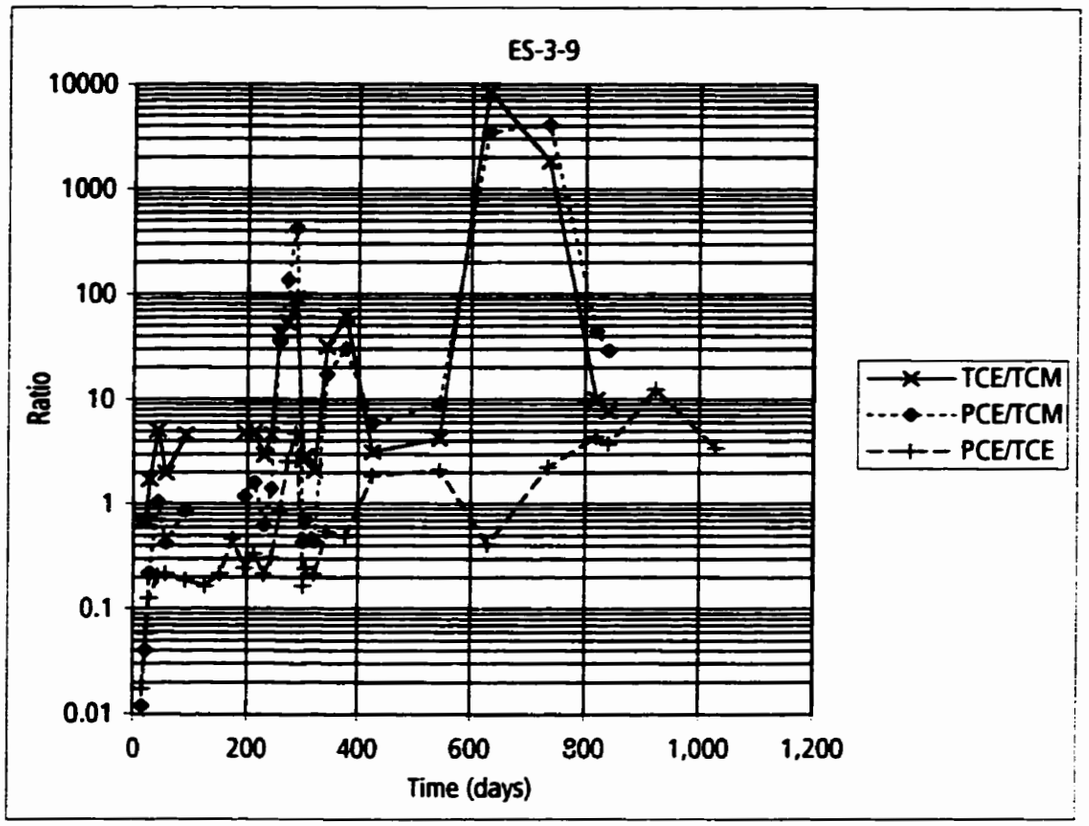

Key:
TCM - Chloroform
TCE - Trichloroethylene
PCE - Tetrachloroethylene

Figure 6-44. Temporal variation in aqueous concentration ratios at monitoring point ES-3-9.

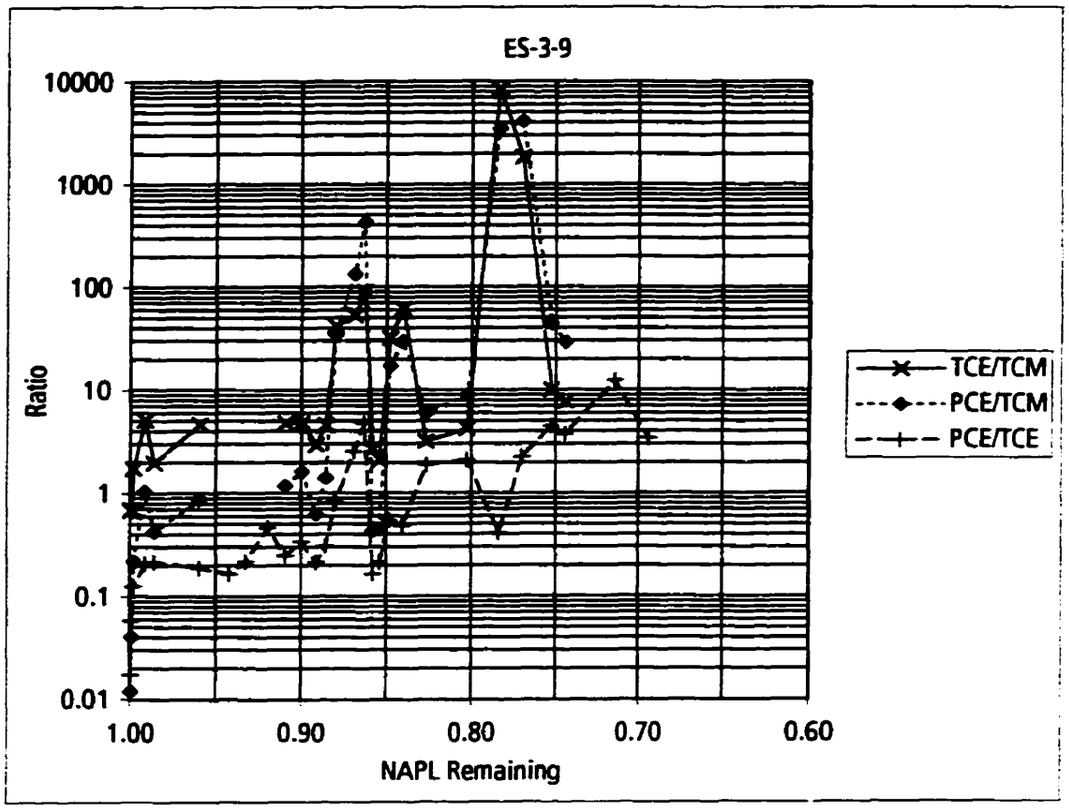

Key:
TCM - Chloroform
TCE - Trichloroethylene
PCE - Tetrachloroethylene

Figure 6-45. Change in aqueous concentration ratios versus NAPL remaining for monitoring point ES-3-9.

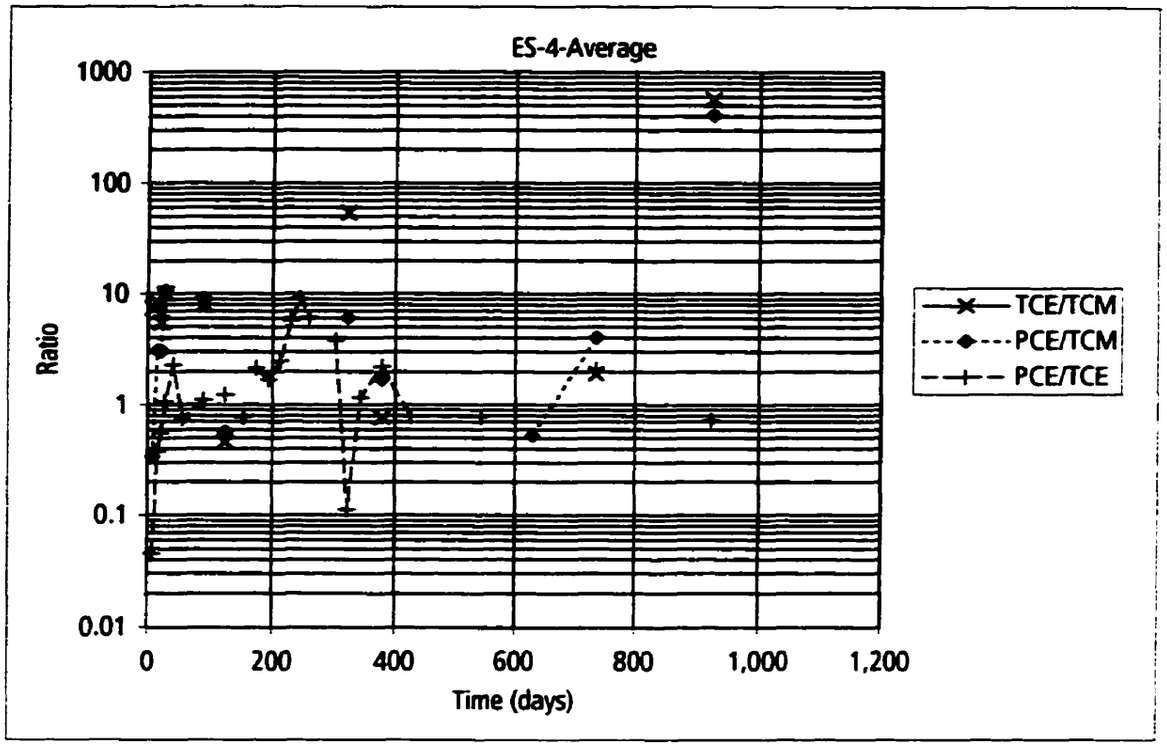

Key:
TCM - Chloroform
TCE - Trichloroethylene
PCE - Tetrachloroethylene

Figure 6-46. Temporal variation in aqueous concentration ratios for concentrations averaged for monitoring location ES-4.

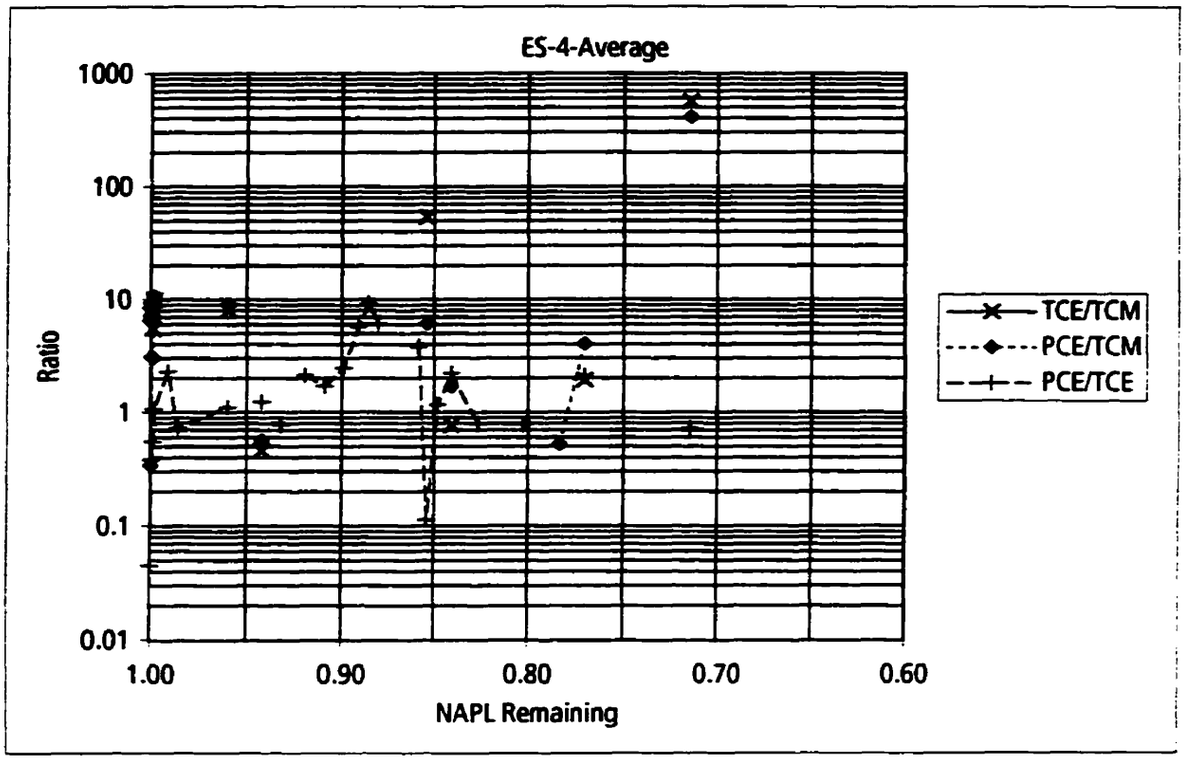

Key:
TCM - Chloroform
TCE - Trichloroethylene
PCE - Tetrachloroethylene

Figure 6-47. Change in aqueous concentration ratios versus NAPL mass remaining for concentrations averaged for monitoring location ES-4.

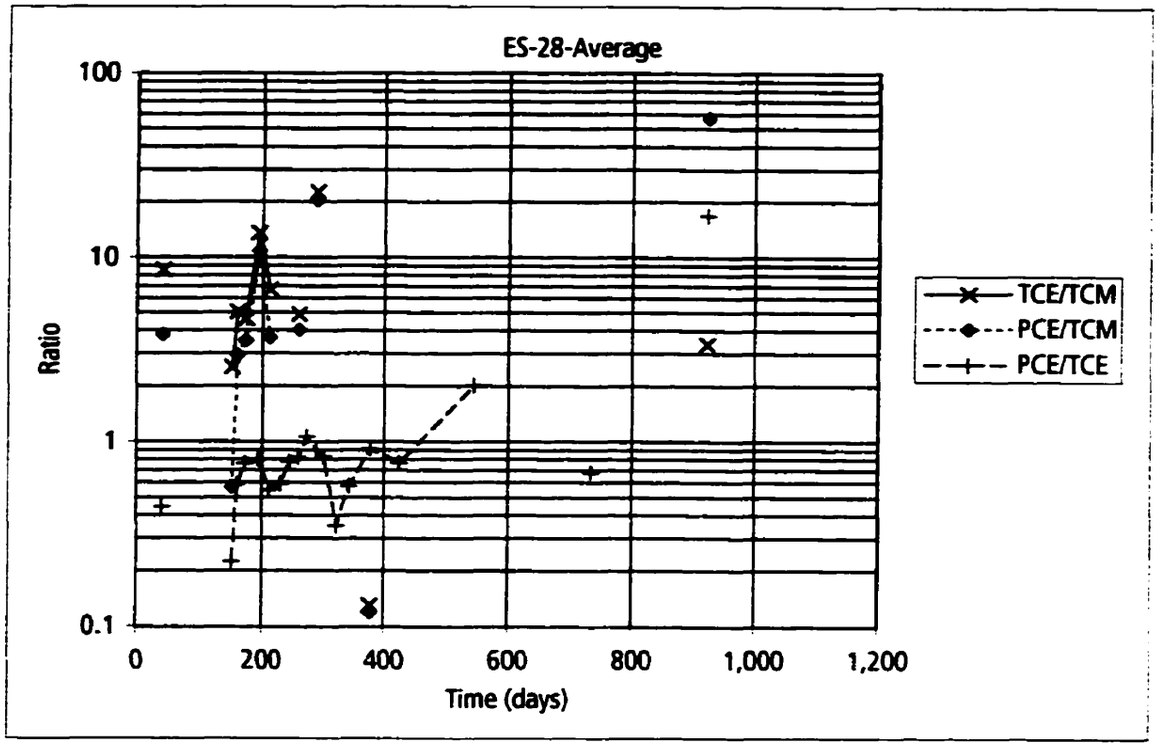

Key:
TCM - Chloroform
TCE - Trichloroethylene
PCE - Tetrachloroethylene

Figure 6-48. Temporal variation in aqueous concentration ratios for concentrations averaged for monitoring location ES-28.

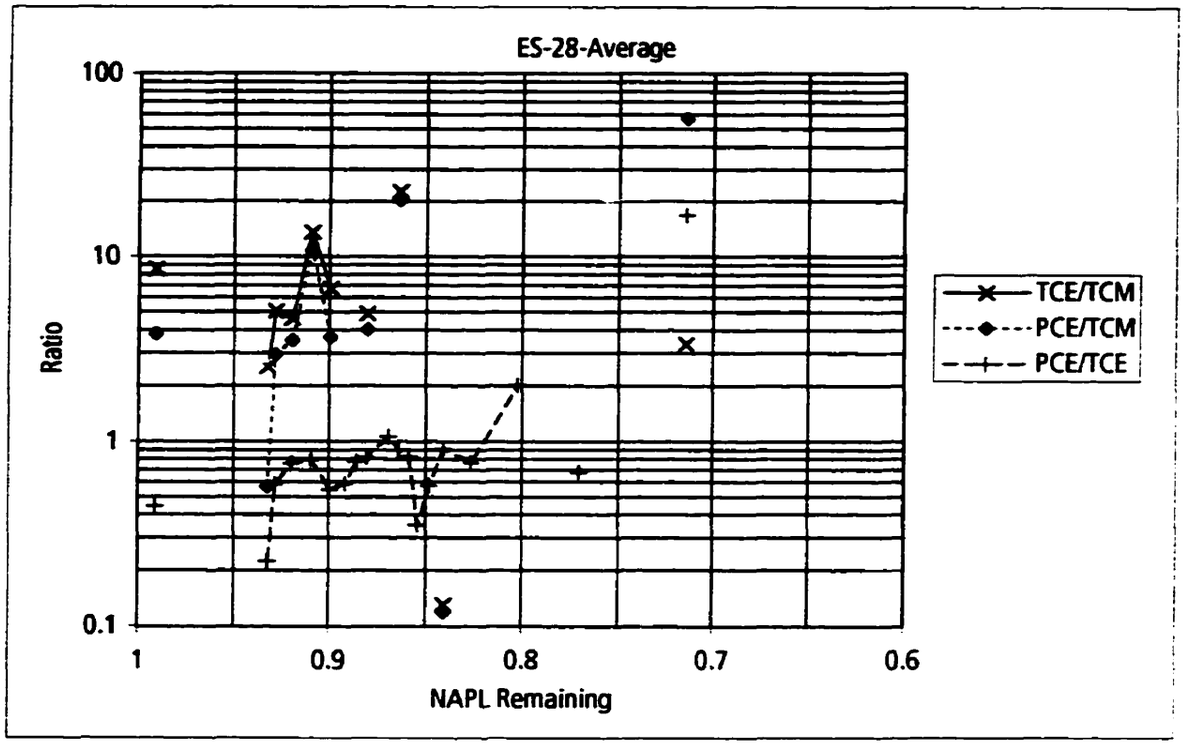

Key:
TCM - Chloroform
TCE - Trichloroethylene
PCE - Tetrachloroethylene

Figure 6-49. Change in aqueous concentration ratios versus NAPL mass remaining for concentrations averaged for monitoring location ES-28.

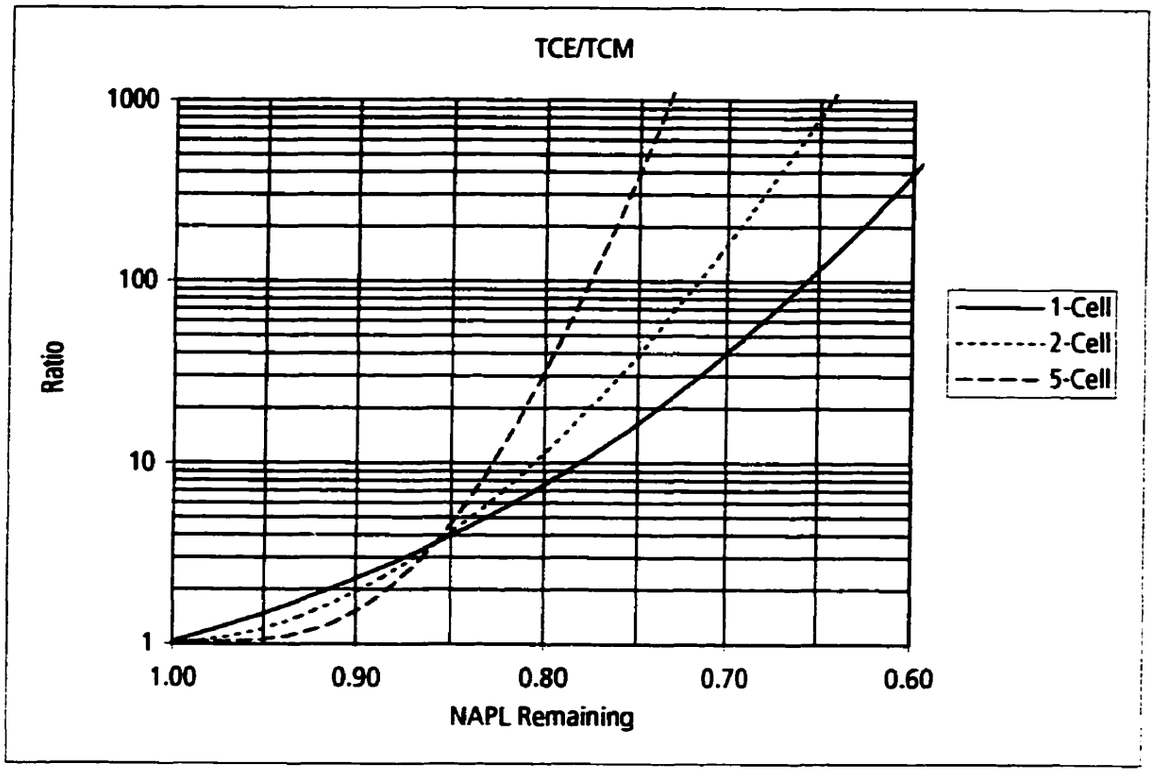

Key:
TCM - Chloroform
TCE - Trichloroethylene
PCE - Tetrachloroethylene

Figure 6-50. Change in TCE/TCM ratio versus NAPL remaining predicted by ESM.

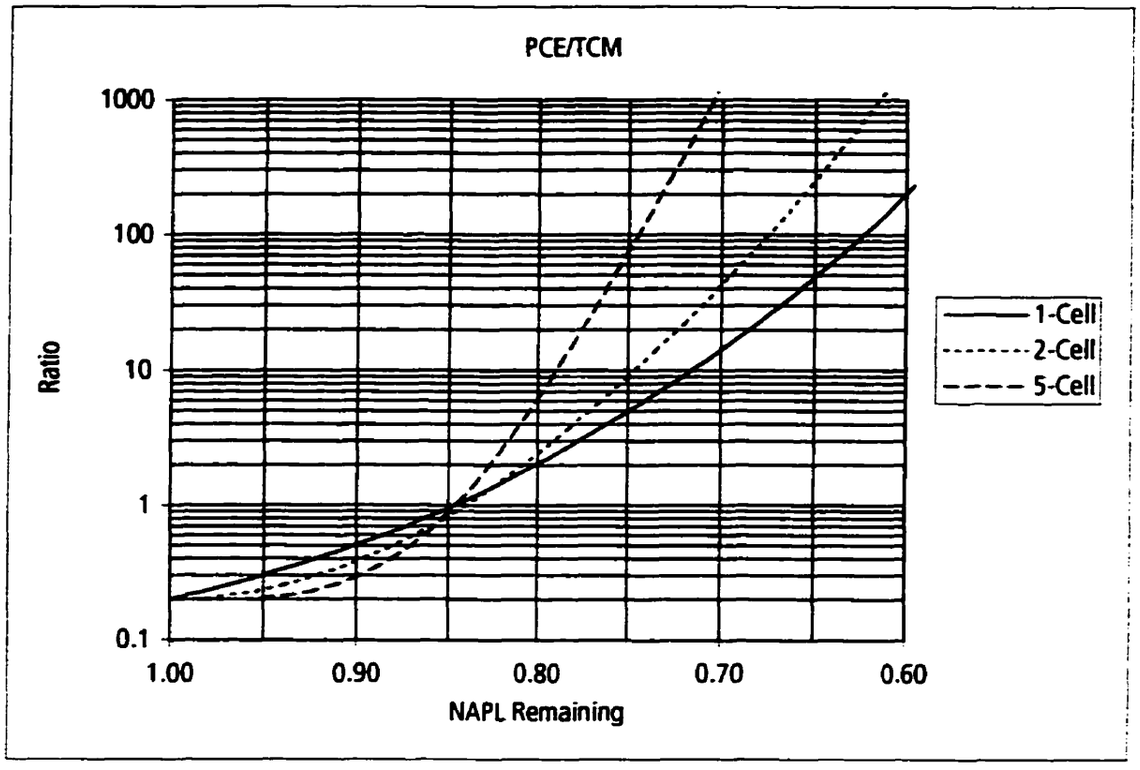

Key:
TCM - Chloroform
TCE - Trichloroethylene
PCE - Tetrachloroethylene

Figure 6-51. Change in PCE/TCM ratio versus NAPL remaining predicted by ESM.

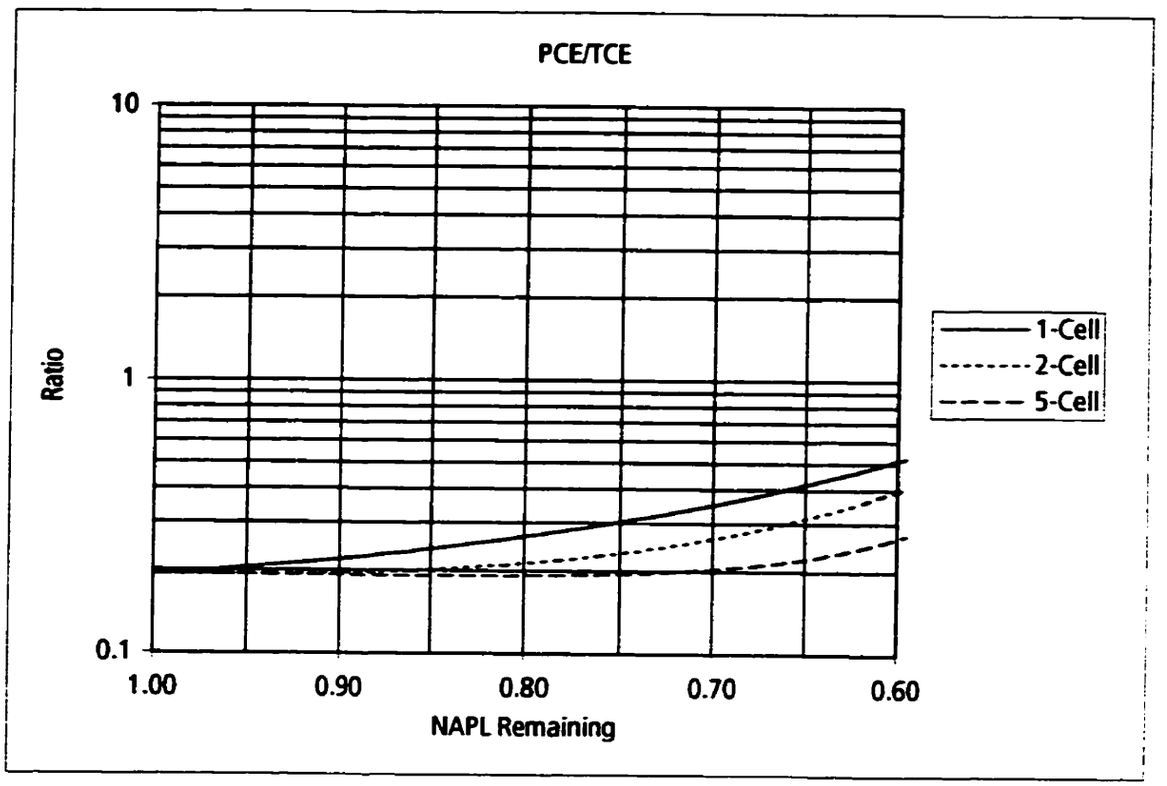

Key:
TCM - Chloroform
TCE - Trichloroethylene
PCE - Tetrachloroethylene

Figure 6-52. Change in PCE/TCE ratio versus NAPL remaining predicted by ESM.

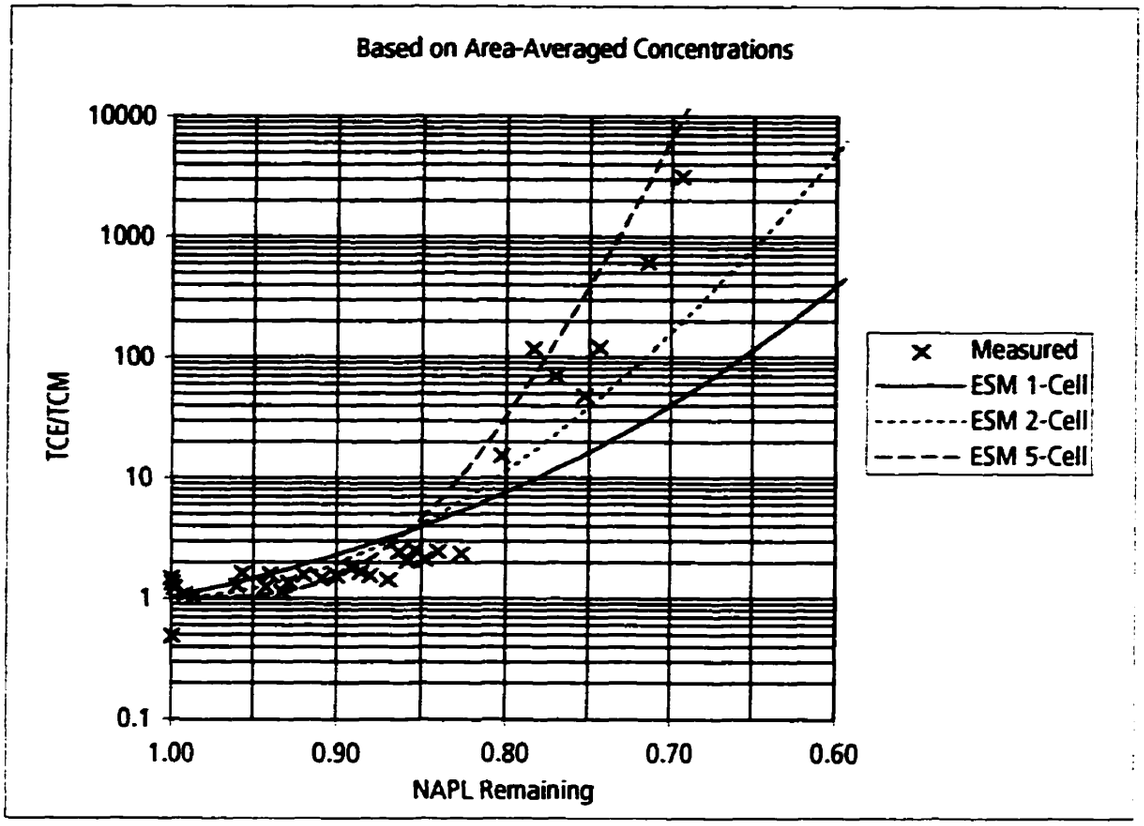

Key:
TCM - Chloroform
TCE - Trichloroethylene
PCE - Tetrachloroethylene

Figure 6-53. Measured TCE/TCM ratios versus NAPL remaining for concentrations averaged over the 1 m Fence compared to ratios predicted by the ESM.

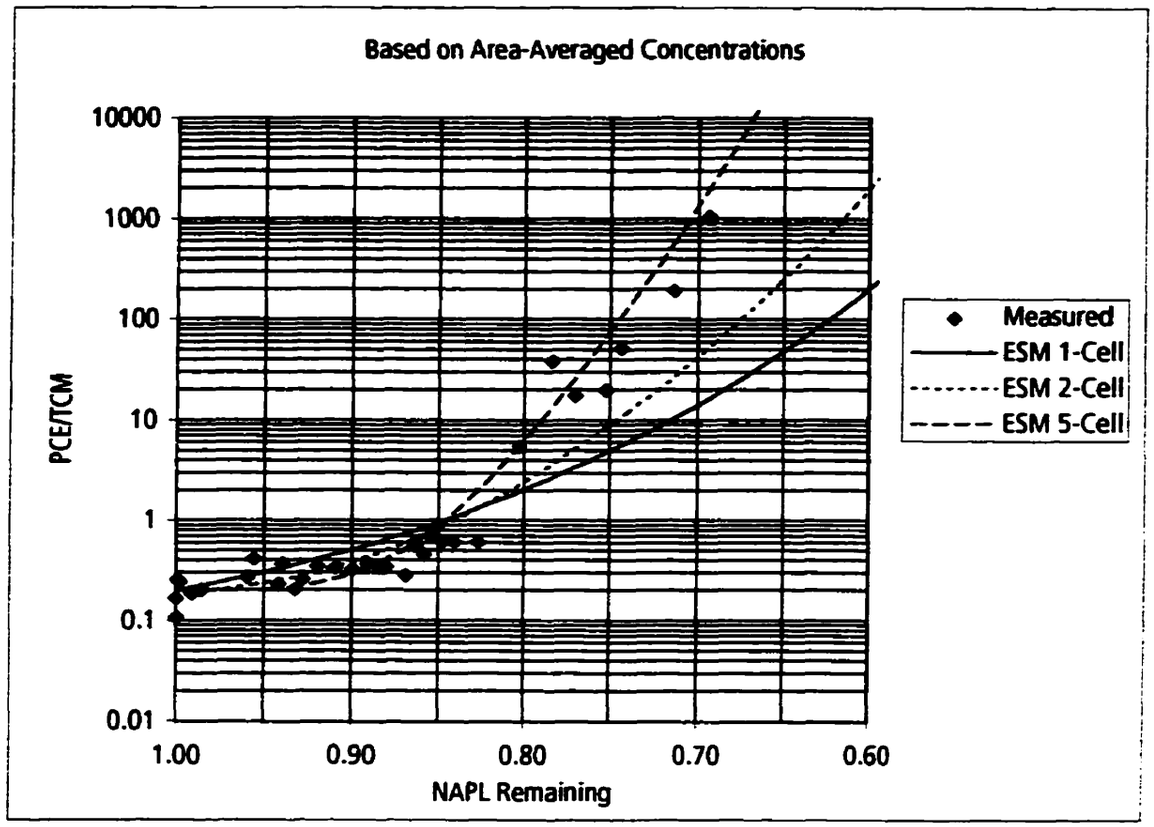

Key:
TCM - Chloroform
TCE - Trichloroethylene
PCE - Tetrachloroethylene

Figure 6-54. Measured PCE/TCM ratios versus NAPL remaining for concentrations averaged over the 1 m Fence compared to ratios predicted by the ESM.

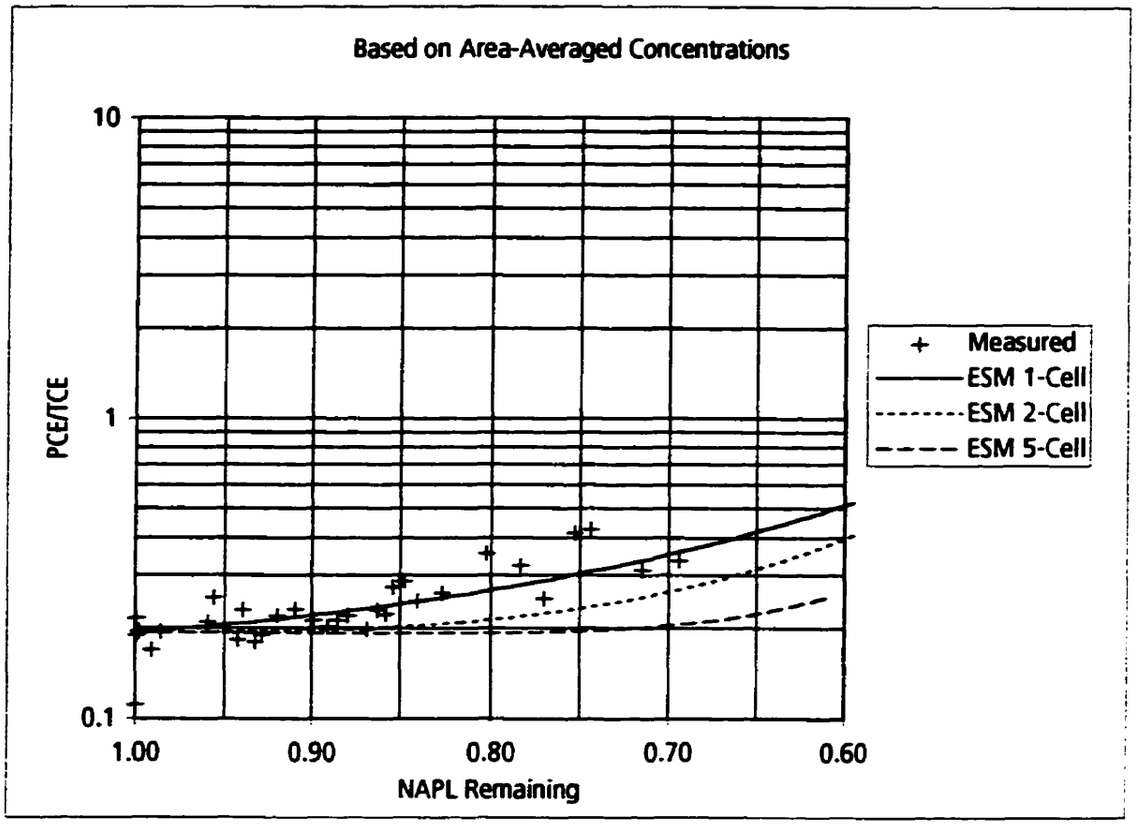

Key:
TCM - Chloroform
TCE - Trichloroethylene
PCE - Tetrachloroethylene

Figure 6-55. Measured PCE/TCE ratios versus NAPL remaining for concentrations averaged over the 1 m Fence compared to ratios predicted by the ESM.

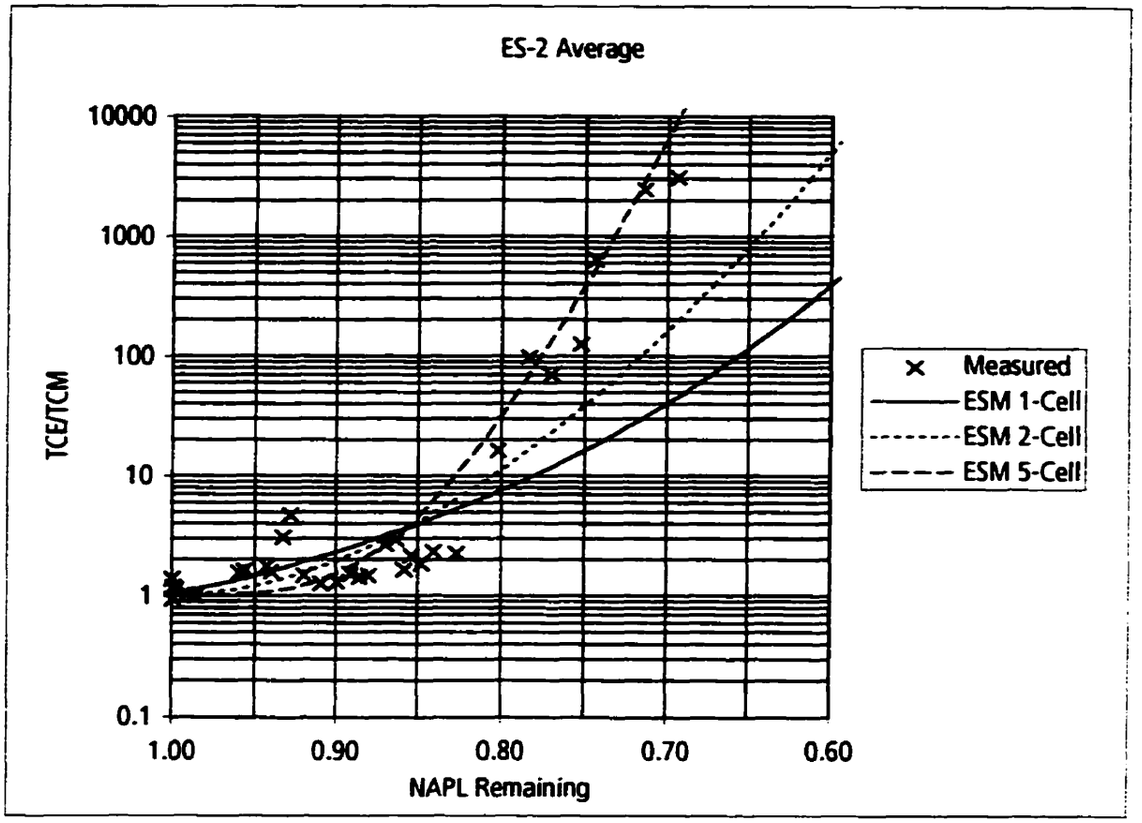

Key:
TCM - Chloroform
TCE - Trichloroethylene
PCE - Tetrachloroethylene

Figure 6-56. Measured TCE/TCM ratios versus NAPL remaining for averaged concentrations at monitoring location ES-2 compared to ratios predicted by the ESM.

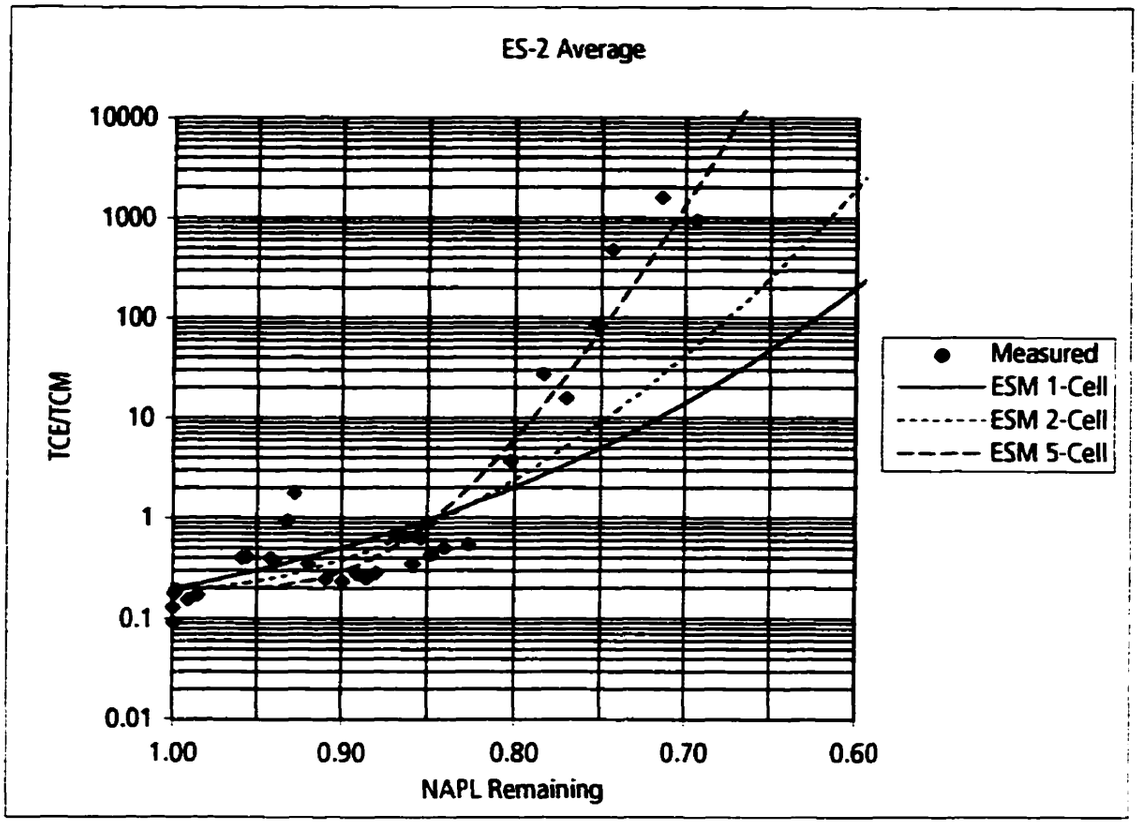

Key:
TCM - Chloroform
TCE - Trichloroethylene
PCE - Tetrachloroethylene

Figure 6-57. Measured PCE/TCM ratios versus NAPL remaining for averaged concentrations at monitoring location ES-2 compared to ratios predicted by the ESM.

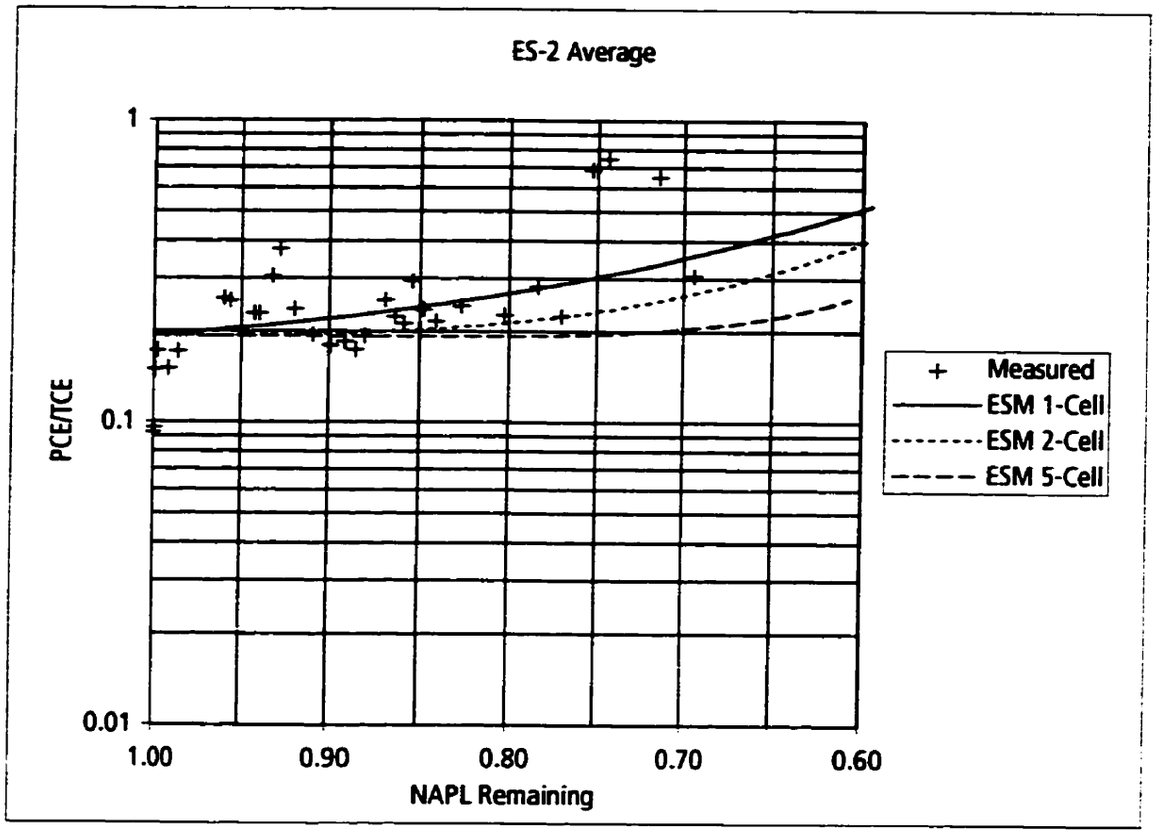

Key:
TCM - Chloroform
TCE - Trichloroethylene
PCE - Tetrachloroethylene

Figure 6-58. Measured PCE/TCE ratios versus NAPL remaining for averaged concentrations at monitoring location ES-2 compared to ratios predicted by the ESM.

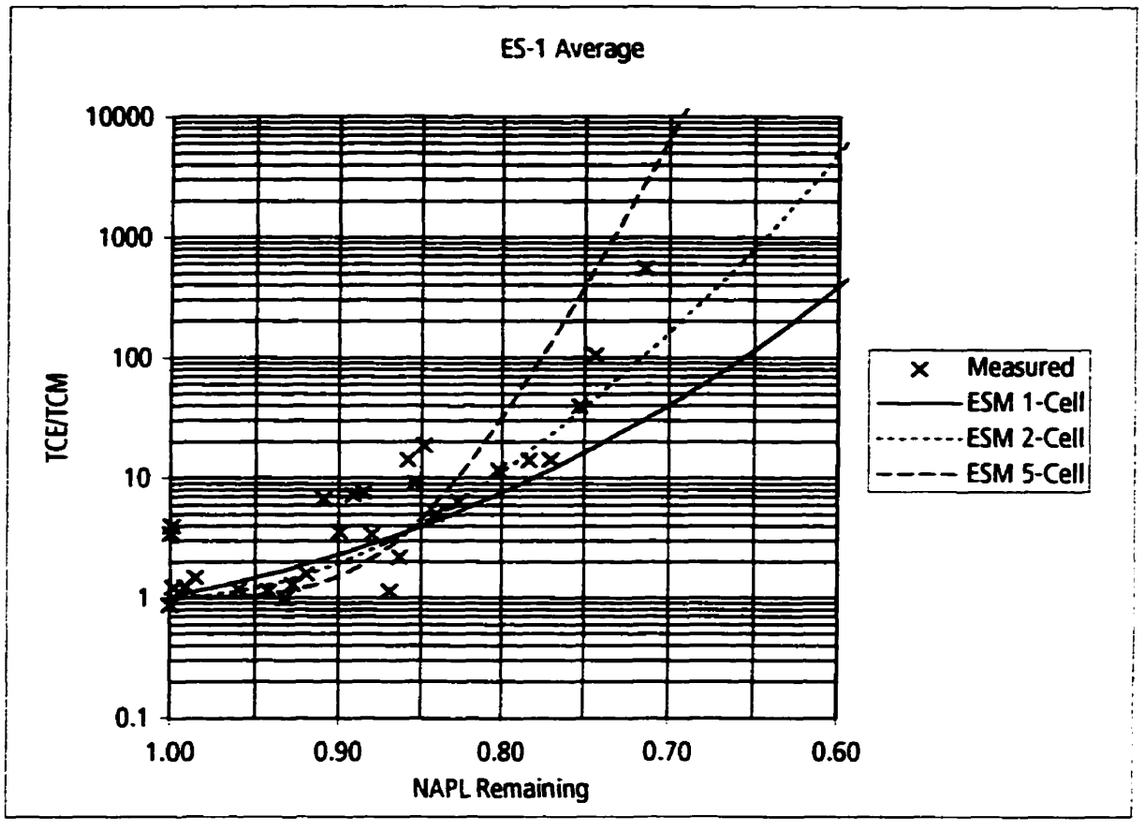

Key:
TCM - Chloroform
TCE - Trichloroethylene
PCE - Tetrachloroethylene

Figure 6-59. Measured TCE/TCM ratios versus NAPL remaining for averaged concentrations at monitoring location ES-1 compared to ratios predicted by the ESM.

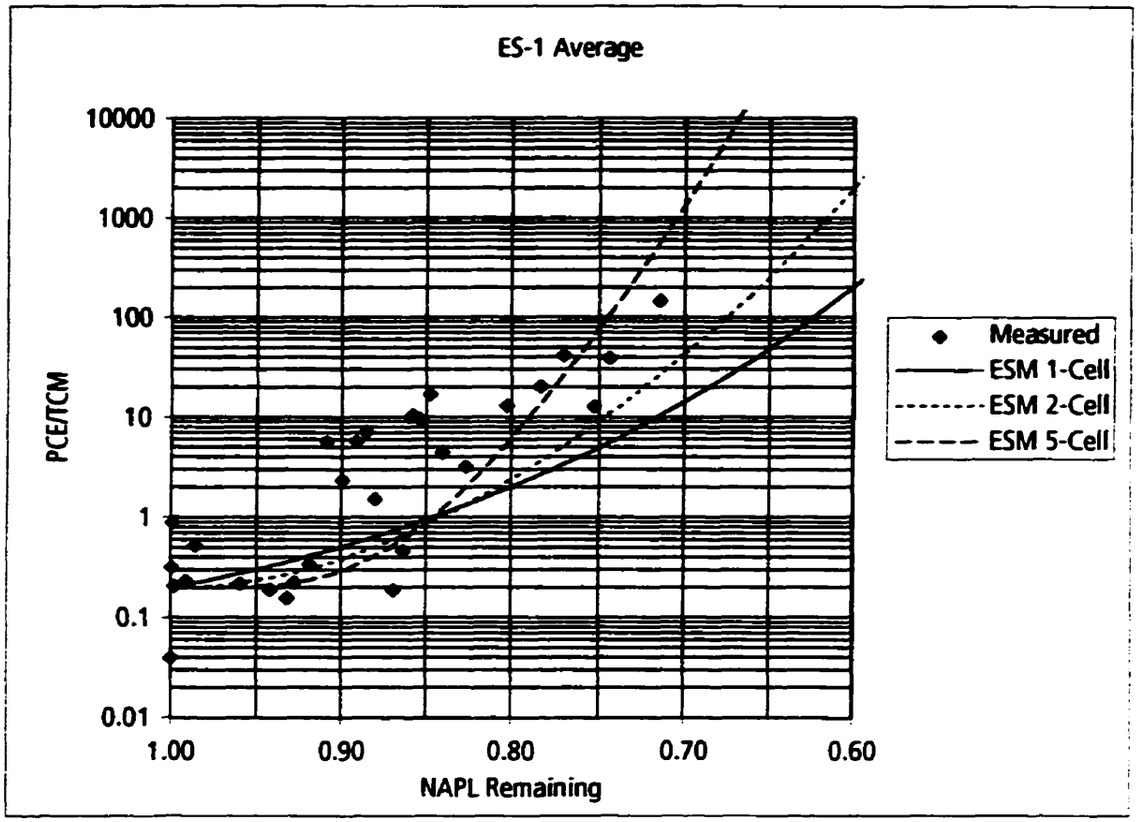

Key:
TCM - Chloroform
TCE - Trichloroethylene
PCE - Tetrachloroethylene

Figure 6-60. Measured PCE/TCM ratios versus NAPL remaining for averaged concentrations at monitoring location ES-1 compared to ratios predicted by the ESM.

File:ES Exp. Equilibrium.EXCL/Plots

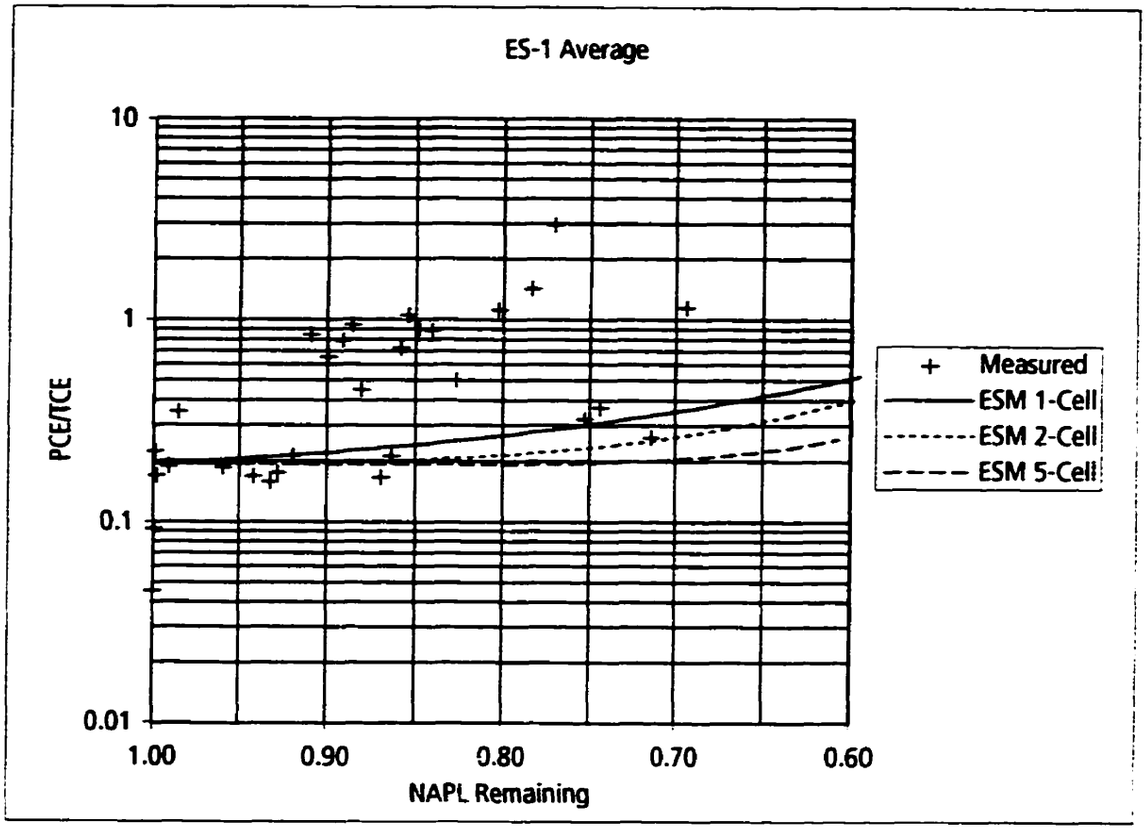

Key:
TCM - Chloroform
TCE - Trichloroethylene
PCE - Tetrachloroethylene

Figure 6-61. Measured PCE/TCE ratios versus NAPL remaining for averaged concentrations at monitoring location ES-1 compared to ratios predicted by the ESM.

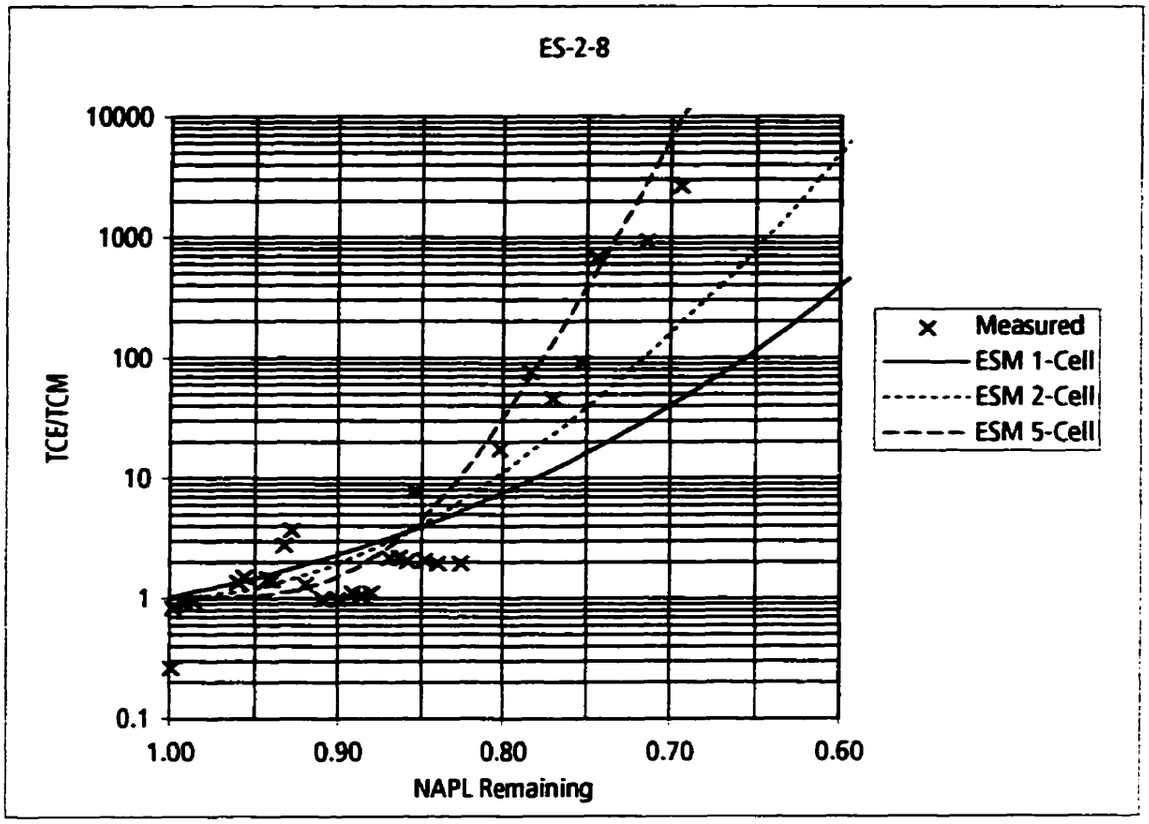

Key:
TCM - Chloroform
TCE - Trichloroethylene
PCE - Tetrachloroethylene

Figure 6-62. Measured TCE/TCM ratios versus NAPL remaining for monitoring point ES-2-8 compared to ratios predicted by the ESM.

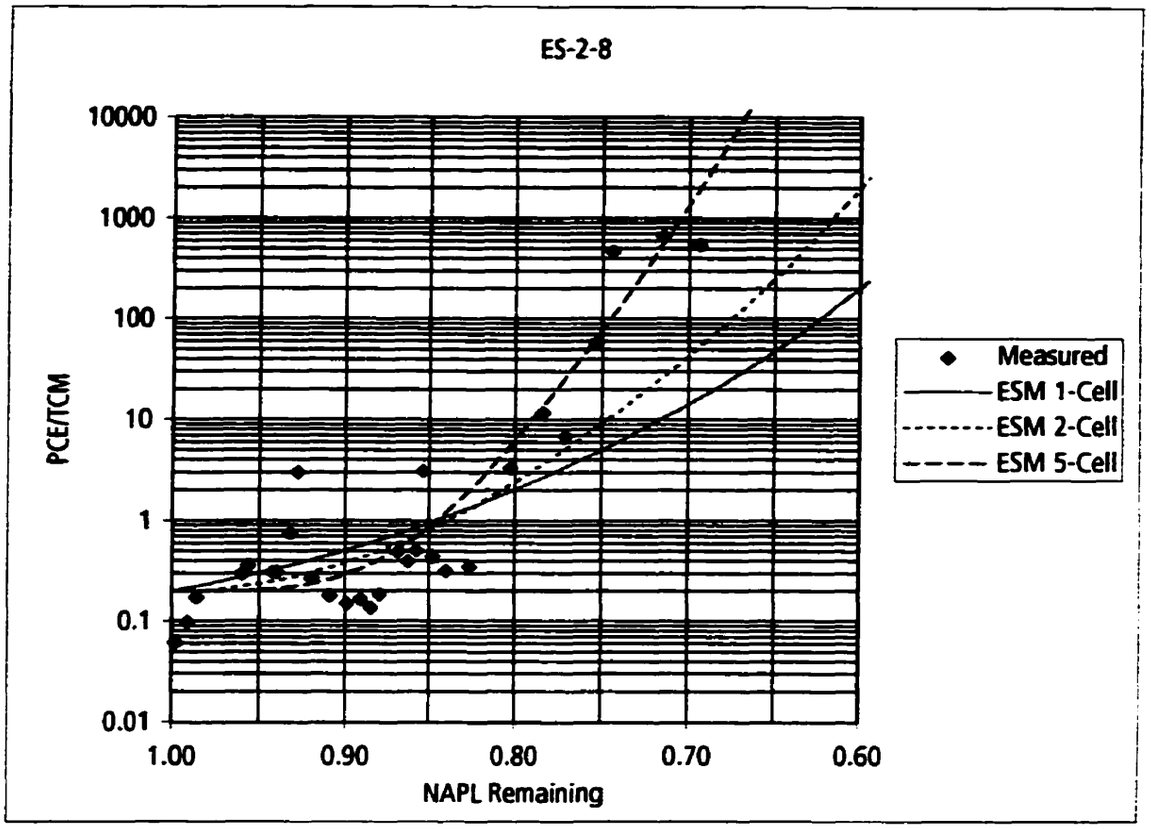

Key:
TCM - Chloroform
TCE - Trichloroethylene
PCE - Tetrachloroethylene

Figure 6-63. Measured PCE/TCM ratios versus NAPL remaining for monitoring point ES-2-8 compared to ratios predicted by the ESM.

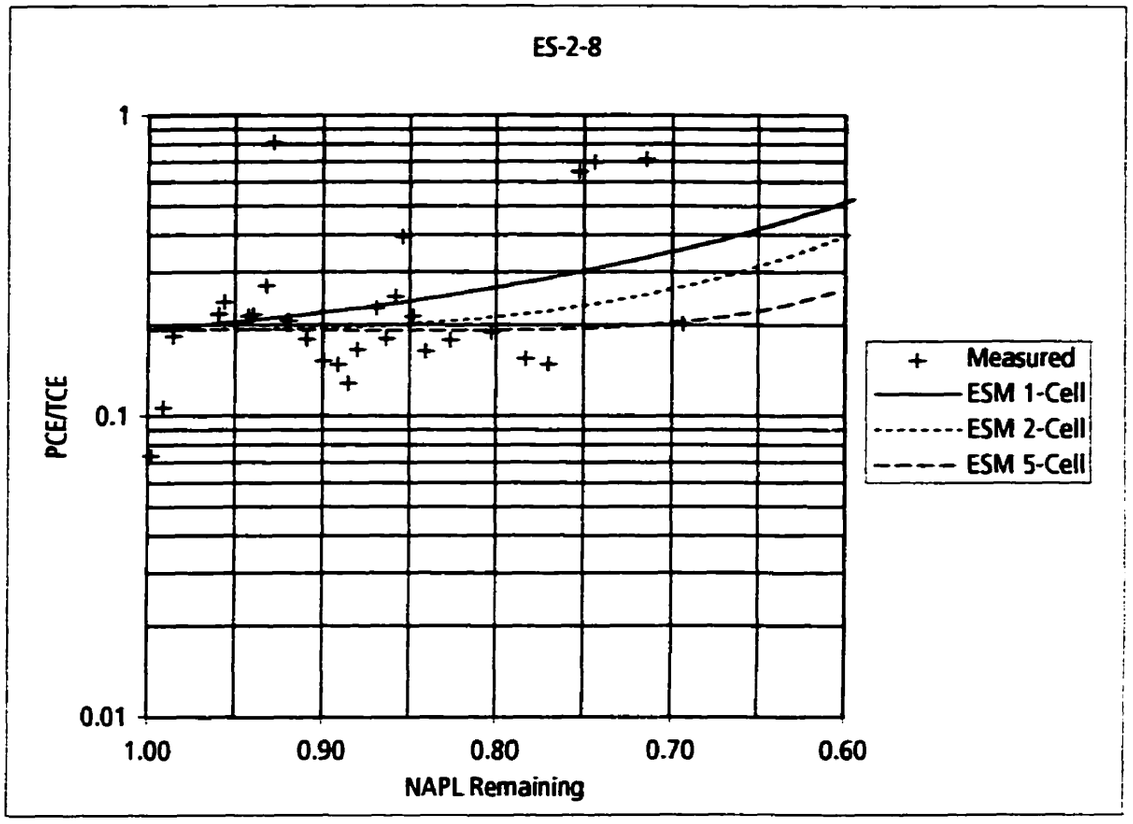

Key:
TCM - Chloroform
TCE - Trichloroethylene
PCE - Tetrachloroethylene

Figure 6-64. Measured PCE/TCE ratios versus NAPL remaining for monitoring point ES-2-8 compared to ratios predicted by the ESM.

7. Controlled Field Study: Free-Release Experiment

7.1 Overview

A second controlled field-scale dissolution experiment, referred to here as the Free-Release (FR) experiment, was conducted to examine the dissolution of a residual NAPL source of chlorinated solvents in the sandy aquifer at the Borden field experimental site beginning in the summer of 1992. A NAPL of known mass and composition was released directly in the groundwater zone inside a steel sheet piling test cell. The NAPL was permitted to distribute itself in the aquifer and form an irregular NAPL zone. Utilization of an irregular NAPL source zone distinguishes this experiment from the Emplaced-Source experiment which utilized a NAPL source zone of regular geometry. Horizontal groundwater flow was induced in the test cell and the aqueous concentrations emitted from the NAPL zone were measured. Aqueous concentration ratios and the NAPL mass remaining were determined from the experimental data. This allowed direct comparison of the experimental results to ESM simulations of NAPL dissolution.

Since 1990, the area around the FR site has been host to other experiments related to the migration and remediation of NAPL in the subsurface (see Figure 7-1). These other experiments were conducted in separate sheet piling test cells.

The FR experiment was designed to examine various aspects of the dissolution of the NAPL source zone. A specific objective of the FR experiment was to examine the dissolution of a multi-component NAPL from an irregular source zone, and evaluate whether temporal changes in aqueous concentration ratios may be used to determine the mass of contaminants contained in NAPL source zones. This is the work described in this chapter.

Other objectives of the FR experiment included: evaluation of whether the spatial distribution of NAPL source zones could be determined from monitoring of aqueous-phase concentrations downgradient of the source; and, evaluation of the effectiveness of methanol-water flush technology for the remediation of NAPL source zones.

7.2 Test Cell Layout and Study Program

The Free-Release (FR) experimental site is situated in an area where the sand aquifer is approximately 2.3 m thick. The aquifer is underlain by 7.5 m thick aquitard comprised of an upper silty clay and a lower clayey sand unit. The experiment was conducted inside a test cell constructed of steel sheet piling. The test cell measured 5.5 m in length and 4.5 m in width (see Figure 7-2). The sheet piling walls extended through the sand aquifer and penetrated 0.3 m into the aquitard. The interlocking joints of the sheet piles were sealed to reduce the permeability of the cell walls (Starr et al., 1992).

Groundwater flow through the cell was controlled by means of 5 injection wells on one side of the cell and 5 extraction wells on the opposite side. Water was introduced to the injection wells at a constant head and water was withdrawn from the extraction wells at a constant rate. Each extraction well operated at a rate of 0.05 L/min. for a total flow rate of 0.25 L/min.

A series of 9 monitoring point arrays were installed 0.7 m upgradient of the extraction wells for the purpose of groundwater sampling. Each sampling array consisted of 20 to 22 sampling tubes installed at different depths in aquifer. The monitoring arrays are shown in section view in Figure 7-3.

Prior to the release of the NAPL, a chloride tracer test was conducted to determine the groundwater velocity in different portions of the test cell. A pulse of sodium chloride solution was introduced into all 5 injection wells and samples collected from the monitoring arrays were analysed.

Groundwater velocities determined from the breakthrough curves of the chloride concentrations.

Injection of the NAPL took place on July 6, 1992. The NAPL was a mixture similar to that used in the Emplaced-Source experiment and contained 9.7% by weight TCM, 37.9% by weight TCE and 52.5% by weight PCE. The NAPL was dyed red in colour by addition of 1 g/L of Sudan IV dye to assist subsequent sampling and analysis of soil at the end of the dissolution experiment. The NAPL was released to a 5-cm diameter polyethylene tube open at a depth of 0.66 m below ground surface and 0.05 m below the water table at the time of the release. A total of 5 L of NAPL mixture was injected over 25 hours at a constant NAPL head of 0.6 m.

Following injection of the NAPL, groundwater flow through the test cell caused dissolution of the NAPL. Groundwater samples were collected periodically over a period of 220 days to examine the dissolution processes. During the dissolution stage of the experiment, about 4,500 groundwater samples were collected. After the dissolution experiment, the NAPL source zone remained in place for a methanol-water flush experiment. A 5.5-day long pulse of 30% methanol - 70% water was introduced to the injection wells and the groundwater sampled in the monitoring arrays periodically for another 71 days. The methanol-water flush experiment is not discussed further here.

Upon completion of the methanol-water flush experiment, the aquifer material in the test cell was excavated to determine the actual spatial distribution of the NAPL remaining in the aquifer by means of visual examination and soil sampling.

7.3 Investigation and Monitoring Methods

7.3.1 Water Table Monitoring

The elevation of the water table was monitored in the extraction wells and, at later times, in 8 piezometers installed across the test cell. Injection and extraction wells consisted of 5-cm diameter PVC casing with 1.82-m long slotted intakes. The injection wells were installed to a depth of 1.97 m and the extraction wells were installed to a depth of 1.87 m. The depth to the top of the aquitard is 2.3 m. The wells were installed inside a temporary casing driven to the applicable depth. The well was held in place while the casing was removed.

Piezometers consisted of 0.64-cm diameter Teflon tubing installed to a depth of 1.0 m below ground surface. The piezometers had 0.1-m long slotted intakes, wrapped with 100-mesh nylon screening. The piezometers were installed inside a steel pipe driven to the applicable depth. The well was held in place while the pipe was removed. The piezometers were not installed until 153 days after the NAPL injection when concern arose regarding the hydraulics of the injection-extraction system.

Water levels were measured using an electric water level finder tape. During the chloride tracer test and NAPL dissolution experiment, water levels were measured in the injection wells on 60 occasions. Water levels were measured in the piezometers on 11 occasions during the dissolution experiment.

7.3.2 Groundwater Sampling

The groundwater monitoring arrays consisted of 0.64-cm diameter stainless steel tubes each installed to a different depth in the aquifer. Each tube had a pointed end and a 1-cm long stainless steel screen intake. The tubes were pushed by hand or hammered to the desired depth. Each array

had 20 or 22 monitoring points. The vertical spacing between monitoring points was 0.1 m. The lateral spacing between monitoring arrays was 0.5 m.

A 14-place manifold system was used to collect groundwater samples simultaneously from up to 14 sampling points in a monitoring array. This sampling system was described by Mackay et al. (1986) and was the same as that used to the Emplaced-Source experiment. The manifold system was attached to the monitoring tubes using lengths of Teflon tubing. Groundwater was drawn by vacuum from the monitoring point tubes into the manifold, where it passed into an 18-mL glass sample vial prior to entering a 125-mL glass vacuum flask. At least 80 mL of groundwater was purged from each point and flushed through the sample vial prior to collection of the sample. After purging the required water volume, the flow-through heads on the glass vials were removed. The glass vials were sealed immediately with a Teflon-lined rubber septa and crimp-on caps, and used for the analysis of chlorinated solvents. Between monitoring array locations, the tubing and fittings of the manifold were blown out with air and wiped dry to prevent cross contamination of samples. In addition, whenever possible, the sequence of sampling proceeded from areas of low aqueous concentrations to areas of higher concentrations. Groundwater samples were collected from the monitoring arrays on 34 occasions during the dissolution portion of the experiment. Samples were collected also from the effluent of the extraction well system.

The analysis of chlorinated solvents in groundwater was performed using a pentane extraction method similar to that described by Glaze et al. (1983). Aliquots of pentane extracts were analysed by direct injection to a Varian 3400 gas chromatograph with electron capture detector. The detection limits were 5 µg/L for TCM and 1 µg/L for both TCE and PCE.

Chloride analyses for the tracer test were performed using a Markson Model 92014 digital pH/mV/Temp meter with an Orion chloride combination electrode.

7.3.3 Aquifer Cores

A total of 3 cores were collected after the methanol-water flush experiment but before excavation of the cell using the piston-coring method of Starr and Ingleton (1992), for the determination of hydraulic conductivity. Aquifer cores were continuous 5-cm diameter cores, each 2.5 m in length. The cores were divided into 5-cm long segments for the laboratory determination of hydraulic conductivity using the falling head permeameter method of Sudicky (1986). Hydraulic conductivity values were corrected to the ambient groundwater temperature of 10°C.

7.3.4 Chloride Tracer Test

Prior to injection of the NAPL, a chloride tracer test was performed to determine the groundwater velocity in different parts of the cell. A pulse of sodium chloride solution, containing 4,100 mg/L chloride, was introduced into all 5 injection wells during a 24 hour period. Clean water continued to be injected following the chloride pulse. Groundwater samples were collected periodically from the monitoring arrays and analysed for chloride. Monitoring continued for about 40 days after introduction of the pulse.

7.3.5 Cell Excavation

Following completion of the methanol-water flush experiment, the aquifer material inside the test cell was excavated to determine the spatial distribution of the remaining NAPL in the source zone. The upper 0.5 m of the cell was removed without specific study. Starting at 0.5 m, sand was carefully removed from the entire central portion of the cell, in 0.05-m vertical increments. The primary means of determining the presence of

NAPL was a visual search for the red-dyed NAPL along the base of the excavation. Excavation of 0.05-m increments continued to a depth of 0.95 m, whereupon excavation continued at 0.1-m increments to a depth of 1.35 m. Several levels of the excavation at depths between 0.5 m and 0.7 m exhibited visual evidence of NAPL

Numerous soil samples were also collected at various levels during the excavation in an attempt to determine the NAPL mass remaining in the test cell. However, no soil samples were collected from what was later determined to be the critical area of the source zone and the soil analyses could not provide useful estimates of the NAPL mass. These soil analyses are not discussed further in this chapter.

7.4 Hydrogeological Conditions

7.4.1 Hydraulic Conductivity

The Borden aquifer at the FR site is similar to the Emplaced-Source site and is comprised of medium-grained to fine-grained glaciolacustrine sand, with occasional beds of coarse sand & gravel or silt, and exhibits distinct laminations or bedding features. Individual beds range from several millimetres to several centimetres in thickness. Bedding is primarily horizontal but convolute bedding features are common.

The hydraulic conductivity of the aquifer at the FR site was found to range from 1.1×10^{-3} cm/s to 8.0×10^{-3} cm/s based on the results of 133 permeameter tests from the 3 cores. These data are shown in Figure 7-4. The geometric average hydraulic conductivity was 2.6×10^{-3} cm/s and the arithmetic average was 2.8×10^{-3} cm/s. This geometric average value is slightly lower than with the geometric average value of 7.2×10^{-3} cm/s obtained by Sudicky (1986) or the value of 6.3×10^{-3} cm/s obtained at the ES site. The 3 cores yielded comparable results. The zones of highest hydraulic

conductivity are at depths of 0.0 m to 0.4 m, and at the bottom of the test cell from 1.7 m to 2.3 m.

7.4.2 Hydraulic Gradient

The water level in the injection wells was maintained at a level of 0.09 m below ground surface during the entire experiment. The total pumping rate in the extraction wells was maintained 0.25 L/min. Initial testing suggested that this system should operate with the difference in hydraulic head along the test cell would be about 0.1 m to yield a hydraulic gradient of about 0.02 while maintaining the water table within 0.2 m of the ground surface. These conditions would yield a groundwater velocity of about 15 cm/day, which is slightly higher than the natural velocities in the Borden aquifer.

However, during the experiment water levels in the extraction wells declined with time, suggesting clogging of the extraction wells, injection wells or both. The wells were re-developed periodically but water levels in the extraction wells varied from 0.16 m to 1.15 m below ground surface. The fluctuation in water levels in the injection and extraction wells are shown in Figure 7-5. Piezometers were installed along the test cell at 153 days to determine the actual water levels and hydraulic gradient without the influence of clogging effects in the wells. Profiles of water levels in the piezometers measured on 3 occasions are shown in Figure 7-6. The water level at the downgradient end of the test cell was similar to the level in the extraction wells, whereas the water level at the upgradient end was much lower than the level in the injection wells. This indicates that the principal loss of hydraulic head occurred at the injection wells. Although the water table in the test cell rose and fell in the entire cell during the experiment, the hydraulic gradient was relatively constant at 0.023.

At the centre of the test cell, the average water table elevation was about 0.5 m below ground surface, but fell to a depth of 0.75 m for a short time during the dissolution test.

7.4.3 Calculated Groundwater Velocity

The velocity of groundwater flow through the test cell was calculated based on the rate of pumping from the extraction wells and measured hydraulic gradient; the measured hydraulic conductivity and hydraulic gradient; and, the chloride tracer test. All three methods yielded similar results.

The total pumping rate was 0.25 L/min. or 360 L/day drawn from a cross-sectional area measuring 4.5 m in width and 1.8 m in depth. Based on a porosity of 0.33, this groundwater flow rate is equivalent to a linear velocity of 13 cm/day.

Based on the average hydraulic conductivity of 2.8×10^{-3} cm/s, hydraulic gradient of 0.023, and porosity of 0.33, the linear groundwater velocity is calculated to be 17 cm/day.

Groundwater velocities were calculated from the breakthrough curves of the chloride concentrations at each monitoring point using the moment technique of Levenspiel (1989). These calculated velocities for monitoring arrays FR-2 through FR-8 are shown in Figure 7-7. Data from FR-1 and FR-9 are not shown because aqueous-phase solvents from the NAPL source zone were never detected at these locations during the dissolution experiment. Velocities based on the tracer test ranged from 4.8 cm/day to 21 cm/day, with an average velocity of 10 cm/day. Although the velocity profiles for arrays FR-2 and FR-3 are relatively constant with depth, arrays FR-4 through FR-8 exhibit notably higher velocities at a depth of 1.7 m to 2.3 m. This trend is consistent with the results of the permeameter tests of the core sample shown in Figure 7-4.

7.4.4 Position of NAPL Source Zone

Excavation and visual examination of the aquifer material at the end of the experiment revealed the actual position of the NAPL source zone. Although not clearly evident from aqueous-phase concentrations in the monitoring arrays, NAPL released from the injection tube did not penetrate downward into the aquifer. During excavation, it was observed that the end of the injection tube was situated in a thin bed of silty sand. The injection pressure of the NAPL was not sufficient to cause entry into this layer and NAPL migrated outward and rose upward along the outside of the injection tube. At a depth of 0.55 m, or 0.11 m above the level of the end of the injection tube, the majority of the NAPL entered a relatively permeable horizon and spread laterally. Smaller volumes of NAPL entered other beds.

The final position of the NAPL is shown in section view in Figure 7-8 and the maximum lateral extent of NAPL is shown in plan view in Figure 7-9. The NAPL was distributed as residual and mobile NAPL in thin layers of less than a centimetre in thickness. Photographs of the most extensive layer at 0.55 m are shown in Feenstra and Cherry (1996). It is known the some of the NAPL was potentially mobile, but was pooled or perched in the layers. When the layer at 0.55 m was intersected by survey rods, stakes or core tubes, a portion of the NAPL in the layer was remobilized and migrated downward along the disturbed zone.

Because of the shallow depth of the NAPL zone from 0.5 m to 0.7 m, the NAPL zone was above the water table as the water table fell to 0.75 m for a period of time during the dissolution experiment. Despite this fact, the NAPL zone likely remained submerged by water in the capillary fringe. The thickness of the capillary fringe in the Borden aquifer is typically 0.3 m to 0.4 m and may be slightly greater in this case. The aquifer at the FR site has a lower hydraulic conductivity than the typical Borden aquifer, presumably due to a finer texture. This would result if a slightly thicker capillary fringe.

Within the capillary fringe, lateral aqueous-phase transport would occur also in response to the hydraulic gradient in the saturated zone.

7.5 Plume Migration

7.5.1 Overview

Following the release of the NAPL, groundwater flow through the NAPL zone and dissolution caused aqueous-phase plumes to develop at the downgradient monitoring arrays. With the position of the NAPL in the centre of the test cell and a groundwater velocity of 10 cm/day to 15 cm/day, a period of 10 days to 30 days was required for aqueous-phase solvents to arrive at the monitoring arrays. Aqueous concentrations reflecting the maximum initial conditions developed at most monitoring points by about 50 days.

The forms of the aqueous-phase plumes across the monitoring arrays are shown in Figure 7-10 on 5 occasions at 43 days, 94 days, 140 days, 174 days and 221 days. These occasions were selected to illustrate the principal changes which occurred in the plumes. The concentration contours were drawn in Spyglass® Transform Version 3.0 using a 0.01 m grid with kernel smoothing.

Several features of the aqueous-phase plumes are evident in Figure 7-10. The portions of the plumes having the highest concentrations were aligned with the central portion of the NAPL zone. However, the plumes generally extended laterally to the full width of the NAPL zone or larger. At times, there were low-concentration lobes of the plumes extending to the left, to the right, or both ways beyond the lateral extent of the NAPL zone. These lateral shifts in the margins of the plumes may have been the result of localized changes in flow direction caused by fluctuations in the water table.

The plumes extended consistently to a depth of about 1.2 m below ground despite the fact that the NAPL source zone resided at a depth of 0.5 m

to 0.7 m. Although the experiment was designed with the intent that groundwater flow through the cell would be strictly horizontal, it is possible that there may have been a vertical component of flow as a result of the zone of higher hydraulic conductivity at the base of the aquifer.

At 43 days, the TCM and TCE plumes had reached their highest concentrations and greatest extent. The PCE did not reach its greatest extent until a later time because it is retarded slightly relative to TCM and TCE due to sorption. During the dissolution experiment, the TCM plume is diminished in concentration and extent as a result of preferential dissolution. The TCE plume also showed a notable decline in concentration. The PCE plume remained relatively consistent during the experiment.

7.5.2 Magnitude of Aqueous Concentrations

The initial effective solubilities of TCM, TCE and PCE are 1,030,000 µg/L, 590,000 µg/L and 110,000 µg/L, respectively, based on the initial NAPL source composition and Raoult's Law. These calculations are shown also in Table 7-1. Aqueous concentrations approaching the initial effective solubility values were observed only in a small number of monitoring points directly downgradient from the central portion of the source zone. Concentrations were lower around the margin of the source zone. Figure 7-11 shows the aqueous concentrations at monitoring point FR-5-7 located in the upper portion of the plume. Peak concentrations of TCM, TCE and PCE were 800,000 µg/L, 670,000 µg/L and 120,000 µg/L, respectively, and compare reasonably well with the calculated initial effective solubilities. This observation supports further the applicability of Raoult's Law for mixtures of chlorinated solvents.

7.5.3 Temporal Changes in Aqueous Concentrations

Aqueous concentrations measured at the arrays varied with time in response to preferential dissolution of the more soluble components of the

NAPL source, and in response to fluctuations in groundwater flow conditions in the test cell. At monitoring point FR-5-7 in the centre of the plumes, TCM and TCE reached their initial input concentrations at about 50 days and PCE reached its initial input concentration at about 75 days. TCE and PCE concentrations remained relatively constant during the remainder of the experiment. TCM concentrations declined markedly from 130 days to 220 days in response to depletion of TCM in the source. This monitoring point was not influenced by fluctuations in the water table or groundwater flow directions. A substantial change in water table elevation occurred at about 140 days (see Figure 7-5), but is not evidenced in the TCE or PCE concentrations.

Monitoring point FR-5-5 (see Figure 7-12) was located in the upper portion of the plumes. Initial input concentrations for TCM and TCE were reached in about 40 days and for PCE at about 60 days. TCM concentrations declined from 60 days to 100 days, likely in response to depletion of the source. However, concentrations of TCM, TCE and PCE all declined from 100 days to 130 days when the water table reached its lowest level. At this time the NAPL zone was likely within the capillary fringe. When the water table rose abruptly at 140 days, concentrations of TCM, TCE and PCE increased.

Monitoring point FR-5-9 (see Figure 7-13) was located in the lower portion of the plumes. After reaching initial input concentration, TCE and PCE concentrations remained steady until 140 days. From 60 days to 140 days TCM concentrations declined, likely due to depletion of the source. However, when the water table rose abruptly at 140 days, concentrations of TCE and PCE declined abruptly. Other monitoring points exhibited similar fluctuations.

7.5.4 Averaged Aqueous Concentrations

Further evaluation of the temporal variation in aqueous concentrations and ratios caused by dissolution was performed on values averaged over the monitoring points in each array. The primary purpose of the averaging was to minimize the effect of temporal variations in aqueous concentrations caused by changes in groundwater flow direction. In addition, aqueous concentrations averaged vertically over all the monitoring points in an array is likely a reasonable approximation of the results that would be obtained from a conventional monitoring well with a intake of moderate length (i.e. several metres).

The monitoring point arrays that exhibited the highest concentrations are FR-6, FR-5 and FR-4. The temporal variations in concentration for these arrays are shown in Figures 7-14, 7-15 and 7-16, respectively. In each case, after initial input concentrations were achieved, TCE and PCE remained relatively constant and TCM declined markedly. Such trends are difficult to discern for arrays FR-7 and FR-3 at the lateral margins of the plumes as shown in Figures 7-17 and 7-18.

Full area-averaged aqueous concentrations for the test cell are provided by the analyses of the effluent from the extraction wells. The results for the cell effluent are shown in Figure 7-19. The cell effluent shows the same trends as arrays FR-6, FR-5 and FR-4 in the central portions of the plumes.

7.6 Determination of NAPL Mass Remaining

The quantity of NAPL mass remaining in the source zone was determined by the difference between the initial mass and the mass removed by the extraction wells. The chemical mass flux for the cell effluent is shown in Figure 7-20. The initial mass flux for TCM reached about 8 g/day and declined steadily as TCM was depleted from the NAPL source. The mass flux

for TCE remained between 4 g/day and 7 g/day. The mass flux for PCE remained between 1 g/day and 2 g/day.

The cumulative chemical mass removed from the cell was calculated from the mass flux values. The decline in NAPL mass remaining versus time is shown in Figure 7-21. The plot of NAPL mass remaining versus time is used Section 7.7 and 7.8 to evaluate the relationship between aqueous concentration ratios and the NAPL mass remaining.

7.7 Temporal Variation in Aqueous Concentration Ratios

The fluctuations in the water table and resultant shifts in position of the aqueous-phase plumes make it difficult to evaluate trends in aqueous concentrations and concentrations ratios at individual monitoring points and at sampler bundles that do not intersect the plumes continually. The most consistent aqueous concentration-time data are derived from the cell effluent and from arrays FR-6, FR-5 and FR-4.

The temporal variation in aqueous concentration ratios for the cell effluent are shown in Figure 7-22. After initial input concentrations are achieved after 50 days, the TCE/TCM and PCE/TCM ratios increased gradually as TCM was dissolved preferentially. PCE/TCE ratios remained relatively constant during the experiment.

These trends in aqueous concentration ratios are those expected for the preferential dissolution of TCM and then TCE from the NAPL source zone. In this controlled field experiment, the change in NAPL mass remaining with time is known from the cell effluent data, and aqueous concentration ratios can be plotted versus NAPL remaining in the manner shown in Chapters 4, 5 and 6. These data are shown in Figure 7-23. In this case, the rate of dissolution of the NAPL source is relatively constant (see Figure 7-21) so that the plot of ratios versus NAPL remaining is similar to the plot of ratios versus time.

Similar plots of aqueous concentration ratios at monitoring arrays FR-6, FR-5 and FR-4 are shown in Figures 7-24, 7-25, 7-26, 7-27, 7-28 and 7-29. These figures show the same consistent increases in TCE/TCM and PCE/TCM ratios as those for the cell effluent. Similar trends are observed in small number of individual monitoring points. Plots of aqueous concentration ratios at monitoring point FR-5-7, FR-5-5 and FR-5-9 are shown in Figures 7-30, 7-31, 7-32, 7-33, 7-34 and 7-35. The consistency of the trends in these data are favourable for comparison to predictions by the ESM.

At monitoring arrays which did not intersect the plumes continually, and at most individual monitoring points, the temporal variation in aqueous concentrations ratios are erratic. Plots of aqueous concentration ratios at monitoring arrays FR-7 and FR-3 are shown in Figures 7-36, 7-37, 7-38 and 7-39. Although these figures show a general increase in TCE/TCM and PCE/TCM ratios, the magnitude of the fluctuations is sufficiently large to preclude comparison of these curves to the predictions of the ESM.

7.8 Comparison of Measured Ratios to ESM

The ESM was used to simulate the changes in aqueous concentration ratios for the dissolution of the NAPL in the FR source zone. The composition of the NAPL and the properties of the components used as input parameters to the ESM are shown in Table 7-2. The aquifer was specified to have a dry bulk density of 1,809 kg/m^3, at total porosity of 0.33 and a fraction organic carbon (f_{OC}) of 0.0002. The initial NAPL content was specified to be 20 L/m^3. Using these parameters values, simulations were performed for 1-cell, 2-cell and 5-cell configurations. The number of cells is the only model input parameter not defined explicitly by the NAPL and aquifer properties.

TCE/TCM, PCE/TCM and PCE/TCE ratios versus NAPL mass remaining predicted by the ESM are shown in Figures 7-40, 7-41 and 7-42, respectively. The predicted ratios were compared to those site monitoring

data that exhibited discernible trends in aqueous concentrations with time. The predicted ratios are compared to the measured ratios for the cell effluent in Figures 7-43, 7-44 and 7-45; for monitoring array FR-6 in Figures 7-46, 7-47 and 7-48; for monitoring array FR-5 in Figures 7-49, 7-50 and 7-51; for monitoring array FR-4 in Figures 7-52, 7-53 and 7-54; and, for monitoring point FR-5-7 in Figures 7-55, 7-56 and 7-57.

The changes in TCE/TCM and PCE/TCM ratios predicted by the ESM compare well with the measured ratios for the cell effluent, monitoring array FR-5 and monitoring point FR-5-7. For the cell effluent and FR-5, the best match between the predicted and measured ratios is provided by the 1-cell configuration of the ESM. This suggests that the size and character of the NAPL zone is not sufficient to cause a chromatographic effect as aqueous-phase solvents exchange with the NAPL present in downgradient portions of the source zone. However, the best match between the predicted and measured ratios for individual point FR-5-7 is provided by the 5-cell configuration of the ESM. This suggests that the character of the NAPL zone upgradient from this specific monitoring point is sufficient to cause a chromatographic effect on the aqueous concentrations emitted from the source zone, but overall, there is little chromatographic effect on the whole plume.

There is a larger degree of scatter in the TCE/TCM and PCE/TCM ratio data from monitoring arrays FR-6 and FR-4 and although trends are comparable to the cell effluent, FR-5 and FR-5-7, it is not possible to match the measured data well with the results of a particular ESM configuration.

It is difficult also to compare the measured PCE/TCE ratios to those predicted by the ESM simulations because the PCE/TCE ratios change by only a factor of 3 times or less during the experiment. The degree of scatter in the PCE/TCE ratios due to analytical variations and fluctuations in groundwater flow is sufficiently large to mask any trends. In contrast, the measured

TCE/TCM and PCE/TCM ratios change during the experiment by a factor of 10 times or more and this change is larger than the scatter in ratio data from analytical and hydrogeologic variations.

7.9 Conclusions Regarding Free-Release Experiment

The results of the Free-Release experiment indicate that the changes in aqueous concentration ratios measured during dissolution of the NAPL source can be predicted with reasonable accuracy using the ESM. This is the case despite the fact that the geometry of the NAPL source zone was complex and contained both residual NAPL and thin NAPL pools. This suggests that the dissolution behaviour of thin NAPL pools can be simulated by the ESM.

Area-averaged and vertically-averaged concentrations provide measured ratios that compared well with the simplest 1-cell configuration of the ESM. However, the ratios measured at a specific monitoring point required a 5-cell configuration of the ESM for the best match. If the 1-cell configuration were used to compare to the data from monitoring point FR-5-7 (see Figure 7-55), at the point where the measured TCE/TCM ratio reached 20, the ESM predicted the NAPL mass remaining to be about 0.68. In comparison, the true NAPL mass remaining was 0.77. This difference is relatively small given the much larger uncertainty in estimating the mass contained in NAPL source zones by direct soil sampling and analysis. This experiment does illustrate that the relationship between aqueous concentration ratios and NAPL remaining may be different at different locations for complex NAPL source zones.

A method for the comparison of field data to ESM simulations in order to select the most appropriate ESM configuration at a particular site is described in the following chapter.

Table 7-1. Calculation of initial effective solubilities of solvents based on initial NAPL source composition and Raoult's Law.

Measurement	TCM	TCE	PCE	Total
Pure-phase Solubility (µg/L)	8,700,000	1,400,000	240,000	
Volume in NAPL Source (L)	0.5	2.0	2.5	5.0
Mass in NAPL Source (g)	740	2,920	4,075	7,735
Weight % in NAPL	9.7	37.9	52.4	100
Mole Fraction in NAPL	0.119	0.420	0.461	1.00
Initial Effective Solubility (µg/L)	1,030,000	590,000	110,000	

Key:
TCM - Chloroform
TCE - Trichloroethylene
PCE - Tetrachloroethylene

Table 7-2. Composition and properties of the components in the NAPL in the source zone used as input parameters in the ESM simulations.

Parameter	TCM	TCE	PCE
Molecular Mass (g/mol)	119.4	131.5	165.8
Density (kg/m^3)	1,490	1,470	1,630
Pure-phase Solubility (µg/L)	8,700,000	1,400,000	240,000
K_{OC} (mL/g)	56	93	302
Composition (wt.%)	9.7	37.9	52.5

Key:
TCM - Chloroform
TCE - Trichloroethylene
PCE - Tetrachloroethylene

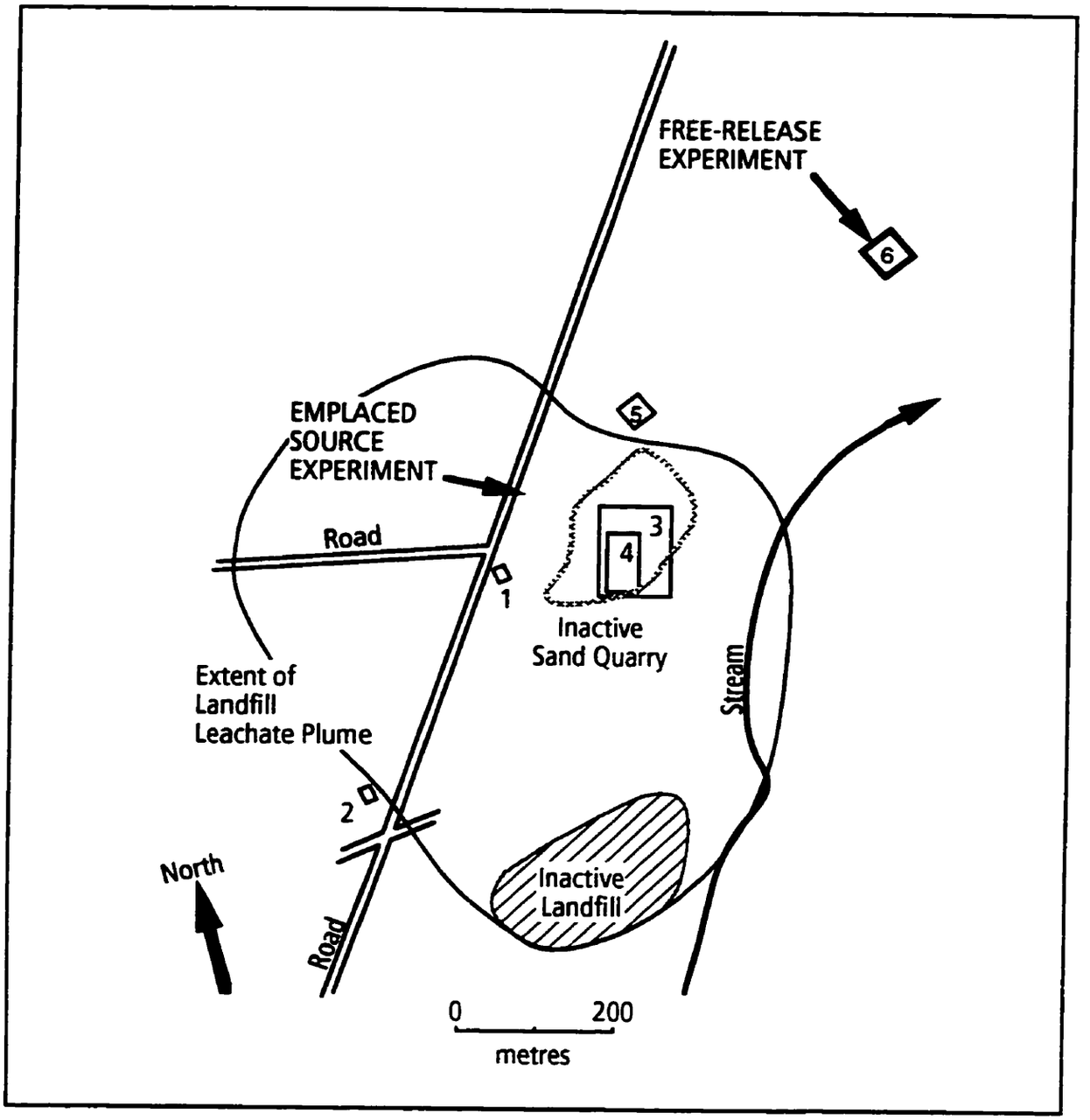

Figure 7-1. Location of the Free-Release experimental site at the Canadian Forces Base Borden.

Other experimental sites shown are:
1. Chloride transport - Sudicky et al., (1983)
2. Organics transport - Sutton and Barker, (1985)
3. Chlorinated solvents transport- Mackay et al., (1986)
4. BTEX transport - Patrick et al., (1986)
5. Vapor transport- Hughes et al. (1990)
6. DNAPL releases- Kueper et al. (1993), Brewster et al., (1995)

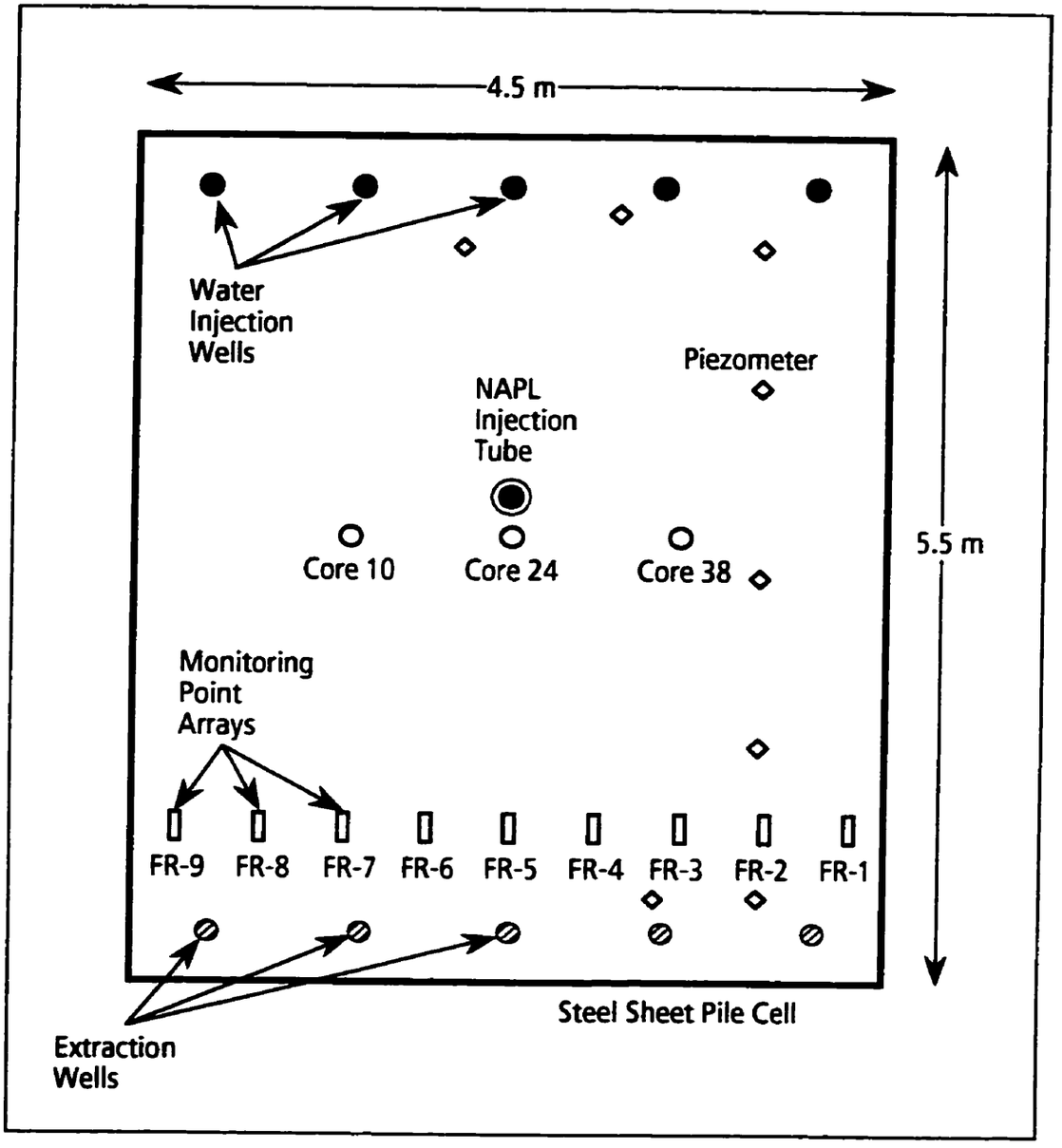

Figure 7-2. Plan map of test cell for the Free-Release Experiment.

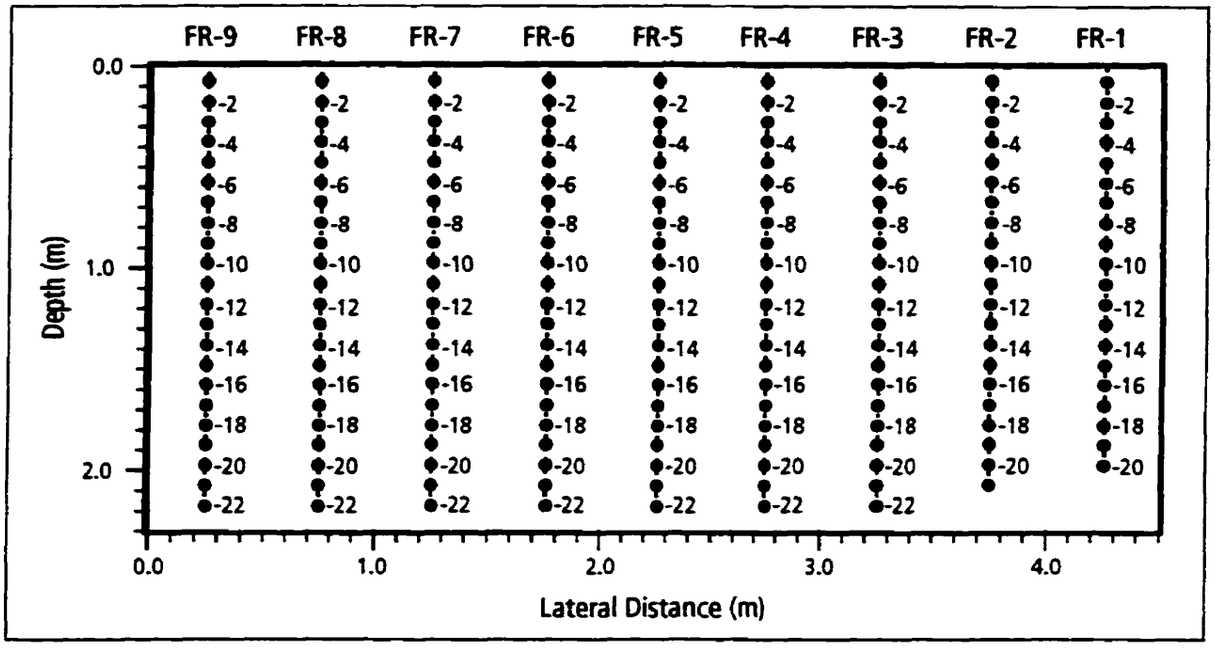

Figure 7-3. Section diagram of monitoring points located downgradient of the NAPL source zone.

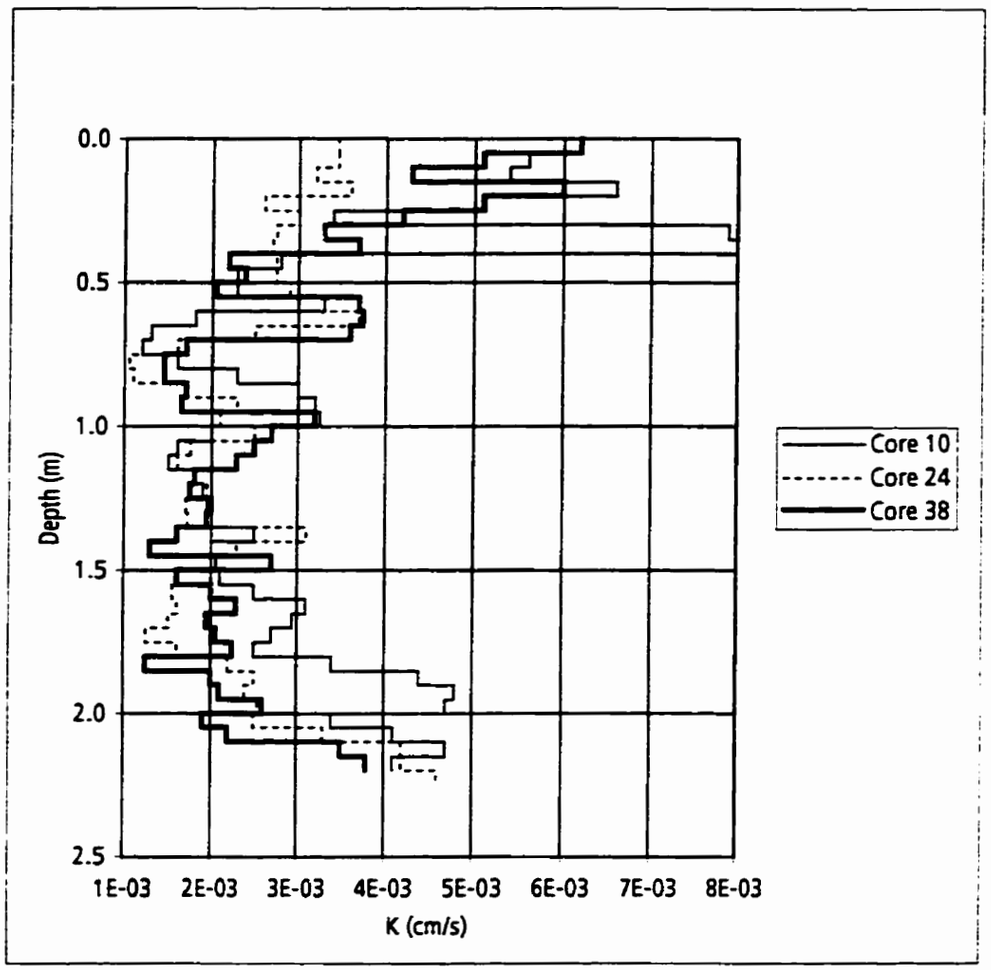

Figure 7-4. Hydraulic conductivity profiles for the aquifer inside the test cell.

Hydraulic conductivity determined in the laboratory
by falling-head permeameter.
Overall Average K= 2.8E-3 cm/s

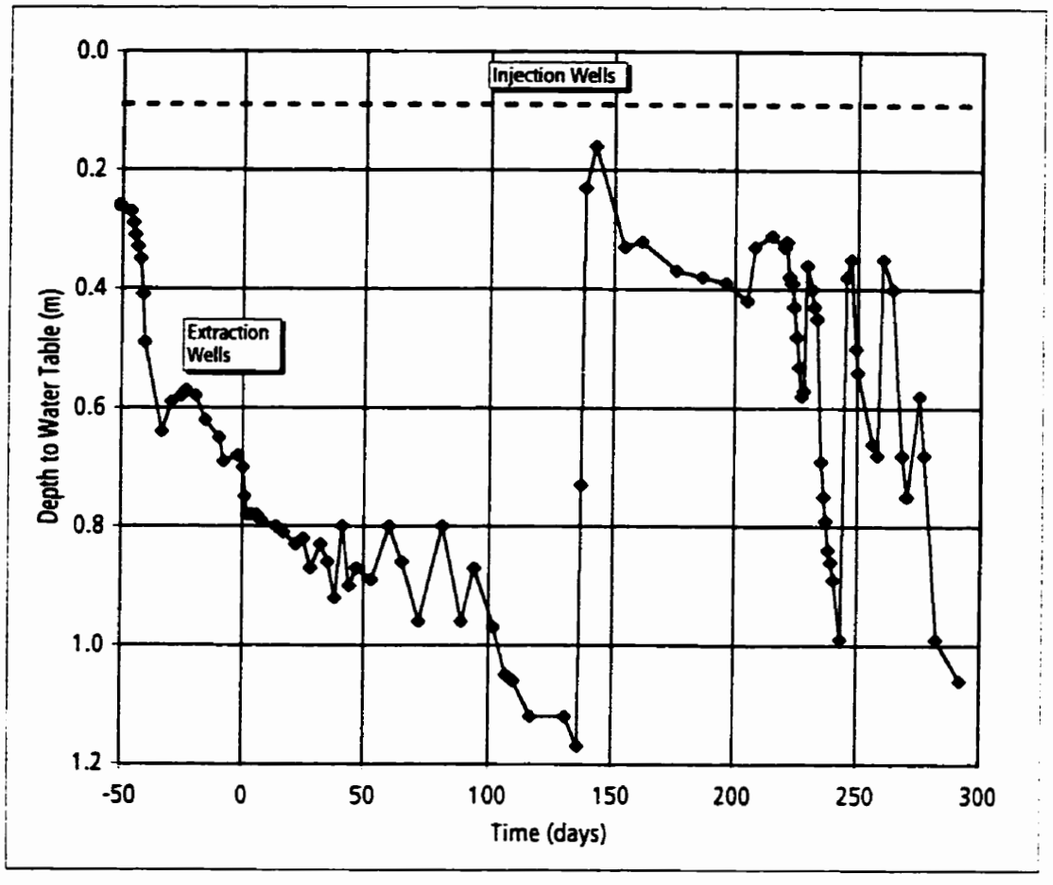

Figure 7-5. Temporal variation in water levels in the extraction wells and injection wells.

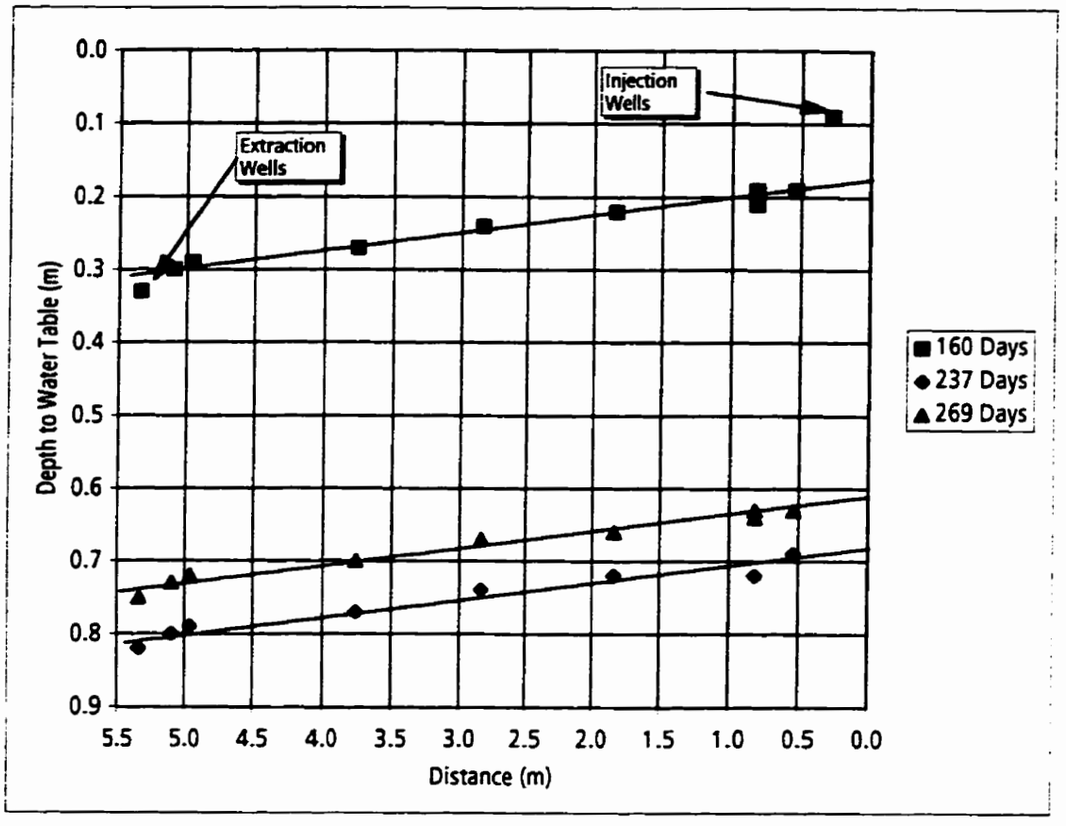

Figure 7-6. Slope of the water table along the test cell. Average hydraulic gradient is 0.023.

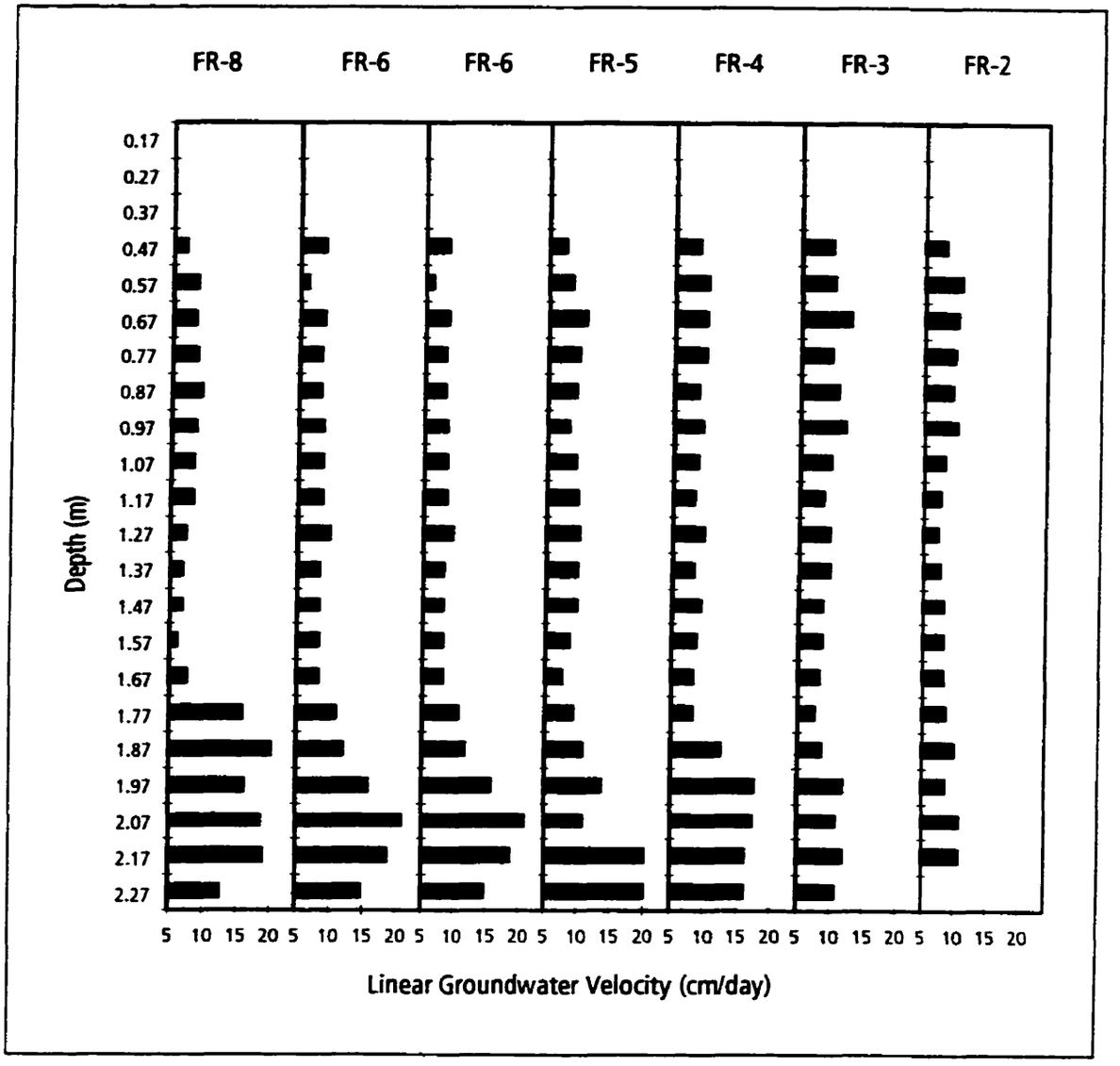

Figure 7-7. Vertical profiles of linear groundwater velocity determined from the arrival of chloride tracer at the monitoring points.

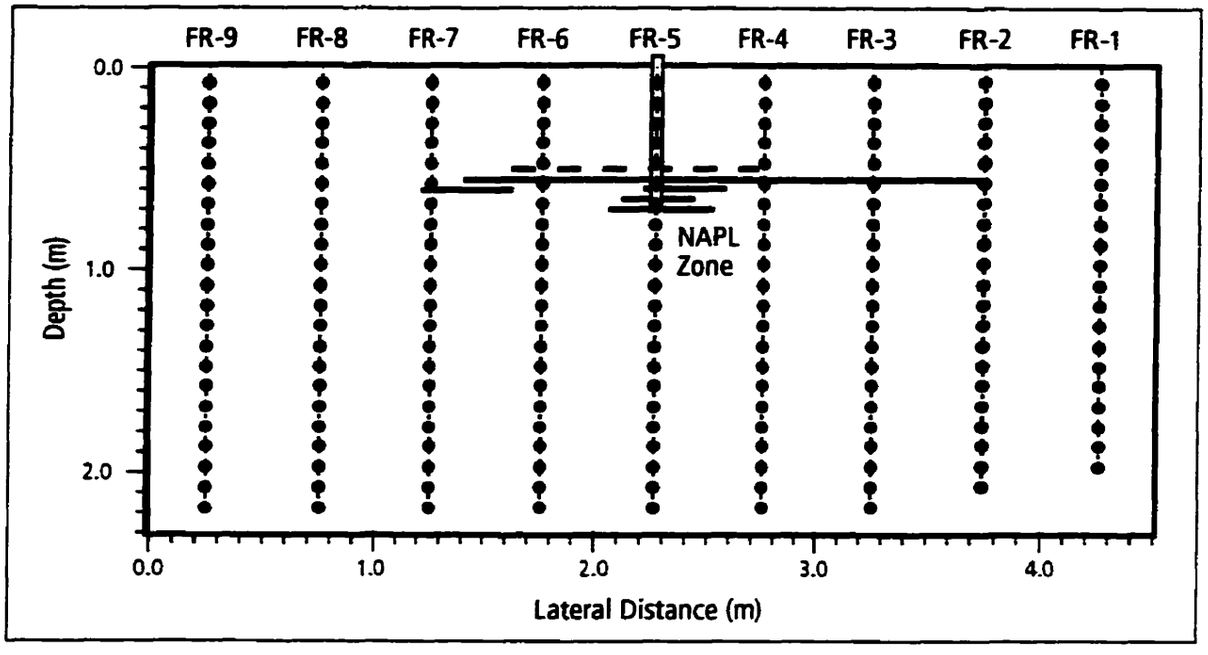

Figure 7-8. Section diagram showing configuration of the NAPL source zone.

Viewed looking upgradient from the monitoring points.

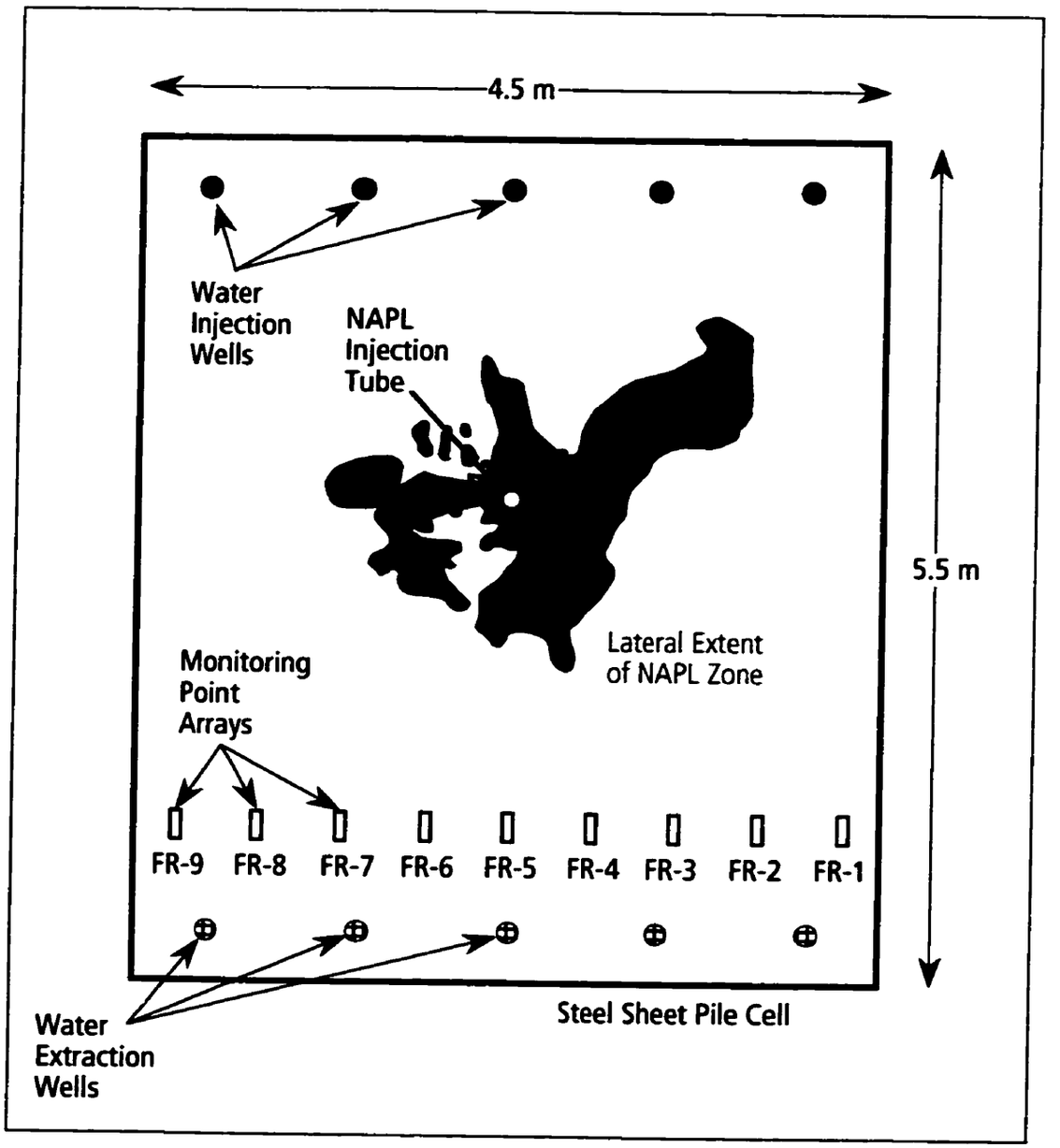

Figure 7-9. Plan map showing lateral extent of NAPL zone.

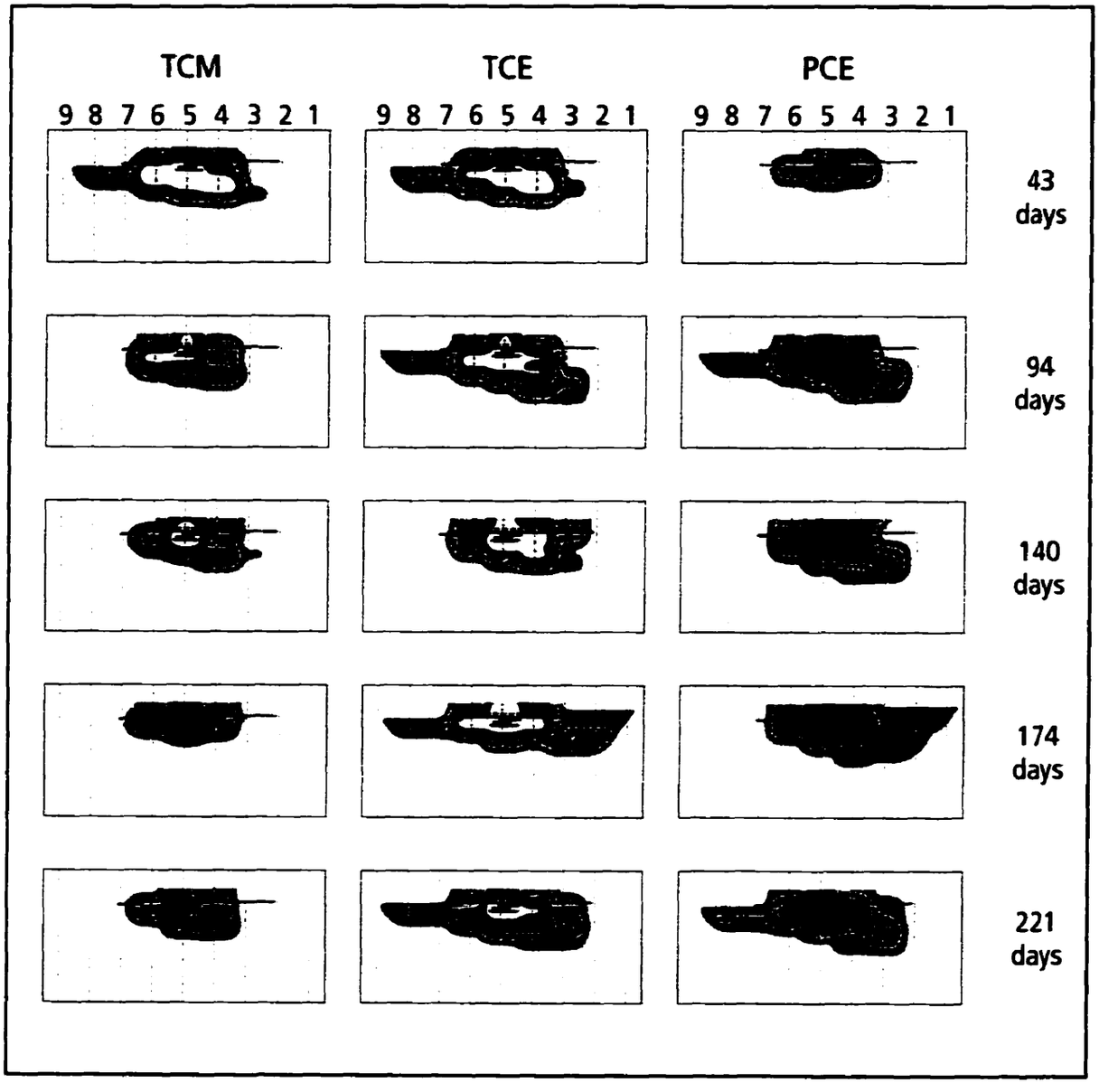

Figure 7-10. Aqueous-phase plumes in the monitoring arrays.

Cell cross-section is 4.5 m wide and 2.3 m deep.
Concentration contours are 1,000 µg/L, 10,000 µg/L, 100,000 µg/L and 300,000 µg/L for chloroform (TCM) and trichloroethylene (TCE); 1,000 µg/L, 10,000 µg/L and 30,000 µg/L for tetrachloroethylene (PCE).

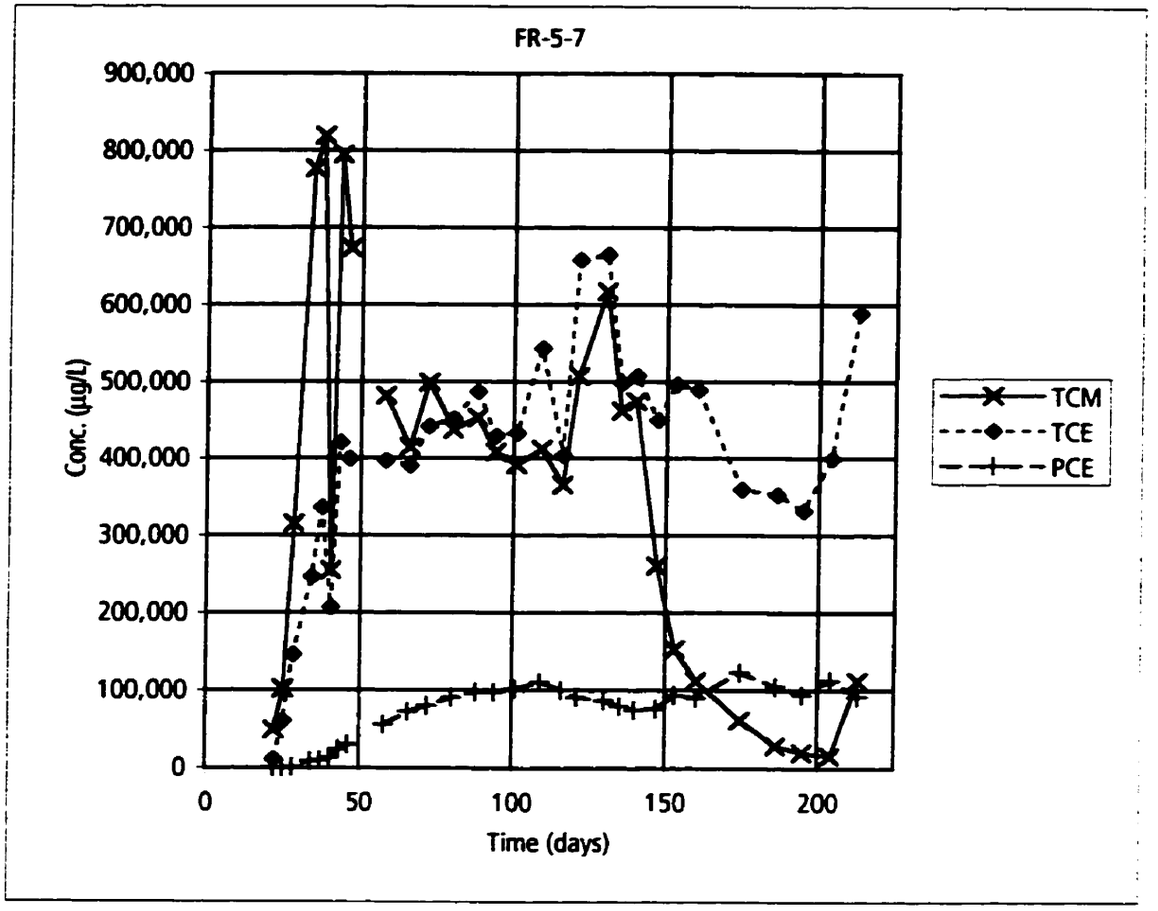

Key:
TCM - Chloroform
TCE- Trichloroethylene
PCE - Tetrachloroethylene

Figure 7-11. Temporal variation in aqueous concentrations at monitoring point FR-5-7.

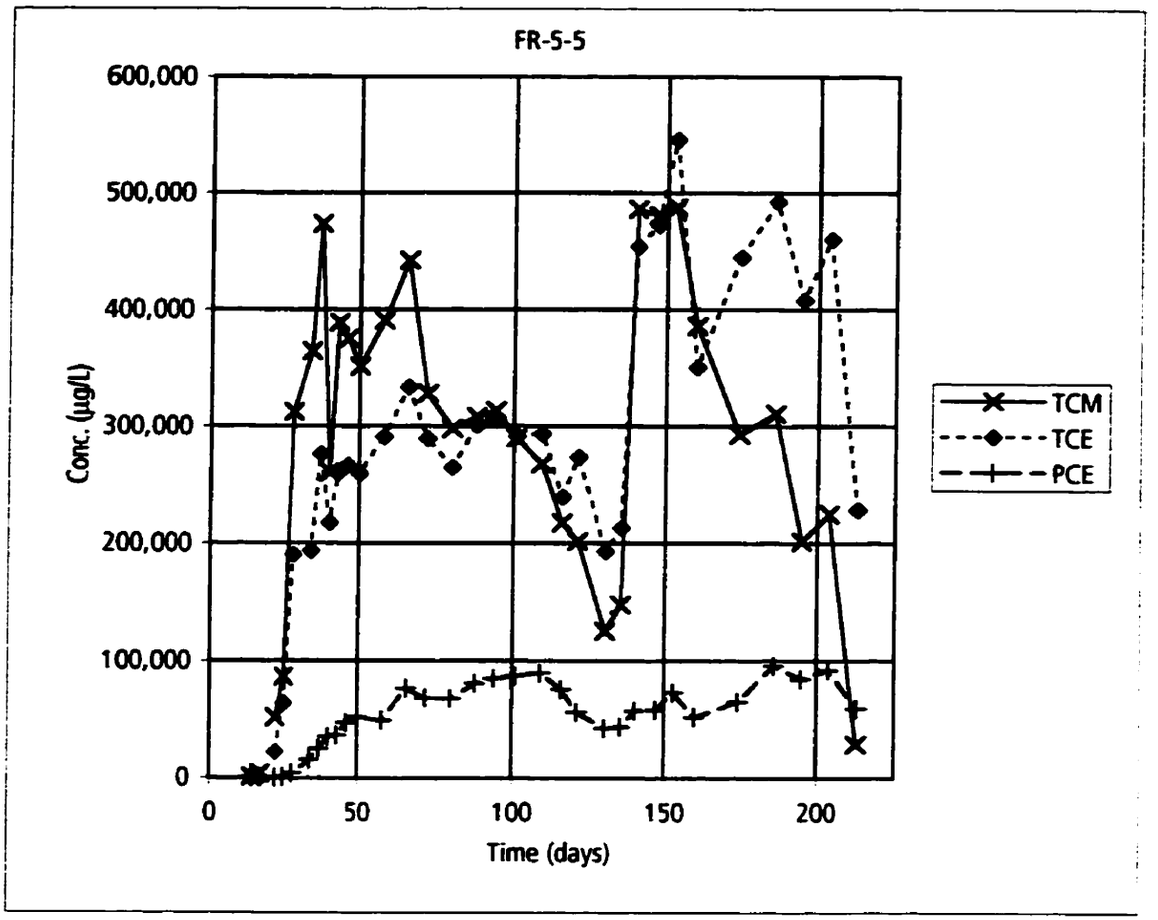

Key:
TCM - Chloroform
TCE- Trichloroethylene
PCE - Tetrachloroethylene

Figure 7-12. Temporal variation in aqueous concentrations at monitoring point FR-5-5.

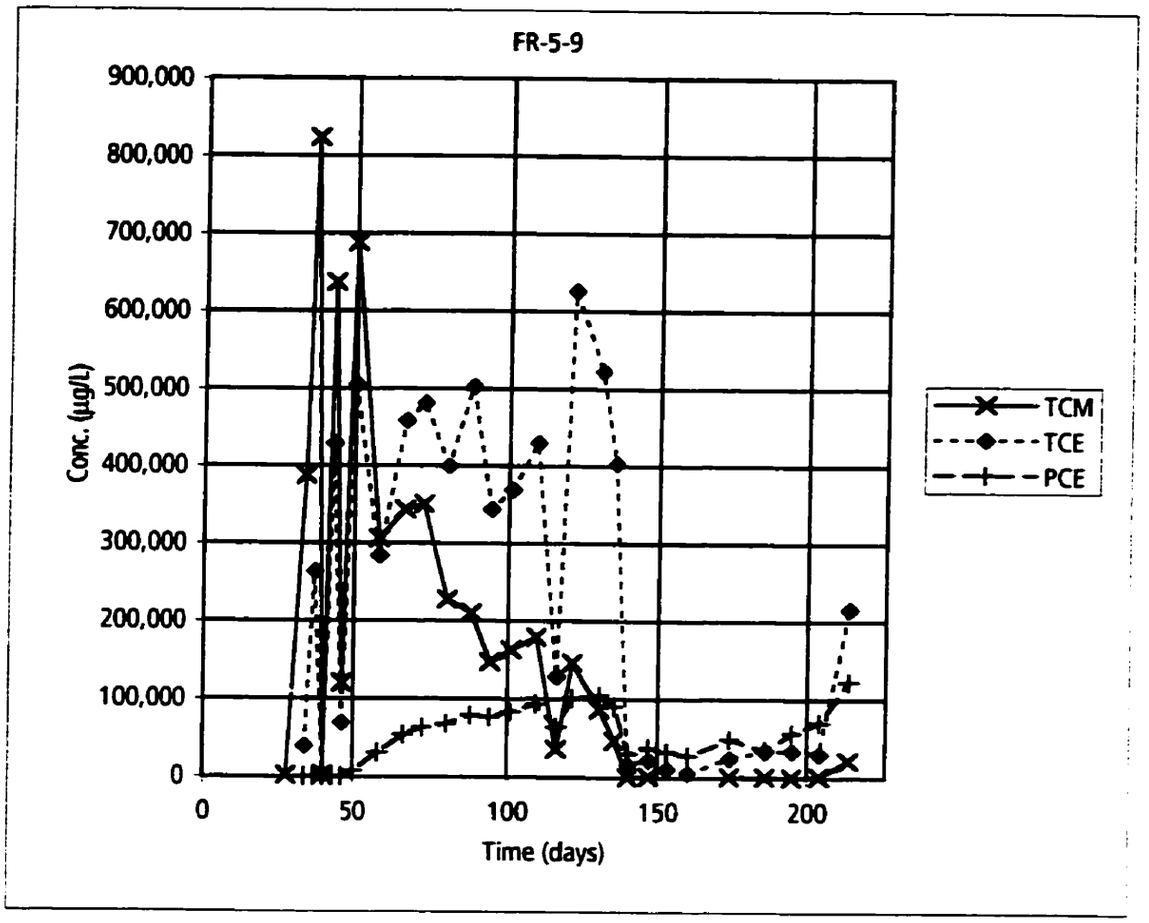

Key:
TCM - Chloroform
TCE- Trichloroethylene
PCE - Tetrachloroethylene

Figure 7-13. Temporal variation in aqueous concentrations at monitoring point FR-5-9.

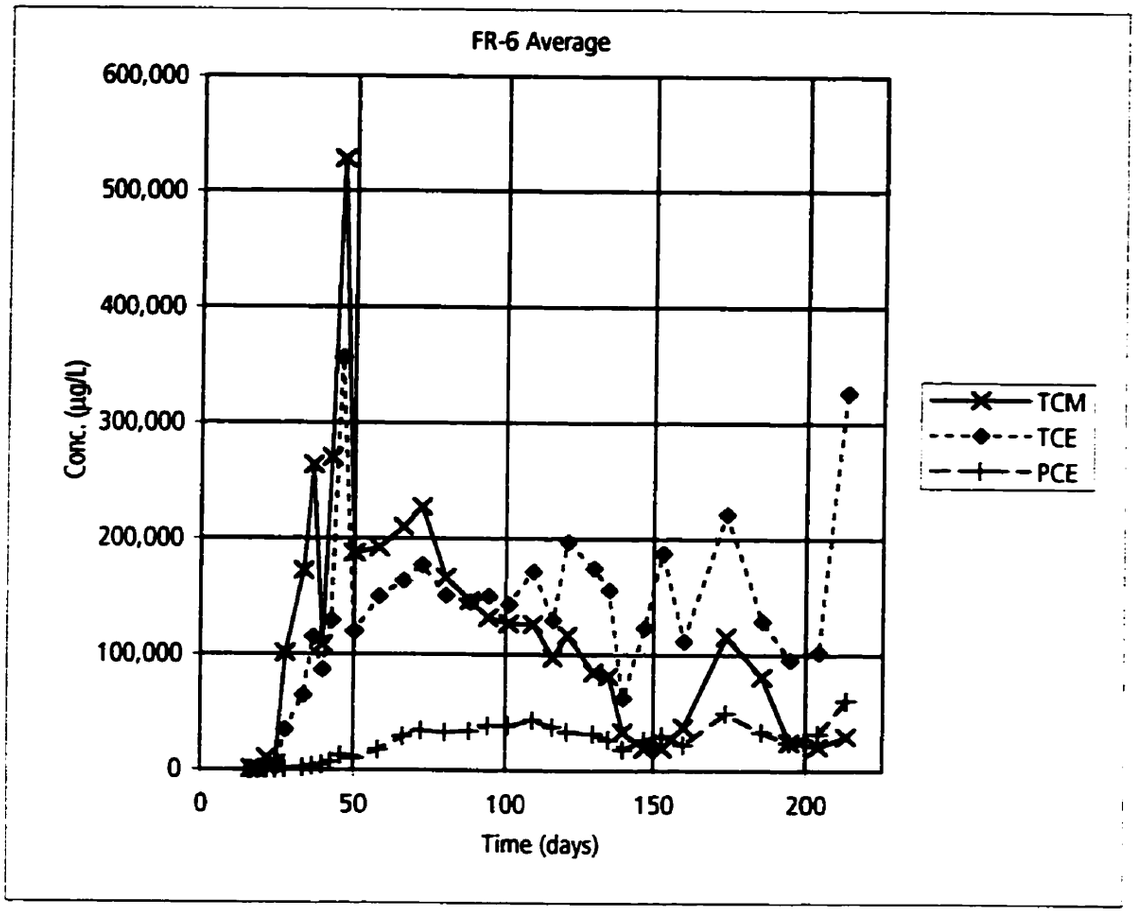

Key:
TCM - Chloroform
TCE- Trichloroethylene
PCE - Tetrachloroethylene

Figure 7-14. Temporal variation in aqueous concentrations averaged for monitoring location FR-6.

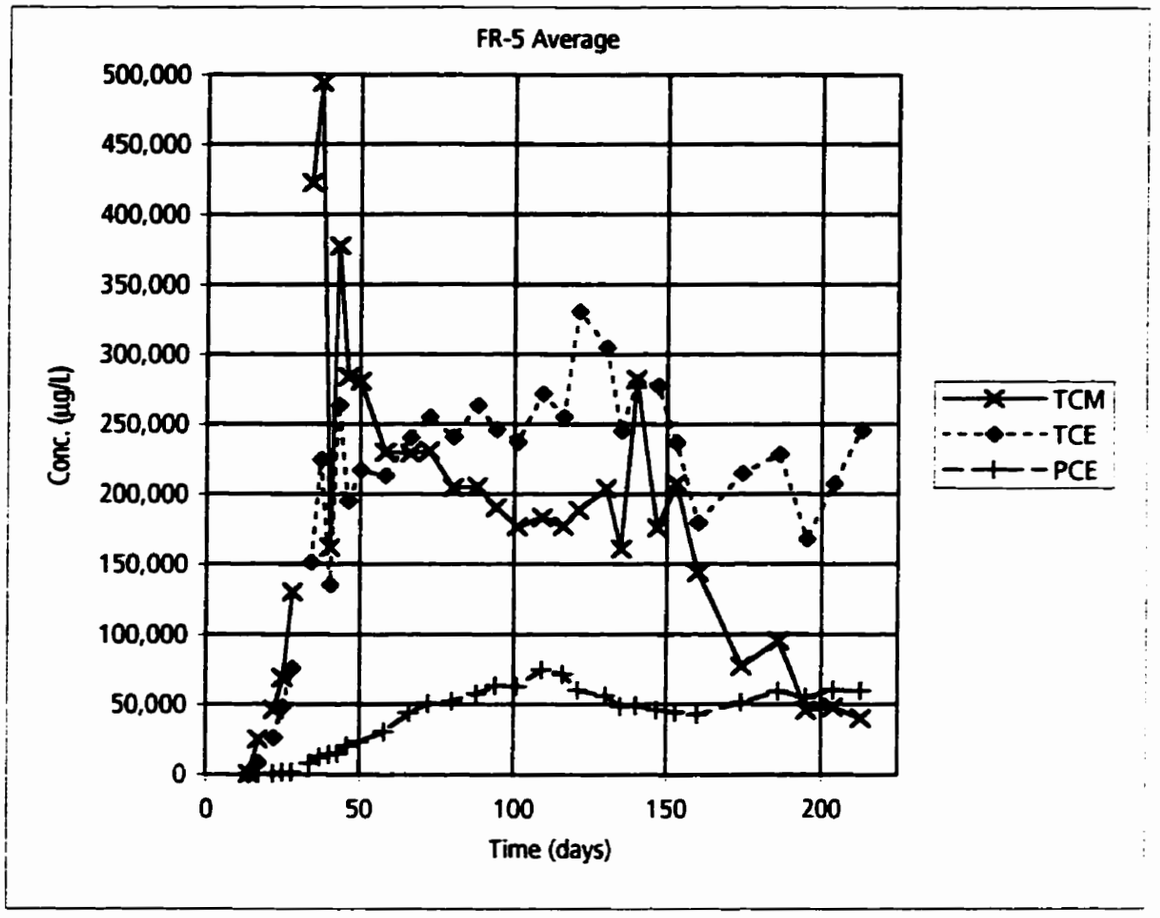

Key:
TCM - Chloroform
TCE- Trichloroethylene
PCE - Tetrachloroethylene

Figure 7-15. Temporal variation in aqueous concentrations averaged for monitoring location FR-5.

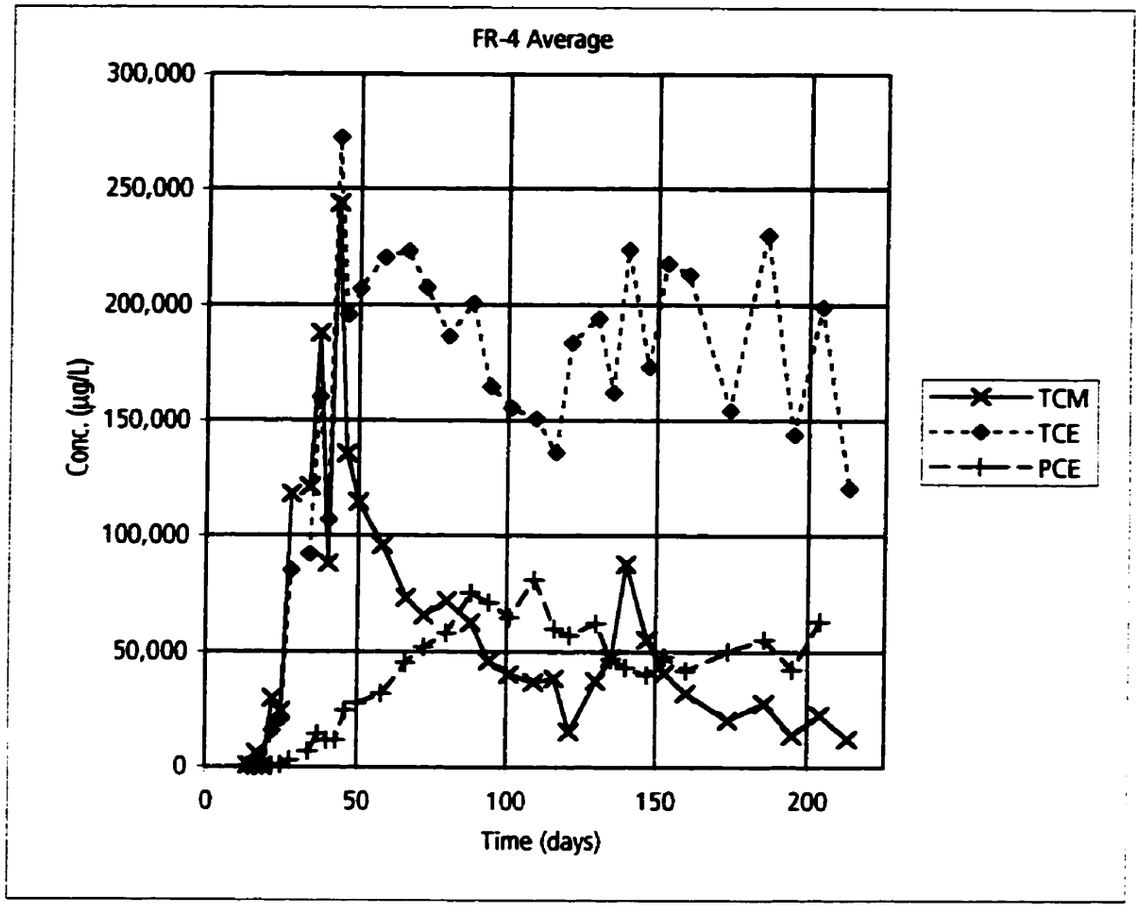

Key:
TCM - Chloroform
TCE- Trichloroethylene
PCE - Tetrachloroethylene

Figure 7-16. Temporal variation in aqueous concentrations averaged for monitoring location FR-4.

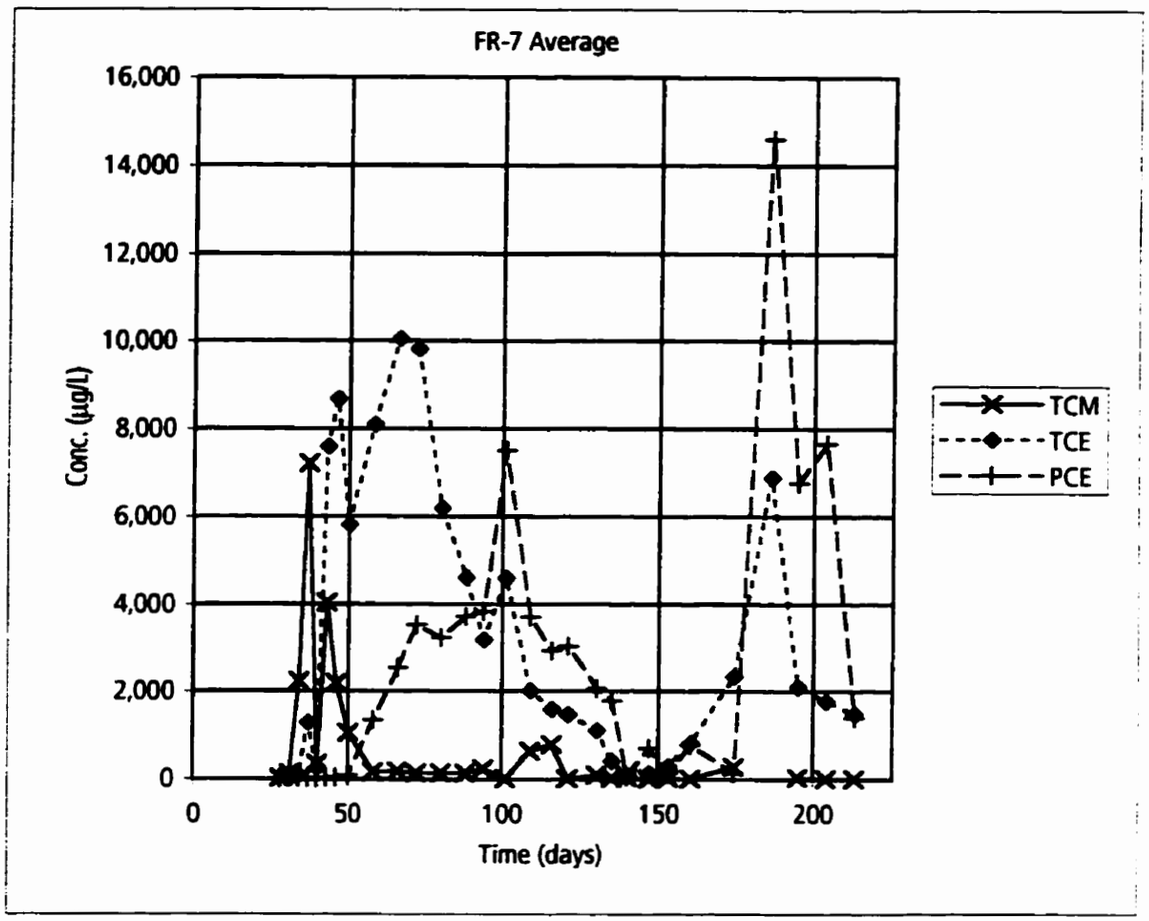

Key:
TCM - Chloroform
TCE- Trichloroethylene
PCE - Tetrachloroethylene

Figure 7-17. Temporal variation in aqueous concentrations averaged for monitoring location FR-7.

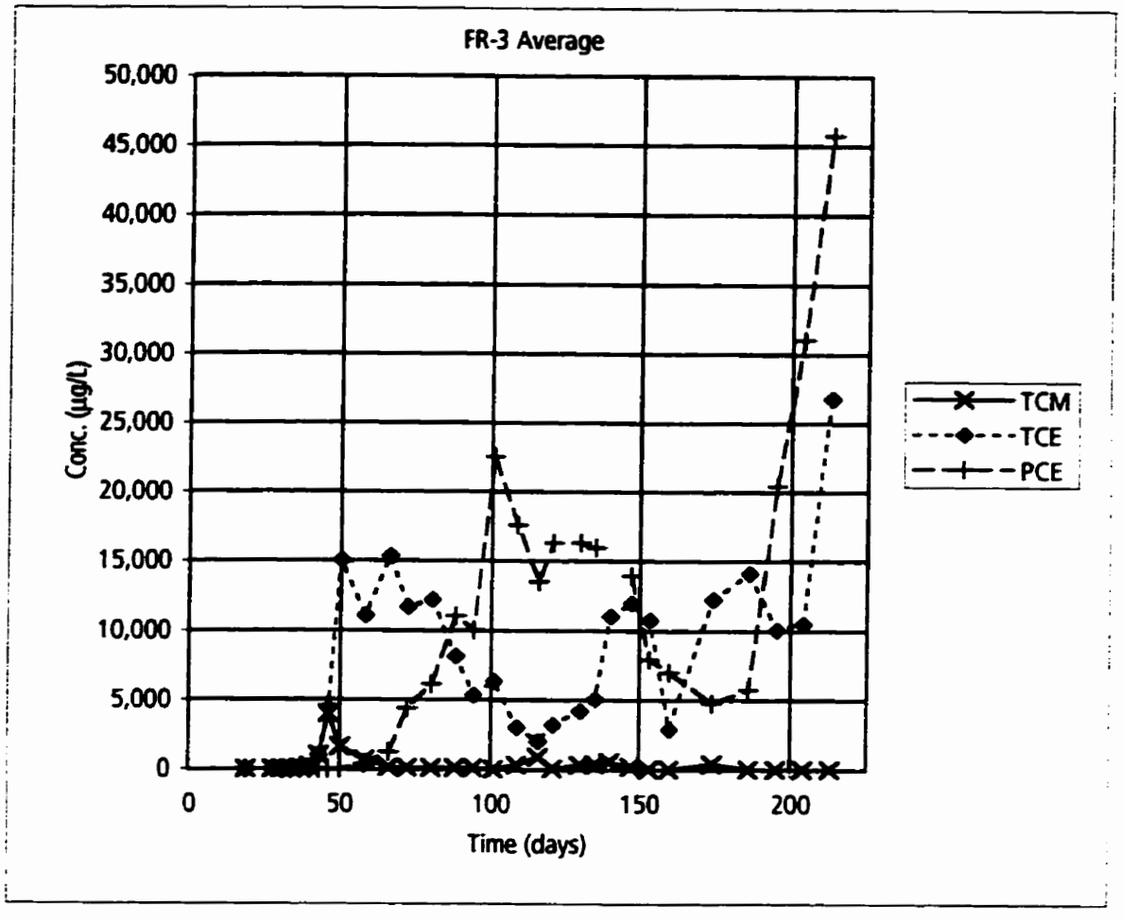

Key:
TCM - Chloroform
TCE- Trichloroethylene
PCE - Tetrachloroethylene

Figure 7-18. Temporal variation in aqueous concentrations averaged for monitoring location FR-3.

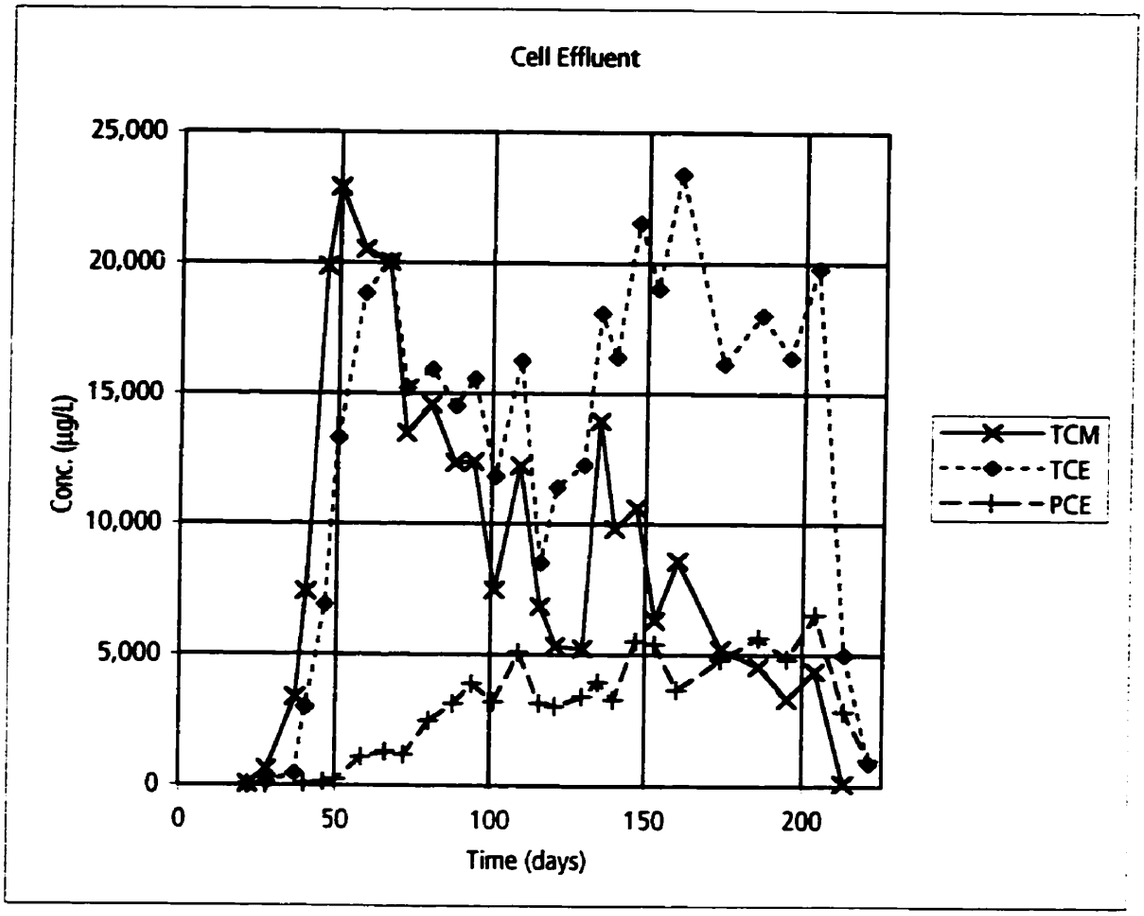

Key:
TCM - Chloroform
TCE - Trichloroethylene
PCE - Tetrachloroethylene

Figure 7-19. Temporal variation in aqueous concentrations in the effluent from the test cell.

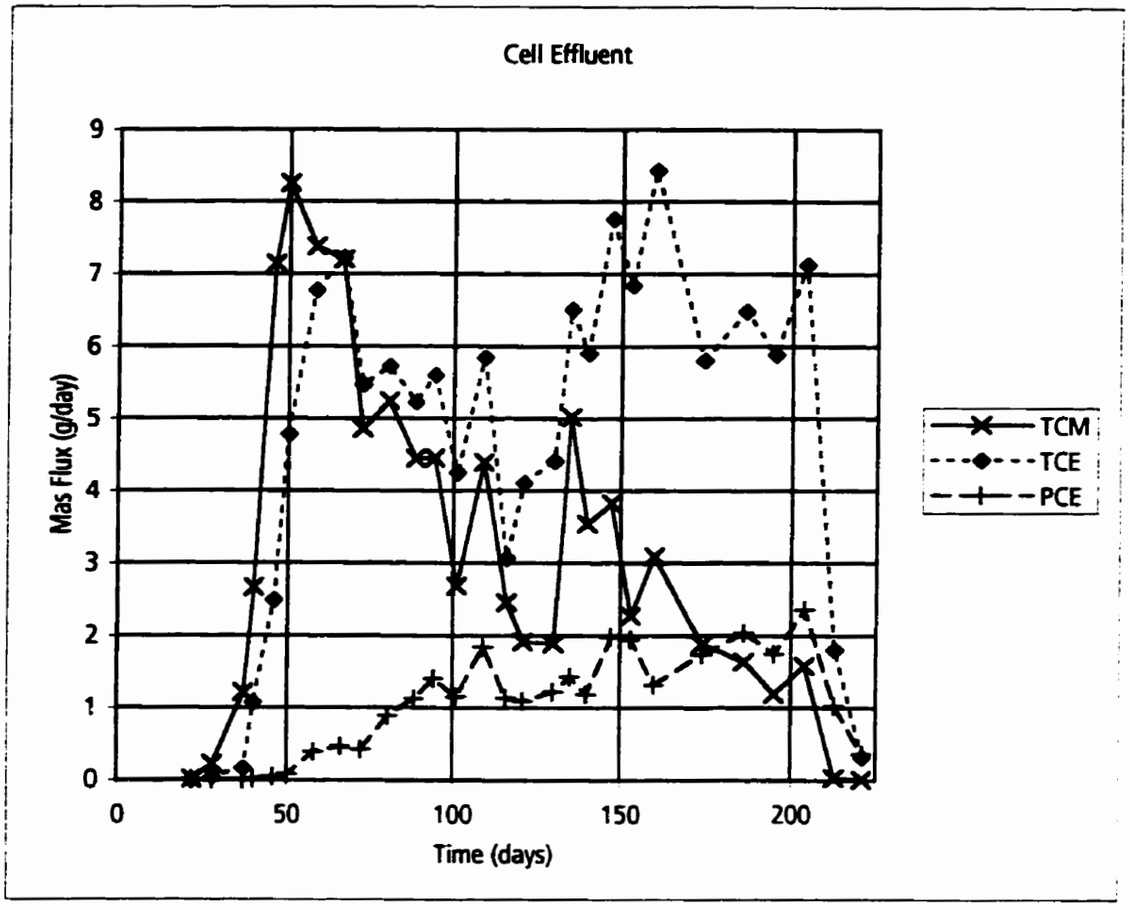

Key:
TCM - Chloroform
TCE - Trichloroethylene
PCE - Tetrachloroethylene

Figure 7-20. Temporal variation in chemical mass flux for the effluent from the test cell.

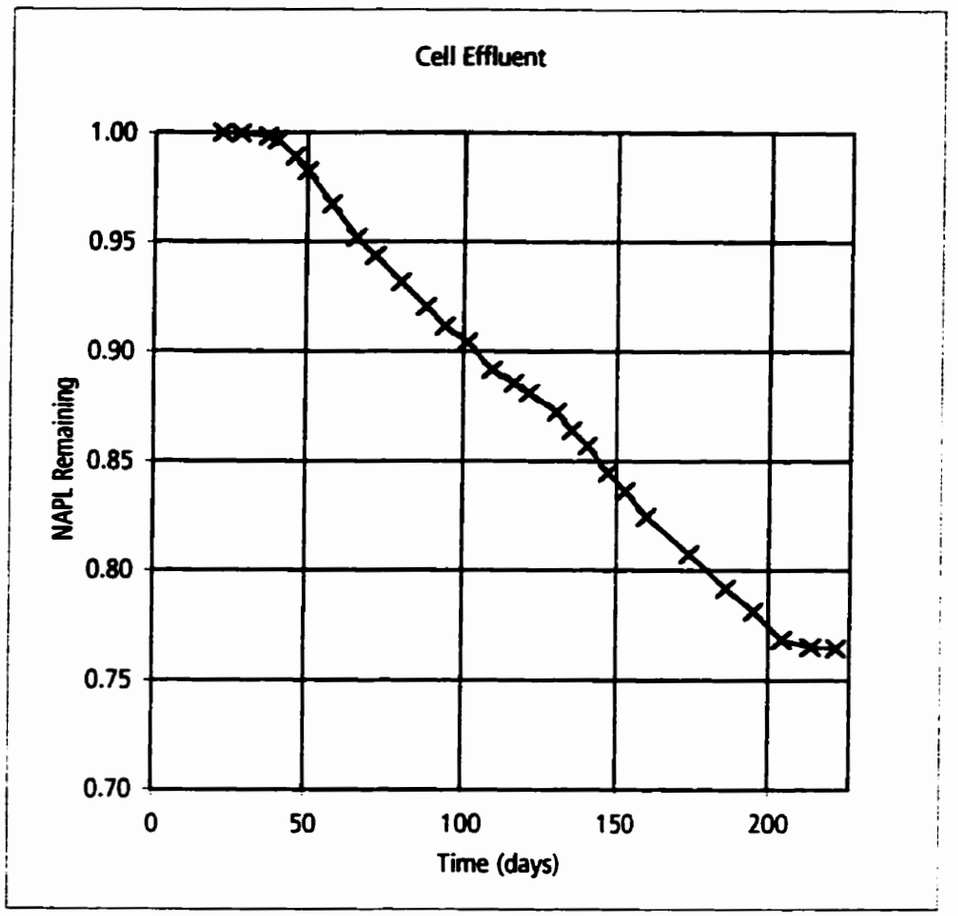

Figure 7-21. Temporal change in NAPL mass remaining based on mass removed in cell effluent.

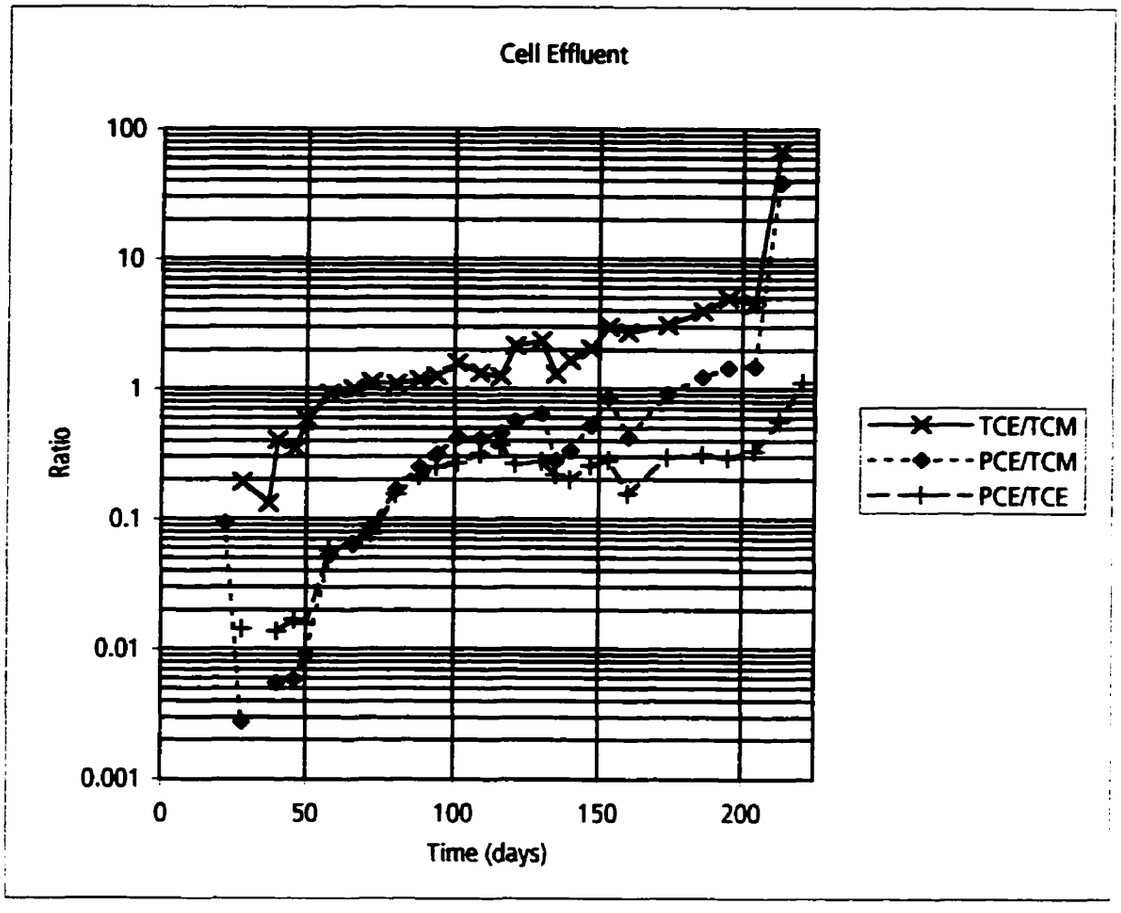

Key:
TCM - Chloroform
TCE - Trichloroethylene
PCE - Tetrachloroethylene

Figure 7-22. Temporal variation in aqueous concentration ratios for the effluent from the test cell.

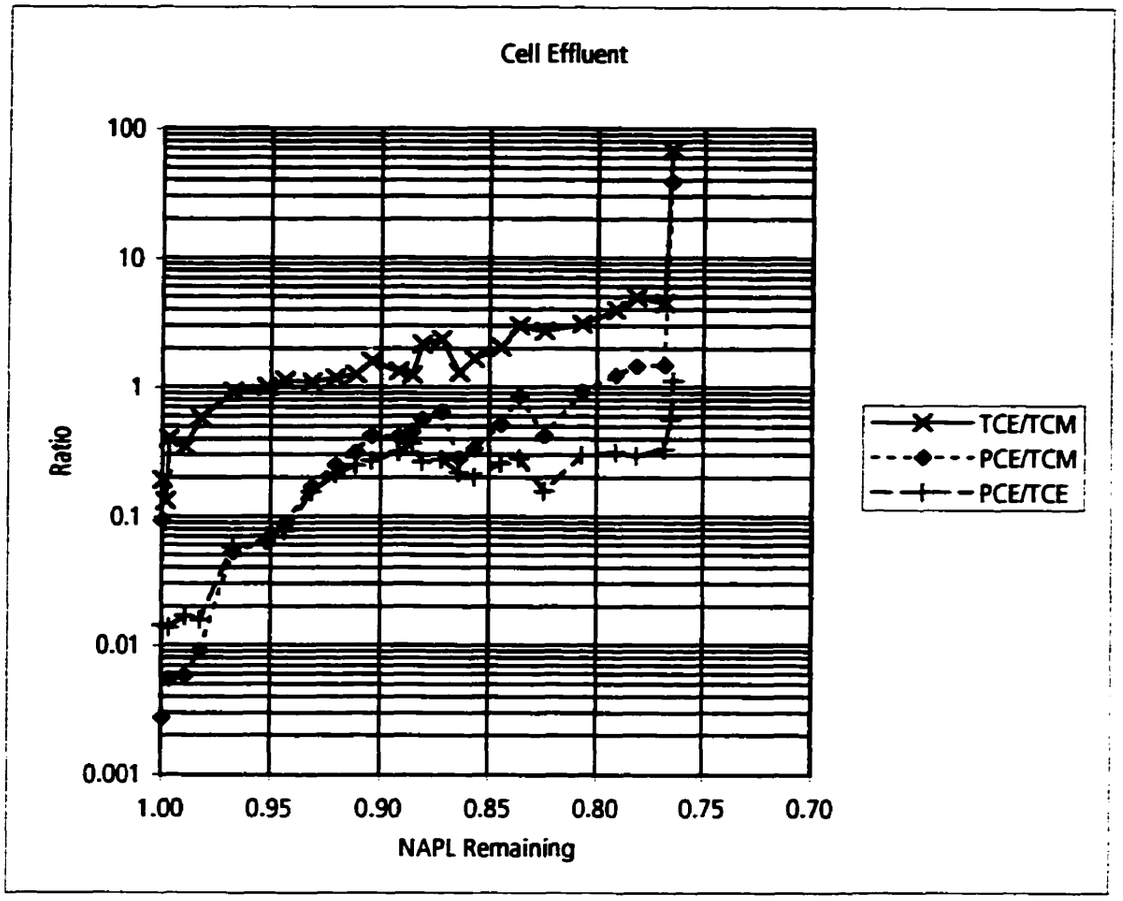

Key:
TCM - Chloroform
TCE - Trichloroethylene
PCE - Tetrachloroethylene

Figure 7-23. Change in aqueous concentration ratios versus NAPL remaining for the effluent from the test cell.

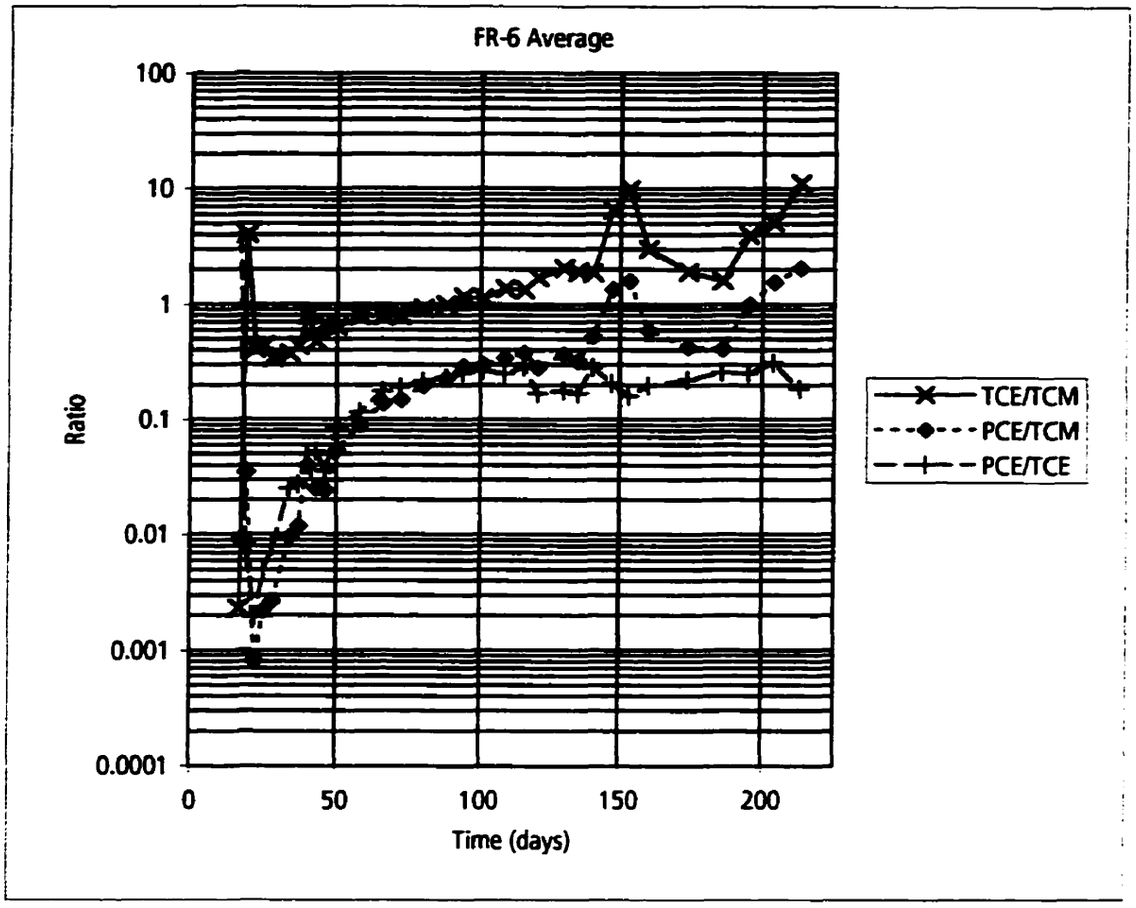

Key:
TCM - Chloroform
TCE- Trichloroethylene
PCE - Tetrachloroethylene

Figure 7-24. Temporal variation in aqueous concentration ratios averaged for monitoring location FR-6.

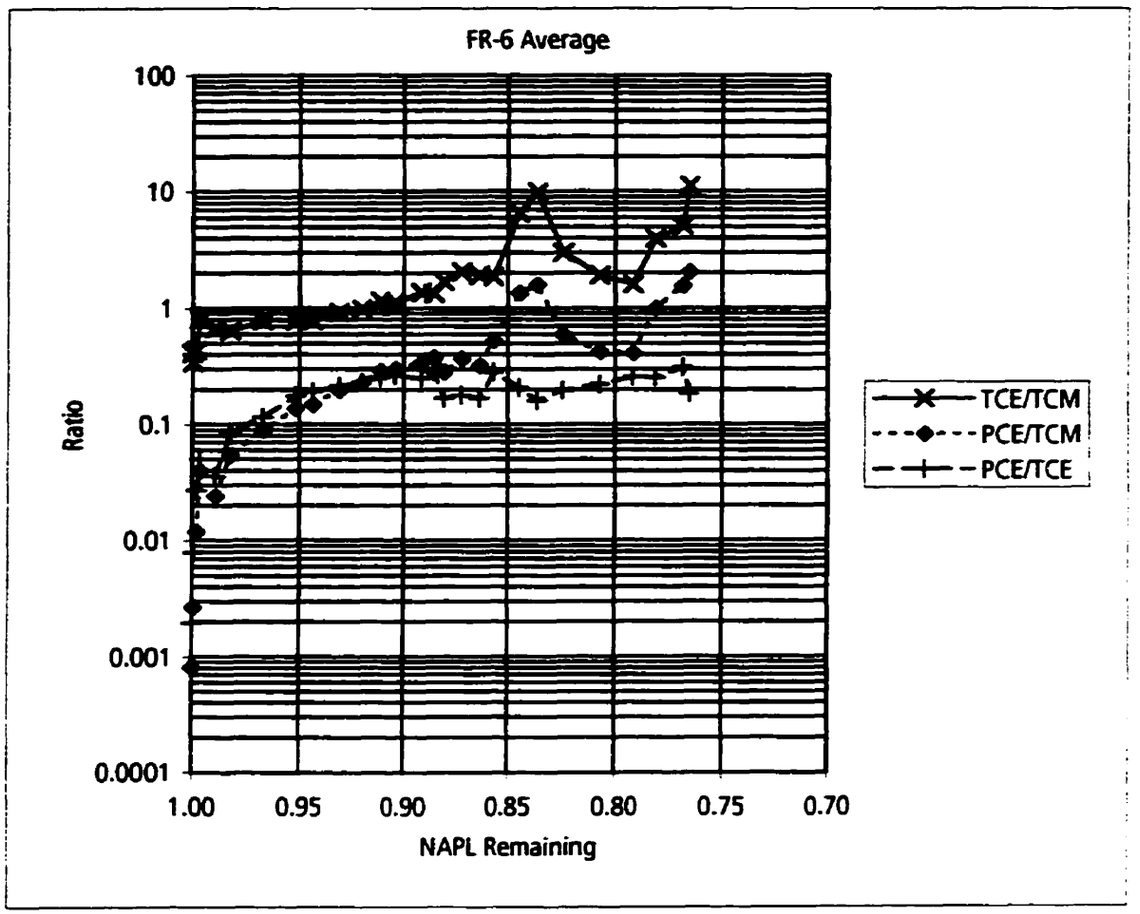

Key:
TCM - Chloroform
TCE- Trichloroethylene
PCE - Tetrachloroethylene

Figure 7-25. Change in aqueous concentration ratios versus NAPL remaining averaged for monitoring location FR-6.

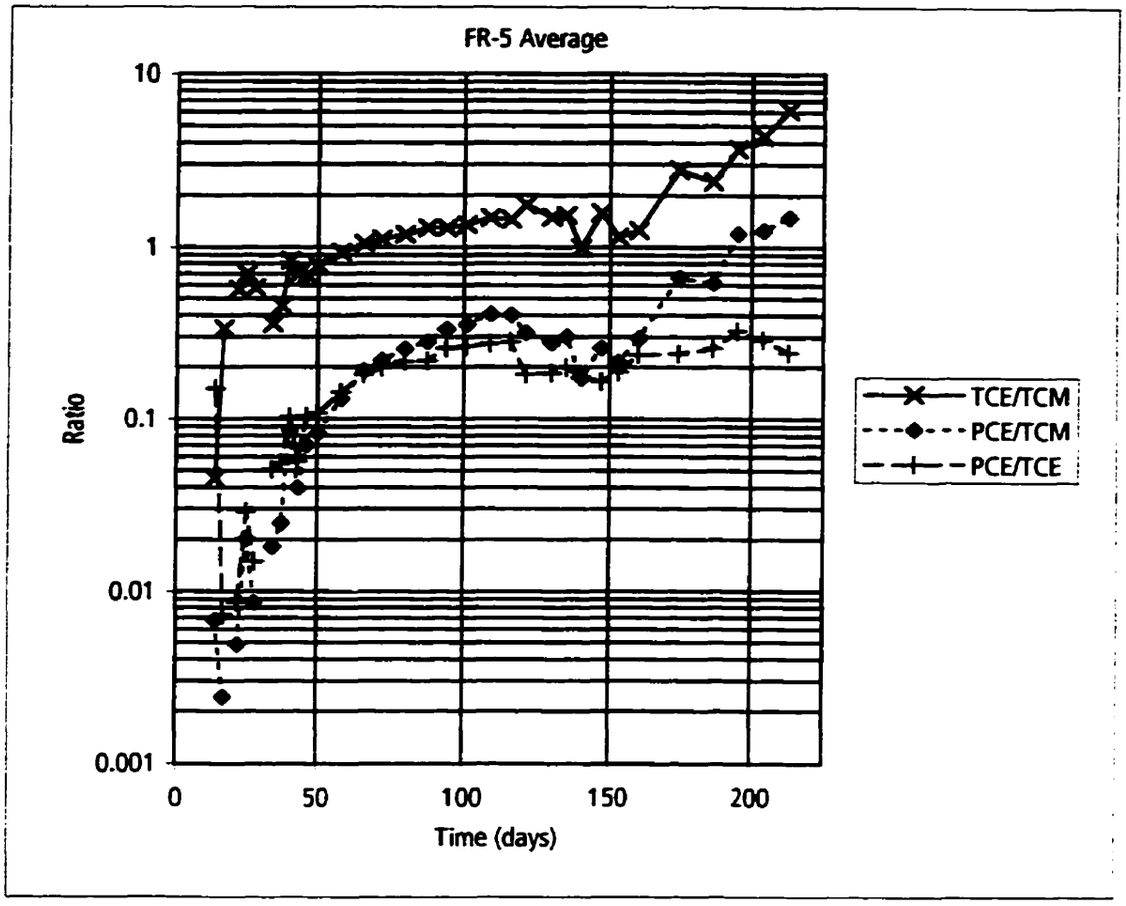

Key:
TCM - Chloroform
TCE- Trichloroethylene
PCE - Tetrachloroethylene

Figure 7-26. Temporal variation in aqueous concentration ratios averaged for monitoring location FR-5.

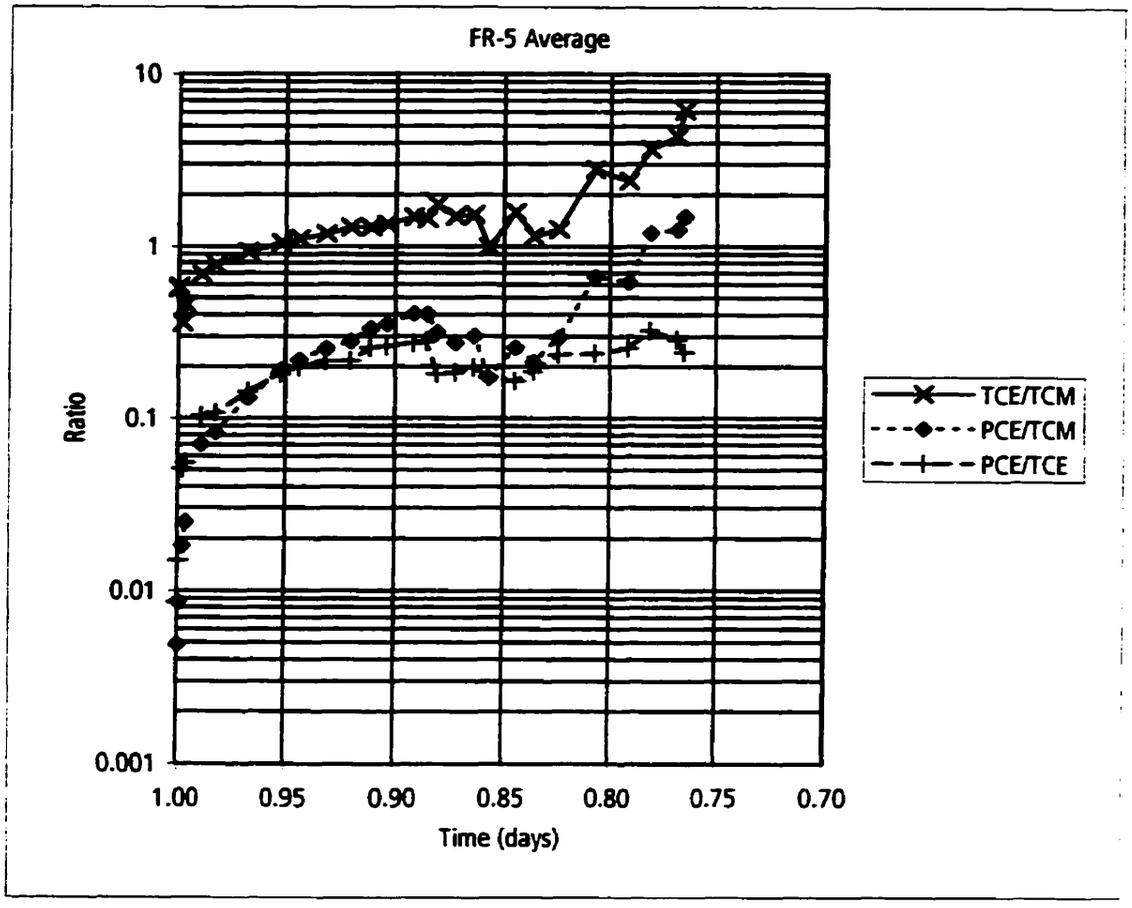

Key:
TCM - Chloroform
TCE- Trichloroethylene
PCE - Tetrachloroethylene

Figure 7-27. Change in aqueous conentration ratios versus NAPL remaining averaged for monitoring location FR-5.

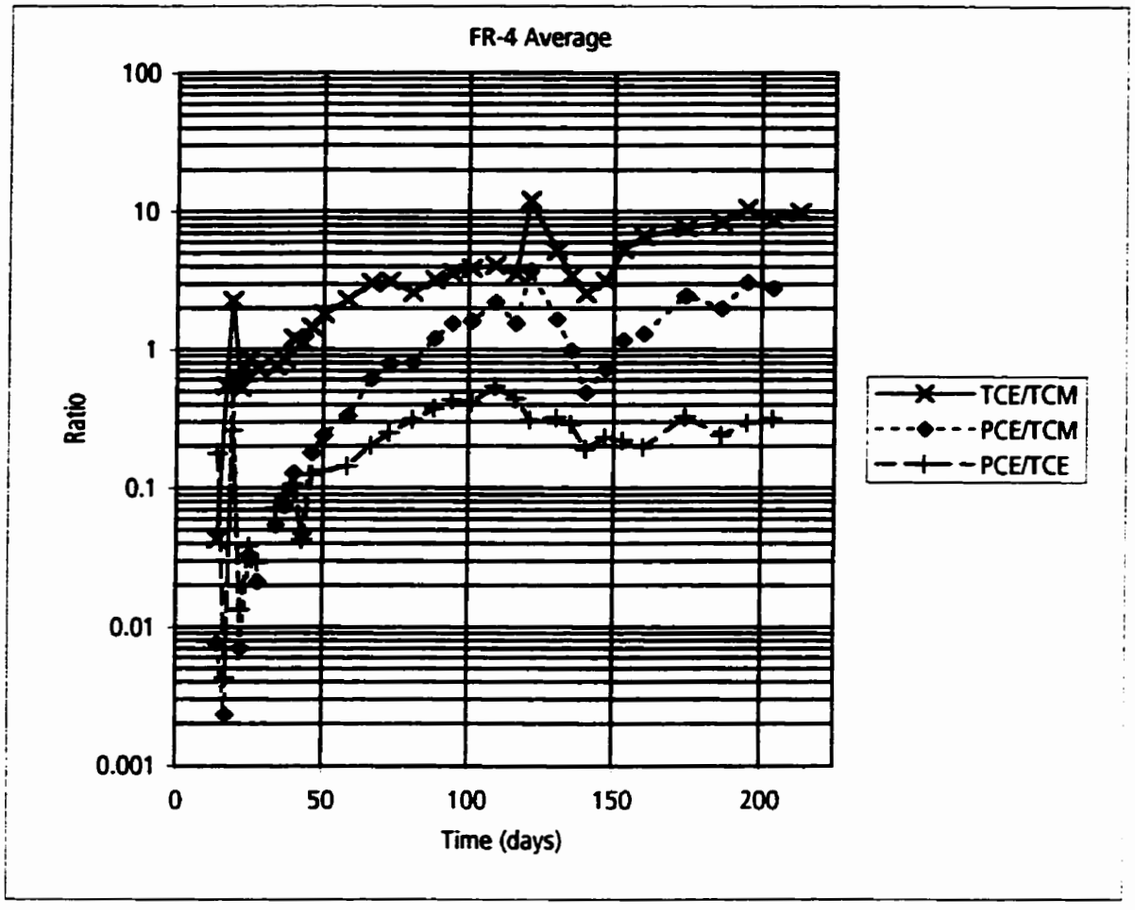

Key:
TCM - Chloroform
TCE- Trichloroethylene
PCE - Tetrachloroethylene

Figure 7-28. Temporal variation in aqueous concentration ratios averaged for monitoring location FR-4.

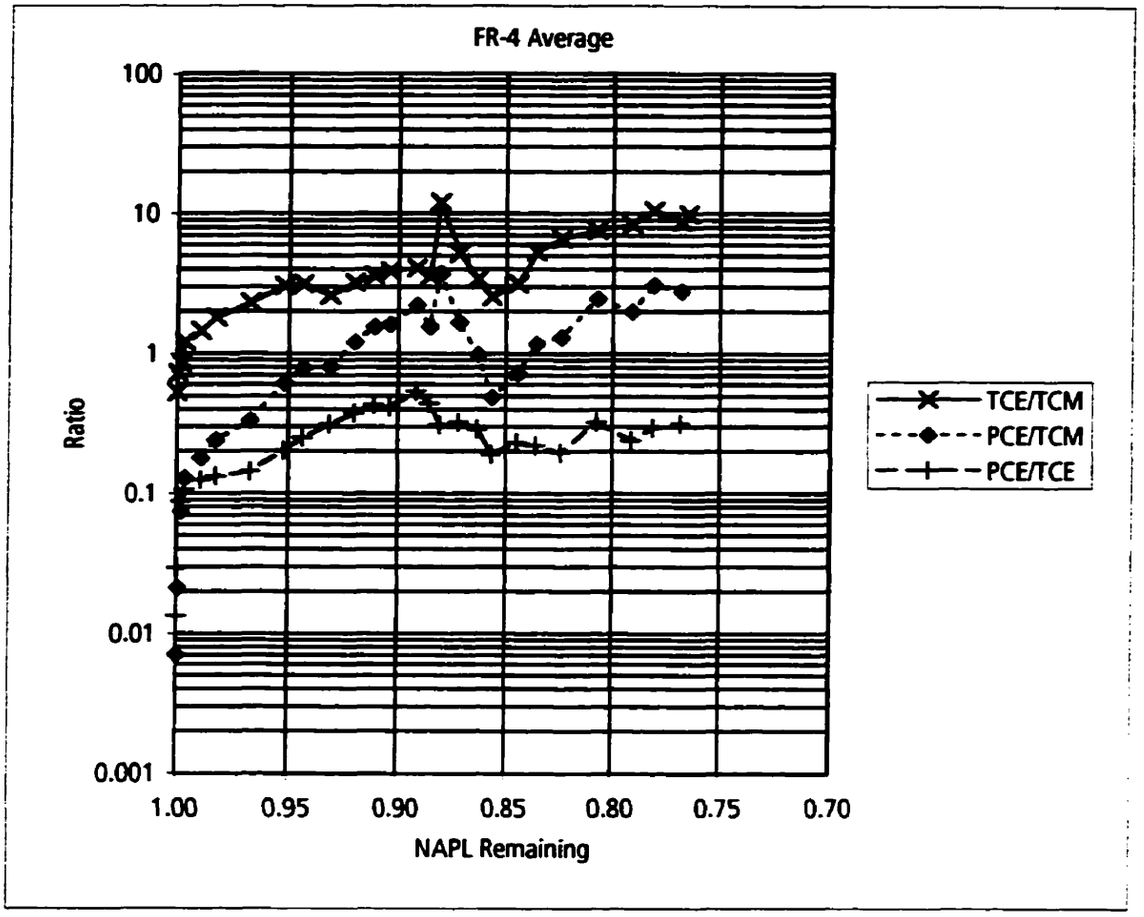

Key:
TCM - Chloroform
TCE- Trichloroethylene
PCE - Tetrachloroethylene

Figure 7-29. Change in aqueous concentration ratios versus NAPL remaining averaged for monitoring location FR-4.

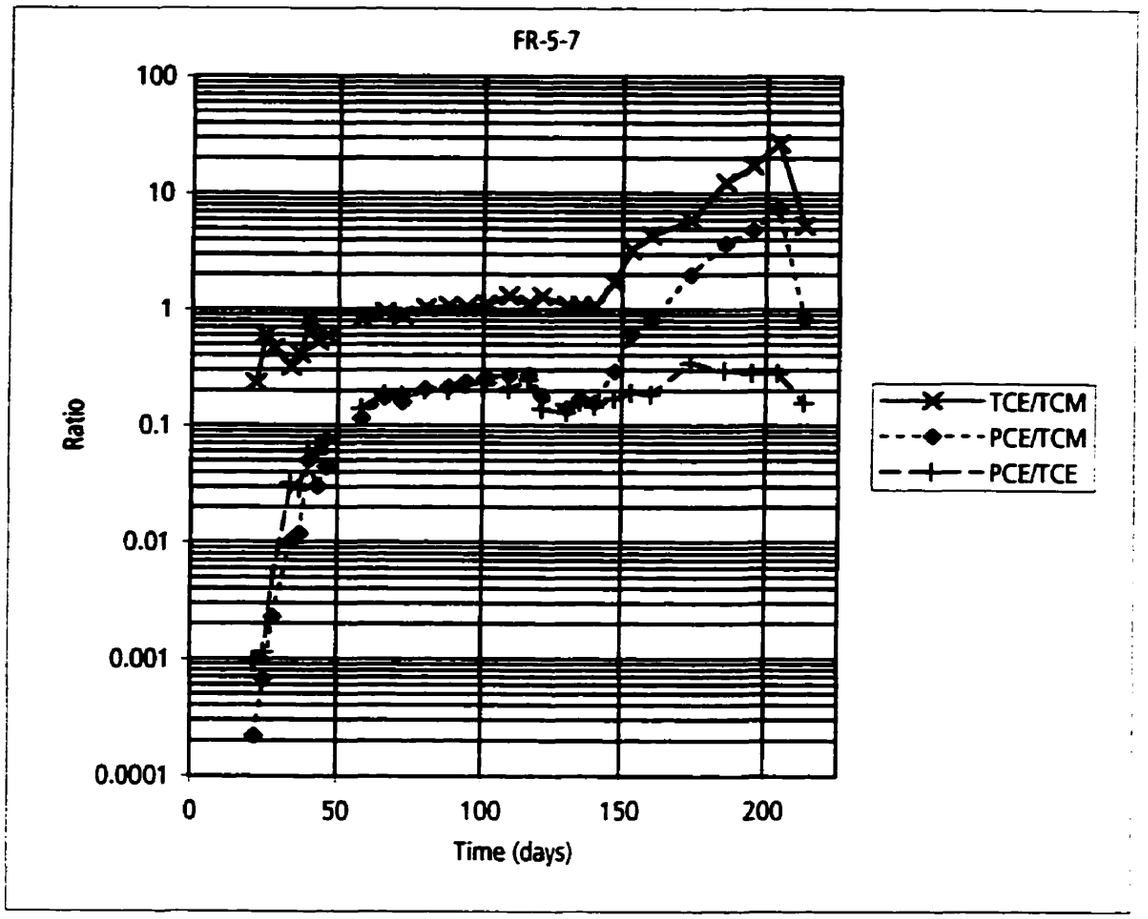

Key:
TCM - Chloroform
TCE- Trichloroethylene
PCE - Tetrachloroethylene

Figure 7-30. Temporal variation in aqueous concentration ratios at monitoring point FR-5-7.

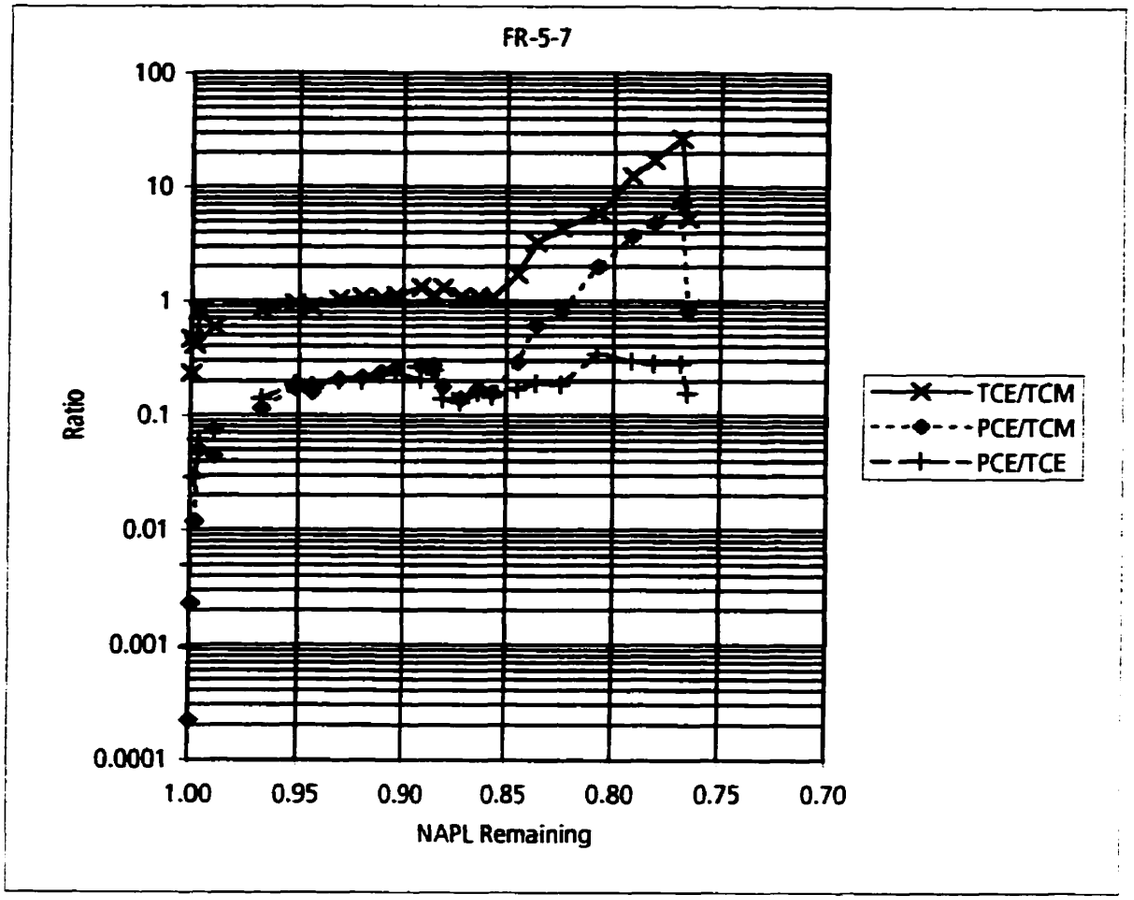

Key:
TCM - Chloroform
TCE- Trichloroethylene
PCE - Tetrachloroethylene

Figure 7-31. Change in aqueous conentration ratios versus NAPL remaining for monitoring point FR-5-7.

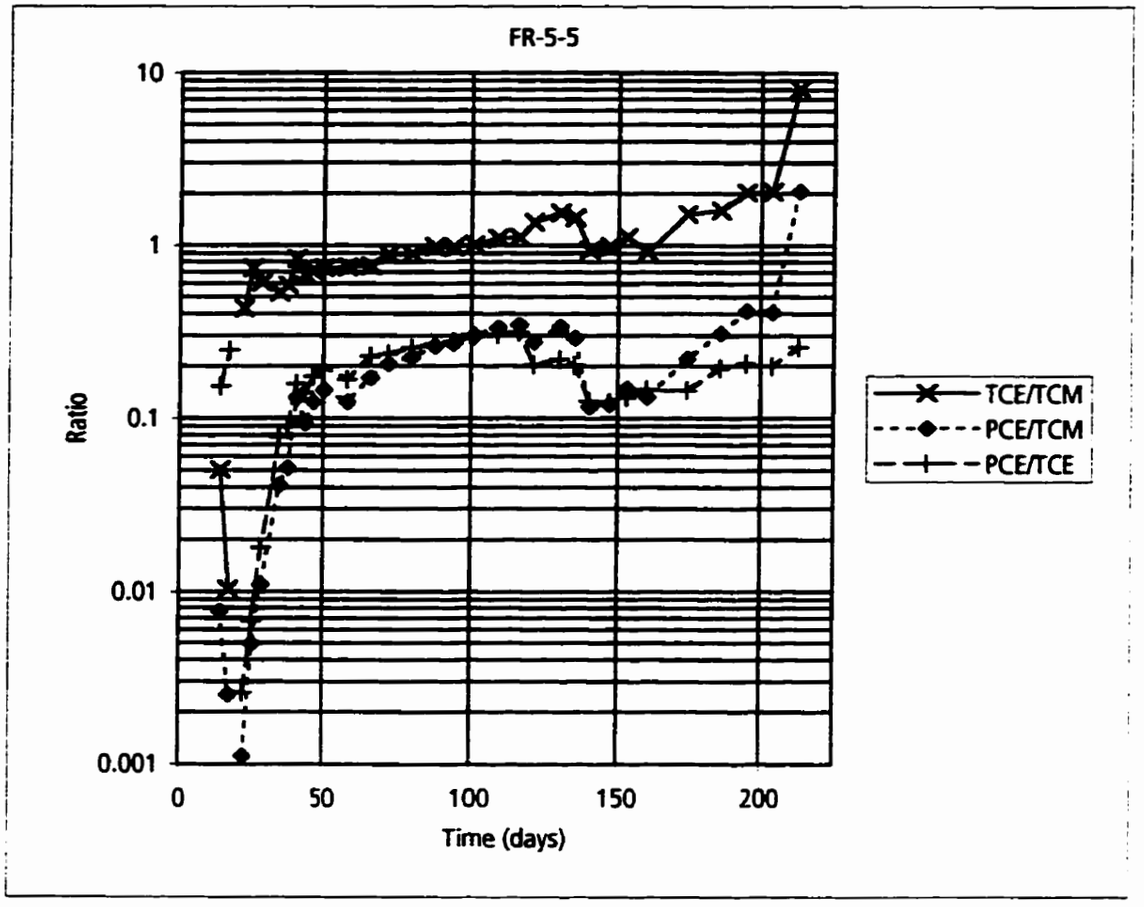

Key:
TCM - Chloroform
TCE- Trichloroethylene
PCE - Tetrachloroethylene

Figure 7-32. Temporal variation in aqueous concentration ratios at monitoring point FR-5-5.

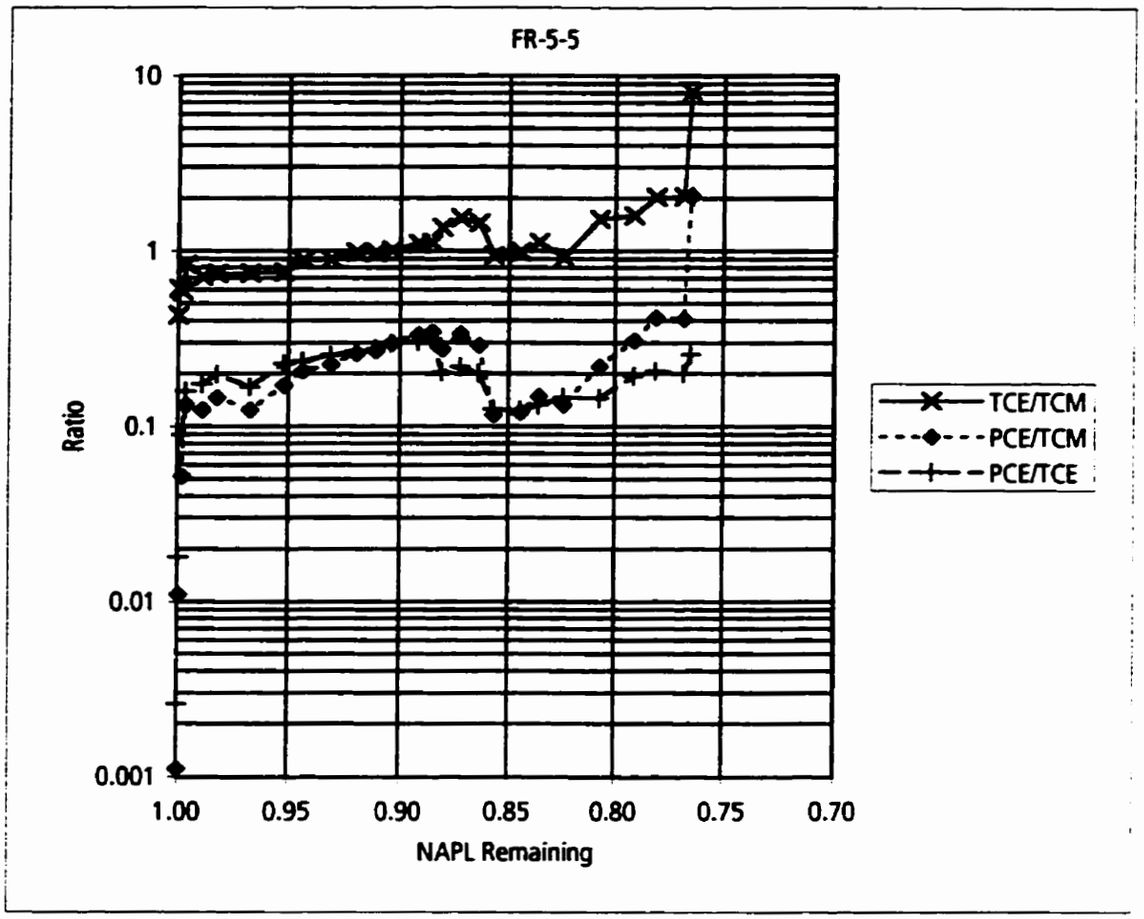

Key:
TCM - Chloroform
TCE- Trichloroethylene
PCE - Tetrachloroethylene

Figure 7-33. Change in aqueous conentration ratios versus NAPL remaining for monitoring point FR-5-5.

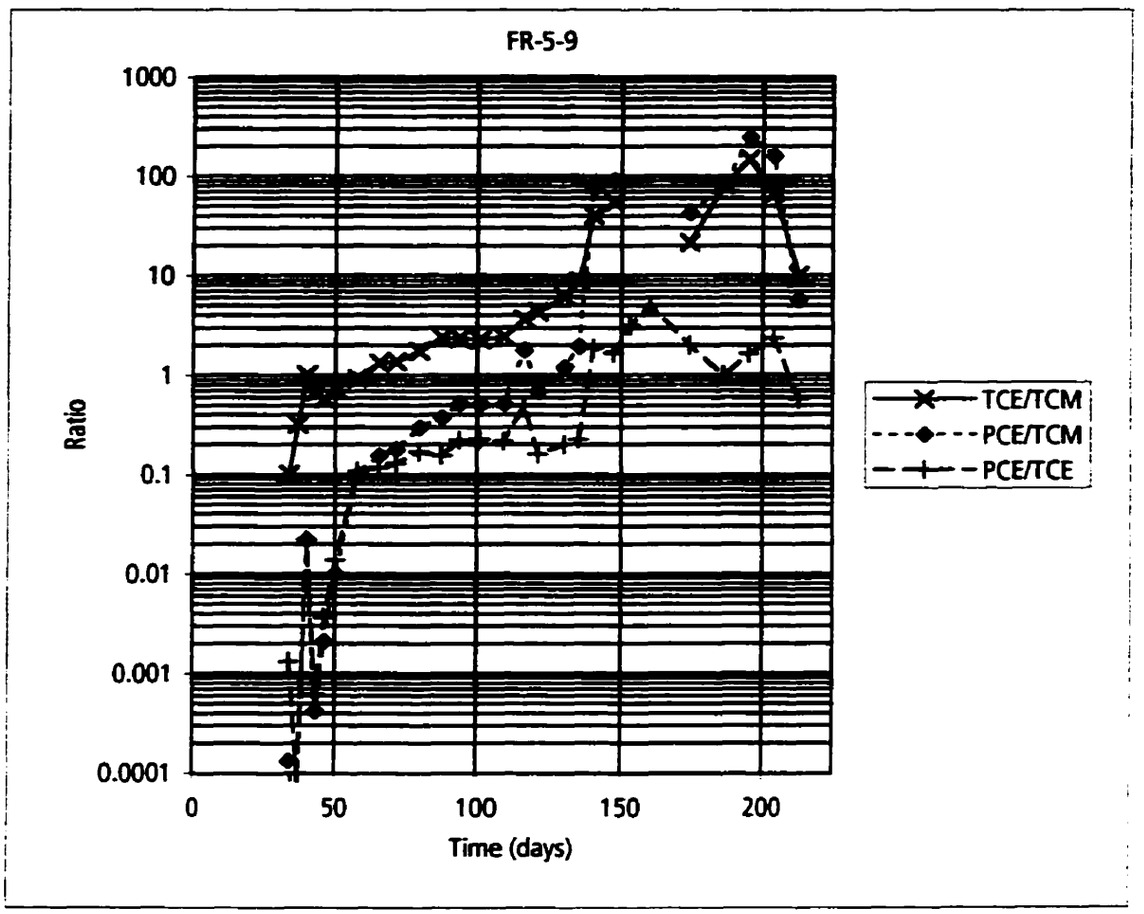

Key:
TCM - Chloroform
TCE- Trichloroethylene
PCE - Tetrachloroethylene

Figure 7-34. Temporal variation in aqueous concentration ratios at monitoring point FR-5-9.

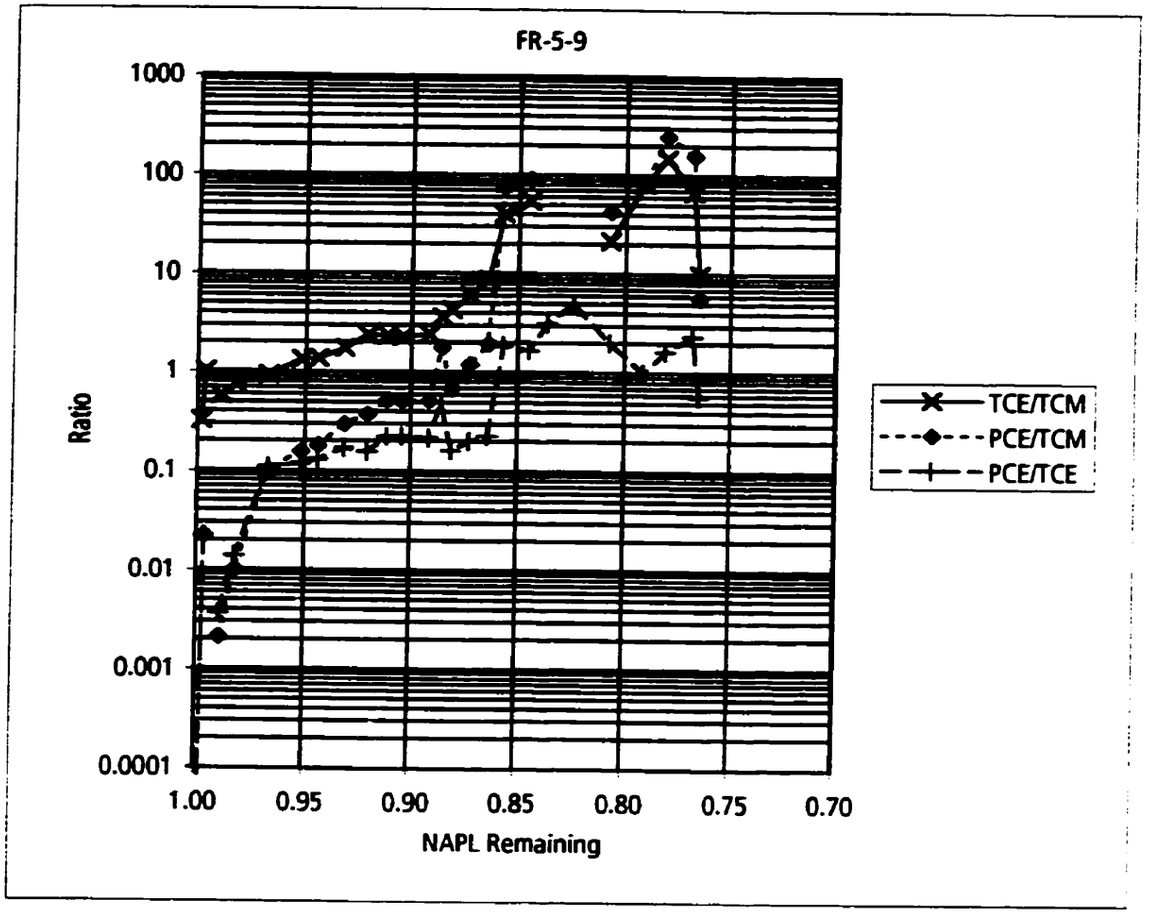

Key:
TCM - Chloroform
TCE- Trichloroethylene
PCE - Tetrachloroethylene

Figure 7-35. Change in aqueous conentration ratios versus NAPL remaining for monitoring point FR-5-9.

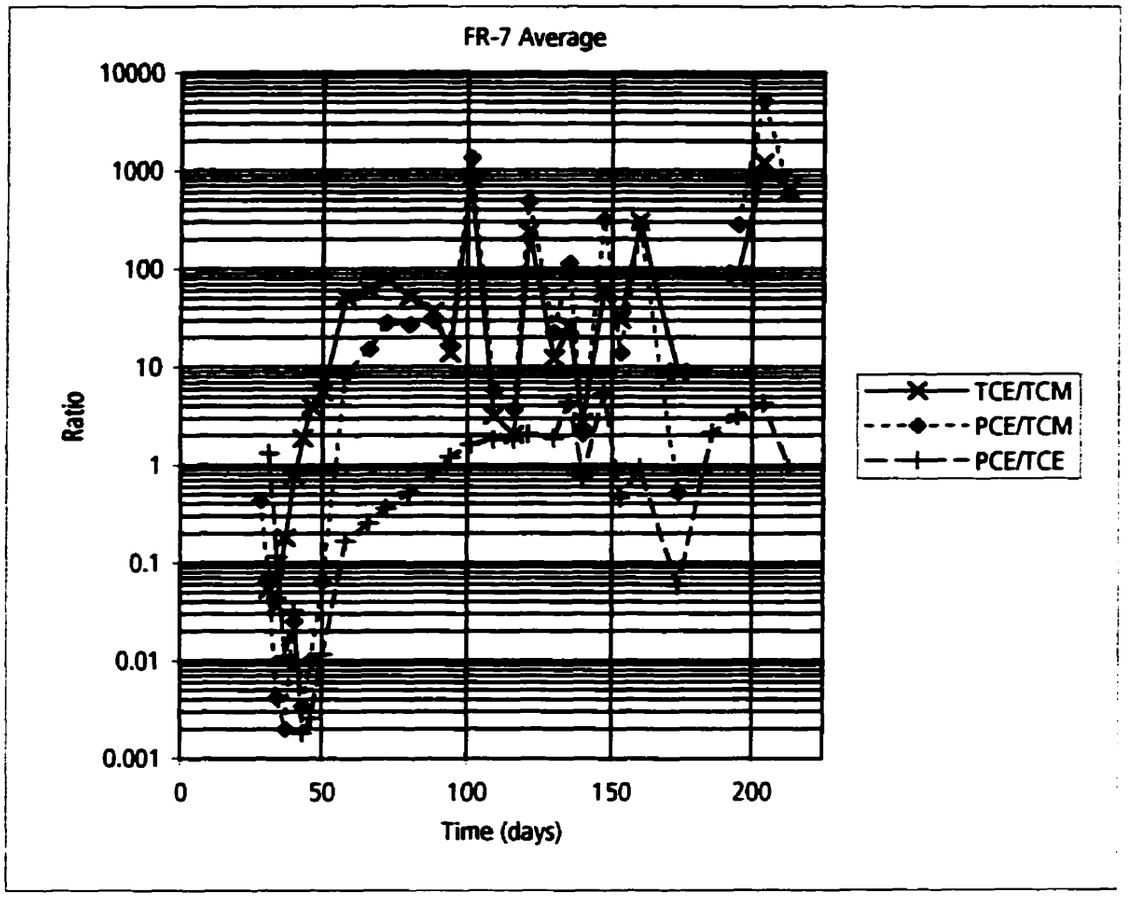

Key:
TCM - Chloroform
TCE- Trichloroethylene
PCE - Tetrachloroethylene

Figure 7-36. Temporal variation in aqueous concentration ratios averaged for monitoring location FR-7.

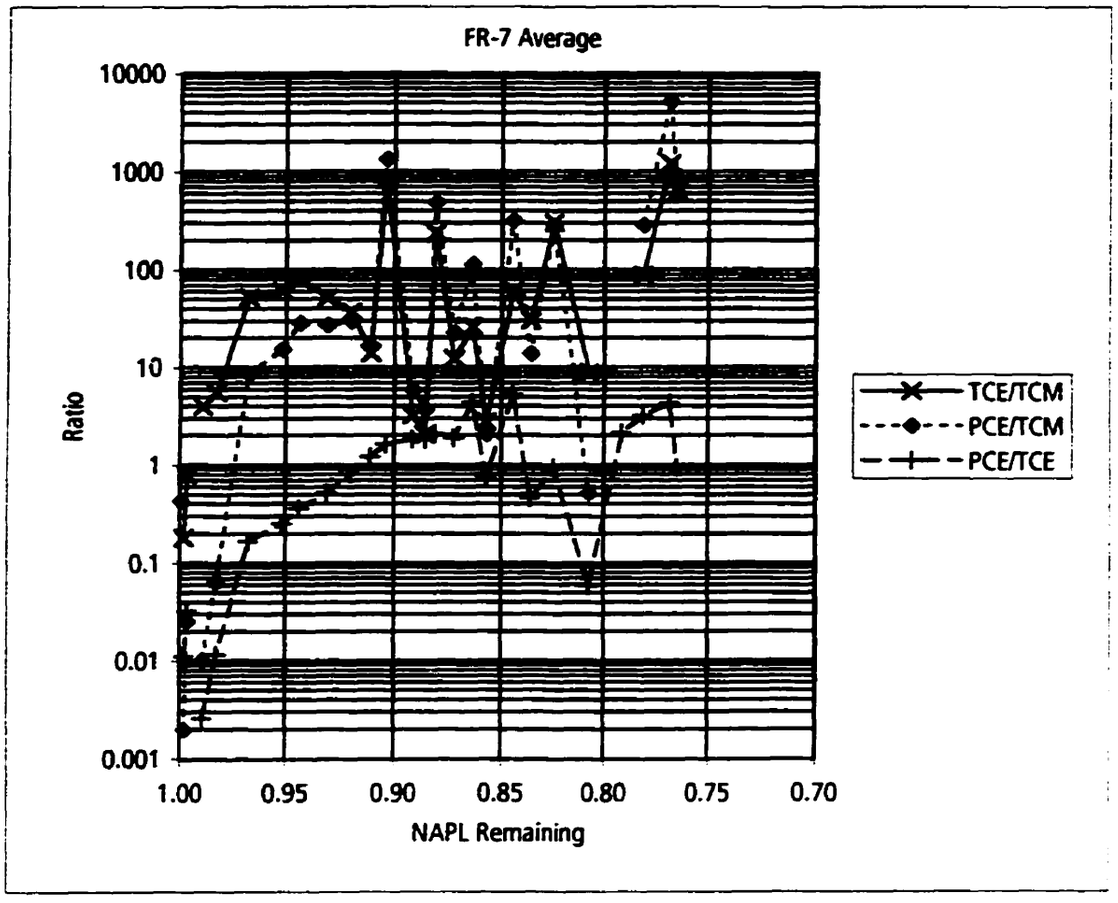

Key:
TCM - Chloroform
TCE- Trichloroethylene
PCE - Tetrachloroethylene

Figure 7-37. Change in aqueous concentration ratios versus NAPL remaining averaged for monitoring location FR-7.

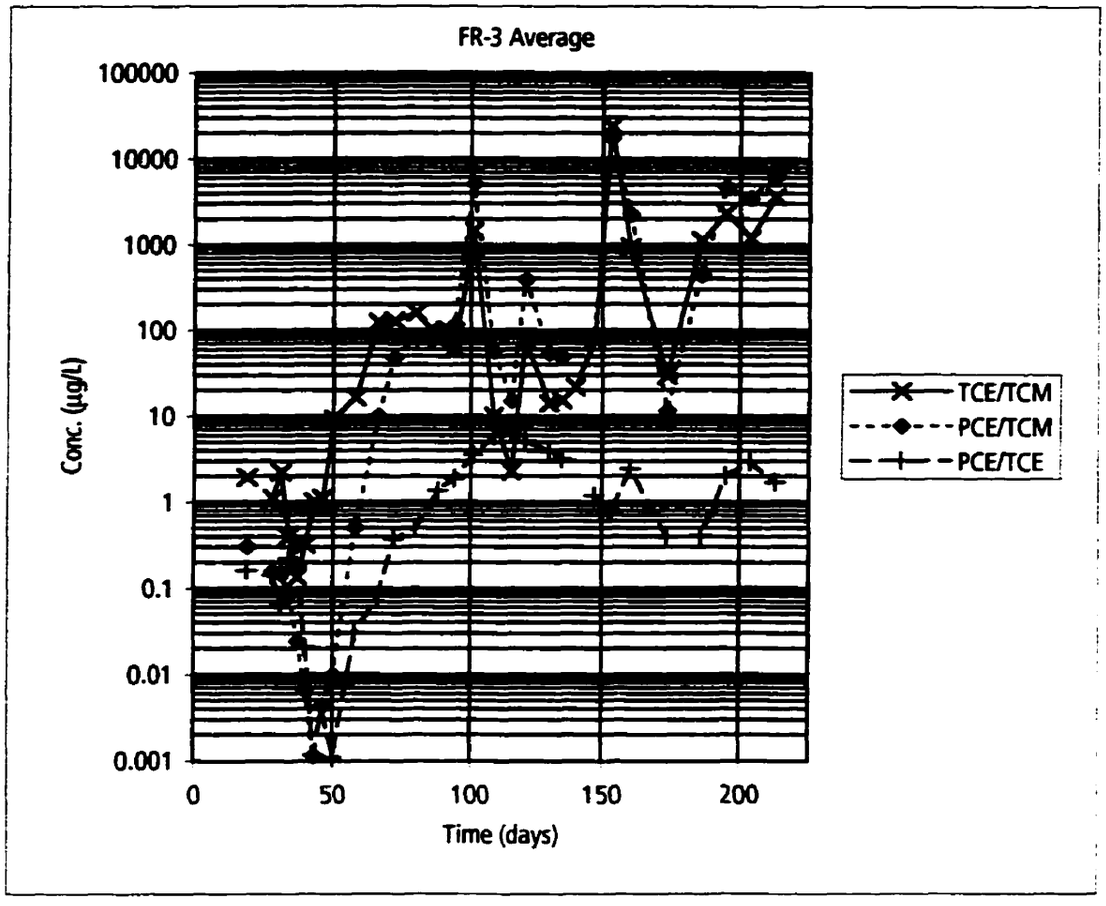

Key:
TCM - Chloroform
TCE- Trichloroethylene
PCE - Tetrachloroethylene

Figure 7-38. Temporal variation in aqueous concentration ratios averaged for monitoring location FR-3.

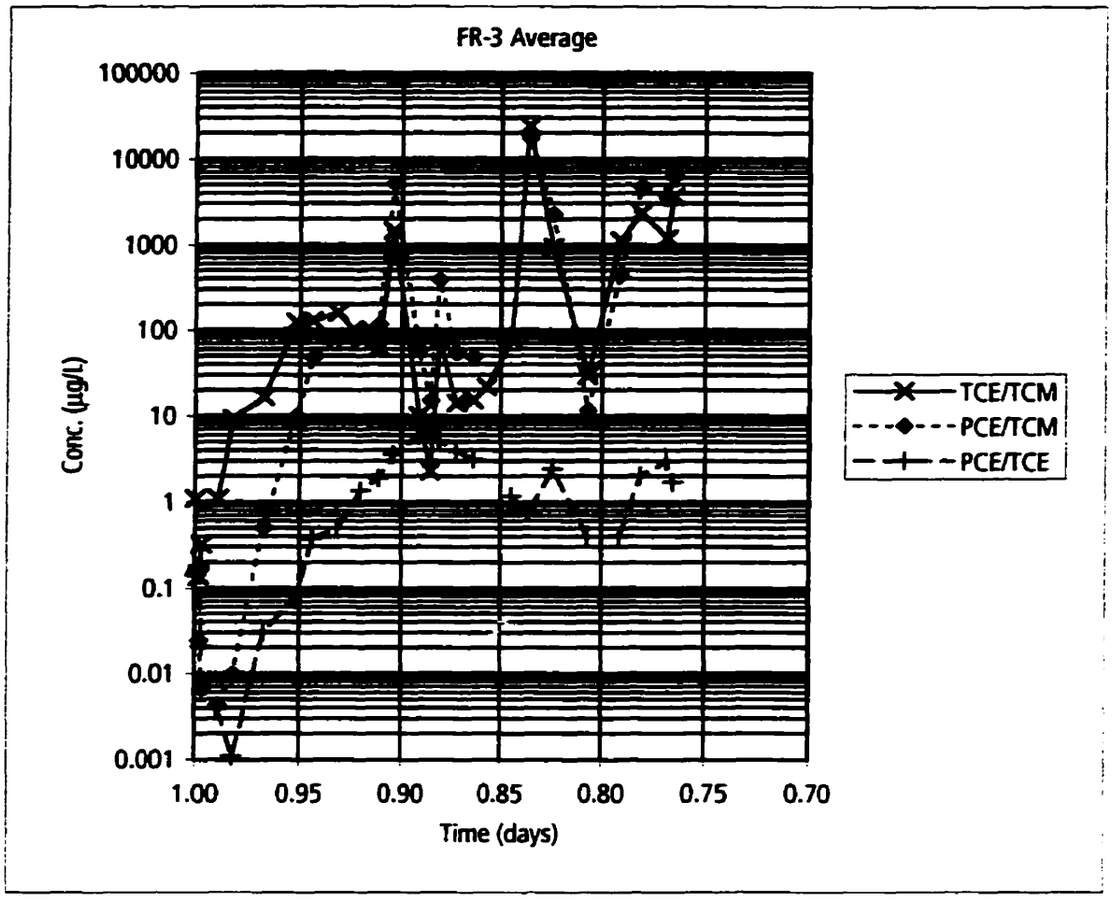

Key:
TCM - Chloroform
TCE- Trichloroethylene
PCE - Tetrachloroethylene

Figure 7-39. Change in aqueous concentration ratios versus NAPL remaining averaged for monitoring location FR-3.

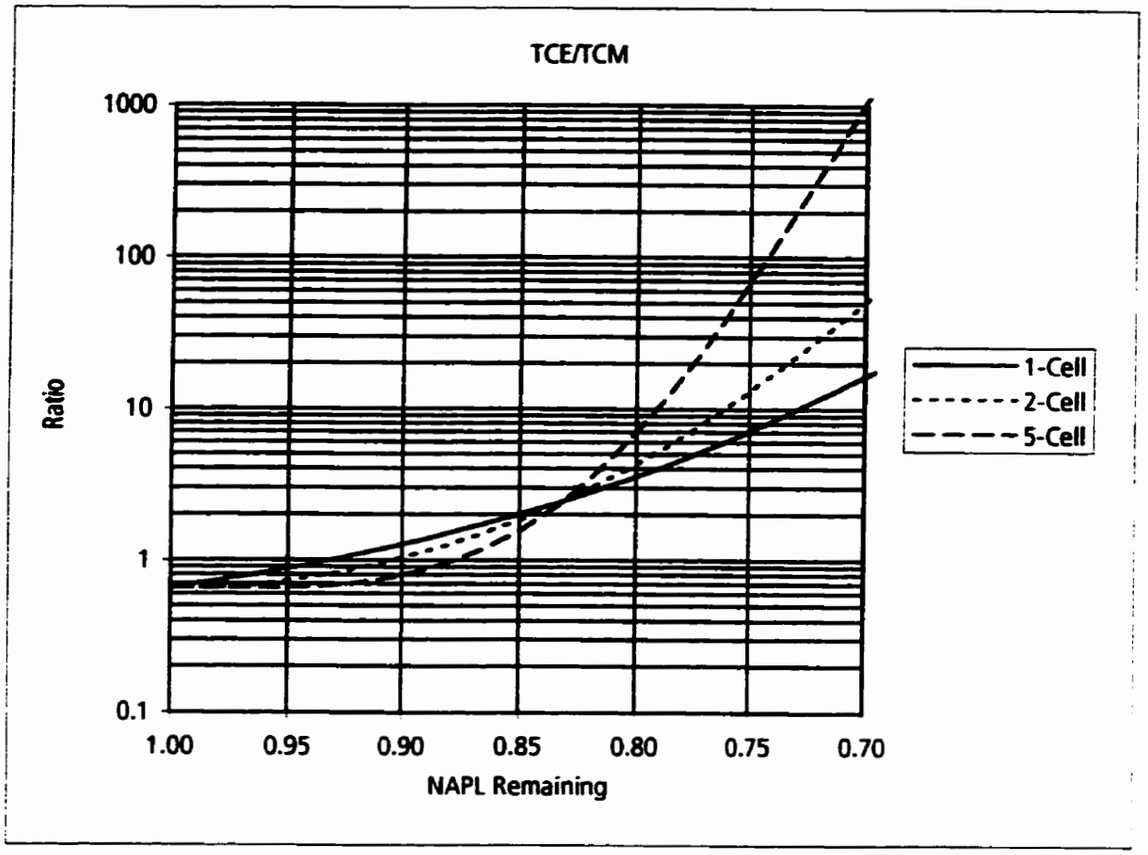

Key:
TCM - Chloroform
TCE - Trichloroethylene
PCE - Tetrachloroethylene

Figure 7-40. Change in TCE/TCM ratio versus NAPL remaining predicted by ESM.

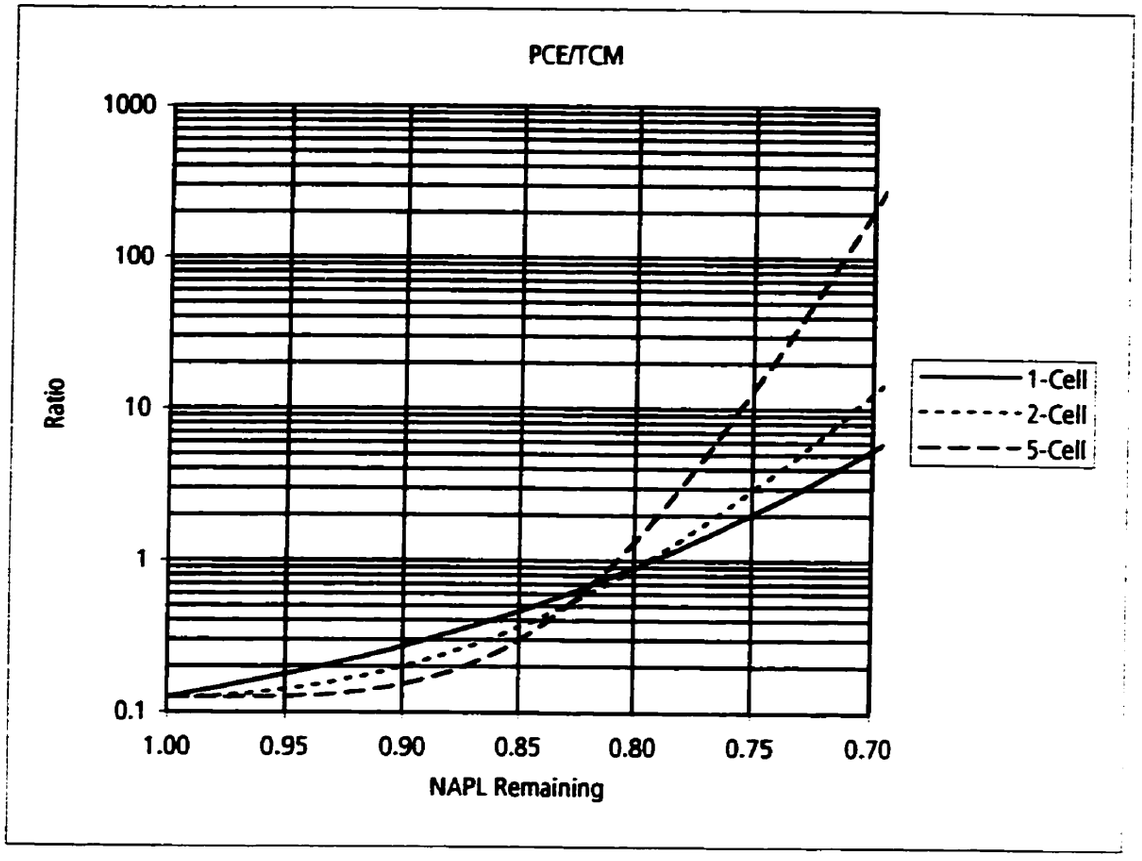

Key:
TCM - Chloroform
TCE - Trichloroethylene
PCE - Tetrachloroethylene

Figure 7-41. Change in PCE/TCM ratio versus NAPL remaining predicted by ESM.

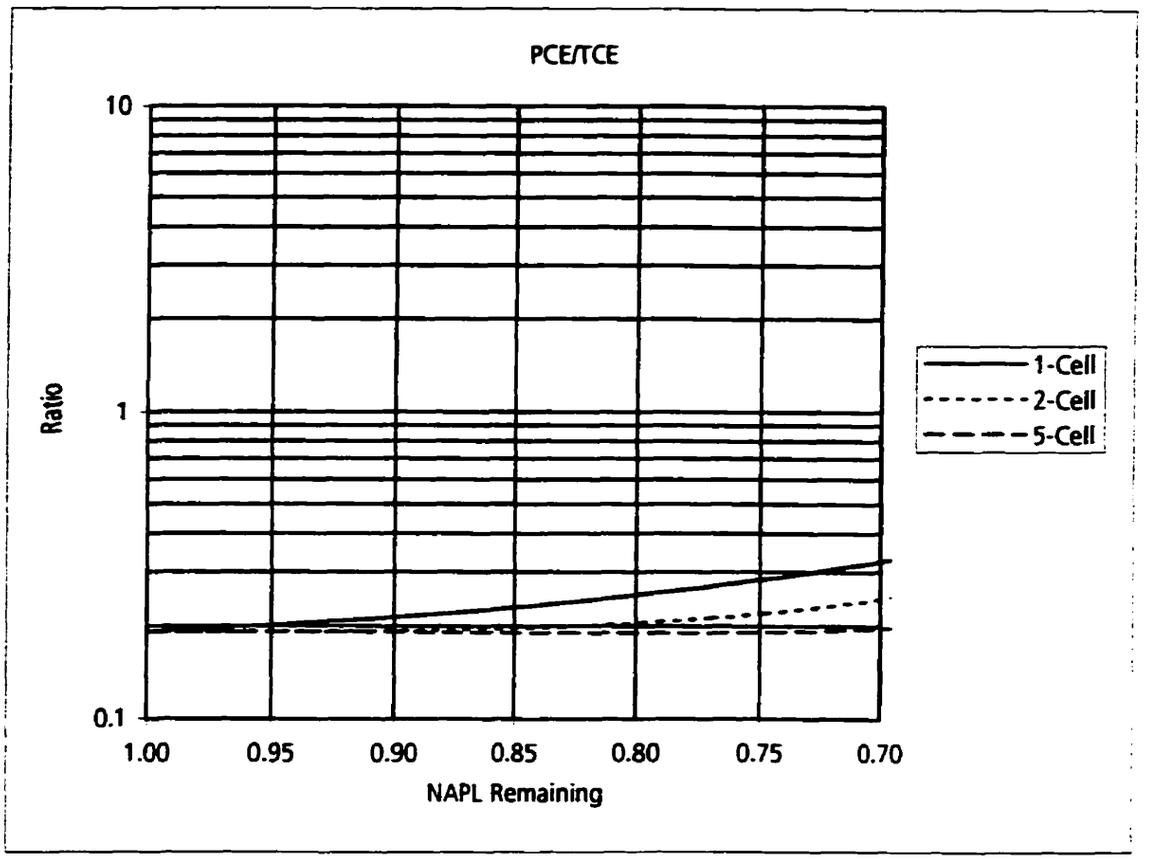

Key:
TCM - Chloroform
TCE - Trichloroethylene
PCE - Tetrachloroethylene

Figure 7-42. Change in PCE/TCE ratio versus NAPL remaining predicted by ESM.

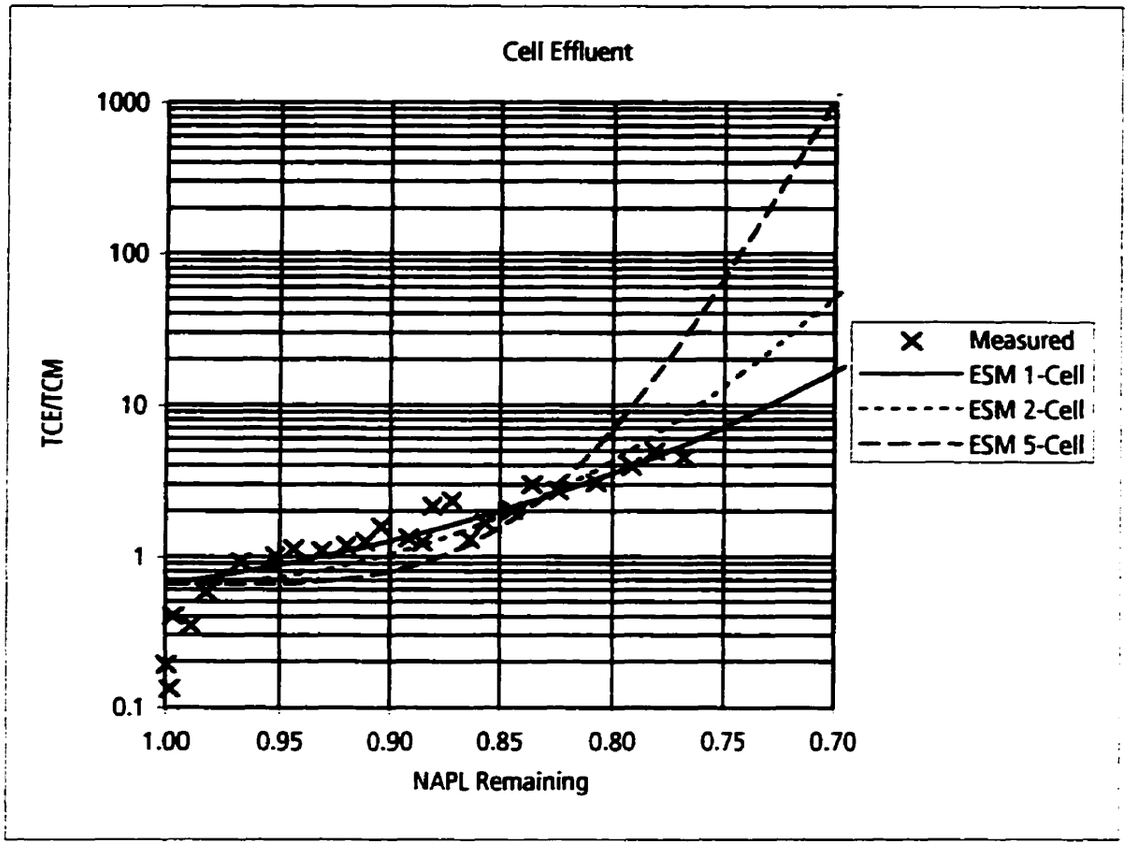

Key:
TCM - Chloroform
TCE - Trichloroethylene
PCE - Tetrachloroethylene

Figure 7-43. Measured TCE/TCM ratios versus NAPL remaining for average concentrations in the cell effluent compared to ratios predicted by ESM.

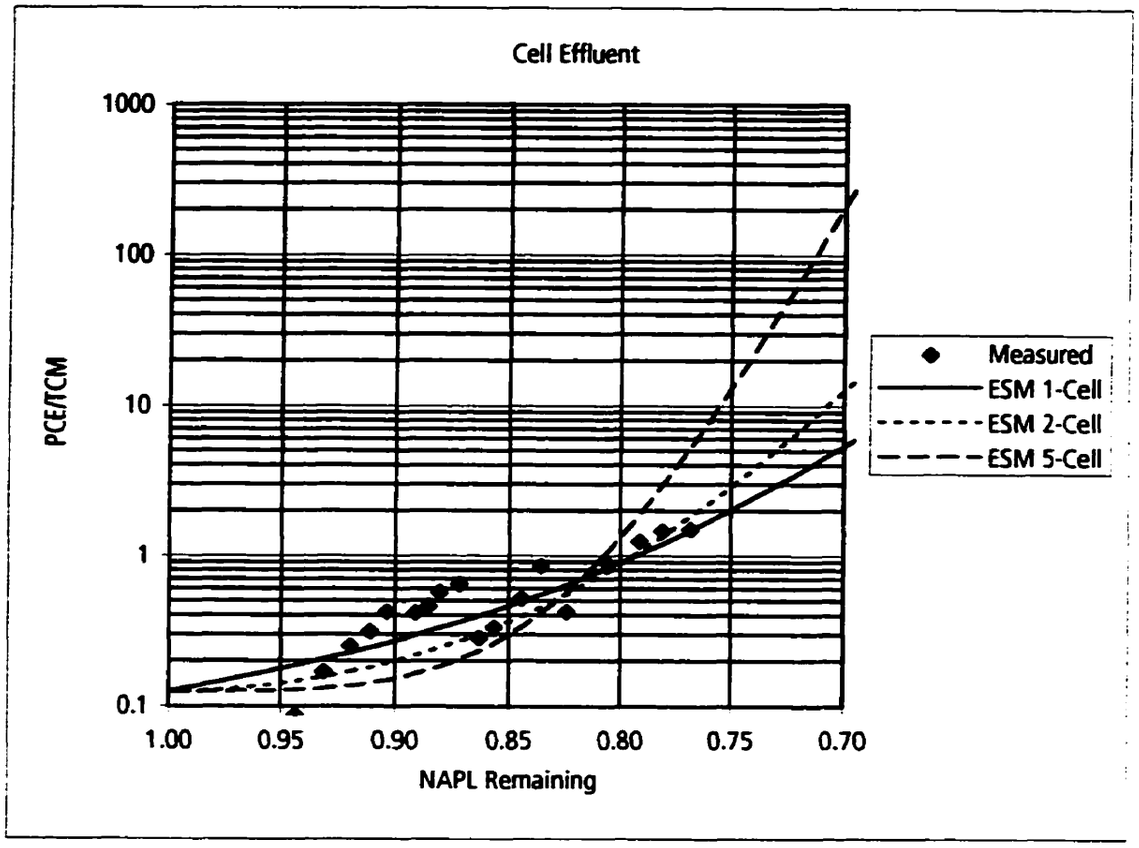

Key:
TCM - Chloroform
TCE - Trichloroethylene
PCE - Tetrachloroethylene

Figure 7-44. Measured PCE/TCM ratios versus NAPL remaining for average concentrations in the cell effluent compared to ratios predicted by ESM.

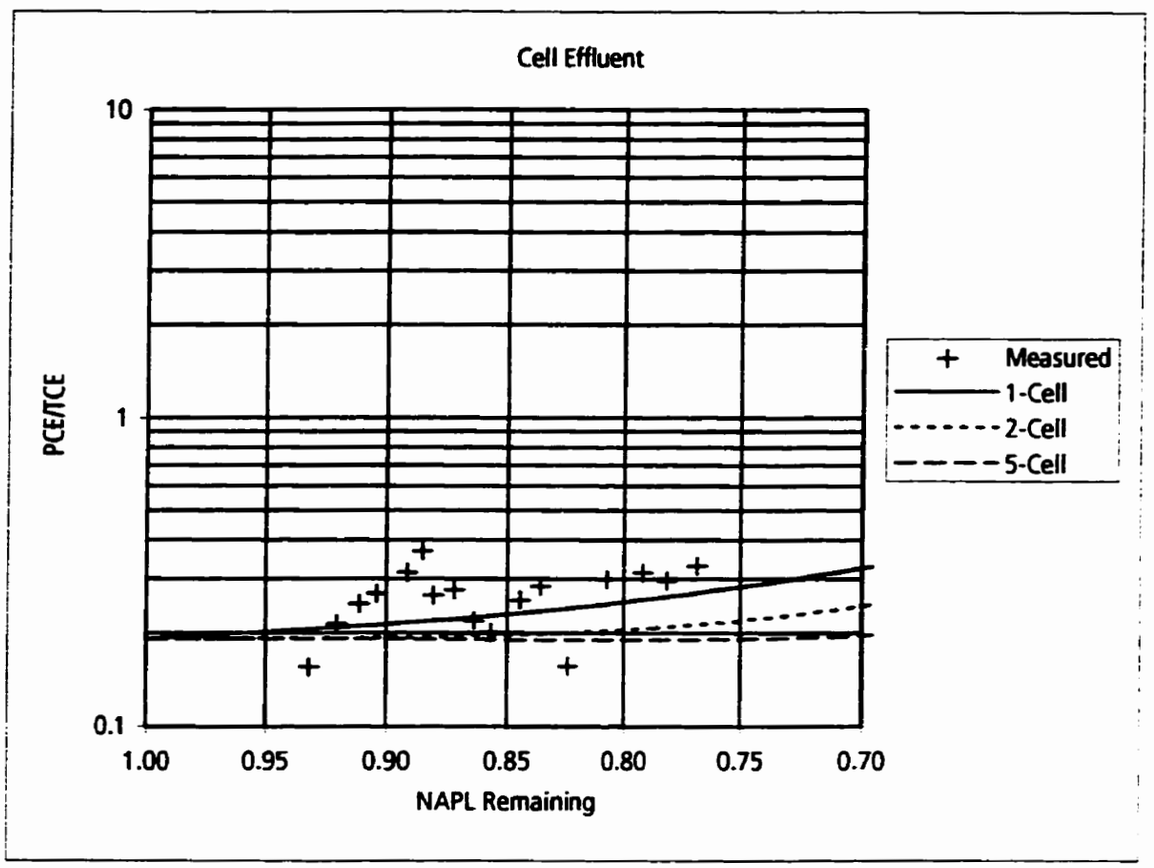

Key:
TCM - Chloroform
TCE - Trichloroethylene
PCE - Tetrachloroethylene

Figure 7-45. Measured PCE/TCE ratios versus NAPL remaining for average concentrations in the cell effluent compared to ratios predicted by ESM.

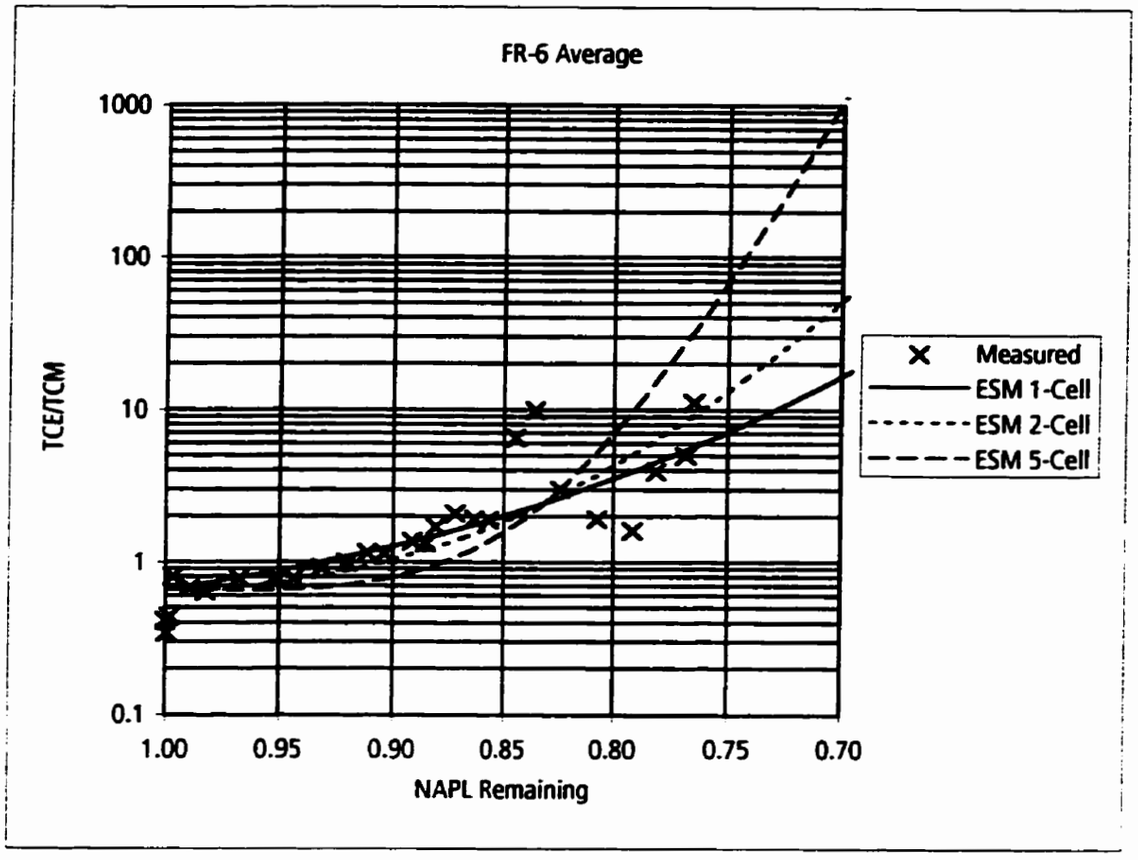

Key:
TCM - Chloroform
TCE - Trichloroethylene
PCE - Tetrachloroethylene

Figure 7-46. Measured TCE/TCM ratios versus NAPL remaining for average concentrations at monitoring location FR-6 compared to ratios predicted by ESM.

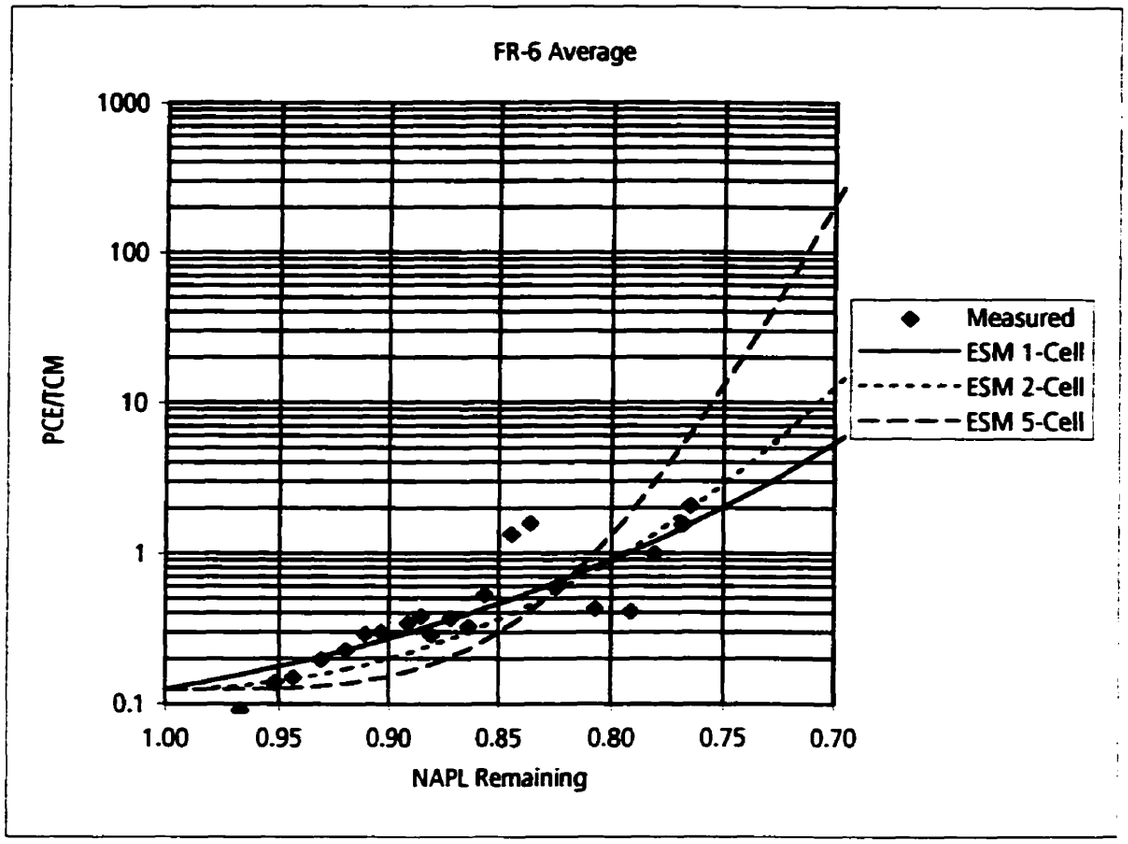

Key:
TCM - Chloroform
TCE - Trichloroethylene
PCE - Tetrachloroethylene

Figure 7-47. Measured PCE/TCM ratios versus NAPL remaining for average concentrations at monitoring location FR-6 compared to ratios predicted by ESM.

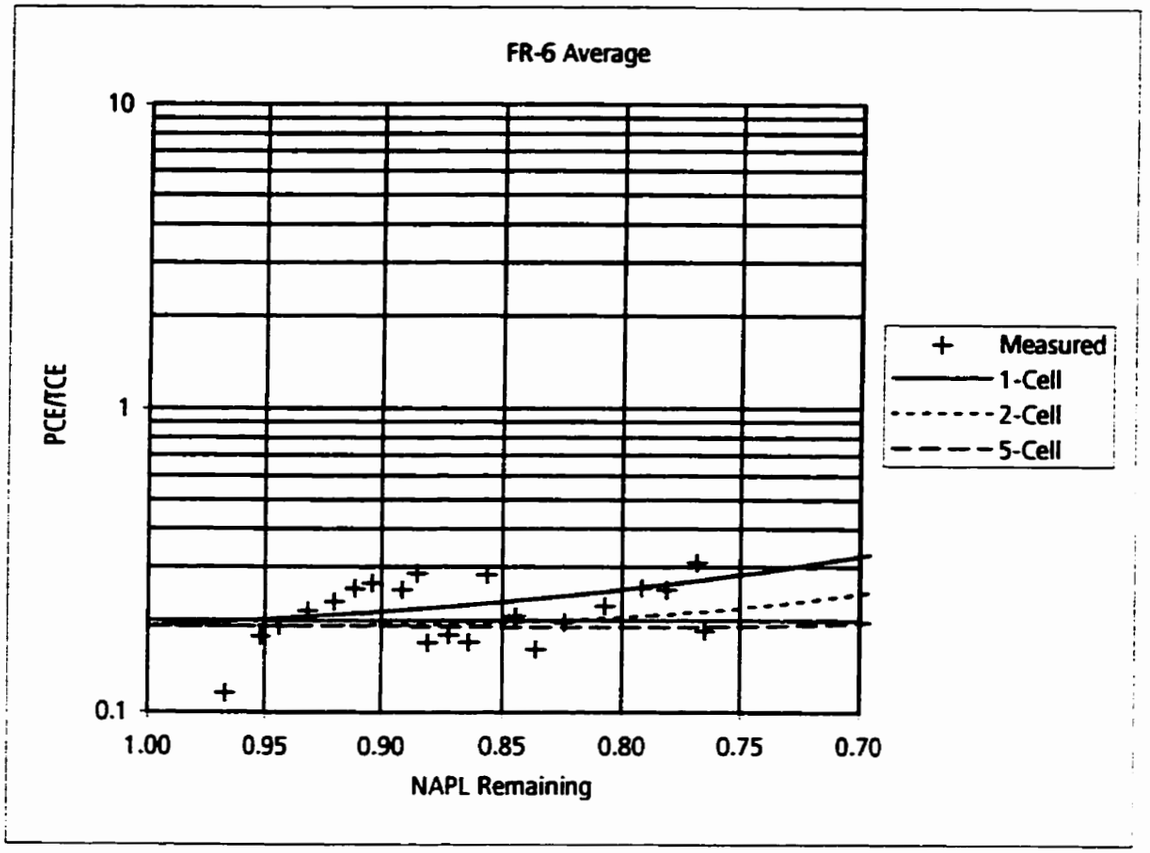

Key:
TCM - Chloroform
TCE - Trichloroethylene
PCE - Tetrachloroethylene

Figure 7-48. Measured PCE/TCE ratios versus NAPL remaining for average concentrations at monitoring location FR-6 compared to ratios predicted by ESM.

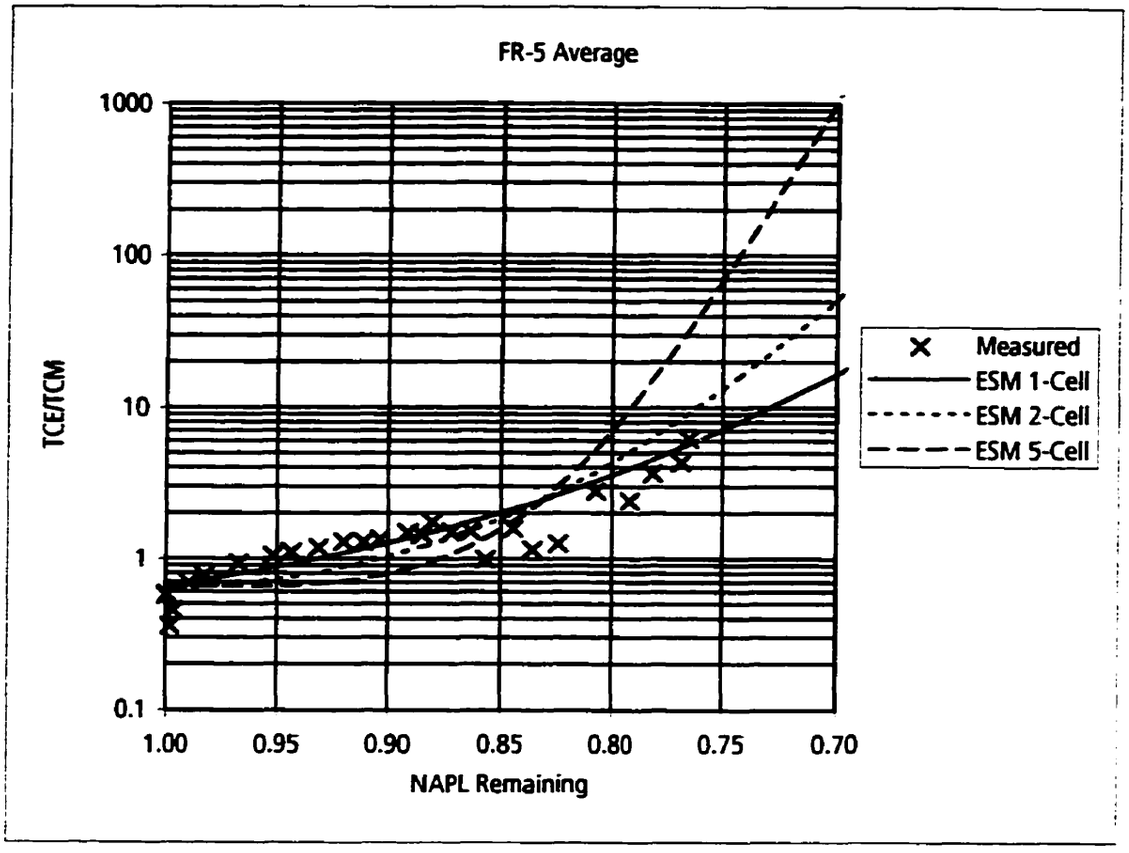

Key:
TCM - Chloroform
TCE - Trichloroethylene
PCE - Tetrachloroethylene

Figure 7-49. Measured TCE/TCM ratios versus NAPL remaining for average concentrations at monitoring location FR-5 compared to ratios predicted by ESM.

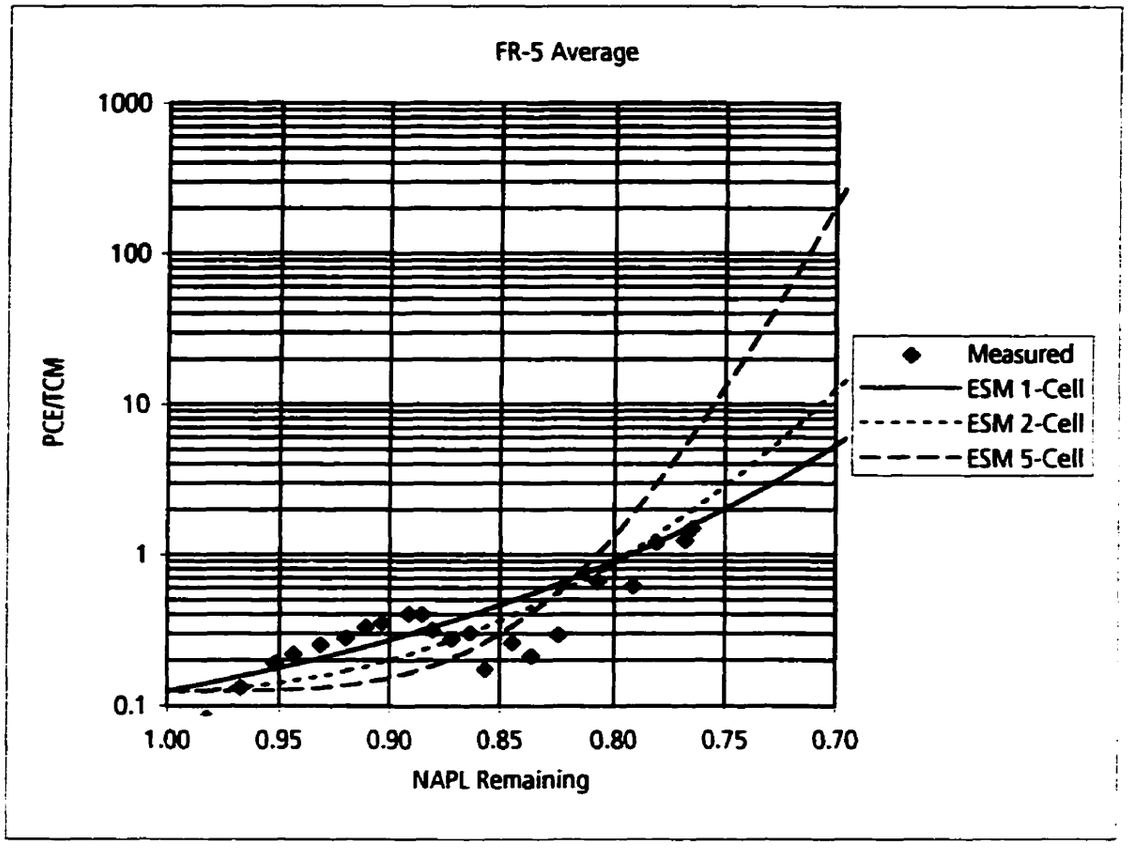

Key:
TCM - Chloroform
TCE - Trichloroethylene
PCE - Tetrachloroethylene

Figure 7-50. Measured PCE/TCM ratios versus NAPL remaining for average concentrations at monitoring location FR-5 compared to ratios predicted by ESM.

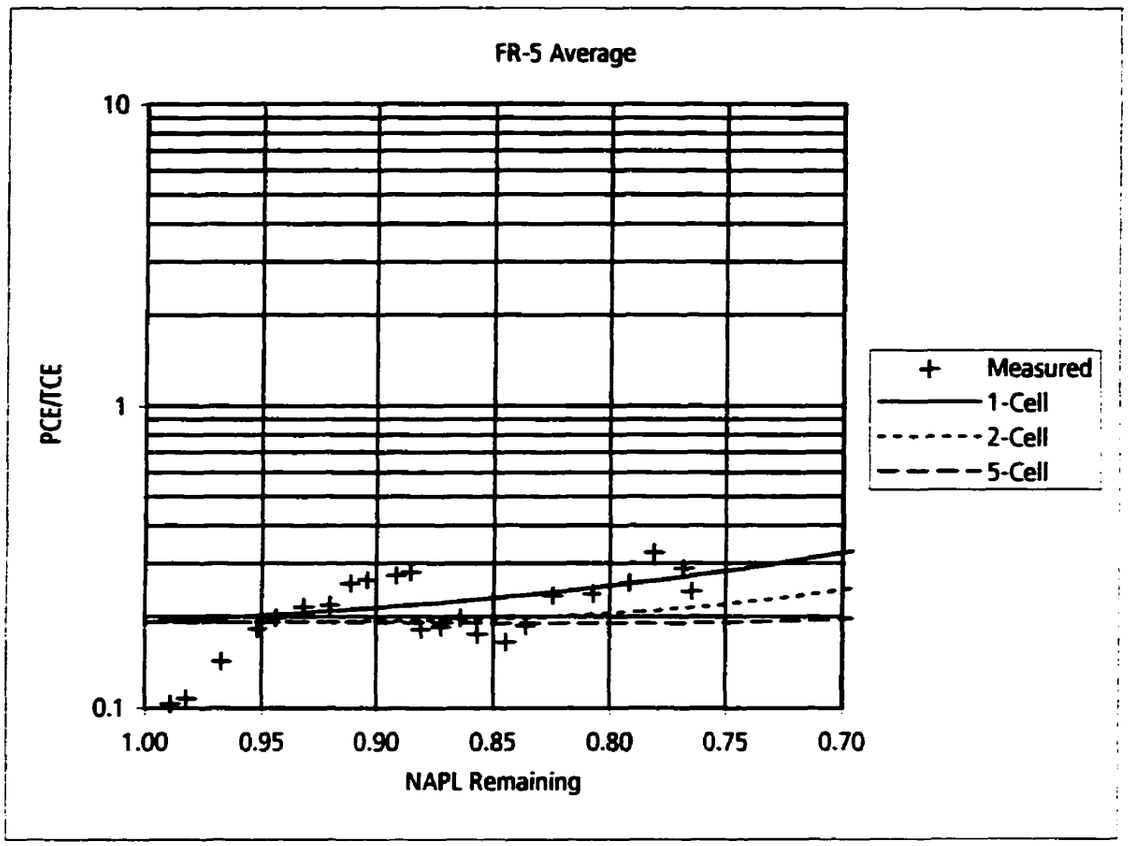

Key:
TCM - Chloroform
TCE - Trichloroethylene
PCE - Tetrachloroethylene

Figure 7-51. Measured PCE/TCE ratios versus NAPL remaining for average concentrations at monitoring location FR-5 compared to ratios predicted by ESM.

File:FR Exp. Equilibrium.EXCL/Plots

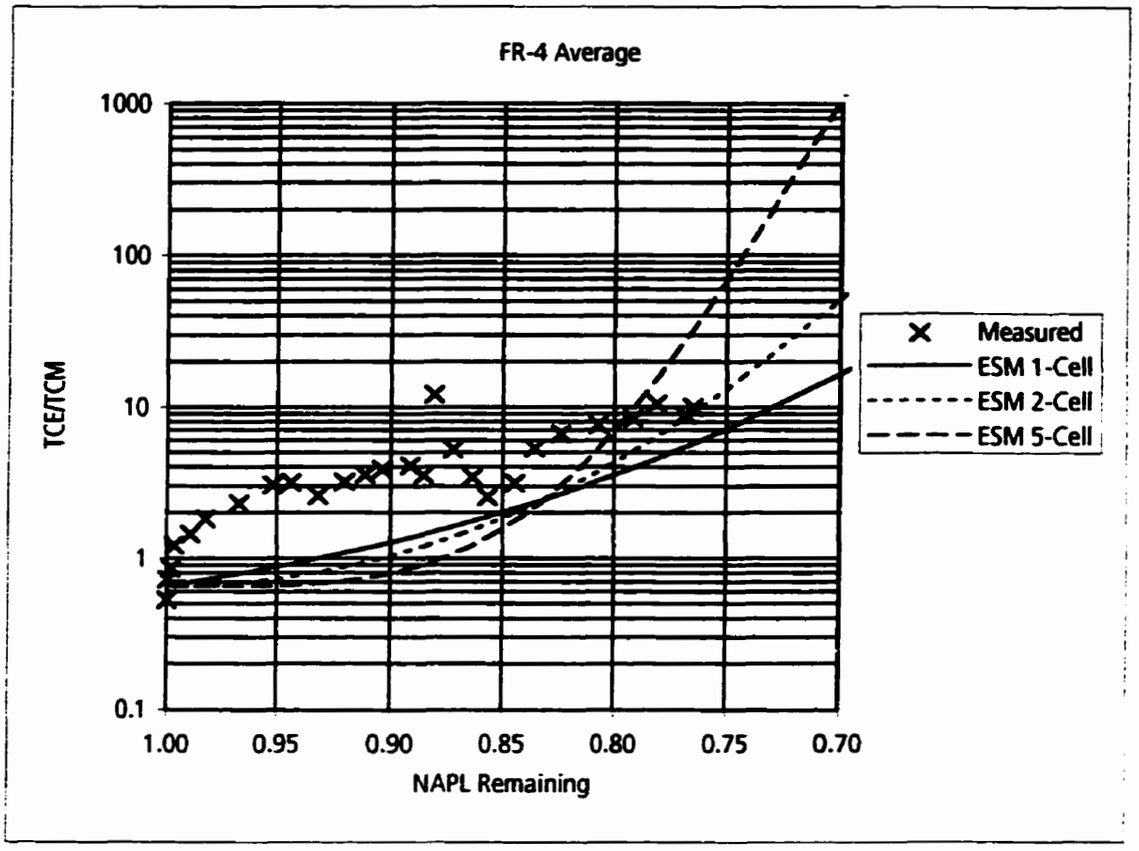

Key:
TCM - Chloroform
TCE - Trichloroethylene
PCE - Tetrachloroethylene

Figure 7-52. Measured TCE/TCM ratios versus NAPL remaining for average concentrations at monitoring location FR-4 compared to ratios predicted by ESM.

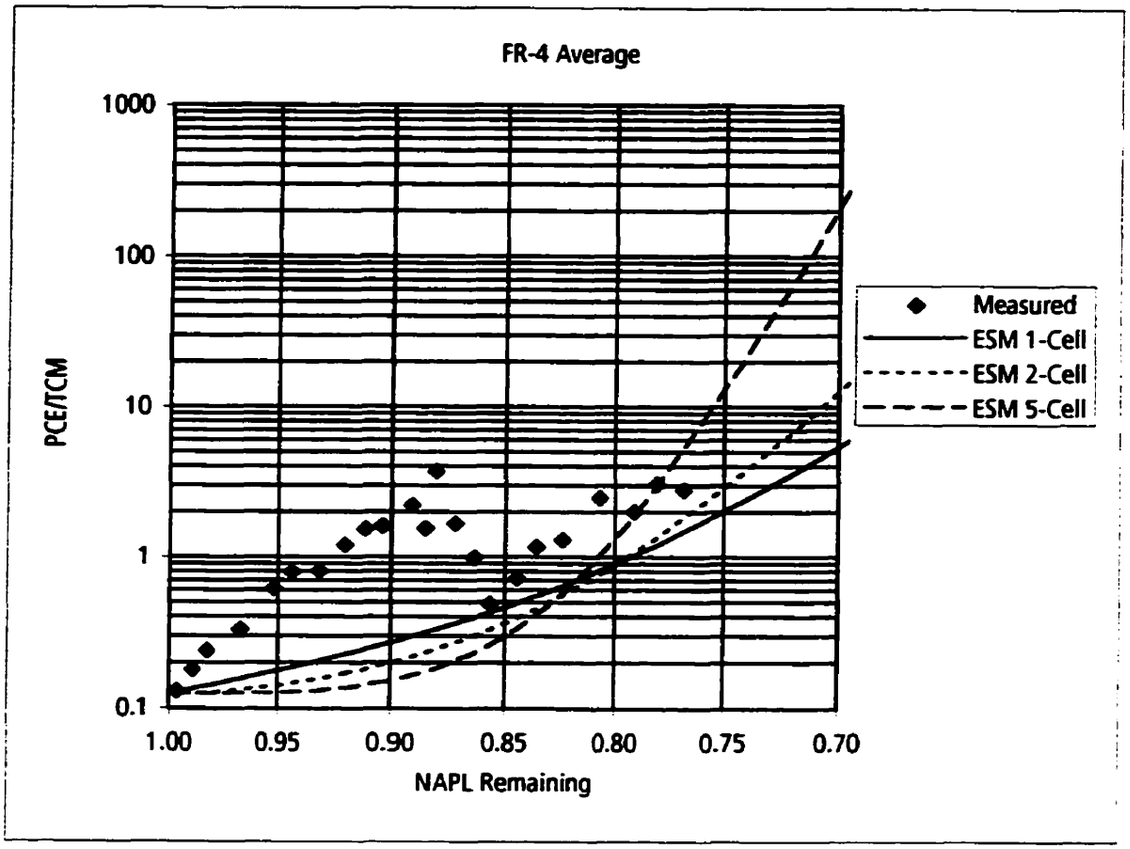

Key:
TCM - Chloroform
TCE - Trichloroethylene
PCE - Tetrachloroethylene

Figure 7-53. Measured PCE/TCM ratios versus NAPL remaining for average concentrations at monitoring location FR-4 compared to ratios predicted by ESM.

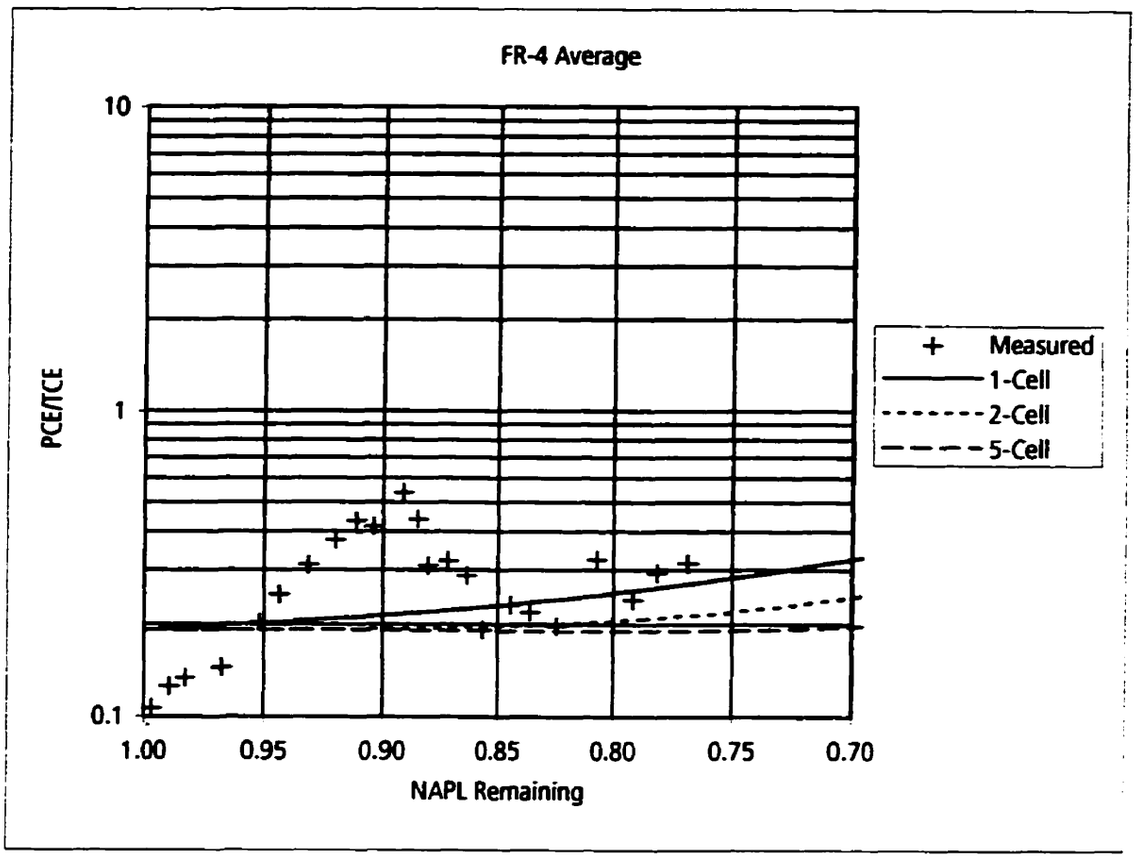

Key:
TCM - Chloroform
TCE - Trichloroethylene
PCE - Tetrachloroethylene

Figure 7-54. Measured PCE/TCE ratios versus NAPL remaining for average concentrations at monitoring location FR-4 compared to ratios predicted by ESM.

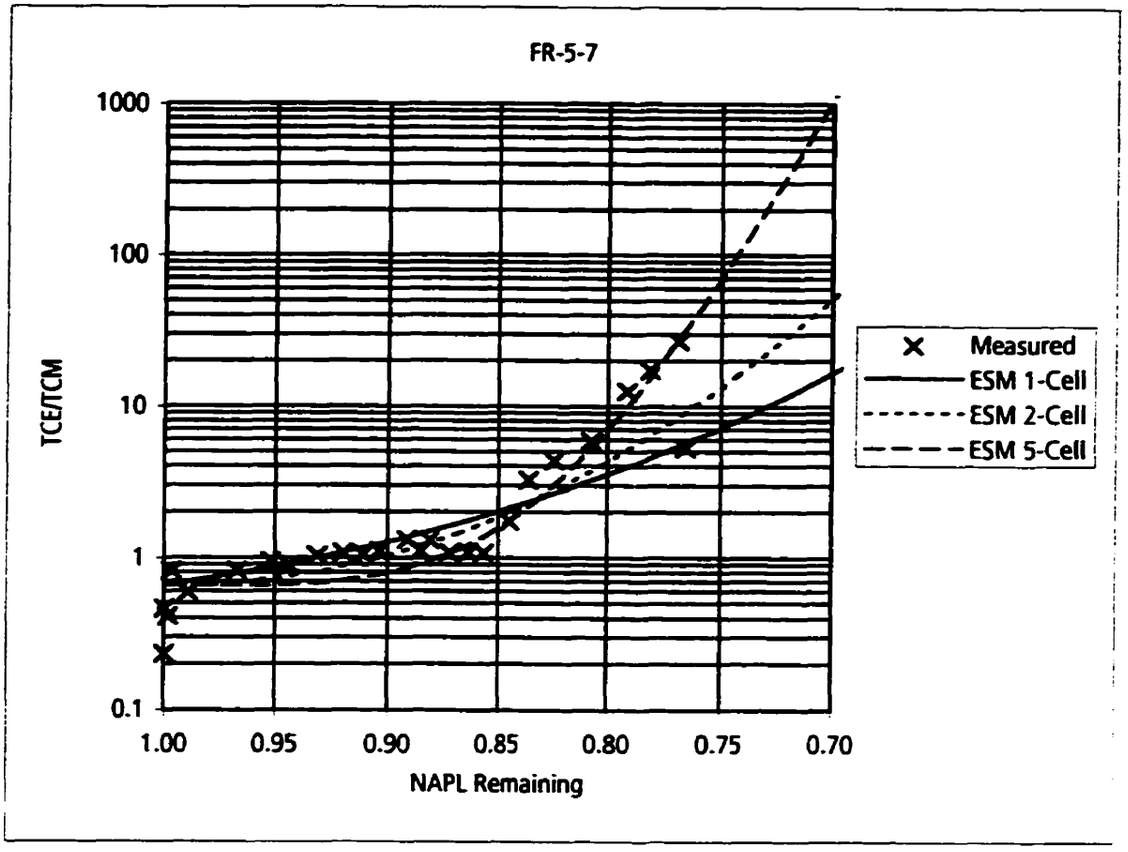

Key:
TCM - Chloroform
TCE - Trichloroethylene
PCE - Tetrachloroethylene

Figure 7-55. Measured TCE/TCM ratios versus NAPL remaining for monitoring point FR-5-7 compared to ratios predicted by ESM.

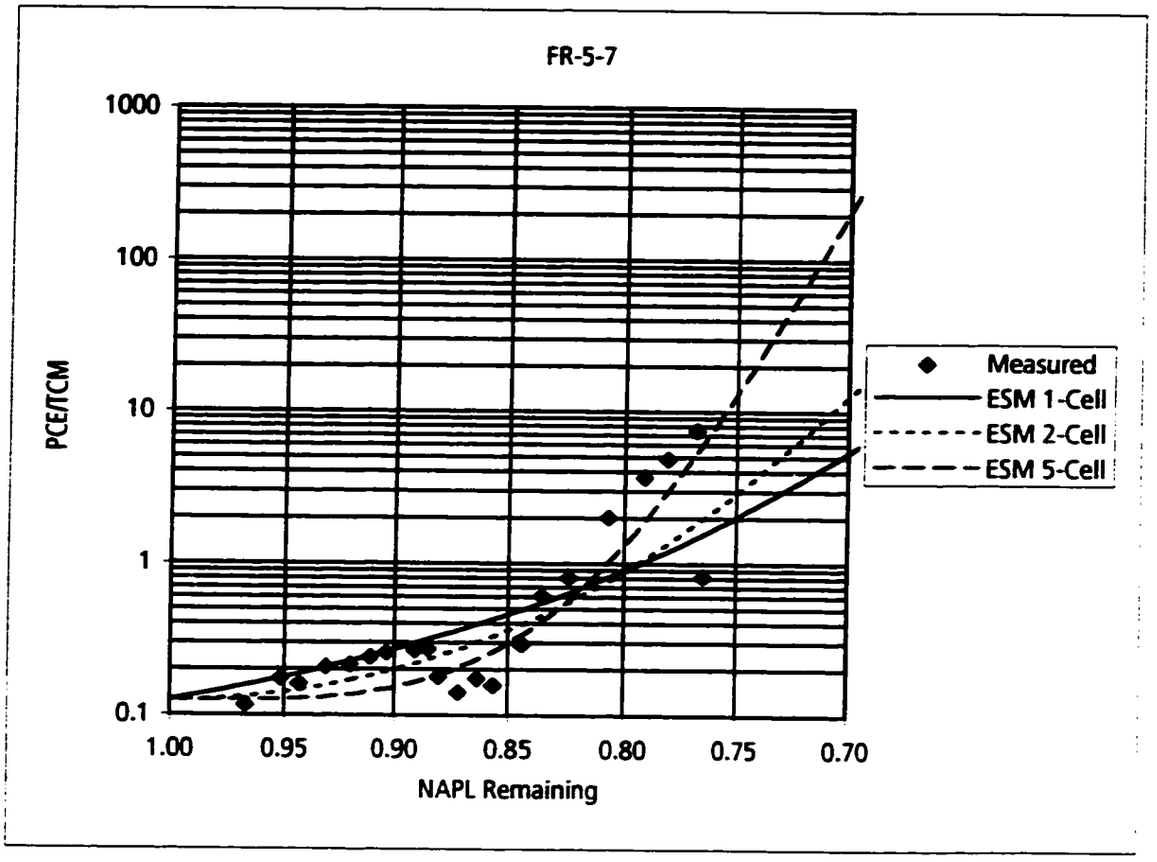

Key:
TCM - Chloroform
TCE - Trichloroethylene
PCE - Tetrachloroethylene

Figure 7-56. Measured PCE/TCM ratios versus NAPL remaining for monitoring point FR-5-7 compared to ratios predicted by ESM.

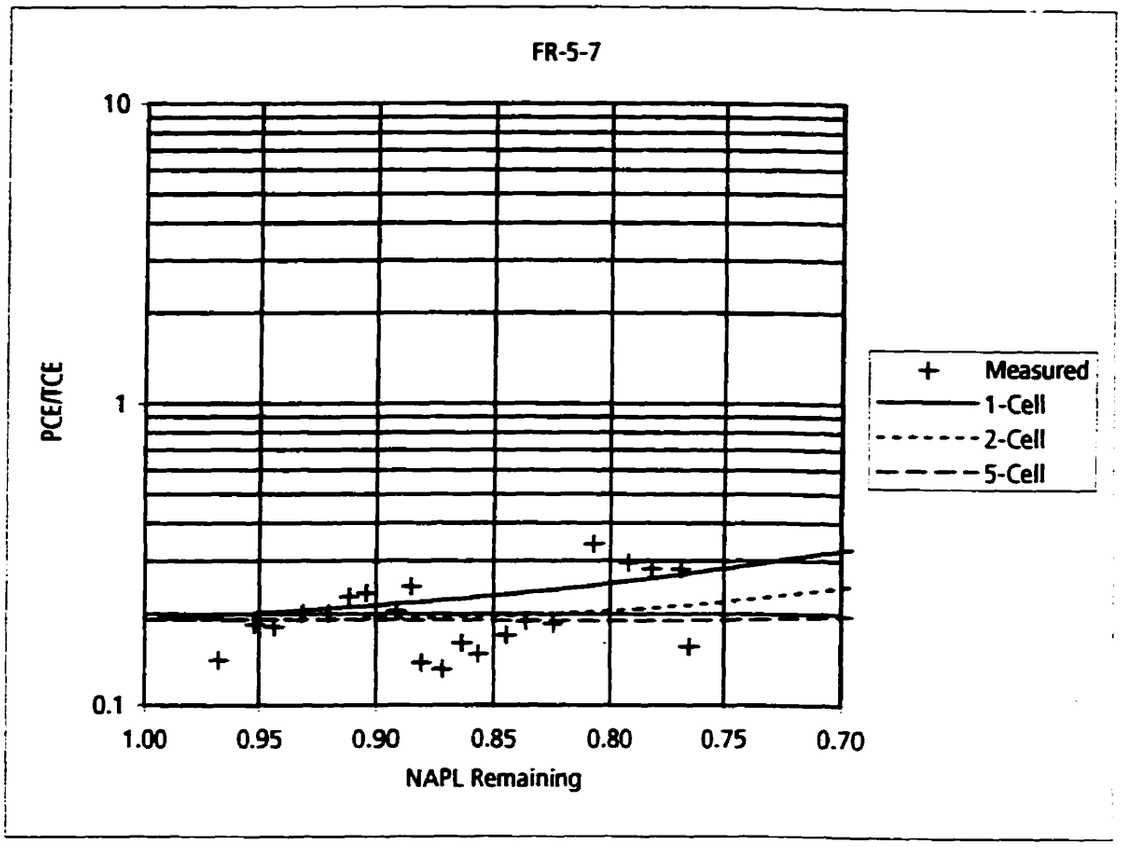

Key:
TCM - Chloroform
TCE - Trichloroethylene
PCE - Tetrachloroethylene

Figure 7-57. Measured PCE/TCE ratios versus NAPL remaining for monitoring point FR-5-7 compared to ratios predicted by ESM.

8. Application of the ESM Method for Evaluation of NAPL Sites

8.1 Methodology

8.1.1 Overview

The preceding chapters have demonstrated how the Effective Solubility Model (ESM) can be used to relate changes in aqueous concentration ratios to the chemical mass remaining in multi-component residual NAPL source zones, for both small-scale laboratory experiments and moderate-scale controlled field experiments.

This chapter describes a methodology for how the ESM could be used, together with groundwater monitoring data, to estimate the quantity of chemical mass remaining in multi-component NAPL residual zones at real sites of groundwater contamination.

8.1.2 Required Field Data

Estimation of the mass in NAPL residual zones using the ESM requires groundwater monitoring data collected over a sufficient period of time to define changes in aqueous concentration ratios and information on the cumulative chemical mass dissolved from the source zone during the corresponding period of time.

These types of data are available readily for sites at which groundwater extraction systems (i.e. pump-and-treat) have been in operation. Monitoring at most such systems include measurement of contaminant concentrations, water flow rates and determination of mass removed. Depending on the NAPL composition, relative solubility of the NAPL components and the groundwater extraction rates, changes in aqueous concentration ratios may be evident within a period of a few years.

At sites with no groundwater extraction system in operation, it is necessary to estimate the cumulative chemical mass dissolved from the source zone on the basis of the natural groundwater flow rates and the aqueous concentrations measured in the plumes.

The collection and analysis of groundwater samples must be sufficiently frequent to allow identification of temporal changes in aqueous concentration ratios amidst other variability in the ratio data. A considerable degree of scatter is to be expected in ratio data for real sites due to fluctuations in groundwater flow conditions, fluctuations in operation of extraction systems, and analytical variability.

Groundwater quality data must be collected from locations judged to be relatively close to the known or suspected NAPL source zones. The ESM describes only the changes in aqueous concentration ratios that result from NAPL dissolution. Processes such as sorption on aquifer solids and biodegradation may also change concentration ratios in the plumes as contaminants migrate away from the source zone. The ESM considers sorption on the soil solids only within the NAPL zone. However, close to the source zone the effects of sorption and biodegradation are likely to be small, particularly for chemicals such as chlorinated solvents which do not sorbed strongly on aquifer material and are not highly susceptible to biodegradation. The potential significance of biodegradation processes can be evaluated based on information regarding reduction-oxidation conditions in the groundwater and the presence of degradation products in the groundwater.

The application of the ESM requires specification of the initial chemical composition of the NAPL. This information may be available directly from analyses of samples of NAPL, or indirectly from groundwater or soil analyses.

The composition of NAPL in a source zone can be determined from the aqueous concentrations in groundwater downgradient of the source using

Raoult's Law. This technique is described by Jackson and Mariner (1995). For aqueous-phase chemicals in equilibrium with a multi-component NAPL, the ratio of their aqueous concentration to their pure-phase solubility equals the mole fraction of the chemical in the NAPL:

$$\frac{C^i}{S^i} = \chi^i_{NAPL} \qquad [8\text{-}1]$$

where :

C^i *is the effective solubility* (M/L^3)

S^i *is the pure – phase solubility* (M/L^3)

χ^i_{NAPL} *is the mole fraction in the NAPL*

Even if the aqueous concentrations in groundwater at a downgradient location have been diluted, the ratio of their concentration to pure-phase solubility provides the relative mole fraction in the NAPL:

$$\frac{C^i_{diluted}}{S^i} = (\chi^i_{NAPL})_{diluted} \qquad [8\text{-}2]$$

where :

$C^i_{diluted}$ *is the groundwater concentration* (M/L^3)

$(\chi^i_{NAPL})_{diluted}$ *is the mole fraction in the NAPL diluted by the same factor as the groundwater concentration*

Because the aqueous concentrations of all the components are diluted to the same degree, the calculated diluted mole fractions can be summed and undiluted mole fractions calculated by:

$$\chi^{i}_{NAPL} = \frac{(\chi^{i}_{NAPL})_{diluted}}{\sum_{i=1}^{n}(\chi^{i}_{NAPL})_{diluted}} \qquad [8\text{-}3]$$

where :

n is the number of components

This method assumes that all the components of the NAPL are detected in the groundwater and incorporated in the analysis. In the case where there are components of the NAPL which go unidentified, the ratios of the identified components are not affected. In addition, the presence of unidentified components in the NAPL does not strongly influence the results of ESM simulations (see Section 4.4). However, estimates of NAPL mass remaining based on the ESM simulations include only the mass represented by the identified components.

The composition of NAPL can be estimated also using the results of soil analyses if suitable samples are available from within the source zone. However, at many sites, spatial variability in the distribution of NAPL in the subsurface may be extreme, making identification and sampling of NAPL source zones a great challenge.

The partitioning calculations of Feenstra et al. (1991) can be used to determine which soil samples have soil concentrations above the threshold concentration which would indicate the presence of NAPL. If the soil concentrations are greater than the calculated threshold concentration by a factor of 10 times or more, it is appropriate to use the total weight-based concentrations to estimate mole fractions for the chemical components. It is possible also to use the partitioning relationships described in Feenstra et al. (1991) to determine the chemical concentrations in the NAPL-, sorbed-, aqueous-, and vapour-phases of the soil from the total concentration to

calculate the component concentrations in the NAPL and mole fractions separately.

The estimation of NAPL composition from soil samples is most applicable to NAPL comprised of semi-volatile and non-volatile components. For NAPL containing volatile compounds such as chlorinated solvents or BTEX compounds, reliable chemical analyses of soil samples can be obtained only if samples are analysed immediately in the field, or using methanol-preservation methods. Soil samples not analysed by these methods cannot be used reliably for estimating NAPL composition because of the large potential error due to loss of volatiles during sample collection, storage and handling. The magnitude of the error associated with analysis of volatiles in soil is described in Smith et al. (1996).

The use of the ESM requires information also on the aquifer properties of total porosity, dry bulk density and organic carbon content. These parameters are measured routinely in many site investigation programs. Even when site-specific values are not available, values for these parameters can usually be estimated with a suitable degree of accuracy. As described in Chapter 4, the results of the ESM are not highly sensitive to the values of these parameters.

8.1.3 Required Model Parameters

The components of the NAPL and the information on the NAPL composition are determined from the field data. In addition, the ESM requires values for the physical and chemical properties of NAPL components including the molecular weight, density, pure-phase solubility, and K_{OC} (organic carbon-water partition coefficient). Values for these parameters are available from the published literature for most common groundwater contaminants.

The ESM also requires that the initial NAPL content be specified for the model calculations. As described in Chapter 4, the results of the ESM are not sensitive to the initial NAPL value provided typical NAPL residual saturations are used.

The only parameter of the ESM that is not defined explicitly by the NAPL or aquifer properties is the number of cells. Although the laboratory and controlled field experiments described in Chapters 5, 6 and 7 suggest that even a 1-cell configuration of the ESM may provide useful estimates of NAPL remaining in source zones, the comparison and matching of field data to multiple-cell configurations is likely to provide more accurate predictions. The following section describes how field data may be compared to ESM simulations.

8.1.4 Model Simulations

The first step in the comparison of field data to the ESM is to perform a series of ESM simulations using the NAPL composition and aquifer properties defined for the site. Simulations should be performed for a range of cell configurations to produce a family of dissolution curves for the NAPL showing the change in aqueous concentration ratios versus the NAPL remaining. For a given NAPL composition, the different curves in a family will have distinctly different shapes as the number of cells increases.

All simulations for a specified NAPL should yield the same initial aqueous concentration ratios. The values can be compared to the measured aqueous concentration ratios at the start of the monitoring period at the site. The predicted initial ratios and measured initial ratios should be identical if the groundwater concentrations were used to back-calculate the NAPL composition. If the NAPL composition was estimated from NAPL samples or soil samples and the predicted and measured initial ratios differ significantly,

the NAPL composition input to the ESM may be adjusted to provide a better match.

If the 1-cell configuration of the ESM were known to be always the most applicable, the aqueous concentration ratio measured at the site at a given time could be related simply to the ratio from the 1- cell curve of ESM and the NAPL remaining determined directly. However, the most appropriate cell configuration is not known *a priori* so that the measured ratios must be compared to the different curves to evaluate the best match.

The data on measured aqueous concentration ratios and corresponding values of cumulative mass removed from the site are used for comparison to the ESM simulations. The cumulative mass removed is expressed as NAPL mass remaining, calculated based on a series of estimates of the initial NAPL mass in the source zone. The measured ratios and corresponding values for calculated NAPL mass remaining are plotted on the same graph at the ESM results for comparison to the family of dissolution curves. These calculations and curve matching are performed easily in an spreadsheet-plotting program. The estimates of initial NAPL mass are adjusted until the best match is obtained between the measured ratios and a particular ESM curve.

For the best match, the initial mass represents the initial NAPL mass in the source zone at the start of the monitoring period. The NAPL mass remaining is given by the value at the final measured ratio data point.

The number of cells required for a match between the measured and predicted ratios provides a generic indication of the length of the groundwater flow path through the NAPL source zone. A larger number of cells is required to simulate the chromatographic effect as aqueous-phase contaminants dissolved from the upgradient portion of the source zone interact with NAPL in the downgradient portion of the source zone. The longer the flow path through the NAPL zone, the greater the

chromatographic effect on the aqueous concentrations. For normal groundwater velocities, a chromatographic effect would be expected in groundwater that passes through zones of NAPL residual more than a few centimetres in length. However, because spatial distribution of NAPL within a source zone may be extremely variable at a scale of centimetres (Poulsen and Kueper, 1992; Kueper et al., 1993; Brewster et al., 1995), the opportunity for aqueous-phase contaminants to exchange with downgradient NAPL may be small, even in large source zones which contain large total amounts of NAPL. A match between measured and predicted ratios with a small number of cells likely reflects a source zone in which NAPL is distributed irregularly on a small scale to minimize the chromatographic effect. A match with a large number of cells likely reflects a source zone in which NAPL is distributed more uniformly.

The following sections provide examples of the application of the methodology to estimate the quantity of chemical mass remaining in the NAPL residual zone at the Emplaced-Source experiment using only the data from pumping well PW-2, and for a NAPL source zone at an industrial site in New Jersey.

8.2 Example: Emplaced-Source Experiment PW-2

Although the monitoring data collected from the groundwater pump-and-treat system could not be used for a rigorous evaluation of the rate of mass depletion from the NAPL source zone, they can be used to illustrate the method for using the ESM to estimate the quantity of chemical mass remaining in the NAPL source zone.

Pumping well PW-2 was located about 25 m downgradient of the source zone (see Figure 6-13). The decline in aqueous concentrations in PW-2 with time is shown in Figure 6-32. Groundwater extraction from PW-2

intercepted the entire width of the plumes emitted from the source zone. The calculated mass flux for PW-2 is shown in Figure 6-33.

TCE/TCM, PCE/TCM and PCE/TCE ratios increased with time as pump-and-treat operations continued. The temporal changes in ratios are shown in Figure 8-1. Data are shown here only for the period from 475 days at the start of operations to about 700 days. After 700 days the aqueous concentrations measured at PW-2 were influenced by the *in situ* treatment wall situated between the source and PW-2. The cumulative chemical mass removed from PW-2 was calculated from the aqueous concentrations and pumping rates, and is plotted versus aqueous concentration ratios in Figure 8-2. The total chemical mass removed from PW-2 was 2,200 g.

Based on the initial aqueous concentrations measured in PW-2, the mole fractions for TCM, TCE and PCE in the NAPL source were calculated using equation 8-3 and converted to weight% concentrations for input to the ESM. The results of these calculations are shown in Table 8-1. This NAPL composition differs somewhat from the original NAPL composition of the source zone. However, the travel time for groundwater to migrate from the source to PW-2 was about 250 days to 300 days. Therefore, by the time PW-2 commenced operation at 475 days, the groundwater arriving at PW-2 represented the groundwater that left the source zone at a time of about 200 days. At that stage, substantial TCM has already be removed from the source zone. This explains why the calculated composition shown in Table 8-1 is depleted in TCM relative to the original source composition.

The properties of the components used as input parameters to the ESM are shown in Table 8-2. The aquifer was specified to have a dry bulk density of 1,809 kg/m^3, a total porosity of 0.33 and a fraction organic carbon (f_{OC}) of 0.0002. The initial NAPL content was specified to be 20 L/m^3. Using these parameters values, simulations were performed for 1-cell, 2-cell and 5-cell configurations.

The values of cumulative mass removed from PW-2 were converted to NAPL mass remaining for assumed initial NAPL source zone masses of 12,000 g, 17,000 g and 22,000 g. These data were combined with the measured aqueous concentration ratios and plotted with the ESM simulations. The measured TCE/TCM ratios for an assumed 17,000 g source zone are shown in Figure 8-3. The measured ratios compare well with the 5-cell configuration curve.

In contrast, measured PCE/TCM and PCE/TCE ratios for an assumed 17,000 g source zone shown in Figure 8-4 and 8-5 do not compare well with any of the ESM simulation curves. This is likely due to the sorption of PCE relative to TCM and TCE over the migration distance of 25 m from the source zone to PW-2. The ESM simulations cannot account for changes in aqueous concentration due to sorption outside the NAPL zone. As a result, the use of PCE/TCM and PCE/TCE ratios are not suitable for estimating the NAPL mass remaining based on the monitoring data from PW-2. The TCE/TCM and PCE/TCM ratios yield similar results for the monitoring location along the 1 m Fence. This indicates that the effect of sorption of PCE is not observed closer to the source zone.

Measured TCE/TCM ratios for assumed NAPL sources of 12,000 g and 22,000 g are shown in Figures 8-6 and 8-7, respectively. These data are substantially different from the assumed 17,000 g source and do not match any of the ESM simulation curves. This evaluation suggests that the best estimate of the initial source zone mass is about 17,000 g. The true source zone mass at 200 days is not known precisely. On the basis of the mass flux measured at the 1 m Fence, the mass in the source zone at 200 days was 20,800 g. However, PW-2 would have drawn back some water and chemical mass that left the source prior to 200 days. The chemical mass removed from PW-3 and PW-4 was about 740 g. If this is assumed to represent the chemical mass that left the source between 0 days and 200 days but not captured by PW-2, then the mass in the source zone at 200 days was 22,200 g. Splitting the

difference between the 20,800 g estimate and the 22,200 g estimate, yields an initial source mass of 21,500 g to compare with the ESM estimate of 17,000 g.

The mass estimated using the 5-cell configuration of the ESM is within 20% of the initial NAPL source zone mass. This estimate could be made using only the measured aqueous concentrations in PW-2, and the general physical and chemical properties for the NAPL components and aquifer. No specific assumptions were required regarding the actual dimensions or geometry of the source zone, groundwater flow conditions through the source zone, or dissolution mass transfer coefficients.

If the maximum measured TCE/TCM ratio of 7 is compared simply to the curve for the 1-cell configuration of the ESM, it is predicted that 0.15 of the NAPL source has been removed. Based on the measured mass removal of 2,200 g, the 1-cell curve yields a predicted source mass of 14,700 g. Consequently, even use of the 1-cell ESM provides an estimate of the NAPL mass within about 30% of the actual value.

8.3 Dayton Case Study

8.3.1 Site Conditions

An industrial plant site near Dayton, New Jersey is a site of groundwater contamination by tetrachloroethylene (PCE) and 1,1,1-trichloroethane (TCA). This section describes the use of the ESM to estimate the quantity of chemical mass remaining the DNAPL source zone at this site. No other methods have been applied at this site to provide such an estimate. A preliminary application of this method was described by Feenstra (1990).

The plant site was used for the manufacture of punch cards for computers and inked printer ribbons. The aquifer consists of about 15 m of coarse sand & gravel overlying a discontinuous layer of interbedded sand and clay about 1 m to 3 m in thickness. The saturated thickness of the aquifer

ranges from 8 to 10 m and the average hydraulic conductivity is about 8×10^{-2} cm/s. In December 1977, PCE and TCA were discovered at concentrations of about 200 µg/L and 600 µg/L, respectively, in a municipal water supply well located about 500 m east of the plant.

During early 1978, plumes of PCE and TCA were found on the plant site with concentrations as high as 6,100 µg/L PCE and 9,500 µg/L TCA (see Figures 8-9a and 8-9b). The maximum observed concentrations in monitoring wells and pumping wells were several percent of the pure-phase solubility of the solvents. Chlorinated solvents had been used at the plant since the 1960's and it was believed that the groundwater contamination originated from releases of solvent product from the chemical off-loading and storage area. Although the plume was directed toward the municipal well located off-site to the east, the plumes were wide compared to the size of the suspected release area. This could be the result of several factors. Time-dependent variations in off-site pumping in the municipal well to the east and other private wells to the north may have acted to draw the plume back and forth. A broad plume of relatively low concentration (10 µg/L to 100 µg/L) in the groundwater could also have resulted initially from the transport of vapors through the vadose radially outward the release area. These vapors would have resulted in a thin, relatively high-concentration groundwater plume immediately at the water table. However, almost all monitoring and groundwater pumping at the site was conducted using wells screened over the entire aquifer thickness. Therefore, the concentrations from any thin plumes at the water table would be diluted significantly during sampling. It is also possible that the broad dissolved plume is a composite plume resulting from several different sources on the site.

Remedial measures commenced in mid-1978 with the removal of the chemical storage tanks, excavation of several tens of cubic metres of soil from around the tanks, and installation of a network of groundwater pumping

wells on the plant site. According to the conceptual model for groundwater contamination at that time, removal of the tanks and shallow soil together with removal of the dissolved plume by groundwater pump-and-treat should have provided full restoration of the aquifer in several years. When the remedial measures were designed in 1978, it was not recognized that the chlorinated solvents were DNAPLs and that it was highly likely that immiscible-phase solvents released into the aquifer would penetrate to a considerable depth below the water table and comprise a long-term source of contamination.

The remedial measures for the overall plume involved on-site pumping wells, off-site pumping wells and a resumption of pumping and treatment of the municipal water supply well. This discussion will only consider the performance of the on-site pumping because this area includes the source zone.

The on-site pumping system consisted of up to 13 wells. Seven of the wells operated almost continuously from mid-1978 until late-1984 when on-site pumping ceased. These wells are shown in Figure 8-9a. The other wells operated for shorter intervals during this time period. Three of the pumping wells yielded from 250 L/min. to 390 L/min. and the remaining 10 wells yielded from 20 L/min. to 40 L/min. A typical pumping rate for the overall system was about 1,100 L/min. The discharge from the pumping system was treated by air stripping and recharged to the aquifer by spray irrigation along the western side of the plant site.

By late 1984, aqueous concentrations in the aquifer zone had been reduced significantly from levels of 1,000 to 2,000 µg/L down to 10 µg/L or less (see Figures 8-10 and 8-10b). During this time period a total of 3,400,000,000 L of groundwater and 4,840 kg of solvents had been removed by the on-site pumping system. Reductions down to low microgram per litre concentrations occurred in monitoring wells and pumping wells throughout

the plume zone except in the area close to the suspected release. Close to the release area or probable source zone, solvent concentrations in 2 pumping wells were also reduced significantly but declined only to concentrations of 300 µg/L to 500 µg/L.

Although it was not recognized in 1984, the continued elevated concentrations in the pumping wells close to the suspected source zone indicated an on-going source of contamination, which is likely DNAPL solvents below the water table. The reduction in concentrations in pumping wells close to the source zone are largely due to dilution of contaminated water from the source zone with uncontaminated or less-contaminated water draw from outside the source zone.

In late 1984, the state environmental regulatory agency determined that the remedial measures had reached the appropriate clean-up target for the majority of the plume area, and had reached the point of diminishing returns for the release area. With this conclusion, groundwater pump-and-treat was ceased.

Within about 6 months to 9 months after groundwater pumping ceased, monitoring indicated that concentrations had begun to rise in the wells close to the source zone. Eventually, concentrations in several of the wells rose to levels higher than were observed in 1978. By mid-1989, about 4.5 years after pumping had ceased, the dissolved solvent plumes extended again beyond the eastern plant boundary (see Figures 8-11a and 8-11b). The regrowth of the plume was clear evidence of a DNAPL source zone below the water table.

Further evidence of the nature of the DNAPL source zone in the aquifer was derived from multi-level monitoring wells. The majority of the monitoring at the site was conducted in well screened over the entire saturated thickness of the aquifer. In 1985, 3 water samplers (42s, 42i and 42d)

was installed in the upper, middle and lower portions of the aquifer within about 10 m to 20 m of the suspected source zone. These samplers were monitored regularly during the period after the groundwater pump-and-treat operations ceased and the results are shown in Figure 8-12. Moderate concentrations occurred in the upper part of the aquifer, very low concentrations occurred in the middle part of the aquifer, and the highest solvent concentrations occurred at the bottom of the aquifer. This suggests that DNAPL exists in the upper and lower portions of the aquifer. The DNAPL in the upper portion of the aquifer is likely in the form of residual and thin pools. The DNAPL in the lower portion of the aquifer may be in the form of a thicker pool on top of the clay aquitard.

In 1990, the groundwater pump-and-treat system was reactivated with a network of 4 pumping wells: one at the source zone, one close to the middle of the plumes, and two at the eastern boundary of the plant site. The goals of this pump-and-treat system are containment of the plumes to prevent further migration off-site and eventual restoration of the aquifer in the plume zone. It is hoped that in several years the aqueous plumes will be again eliminated and containment of the source zone can be provided by pumping of the one well near the source zone.

8.3.2 DNAPL Source Zone

The DNAPL source zone remaining in the aquifer likely consists of residual and multiple pools or layers at various depths within the aquifer as well as at the bottom of the aquifer. Because of the expected spatial variability of the DNAPL distribution, an inordinately detailed program of soil borings and soil sampling would be necessary to attempt to define the distribution and mass of the DNAPL zone and is not feasible.

There are no records from the industrial facility regarding leaks or spills which would permit an estimate of the possible chemical mass present

in the aquifer. The only information on the magnitude of the DNAPL source zone is that a total of 4,840 kg of aqueous-phase solvents were removed from the groundwater pumping system from 1978 to 1984. Of this total, 2,150 kg were removed from pumping well GW-32 adjacent to the expected source area. In crude terms, mass removed from GW-32 represents the mass dissolved from the source zone from 1978 to 1984. The difference between the total mass removed and the mass removed from GW-32, about 2,690 kg, represents the mass dissolved from the source prior to 1978. Although the regrowth of the plumes and the vertical pattern of groundwater contamination confirms that substantial DNAPL remains in the aquifer, the chemical mass remaining is not known.

8.3.3 Aqueous Concentrations and Ratios in GW-32

During operation of the groundwater pumping system from 1978 to 1984, the PCE and TCA concentrations in GW-32 declined. These data are shown in Figure 8-13. It is evident also from this figure that the relative proportion of TCA in the groundwater in GW-32 declined with time relative to PCE. TCA is the more soluble of the two compounds so that the preferential removal of TCA would be expected for the dissolution of a PCE-TCA NAPL source zone.

The change in PCE/TCA ratio versus time is shown in Figure 8-14. The initial PCE/TCA ratio was about 0.5 and increased to about 5 during pumping. The change in PCE/TCA ratio versus chemical mass removed is shown in Figure 8-15.

Based on the initial aqueous concentrations measured in GW-32, the mole fractions for TCA and PCE were calculated using equation 8-3 and converted to weight% concentrations for input to the ESM. The results of these calculations are shown in Table 8-3. The DNAPL source zone was estimated to be comprised of 26% TCA and 74% PCE.

The properties of the components used as input parameters to the ESM are shown in Table 8-4. The aquifer was assumed to have a dry bulk density of 1,809 kg/m^3, at total porosity of 0.33 and a fraction organic carbon (f_{OC}) of 0.0002. The initial NAPL content was assumed to be 20 L/m^3. Using these parameters values, simulations were performed for 1-cell, 2-cell and 5-cell configurations. The results of these simulations are shown in Figure 8-16.

The values of cumulative mass removed from GW-32 were converted to NAPL mass remaining for assumed initial NAPL source zone masses 4,000 kg, 5,000 kg and 6,000 kg. These data were combined with the measured aqueous concentration ratios and plotted with the ESM simulations. The measured PCE/TCA ratios for an assumed 5,000 kg source zone are shown in Figure 8-17. The measured ratios compare best with the 5-cell configuration curve.

Measured PCE/TCA ratios for assumed NAPL sources of 6,000 kg and 4,000 kg are shown in Figures 8-18 and 8-19, respectively. These data are substantially different from the assumed 5,000 kg source and do not match well with any of the ESM simulation curves. This evaluation suggests that the best estimate of the initial source zone mass is about 5,000 kg. With the removal of 2,150 kg from the pumping of GW-32, this suggests that a NAPL source of 2,850 kg (57% of the initial mass) remained in the source zone at the end of pumping in 1984.

If the maximum measured PCE/TCA ratio of 8 is compared simply to the curve for the 1-cell configuration of the ESM, it is predicted that 0.55 of the NAPL source has been removed. Based on the measured mass removal from GW-32 of 2,150 kg, the 1-cell curve yields an estimated source mass of 3,900 kg. This value does not differ greatly from the value of 5,000 kg estimated from the 5-cell configuration.

In this particular case, these mass estimates must be considered as minimum values because of the high likelihood of the presence of a thick (i.e. greater than several centimetres) DNAPL pool at the bottom of the aquifer. For a thick pool of DNAPL, PCE/TCA ratios in the groundwater may change in response to changes in NAPL composition and mass depletion at the top of the pool, but not deeper in the pool. As a result, the presence of the chemical mass deeper in the pool will not be reflected in the NAPL mass estimated from the aqueous concentration ratios.

Unlike the laboratory experiments and controlled field experiments described in Chapters 5, 6 and 7, there is no knowledge of the actual source mass at the Dayton site with which to compare the ESM estimates. This will be the case at almost all real sites of NAPL contamination because of uncertainty in the quantity of NAPL released and difficulty in direct sampling and analysis of NAPL source zones.

8.4 Conditions for Application of the ESM Method

On the basis of the favourable comparison to laboratory and controlled field experiments, it is evident that the Effective Solubility Model (ESM) may provide a useful tool to relate changes in aqueous concentration ratios to the chemical mass remaining in multi-component NAPL residual. The ESM, together with groundwater monitoring data, has the potential to provide estimates of the chemical mass contained in NAPL residual zones.

For the case of the Emplaced-Source experiment, using only the monitoring results from pumping well PW-2 situated 25 m downgradient of the source zone, the NAPL source mass estimated using the ESM was within 30% of the actual NAPL mass using the 1-cell configuration of the ESM, and within 20% using the 5-cell configuration of the ESM which provided a better match between the measured and predicted ratios. This degree of error is far less than would be expected for mass estimates based on the sampling and

analysis of soil samples. The mass estimate using the ESM could be made using only the measured aqueous concentrations in PW-2, and the general physical and chemical properties for the NAPL components and aquifer. No specific assumptions were required regarding the actual dimensions or geometry of the source zone, groundwater flow conditions through the source zone, or dissolution mass transfer coefficients.

At the Dayton site, the presence of a DNAPL source zone was clearly indicated by the regrowth of the aqueous-phase plumes after the cessation of pumping in 1984. The use of the ESM with the measured PCE/TCA ratios yielded an estimate of 5,000 kg for the NAPL source zone, reflecting the removal of 43% of the mass by GW-32 during pumping. This means that an estimated 2,850 kg, or 57% of the source zone, remained in the aquifer at the end of 1984. This method is, at present, the only means that has been applied to estimate the mass of the DNAPL source zone.

This research has illustrated the potential for the ESM method to provide useful estimates of the chemical mass contained in multi-component NAPL residual zones in porous media. In many situations, the ESM method could be employed for estimation of mass in NAPL zones with existing groundwater monitoring data, especially for sites with operating groundwater extraction systems close to NAPL source zones. In contrast, programs for sampling and analysis of soil, or partitioning interwell tracer tests for estimates of the mass in NAPL zones will require specific field studies which are likely to be costly, especially for large suspected NAPL source zones.

However, it must be recognized that the ESM method has been tested only for small-scale laboratory studies and for two moderate-scale field experiments in sandy aquifer materials. There are numerous specific conditions required for its application which include the following:

- The NAPL must consist of multiple components and occur in porous media. The ESM method is not applicable for single-component NAPL, or for fractured media, or fractured porous media.

- There must be sufficient differences in the solubilities of the NAPL components to result in preferential dissolution of the more soluble components.

- Raoult's Law must be suitable for determining the effective solubility of the NAPL components. The ESM method will be most suitable for relatively simple mixtures of chlorinated solvents or hydrocarbons.

- The NAPL source zone must not contain different NAPLs of different chemical composition. Site history and groundwater monitoring data may provide information on the nature of NAPL releases to assess this condition.

- The record of groundwater monitoring must be of sufficient duration and detail to define trends in aqueous concentration ratios and chemical mass released from the NAPL source zone. This is best accomplished for a groundwater extraction system which captures the entire mass flux from the NAPL source zone.

- Aqueous concentration ratios measured in the groundwater must not have been altered by sorption processes in the aquifer between the source zone and monitoring location. This condition is most likely to be satisfied at monitoring locations close to the source zone, or for contaminants such as chlorinated solvents and low molecular weight hydrocarbons which do not sorb strongly on most geologic materials.

- Aqueous concentration ratios measured in the groundwater must not have been altered by biodegradation processes within the NAPL source zone or in the aquifer between the source zone and monitoring location. Groundwater monitoring data may provide information on whether biodegradation reactions have occurred, or are likely to occur.

- NAPL must occur as residual or thin pools. The ESM method is not applicable to thick NAPL pools.

- NAPL residual must be available for dissolution into groundwater flowing through the source zone. The ESM method is not applicable in situations where a significant portion of the NAPL mass is contained in zones of lower permeability. In such situations, estimates of NAPL mass using aqueous concentration ratios will reflect the NAPL mass contained in areas accessible to groundwater flow and will underestimate the total NAPL mass.

For the majority of the aforementioned conditions, it will be possible to render a reasonable judgment as to whether they are satisfied at a particular site of NAPL contamination. However, this is not likely to be the case for conditions related to the physical distribution of the NAPL. Investigations of the geologic conditions and chemical distribution within NAPL source zones are rarely sufficient to establish whether thick NAPL pools or zones of NAPL isolated in lower permeability zones are present or absent.

Table 8-1. Calculation of initial NAPL source composition based on aqueous concentrations in PW-2.

Measurement	TCM	TCE	PCE	Total
Initial Concentration in PW-2 (µg/L)	2,800	4,100	700	
Pure-phase Solubility (µg/L)	8,700,000	1,400,000	240,000	
Concentration/Solubility Ratio	3.2×10^{-4}	2.9×10^{-3}	2.9×10^{-3}	
Calculated Mole Fraction in NAPL	0.052	0.474	0.474	1.000
Weight % in NAPL	4.2	42.4	53.4	100.0

18

Key:
TCM - Chloroform
TCE - Trichloroethylene
PCE - Tetrachloroethylene

Table 8-2. Composition and properties of the components in the NAPL in the source zone used as input parameters in the ESM simulations for the PW-2 data.

Parameter	TCM	TCE	PCE
Molecular Mass (g/mol)	119.4	131.5	165.8
Density (kg/m^3)	1,490	1,470	1,630
Pure-phase Solubility (µg/L)	8,700,000	1,400,000	240,000
K_{OC} (mL/g)	56	93	302
Composition (wt.%)	4.2	42.4	53.4

Key:
TCM - Chloroform
TCE - Trichloroethylene
PCE - Tetrachloroethylene

Table 8-3. Calculation of initial NAPL source composition based on aqueous concentrations in GW-32.

Measurement	TCA	PCE	Total
Initial Concentration in PW-32 (µg/L)	2,750	1,240	
Pure-phase Solubility (µg/L)	1,250,000	240,000	
Concentration/Solubility Ratio	2.2×10^{-3}	5.2×10^{-3}	
Calculated Mole Fraction in NAPL	0.30	0.70	1.000
Weight % in NAPL	26	74	100

Key:
TCA - 1,1,1-Trichloroethane
PCE - Tetrachloroethylene

Table 8-4. Composition and properties of the components in the NAPL in the source zone used as input parameters in the ESM simulations for the Dayton data.

Parameter	TCA	PCE
Molecular Mass (g/mol)	133.4	165.8
Density (kg/m^3)	1,370	1,630
Pure-phase Solubility (µg/L)	1,400,000	240,000
K_{OC} (mL/g)	126	302
Composition (wt.%)	26	74

Key:
TCA - 1,1,1-Trichloroethane
PCE - Tetrachloroethylene

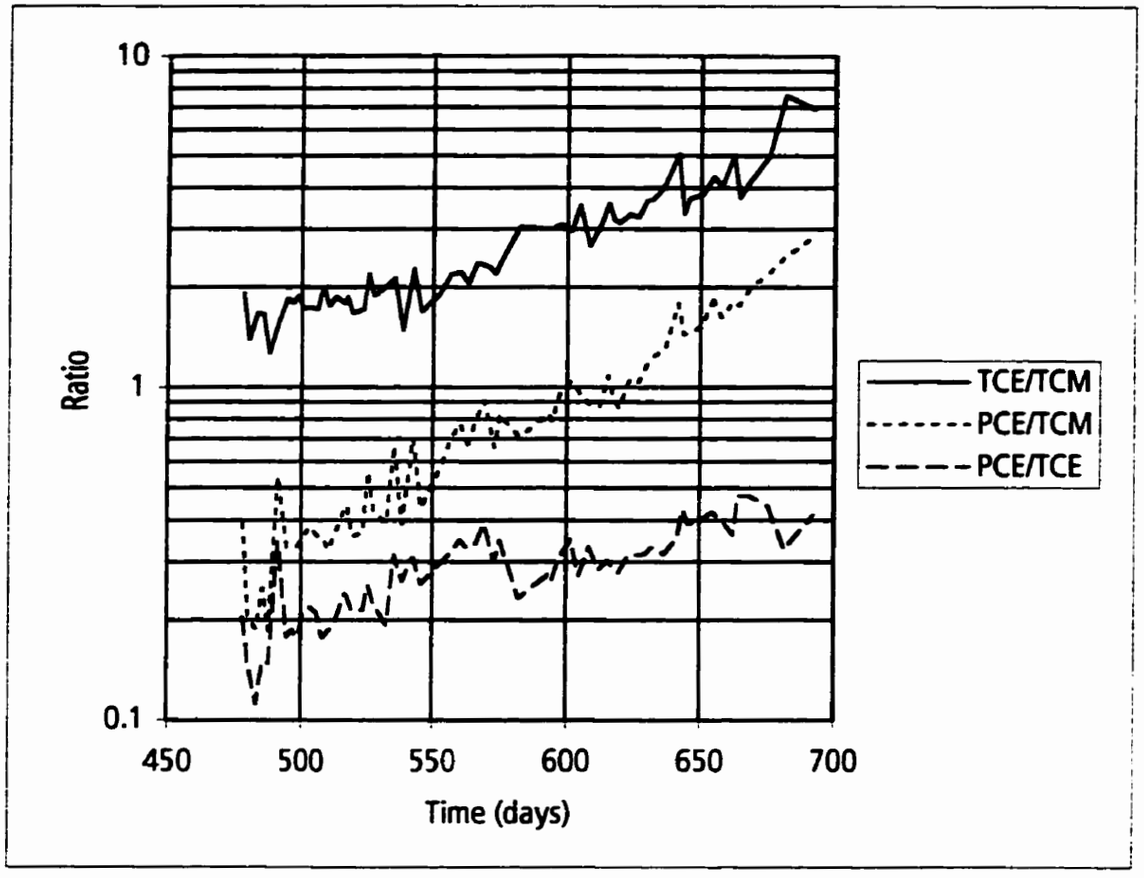

Key:
TCM - Chloroform
TCE - Trichloroethylene
PCE - Tetrachloroethylene

Figure 8-1. Change in aqueous concentration ratios versus time at the pumping well PW-2.

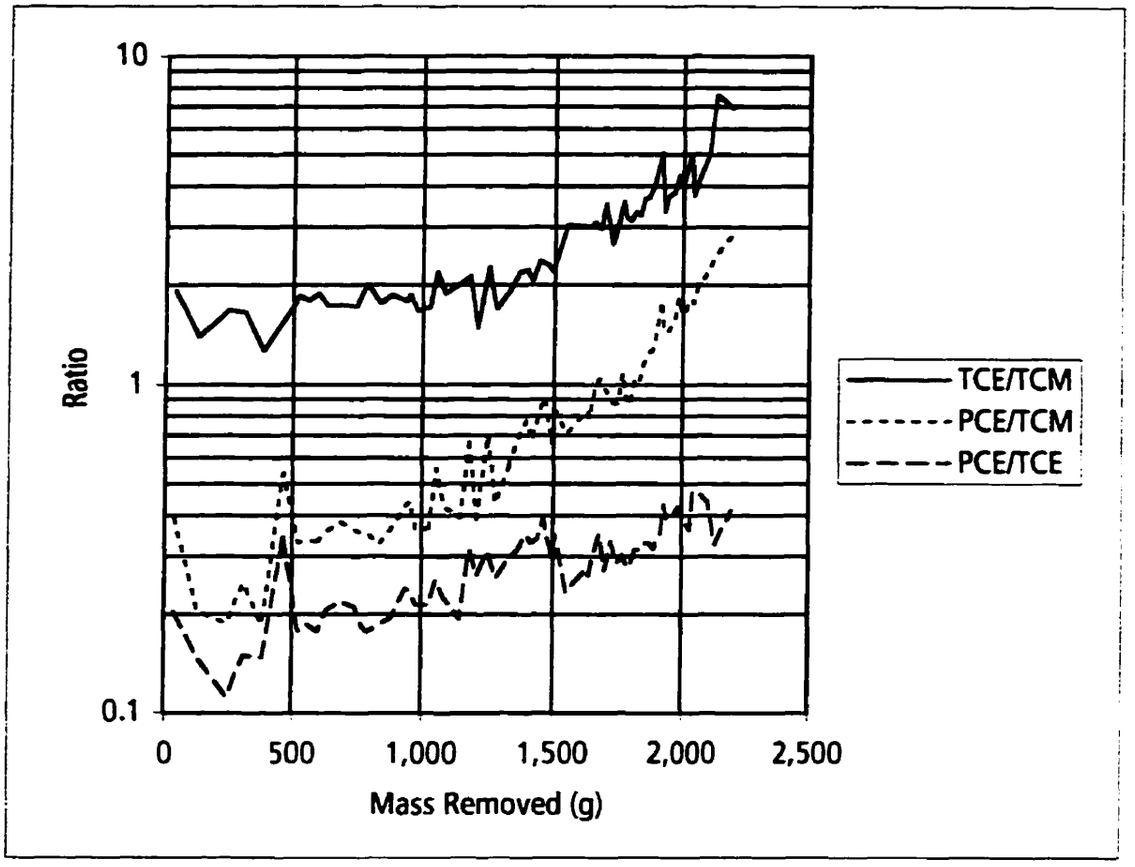

Key:
TCM - Chloroform
TCE - Trichloroethylene
PCE - Tetrachloroethylene

Figure 8-2. Change in aqueous concentration ratios versus chemical mass removed at the pumping well PW-2.

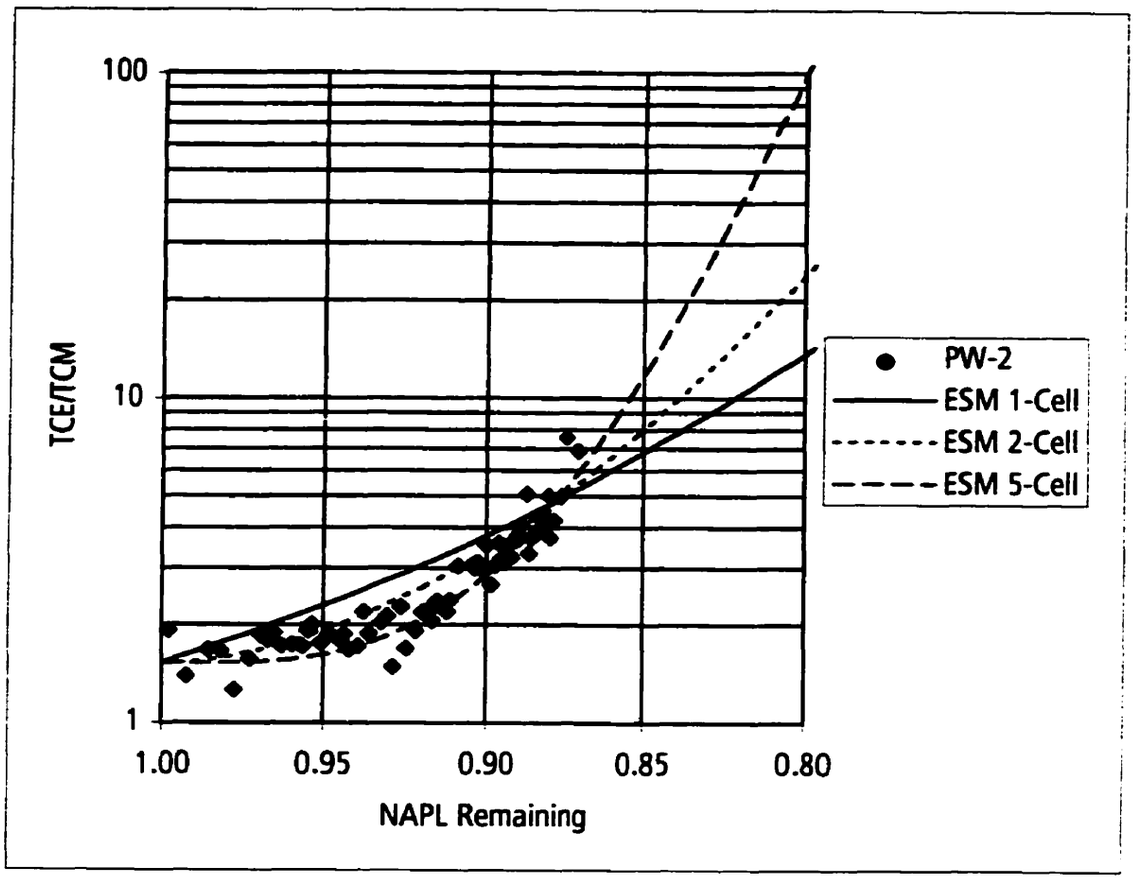

Key:
TCM - Chloroform
TCE - Trichloroethylene
PCE - Tetrachloroethylene

Figure 8-3. Measured TCE/TCM ratios for a 17,000 g NAPL source compared to the ratios predicted by ESM.

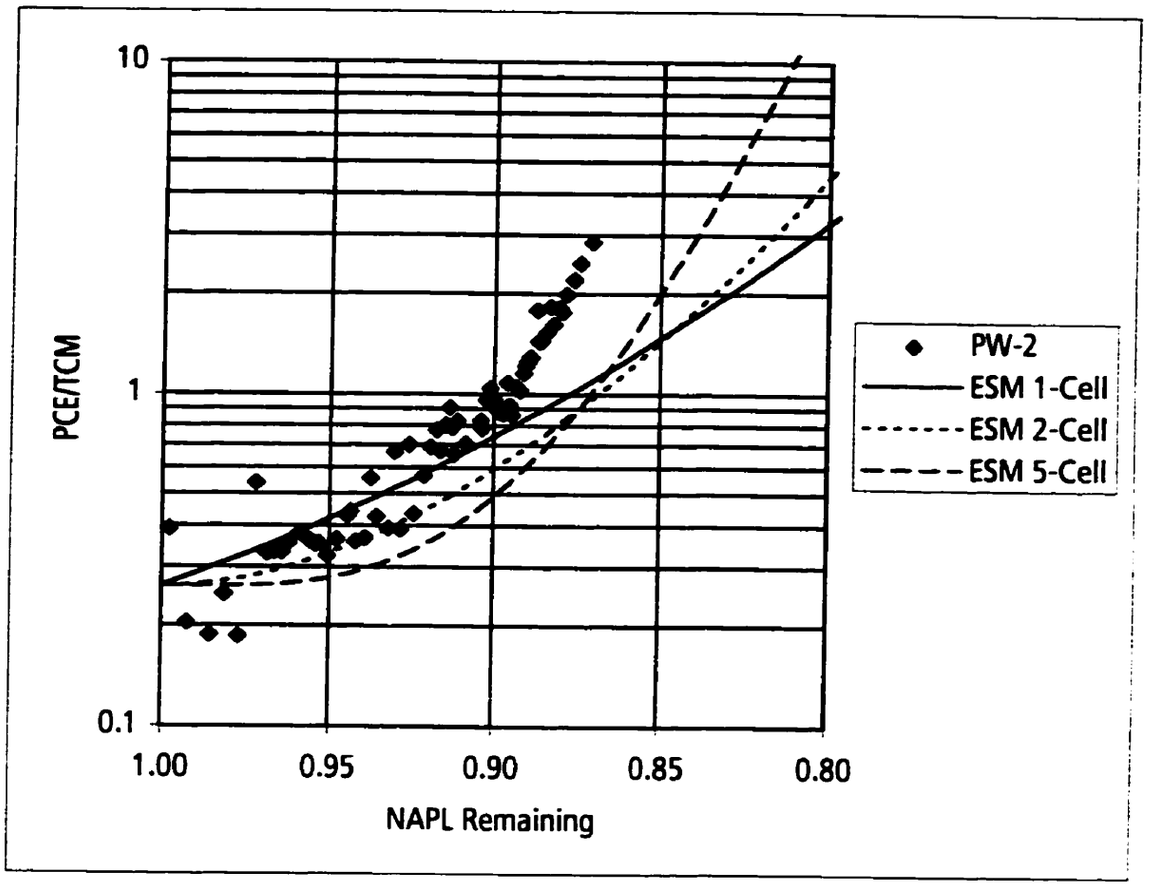

Key:
TCM - Chloroform
TCE - Trichloroethylene
PCE - Tetrachloroethylene

Figure 8-4. Measured PCE/TCM ratios for a 17,000 g NAPL source compared to the ratios predicted by ESM.

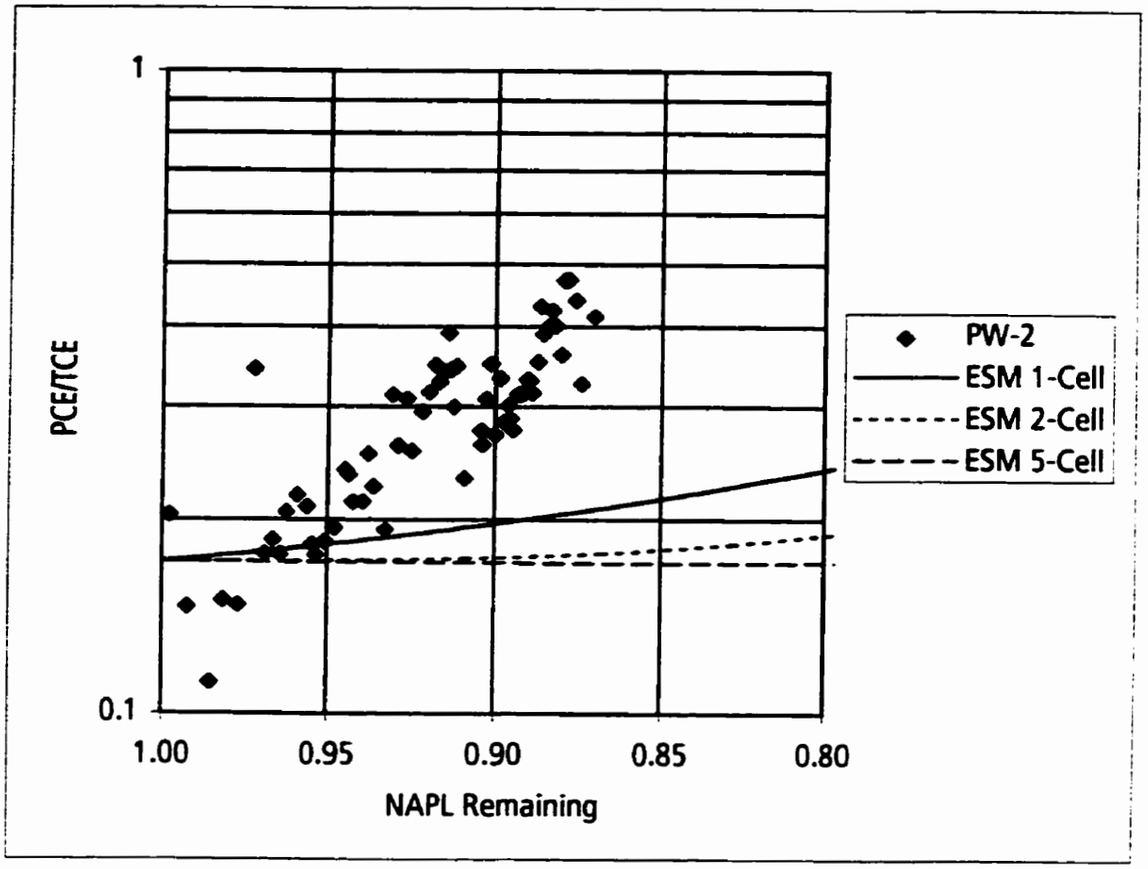

Key:
TCM - Chloroform
TCE - Trichloroethylene
PCE - Tetrachloroethylene

Figure 8-5. Measured PCE/TCE ratios for a 17,000 g NAPL source compared to the ratios predicted by ESM.

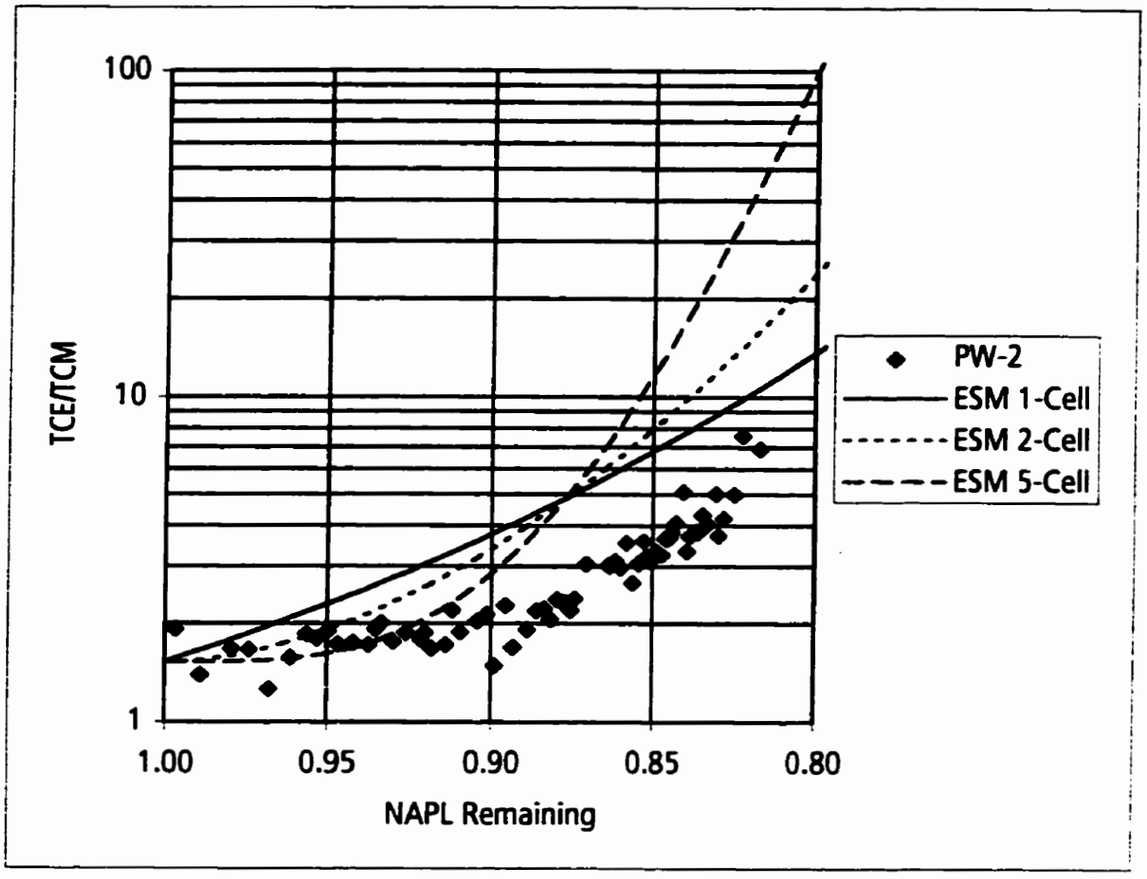

Key:
TCM - Chloroform
TCE - Trichloroethylene
PCE - Tetrachloroethylene

Figure 8-6. Measured TCE/TCM ratios for a 12,000 g NAPL source compared to the ratios predicted by ESM.

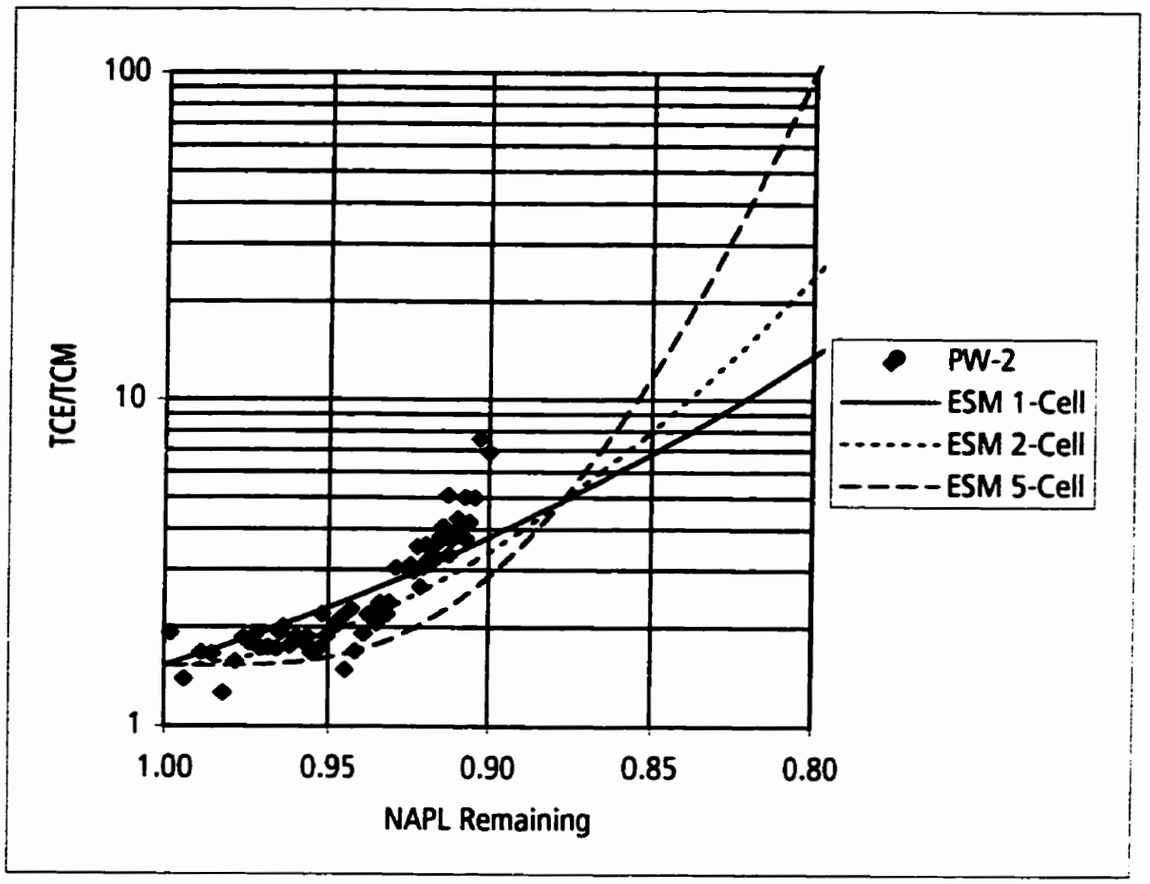

Key:
TCM - Chloroform
TCE - Trichloroethylene
PCE - Tetrachloroethylene

Figure 8-7. Measured TCE/TCM ratios for a 22,000 g NAPL source compared to the ratios predicted by ESM.

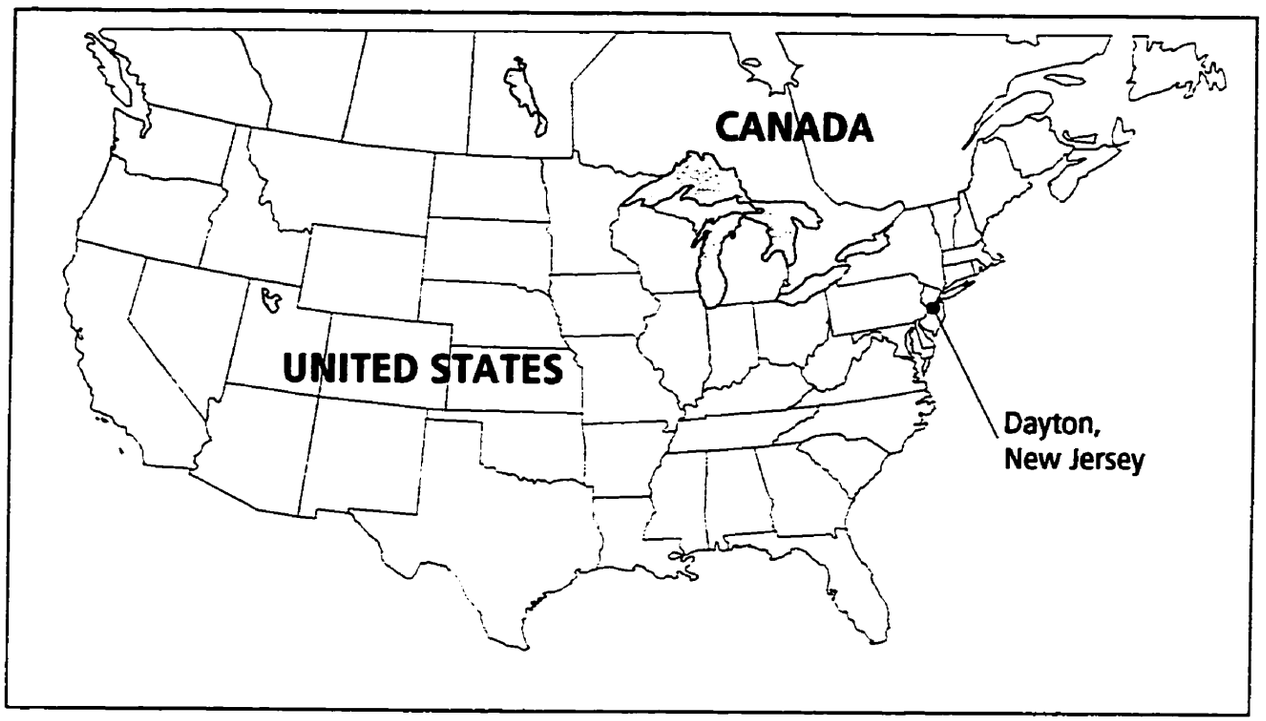

Figure 8-8. Location of the Dayton, New Jersey site.

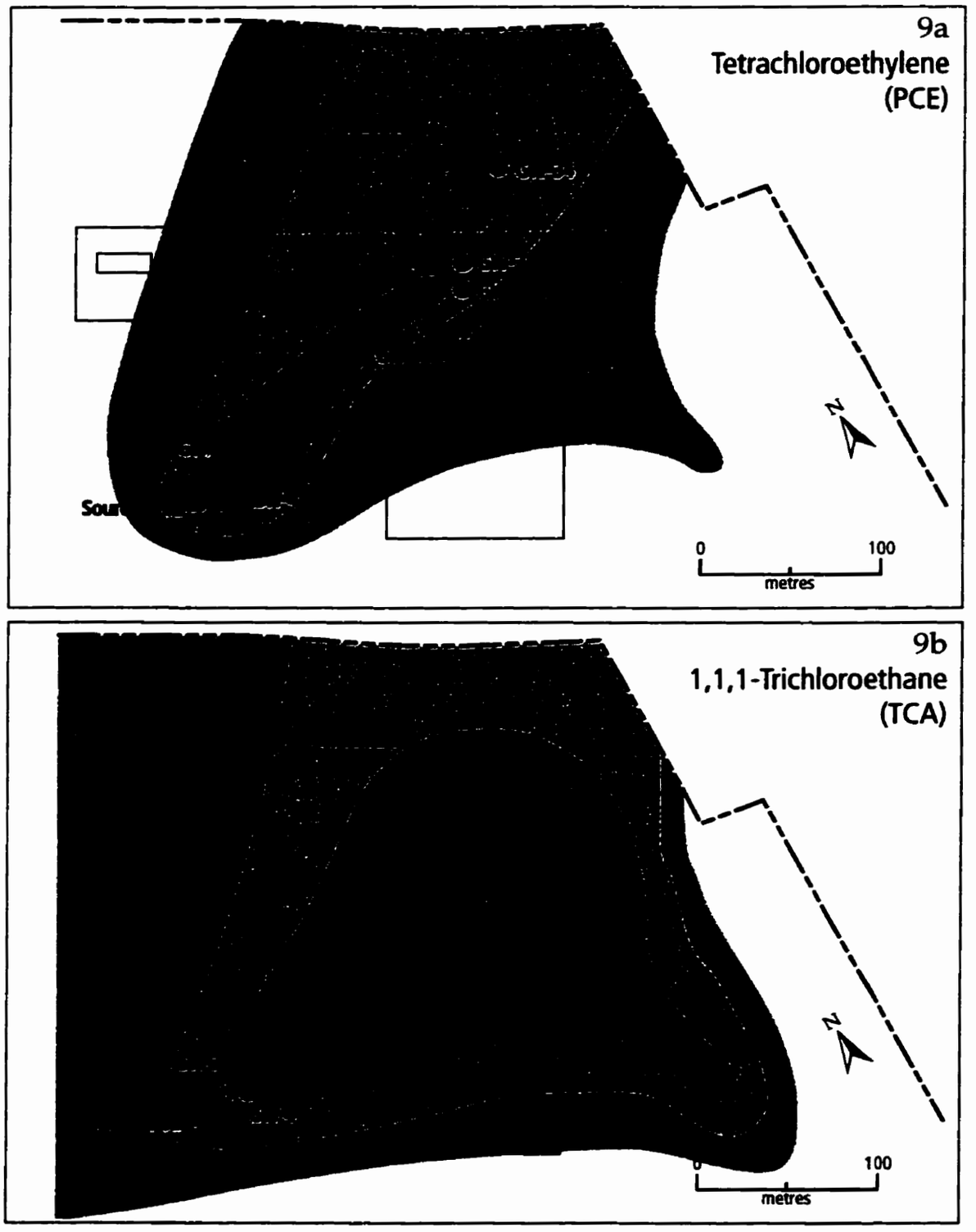

Figure 8-9. Aqueous-phase plumes at the Dayton site in April 1978 before the start of groundwater pumping. Concentration contours 10 µg/L, 100 µg/L and 1,000 µg/L.

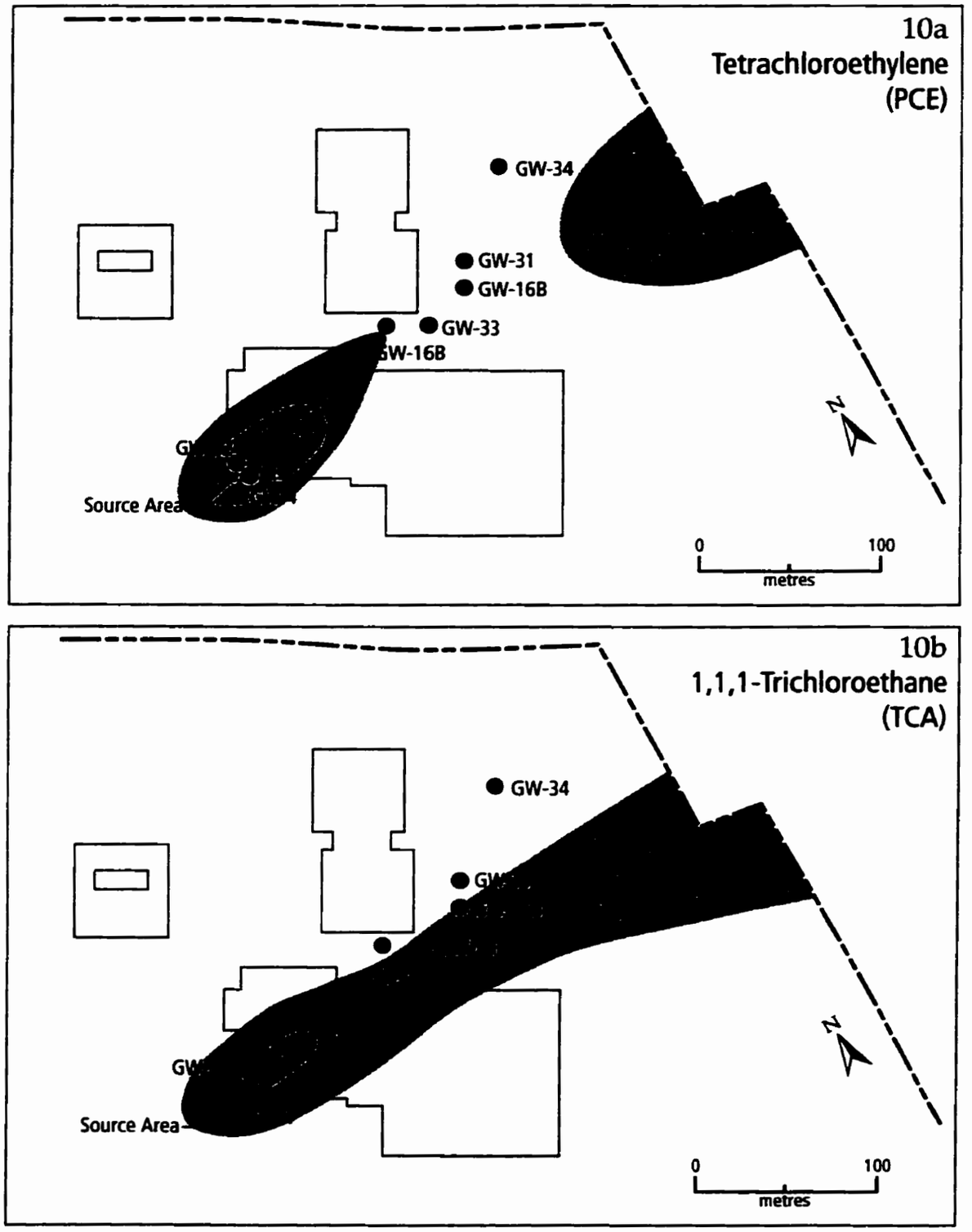

Figure 8-10. Aqueous-phase plumes at the Dayton site in March 1984 at the end of groundwater pumping. Concentration contours 10 µg/L, 100 µg/L and 1,000 µg/L.

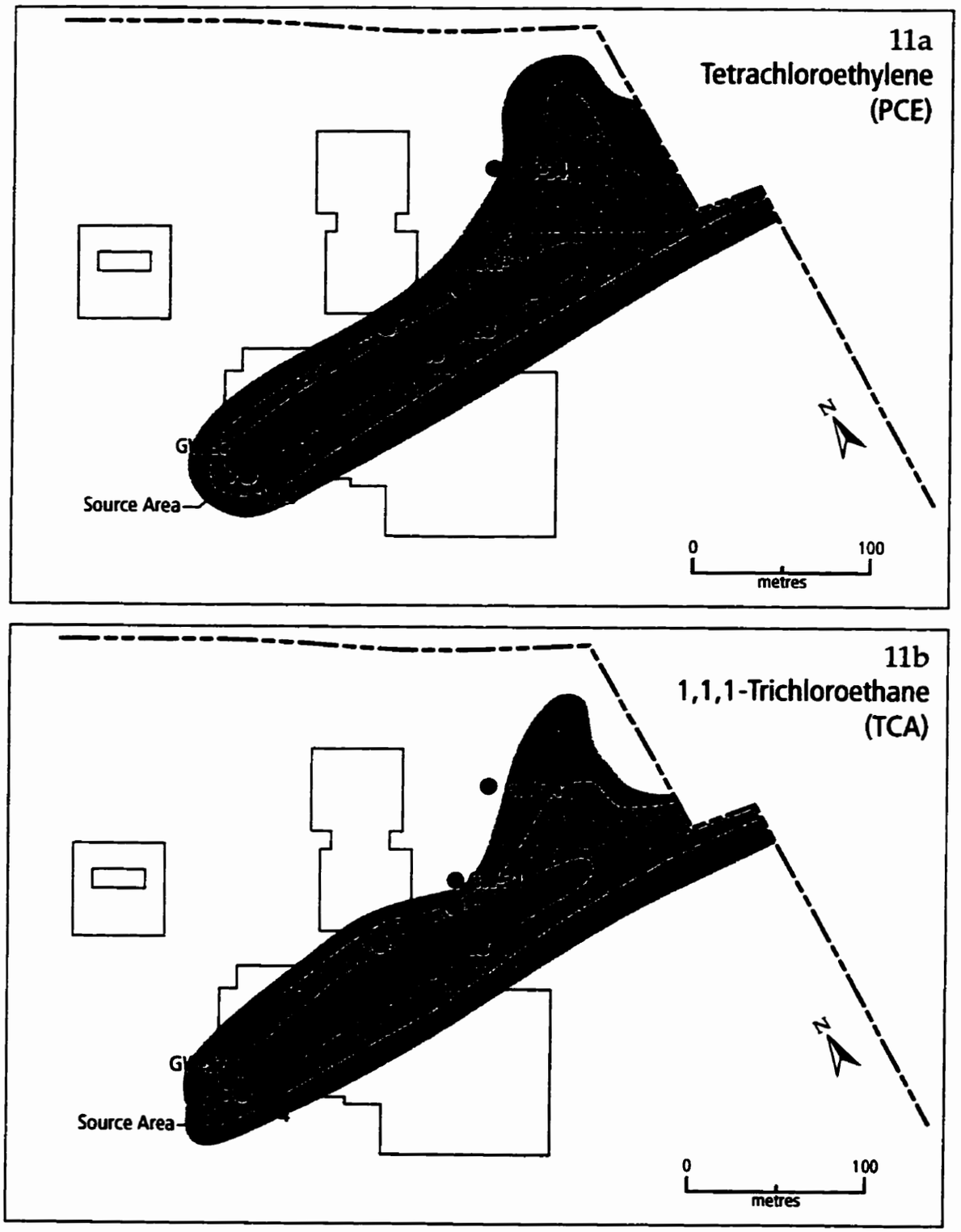

Figure 8-11. Aqueous-phase plumes at the Dayton site in June 1989. Concentration contours 10 µg/L, 100 µg/L and 1,000 µg/L.

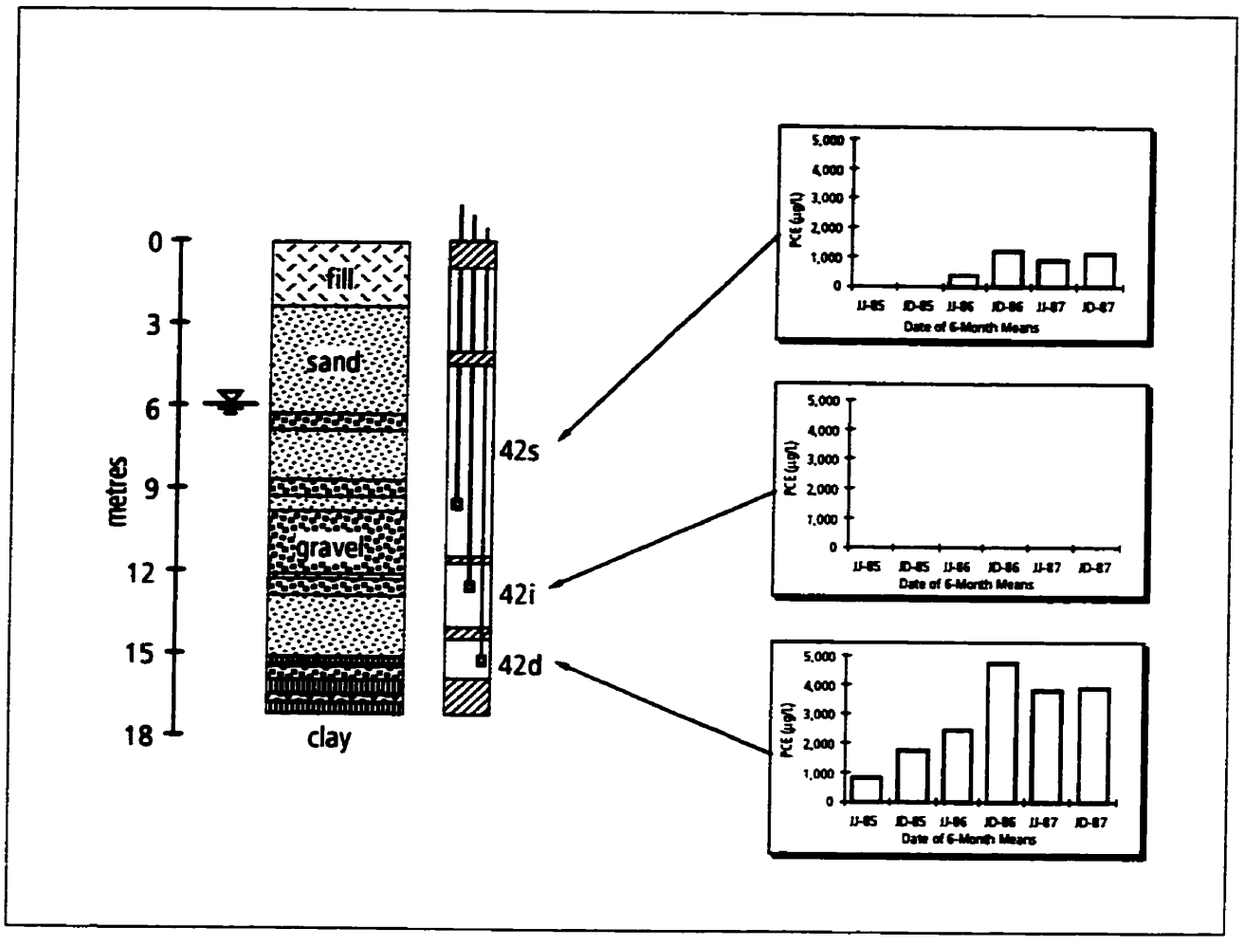

Figure 8-12. PCE concentrations in multi-level monitoring installation adjacent to the source area.

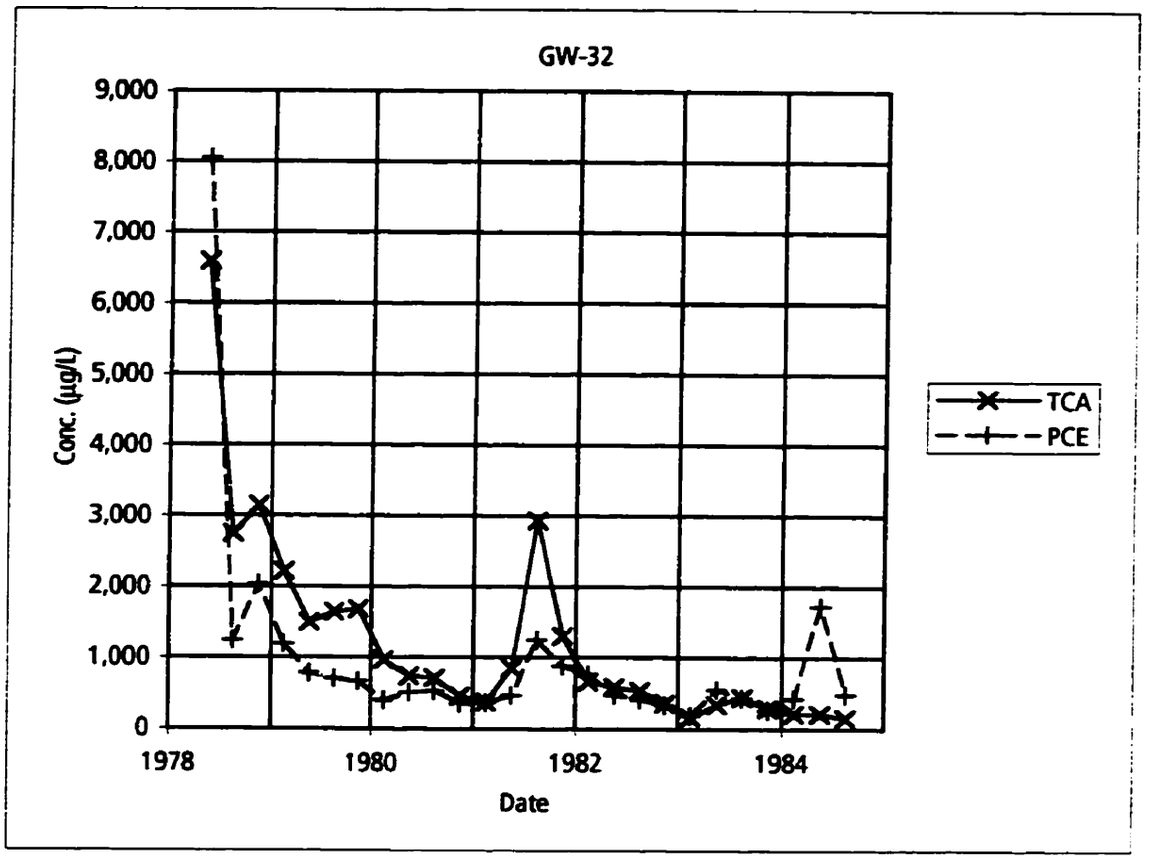

Key:
PCE - Tetrachloroethylene
TCA - 1,1,1-Trichloroethane

Figure 8-13. Temporal variation in aqueous concentrations measured in pumping well GW-32

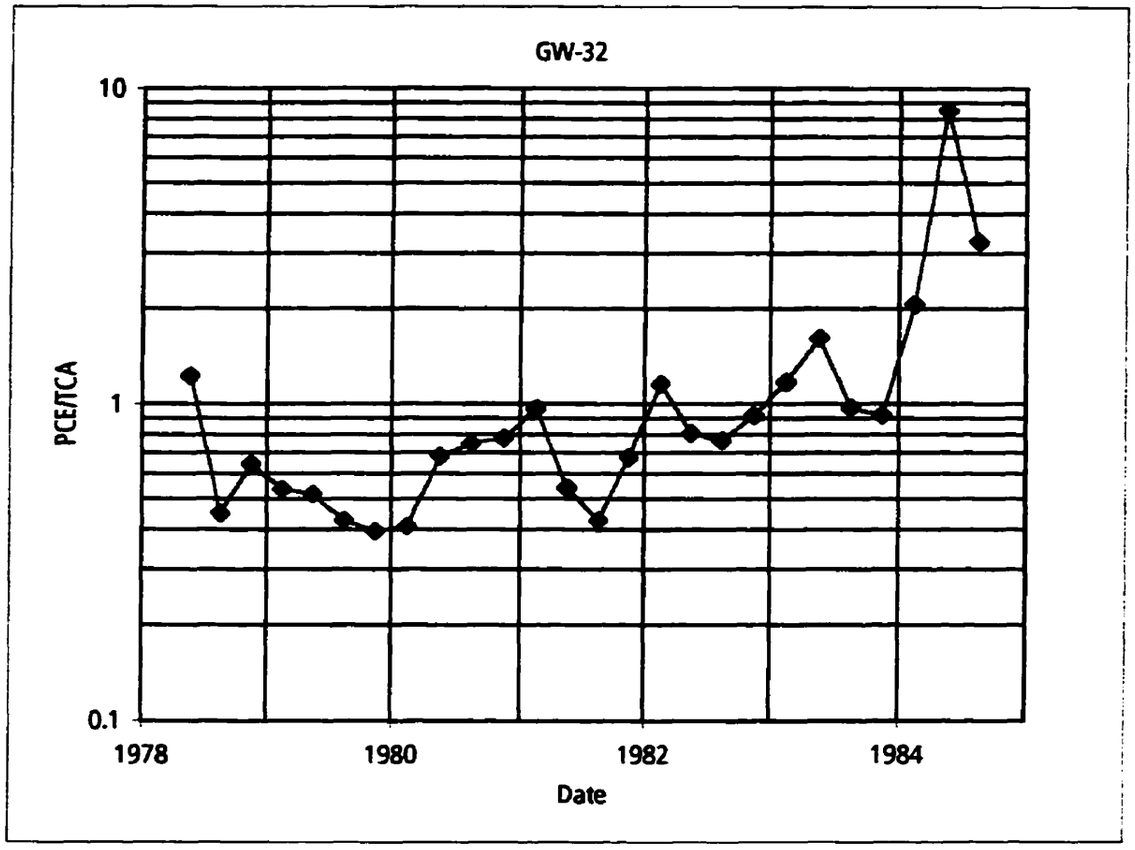

Key:
PCE - Tetrachloroethylene
TCA - 1,1,1-Trichloroethane

Figure 8-14. Variation in PCE/TCA ratio versus time for pumping well GW-32.

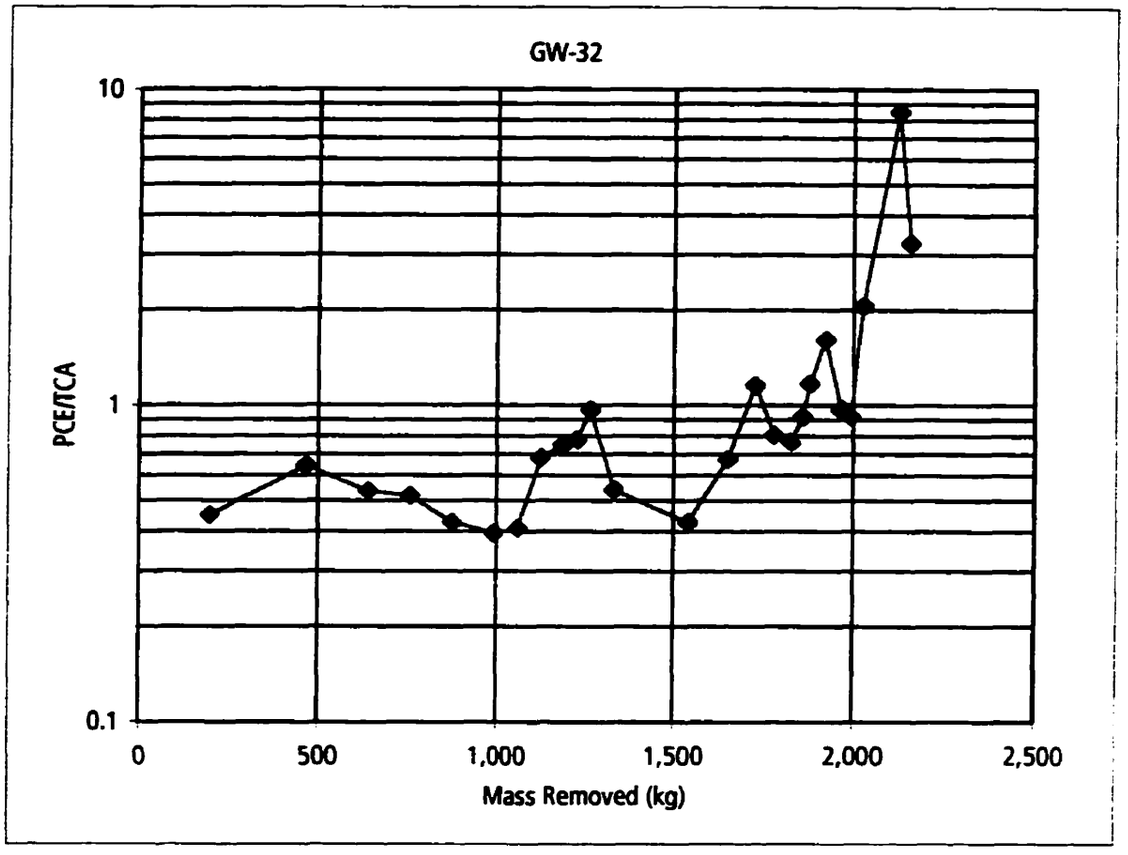

Key:
PCE - Tetrachloroethylene
TCA - 1,1,1-Trichloroethane

Figure 8-15. Variation in PCE/TCA ratio versus mass removed for pumping well GW-32.

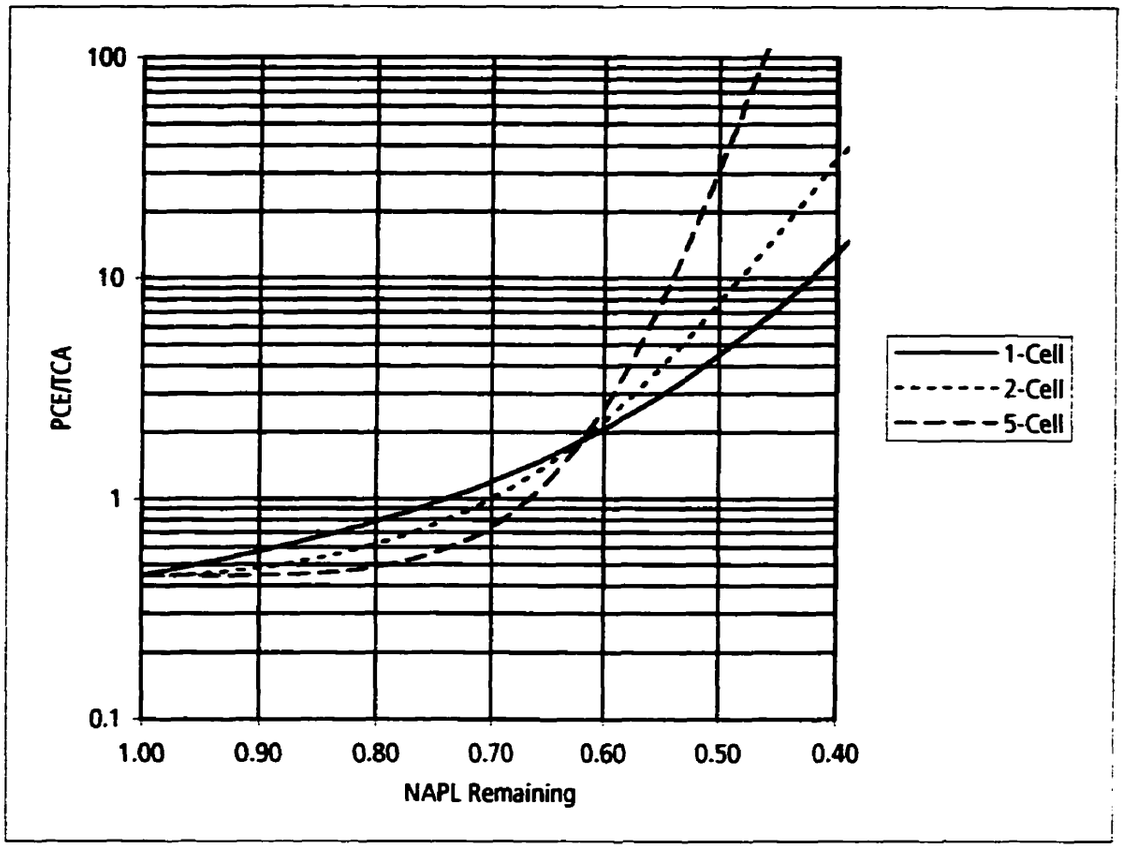

Key:
PCE - Tetrachloroethylene
TCA - 1,1,1-Trichloroethane

Figure 8-16. Change in aqueous concentration ratios versus NAPL remaining predicted for the Dayton site by ESM for 1-cell, 2-cell and 5-cell configurations.

File:Dayton. Equilibrium.EXCL/Plots

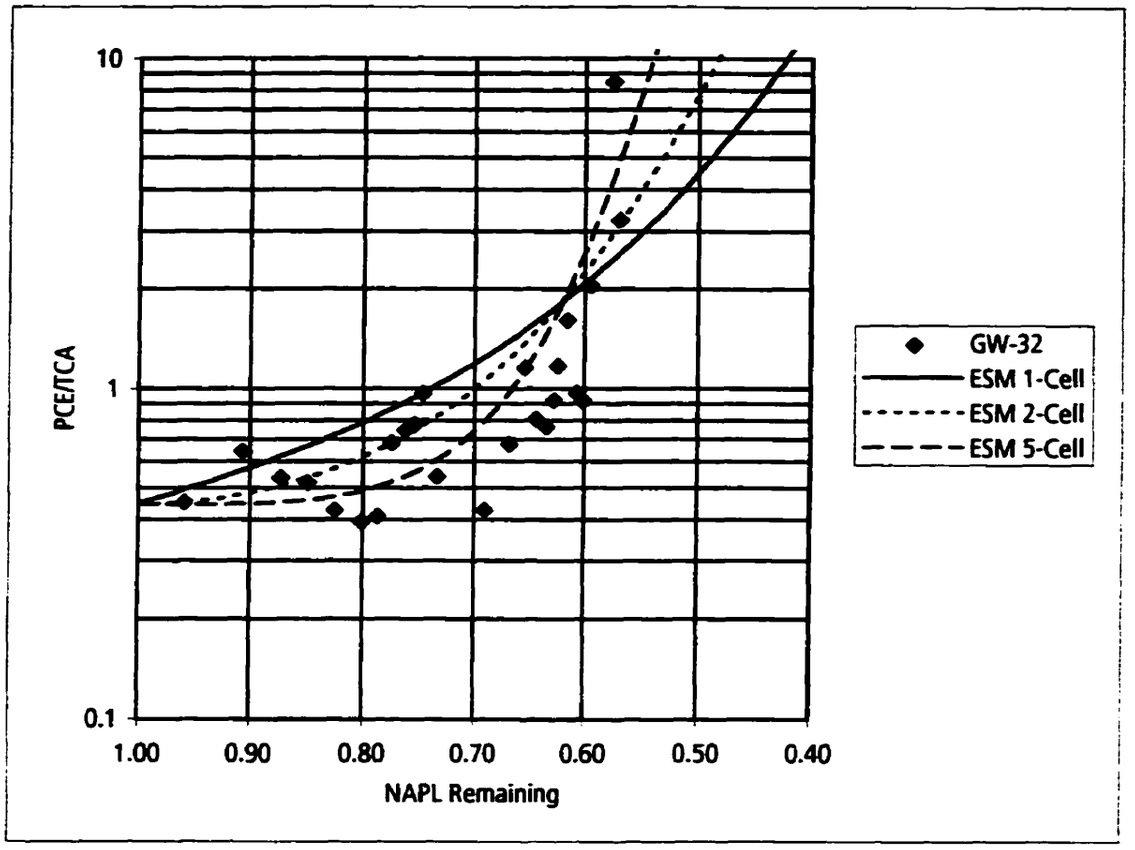

Key:
PCE - Tetrachloroethylene
TCA - 1,1,1-Trichloroethane

Figure 8-17. Measured PCE/TCA ratio versus NAPL mass remaining for extraction well GW-32, for a 5,000 kg source, compared to ratios predicted by ESM.

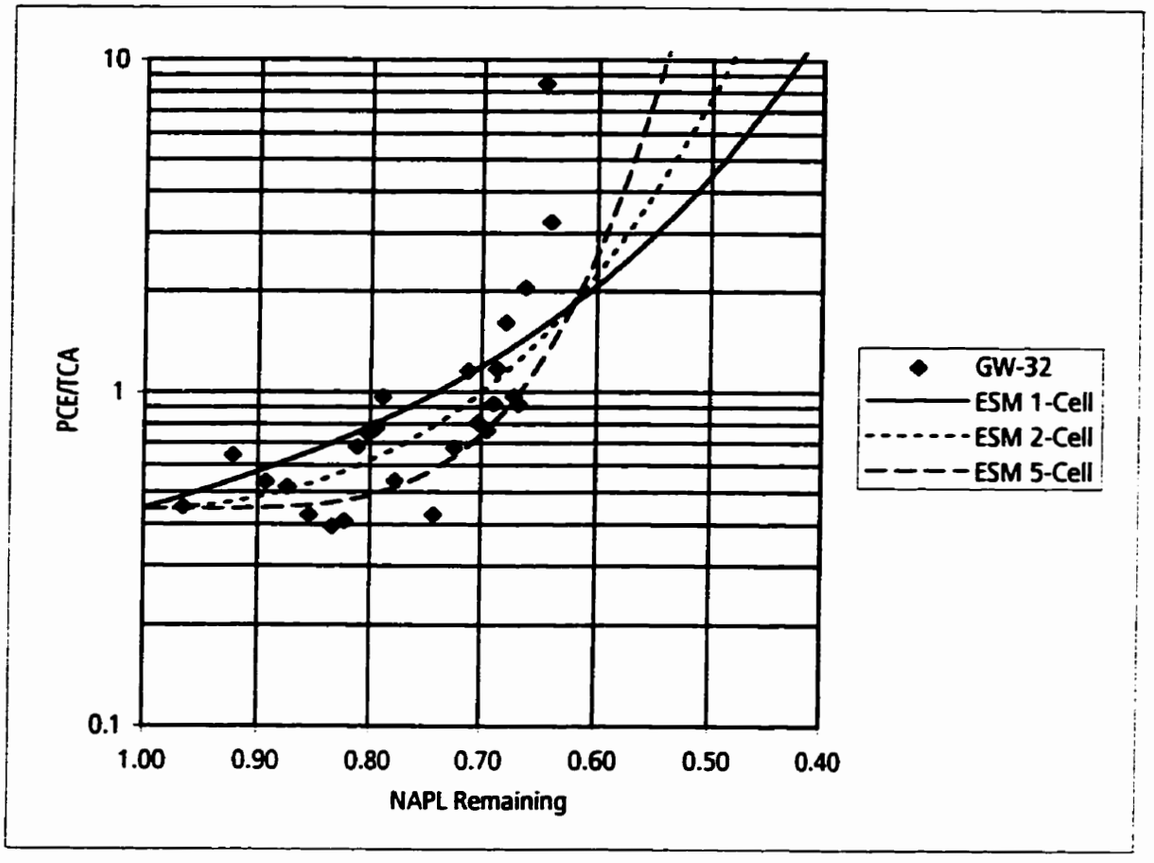

Key:
PCE - Tetrachloroethylene
TCA - 1,1,1-Trichloroethane

Figure 8-18. Measured PCE/TCA ratio versus NAPL mass remaining for extraction well GW-32, for a 6,000 kg source, compared to ratios predicted by ESM.

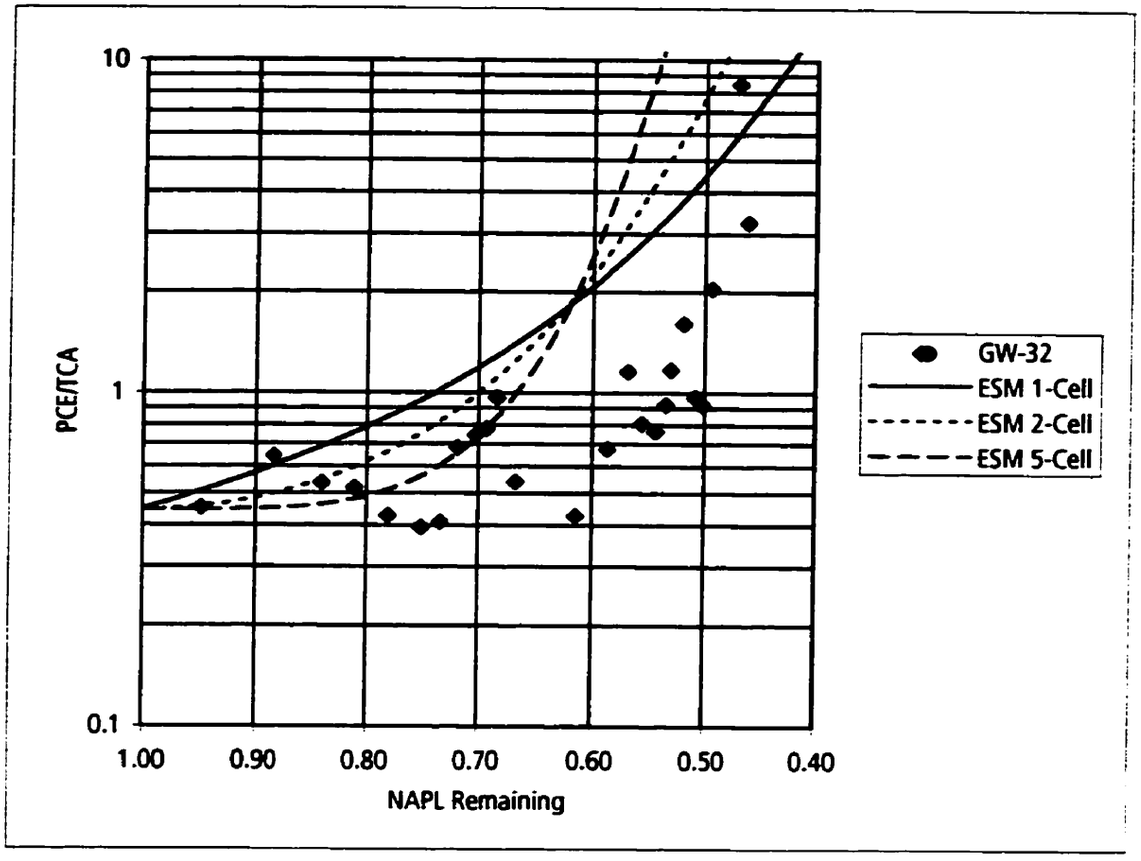

Key:
PCE - Tetrachloroethylene
TCA - 1,1,1-Trichloroethane

Figure 8-19. Measured PCE/TCA ratio versus NAPL mass remaining for extraction well GW-32, for a 4,000 kg source, compared to ratios predicted by ESM.

9. Summary and Conclusions

This thesis has described the development and evaluation of a method to estimate the mass of chemicals contained in NAPL zones. The principal tool of this method is the Effective Solubility Model (ESM) which is used to relate changes in aqueous concentration ratios in groundwater emitted by dissolution of residual NAPL to the mass remaining in the NAPL. Changes in aqueous concentration ratios measured in groundwater near a NAPL source zone are compared to the results of ESM simulations to estimate the chemical mass contained in the NAPL zone.

9.1 Determination of Effective Solubility

The ESM relies on the principle that the aqueous concentration, or effective solubility, of contaminants in groundwater in equilibrium with a multi-component NAPL can be determined from the chemical composition of the NAPL according to Raoult's Law. Based on laboratory studies it is evident that Raoult's Law provides a relatively accurate means for the calculation of effective solubility for mixtures of structurally similar compounds such chlorinated solvents or chlorinated benzenes. Raoult's Law predictions of effective solubility vary from measured values by 10% to 30%, or less, for such mixtures. Predictions vary from measured values by 25% to 50%, or less, for mixtures of structurally dissimilar compounds such as aromatic and aliphatic hydrocarbons, typified by gasoline. The potential error in effective solubility values predicted by Raoult's Law is comparable to, or smaller than the uncertainty associated with the chemical analysis of groundwater samples.

Raoult's Law is less suitable for NAPL comprised of coal tar, creosote, chlorophenols, nitrophenols and high molecular weight hydrocarbons. Raoult's Law will not be suitable when the groundwater contains high

concentrations of total dissolved solids, miscible co-solvents, surfactants or dissolved organic matter.

Predictions of effective solubility using activity coefficients calculated by UNIFAC are not substantially more accurate than simple Raoult's Law predictions for most simple or complex NAPL mixtures. In the majority of circumstances in groundwater, Raoult's Law will be the most reliable method for the prediction of effective solubility of organic contaminants derived from the dissolution of multi-component NAPL.

9.2 Principles for Dissolution of Multi-Component NAPL

Theoretical pore-scale models and empirical laboratory models of NAPL dissolution suggest that the rate of mass transfer and resultant aqueous concentrations emitted by dissolution of multi-component NAPL residual will be determined primarily by the effective solubility of the NAPL components, for a given NAPL source and set of water flow conditions. The effective solubilities of NAPL components are determined by the NAPL composition.

Changes in the NAPL composition due to preferential dissolution of higher-solubility components will be reflected in the aqueous concentrations emitted from the NAPL residual at later times. However, in a field setting it will not be possible to relate the magnitude of aqueous concentrations in the groundwater to the composition of the NAPL residual zone because of uncertainty in the exact size and geometry of NAPL residual zones, and the unknown degree of dilution reflected in the contaminant concentrations found in monitoring or extraction wells. In addition, non-equilibrium mass transfer may occur under conditions of low NAPL residual saturation or high groundwater velocity. However, because dilution and non-equilibrium mass transfer should affect all dissolved contaminants to the same degree,

information about the composition of NAPL residual reflected in the ratios of aqueous concentrations may be preserved.

The preliminary study by Feenstra (1990) suggested that estimates of the chemical mass in NAPL residual zones may be possible using changes in measured aqueous concentration ratios in groundwater, together with predicted changes derived from a 1-cell configuration of the Effective Solubility Model (ESM).

For dissolution of multi-component NAPL in short-length laboratory column experiments or shake-flask experiments, the composition of the NAPL may change with time but it is relatively homogeneous at any point in time. However, at real sites of NAPL contamination, the flow path of groundwater through the NAPL residual zone may be sufficiently long that the aqueous concentrations and NAPL composition in the upgradient portion of the NAPL zone may differ from that in the downgradient portion of the NAPL zone. Aqueous concentrations emitted from the upgradient portion of the NAPL residual may be modified by exchange with NAPL of different composition in the downgradient portion of the NAPL zone. This potential effect is referred to as a "chromatographic effect". ESM must be extended to account for different conditions along the groundwater flow path through the NAPL zone in order to simulate this effect.

The ESM relies on the principle that the aqueous concentrations in the groundwater can be determined from the chemical composition of the NAPL. This principle is applicable for zones of NAPL residual. It may applicable also for thin NAPL pools, but will not be applicable for thick NAPL pools. Dissolution of NAPL pools takes place along the top of the pool. Aqueous concentrations extend upward into the aquifer as a result of vertical dispersion. Because this vertical dispersion is essentially a dilution effect, the average aqueous concentration ratios in the groundwater flowing over the NAPL pool may reflect the NAPL composition within the NAPL layer

provided that the pool has a uniform chemical composition throughout its thickness. This may occur for thin pools where the diffusion within the NAPL is sufficiently rapid to replenish the more soluble contaminants dissolved from the top of the pool. This is unlikely to be the case for thick pools, so that the aqueous concentrations in groundwater at the top of the pool will not reflect the overall chemical composition of the pool. Consequently, the ESM is not applicable to NAPL pools.

9.3 Effective Solubility Model (ESM)

The Effective Solubility Model (ESM) was developed to provide a method of describing the changes in aqueous concentrations of organic contaminants emitted from the dissolution of a multi-component zone of NAPL residual. In its simplest form, the ESM represents a single cell, of unit volume, in which clean water enters the cell and equilibrates with NAPL. Aqueous concentrations are calculated according to Raoult's Law and the NAPL composition. The water leaves the cell, the masses of the components transferred to the water from the NAPL are calculated, and a new NAPL composition is determined.

A 1-cell configuration of the ESM cannot simulate the chromatographic effect on aqueous concentrations expected in NAPL residual zones where the groundwater flow path is long. To account for this effect, the ESM was extended to simulate a series of equilibration cells linked sequentially. The equilibration calculations within each cell take the total chemical mass and allocate appropriate proportions to the NAPL, sorbed and aqueous-phases according Raoult's Law and linear partitioning relationships. For each equilibration step for each cell, the calculated sorbed-phase and NAPL-phase chemical mass is retained within the cell and the calculated aqueous-phase chemical mass is passed to the next downgradient cell for the next equilibration step.

The results of ESM simulations are most sensitive to the NAPL composition, the pure-phase solubilities of the NAPL components, and the number of equilibration cells specified in the model. The number of cells reflects, generically, the length of NAPL residual zone and the degree of the chromatographic effect on the aqueous concentrations. The results of the ESM simulations are insensitive to the other model input parameters: fraction organic carbon in the aquifer, porosity or initial NAPL content.

9.4 Comparison to Laboratory Studies

ESM simulations were compared to the results of three published laboratory column dissolution experiments. In each experiment, the NAPL composition and mass of NAPL placed in the column was known, and the aqueous concentrations emitted from the column were measured. Aqueous concentration ratios and the NAPL mass remaining were determined from the experimental data. For two of the laboratory experiments, the measured aqueous concentration ratios compared favourably with the concentration ratios predicted by 1-cell or 2-cell configurations of the ESM. These results indicate little or no chromatographic effect on the aqueous concentrations during flow through the NAPL residual. For one of the experiments, the measured ratios compared most favourably with ratios predicted by a 10-cell configuration of the ESM. This indicates a chromatographic effect during flow through the NAPL residual.

9.5 Comparison to the Emplaced-Source Experiment

A controlled field-scale dissolution experiment, referred to here as the Emplaced-Source Experiment, was conducted to examine the dissolution of a residual NAPL source of chlorinated solvents in a sandy aquifer. This experiment allowed examination of the dissolution of a NAPL source zone larger than those represented in laboratory experiments. A residual NAPL source zone of known mass, composition and geometry was emplaced

directly in the groundwater zone, and the aqueous concentrations emitted from the NAPL zone were measured. Aqueous concentration ratios and the NAPL mass remaining were determined from the experimental data.

The results of the Emplaced-Source experiment indicate that the changes in aqueous concentration ratios measured during dissolution of the NAPL source can be predicted with reasonable accuracy using a 5-cell configuration of the ESM. This indicates a chromatographic effect on the aqueous concentrations during flow through the source zone. Despite the fact that NAPL source zone in the field experiment was larger in size than the NAPL zones considered in laboratory experiments, a larger number of cells was not required. This suggests that the length of size of the NAPL zone is not the only factor which will determine whether a chromatographic effect results during flow through NAPL residual. Other factors such as the pore-scale distribution of NAPL and pattern of groundwater flow also likely determine whether a chromatographic effect occurs within a NAPL source zone.

9.6 Comparison to Free-Release Experiment

A second controlled field-scale dissolution experiment, referred to here as the Free-Release Experiment, was conducted to examine the dissolution of a residual NAPL source of chlorinated solvents in the sandy aquifer at the Borden. A NAPL of known mass and composition was released directly in the groundwater zone inside a steel sheet piling test cell. The NAPL was permitted to distribute itself in the aquifer and form an irregular NAPL zone. Utilization of an irregular NAPL source zone distinguishes this experiment from the Emplaced-Source experiment which utilized a NAPL source zone of regular geometry. Horizontal groundwater flow was induced in the test cell and the aqueous concentrations emitted from the NAPL zone were measured. Aqueous concentration ratios and the NAPL mass remaining were determined from the experimental data.

The results of the Free-Release experiment indicate that the changes in aqueous concentration ratios measured during dissolution of the NAPL source can be predicted with reasonable accuracy using a 1-cell configuration of the ESM. This is the case despite the fact that the geometry of the NAPL source zone was complex and contained both residual NAPL and thin NAPL pools.

Area-averaged and vertically-averaged concentrations provide measured ratios that compared well with the 1-cell configuration of the ESM. However, the ratios measured at a specific monitoring point in the aqueous-phase plume required a 5-cell configuration of the ESM for the best match. This experiment illustrates that the relationship between aqueous concentration ratios and NAPL remaining may be different at different locations for complex NAPL source zones. In such circumstances, area-weighted averaged concentrations such as reflected in a groundwater extraction well would be preferable to concentrations measured in individual monitoring wells.

9.7 Application of the ESM Method for Evaluation of NAPL Sites

A methodology was developed for how the ESM can be used, together with groundwater monitoring data, to estimate the chemical mass contained in multi-component NAPL residual zones.

The first step in the comparison of field data to the ESM is to perform a series of ESM simulations using the NAPL composition and aquifer properties defined for the site. Simulations should be performed for a range of cell configurations to produce a family of dissolution curves for the NAPL showing the change in aqueous concentration ratios versus the NAPL remaining. For a given NAPL composition, the different curves in a family will have distinctly different shapes as the number of cells increases.

If the 1-cell configuration of the ESM were known to be always the most applicable, the aqueous concentration ratio measured at the site at a given time could be related simply to the ratio from the 1- cell curve of ESM and the NAPL remaining determined directly. However, the most appropriate cell configuration is not known *a priori* so that the measured ratios must be compared to the different curves to evaluate the best match.

The data on measured aqueous concentration ratios and corresponding values of cumulative mass removed from the site are used for comparison to the ESM simulations. The cumulative mass removed is expressed as NAPL mass remaining, calculated based on a series of estimates of the initial NAPL mass in the source zone. The measured ratios and corresponding values for calculated NAPL mass remaining are plotted on the same graph at the ESM results for comparison to the family of dissolution curves. The estimates of initial NAPL mass are adjusted until the best match is obtained between the measured ratios and a particular ESM curve. For the best match, the initial mass represents the initial NAPL mass in the source zone at the start of the monitoring period. The NAPL mass remaining is given by the value at the final measured ratio data point.

The number of cells required for a match between the measured and predicted ratios provides a generic indication of the length of the groundwater flow path through the NAPL source zone. A larger number of cells is required to simulate the chromatographic effect as aqueous-phase contaminants dissolved from the upgradient portion of the source zone interact with NAPL in the downgradient portion of the source zone. The longer the flow path through the NAPL zone, the greater the chromatographic effect on the aqueous concentrations.

For the case of the Emplaced-Source experiment, using only the monitoring results from pumping well PW-2 situated 25 m downgradient of the source zone, the NAPL source mass estimated within 30% of the actual

NAPL mass using the 1-cell configuration of the ESM, and within 20% using the 5-cell configuration of the ESM which provided a better match between the measured and predicted ratios. This degree of error is far less than would be expected for mass estimates based on the sampling and analysis of soil samples. The mass estimate using the ESM could be made using only the measured aqueous concentrations in PW-2, and the general physical and chemical properties for the NAPL components and aquifer. No specific assumptions were required regarding the actual dimensions or geometry of the source zone, groundwater flow conditions through the source zone, or dissolution mass transfer coefficients.

This research has illustrated the potential for the ESM method to provide useful estimates of the chemical mass contained in multi-component NAPL residual zones in porous media. However, it must be recognized that, at this time, the ESM method has been tested only for small-scale laboratory experiments and two moderate-scale field experiments in sandy aquifer materials. There are numerous specific conditions required for its application which include:

- Multi-component NAPL in porous media. The method is not applicable to fractured media or fractured porous media.
- Sufficient difference in solubility of components to result in preferential dissolution of the more soluble components.
- Raoult's Law must be suitable for determining the effective solubility of the NAPL components.
- Source zone must not consist of different NAPLs having substantially different chemical compositions.

- Sufficient record of groundwater monitoring data to define trends in aqueous concentration ratios and the chemical mass released from the source zone.

- Aqueous concentration ratios must not be altered by sorption processes outside of the NAPL source zone.

- Aqueous concentration ratios must not be altered by biodegradation processes.

- NAPL residual or thin pools in porous media. The method is not applicable to thick pools of NAPL.

- NAPL must be available for dissolution by groundwater flowing through the NAPL source zone. The method is not applicable where a significant portion of the NAPL mass is isolated in lower permeability zones.

In most circumstances, site-specific information can be used to determine whether these conditions are satisfied. For example, the analyses of soil and groundwater samples can be used to identify the contaminants and estimate the likely composition of NAPL. Information on the wastes or chemicals released to the subsurface, together with analyses of soil and groundwater can be used to determine the likelihood of NAPLs with different compositions in different areas of the site. General information on the chemical properties of the contaminants and site-specific information of the migration and fate of contaminants can be used to determine whether Raoult's Law is applicable, and whether sorption or biodegradation processes are likely to have affected aqueous concentration ratios.

The greatest uncertainty in the application of the ESM method relates to the requirement that not NAPL occur in thick pools or isolated in lower permeability zones. At most sites, the general location of the NAPL source

zone may be known but there is seldom information available on the nature of the NAPL distribution. If thick NAPL pools or areas of isolated NAPL are present in the source zone and contain significant mass compared to the residual zones, the ESM method will underestimate the total chemical mass present in the source zone.

10. References

Banerjee, S. (1984). Solubility of organic mixtures in water. Environmental Science & Technology, v. 18, no. 8, pp. 587-591.

Bastien, F., Muntzer, P., and Zilliox, L. (1977). Pollution par les produits petroliers. In: Colloque du Service Geologique National, Orleans-La-Source, France.

Benvenue, A., and Beckman, H. (1963). Pentachlorophenol: A discussion of its properties and its occurrence as a residue in human and animal tissues. Residue Reviews, v. 19, pp. 83-114.

Bonolli, L., and Witherspoon, P. A. (1968). Diffusion of aromatic and cycloparaffin compounds in water at 20°C to 60°C. Journal of Physical Chemistry, v. 72, pp. 2532-2534.

Brewster, M. L., Annan, A. P., Greenhouse, J. P., Kueper, B. H., Olhoeft, G. R., Redman, J. D., and Sander, K. A. (1995). Observed migration of a controlled DNAPL release by geophysical methods. Ground Water, v. 33, no. 6, p. 977-987.

Broholm, K., and Feenstra, S. (1995). Laboratory measurements of the aqueous solubility of mixtures of chlorinated solvents. Environmental Toxicology and Chemistry, v. 14, no. 1, pp. 9-15.

Burris, D. R., and MacIntyre, W. G. (1985). Water solubility behavior of binary hydrocarbon mixtures. Environmental Toxicology and Chemistry, v. 4, pp. 371-377.

Burris, D. R., and MacIntyre, W. G. (1986a). A thermodynamic study of solutions of liquid hydrocarbon mixtures in water. Geochimica et Cosmochimica Acta, v. 50, pp. 1545-1549.

Burris, D. R., and MacIntyre, W. G. (1986b). Water solubility behavior of hydrocarbon mixtures - Implications for petroleum dissolution. In: Oil in Freshwater: Chemistry, Biology, Countermeasure Technology, Editors: Vandermeulen, J. H. and Hrudey, S. E., Edmonton, Alberta, Pergamon Press, pp. 85-94.

Burris, D. R., and MacIntyre, W. G. (1986c). Solution of hydrocarbons in a hydrocarbon-water system with changing phase composition due to evaporation. Environmental Science & Technology, v. 20, no. 3, pp. 296-299.

Cline, P. V., Delfino, J. J., and Rao, P. S. C. (1991). Partitioning of aromatic constituents into water from gasoline and other complex solvent mixtures. Environmental Science & Technology, v. 25, no. 5, pp. 914-920.

Dankwerts, P. W. (1951). Significance of liquid-film coefficients in gas absorption. Industrial Engineering Chemistry, Process Design Development, v. 43, pp. 1460-1467.

Dean, J. A. (1985). Lange's Handbook of Chemistry. New York, McGraw-Hill Book Company, New York.

Edwards, D. A., Luthy, R. G., and Liu, Z. (1991). Solubilization of polycyclic aromatic hydrocarbons in micellar nonionic surfactant solutions. Environmental Science & Technology, v. 25, no. 1, pp. 127-133.

Enfield, C. G., and Bengtsson, G. (1988). Macromolecular transport of hydrophobic contaminants in aqueous environments. Ground Water, v. 26, no. 1, pp. 64-70.

Enfield, C. G., Bengtsson, G., and Lindqvist, R. (1989). Influence of macromolecules on chemical transport. Environmental Science & Technology, v. 23, no. 10, pp. 1278-1286.

ERM (1992). Off-Site Operable Unit Remedial Investigations - Fourth Addendum Investigation and Ground Water Remediation Strategy Report, Tyson's Site, Montgomery County, Pennsylvania. Submitted to US Environmental Protection Agency, Region III, Philadelphia, Pennsylvania. Prepared by Environmental Resources Management, Inc. for CIBA-GEIGY Corporation.

Feenstra, S. (1986). Subsurface contamination from spills of dense non-aqueous phase liquid (DNAPL) chemicals. In: Technical Seminar on Chemical Spills, Environment Canada, Montreal, Quebec, pp. 11-22.

Feenstra, S. (1990). Evaluation of multi-component DNAPL sources by monitoring of dissolved-phase concentrations. In: International Conference on Subsurface Contamination by Immiscible Fluids, Editor: Weyer, K. U., Calgary, Alberta, A. A. Balkema, pp. 65-72.

Feenstra, S., Mackay, D. M., and Cherry, J. A. (1991). A method for assessing residual NAPL based on organic chemical concentrations in soil samples. Ground Water Monitoring Review, v. 11, no. 2, pp. 128-136.

Feenstra, S., and Cherry, J. A. (1996). Diagnosis and Assessment of DNAPL Sites. In: Dense Chlorinated Solvents and other DNAPLs in Groundwater, Editors: Pankow, J. F. and Cherry, J. A., Waterloo Press, Portland Oregon, pp. 395-473.

Feenstra, S., Cherry, J. A., and Parker, B. (1996). Conceptual Models for Dense Chlorinated Solvents in Groundwater. In: Dense Chlorinated Solvents and other DNAPLs in Groundwater, Editors: Pankow, J. F. and Cherry, J. A., Waterloo Press, Portland Oregon, pp. 53-88.

Fredenslund, A., Gmehling, J., and Rasmussen, P. (1977). Vapor-liquid equilibrium using UNIFAC. Elsevier Scientific Publishing Co., Amsterdam.

Fried, J. J., Muntzer, P., and Zilliox, L. (1979). Ground-water pollution by transfer of oil hydrocarbons. Ground Water, v. 17, no. 6, pp. 586-594.

Geller, J. T., and Hunt, J. R. (1993). Mass transfer from nonaqueous phase organic liquids in water-saturated porous media. Water Resources Research, v. 29, no. 4, pp. 833-845.

Gillham, R. W. (1996). In situ treatment of groundwater: Metal-enhanced degradation of chlorinated organic contaminants. In: Advances in Groundwater Pollution Control and Remediation, Editor: Aral, M. M., Kluwer Academic Publishers, Amsterdam, Netherlands, pp. 249-274.

Glaze, W. C., Lin, C. C., Burleson, J. L., Henderson, J. E., Mapel, D., Rawkey, R., and Scott, D. R. (1983). Optimization of liquid-liquid extraction methods for analysis of organics in water. US Environmental Protection Agency, Environmental Monitoring and Support Laboratory, Report No. CR-808562, Cincinatti, Ohio.

Guiguer, N. (1993). Dissolution and Mass Transfer Processes for Residual Organics in the Saturated Groundwater Zone: Numerical Modelling. Ph. D. Thesis, Department of Earth Sciences, University of Waterloo, Waterloo, Ontario.

Higbie, R. (1935). The rate of absorption of a pure gas into a still liquid during short periods of exposure. Transactions of the American Institute of Chemical Engineers, v. 31, pp. 365-385.

Horvath, A. L. (1982). Halogenated Hydrocarbons: Solubility-Miscibility with Water. Marcel Dekker, Inc., New York.

Hunt, J. R., Sitar, N., and Udell, K. S. (1988). Non-aqueous phase liquid transport and cleanup. 1. Analysis and mechanisms. Water Resources Research, v. 24, no. 8, pp. 1247-1259.

Imhoff, P. T., Jaffe, P. R., and Pinder, G. F. (1993). An experimental study of complete dissolution of a nonaqueous phase liquid in saturated porous media. Water Resources Research, v. 30, no. 2, pp. 307-320.

Jackson, R. E., and Mariner, P. E. (1995). Estimating DNAPL composition and VOC dilution from extraction well data. Ground Water, v. 33, no. 3, pp. 407-414.

Jin, M., Delshad, M., Dwarakanath, V., McKinney, D. C., Pope, G. A., Sepehrnoori, K., Tilburg, C. E., and Jackson, R. E. (1995). Partitioning tracer test for detection, estimation and remediation performance assessment of subsurface non aqueous phase liquids. Water Resources Research, v. 31, no. 5, pp. 1201-1211.

Johnson, R. L., and Pankow, J. F. (1992). Dissolution of dense chlorinated solvents in groundwater. 2. Source functions for pools of solvents. Environmental Science & Technology, v. 26, pp. 896-901.

Kile, D. E., and Chiou, C. T. (1989). Water solubility enhancements of DDT and trichlorobenzene by some surfactants below and above the critical micelle concentration. Environmental Science & Technology, v. 23, no. 7, pp. 832-838.

Kreamer, D. K., and Stetzenbach, K. J. (1990). Development of a standard, pure-compound base gasoline for use as a reference in field and laboratory experiments. Ground Water Monitoring Review, v. 10, no. 2, pp. 135-145.

Kueper, B. H., and Frind, E. O. (1991a). Two-phase flow in heterogeneous porous media. 1. Model development. Water Resources Research, v. 27, pp. 1049-1057.

Kueper, B. H., and Frind, E. O. (1991b). Two-phase flow in heterogeneous porous media. 2. Model application. Water Resources Research, v. 27, pp. 1059-1070.

Kueper, B. H., Redman, D., Starr, R. C., Reitsma, S. and Mah, M. (1993). A field experiment to study the behavior of tetrachloroethylene below the water table: Spatial distribution of residual and pooled DNAPL. Ground Water, v. 31, no. 5, pp. 756-766.

Kueper, B. H., and Gerhard, J. I. (1995). Variability of point source infiltration rates for two-phase flow in heterogeneous porous media. Water Resources Research, v. 31, no. 12, pp. 2971-2980.

Lee, L. S., Rao, P. S. C., Nkedi-Kizza, P., and Delfino, J. J. (1990). Influence of solvent and sorbent characteristics on distribution of pentachlorophenol in octanol-water and soil-water systems. Environmental Science & Technology, v. 24, no. 5, pp. 654-661.

Lee, L. S., Rao, P. S. C., and Okuda, I. (1992a). Equilibrium partitioning of polycyclic aromatic hydrocarbons from coal tar into water. Environmental Science & Technology, v. 26, no. 11, pp. 2110-2115.

Lee, L. S., Hagwall, M., Delfino, J. J., and Rao, P. S. C. (1992b). Partitioning of polycyclic aromatic hydrocarbons from diesel fuel into water. Environmental Science & Technology, v. 26, no. 11, pp. 2104-2110.

Leinonen, P. J., and Mackay, D. (1973). The multicomponent solubility of hydrocarbons in water. Canadian Journal of Chemical Engineering, v. 51, pp. 230-233.

Levenspiel, O. (1989). The Chemical Reactor Omnibook. Oregon State University Book Stores, Inc., Corvallis, Oregon.

Lyman, W. J., Reehl, W. F., & Rosenblatt, D. H. (1990). Handbook of chemical property estimation methods - Environmental behavior of organic compounds. American Chemical Society, Washington, D.C.

Mackay, D., Shiu, W. Y., Bobra, A., Billington, J., Chau, E., Yuen, A., Ng, C., and Szeto, F. (1982). Volatilization of Organic Pollutants from Water US Environmental Protection Agency, Report No. EPA 600/3-82-019).

Mackay, D. M., Freyburg, D. L., Roberts, P. V., and Cherry, J. A. (1986). A natural gradient experiment on solute transport in a sand aquifer, 1. Approach and overview of plume movement. Water Resources Research, v. 22, no. 13, pp. 2017-2029.

Mackay, D., Shiu, W. Y., Maijanen, A., and Feenstra, S. (1991). Dissolution of non-aqueous phase liquids in groundwater. Journal of Contaminant Hydrology, v. 8, pp. 23-42.

Mackay, D., Shiu, W. Y., and Ma, K. C. (1992a). Illustrated Handbook of Physical-Chemical Properties and Environmental Fate for Organic Chemicals Volume I. Lewis Publishers, Inc., Boca Raton, Florida.

Mackay, D., Shiu, W. Y., and Ma, K. C. (1992b). Illustrated Handbook of Physical-Chemical Properties and Environmental Fate for Organic Chemicals Volume II. Lewis Publishers, Inc., Boca Raton, Florida.

Mackay, D., Shiu, W. Y., and Ma, K. C. (1993). Illustrated Handbook of Physical-Chemical Properties and Environmental Fate for Organic Chemicals Volume III. Lewis Publishers, Inc., Boca Raton, Florida.

Mackay, D., Shiu, W. Y., and Ma, K. C. (1995). Illustrated Handbook of Physical-Chemical Properties and Environmental Fate for Organic Chemicals Volume IV. Lewis Publishers, Inc., Boca Raton, Florida.

Magee, B. R., Lion, L. W., and Lemley, A. T. (1991). Transport of dissolved organic macromolecules and their effect on the transport of phenanthrene in porous media. Environmental Science & Technology, v. 25, no. 2, pp. 323-331.

McWhorter, D. B. and Kueper, B. H. (1996). Mechanics and Mathematics of the Movement of Dense Non-Aqueous Phase Liquids (DNAPLs) in Porous Media. In: Dense Chlorinated Solvents and other DNAPLs in Groundwater, Editors: Pankow, J. F. and Cherry, J. A., Waterloo Press, Portland Oregon, pp. 89-129.

Miller, M. M., Wasik, S. P., Huang, G. L., Shiu, W. Y., and Mackay, D. (1985). Relationships between octanol-water partition coefficient and aqueous solubility. Environmental Science & Technology, v. 19, pp. 522-529.

Miller, C. T., Poirier-McNeill, M. M., and Mayer, A. S. (1990). Dissolution of trapped nonaqueous phase liquids: Mass transfer characteristics. Water Resources Research, v. 26, no. 11, pp. 2783-2796.

Mukehrji, S., Peters, C. A., and Weber, W. J. (1997). Mass transfer of polynuclear aromatic hydrocarbons from complex DNAPL mixtures. Environmental Science & Technology, v. 31, no. 2, pp. 416-423.

Nelson, N. T., and Brusseau, M. L. (1996). Field study of the partitioning tracer method for detection of dense non-aqueous phase liquid in a trichloroethene-contaminated aquifer. Environmental Science & Technology, v. 30, no. 9, pp. 2859-2863.

Nernst, W. (1904). Zeitschrift fur Physikalische Chemie, v. 47, pp. 52.

Nkedi-Kizza, P., Rao, P. S. C., and Hornsby, A. G. (1985). Influence of organic cosolvents on sorption of hydrophobic organic chemicals by soils. Environmental Science & Technology, v. 19, no. 10, pp. 975-979.

Occidental Chemical Corporation, Inc. (1988). "S-Area" Remedial Program - Chemical Monitoring Program. Submitted to US Environmental Protection Agency, Region II, New York, New York.

Okouchi, S., Saegusa, H., and Noijima, O. (1992). Prediction of environmental parameters by adsorbability index: Water solubulities of hydrophobic pollutants. Environment International, v. 18, pp. 249-261.

Pearce, A. E., Voudrias, E. A., and Whelan, M. P. (1994). Dissolution of TCE and TCA pools in saturated subsurface systems. Journal of Environmental Engineering, v. 120, no. 5, pp. 1191-1206.

Perrin, D. D. (1972). Dissociation Constants of Organic Bases in Aqueous Solutions. Butterworth, London, UK.

Perry's Chemical Engineering Handbook (1984). Sixth Edition. McGraw-Hill Book Company, Toronto.

Polak, J., and Lu, B. C. Y. (1973). Mutual solubilities of hydrocarbons and water at 0°C and 25°C. Canadian Journal of Chemistry, v. 51, pp. 4108-4023.

Poulsen, M., and Kueper, B. H. (1992). A field experiment to study the behavior of tetrachloroethylene in unsaturated porous media. Environmental Science & Technology, v. 26, pp. 899-895.

Poulsen, M., Lemon, L., and Barker, J. F. (1992). Dissolution of monoaromatic hydrocarbons into groundwater from gasoline-oxygenate mixtures. Environmental Science & Technology, v. 26, no. 12, pp. 2483-2489.

Powers, S. E., Abriola, L. M., and Weber, W. J. (1992). An experimental investigation of nonaqueous phase liquid dissolution in saturated subsurface systems: Steady state mass transfer rates. Water Resources Research, v. 28, no. 10, pp. 2691-2705.

Powers, S. E., Abriola, L. M., and Weber, W. J. (1994). An experimental investigation of nonaqueous phase liquid dissolution in saturated subsurface systems: Transient mass transfer rates. Water Resources Research, v. 30, no. 2, pp. 321-332.

Priddle, M. W., and MacQuarrie, K. T. B. (1994). Dissolution of creosote in groundwater: An experimental and modeling investigation. Journal of Contaminant Hydrology, v. 12, pp. 27-55.

Ramanantsoa, B., Munzter, P., and Zilliox, L. (1986). Dissolution selective d'un melange d'hydrocarbures par l'eau en milieu poreux sature. Application a la pollution des eaux souterraines par les produits petrolier. Sciences de L'eau, v. 5, pp. 149-168.

Rao, P. S. C., Hornsby, A. G., Kilcrease, D. P., and Nkedi-Kizza, P. (1985). Sorption and transport of hydrophobic organic chemicals in aqueous and mixed solvent systems: Model development and preliminary evaluation. Journal of Environmental Quality, v. 14, no. 3, pp. 376-383.

Ripp, J., Taylor, B., Mauro, D., and Young, M. (1993). Chemical and physical characteristics of tar samples from selected manufactured gas plant (MGP) sites . Electric Power Research Institute, Report No. TR-102184, Research Project 2879-12).

Rivett, M. O., Feenstra, S., and Cherry, J. A. (1991). Field experimntal studies of a residual solvent source emplaced in the groundwater zone. In: Conference on Petroleum Hydrocarbons and Organic Chemicals in Ground Water, National Water Well Association, Houston, Texas, pp. 283-299.

Rivett, M. O., Feenstra, S., and Cherry, J. A. (1992). Groundwater zone transport of chlorinated solvents: A field experiment. In: IAH

Conference on Modern Trends in Hydrogeology, International Association of Hydrogeologists, Hamilton, Ontario.

Rivett, M. O. (1993). A field evaluation of pump-and-treat remediation. In: The Joint CSCE-ASCE National Conference on Environmental Engineering, American Society of Civil Engineers, Montreal, Quebec, pp. 1171-1178.

Rivett, M. O., Feenstra, S., and Cherry, J. A. (1994a). Comparison of Borden natural gradient tracer tests. In: IAHR/AIRH Symposium on Transport and Reactive Processes in Aquifers, Editors: Dracos, T., and Stauffer, F., Zurich, Switzerland: A. A. Balkema, pp. 283-288.

Rivett, M. O., Feenstra, S., and Cherry, J. A. (1994b). Transport of a dissolved-phase plume from a residual solvent source in a sand aquifer. Journal of Hydrology, v. 159, pp. 27-41.

Rivett, M. O. (1995). Soil-gas signatures from volatile chlorinated solvents: Borden field experiments. Ground Water, v. 33, no. 1, pp. 84-98.

Rosen, M. J. (1989). Surfactants and Interfacial Phenomena. J. Wiley & Sons, Toronto.

Schwarzenbach, R. P., Gschwend, P. M., and Imboden, D. M. (1992). Environmental Organic Chemistry. J. Wiley & Sons, Inc., Toronto.

Schwille, F. (1967). Petroleum contamination of the subsoil - A hydrogeological problem. In: The Joint Problems of the Soil and Water Industries, Institute of Petroleum, Brighton, UK, pp. 23-54.

Schwille, F. (1981). Groundwater pollution in porous media by fluids immiscible with water. Science of the Total Environment, v. 21, pp. 173-185.

Schwille, F. (1988). Dense Chlorinated Solvents in Porous and Fractured Media - Model Experiments. Translator: Pankow, J. F., Lewis Publishers, Inc., Boca Raton, Florida.

Setschenow, J. (1889). Uber die konstitution der salzosungen auf grund ihres verhaltens zu Kohlensaure. Z. Phys. Chem., Vieter Band, v. 1, pp. 117-125.

Shiau, B. J., Sabatini, D. A., and Harwell, J. H. (1994). Solubilization and microemulsification of chlorinated solvents using direct food additive (edible) surfactants. Ground Water, v. 32, no. 4, pp. 561-569.

Shiu, W. Y., Maijanen, A., Ng, A. L. Y., and Mackay, D. (1988). Preparation of aqueous solutions of sparingly soluble organic substances: II. Multicomponent systems - Hydrocarbon mixtures and petroleum products. Environmental Toxicology and Chemistry, v. 7, pp. 125-137.

Smith, J. S., Eng, L., Comeau, J., Rose, C., Schulte, R. M., Barcelona, M. J., Klopp, K., Pilgrim, M. J., Minnich, M., Feenstra, S., Urban, M. J., Moore, M. B., Maskarinec, M. P., Siegrist, R., Parr, J., and Claff, R. E. (1996). Volatile organic compounds in soil: Accurate and representative analysis. In: Principles of Environmental Sampling, Editor: Keith, L. H., American Chemical Society, Washington, D.C., pp. 693-704.

Starr, R. C., and Ingleton, R. A. (1992). A new method for collecting core samples without a drill rig. Ground Water Monitoring Review, v. 12, no. 1, pp. 91-95.

Sudicky, E. A. (1986). A natural gradient experiment on solute transport in a sand aquifer: Spatial variability of hydraulic conductivity and its role in the dispersion process. Water Resources Research, v. 22, no. 13, pp. 2069-2082.

Sutton, C., and Calder, J. A. (1975). Solubility of alkylbenzenes in distilled water and seawater at 25°C. Journal of Chemical Engineering Data, v. 20, pp. 320-322.

TRC Environmental Consultants, Inc. (1985). Laboratory study on solubilities of petroleum hydrocarbons in groundwater. American Petroleum Institute, API Publication No. 4395.

van der Waarden, M., Bridie, A. L. A. M., and Groenewoud, W. M. (1971). Transport of mineral oil components to groundwater - 1. Model experiments on the transfer of hydrocarbons from a residual oil zone to trickling water. Water Research, v. 5, pp. 213-226.

Voudrias, A. E., and Yeh, M. F. (1994). Dissolution of a toluene pool under constant and variable hydraulic gradients with implications for aquifer remediation. Ground Water, v. 32, no. 2, pp. 305-311.

Webb, R. G., and McCall, A. C. (1973). Quantitative PCB standards for electron capture chromatography. Journal of Chromatographic Science, v. 11, pp. 366-371.

Whelan, M. P., Voudrias, A. E., and Pearce, A. E. (1994). DNAPL pool dissolution in saturated porous media: Procedure development and preliminary results. Journal of Contaminant Hydrology, v. 15, pp. 223-237.

Wilson, R. D., and Mackay, D. M. (1995). Direct detection of residual non aqueous phase liquid in the saturated zone using SF_6 as a partitioning tracer. Environmental Science & Technology, v. 29, no. 5, pp. 1255-1258.

Yalkowsky, S. H., and Valvani, S. C. (1979). Solubilities and partitioning, 2. Relationships between aqueous solubilities, partitioning coefficients, and molecular surface areas of rigid aromatic hydrocarbons. Journal of Chemical Engineering Data, v. 24, pp. 127-129.

Yalkowsky, S. H. and Banerjee, S. (1992). Aqueous Solubility - Methods of Estimation for Organic Compounds. Marcel Dekker, Inc., New York.

Appendix A

Evaluation of the Assumption that $\gamma_{aq}^{i} = \gamma_{aq}^{p}$

As described in Section 2.2, the assumption that $\gamma_{aq}^{i} = \gamma_{aq}^{p}$ simplifies the application of Raoult's Law. In order to evaluate the validity of this assumption, UNIFAC was used to calculate γ_{aq}^{p} for various chlorinated organic compounds and BTEX compounds, and γ_{aq}^{i} for various mixtures of chlorinated organic compounds, BTEX compounds and high-solubility organic compounds.

A total of 12 binary mixtures, one ternary mixture and one quaternary mixture of organic compounds dissolved in water were considered. These mixtures included:

Trichloroethylene + Dichloromethane

Trichloroethylene + 1,2-Dichloroethane

Trichloroethylene + 1,1,1-Trichloroethane

Trichloroethylene + Tetrachloroethylene

Trichloroethylene + 1,2-Dichlorobenzene

Trichloroethylene + Isopropanol

Trichloroethylene + Acetone

Trichloroethylene + 1,1,1-Trichloroethane + Tetrachloroethylene

For most of the binary and ternary mixtures, the aqueous concentration of each organic compound was assumed to be 10% of its respective pure-phase solubility value. Aqueous concentrations ranging from 0.2% to 10% were

used for isopropanol and acetone. For the quaternary mixture of benzene, toluene, ethyl benzene and xylene, the aqueous concentrations were selected to approximate the maximum concentrations that would in expected in groundwater in equilibrium with gasoline.

In each case, the aqueous-phase activity coefficient for each component in the mixture was compared to the aqueous-phase activity coefficient for the pure compound at infinite dilution. All activity coefficients were calculated using the computer code PC-UNIFAC Version 4.0[1]. The results of these calculations are shown in Tables A-1, A-2 and A-3.

In all cases where the aqueous concentrations of the components are less than about 1,000 mg/L, the difference between the aqueous-phase activity coefficient for the mixture and the activity coefficient for the pure compound is less than 1% (or a ratio of 0.99 to 1.01). For such cases it is appropriate to assume that $\gamma_{aq}^{i} = \gamma_{aq}^{p}$.

For mixtures in which the aqueous concentrations exceed 1,000 mg/L, the differences are greater between the aqueous-phase activity coefficient for the mixture and the activity coefficient for the pure compound. In the cases for miscible organic compounds such as isopropanol and acetone at percent-level concentrations, the aqueous-phase activity coefficients in the mixture may be reduced from the activity coefficient of the pure compound by a factor of 5 times.

[1] PC-UNIFAC Version 4.0 (1993). Available commercially from bri, inc., P.O. Box 7834, Atlanta, Georgia 30357-0834.

Table A-1. Comparison of aqueous-phase activity coefficients (γ_{aq}^{i}) in mixtures with aqueous-phase activity coefficients for pure organic compounds (γ_{aq}^{p}) at infinite dilution.

Compound	Aqueous Conc. (mg/L)	γ_{aq}^{i}	γ_{aq}^{p}	Ratio $\gamma_{aq}^{p}/\gamma_{aq}^{i}$
Mixture 1				
Trichloroethylene	140	15,010	15,290	1.019
Dichloromethane	2,000	106.4	107.1	1.007
Mixture 2				
Trichloroethylene	140	15,110	15,290	1.012
1,2-Dichloroethane	870	663.1	666.8	1.006
Mixture 3				
Trichloroethylene	140	15,240	15,290	1.003
1,1,1-Trichloroethane	125	4,823	4,835	1.002
Mixture 4				
Trichloroethylene	140	15,260	15,290	1.002
Tetrachloroethylene	24	86,930	87,150	1.003
Mixture 5				
Trichloroethylene	140	15,250	15,290	1.003
1,2-Chlorobenzene	10	165,400	165,800	1.002

Table A-2. Comparison of aqueous-phase activity coefficients (γ_{aq}^{i}) in mixtures with aqueous-phase activity coefficients for pure organic compounds (γ_{aq}^{p}) at infinite dilution.

Compound	Aqueous Conc. (mg/L)	γ_{aq}^{i}	γ_{aq}^{p}	Ratio $\gamma_{aq}^{p}/\gamma_{aq}^{i}$
Mixture 6				
Trichloroethylene	140	3,132	15,290	4.88
Isopropanol	100,000	-	-	-
Mixture 7				
Trichloroethylene	140	12,730	15,290	1.20
Isopropanol	10,000	-	-	-
Mixture 9				
Trichloroethylene	140	14,710	15,290	1.039
Isopropanol	2,000	-	-	-
Mixture 10				
Trichloroethylene	140	3,545	15,290	4.31
Acetone	100,000	-	-	-
Mixture 11				
Trichloroethylene	140	12,980	15,290	1.18
Acetone	10,000	-	-	-
Mixture 12				
Trichloroethylene	140	14,770	15,290	1.035
Acetone	2,000	-	-	-

Table A-3. Comparison of aqueous-phase activity coefficients (γ_{aq}^{i}) in mixtures with aqueous-phase activity coefficients for pure organic compounds (γ_{aq}^{p}) at infinite dilution.

Compound	Aqueous Conc. (mg/L)	γ_{aq}^{i}	γ_{aq}^{p}	Ratio $\gamma_{aq}^{p}/\gamma_{aq}^{i}$
Mixture 13				
Trichloroethylene	140	15,240	15,290	1.003
1,1,1-Trichloroethane	125	4,822	4,835	1.003
Tetrachloroethylene	24	86,800	87,150	1.004
Mixture14				
Benzene	43	2,413	2,417	1.002
Toluene	69	12,070	12,100	1.002
Ethyl Benzene	3.2	69,110	69,290	1.003
Xylenes	5.6	56,370	56,500	1.002

PLEASE NOTE

Page(s) missing in number only; text follows. filmed as received.

532

UMI

Appendix B

ESM Implementation

The Effective Solubility Model (ESM) was implemented as an executable macro programmed in Visual Basic in the spreadsheet Microsoft Excel Version 5.0. The macro consists of three modules. The module "CopytheData", shown in Listing B-1, reads the input data from worksheet named "Input" and prepares worksheets named "Output" and "Dissolved Concentrations". The worksheet "Output" confirms the input data and presents in initial mass of the NAPL components. The worksheet "Dissolved Concentrations" presents the calculated aqueous concentrations for each equilibration step. The "Equilibrium" module, shown in Listing B-2, uses the input data to perform the equilibrium partitioning calculations for a given time, or equilibrium, step. The "Multistep" subroutine module, shown in Listing B-3, takes the results of the calculations from the "Equilibrium" module and sends output to the "Dissolved Concentrations" worksheet, or back to the "Equilibrium" module depending on the number of cells specified and the number of equilibration steps specified.

An example of the "Input" worksheet is shown in Table B-1. The input data include the chemical and physical properties of the NAPL components; the soil properties; the initial NAPL composition; the number of time, or equilibration, steps; and the number of cells.

An example of the "Output" worksheet is shown in Table B-2. An example of the "Dissolved Concentrations" worksheet is shown in Table B-3. The number of pore volumes present the number of time, or equilibration, steps. The calculated water:NAPL ratio (Q), the proportion NAPL mass remaining, and the aqueous concentrations of each component, are shown for each equilibration step. After the ESM macro is run, the aqueous concentration ratios are calculated and plotted within Excel.

Table B-1. Example worksheet for input data.

Program Listing Example			
Component	CHex	DMB	Hex
Molecular Mass	84.2	86.2	86.2
Solubility	56.4	20.2	12.3
Koc	2750	6600	12900
Density	779	649	660
Soil Density	1809		
foc	0.0001		
Porosity	330		
Initial Conditions			
Initial NAPL Volume	1		
Initial NAPL Composition	0.37	0.31	0.32
Number of Timesteps	40		
Number of Cells	1		

Table B-2. Example worksheet for model output data.

Program Listing Example			
Names of Components	**CHex**	**DMB**	**Hex**
Molecular Mass (g/mole)	84.2	86.2	86.2
Solubility (mg/L)	56.4	20.2	12.3
Koc (mL/g)	2750	6600	12900
Kd (mL/g)	0.275	0.66	1.29
Density (kg/m3)	779	649	660
Initial NAPL Composition	0.37	0.31	0.32
Initial NAPL Mass (g)	257	216	223
Soil Density (kg/m3)	1809		
foc	0.0001		
Porosity (L/m3)	330		
Initial NAPL Volume (L/m3)	1		
Initial NAPL Density (kg/m3)	696		
Initial Water Volume (L/m3)	329		
Number of Timesteps	40		
Number of Cells	1		

Table B-3. Example of worksheet for dissolved concentrations calculated by the model.

CURRENT TIMESTEP IS			40	OF 40	
Program Listing Example					
		Dissolved Concentrations (mg/L)			
Pore Volumes	Q	NAPL Remaining	CHex	DMB	Hex
0	347	1.00	20.88	6.27	3.93
1	695	0.98	20.62	6.30	3.97
2	1,042	0.97	20.36	6.34	4.00
3	1,390	0.95	20.10	6.37	4.04
4	1,737	0.94	19.83	6.40	4.08
5	2,084	0.92	19.56	6.44	4.11
6	2,432	0.91	19.29	6.47	4.15
7	2,779	0.89	19.02	6.51	4.19
8	3,127	0.88	18.74	6.54	4.23
9	3,474	0.86	18.46	6.57	4.27
10	3,822	0.85	18.18	6.61	4.31
11	4,169	0.84	17.90	6.64	4.35
12	4,517	0.82	17.61	6.68	4.39
13	4,864	0.81	17.33	6.71	4.44
14	5,212	0.79	17.04	6.74	4.48
15	5,560	0.78	16.75	6.78	4.52
16	5,907	0.77	16.45	6.81	4.57
17	6,255	0.75	16.16	6.84	4.61
18	6,602	0.74	15.86	6.87	4.66
19	6,950	0.72	15.56	6.91	4.70
20	7,298	0.71	15.26	6.94	4.75
21	7,645	0.70	14.96	6.97	4.79
22	7,993	0.68	14.65	7.00	4.84
23	8,341	0.67	14.35	7.03	4.89
24	8,688	0.66	14.04	7.06	4.94
25	9,036	0.64	13.73	7.09	4.99
26	9,384	0.63	13.42	7.12	5.04
27	9,731	0.62	13.11	7.15	5.09
28	10,079	0.61	12.80	7.18	5.14
29	10,427	0.59	12.49	7.21	5.19
30	10,775	0.58	12.18	7.24	5.24
31	11,123	0.57	11.87	7.26	5.29
32	11,470	0.56	11.55	7.29	5.34
33	11,818	0.55	11.24	7.31	5.40
34	12,166	0.53	10.93	7.34	5.45
35	12,514	0.52	10.62	7.36	5.50
36	12,862	0.51	10.31	7.38	5.56
37	13,209	0.50	10.00	7.40	5.61
38	13,557	0.49	9.69	7.42	5.67
39	13,905	0.48	9.38	7.44	5.73

Listing B-1. CopytheData Module.

```
Const ROWOFHEADER = 1
Const ROWOFTITLES = 3
Const ROWOFMOLECULARMASS = 4
Const ROWOFSOLUBILITY = 5
Const ROWOFKOC = 6
Const ROWOFDENSITY = 7
Const ROWOFSOILDENSITY = 9
Const ROWOFFOC = 10
Const ROWOFPOROSITY = 11
Const ROWOFINITIALNAPLVOLUME = 14
Const ROWOFINITIALNAPLCOMPOSITION = 15
Const ROWOFNUMBEROFTIMESTEPS = 17
Const ROWOFNUMBEROFCELLS = 18
Const NUMBEROFCOMPONENTS = 3
Const FIRSTCOLUMN = 2
Const STARTROWOFOUTPUT = 3
Const OUTPUTROWOFHEADER = 1
Const FIRSTOUTPUTCOLUMN = 1
'
Sub CopyTheData()
'
Dim Header As String
Dim NamesofComponents(1 To 20) As String
Dim MolecularMass(1 To 20) As Double
Dim Solubility(1 To 20) As Double
Dim Density(1 To 20) As Double
Dim Kd(1 To 20) As Double
Dim Koc(1 To 20) As Double
Dim InitialNAPLComposition(1 To 20) As Double
Dim InitialNAPLMass(1 To 20) As Double
'
Dim SoilDensity As Double
Dim foc As Double
Dim Porosity As Double
Dim InitialNAPLVolume As Double
Dim InitialNAPLDensity As Double
Dim InitialWaterVolume As Double
'
Dim ComponentCounter As Integer
Dim NumberofTimesteps As Integer
Dim NumberofCells As Integer
'
'Read starting values from the spread sheet
'
Header = Cells(ROWOFHEADER, FIRSTCOLUMN - 1)
SoilDensity = Cells(ROWOFSOILDENSITY, FIRSTCOLUMN)
foc = Cells(ROWOFFOC, FIRSTCOLUMN)
Porosity = Cells(ROWOFPOROSITY, FIRSTCOLUMN)
InitialNAPLVolume = Cells(ROWOFINITIALNAPLVOLUME, FIRSTCOLUMN)
NumberofTimesteps = Cells(ROWOFNUMBEROFTIMESTEPS, FIRSTCOLUMN)
NumberofCells = Cells(ROWOFNUMBEROFCELLS, FIRSTCOLUMN)

'
'Read component dependent starting values from the spreadsheet
```

```
'
For ComponentCounter = 1 To NUMBEROFCOMPONENTS
   NamesofComponents(ComponentCounter) = Cells(ROWOFTITLES, _
   FIRSTCOLUMN + ComponentCounter - 1)
   MolecularMass(ComponentCounter) = Cells(ROWOFMOLECULARMASS, _
   FIRSTCOLUMN + ComponentCounter - 1)
   Solubility(ComponentCounter) = Cells(ROWOFSOLUBILITY, FIRSTCOLUMN _
   + ComponentCounter - 1)
   Koc(ComponentCounter) = Cells(ROWOFKOC, FIRSTCOLUMN + _
   ComponentCounter - 1)
   Density(ComponentCounter) = Cells(ROWOFDENSITY, FIRSTCOLUMN _
   + ComponentCounter - 1)
   InitialNAPLComposition(ComponentCounter) = _
   Cells(ROWOFINITIALNAPLCOMPOSITION, FIRSTCOLUMN + _
   ComponentCounter - 1)
Next ComponentCounter
'
' Calculate initial starting values for Kd, Initial Water Volume, Initial NAPL Density,
' Initial NAPL Mass for each component
'
InitialNAPLDensity = 0#
For ComponentCounter = 1 To NUMBEROFCOMPONENTS
   Kd(ComponentCounter) = Koc(ComponentCounter) * foc
   InitialNAPLDensity = InitialNAPLDensity + _
   (InitialNAPLComposition(ComponentCounter) / Density(ComponentCounter))
Next ComponentCounter
InitialWaterVolume = Porosity - InitialNAPLVolume
InitialNAPLDensity = 1# / InitialNAPLDensity
For ComponentCounter = 1 To NUMBEROFCOMPONENTS
  InitialNAPLMass(ComponentCounter) = _
  InitialNAPLComposition(ComponentCounter) * InitialNAPLDensity _
  * InitialNAPLVolume
Next ComponentCounter
'
'Add a new sheet to the workbook and display the output values
'
Sheets.Add
With ActiveSheet
   .Name = "Output"
End With
'
'Titles go in the first column of the output sheet

Cells(OUTPUTROWOFHEADER, FIRSTOUTPUTCOLUMN) = Header
Cells(STARTROWOFOUTPUT, FIRSTOUTPUTCOLUMN) = "Names of Components"
Cells(STARTROWOFOUTPUT + 1, FIRSTOUTPUTCOLUMN) = "Molecular Mass"
Cells(STARTROWOFOUTPUT + 2, FIRSTOUTPUTCOLUMN) = "Solubility"
Cells(STARTROWOFOUTPUT + 3, FIRSTOUTPUTCOLUMN) = "Koc"
Cells(STARTROWOFOUTPUT + 4, FIRSTOUTPUTCOLUMN) = "Kd"
Cells(STARTROWOFOUTPUT + 5, FIRSTOUTPUTCOLUMN) = "Density"
Cells(STARTROWOFOUTPUT + 6, FIRSTOUTPUTCOLUMN) = "Initial NAPL Composition"
Cells(STARTROWOFOUTPUT + 7, FIRSTOUTPUTCOLUMN) = "Initial NAPL Mass"
For ComponentCounter = 1 To NUMBEROFCOMPONENTS
   Cells(STARTROWOFOUTPUT, FIRSTCOLUMN + ComponentCounter - 1) = _
   NamesofComponents(ComponentCounter)
   Cells(STARTROWOFOUTPUT + 1, FIRSTOUTPUTCOLUMN + ComponentCounter) = _
   MolecularMass(ComponentCounter)
```

```
        Cells(STARTROWOFOUTPUT + 2, FIRSTOUTPUTCOLUMN + ComponentCounter) = _
        Solubility(ComponentCounter)
        Cells(STARTROWOFOUTPUT + 3, FIRSTOUTPUTCOLUMN + ComponentCounter) = _
        Koc(ComponentCounter)
        Cells(STARTROWOFOUTPUT + 4, FIRSTOUTPUTCOLUMN + ComponentCounter) = _
        Kd(ComponentCounter)
        Cells(STARTROWOFOUTPUT + 5, FIRSTOUTPUTCOLUMN + ComponentCounter) = _
        Density(ComponentCounter)
        Cells(STARTROWOFOUTPUT + 6, FIRSTOUTPUTCOLUMN + ComponentCounter) = _
        InitialNAPLComposition(ComponentCounter)
        Cells(STARTROWOFOUTPUT + 7, FIRSTOUTPUTCOLUMN + ComponentCounter) = _
        InitialNAPLMass(ComponentCounter)
    Next ComponentCounter
    Cells(STARTROWOFOUTPUT + 9, FIRSTOUTPUTCOLUMN) = "Soil Density"
    Cells(STARTROWOFOUTPUT + 10, FIRSTOUTPUTCOLUMN) = "foc"
    Cells(STARTROWOFOUTPUT + 11, FIRSTOUTPUTCOLUMN) = "Porosity"
    Cells(STARTROWOFOUTPUT + 12, FIRSTOUTPUTCOLUMN) = "Initial NAPL Volume"
    Cells(STARTROWOFOUTPUT + 13, FIRSTOUTPUTCOLUMN) = "Initial NAPL Density"
    Cells(STARTROWOFOUTPUT + 14, FIRSTOUTPUTCOLUMN) = "Initial Water Volume"
    Cells(STARTROWOFOUTPUT + 16, FIRSTOUTPUTCOLUMN) = "Number of Timesteps"
    Cells(STARTROWOFOUTPUT + 17, FIRSTOUTPUTCOLUMN) = "Number of Cells"
    '
    Cells(STARTROWOFOUTPUT + 9, FIRSTOUTPUTCOLUMN + 1) = SoilDensity
    Cells(STARTROWOFOUTPUT + 10, FIRSTOUTPUTCOLUMN + 1) = foc
    Cells(STARTROWOFOUTPUT + 11, FIRSTOUTPUTCOLUMN + 1) = Porosity
    Cells(STARTROWOFOUTPUT + 12, FIRSTOUTPUTCOLUMN + 1) = InitialNAPLVolume
    Cells(STARTROWOFOUTPUT + 13, FIRSTOUTPUTCOLUMN + 1) = InitialNAPLDensity
    Cells(STARTROWOFOUTPUT + 14, FIRSTOUTPUTCOLUMN + 1) = InitialWaterVolume
    Cells(STARTROWOFOUTPUT + 16, FIRSTOUTPUTCOLUMN + 1) = NumberofTimesteps
    Cells(STARTROWOFOUTPUT + 17, FIRSTOUTPUTCOLUMN + 1) = NumberofCells
    '
    'Make the title column wide enough
    '
    Columns(FIRSTOUTPUTCOLUMN).Select
    Selection.ColumnWidth = 25
    Cells(1, 1).Select

    MultiSteps NumberofTimesteps, NumberofCells, NUMBEROFCOMPONENTS, _
    NamesofComponents, Header, MolecularMass, Solubility, Kd, Density, _
    InitialNAPLMass, InitialWaterVolume, Porosity, SoilDensity
End Sub
```

Listing B-2. Equilibrium Module.

```
Sub Equilibrium(Components, MolecularMass, Solubility, Kd, Density, InitialNAPLMass, _
InitialWaterVolume, Porosity, SoilDensity, NAPLMass, DissolvedMass, SorbedMass, _
DissolvedConcentration, WaterVolume)
    '
    Const TOLERANCE = 1E-30
    Const MGTOGRAMCONVERSION = 1000
    Const TITLEROWS = 3
    Const DEBUGPRINTFLAG = False
    Const PRECISIONOFSOLUTION = 0.0000001

    Dim MolarConcentration(1 To 20) As Double
    Dim MoleFraction(1 To 20) As Double
    Dim PreviousDissolvedConcentration(1 To 20) As Double
    Dim Volume(1 To 20) As Double
    Dim NAPLVolume As Double
    Dim TotalMoles As Double
    Dim SumofMoleFractions As Double
    Dim DissolvedDifference As Boolean
    Dim ChangeinPrecison As Double
    Dim temp As Double

    '
    Dim CCount As Integer
    Dim NumberIterations As Integer
    '
    'Start of first iteration
    'Assume all the mass is in the NAPL
    'Calculate the molar concentration of each component in the NAPL based _
    on the initial NAPL Mass values
    '

    'Initialize the iterative variables with start values
    '
    WaterVolume = InitialWaterVolume
    For CCount = 1 To Components
        NAPLMass(CCount) = InitialNAPLMass(CCount)
        DissolvedConcentration(CCount) = 1#
        DissolvedMass(CCount) = 0#
        SorbedMass(CCount) = 0#
    Next CCount


    If DEBUGPRINTFLAG Then
        Sheets.Add

        Cells(TITLEROWS - 1, 1) = "Iteration"
        Cells(TITLEROWS - 1, 2) = "Water Volume"
        Cells(TITLEROWS, 2) = InitialWaterVolume

        For CCount = 1 To Components
            Cells(TITLEROWS - 2, (CCount - 1) * 4 + 3) = "Component"
            Cells(TITLEROWS - 2, (CCount - 1) * 4 + 4) = CCount
            Cells(TITLEROWS - 1, (CCount - 1) * 4 + 3) = "NAPL Mass"
            Cells(TITLEROWS - 1, (CCount - 1) * 4 + 4) = "Dissolved Mass"
            Cells(TITLEROWS - 1, (CCount - 1) * 4 + 5) = "Sorbed Mass"
```

```
        Cells(TITLEROWS - 1, (CCount - 1) * 4 + 6) = "Dissolved Concentration"
        Cells(TITLEROWS, (CCount - 1) * 4 + 3) = NAPLMass(CCount)
    Next CCount
    End If

'
'The sum of the mole fractions should equal 1.0
'If mole fractions of all components equal zero, the mole fraction will equal zero _
and no NAPL remains
'
' Calculate the dissolved concentration based on the NAPL mole fractions for as _
long as the mole fraction is greater than 0

NumberIterations = 1
Do
    TotalMoles = 0
    For CCount = 1 To Components
        PreviousDissolvedConcentration(CCount) = DissolvedConcentration(CCount)
        MolarConcentration(CCount) = NAPLMass(CCount) / MolecularMass(CCount)
        TotalMoles = TotalMoles + MolarConcentration(CCount)
    Next CCount

    SumofMoleFractions = 0
    For CCount = 1 To Components
        If TotalMoles > TOLERANCE Then
            MoleFraction(CCount) = MolarConcentration(CCount) / TotalMoles
        Else MoleFraction(CCount) = 0#
        End If
        SumofMoleFractions = SumofMoleFractions + MoleFraction(CCount)
    Next CCount


    For CCount = 1 To Components
        MolarConcentration(CCount) = NAPLMass(CCount) / MolecularMass(CCount)
    '
    'If the mole fraction of a component equals zero,
    'then the total mass of each component can be partititoned
    'exactly into the dissolved phase and sorbed phase
    'No more iterations required for this component
    '
        If MoleFraction(CCount) < TOLERANCE Then
            temp = WaterVolume / (SoilDensity * Kd(CCount))
            DissolvedConcentration(CCount) = (InitialNAPLMass(CCount) * _
            (temp / (1 + temp))) / WaterVolume
        Else DissolvedConcentration(CCount) = MoleFraction(CCount) * _
        Solubility(CCount) / MGTOGRAMCONVERSION
        End If
    '
    '
    'Calculate dissolved mass based on dissolved concentrations
    '
        DissolvedMass(CCount) = DissolvedConcentration(CCount) * WaterVolume
    '
    ' Calculate sorbed mass based on dissolved concentrations and Kd.
    '
        SorbedMass(CCount) = DissolvedConcentration(CCount) * Kd(CCount) * _
        SoilDensity
    '
```

```
    ' Calculate NAPL Mass
    '
        NAPLMass(CCount) = InitialNAPLMass(CCount) - DissolvedMass(CCount) - _
        SorbedMass(CCount)
        If NAPLMass(CCount) < 0 Then NAPLMass(CCount) = 0#
    '
    'Calculate NAPL Volume for each component
    '
        Volume(CCount) = NAPLMass(CCount) / Density(CCount)
    Next CCount
'
'Calculate total NAPL Volume
'
    NAPLVolume = 0#
    DissolvedDifference = True
    For CCount = 1 To Components
        NAPLVolume = NAPLVolume + Volume(CCount)

        If PreviousDissolvedConcentration(CCount) < TOLERANCE Then
            ChangeinPrecision = Abs(DissolvedConcentration(CCount))
        Else
            ChangeinPrecision = Abs(DissolvedConcentration(CCount) - _
            PreviousDissolvedConcentration(CCount)) / _
            PreviousDissolvedConcentration(CCount)
        End If
        DissolvedDifference = DissolvedDifference And _
        (ChangeinPrecision < PRECISIONOFSOLUTION)
    Next CCount
'
'Calculate new volume of water based on porosity and new NAPL volume
'
    WaterVolume = Porosity - NAPLVolume
'
'Print Output Array on a New Spreadsheet
'
'
If DEBUGPRINTFLAG Then
    Cells(NumberIterations + TITLEROWS, 1) = NumberIterations
    Cells(NumberIterations + TITLEROWS, 2) = WaterVolume
    For CCount = 1 To Components
        Cells(NumberIterations + TITLEROWS, (CCount - 1) * 4 + 3) = _
        NAPLMass(CCount)
        Cells(NumberIterations + TITLEROWS, (CCount - 1) * 4 + 4) = _
        DissolvedMass(CCount)
        Cells(NumberIterations + TITLEROWS, (CCount - 1) * 4 + 5) = _
        SorbedMass(CCount)
        Cells(NumberIterations + TITLEROWS, (CCount - 1) * 4 + 6) = _
        DissolvedConcentration(CCount)
    Next CCount
End If

    NumberIterations = NumberIterations + 1
    If NumberIterations > 20 Then Exit Sub

Loop Until DissolvedDifference
Exit Sub
End Sub
```

Listing B-3. Multistep Subroutine Module.

```
Sub MultiSteps(NumberofTimesteps, NumberofCells, Components, NamesofComponents, _
Header, MolecularMass, Solubility, Kd, Density, InitialNAPLMass, InitialWaterVolume, _
Porosity, SoilDensity)
'
  'Note that there should be a minimum to 5 header rows
  Const TITLEROWS = 5
  Const FIRSTCOLUMN = 1
  Const DEBUGPRINTFLAG = False
  Const OUTPUTPRECISION = 1000
  Const TOTALNUMBERROWS = 15000

  Dim NAPLMass(1 To 20) As Double
  Dim DissolvedMass(1 To 20) As Double
  Dim SorbedMass(1 To 20) As Double
  Dim DissolvedConcentration(1 To 20) As Double
  Dim InputNAPLMass(1 To 20) As Double
  Dim RetainedNAPLMass(1 To 20, 1 To 100) As Double
  Dim LasttimeExportedNAPLMass(1 To 20, 1 To 100) As Double
  Dim ThistimeExportedNAPLMass(1 To 20, 1 To 100) As Double
  Dim RetainedWaterVolume(1 To 100) As Double
  Dim InputWaterVolume As Double
  Dim WaterVolume As Double
  Dim SumofNAPLMass(1 To 20) As Double
  Dim TotalNAPLinfirstcell As Double
  Dim NAPLRemainingFraction As Double
  Dim InitialNAPLVolume As Double
  Dim WaterVolumeSummary As Double

  Dim Timestep As Integer
  Dim CCount As Integer
  Dim CellCounter As Integer
  Dim Rownumber As Integer
  Dim PanelCounter As Integer
  Dim TotalNumberofColumns As Integer
  Dim TotalNumberofPanels As Integer
  Dim ColumnOffset As Integer
  Dim RowOffset As Integer

  If DEBUGPRINTFLAG Then
    Sheets.Add
    With ActiveSheet
      .Name = "Debug Multistep"
    End With

    Cells(TITLEROWS, 1) = "Time Step"
    Cells(TITLEROWS, 2) = "Cell Number"
    Cells(TITLEROWS, 3) = "Initial Water Volume"
    Cells(TITLEROWS, 4) = "Water Volume"

    For CCount = 1 To Components
      Cells(TITLEROWS - 1, (CCount - 1) *5 + 5) = "Component"
      Cells(TITLEROWS - 1, (CCount - 1) * 5 + 6) = CCount
      Cells(TITLEROWS, (CCount - 1) *5 + 5) = "Initial NAPL Mass"
      Cells(TITLEROWS, (CCount - 1) * 5 + 6) = "NAPL Mass"
      Cells(TITLEROWS, (CCount - 1) * 5 + 7) = "Dissolved Mass"
```

```
    Cells(TITLEROWS, (CCount - 1) * 5 + 8) = "Sorbed Mass"
    Cells(TITLEROWS, (CCount - 1) * 5 + 9) = "Dissolved Concentration"
Next CCount
End If
' Calculate the number of panels
' Total number of columns in each panel is 3 (timestep number or pore volume, _
Q, and NAPL remaining)
' plus the total number of components
If NumberofTimesteps <= TOTALNUMBERROWS Then _
TotalNumberofPanels = 1
If NumberofTimesteps > TOTALNUMBERROWS Then _
TotalNumberofPanels = NumberofTimesteps \ TOTALNUMBERROWS + 1

TotalNumberofColumns = 3 + Components
If (TotalNumberofPanels * TotalNumberofColumns) > 256 Then
MsgBox ("Output sheet will occupy more than 256 columns." & Chr(13) & _
"Total Number of Rows Allowed by Multistep Subroutine is " & _
TOTALNUMBERROWS & Chr(13) & _
"Change the constant TOTALNUMBERROWS in the Multistep subroutine." & Chr(13) & _
"Excel may not allow more than 16,638 rows in a sheet.")
Exit Sub
End If

Sheets.Add
With ActiveSheet
   .Name = "Dissolved Concentrations"
End With
Cells(TITLEROWS - 4, FIRSTCOLUMN) = "CURRENT TIMESTEP IS"
Cells(TITLEROWS - 4, FIRSTCOLUMN + 4) = "OF " & NumberofTimesteps

For PanelCounter = 1 To TotalNumberofPanels
   ColumnOffset = (PanelCounter - 1) * TotalNumberofColumns
   Cells(TITLEROWS - 2, FIRSTCOLUMN + ColumnOffset) = Header
   Cells(TITLEROWS - 1, FIRSTCOLUMN + 3 + ColumnOffset) = _
   "Dissolved Concentrations (mg/L)"
   Cells(TITLEROWS, FIRSTCOLUMN + ColumnOffset) = "Pore Volumes"
   Cells(TITLEROWS, FIRSTCOLUMN + 1 + ColumnOffset) = "Q"
   Cells(TITLEROWS, FIRSTCOLUMN + 2 + ColumnOffset) = "NAPL Remaining"
   For CCount = 1 To Components
      Cells(TITLEROWS, FIRSTCOLUMN + 2 + CCount + ColumnOffset) = _
      NamesofComponents(CCount)
   Next CCount
Next PanelCounter

With Rows(TITLEROWS - 4)
.Font.Bold = True
.Font.Size = 14
End With

 With Rows(TITLEROWS - 2)
.Font.Size = 14
End With

With Rows(TITLEROWS)
   .Font.Bold = True
End With

For CellCounter = 1 To NumberofCells
```

```
      For CCount = 1 To Components
        RetainedNAPLMass(CCount, CellCounter) = InitialNAPLMass(CCount)
        LasttimeExportedNAPLMass(CCount, CellCounter) = 0#
        ThistimeExportedNAPLMass(CCount, CellCounter) = 0#
      Next CCount
      RetainedWaterVolume(CellCounter) = InitialWaterVolume
    Next CellCounter

    TotalNAPLinfirstcell = 0#
    WaterVolumeSummary = 0#

For Timestep = 1 To NumberofTimesteps

  For CCount = 1 To Components
    SumofNAPLMass(CCount) = 0#
  Next CCount

  For CellCounter = 1 To NumberofCells

    For CCount = 1 To Components
      If CellCounter > 1 And Timestep > 1 Then
      InputNAPLMass(CCount) = RetainedNAPLMass(CCount, CellCounter) + _
      LasttimeExportedNAPLMass(CCount, CellCounter - 1)
      Else
      InputNAPLMass(CCount) = RetainedNAPLMass(CCount, CellCounter)
      End If
      Next CCount
    InputWaterVolume = RetainedWaterVolume(CellCounter)

    Equilibrium Components, MolecularMass, Solubility, Kd, Density, InputNAPLMass, _
    InputWaterVolume, Porosity, SoilDensity, NAPLMass, DissolvedMass, SorbedMass, _
    DissolvedConcentration, WaterVolume

    For CCount = 1 To Components
      RetainedNAPLMass(CCount, CellCounter) = NAPLMass(CCount) + _
      SorbedMass(CCount)
      ThistimeExportedNAPLMass(CCount, CellCounter) = DissolvedMass(CCount)
      SumofNAPLMass(CCount) = SumofNAPLMass(CCount) + NAPLMass(CCount)
      If Timestep = 1 And CellCounter = 1 Then
        TotalNAPLinfirstcell = TotalNAPLinfirstcell + NAPLMass(CCount)
        InitialNAPLVolume = Porosity - WaterVolume
      End If
    Next CCount
    RetainedWaterVolume(CellCounter) = WaterVolume

    If DEBUGPRINTFLAG Then
    Worksheets("Debug Multistep").Activate
      Rownumber = (Timestep - 1) * NumberofCells + CellCounter + TITLEROWS
      Cells(Rownumber, 1) = Timestep
      Cells(Rownumber, 2) = CellCounter
      Cells(Rownumber, 3) = InputWaterVolume
      Cells(Rownumber, 4) = WaterVolume
      For CCount = 1 To Components
        Cells(Rownumber, (CCount - 1) * 5 + 5) = InputNAPLMass(CCount)
        Cells(Rownumber, (CCount - 1) * 5 + 6) = NAPLMass(CCount)
        Cells(Rownumber, (CCount - 1) * 5 + 7) = DissolvedMass(CCount)
        Cells(Rownumber, (CCount - 1) * 5 + 8) = SorbedMass(CCount)
        Cells(Rownumber, (CCount - 1) * 5 + 9) = DissolvedConcentration(CCount)
```

```
            Next CCount
          End If

        Next CellCounter

        For CellCounter = 1 To NumberofCells
          For CCount = 1 To Components
            LasttimeExportedNAPLMass(CCount, CellCounter) = _
            ThistimeExportedNAPLMass(CCount, CellCounter)
          Next CCount
        Next CellCounter

        WaterVolumeSummary = WaterVolumeSummary + WaterVolume
        NAPLRemainingFraction = 0#

        For CCount = 1 To Components
          NAPLRemainingFraction = NAPLRemainingFraction + SumofNAPLMass(CCount)
        Next CCount
        NAPLRemainingFraction = NAPLRemainingFraction / (TotalNAPLinfirstcell * _
        NumberofCells)


        Worksheets("Dissolved Concentrations").Activate
        Cells(TITLEROWS - 4, FIRSTCOLUMN + 3) = Timestep
        PanelCounter = (Timestep - 1) \ TOTALNUMBERROWS + 1
        RowOffset = Timestep - (PanelCounter - 1) * TOTALNUMBERROWS
        ColumnOffset = (PanelCounter - 1) * TotalNumberofColumns
        Cells(TITLEROWS + RowOffset, FIRSTCOLUMN + ColumnOffset) = _
        Timestep - 1
        Cells(TITLEROWS + RowOffset, FIRSTCOLUMN + 1 + ColumnOffset) = _
        WaterVolumeSummary / (InitialNAPLVolume * NumberofCells)
        Cells(TITLEROWS + RowOffset, FIRSTCOLUMN + 2 + ColumnOffset) = _
        NAPLRemainingFraction
        For CCount = 1 To Components
          Cells(TITLEROWS + RowOffset, FIRSTCOLUMN + CCount + 2 + ColumnOffset) = _
          DissolvedConcentration(CCount) * OUTPUTPRECISION
        Next CCount

      Next Timestep

    End Sub
```